U.F.R. des Sciences d'Orsay

Mémoire
d'HABILITATION A DIRIGER DES RECHERCHES
de l'UNIVERSITE PARIS-SUD 11

présenté par

Laurent DANIEL

Approche multi-échelle du comportement électro-magnéto-mécanique

Travaux soutenus le 8 juin 2011 devant le jury composé de :

Francis Piriou	Professeur des Universités	Président, rapporteur
Gérard Maugin	Directeur de Recherche	Rapporteur
Ari Sihvola	Professeur des Universités	Rapporteur
Oriano Bottauscio	Directeur de Recherche	Examinateur
Frédéric Bouillault	Professeur des Universités	Examinateur
Pierre Gilormini	Directeur de Recherche	Examinateur
Nelson Sadowski	Professeur des Universités	Examinateur
Philip Withers	Professeur des Universités	Invité

Laboratoire de Génie Électrique de Paris
CNRS UMR 8507 ; Supelec ; UPMC ; Univ Paris-Sud
11 rue Joliot-Curie, F-91192 GIF-SUR-YVETTE CEDEX

Préambule

Ce document décrit les activités professionnelles que j'ai menées depuis environ dix ans. Il est divisé en trois parties.

- La première partie est un curriculum vitæ détaillé décrivant mon parcours et les grandes lignes de mes activités d'enseignement et de recherche.
- La deuxième partie est un recueil de publications donnant un aperçu plus précis de ma thématique de recherche. J'ai tenté d'articuler ce recueil en trois parties, en introduisant à chaque fois les articles proposés, de façon à mettre en avant le fil directeur de mes activités sur les phénomènes de couplage multiphysique.
- La troisième partie enfin propose quelques pistes de recherche pour les années à venir.

Résumé des travaux de recherche

Mes travaux de recherche portent sur l'étude et la modélisation multi-échelle des phénomènes de couplage multiphysique, et plus particulièrement entre propriétés mécaniques et électromagnétiques.

Ils abordent de manière complémentaire les aspects numériques et théoriques, et les aspects expérimentaux. Du point de vue de la modélisation, on cherche à décrire le comportement à l'échelle des mécanismes physiques qui permettent de l'expliquer. La démarche consiste ensuite à tirer parti des outils d'homogénéisation développés pour les comportements découplés et à les adapter au cas des comportements couplés. Cette approche a permis de décrire certains effets d'hétérogénéité et de microstructure dans les matériaux du Génie Electrique, et de proposer des modèles prédictifs pour les comportements couplés. Des outils de modélisation par éléments finis ont également été proposés pour le dimensionnement de structures. Du point de vue expérimental, des dispositifs de caractérisation du comportement magnéto-mécanique ont été développés pour permettre la construction, l'identification et la validation des modèles proposés.

Un effort particulier a été fait sur la description et la caractérisation du comportement magnéto-mécanique, mais le comportement piézoélectrique a également été abordé, notamment pour permettre l'étude de l'effet magnéto-électrique dans les matériaux composites à constituants magnétostrictifs et piézoélectriques.

La gamme des matériaux utilisés va des matériaux polycristallins classiquement utilisés pour les dispositifs électrotechniques aux composites magnéto-électriques pour capteurs de champ magnétique, en passant par les matériaux à magnétostriction géante pour la conception d'actionneurs.

Ces travaux sont décrits dans la partie 2 de ce document.

Remerciements

Je tiens tout d'abord à remercier Oriano Bottauscio, Frédéric Bouillault, Pierre Gilormini, Gérard Maugin, Francis Piriou, Nelson Sadowski, Ari Sihvola et Philip Withers pour leur participation à mon jury d'habilitation, pour le travail qu'a représenté l'étude de mon mémoire et pour les échanges qui ont suivi ma soutenance. La diversité de leurs horizons, géographiques mais surtout disciplinaires, représentait pour moi un défi, et je suis très honoré de leur intérêt pour mes travaux.

Ce document est un point d'étape d'un parcours jalonné de nombreuses rencontres. Il m'est impossible de toutes les mentionner, mais certaines ont été essentielles.
Je suis très redevable à René Billardon, Olivier Hubert et plus généralement à toute l'équipe "magnétisme" du LMT-Cachan qui m'ont fait découvrir le domaine des couplages magnéto-élastiques.
Le département MOCOSEM, en faisant le pari d'accueillir un "mécanicien" dans un laboratoire de Génie Electrique, m'a donné l'opportunité d'apporter un regard que j'espère original sur les phénomènes de couplage dans les dispositifs électromagnétiques. J'ai appris beaucoup au contact de cette nouvelle culture. J'ai en plus trouvé au LGEP un environnement propice à la réflexion, au débat, à la controverse, mais aussi à la détente. Je remercie le personnel du LGEP avec une pensée spéciale pour mon compère Yves Bernard avec qui je détiens mon record de consommation de caféine. Je souhaite aussi remercier les nombreux collègues du département de Physique et de Polytech'Paris-Sud qui m'ont accompagné dans ce parcours transdisciplinaire. Cette expérience me conforte dans la conviction que ni la recherche ni l'enseignement ne doivent être une aventure individuelle.

Le travail présenté dans ce document est un travail collectif, fruit de nombreux échanges.
Les collaborations internes au LGEP ont été nombreuses, de nouvelles se lancent. Je remercie mes collègues du département MOCOSEM et plus spécifiquement les participants au thème "Comportement multiphysique des Matériaux" avec lesquels les discussions ont été riches. Je dois beaucoup aux étudiants avec qui j'ai pu travailler, en particulier les doctorants : Nicolas Galopin, Romain Corcolle, Karl-Joseph Rizzo, Thu Trang Nguyen, András Bartók, Valentin Préault et Mahmoud Rekik. Ils ont, chacun à leur façon, contribué à mon évolution sur ce parcours.
Mes travaux se sont également nourris des liens que j'ai pu tisser à l'extérieur du laboratoire.
J'ai eu notamment la chance de travailler avec les équipes du LMT-Cachan, du LPCES, du LPMTM et de l'IEF. J'ai également eu de nombreux échanges avec des collègues plus éloignés géographiquement, en France, en Finlande, au Vietnam, au Brésil, au Royaume-Uni ou ailleurs. J'apprécie toutes ces rencontres, j'ai conscience de leur importance, et elles représentent pour moi une grande stimulation.

Enfin, je dédie ce mémoire à Laure, Maël et Romane, pour les expériences partagées, et celles à venir.

FIGURE 1 – "La famille d'Angleterre", Maël, juillet 2011.

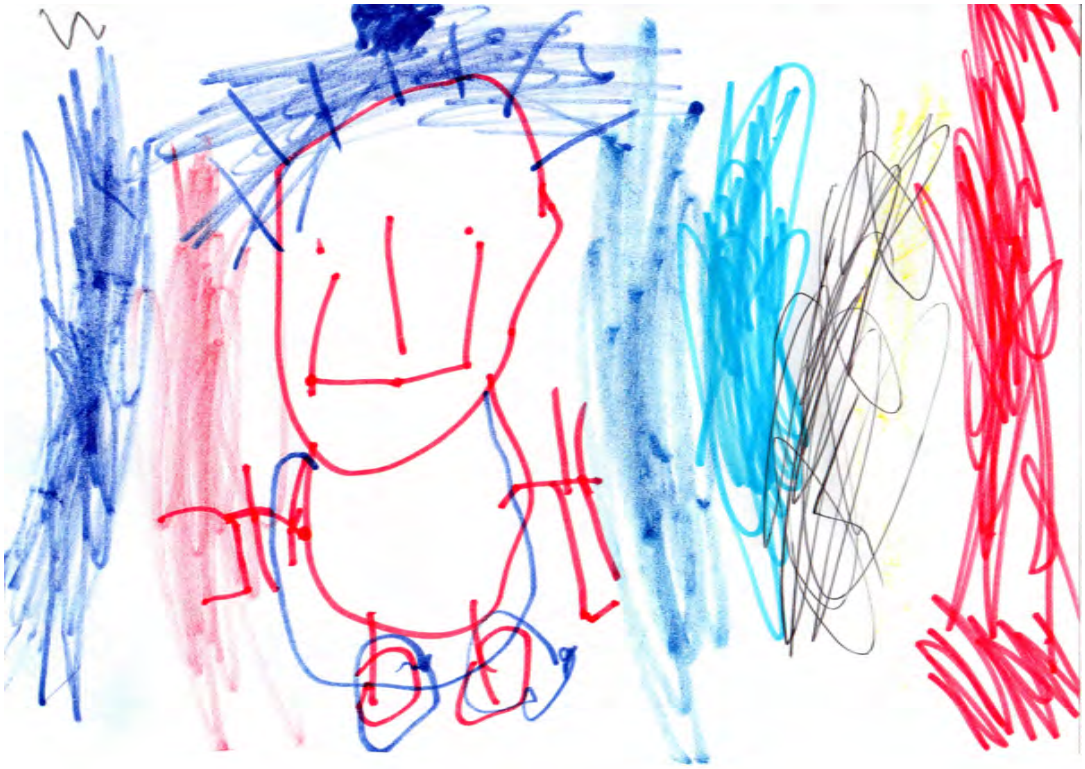

FIGURE 2 – "Mon rouge", Romane, juillet 2011.

Table des matières

Abbréviations

Quelques abbréviations utilisées dans le document sont indiquées sur cette page.

ANR	Agence Nationale de la Recherche (organisme de financement de projets de recherche).
FUI	Fonds Unique Interministériel (organisme de financement de projets de recherche).
3MT	Matériaux Magnétiques pour Machines et Transformateurs, projet FUI.
MAEL	MAgneto-ELastic behaviour characterisation and multiscale modelling Programme ANR Blanc BLAN08-2_367373.
SYRENA	SYstème de REgulation Nouvelle Architecture, projet FUI.
CEA	Commissariat à l'Energie Atomique.
CNRS	Centre National de la Recherche Scientifique.
ECP	Ecole Centrale Paris.
ENS de Cachan	Ecole Normale Supérieure de Cachan.
ENSAM	Ecole Nationale Supérieure d'Arts et Métiers.
ENSMP	Ecole Nationale Supérieure des Mines de Paris.
INRETS	Institut National de Recherche sur les Transports et leur Sécurité.
INSA	Institut National des Sciences Appliquées.
MENRT	Ministère de l'Education Nationale, de la Recherche et de la Technologie.
UPMC	Université Pierre et Marie Curie.
UVSQ	Université de Versailles Saint Quentin.
X	Ecole Polytechnique.
CCSU	Commission Consultative de Spécialistes de l'Université.
DEA	Diplôme d'Etudes Approfondies (éq. Master of Science).
GDR	Groupement de Recherche.
UFR	Unité de Formation et de Recherche.
UMR	Unité Mixte de Recherche.
IEF	Institut d'Electronique Fondamentale, Orsay.
LGEP	Laboratoire de Génie Electrique de Paris, Gif-sur-Yvette.
LMA	Laboratoire de Mécanique et d'Acoustique, Marseille.
LMM	Laboratoire de Modélisation en Mécanique, Paris.
LMT	LMT-Cachan (Laboratoire de Mécanique et Technologie), Cachan.
LPCES	Laboratoire de Physico-Chimie de l'Etat Solide, Orsay.
LPMTM	Laboratoire des Propriétés Mécaniques et Thermodynamiques des Matériaux, Villetaneuse.
MECAMAT	Association Mécanique et Matériaux.
SEEDS	Les Systèmes d'Energie Electrique dans leurs Dimensions Sociétales. (Groupement de recherche en Génie Electrique).
GO	Tôles à grains orientés.
NO	Tôles à grains non orientés.
AMR	Magnétorésistance anisotrope (anisotropic magnetoresistance).
FFT	Transformée de Fourier Rapide.
MEF	Méthode des Eléments Finis.
MHE	Milieu homogène équivalent.
VER	Volume Elémentaire Représentatif.

Partie 1

Parcours professionnel

Sommaire

1.1 Fiche synthétique

Laurent DANIEL - 35 ans
Maître de conférences à l'*Université Paris-Sud*
Chercheur au *Laboratoire de Génie Électrique de Paris* (LGEP)
Chercheur invité à la *School of Materials* (Université de Manchester, Royaume-Uni) depuis le 1^{er} mars 2011.

Formation et diplômes

2000-2003 : Thèse de doctorat au LMT-Cachan soutenue le 8 septembre 2003
1999-2000 : D.E.A. Mécanique & Matériaux
1996-1999 : Elève à l'Ecole Nationale Supérieure d'Arts & Métiers, diplômé en Juillet 1999

Activités d'enseignement

Depuis 2004 : 192 heures par an à l'Université Paris-Sud
Département de Physique de l'UFR des Sciences et Polytech'Paris-Sud
Génie Electrique, Electrocinétique, Sciences des Matériaux, Mécanique

2003-2004 : 192 heures au Département Génie Mécanique de l'ENS de Cachan
Science des Matériaux, Technologie Mécanique

2000-2003 : environ 230h sur 3 ans
Mécanique - Ecole d'ingénieurs en alternance, Cefipa, Bagneux (92)
Maîtrise Statistique des Procédés - Ingénieurs 2000, Univ. Marne-la-Vallée (77)

Activités de recherche

Méthodes multi-échelles pour la modélisation de comportements multi-physiques

Mes travaux de recherche portent sur l'étude et la modélisation des phénomènes de couplage multiphysique, et plus particulièrement sur le comportement électro-magnéto-mécanique. Ils abordent à la fois les aspects numériques, en particulier à travers le développement d'outils de modélisation multi-échelle, et les aspects expérimentaux, avec la mise en place de dispositifs de caractérisation de comportements couplés. Les matériaux étudiés vont des matériaux traditionnels du Génie Electrique pour la conception de matériel électrique jusqu'aux matériaux actifs pour la conception de capteurs ou d'actionneurs. Ces travaux ont pour objectif de fournir des relations de comportement couplé à destination des outils de conception, de dimensionnement et d'optimisation des dispositifs électromagnétiques.

Publications

Articles dans des revues internationales à comité de lecture : 31
Actes de colloques internationaux avec comité de lecture : 29
Colloques nationaux avec actes : 24

Activités d'animation scientifique et/ou d'intérêt collectif

Responsable du thème "*Comportement Multiphysique des Matériaux*" au LGEP
Coordinateur du projet ANR MAEL (BLAN08-2_367373) www.lgep.supelec.fr/mael
Rapporteur occasionnel pour les revues *Eur. Phys. J. Appl. Phys.*, *IEEE Trans. Magn.*, *J. Appl. Phys.*, *Appl. Phys. Lett.*, *Eur. J. Mech. A/Solids*, *Int. J. Solids Struct.*, *J. Zhejiang Univ-Sci. A.*

1.2 Curriculum Vitae

Laurent DANIEL né le 19 février 1976 (35 ans) **laurent.daniel@u-psud.fr**

Adresse professionnelle : **LGEP** (CNRS (UMR 8507) / SUPELEC / Univ Paris-Sud / UPMC)
11 rue Joliot Curie, Plateau de Moulon - 91192 Gif sur Yvette Cedex - Tél. : 01 69 85 16 39 - Fax : 01 69 41 83 18

Maître de conférences à l'Université Paris-Sud
Chercheur au Laboratoire de Génie Electrique de Paris

Formation

2000-2003 :	**Thèse au *LMT-Cachan*** (ENS de Cachan / CNRS (UMR 8535) / UPMC) Secteur Mécanique & Matériaux, sous la direction de R. Billardon et O. Hubert
Septembre 2003 :	Doctorat de l'***ENS de Cachan***, mention *Très honorable avec les félicitations du jury*
1999-2000 :	**D.E.A.** Mécanique & Matériaux (Université Paris 13) Option Mécanique et Mécanismes de la plasticité et de la mise en forme
Juillet 2000 :	Diplôme de DEA *mention Bien* ($4^{\text{ème}}$)
1996-1999 :	Etudes à l'Ecole Nationale Supérieure d'Arts & Métiers Centres de Lille (59) puis Paris (75)
Juillet 1999 :	Diplôme d'**ingénieur ENSAM**
1993-1996 :	Lycée Raspail, Paris (75) - Classes Préparatoires Technologiques
Juillet 1996 :	Admis à l'ENSAM, rang : $19^{\text{ème}}$
Juin 1993 :	Baccalauréat, Série C

Expériences professionnelles

Depuis 2004 :	Maître de conférences à l'***Université Paris-Sud*** (département de Physique - Orsay) Chercheur au ***LGEP*** (CNRS (UMR 8507) / Supelec / Univ Paris-Sud / UPMC) Département ***MOCOSEM*** (Modélisation et Contrôle de Systèmes Electromagnétiques) Animateur du thème "Comportement Multiphysique des Matériaux" (2006-2011) Bénéficiaire de la Prime d'Encadrement Doctoral et de Recherche (PEDR) (2006-2010) Coordinateur du projet ANR Blanc MAEL (janvier 2009 - décembre 2011) : « Magneto-elastic behaviour characterisation and multiscale modelling » Membre du bureau du département Matériaux de Polytech'Paris-Sud (2008-2011) Membre élu du Conseil de Laboratoire du LGEP (2010-2011) Membre élu de la C.C.S.U. de l'Université Paris-Sud, $63^{\text{ème}}$ section (2010-2011)
2010-2011 :	Accueilli en délégation au ***CNRS*** à mi-temps, affecté au LGEP
03/2011 - ... :	Chercheur invité, School of Materials, ***University of Manchester***, Royaume-Uni
2003-2004 :	Attaché Temporaire d'Enseignement et de Recherche à l'***ENS de Cachan***
2000-2003 :	Allocataire de recherche (MENRT) à l'***ENS de Cachan*** Enseignant vacataire à l'Université de Marne-la-Vallée (77) et au Centre de Formation des Ingénieurs Par l'Apprentissage (92)
Mars-Juin 2000 :	Stage de DEA au LMT-Cachan (ENS de Cachan / CNRS (UMR 8535) / UPMC) "Modélisation multi-échelle de la déformation de magnétostriction d'un polycristal"
Mars-Juin 1999 :	Projet de fin d'études au Lab. de Transformation et de Vieillissement des Polymères (LTVP) du centre ENSAM de Paris "Etude et modélisation de la diffusion de l'eau dans un matériau composite"

Langues

Anglais : Courant
Espagnol : Lu, écrit, parlé

1.3 Titres universitaires - Diplômes

Doctorat de l'Ecole Normale Supérieure de Cachan

Année : 2003
Spécialité : Mécanique - Génie Mécanique - Génie Civil
Laboratoire : Laboratoire de Mécanique et Technologie
Titre : Modélisation multi-échelle du comportement magnéto-mécanique des matériaux ferromagnétiques texturés
Soutenance : le 8 septembre 2003 à l'*ENS de Cachan*
Mention : *Très honorable avec les félicitations du jury*
Composition du jury

Rapporteurs :	Gérard MAUGIN, Directeur de Recherche au CNRS - LMM - Paris
	Paul VAN HOUTTE, Professeur à l'Université Catholique de Louvain
Examinateurs :	Jacques DEGAUQUE, Professeur à l'Université Paul Sabatier - Toulouse
	Yves-Patrick PELLEGRINI, Ingénieur au CEA - Bruyère-Le-Chatel
	Pierre SUQUET, Directeur de Recherche au CNRS - LMA - Marseille
Président :	André PINEAU, Professeur à l'Ecole des Mines de Paris
Encadrants :	René BILLARDON, Professeur à l'Université Paris VI
	Olivier HUBERT, Maître de Conférences à l'Université Paris VI

Résumé :
La thèse porte sur la caractérisation expérimentale et la modélisation des phénomènes de couplage magnéto-mécanique. On s'intéresse principalement à l'effet des contraintes sur le comportement magnétique et à la déformation de magnétostriction, qui est la déformation spontanée induite par la présence d'un champ magnétique. La très forte anisotropie des comportements couplés est mise en évidence, et une modélisation multi-échelle, considérant successivement l'équilibre d'un domaine magnétique, d'un monocristal (ou grain), et enfin d'un volume élémentaire représentatif est mise en œuvre. On montre notamment que l'état initial des matériaux, en particulier la configuration en domaines magnétiques à l'état désaimanté et l'état de contraintes résiduelles, a une grande influence sur le comportement macroscopique.

Mots-clefs : couplages magnéto-élastiques, déformation de magnétostriction, anisotropie, texture, homogénéisation, polycristal, fer-silicium.

Diplôme d'Etudes Approfondies

Année : 2000
DEA : Mécanique & Matériaux
Option : Mécanique et mécanismes de la plasticité et de la mise en forme
Etablissements : ECP - ENSAM - ENS de Cachan - ENSMP - Université Paris 13 - X
Mention : bien ($4^{\text{ème}}$)

Diplôme d'ingénieur

Année : 1999
Etablissement : Ecole Nationale Supérieure d'Arts & Métiers (ENSAM)

Baccalauréat

Année : 1993
Série : C

1.4 Bilan d'activités : Enseignement *

Université Paris-Sud - Département de Physique et Polytech'Paris-Sud

Période 2004-2011 (192 heures par an)
TP, TD Electrotechnique - L3 - 48 heures (2004-2006)
TP Ondes - Polytech'Paris-Sud - I1TC - 48 heures (2004-2006)
C, TD, TP Electrocinétique - L2 - 36 heures (2004-2009)
TD Simulation Numérique en Résistance des Matériaux^R - I2M - 30 heures (2004-2010)
C, TD, TP Sciences des Matériaux ("Véhicule du Futur")^R - I1TC - 60 heures (2005-2010)
C, TD Matériaux Composites^R - I3M - 22 heures (2006-2011)
C, TD, TP Méthodes Numériques^R - M1, PUF Hanoi - 40 heures (2006-2010)
C, TD Résistance des Matériaux^R - I2M - 28 heures (2009-2011)
C,TD Mécanique Statique - I1M - 15 heures (2009-2011)
C, TD, TP Couplages Multiphysiques^R - I3M - 25 heures (2009-2011)
C Initiation à la Mécanique du Solide - M2R PIE - 12 heures (2010-2011)
Participation aux entretiens de recrutement à Polytech'Paris-Sud
Encadrement et tutorat de stagiaires et de moniteurs (Polytech'Paris-Sud et Département de Physique)
Responsabilité du Laboratoire de TP commun Département de Chimie - Polytech'Paris-Sud (2007-2010)
Membre du bureau du Département Matériaux de Polytech'Paris-Sud (2008-2011)

Ecole Normale Supérieure de Cachan - Département de Génie Mécanique

Période 2003-2004 (192 heures)
TD, TP de Matériaux - L3 - 38 heures
TD de Spécifications géométriques - L3 - 10 heures
TD d'Analyse de l'Existant Technique - L3 - 16 heures
TD, TP de Mécanique du contact - L3 - 36 heures
TD de Conception Mécanique Assistée par Ordinateur - L3 - 28 heures
TD, TP de Science des Matériaux - M1 - 40 heures
Encadrement de TER en L3

Université de Marne-la-Vallée - Formation Ingénieurs 2000

Période 2000-2003 (160 heures sur 3 ans)
C, TD, TP de Maîtrise Statistique des Procédés^R
Etudiants en deuxième année d'école d'ingénieurs, formation en alternance.

Centre de Formation des Ingénieurs Par l'Apprentissage (Cefipa) - Bagneux

Période 2000-2003 (70 heures sur 3 ans)
C, TD de remise à niveau en mécanique des solides rigides (statique)
Etudiants en première année d'école d'ingénieurs, formation en alternance.

∗. Sauf mention contraire les volumes horaires s'entendent en heures équivalent TD par an.
C : cours, TD : travaux dirigés, TP : travaux pratiques, TER : Travaux Encadrés de Recherche.
L1, L2, L3 : Licence 1ère, 2ème, 3ème année,
M1, M2 : Master 1ère, 2ème année,
I1TC : Polytech'Paris-Sud - Cycle ingénieur 1ère année - Tronc Commun,
I1M, I2M, I3M : Polytech'Paris-Sud - Cycle ingénieur Matériaux 1ère, 2ème, 3ème année,
PUF Hanoi : Pôle Univesritaire Français à Hanoi, Master IST (Information, Systèmes et Technologie).
M2R PIE : Master 2 Recherche, Physique et Ingénierie de l'Energie, Univ Paris-Sud.
L'exposant ^{R} après l'intitulé signale la responsabilité ou co-responsabilité du module.

1.5 Bilan d'activités : Encadrement

Participation à l'encadrement de doctorants

Année (soutenance)	**Etudiant**	**Taux d'encadrement**	**Co-encadrement**	**Sujet**
2013 (prév.)	V. Préault	50%	R. Corcolle L. Pichon	Modélisation et caractérisation de matériaux composites pour boîtier d'équipement électronique
2013 (prév.)	M. Rekik	50%	O. Hubert	Mesure et modélisation du comportement magnéto-mécanique dissipatif des matériaux ferromagnétiques à haute limite d'élasticité sous chargement multiaxial
2012 (prév.)	A. Bartók	80%	A. Razek	Modélisation du comportement de dispositifs électromagnétiques sous sollicitations multi-physiques
2011 (prév.)	T.T. Nguyen	40%	X. Mininger F. Bouillault	Modélisation et caractérisation de l'effet magnéto-électrique au sein de matériaux composites
2011 (prév.)	K.J. Rizzo	40%	O. Hubert	Modélisation multi-échelle du comportement magnéto-mécanique : prise en compte des phénomènes d'hystérésis
2009	R. Corcolle [a]	80%	F. Bouillault	Détermination de lois de comportement couplé par des techniques d'homogénéisation : Application aux matériaux du Génie Electrique
2007	N. Galopin [b]	60%	F. Bouillault	Modélisation et caractérisation de matériaux actifs pour la conception de dispositifs magnéto-électriques

a. Actuellement maître de conférences à l'Université Paris-Sud, Orsay, France.
b. Actuellement maître de conférences à l'Université Joseph Fourier, Grenoble, France.

Participation à l'encadrement de stagiaires

Année	**Formation** (durée du stage)	**Etudiant**	**Taux d'encadrement** (co-encadrant)	**Sujet**
2010	Licence 3 Stage non obligatoire (10 semaines)	A. Al-Ganad	100%	Caractérisation du comportement magnéto-mécanique de matériaux magnétiques
2010	Magistère de Physique (9 semaines)	Y. Zhang	40% (G. Krebs)	Conception de machine électrique intégrant l'effet des contraintes mécaniques sur la perméabilité magnétique des matériaux
2009	I3M [a] Stage court (5 semaines)	L. Anagonou Y. Dezac	50% (Y. Bernard)	Modélisation par élements finis d'un dispositif de lévitation magnétique
2009	I3M Stage court (5 semaines)	J. Barnerias R. Guillory	50% (R. Corcolle)	Validation des résultats d'homogénéisation par génération aléatoire de microstructures en éléments finis
2009	Licence 2 Stage non obligatoire (3 semaines)	A. Al-Ganad	50% (G. Krebs)	Prise en compte de l'effet des contraintes mécaniques dans le logiciel Simap

a. Polytech'Paris-Sud - Cycle ingénieur Matériaux 3$^{\text{ème}}$ année.

Participation à l'encadrement de stagiaires (suite)

Année	**Formation** (durée du stage)	**Etudiant**	**Taux d'encadrement** (co-encadrant)	**Sujet**
2008	Master IST [a] Stage M2R (16 semaines)	T.H. Nguyen	50% (X. Mininger)	Contrôle mécanique de structures antennaires embarquées par actionnement actif
2008	Magistère de Physique Stage 1ère année (8 semaines)	V. Berionni	100%	Modélisation du comportement magnéto-élastique de matériaux ferromagnétiques amorphes
2007	I2M [b] Stage recherche (16 semaines)	J.S. Jeong	100%	Modélisation du comportement de matériaux ferromagnétiques amorphes
2007	Master MPF [c] Stage M2R (16 semaines)	K.J. Rizzo	30% (O. Hubert)	Modélisation multi-échelle de l'hystérésis magnéto-mécanique. Application à la mesure des contraintes au cours d'un impact par barre d'Hopkinson
2007	Master PA [d] Stage M1 (14 semaines)	T. Charron	50% (N. Galopin)	Caractérisation d'un matériau à magnétostriction géante : le Galfenol
2007	I3M Stage court (5 semaines)	D. Estève P. Hugel	50% (R. Corcolle)	Résolution de problèmes d'inclusion en magnétostatique non-linéaire à l'aide du logiciel éléments finis COMSOL MULTIPHYSICS
2006	Master PA Stage M2R (16 semaines)	A. Ribeiro	100%	Modélisation du comportement magnéto-élastique de monocristaux ferromagnétiques
2006	Master PA Stage M2R (16 semaines)	I. Estevez	50% (Y. Bernard)	Caractérisation d'un matériau piézoélectrique sous contraintes
2005	Master PA Stage M1 (9 semaines)	A. Ribeiro	100%	Modélisation du comportement magnétique du Terfenol-D : prise en compte de l'hystérésis
2005	Master PA Stage M1 (9 semaines)	C. Ketchazo	100%	Modélisation multi-échelle du comportement magnéto-élastique du Terfenol-D
2004	DEA M&M [e] Stage DEA (16 semaines)	O. Cerri	30% (O. Hubert)	Comportement magnéto-mécanique d'une ferrite Ni-Zn. Aspects expérimentaux et numériques
2003	DEA S3M [f] Stage DEA (16 semaines)	S. Dossin	40% (O. Hubert)	Suivi par mesures magnétiques de l'anisotropie de transformation de phase dans un acier TRIP : aspects expérimentaux et numériques
2002	DEA S3M AEN [g] (10 jours)	N. Jendly	40% (O. Hubert)	Plasticité et microplasticité des alliages de fer-silicium lors de sollicitations de traction et de flexion pure
2001	DEA S3M AEN (10 jours)	N. Derouiche	40% (O. Hubert)	Mise en évidence de l'anisotropie magnéto-élastique d'un alliage de fer silicium

a. Master Information, Systèmes et Technologie, parcours "Composants et antennes pour les télécommunications", Univ Paris-Sud.
b. Polytech'Paris-Sud - Cycle ingénieur Matériaux 2ème année.
c. Master Matériaux et Procédés de Fabrication, UPMC.
d. Master Physique et Applications, UPMC.
e. DEA Mécanique et Matériaux, UPMC.
f. DEA Solides, Structures et Systèmes Mécaniques, option "Couplages multi-physiques", UPMC.
g. Atelier expérimental et Numérique.

1.6 Bilan d'activités : Recherche *

Mes travaux de recherche portent sur l'étude et la modélisation des phénomènes de couplage multiphysique. Ils abordent à la fois les aspects numériques, en particulier à travers le développement d'outils de modélisation multi-échelle, et les aspects expérimentaux, avec la mise en place de dispositifs de caractérisation du comportement des matériaux du génie électrique ou des matériaux actifs.

Contexte

Les méthodes de calcul numérique ont fait durant ces dernières dizaines d'années des progrès considérables, qui ont rendu possible la modélisation de dispositifs de géométrie complexe. Les lois de comportement qui alimentent ces outils de calcul numérique ont en revanche relativement peu évolué. Si on s'intéresse aux phénomènes de couplage multiphysique, on s'aperçoit que ces relations de comportement sont encore assez rudimentaires, le plus souvent linéaires. L'un des verrous majeurs pour une modélisation fine des dispositifs électromagnétiques réside aujourd'hui dans la pauvreté des modèles de comportement. Avec le développement rapide des dispositifs basés sur l'utilisation de matériaux actifs, le besoin de modèles pour décrire les phénomènes de couplage multi-physique est de plus en plus fort. Les approches macroscopiques phénoménologiques - classiquement utilisées pour la description des phénomènes découplés - échouent bien souvent à décrire avec précision les comportements couplés. Cette faiblesse est probablement en partie responsable du retard dans la description des dispositifs exploitant les propriétés - souvent non-linéaires - de matériaux actifs. Dans ce domaine, les méthodes d'homogénéisation ouvrent des perspectives prometteuses pour faire évoluer significativement les outils de modélisation des dispositifs électromagnétiques.

Ces démarches de modélisation multi-échelle s'appuient sur le principe que l'échelle pertinente de modélisation d'un phénomène physique (ou multi-physique) est l'échelle des mécanismes qui sous-tendent ce phénomène. Cette échelle est souvent bien plus petite que la taille caractéristique des objets que l'on cherche à modéliser. C'est la raison pour laquelle il est nécessaire de définir des règles de changement d'échelle pour effectuer le passage des lois de comportement de l'échelle de description physique à l'échelle macroscopique, qui sera l'échelle de modélisation finale.

Dans ce contexte mes travaux de recherche se sont attachés à élaborer des règles de changement d'échelle adaptées aux phénomènes de couplage multiphysique. Cette démarche permet d'obtenir des lois de comportement homogénéisées pour les matériaux hétérogènes. Ces travaux ont permis de mettre en place une méthodologie générique d'homogénéisation pour les comportements découplés [RI.11] puis pour les comportements couplés [RI.17]. Des outils de modélisation ont également été développés pour accéder aux fluctuations intraphases dans les matériaux composites [RI.23], de manière à ne plus se contenter dans les modélisations du comportement moyen des constituants. Mes travaux de recherches se sont concentrés jusqu'à présent sur deux types de couplage multiphysique : le comportement magnéto-mécanique et l'effet magnéto-électrique.

Comportement magnéto-mécanique

Le couplage magnéto-mécanique dans les matériaux magnétiques présente deux manifestations principales. La première de ces manifestations est l'effet de l'application d'une sollicitation mécanique sur le comportement magnétique. On sait en effet que l'application d'une contrainte modifie les propriétés magnétiques, ce qui conduit souvent à une baisse de rendement dans les systèmes électromagnétiques de conversion d'énergie. Or, les sources potentielles de l'apparition de contraintes sont nombreuses, de l'élaboration des matériaux à leur mise en service, en passant par les traitements thermo-mécaniques, le transport, le stockage et l'assemblage du matériel. On cherche donc, une fois connues les contraintes subies par le matériau, à en identifier les effets, afin de les maîtriser ou de les exploiter. La deuxième manifestation des phénomènes de couplage magnéto-mécanique est la déformation de magnétostriction. Cette déformation est la déformation spontanée induite dans les matériaux ferromagnétiques par la présence d'un champ magnétique. Elle permet notamment la fabrication d'actionneurs ou de capteurs magnétostrictifs qui transforment un signal magnétique en déplacement, ou inversement. L'amplitude de la déformation de magnétostriction est elle-même très sensible à l'application d'un état de contraintes. On souhaite donc disposer de modèles permettant de quantifier l'amplitude de cette déformation en fonction des sollicitations extérieures.

∗. Les références utilisées dans cette partie renvoient à la codification de la liste des publications.

La description des mécanismes de couplage magnéto-mécanique fait intervenir différentes échelles, de celle de l'atome ou du groupement d'atomes, à laquelle on définit de façon fondamentale les mécanismes physiques du comportement, à celle de la structure qui intéresse finalement les utilisateurs de dispositifs électromagnétiques. Le couplage magnéto-mécanique se prête donc particulièrement à la démarche de modélisation multi-échelle. Un modèle de comportement magnéto-mécanique pour les matériaux polycristallins, s'appuyant sur trois échelles intermédiaires (domaine magnétique, monocristal (ou grain) et Volume Elémentaire Représentatif (VER)) a été proposé [RI.14,RI.15]. Cette approche de modélisation a été accompagnée de nombreux travaux expérimentaux, souvent menés en collaboration, afin d'alimenter, d'identifier et de valider les modèles proposés. Un banc de caractérisation des matériaux actifs a notamment été mis en place au LGEP [RI.9].

Cette démarche a été mise en œuvre pour étudier le comportement de nombreux matériaux ou dispositifs. Des études on été menées sur les alliage de fer à 3% de silicium à grains non-orientés (NO) concernant les effets d'anisotropie [RI.1], l'importance des surfaces libres ou de la texture cristallographique [RI.2, RI.3], ou encore l'effet de la micro-plasticité sur le comportement magnétique [RI.5] ou magnétostrictif [RI.8]. Des mesures de comportement magnétique et de déformation de magnétostriction sous contraintes accompagnées des modélisations correspondantes ont été obtenues sur des tôles de fer-silicium à grains orientés (GO) [RI.12], sur des monocristaux de fer-silicium [RI.24], sur des alliages de fer-cobalt [RI.7], sur des ferrites Nickel-Zinc [RI.10], ou sur des échantillons de Terfenol-D [RI.15]. Nous nous sommes aussi intéressés à l'étude de dispositifs électromagnétiques à base de matériaux à magnétostriction géante [RN.1, RN.2, RI.16]. Des travaux ont également été menés afin d'évaluer le comportement magnéto-élastique des matériaux magnétiques sous sollicitations multi-axiales [RI.7]. La partie expérimentale est organisée en partenariat avec le LMT-Cachan autour de la machine triaxiale Astree. Ces travaux ont déjà permis de fournir des pistes de modélisation, qu'il s'agisse d'une approche par contrainte équivalente [RI.20, RI.26] ou de l'utilisation de modèles simplifiés [RI.30]. Enfin, des versions simplifiées du modèle multi-échelle ont permis l'étude de certains aspects particuliers du comportement magnéto-élastique, comme l'effet ΔE, qui est une perte apparente de linéarité dans le comportement élastique des matériaux magnétiques désaimantés. Ces résultats ont été confrontés avec succès à des résultats expérimentaux sur divers matériaux [RI.21, RI.25].

Comportement magnéto-électrique

Les matériaux magnéto-électriques présentent un effet de couplage entre grandeurs magnétiques et électriques, même en régime statique. Certains matériaux homogènes multiferroïques sont le siège d'un effet magnéto-électrique, mais l'obtention de coefficients de couplage exploitables est en général obtenue par l'association dans un matériau composite de phases piézoélectriques et magnétostrictives. Le couplage magnéto-électrique résulte alors de l'interaction mécanique entre les phases. Par exemple dans le cas de l'effet magnéto-électrique direct, la phase magnétostrictive se déforme sous l'action du champ magnétique extérieur. Cette déformation se transmet à la phase piézoélectrique (interactions élastiques) qui se polarise. Une explication analogue permet d'expliquer l'effet inverse : l'aimantation (ou la perméabilité) du composite est modifiée par l'application d'un champ électrique. L'effet magnéto-électrique est alors dit extrinsèque car il apparaît macroscopiquement mais n'est présent localement dans aucune des phases. Les méthodes d'homogénéisation sont particulièrement adaptées à ce type de matériaux composites. Des travaux de modélisation de dispositifs magnéto-électriques ont été entrepris, sur la base des méthodes par éléments finis [RI.13, RI.19, RI.28], ou sur celles des outils d'homogénéisation semi-analytiques [RI.17, RI.22].

Collaborations nationales et internationales récentes

Ces travaux m'ont donné l'opportunité de mettre en place ou de participer à des collaborations nationales ou internationales. En particulier, des liens ont été tissés avec l'Université Technologique d'Helsinki (A. Arkkio, A. Belahcen, Laboratory of Electromechanics) sur le thème de l'identification des modèles macroscopiques pour le comportement magnéto-mécanique. Dans le cadre de cette collaboration, j'ai effectué un séjour d'une semaine dans ce laboratoire en juin 2007, et une doctorante, Katarzyna Fonteyn [*thèse soutenue en 2010*], a été reçue au LGEP sous ma responsabilité du 1^{er} octobre 2007 au 31 janvier 2008.
J'ai également pu bénéficier des liens, antérieurs à mon arrivée au LGEP, avec l'Université de Tokyo (T. Ueno, Advanced Mechatronics Laboratory) sur la conception d'actionneurs et de capteurs basés sur l'utilisation de matériaux actifs (matériaux à magnétostriction géante et matériaux piézoélectriques).
Par ailleurs, nous mettons en place une collaboration entre le LGEP, l'IEF (Institut d'Electronique Fondamentale, Orsay) et le Coltech (College of Technology, Vietnam National University, Hanoi) pour l'étude de dispositifs d'assistance au changement d'aimantation par application de contrainte. Les dispositifs visés ici sont de taille beaucoup plus réduite que ceux traités jusqu'à présent. Dans le cadre de cette collaboration, T.T. Nguyen,

doctorante au LGEP a séjourné un mois au Coltech, et D.T. Huong Giang, maître de conférences au Coltech, a obtenu un financement post-doctoral à l'Université Paris-Sud à compter de novembre 2010.
Des contacts ont également été pris avec le GRUCAD (Grupo de Concepção e Análise de Dispositivos Eletromagnéticos, Universidade Federal de Santa Catarina (UFSC), Florianopolis) sur le thème de la modélisation de dispositifs électromagnétiques sous sollicitation mécanique. Dans ce cadre, j'ai été invité à séjourner deux semaines au GRUCAD en octobre 2010, et Jhoe Batistela, professeur à l'UFSC a obtenu un mois de professeur invité à l'Université Paris-Sud pour l'année 2010-2011.
Enfin, un partenariat se développe avec l'Université de Manchester, et plus particulièrement la School of Materials, sur le développement d'outils de caractérisation et de modélisation micromécanique du comportement ferroélectrique, avec pour objectif le développement de matériaux ferroélectriques sans plomb. Je viens d'entamer dans ce cadre un séjour de longue durée à l'Université de Manchester.

Sur le plan national, une collaboration a été mise en place (dans le cadre d'un projet exploratoire financé par SEEDS pour la période 2007-2008) avec le Laboratoire de Génie Electrique et de Ferroélectricité de l'INSA de Lyon pour la synthèse, la caractérisation et la modélisation de matériaux composites magnéto-électriques.
Par ailleurs, je suis coordinateur du projet blanc ANR MAEL (BLAN08-2_367373), débuté en janvier 2009 pour une durée de trois ans, visant à quantifier les mécanismes physiques à l'origine des phénomènes de couplages magnéto-mécaniques à l'échelle de monocristaux. Ce projet doit permettre d'identifier des modèles de comportement pertinents à une échelle locale (typiquement la dizaine de micromètres) de manière à les introduire dans des outils de modélisation multi-échelle. L'objectif final est de mieux cerner les relations entre microstructure et propriétés macroscopiques, afin de mettre en place des microstructures optimales pour le comportement magnéto-mécanique. Aux compétences du LGEP dans le domaine du Génie Electrique, ce projet fortement pluri-disciplinaire associe celles d'équipes de physiciens, de métallurgistes et de mécaniciens.
Enfin, je participe à différents projets de recherche financés par le Fonds Unique Interministériel (FUI) parmi lesquels le projet 3MT (Matériaux Magnétiques pour Machines et Transformateurs) soutenu par le pôle de compétitivité ASTech, et le projet SYRENA (SYstème de REgulation Nouvelle Architecture) soutenu par les pôles de compétitivité ASTech et Aerospace Valley.

1.7 Activités d'animation scientifique et/ou d'intérêt collectif

- Membre du bureau du Département Matériaux de Polytech'Paris-Sud (2008-2011).
- Responsable du laboratoire commun Polytech'Paris-Sud - Département de Chimie de Travaux Pratiques en Sciences des Matériaux 2007-2010).
- Membre élu de la Commission Consultative de Spécialistes de l'Université Paris-Sud (C.C.S.U.), 63$^{\text{ème}}$ section (2010-2011).
- Participation à des Comités de Sélection pour le recrutement d'enseignants-chercheurs :
  - Polytech'Paris-Sud, 2006, maître de conférences : poste 33MCF670
  - INRETS /UVSQ, 2010, Chaire Organisme-Université : poste 28MCF1265
- Membre élu du Conseil de Laboratoire du LGEP (2010-2011).
- Animateur du thème "*Comportement Multiphysique des Matériaux*" au LGEP depuis 2006 (10 chercheurs ou enseignants-chercheurs et 10 doctorants ou post-doctorants au 1/12/2010). www.lgep.supelec.fr/muphy.
- Coordinateur du projet ANR MAEL (BLAN08-2_367373, Période 2009-2011). www.lgep.supelec.fr/mael.
- Responsable scientifique du projet FUI SYRENA (SYstème de REgulation Nouvelle Architecture, Période 2010-2013), pôles de compétitivité ASTech et Aerospace Valley.
- Rapporteur occasionnel pour les revues
  - *Eur. Phys. J. Appl. Phys.*,
  - *IEEE Trans. Magn.*,
  - *J. Appl. Phys.*,
  - *Appl. Phys. Lett.*,
  - *Eur. J. Mech. A/Solids*,
  - *Int. J. Solids Struct.*,
  - *J. Zhejiang Univ-Sci. A*.
- Membre de l'équipe enseignante de l'Ecole d'Eté CE2M10 "Changement d'Echelles en Mécanique des Matériaux". http ://www.f2m.cnrs-bellevue.fr/spip.php ?rubrique75.
- Membre du comité d'organisation de la conférence PIERS 2011 (Progress In Electromagnetics Research Symposium) à Marrakech, Maroc. http ://directevent.net/piers/.
  Co-organisateur de la session "Smart Materials".
- Co-organisateur du colloque MECAMAT Aussois 2012 : "Mécanique, électricité et magnétisme : mécanismes, couplages, matériaux et applications".

1.8 Publications et communications

Articles dans des revues internationales avec comité de lecture

[RI.31] A. Bartók, L. Daniel, A. Razek, "Micro-macro modeling of stress-dependent anisotropic magnetoresistance", *Journal of Physics D : Applied Physics*, **44** :135001, 2011.

[RI.30] L. Bernard, X. Mininger, L. Daniel, G. Krebs, F. Bouillault and M. Gabsi, "Effect of stress on switched reluctance motors : A magneto-elastic finite element approach based on multiscale constitutive laws", *IEEE Transactions on Magnetics*, 2011 (accepté).

[RI.29] O. Hubert, L. Daniel, "Energetical and multiscale approaches for the definition of an equivalent stress for magneto-elastic couplings", *Journal of Magnetism and Magnetic Materials*, **323(13)** :1766-1781, 2011.

[RI.28] T.T. Nguyen, F. Bouillault, L. Daniel, X. Mininger, "Finite element modeling of magnetic field sensors based on nonlinear magnetoelectric effect", *Journal of Applied Physics*, **109(8)** :084904, 2011.

[RI.27] T.T. Nguyen, X. Mininger, F. Bouillault, L. Daniel, "Finite element harmonic modeling of magnetoelectric effect", *IEEE Transactions on Magnetics*, **47(5)** :1142-1145, 2011.

[RI.26] L. Daniel, O. Hubert, "Equivalent stress criteria for the effect of stress on magnetic behavior", *IEEE Transactions on Magnetics*, **46(8)** :3089-3092, 2010.

[RI.25] O. Hubert, L. Daniel, "Measurement and analytical modeling of the ΔE effect in a bulk iron-cobalt alloy", *IEEE Transactions on Magnetics*, **46(2)** :401-404, 2010.

[RI.24] K.J. Rizzo, O. Hubert, L. Daniel, "Magnetic and magnetostrictive behavior of iron-silicon single crystals under uniaxial stress", *IEEE Transactions on Magnetics*, **46(2)** :270-273, 2010.

[RI.23] R. Corcolle, L. Daniel, F. Bouillault, "Intraphase fluctuations in heterogeneous magnetic materials", *Journal of Applied Physics*, **105(12)** :123913 (8p), 2009.

[RI.22] R. Corcolle, L. Daniel, F. Bouillault, "Modeling of magnetoelectric composites using homogenization techniques", *Sensor Letters*, **7** :446-450, 2009.

[RI.21] L. Daniel, O. Hubert, "An analytical model for the ΔE effect in magnetic materials", *The European Physical Journal - Applied Physics*, **45** :31101 (11p), 2009.

[RI.20] L. Daniel, O. Hubert, "An equivalent stress for the influence of multiaxial stress on the magnetic behavior", *Journal of Applied Physics*, **105(7)** :07A313 (3p), 2009.

[RI.19] N. Galopin, X. Mininger, F. Bouillault, L. Daniel, "Magneto-electric composite structures", *European Journal of Electrical Engineering*, **12(4)** :461-474, 2009.

[RI.18] K.J. Rizzo, O. Hubert, L. Daniel, "A multiscale model for piezomagnetic behavior", *European Journal of Electrical Engineering*, **12(4)** :525-540, 2009.

[RI.17] R. Corcolle, L. Daniel, F. Bouillault, "Generic formalism for homogenization of coupled behaviors : application to magnetoelectroelastic behavior", *Physical Review B*, **78(21)** :214110 (12p), 2008.

[RI.16] R. Corcolle, L. Daniel, F. Bouillault, "Optimal design of magnetostrictive composites : an analytical approach", *IEEE Transactions on Magnetics*, **44(1)** :17-23, 2008.

[RI.15] L. Daniel, N. Galopin, "A constitutive law for magnetostrictive materials and its application to Terfenol-D single and polycrystals", *The European Physical Journal - Applied Physics*, **42(2)** :153-159, 2008.

[RI.14] L. Daniel, O. Hubert, N. Buiron, R. Billardon, "Reversible magneto-elastic behavior : a multiscale approach", *Journal of the Mechanics and Physics of Solids*, **56(3)** :1018-1042, 2008.

[RI.13] N. Galopin, X. Mininger, F. Bouillault, L. Daniel, "Finite element modelling of magneto-electric sensors", *IEEE Transactions on Magnetics*, **44(6)** :834-837, 2008.

[RI.12] O. Hubert, L. Daniel, "Multiscale modeling of the magneto-mechanical behavior of Grain Oriented Silicon Steels", *Journal of Magnetism and Magnetic Materials*, **320(7)** :1412-1422, 2008.

[RI.11] L. Daniel, R. Corcolle, "A note on the effective magnetic permeability of polycrystals", *IEEE Transactions on Magnetics*, **43(7)** :3153-3158, 2007.

[RI.10] L. Daniel, O. Hubert, B. Vieille, "Multiscale strategy for the determination of magneto-elastic behaviour : discussion and application to Ni-Zn ferrites", *International Journal of Applied Electromagnetics and Mechanics*, **25** :31-36, 2007.

[RI.9] N. Galopin, L. Daniel, F. Bouillault et M. Besbes, "Numerical analysis for the design of a magneto-elastic characterization device", *Prezgląd Elektrotechniczny*, **83(6)** :44-47, 2007.

[RI.8] O. Hubert, L. Daniel, "Effect of plastic straining on magnetostriction of ferromagnetic polycrystals - experiments and multiscale modelling", *Journal of Magnetism and Magnetic Materials*, **304(2)** :489-491, 2006.

[RI.7] O. Hubert, M. Chaabane, J. Jumel, V. Maurel, F. Alvès, A.D. Bensalah, M. Besbes, K. Azoum, L. Daniel, F. Bouillault, "A new experimental set-up for the characterisation of magneto-mechanical behaviour of materials submitted to biaxial stresses. Application to FeCo alloys", *Prezgląd Elektrotechniczny*, **81(5)** :19-23, 2005.

[RI.6] O. Hubert, L. Daniel, R. Billardon, "Magneto-elastic multiscale approach for the modelling of multiaxial stress state and plasticity - Experimental and numerical aspects", *Prezgląd Elektrotechniczny*, **81(5)** :82-86, 2005.

[RI.5] O. Hubert, N. Jendly, L. Daniel, "Modelling of the influence of micro-plasticity on the magnetic behaviour of ferromagnetic polycrystals through a multiscale approach", *Steel Research International*, **76(6)** :440-447, 2005.

[RI.4] L. Daniel, O. Hubert, R. Billardon, "Homogenisation of magneto-elastic behaviour : from the grain to the macro scale", *Computational and Applied Mathematics*, **23(2-3)** :285-308, 2004.

[RI.3] L. Daniel, O. Hubert, R. Billardon, "Magnetic behaviour of electrical steels : demagnetising surface effect and texture gradient", *International Journal of Applied Electromagnetics and Mechanics*, **1-4(19)** :293-297, 2004.

[RI.2] L. Daniel, O. Hubert, F. Ossart, R. Billardon, "Experimental analysis and multiscale modelling of the anisotropic mechanical and magnetostrictive behaviours of electrical steels", *J. Phys. IV*, **105** :247-253, 2003.

[RI.1] O. Hubert, L. Daniel, R. Billardon, "Experimental analysis of the magnetoelastic anisotropy of a non-oriented silicon iron alloy". *Journal of Magnetism and Magnetic Materials*, **254-255C** :352-354, 2003.

Participation à des conférences internationales avec comité de lecture *

[CI.29] R. Corcolle, L. Daniel, "Mean field homogenization methods for piezoelectric composites", *Progress In Electromagnetics Research Symposium (PIERS 2011)*, mars 2011, Marrakech, Maroc.

[CI.28] T.T. Nguyen, L. Daniel, X. Mininger, F. Bouillault, "Finite Element Modeling of Magnetoelectric Sensors", *Progress In Electromagnetics Research Symposium (PIERS 2011)*, mars 2011, Marrakech, Maroc.

[CI.27] G. Krebs, L. Daniel, "A magneto-elastic proposal for field weakening in PMSM", *14th International IGTE Symposium on Numerical Field Calculation in Electrical Engineering (IGTE2010)*, septembre 2010, Graz, Autriche.

[CI.26] (*) T.T. Nguyen, X. Mininger, F. Bouillault, L. Daniel, "Finite element harmonic modeling of Magnetoelectric Effect for bilayer composite", *14th Biennial IEEE Conference on Electromagnetic Field Computation (CEFC2010)*, mai 2010, Chicago, USA.

[CI.25] R. Corcolle, L. Daniel, F. Bouillault, "Modeling of magnetoelectric effect : A comparison between homogenization and finite element techniques", *Compumag 2009*, novembre 2009, Florianopolis, Brésil.

[CI.24] (*) L. Daniel, O. Hubert, "Equivalent stress criteria for the effect of stress on magnetic behavior", *Compumag 2009*, novembre 2009, Florianopolis, Brésil.

[CI.23] X. Mininger, L. Daniel, L. Bernard, F. Bouillault, "Magneto-elastic finite element modeling based on a multiscale approach", *Compumag 2009*, novembre 2009, Florianopolis, Brésil.

[CI.22] (*) O. Hubert, L. Daniel, R. Waberi, "Measurement and analytical modeling of the ΔE effect in a bulk iron-cobalt alloy", *17th International Conference on Soft Magnetic Materials (SMM19)*, septembre 2009, Torino, Italie.

[CI.21] (*) K.J. Rizzo, O. Hubert, L. Daniel, "Magnetic and magnetostrictive behavior of iron-silicon single crystals under uniaxial stress", *17th International Conference on Soft Magnetic Materials (SMM19)*, septembre 2009, Torino, Italie.

[CI.20] R. Corcolle, L. Daniel, F. Bouillault, "An Homogenization Model for Coupled Behavior. Application to Three Phase Electro-Magneto-Elastic Composites", *3rd International Conference on Computational Methods for Coupled Problems in Science and Engineering (COUPLED PROBLEMS 2009)*, juin 2009, Ischia, Italie.

[CI.19] L. Daniel, R. Corcolle, "An homogenization framework based on inclusion problems", *53rd Magnetism and Magnetic Materials Conference (MMM 2008)*, novembre 2008, Austin, Texas.

∗. Les références précédées d'une étoile (*) désignent des résumés dont l'article correspondant a par la suite été accepté en version étendue dans une revue internationale (voir partie *"Articles dans des revues internationales avec comité de lecture"*).

[CI.18] (*) L. Daniel, O. Hubert, "An equivalent stress for the influence of multiaxial stress on the magnetic behavior", *53rd Magnetism and Magnetic Materials Conference (MMM 2008)*, novembre 2008, Austin, Texas.

[CI.17] (*) R. Corcolle, L. Daniel, F. Bouillault, "Modeling of magneto-electric composites using homogenization techniques", *8th European Magnetic Sensors & Actuators Conference (EMSA 2008)*, juin-juillet 2008, Caen, France.

[CI.16] (*) N. Galopin, X. Mininger, F. Bouillault, L. Daniel, "Finite element modelling of magneto-electric sensors", *16th Conference on the Computation of Electromagnetic Fields (COMPUMAG 2007)*, juin 2007, Aachen, Allemagne.

[CI.15] (*) N. Galopin, L. Daniel, F. Bouillault et M. Besbes, "Numerical analysis for the design of a magneto-elastic characterization device", *9th International Workshop on 1&2 - Dimensional Magnetic Measurement and Testing (2DM)*, septembre 2006, Czestochowa, Pologne.

[CI.14] R. Billardon, O. Hubert, L. Daniel, "Multi-scale analysis of magneto-elastic couplings", *6th European Solid Mechanics Conference (ESMC6)*, août 2006, Budapest, Hongrie ***(communication invitée)***.

[CI.13] L. Daniel, O. Hubert, R. Billardon, "Magneto-elastic behaviour of iron-cobalt alloys : a multiscale approach", *6th European Solid Mechanics Conference (ESMC6)*, août 2006, Budapest, Hongrie.

[CI.12] O. Hubert, L. Daniel, R. Billardon, "Multiscale modelling of the effect of plasticity on magneto-mechanical behaviour of ferromagnetic polycrystals", *6th European Solid Mechanics Conference (ESMC6)*, août 2006, Budapest, Hongrie.

[CI.11] N.Galopin, K.Azoum, M. Besbes, F. Bouillault, L.Daniel, "Design and modelling of displacement control device using giant magnetostrictive material", *Sensors & Actuators for Advanced Automotive Applications (SENSACT2005)*, décembre 2005, Noisy-le-Grand, France.

[CI.10] (*) L. Daniel, O. Hubert, B. Vieille, "Multiscale strategy for the determination of magneto-elastic behaviour : discussion and application to Ni-Zn ferrites", *12th International Symposium on Applied Electromagnetics and Mechanics (ISEM2005)*, septembre 2005, Bad Gastein, Autriche.

[CI.9] (*) O. Hubert, L. Daniel, "Effect of plastic straining on magnetostriction of ferromagnetic polycrystals - experiments and multiscale modelling" *17th International Conference on Soft Magnetic Materials (SMM17)*, septembre 2005, Bratislava, Slovaquie.

[CI.8] (*) O. Hubert, M. Chaabane, J. Jumel, V. Maurel, F. Alves, A. Benssalah, M. Besbes, K. Azoum, L. Daniel, F. Bouillault, "Magneto-mechanical behaviour of Fe-Co alloys submitted to biaxial stresses", *8th International Workshop on 1&2-Dimensional Magnetic Measurement and Testing (2DM)*, septembre 2004, Gand, Belgique.

[CI.7] (*) O. Hubert, L. Daniel, R. Billardon, "Magneto-elastic multiscale approach for the modelling of multiaxial stress state and plasticity - experimental and numerical aspects", *8th International Workshop on 1&2-Dimensional Magnetic Measurement and Testing (2DM)*, septembre 2004, Gand, Belgique ***(communication invitée)***.

[CI.6] O. Hubert, L. Daniel, R. Billardon, "Multiscale modelling and demagnetising surface effect : application to the prediction of magnetostriction of Grain Oriented silicon irons", *16th International Conference on Soft Magnetic Materials (SMM16)*, septembre 2003, Düsseldorf, Allemagne.

[CI.5] (*) O. Hubert, N. Jendly, L. Daniel, "Modelling of the influence of micro-plasticity on the magnetic behaviour of ferromagnetic polycrystals through a multiscale approach", *16th International Conference on Soft Magnetic Materials (SMM16)*, septembre 2003, Düsseldorf, Allemagne.

[CI.4] (*) L. Daniel, O. Hubert, R. Billardon, "Magnetic behaviour of electrical steels : demagnetising surface effect and texture gradient", *11th International Symposium on Applied Electromagnetics and Mechanics (ISEM2003)*, mai 2003 , Versailles, France.

[CI.3] (*) L. Daniel, O. Hubert, F. Ossart, R. Billardon, "Experimental analysis and multiscale modeling of the anisotropic mechanical and magnetostrictive behaviours of electrical steels", *Sixth European Mechanics of Materials Conference (EMMC6), « Non linear mechanics of anisotropic materials »*, septembre 2002, Liège, Belgique.

[CI.2] L. Daniel, O. Hubert, R. Billardon, "Homogenisation of magneto-elastic behaviour : from the grain to the macro scale", *Multiscale 2002*, août 2002, Petropolis, Brésil.

[CI.1] (*) O. Hubert, L. Daniel, R. Billardon, "Experimental analysis of the magnetoelastic anisotropy of a non-oriented silicon iron alloy", *15th International Conference on Soft Magnetic Materials (SMM15)*, septembre 2001, Bilbao, Espagne.

Articles dans des revues nationales

[RN.2] N. Galopin, K. Azoum, M. Besbes, F. Bouillault, L. Daniel, O. Hubert, F. Alves, "Caractérisation et modélisation des déformations induites par les forces magnétiques et par la magnétostriction", *Revue Internationale de Génie Electrique*, **9(4/5)** :499-514, 2006.

[RN.1] N. Galopin, K. Azoum, M. Besbes, F. Bouillault, L. Daniel (2006), "Conception et modélisation d'un dispositif de contrôle de déplacement utilisant un matériau à magnétostriction géante", *Revue de l'Electricité et de l'Electronique*, **10** :44-51.

Colloques nationaux avec actes

[CN.24] O. Hubert, L. Daniel, K. Lavernhe-Taillard, "Vers une contrainte équivalente multiphysique", *Matériaux 2010*, octobre 2010, Nantes, France.

[CN.23] K.J. Rizzo, O. Hubert, L. Daniel, D. Solas, "Mesure et modélisation du comportement magnéto-mécanique de monocristaux de fer-silicium sous contrainte", *Matériaux 2010*, octobre 2010, Nantes, France.

[CN.22] I. Drouelle, A.L. Etter, D. Solas, L. Daniel, O. Hubert, T. Baudin, "Maîtrise des microstructures et des textures du fer ARMCO pour la modélisation multi-échelle du comportement magnéto-élastique", *Matériaux 2010*, octobre 2010, Nantes, France.

[CN.21] T.T. Nguyen, L. Daniel, F. Bouillault, X. Mininger, "Modélisation d'un capteur magnétoélectrique par la méthode des éléments finis", *5ème Colloque sur les Matériaux en Génie Electrique - MGE 2010*, août-septembre 2010, Montpellier, France.

[CN.20] K.J. Rizzo, O. Hubert, L. Daniel, "Effet d'une contrainte de traction sur le comportement magnéto-mécanique d'un monocristal de FeSi", *Dix-neuvième Congrès Français de Mécanique*, août 2009, Marseille, France.

[CN.19] R. Corcolle, L. Daniel, F. Bouillault, "Homogénéisation du comportement de milieux hétérogènes magnétiques : détermination des fluctuations intraphases", *Conférence sur les Matériaux du Génie Electrique - MGE 2008*, mai 2008, Toulouse, France.

[CN.18] L. Daniel, O. Hubert, "Identification et modélisation de l'effet ΔE", *Conférence sur les Matériaux du Génie Electrique - MGE 2008*, mai 2008, Toulouse, France.

[CN.17] N. Galopin, X. Mininger, F. Bouillault, L. Daniel, "Structures composites magnéto-électriques", *Conférence sur les Matériaux du Génie Electrique - MGE 2008*, mai 2008, Toulouse, France.

[CN.16] O. Hubert, L. Daniel, "Mesure et modélisation de la magnétostriction de tôles de fer-silicium à grains orientés", *Conférence sur les Matériaux du Génie Electrique - MGE 2008*, mai 2008, Toulouse, France.

[CN.15] K.J. Rizzo, O. Hubert, L. Daniel, "Comportement piézomagnétique d'un acier bas carbone - Application à la mesure des contraintes", *Conférence sur les Matériaux du Génie Electrique - MGE 2008*, mai 2008, Toulouse, France.

[CN.14] N. Galopin, X. Mininger, F. Bouillault, L. Daniel, "Effet magnéto-électrique pour capteur de position", *Conférence sur les Sciences et Applications des Matériaux Electroactifs - C'SAME 2007*, septembre 2007, Toulouse, France.

[CN.13] N. Galopin, L. Daniel, F. Bouillault, A. Poizat, "Dispositif de caractérisation du comportement magnéto-élastique", *Matériaux 2006*, novembre 2006, Dijon, France.

[CN.12] N. Galopin, X. Mininger, F. Bouillault, L. Daniel, "Modélisation par éléments finis de dispositifs basés sur l'utilisation de matériaux actifs", *Matériaux 2006*, novembre 2006, Dijon, France.

[CN.11] O. Hubert, L. Daniel, B. Vieille, R. Billardon, "Influence de l'état mécanique multiaxial élastique(-plastique) sur le comportement magnéto-mécanique d'alliages ferromagnétiques - Résultats expérimentaux et modélisation", *Colloque National MECAMAT « Approches multiéchelles en mécanique des matériaux »*, janvier 2006, Aussois, France ***(communication invitée)***.

[CN.10] N. Galopin, K. Azoum, M. Besbes, L. Daniel, F. Bouillault, F. Alves, O. Hubert, "Dispositif expérimental pour la caractérisation magneto-élastique : comparaison des déformations induites par les forces magnétiques et par la magnétostriction", *Matériaux du Génie Electrique (MGE2005)*, décembre 2005, Lyon, France.

[CN.9] Sunyoto, Y. Bernard, L. Daniel, A. Razek, "Dimensionnement d'une pince d'un actionneur piézoélectrique", *Matériaux du Génie Electrique (MGE2005)*, décembre 2005, Lyon, France.

[CN.8] Y. Bernard, Sunyoto, L. Daniel, "Caractérisation électromécanique d'un actionneur piézoélectrique", *Dix-septième Congrès Français de Mécanique*, août 2005, Troyes, France.

[CN.7] B. Vieille, L. Daniel, O. Cerri, N. Buiron, O. Hubert, R. Billardon, "Modélisation multi-échelle du comportement magnéto-élastique des ferrites ferrimagnétiques", *Colloque National MECAMAT « Mécanismes et Mécanique des Matériaux et Structures à Longueur Interne : Comportement et Effets d'Echelles »*, p.525-528, janvier 2004, Aussois, France.

[CN.6] L. Daniel, O. Hubert, R. Billardon, "Homogénéisation du comportement magnéto-élastique des matériaux ferromagnétiques doux", *Seizième Congrès Français de Mécanique*, septembre 2003, Nice, France.

[CN.5] N. Buiron, L. Daniel, O. Hubert, R. Billardon, "Modélisations à différentes échelles du comportement magnéto-élastique des matériaux magnétiques doux", *Colloque National Matériaux 2002*, octobre 2002, Tours, France.

[CN.4] O. Hubert, L. Daniel, N. Buiron, R. Billardon, "Modélisation et identification du comportement magnéto-élastique d'une tôle de fer-silicium", *Colloque National Matériaux 2002*, octobre 2002, Tours, France.

[CN.3] L. Daniel, O. Hubert, R. Billardon, "Modélisation du comportement élastique d'un polycristal texturé. Application à la déformation de magnétostriction", *Colloque National MECAMAT « Mécanismes et déformations dans les matériaux multi-constituants »*, p.227-230, janvier 2002, Aussois, France.

[CN.2] L. Daniel, O. Hubert, N. Buiron, R. Billardon, "Description par éléments finis d'un polycristal anisotrope", *Quinzième Congrès Français de Mécanique*, septembre 2001, Nancy, France.

[CN.1] L. Daniel, O. Hubert, N. Buiron, R. Billardon, "Modélisation multi-échelle de la déformation de magnétostriction d'un polycristal", *Colloque National MECAMAT « Multi-approches en mécanique des matériaux »*, p.291-294, janvier 2001, Aussois, France.

Thèse de doctorat

[T.1] L. Daniel, "Modélisation multi-échelle du comportement magnéto-mécanique des matériaux ferromagnétiques texturés", Thèse de doctorat, *Ecole Normale Supérieure de Cachan*, 2003.

Autres communications récentes

[Div.15] L. Daniel, "Modélisation multi-échelle du comportement magnéto-mécanique des matériaux magnétiques", *Séminaire au Technocentre Renault*, novembre 2010, Guyancourt, France.

[Div.14] L. Daniel, L. Bernard, "Multiscale constitutive laws and finite element modelling of Magnetic materials under magneto-mechanical loading", *Séminaire du GRUCAD, Universidade Federal de Santa Catarina*, octobre 2010, Florianopolis, Brésil.

[Div.13] L. Daniel, R. Corcolle, "Outils d'homogénéisation pour les comportements couplés", *Séminaire du soir, Ecole d'Eté CE2M10 "Changement d'Echelles en Mécanique des Matériaux"*, août 2010, Briançon, France.

[Div.12] L. Bernard, X. Mininger, L. Daniel "Modélisation par éléments finis de problèmes magnéto-élastiques : application à l'effet des contraintes sur les machines tournantes", *Commission Energie, Supelec*, juillet 2010, Gif-sur-Yvette, France.

[Div.11] L. Daniel, O. Hubert "Modélisation multi-échelle du comportement magnéto-élastique", *Commission Energie, Supelec*, juillet 2010, Gif-sur-Yvette, France.

[Div.10] L. Daniel, "Effets d'inertie dans les machines tournantes - Outils de conception magnéto-mécanique", *Réunion DAS Systèmes Mécatroniques d'Electrification du véhicule*, mai 2010, Paris, France.

[Div.9] L. Daniel, "Une approche multi-échelle pour la modélisation des phénomènes de couplage magnéto-mécanique", *Séminaire du LMS, Ecole Polytechnique*, mars 2010, Palaiseau, France.

[Div.8] Y. Bernard, L. Daniel, L. Santandrea, "Conception d'une soucoupe volante (ou illustration du phénomène de lévitation magnétique)", *Colloque sur l'Enseignement des Technologies et des Sciences de l'Information et des Systèmes (CETSIS)*, mars 2010, Grenoble, France.

[Div.7] L. Daniel, R. Corcolle, "Modélisation de l'effet Magnéto-Electrique dans les matériaux composites", *Journée SPEELabs*, novembre 2009, Cachan, France.

[Div.6] O. Hubert, L. Daniel, S. Lazreg, "Déformation d'origine magnétique, magnétostriction, piézomagnétisme : mesure et modélisation", *Journée du Groupement de Travail MECAMAT « Couplages multiphysiques » sur les déformations et contraintes d'origine électrique et magnétique*, novembre 2008, Cachan, France.

[Div.5] L. Daniel, "Méthodes multi-échelles pour la modélisation des phénomènes de couplage magnéto-mécanique", *Journée SEEDS sur la modélisation multiphysique*, mars 2008, Paris, France.

[Div.4] L. Daniel, "Sollicitations mécaniques dans les machines rapides : élasticité, fatigue et effets magnéto-mécaniques", *Journée SEEDS-Transports sur les machines rapides*, février 2008, Cachan, France.

[Div.3] L. Daniel, "A multiscale constitutive law for magneto-elastic behaviour", *Séminaire au Laboratory of Electromechanics, Université Technologique d'Helsinki (TKK)*, mai 2007, Helsinki, Finlande.

[Div.2] N. Galopin, L. Daniel, F. Bouillault, "Caractérisation et modélisation des matériaux à magnétostriction géante", *Revue de la recherche - SUPELEC*, 2006-2007, France.

[Div.1] L. Daniel, "Phénomènes de couplage magnéto-élastique : une approche multi-échelle", *Séminaire du LPMTM*, mai 2006, Villetaneuse, France.

Partie 2

Bilan des travaux de recherche : modélisation multi-échelle des phénomènes de couplage multiphysique

Sommaire

Introduction

Ce travail de recherche est une contribution à l'étude des phénomènes de couplage multiphysique dans les matériaux fonctionnels. Les matériaux fonctionnels, de manière générale, sont des matériaux dont la fonction principale n'est pas une fonction de structure. Dans le cadre de mes travaux, je me suis intéressé à des matériaux fonctionnels dont la fonction principale est de nature électromagnétique.

Au cours des dernières dizaines d'années, un intérêt grandissant s'est porté sur l'étude des phénomènes de couplage multiphysique dans ces matériaux. En effet, la réponse d'un matériau magnétique ou diélectrique, si elle est bien sûr fortement pilotée par le champ magnétique ou le champ électrique, dépend aussi très fortement de la température ou des contraintes appliquées. Ces effets de couplage peuvent parfois constituer une nuisance. Ils sont par exemple responsables d'une partie des vibrations des machines tournantes ou du bruit émis par les transformateurs électriques. Dans le domaine de l'électrotechnique, la volonté de repousser les limites de fonctionnement des machines, souvent dans le but de minimiser la masse des dispositifs, conduit à solliciter les matériaux dans des conditions sévères en terme de température et de contraintes mécaniques. Ces modes de fonctionnement extrêmes conduisent à revisiter les modèles utilisés de manière à tenir compte de ces effets de couplage jusqu'alors négligés. Les phénomènes de couplage multiphysique peuvent également être un atout à exploiter pour servir de base à la conception de dispositifs innovants pour la conversion d'énergie ou l'électronique. Quel que soit le contexte - nuisance ou potentialité - le manque d'outils de modélisation performants est un handicap pour l'optimisation des dispositifs électromagnétiques, mais aussi pour le développement de nouveaux matériaux.

Par ailleurs, les matériaux pour usage électromagnétique, comme les autres, sont des matériaux hétérogènes. Les matériaux classiques du Génie Electrique sont souvent des alliages polycristallins. On y retrouve les hétérogénéités liées à la structure en grains. A ce niveau de microstructure peut s'ajouter une microstructure en domaines (magnétiques ou ferroélectriques) qui s'imbrique avec la première. La compréhension des effets d'hétérogénéité dans le comportement macroscopique pourrait permettre la définition de microstructures optimisées pour certaines applications. Le développement des matériaux composites - relativement récent en électromagnétisme - renforce la prise de conscience de l'importance des effets d'hétérogénéité dans la compréhension du comportement macroscopique des matériaux.

Dans ce contexte, mes travaux de recherche portent sur la définition de lois de comportement pour les phénomènes de couplage multiphysique dans les matériaux du Génie Electrique. Un accent particulier est mis sur le traitement de l'hétérogénéité de ces matériaux. La non-linéarité du comportement et les effets d'anisotropie font également partie des aspects abordés par ce travail.

2.1 Règles de changement d'échelle

Lorsqu'on s'intéresse à la définition du comportement effectif d'un matériau hétérogène, deux principaux types de modélisation se distinguent.

Les approches "en champ complet" reposent sur la description complète de la microstructure, sous une forme discrétisée, associée à des méthodes de résolution numérique. Ces approches constituent la majorité des applications rencontrées dans le domaine de la modélisation des comportements couplés. La méthode des éléments finis (MEF) est la plus utilisée [1], et on trouve de nombreuses applications dans le cas des couplages magnéto-mécanique [2–7], électro-mécanique [8–13] ou encore magnéto-électrique [14, 15]. Plus récemment, les méthodes basées sur les transformées de Fourier (FFT) développées dans le cadre du comportement mécanique [16] ont été appliquées avec succès au comportement piézo-électrique et magnéto-électrique [17, 18]. Ces approches en champ complet, comme leur nom l'indique, ont l'avantage de fournir une description complète des champs, ce qui peut être utile pour l'étude des phénomènes physiques associés à des mécanismes locaux. L'inconvénient est que ces méthodes nécessitent une discrétisation complète de la microstructure. Or, ces microstructures sont rarement connues de manière exacte, elles sont souvent difficiles à caractériser (notamment en 3D) et présentent en général un caractère aléatoire. Le modélisateur est alors condamné à ne s'intéresser qu'à une réalisation particulière de cette microstructure, ou à réaliser un grand nombre de calculs pour en tirer ensuite une moyenne (ce qui amoindrit l'intérêt de disposer des champs complets). De plus les microstructures à modéliser peuvent être complexes, et la mise en données du problème, par exemple pour un matériau polycristallin peut s'avérer difficile. Ceci est particulièrement vrai pour certains phénomènes couplés pour lesquels la taille du volume élémentaire représentatif peut-être très grande. C'est notamment le cas pour la déformation de magnétostriction [19]. On notera enfin que, en plus des temps de mise en données, et malgré l'augmentation de la puissance des outils de calcul, ces approches sont associées à des temps de calcul importants.

Les approches "en champ moyen" reposent quant à elles sur une description partielle, statistique, de la microstructure [20]. Elles ne permettent pas de définir les champs locaux mais fournissent des informations statistiques représentatives de ces champs (valeur moyenne, variance, ...). En contrepartie, les moyens numériques mis en œuvre sont significativement allégés. Un des avantages de ces approches est qu'elles fournissent des modèles plus simples à inverser, ouvrant la voie à l'optimisation de microstructure, ou à l'identification de loi de comportement local à partir d'essais macroscopiques. Quoique les approches en champ moyen aient initialement été développées pour le comportement électromagnétique [21, 22], ces méthodes sont largement répandues pour l'étude de problèmes mécaniques [23, 24]. Etudiées également en électromagnétisme [25], leur utilisation dans le domaine du Génie Electrique reste encore assez marginale [26–28].

L'essentiel des résultats présentés dans ce mémoire relèvent des approches en champ moyen. Cependant, en raison de l'activité historique de mon département dans le domaine des approches en champ complet, j'ai pu participer à des travaux de modélisation par éléments finis qui ont notamment permis d'effectuer des comparaisons entre ces deux approches complémentaires.

2.1.1 Approches en champ moyen *

Le principe de modélisation utilisé dans les travaux qui font l'objet de ce mémoire est basé sur une représentation du problème permettant de se ramener à la résolution de problèmes élémentaires d'inclusion, pour lesquels des solutions simples, souvent analytiques, sont connues. Le principe, illustré par la figure 2.1 est brièvement exposé ci-après.

Un milieu hétérogène à n phases (une phase peut correspondre à une phase d'un matériau composite ou à une orientation d'un ensemble de grains dans un polycristal) est représenté sous la forme de n problèmes d'inclusion *a priori* décorrélés. Chacune des phases du matériau est supposée se comporter "en moyenne" comme une inclusion, ellipsoïdale en général, plongée dans un milieu infini. Le choix des propriétés du milieu infini est un degré de liberté du problème, il permet de définir un "niveau moyen" d'interactions entre phases.

Chacun des problèmes d'inclusion va permettre de définir des opérateurs de localisation $\mathcal{A}_i$ et $\mathcal{B}_i$, qui relient les champs macroscopiques aux valeurs moyennes des champs par phase. Dans le cas du comportement magnétique, les champs considérés sont le champ magnétique $\mathbf{H}$ et l'induction magnétique $\mathbf{B}$. Les relations de localisation s'écrivent sous la forme :

$$\forall i \in [1,n], \quad \left\{ \begin{array}{l} \mathbf{H}_i = \langle \mathbf{H}(\mathbf{x}) \rangle_i = \mathcal{A}_i : \overline{\mathbf{H}} = \mathcal{A}_i : \langle \mathbf{H}(\mathbf{x}) \rangle \\ \mathbf{B}_i = \langle \mathbf{B}(\mathbf{x}) \rangle_i = \mathcal{B}_i : \overline{\mathbf{B}} = \mathcal{B}_i : \langle \mathbf{B}(\mathbf{x}) \rangle \end{array} \right. \tag{2.1}$$

Les propriétés magnétiques, définies par le tenseur de perméabilité $\mathbb{\mu}$ sont uniformes par phase. La relation de comportement des phases s'écrit donc :

$$\mathbf{B}_i = \mathbb{\mu}_i \cdot \mathbf{H}_i \tag{2.2}$$

La loi de comportement homogénéisée en magnétisme s'écrit à l'aide du tenseur de perméabilité effective $\widetilde{\mathbb{\mu}}$:

$$\overline{\mathbf{B}} = \widetilde{\mathbb{\mu}} \cdot \overline{\mathbf{H}} \tag{2.3}$$

Ce tenseur effectif est déduit des opérateurs de localisation par l'une ou l'autre des équations suivantes :

$$\begin{array}{rcl} \widetilde{\mathbb{\mu}} & = & \langle \mathbb{\mu}_i \cdot \mathcal{A}_i \rangle \\ \widetilde{\mathbb{\mu}}^{-1} & = & \langle \mathbb{\mu}_i^{-1} \cdot \mathcal{B}_i \rangle \end{array} \tag{2.4}$$

On remarque au passage que les deux tenseurs de localisation moyens par phase $\mathcal{A}_i$ et $\mathcal{B}_i$ sont reliés par la relation :

$$\mathcal{B}_i = \mathbb{\mu}_i \cdot \mathcal{A}_i \cdot \widetilde{\mathbb{\mu}}^{-1} \tag{2.5}$$

Par ailleurs, et contrairement à ce que pourrait laisser croire leur appellation, les approches en champ moyen fournissent des informations non seulement sur les champs moyens par phase mais également sur les fluctuations de ces champs. Ainsi, les moments d'ordre 2 du champ magnétique sont définis par la relation suivante [24, 29] :

$$\langle \mathbf{H}(\mathbf{x}) \otimes \mathbf{H}(\mathbf{x}) \rangle_i = \frac{1}{f_i} \overline{\mathbf{H}} \cdot \frac{\partial \widetilde{\mathbb{\mu}}}{\partial \mathbb{\mu}_i} \cdot \overline{\mathbf{H}} \tag{2.6}$$

où le tenseur $\langle \mathbf{H}(\mathbf{x}) \otimes \mathbf{H}(\mathbf{x}) \rangle_i$ est un tenseur d'ordre 2 représentant les moments d'ordre 2. Dans la base (x, y, z) où le champ magnétique est égal à $\mathbf{H}(\mathbf{x}) = {}^t(\begin{array}{ccc} H_x(\mathbf{x}) & H_y(\mathbf{x}) & H_z(\mathbf{x}) \end{array})$, le tenseur (symétrique) des moments d'ordre 2 est égal à :

$$\langle \mathbf{H}(\mathbf{x}) \otimes \mathbf{H}(\mathbf{x}) \rangle_i = \begin{pmatrix} \langle H_x(\mathbf{x})^2 \rangle_i & \langle H_x(\mathbf{x}) \cdot H_y(\mathbf{x}) \rangle_i & \langle H_x(\mathbf{x}) \cdot H_z(\mathbf{x}) \rangle_i \\ \langle H_x(\mathbf{x}) \cdot H_y(\mathbf{x}) \rangle_i & \langle H_y(\mathbf{x})^2 \rangle_i & \langle H_y(\mathbf{x}) \cdot H_z(\mathbf{x}) \rangle_i \\ \langle H_x(\mathbf{x}) \cdot H_z(\mathbf{x}) \rangle_i & \langle H_y(\mathbf{x}) \cdot H_z(\mathbf{x}) \rangle_i & \langle H_z(\mathbf{x})^2 \rangle_i \end{pmatrix} \tag{2.7}$$

De manière duale, il est possible de déterminer le moment d'ordre 2 de l'induction magnétique :

$$\langle \mathbf{B}(\mathbf{x}) \otimes \mathbf{B}(\mathbf{x}) \rangle_i = \frac{1}{f_i} \overline{\mathbf{B}} \cdot \frac{\partial \widetilde{\mathbb{\mu}}^{-1}}{\partial \mathbb{\mu}_i^{-1}} \cdot \overline{\mathbf{B}} \tag{2.8}$$

Ma contribution dans le domaine des méthodes d'homogénéisation a consisté en l'application des méthodes classiques aux problèmes du comportement magnétique de matériaux hétérogènes. Des développements spécifiques ont été proposés pour tenir compte de la symétrie cubique des monocristaux d'un grand nombre de matériaux magnétiques. Ces travaux sont présentés dans la publication [30] jointe ci-après. Des travaux sur la détermination des fluctuations intraphases ont également été menés, conduisant à la construction de bornes sur les fluctuations intraphases dans le cas des matériaux bi-phasés. Ces résultats sont présentés dans la publication [31] ci-après. Enfin, l'application des règles de localisation et d'homogénéisation au cas des comportements couplés a été proposée dans [32] en s'appuyant sur un principe de décomposition des champs.

∗. Les travaux présentés dans ce chapitre ont pour une grande part été menés dans le cadre de la thèse de Romain Corcolle [29].

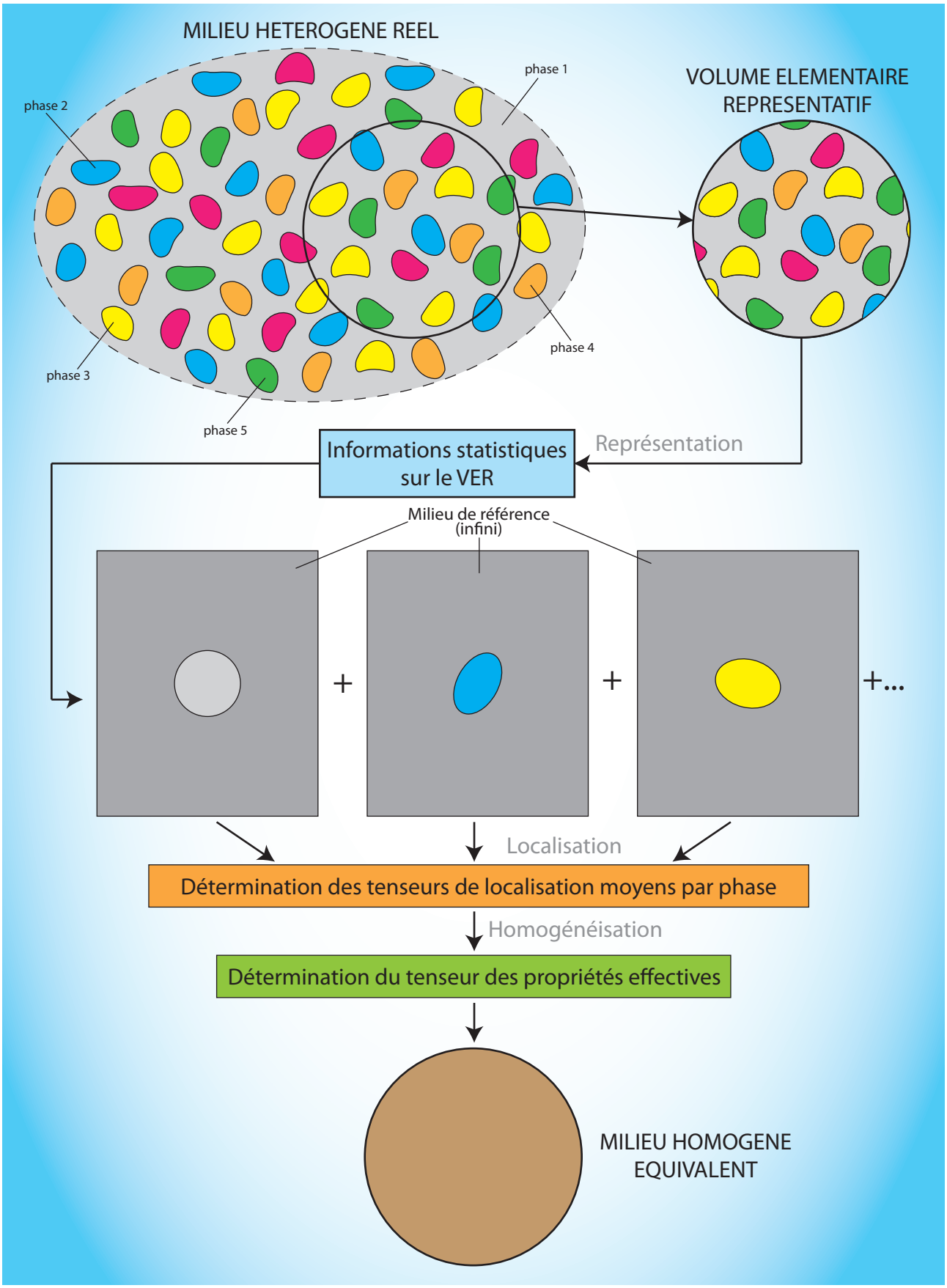

FIGURE 2.1 – Principe du modèle d'homogénéisation basé sur les problèmes d'inclusion.

Publications jointes

[RI.11, 30] : L. Daniel, R. Corcolle, "A note on the effective magnetic permeability of polycrystals", *IEEE Transactions on Magnetics*, **43(7)** :3153-3158, 2007.

[RI.23, 31] : R. Corcolle, L. Daniel, F. Bouillault, "Intraphase fluctuations in heterogeneous magnetic materials", *Journal of Applied Physics*, **105(12)** :123913 (8p), 2009.

[RI.17, 32] : R. Corcolle, L. Daniel, F. Bouillault, "Generic formalism for homogenization of coupled behaviors : application to magnetoelectroelastic behavior", *Physical Review B*, **78(21)** :214110 (12p), 2008.

A Note on the Effective Magnetic Permeability of Polycrystals

Laurent Daniel and Romain Corcolle

Laboratoire de Génie Electrique de Paris (LGEP), CNRS (UMR 8507); Supelec; Univ Paris Sud; UPMC- Paris, Plateau de Moulon, 91192 Gif sur Yvette Cedex, France

Many classical estimates for the effective behavior of heterogeneous materials can be reinterpreted in terms of inclusion problems. However, in the case of cubic polycrystals, a cubic permeability tensor for single crystals has to be written. In the framework of linear behavior, the description of the cubic symmetry reduces to isotropy. The heterogeneity of polycrystals, which results from single crystal anisotropy, cannot be described, and the classical estimates for the overall behavior of heterogeneous materials cannot be used. In this paper, we propose a particular description of the cubic symmetry for the magnetic permeability. We then derive estimates for the effective permeability of polycrystals from the solution of the basic inclusion problem, for both macroscopically isotropic and anisotropic polycrystals.

***Index Terms*—Cubic symmetry, effective properties, homogenization, inclusion, magnetic permeability, polycrystal.**

I. Introduction

THE determination of the effective properties of heterogeneous materials is a long-standing problem in many fields of physics. The purpose is to deduce the material constants of a fictive homogeneous material equivalent to the heterogeneous real one from the properties of its constituents and some assumptions on the microstructure. In the case of magnetic properties, the problem can be presented in the following way: the material is constituted of n phases i for which the behavior is known. Under the assumption of linear magnetic properties, the constitutive law is written:

$$\mathbf{B^i} = \underline{\underline{\mu}}^{\mathbf{i}}\mathbf{H^i} \tag{1}$$

where $\mathbf{B^i}$ and $\mathbf{H^i}$ are the magnetic induction and the magnetic field in the phase i and $\underline{\underline{\mu}}^{\mathbf{i}}$ its magnetic permeability.[1] The objective is to define the effective permeability tensor $\underline{\underline{\mu}}^{\mathbf{eff}}$ of the heterogeneous material, linking the mean magnetic induction in the material $\overline{\mathbf{B}}$ to the mean magnetic field in the material $\overline{\mathbf{H}}$, according to (2)[2]:

$$\overline{\mathbf{B}} = \langle \mathbf{B^i} \rangle = \underline{\underline{\mu}}^{\mathbf{eff}}\overline{\mathbf{H}} = \underline{\underline{\mu}}^{\mathbf{eff}}\langle \mathbf{H^i} \rangle. \tag{2}$$

The simplest general estimates, the Wiener bounds [1], are obtained assuming uniform magnetic field [$\mathbf{H^i} = \overline{\mathbf{H}}$, see (3)] or magnetic induction [$\mathbf{B^i} = \overline{\mathbf{B}}$, see (4)] within the material

$$\overline{\mathbf{B}} = \langle \mathbf{B^i} \rangle = \langle \underline{\underline{\mu}}^{\mathbf{i}}\mathbf{H^i} \rangle = \langle \underline{\underline{\mu}}^{\mathbf{i}} \rangle \overline{\mathbf{H}} \tag{3}$$

$$\overline{\mathbf{H}} = \langle \mathbf{H^i} \rangle = \left\langle \underline{\underline{\mu}}^{\mathbf{i}^{-1}}\mathbf{B^i} \right\rangle = \left\langle \underline{\underline{\mu}}^{\mathbf{i}^{-1}} \right\rangle \overline{\mathbf{B}}. \tag{4}$$

The Wiener lower and upper bounds are thus given by relation (5):

$$\underline{\underline{\mu}}^{\mathbf{eff}}_{W-} = \left\langle \underline{\underline{\mu}}^{\mathbf{i}^{-1}} \right\rangle^{-1} \quad \text{and} \quad \underline{\underline{\mu}}^{\mathbf{eff}}_{W+} = \langle \underline{\underline{\mu}}^{\mathbf{i}} \rangle. \tag{5}$$

An alternative estimate can be obtained assuming uniform magnetization within the material[3] ($\mathbf{M^i} = \overline{\mathbf{M}}$):

$$\overline{\mathbf{H}} = \langle \mathbf{H^i} \rangle = \left\langle \underline{\underline{\chi}}^{\mathbf{i}^{-1}}\mathbf{M^i} \right\rangle = \left\langle \underline{\underline{\chi}}^{\mathbf{i}^{-1}} \right\rangle \overline{\mathbf{M}} \tag{6}$$

leading to the following estimate for the effective permeability tensor:

$$\underline{\underline{\mu}}^{\mathbf{eff}}_{UM} = \mu_0 \underline{\underline{I}} + \langle (\underline{\underline{\mu}}^{\mathbf{i}} - \mu_0 \underline{\underline{I}})^{-1} \rangle^{-1}. \tag{7}$$

Hashin and Shtrikman [2] derived more restrictive bounds in the case of isotropic biphasic composites. Another estimate, based on a geometric averaging operation, has been proposed by Lichtenecker [3]. Other estimates, based on more complicated hypotheses on the microstructure, have been proposed [4]–[8]. These bounds or estimates have been mainly developed for composite materials, with a limited number of distinct phases, mostly biphasic materials. The problem of polycrystalline media is rarely treated.[4] Some authors addressed the case of polycrystalline media [9]–[12], but the crystalline symmetry is limited to transverse isotropy in these contributions. The cubic symmetry is not taken into account. A way to describe the cubic crystalline symmetry for the magnetic behavior is proposed in this paper (Section IV). Based on the classical solution for the inclusion problem (Section II), several estimates for the effective behavior of heteregeneous materials can be found. The classical bounds and estimates for biphasic materials are recovered (Section III) and estimates for polycrystals with cubic crystalline symmetry are derived (Section V).

Digital Object Identifier 10.1109/TMAG.2007.896228

Color versions of one or more of the figures in this paper are available online at http://ieeexplore.ieee.org.

[1] In the anisotropic case, the magnetic permeability is a second order tensor.

[2] The operator $\langle \cdot \rangle$ denotes an average operation over the volume.

[3] $\mathbf{M^i}$ and $\overline{\mathbf{M}}$ are the magnetization vectors respectively in phase i and in the material. $\underline{\underline{\chi}}^{\mathbf{i}}$ denotes the second order susceptibility tensor of phase i, verifying: $\mu_0 \underline{\underline{\chi}}^{\mathbf{i}} = \underline{\underline{\mu}}^{\mathbf{i}} - \mu_0 \underline{\underline{I}}$. $\underline{\underline{I}}$ denotes the second order identity tensor, and μ_0 the vacuum permeability ($\mu_0 = 4\pi\, 10^{-7}$ H/m).

[4] In the case of anisotropic single crystal behavior, the polycrystal can be seen as a n-phasic material. Each phase differs from another only by its crystallographic orientation.

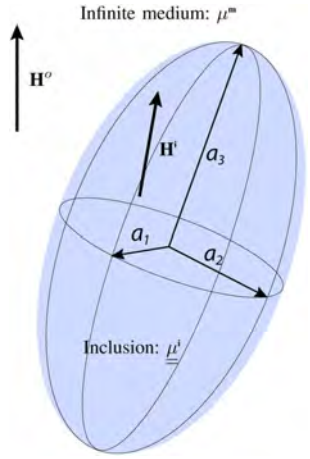

Fig. 1. Basic inclusion problem.

II. Basic Inclusion Problem

Many homogenization models are based on the resolution of the problem of an ellipsoidal inclusion embedded in an infinite medium. The solution of this problem is briefly reminded hereafter.

The infinite medium, as well as the inclusion, is supposed to be homogeneous. The magnetic behavior is supposed linear and, in the case of the infinite medium, isotropic (permeability $\mu^{\mathbf{m}}$ and $\underline{\underline{\mu}}^{\mathbf{i}}$). In such conditions, the magnetic field $\mathbf{H}^{\mathbf{i}}$ in the inclusion is homogeneous and can be derived as a function of the applied field $\mathbf{H}^o$ (8)

$$\mathbf{H}^{\mathbf{i}} = \mu^{\mathbf{m}} \left(\mu^{\mathbf{m}}(\underline{\underline{I}} - \underline{\underline{N}}) + \underline{\underline{N}}\underline{\underline{\mu}}^{\mathbf{i}}\right)^{-1} \mathbf{H}^o. \tag{8}$$

The tensor $\underline{\underline{N}}$ is diagonal and called the demagnetizing tensor. The demagnetizing factors $N_j\,(j = \{1,2,3\})$ are computed from the following elliptic integral [13]:

$$N_j = \frac{a_1 a_2 a_3}{2} \int_0^\infty \frac{ds}{\left(s + a_j^2\right)\sqrt{\left(s + a_1^2\right)\left(s + a_2^2\right)\left(s + a_3^2\right)}} \tag{9}$$

where a_1, a_2, and a_3 denote the ellipsoid's semi-axes (see Fig. 1). One can notice $N_1 + N_2 + N_3 = 1$. In the general case, numerical computations are needed to obtain the demagnetizing factors. In the case of a spherical inclusion, the expression of the demagnetizing factors can be derived analytically

$$\underline{\underline{N}} = \frac{1}{3}\underline{\underline{I}}. \tag{10}$$

For the sake of simplicity, we will focus our study on that case. The magnetic field $\mathbf{H}^{\mathbf{i}}$ in the inclusion can then be written:

$$\mathbf{H}^{\mathbf{i}} = 3\mu^{\mathbf{m}}(2\mu^{\mathbf{m}}\underline{\underline{I}} + \underline{\underline{\mu}}^{\mathbf{i}})^{-1}\mathbf{H}^o. \tag{11}$$

The effective behavior of an heterogeneous medium can be defined through the definition of its magnetic induction $\overline{\mathbf{B}}$, considering that each phase behaves as an inclusion[5] embedded in an infinite medium with permeability $\mu^{\mathbf{m}}$ (12)

$$\begin{aligned}\overline{\mathbf{B}} &= \underline{\underline{\mu}}^{\mathbf{eff}}\langle\mathbf{H}^{\mathbf{i}}\rangle \\ &= \langle\underline{\underline{\mu}}^{\mathbf{i}}\mathbf{H}^{\mathbf{i}}\rangle \\ &= \left\langle 3\mu^{\mathbf{m}}\underline{\underline{\mu}}^{\mathbf{i}}\left(2\mu^{\mathbf{m}}\underline{\underline{I}} + \underline{\underline{\mu}}^{\mathbf{i}}\right)^{-1}\mathbf{H}^o\right\rangle \\ &= \left\langle 3\mu^{\mathbf{m}}\underline{\underline{\mu}}^{\mathbf{i}}\left(2\mu^{\mathbf{m}}\underline{\underline{I}} + \underline{\underline{\mu}}^{\mathbf{i}}\right)^{-1}\right\rangle \mathbf{H}^o.\end{aligned} \tag{12}$$

The applied field in the inclusion problem $\mathbf{H}^o$ (different from the mean magnetic field $\overline{\mathbf{H}}$ in the real heterogeneous material) is defined with respect to (13):

$$\mathbf{H}^o \quad / \quad \langle\mathbf{H}^{\mathbf{i}}\rangle = \left\langle 3\mu^{\mathbf{m}}\left(2\mu^{\mathbf{m}}\underline{\underline{I}} + \underline{\underline{\mu}}^{\mathbf{i}}\right)^{-1}\right\rangle \mathbf{H}^o = \overline{\mathbf{H}}. \tag{13}$$

$\mathbf{H}^o$ is then given by (14):

$$\mathbf{H}^o = \left\langle 3\mu^{\mathbf{m}}\left(2\mu^{\mathbf{m}}\underline{\underline{I}} + \underline{\underline{\mu}}^{\mathbf{i}}\right)^{-1}\right\rangle^{-1} \overline{\mathbf{H}}. \tag{14}$$

Using (12) and (14), the effective permeability is defined according to (15):

$$\underline{\underline{\mu}}^{\mathbf{eff}} = \left\langle \underline{\underline{\mu}}^{\mathbf{i}}(2\mu^{\mathbf{m}}\underline{\underline{I}} + \underline{\underline{\mu}}^{\mathbf{i}})^{-1}\right\rangle \cdot \left\langle \left(2\mu^{\mathbf{m}}\underline{\underline{I}} + \underline{\underline{\mu}}^{\mathbf{i}}\right)^{-1}\right\rangle^{-1}. \tag{15}$$

Several estimates of the effective permeability can be obtained through different choices of the permeability $\mu^{\mathbf{m}}$ of the infinite medium. The appropriate choice will depend on the microstructure of the heterogeneous material. This approach enables to recover classical estimates in the case of biphasic composites (Section III). However, as shown in Section IV, it cannot be applied to most of polycrystals unless a definition for a cubic single crystal permeability is proposed.

III. Permeability of Biphasic Composites

In the case of a biphasic material with isotropic constituents (phase 1 with volumetric fraction f_1 together with phase 2 with volumetric fraction $f_2\,(f_1 + f_2 = 1)$), (15) can be written:

$$\mu^{\mathbf{eff}} = \frac{f_1\dfrac{\mu_1}{2\mu^{\mathbf{m}} + \mu_1} + (1 - f_1)\dfrac{\mu_2}{2\mu^{\mathbf{m}} + \mu_2}}{\dfrac{f_1}{2\mu^{\mathbf{m}} + \mu_1} + \dfrac{1 - f_1}{2\mu^{\mathbf{m}} + \mu_2}}. \tag{16}$$

Any value of $\mu^{\mathbf{m}}$ (from 0 to infinity) can be considered, representing various kinds of microstructure for the composite. It can be noticed that in the case of an homogeneous medium, for which $f_1 = 1$ (resp. $f_1 = 0$), (16) defines an effective permeability $\mu^{\mathbf{eff}} = \mu_1$ (resp. $\mu^{\mathbf{eff}} = \mu_2$), whatever the choice of $\mu^{\mathbf{m}}$.

In the general case of biphasic materials, some particular choices of $\mu^{\mathbf{m}}$ allow to recover some classical estimates.

[5]The shape chosen for the inclusion depends on the distribution of the phases in the composite. Spherical inclusions are associated to an isotropic distribution and ellipsoidal inclusions to an anisotropic one. This distribution of the phases is not related to the shape of the phases in the real material.

1) Wiener lower and upper bounds are obtained choosing respectively $\mu^{\mathbf{m}} = 0$ and $\mu^{\mathbf{m}} \to \infty$:

$$\mu^{\mathbf{eff}}{}_{W-} = \frac{1}{\dfrac{f_1}{\mu_1} + \dfrac{1-f_1}{\mu_2}} \tag{17}$$

$$\mu^{\mathbf{eff}}{}_{W+} = f_1\mu_1 + (1-f_1)\mu_2. \tag{18}$$

2) Hashin and Shtrikman lower and upper bounds are obtained choosing respectively (assuming $\mu_1 < \mu_2$) $\mu^{\mathbf{m}} = \mu_1$ and $\mu^{\mathbf{m}} = \mu_2$:

$$\mu^{\mathbf{eff}}{}_{HS-} = \frac{2f_1\mu_1 + (3-2f_1)\mu_2}{(3-f_1)\mu_1 + f_1\mu_2}\mu_1 \tag{19}$$

$$\mu^{\mathbf{eff}}{}_{HS+} = \frac{(1+2f_1)\mu_1 + 2(1-f_1)\mu_2}{(1-f_1)\mu_1 + (2+f_1)\mu_2}\mu_2. \tag{20}$$

As mentioned in [14], Maxwell-Garnett estimates are equivalent to Hashin and Shtrikman bounds.

3) Bruggeman estimate is obtained choosing $\mu^{\mathbf{m}} = \mu^{\mathbf{eff}}$. $\mu^{\mathbf{eff}}$ is then the solution of the following self-consistent equation:

$$f_1\frac{\mu_1 - \mu^{\mathbf{eff}}}{2\mu^{\mathbf{eff}} + \mu_1} + (1-f_1)\frac{\mu_2 - \mu^{\mathbf{eff}}}{2\mu^{\mathbf{eff}} + \mu_2} = 0. \tag{21}$$

According to these results, the classical estimates for the magnetic behavior of biphasic composites can be reinterpreted as inclusion based models. The application of such an approach to polycrystalline media is then expected to produce several estimates for polycrystal behavior. However, since the heterogeneity of polycrystals is related to single crystal anisotropy, this anisotropy has to be described.

IV. Cubic Permeability

Most ferromagnetic single crystals exhibit a body cubic centered (BCC) or face cubic centered (FCC) structure. For both structures, the magnetic behavior of the single crystal exhibits a cubic symmetry. Let us try to define the magnetic permeability second order tensor $\underline{\underline{\mu}}^{\mathbf{i}}$ of such a material, following (22), written in the crystallographic frame:

$$\mathbf{B^i} = \underline{\underline{\mu}}^{\mathbf{i}}\mathbf{H^i} \tag{22}$$

with

$$\underline{\underline{\mu}}^{\mathbf{i}} = \begin{pmatrix} \mu_{11} & \mu_{12} & \mu_{13} \\ \mu_{21} & \mu_{22} & \mu_{23} \\ \mu_{31} & \mu_{32} & \mu_{33} \end{pmatrix}_{CF}. \tag{23}$$

Since the induction $\mathbf{B^i}$ has to be parallel to the applied field $\mathbf{H^i}$ when the field is along a symmetry axis, and considering a field along $\langle 100\rangle$ directions, all extra-diagonal terms of $\underline{\underline{\mu}}^{\mathbf{i}}$ vanish. Moreover, according to the cubic symmetry, the behavior of all $\langle 100\rangle$ directions has to be identical. Then, it appears that $\mu_{11} = \mu_{22} = \mu_{33}$, and (22) reduces to

$$\mathbf{B^i} = \mu^{\mathbf{i}}\mathbf{H^i} \tag{24}$$

TABLE I
Pure Iron Single Crystal Permeability Along $\langle 100\rangle$, $\langle 110\rangle$, and $\langle 111\rangle$ Directions, According to Webster Experimental Measurements [15]

Magnetic field (A/m)	$\frac{\mu_{100}}{\mu_0}$	$\frac{\mu_{111}}{\mu_0}$	$\frac{\mu_{110}}{\mu_0}$	$\frac{3\mu_{111}+\mu_{100}}{4\mu_0}$
400	2750	1625	1800	1905
2000	835	525	615	605

with $\mu^{\mathbf{i}}$ a scalar value. Cubic symmetry is then reduced to isotropy. Magnetic permeability is on that point analogous to the compressibility modulous in elasticity: if the behavior is identical in three perpendicular directions, then it is isotropic. This conclusion points out a limitation of the use of constant second order tensors for the description of magnetic behavior. Indeed, many experimental observations reveal that cubic single crystals are not magnetically isotropic (see for instance [15] for iron and nickel or [16] for Terfenol-D). In such conditions, the definition of the effective magnetic behavior of polycrystals has no relevance since a polycrystal is defined as an aggregate of isotropic identical phases, meaning a homogeneous material.

Still in the framework of linear behavior, a particular expression for the permeability, in accordance with the cubic symmetry, can be suggested. This expression is inspired from the definition of the magneto-crystalline anisotropy energy of cubic crystals (see for instance [17]):

$$\mu^{\mathbf{i}}{}_{\gamma} = \mu_{100} + 3(\mu_{111} - \mu_{100})\left(\gamma_1^2\gamma_2^2 + \gamma_2^2\gamma_3^2 + \gamma_3^2\gamma_1^2\right) \tag{25}$$

where $[\gamma_1, \gamma_2, \gamma_3]$ are the direction cosines of the considered direction $\boldsymbol{\gamma}$. μ_{100} and μ_{111} are the extremal values of the permeability respectively along the $\langle 100\rangle$ and $\langle 111\rangle$ directions. Under this assumption, the permeability in $\langle 110\rangle$ is defined by relation (26):

$$\mu_{110} = \frac{1}{4}(3\mu_{111} + \mu_{100}). \tag{26}$$

The values of the permeability of the iron single crystal, following a secant definition, identified from Webster experimental results [15] are given in Table I.

The spatial representation of the permeability is shown in Fig. 2 for an iron single crystal under an applied field of 400 A/m.

A more refined description introduces the permeability μ_{110} in $\langle 110\rangle$ directions as a parameter:

$$\mu^{\mathbf{i}}{}_{\gamma} = \mu_{100} + 4(\mu_{110} - \mu_{100})\left(\gamma_1^2\gamma_2^2 + \gamma_2^2\gamma_3^2 + \gamma_3^2\gamma_1^2\right) + 9(3\mu_{111} + \mu_{100} - 4\mu_{110})\left(\gamma_1^2\gamma_2^2\gamma_3^2\right). \tag{27}$$

However, as shown in Fig. 3, the introduction of an additional parameter does not significantly modify the definition of the cubic permeability in the case of iron, since μ_{110} is close to expression (26).

Using the cubic definition of the permeability of the single crystal given by (25), estimates for the behavior of polycrystals can be derived from (15).

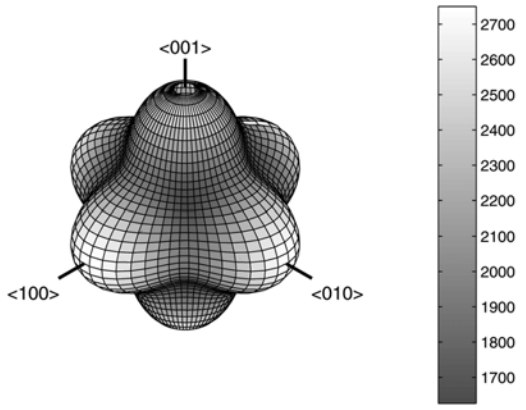

Fig. 2. Spatial representation of the relative permeability $(\mu^{\mathbf{i}}{}_{\gamma}/\mu_0)$ of an iron single crystal for $H = 400$ A/m, using a representation with two parameters.

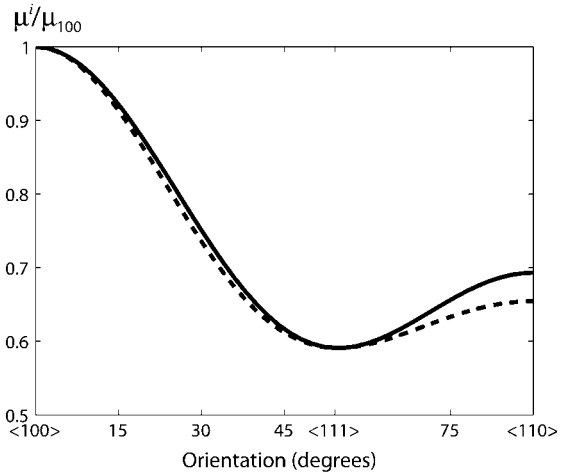

Fig. 3. Comparison between the permeability obtained using a representation with two parameters (line) and with three parameters (dashed line) for an applied field level of 400 A/m. Projection in the plane $y = z$, including directions [100], [111], and [011].

V. Permeability of Polycrystals

The effective permeability in the direction $\boldsymbol{\gamma}$ can be obtained through a projection of relation (15) along $\boldsymbol{\gamma}$:

$$\mu^{\mathbf{eff}}{}_{\gamma} = \frac{\left\langle \dfrac{\mu^{\mathbf{i}}{}_{\gamma}}{2\mu^{\mathbf{m}} + \mu^{\mathbf{i}}{}_{\gamma}} \right\rangle}{\left\langle \dfrac{1}{2\mu^{\mathbf{m}} + \mu^{\mathbf{i}}{}_{\gamma}} \right\rangle}. \tag{28}$$

If the self-consistent method is chosen, the infinite medium permeability is not a constant but the effective permeability $(\mu^{\mathbf{m}} = \mu^{\mathbf{eff}}{}_{\gamma})$, so that (15) becomes:

$$\mu^{\mathbf{eff}}{}_{\gamma} = \frac{\left\langle \dfrac{\mu^{\mathbf{i}}{}_{\gamma}}{2\mu^{\mathbf{eff}}{}_{\gamma} + \mu^{\mathbf{i}}{}_{\gamma}} \right\rangle}{\left\langle \dfrac{1}{2\mu^{\mathbf{eff}}{}_{\gamma} + \mu^{\mathbf{i}}{}_{\gamma}} \right\rangle}. \tag{29}$$

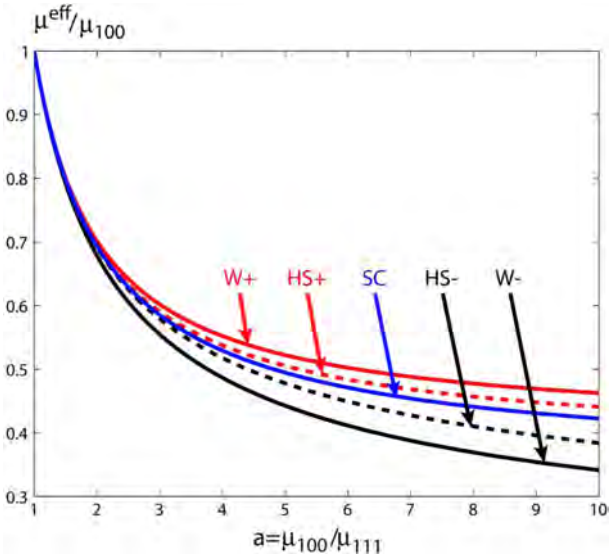

Fig. 4. Normalized effective magnetic permeability of an isotropic polycrystal as a function of the single crystal anisotropy ratio $a = \mu_{100}/\mu_{111}$: Wiener, Hashin & Shtrikman bounds and self-consistent estimate.

Equation (29) can be written in the form of the classical Bruggeman relation (30)

$$\left\langle \frac{\mu^{\mathbf{i}}{}_{\gamma} - \mu^{\mathbf{eff}}{}_{\gamma}}{2\mu^{\mathbf{eff}}{}_{\gamma} + \mu^{\mathbf{i}}{}_{\gamma}} \right\rangle = 0. \tag{30}$$

A. Isotropic Polycrystals

If the crystallographic orientation of grains in the polycrystal is random, the macroscopic behavior is isotropic. The magnetic permeability is then defined by a scalar value $\mu^{\mathbf{eff}}$. The value of $\mu^{\mathbf{eff}}$ has been estimated according to several homogenization schemes (Wiener, Hashin and Shtrikman, self-consistent) as a function of the single crystal anisotropy ratio $a(a = \mu_{100}/\mu_{111})$. The results are presented in Fig. 4. The case of the upper Wiener bound is particularly easy to calculate analytically and can be expressed as follows:

$$\mu^{\mathbf{eff}}{}_{W+} = \frac{2}{5}\mu_{100} + \frac{3}{5}\mu_{111}. \tag{31}$$

As far as low anisotropy ratio $(a < 2)$ are considered, the Wiener lower and upper bounds are very close, and all the homogenization schemes give similar results. When considering higher single crystal anisotropy ratio, the differences between the schemes become more sensitive: for $a = 5$, the difference between the Wiener lower and upper bounds is more than 15%.

B. Anisotropic Polycrystals

In most cases, the macroscopic anisotropy of polycrystals is the result of the combination of the single crystal anisotropy to crystallographic texture. The crystallographic texture is described through an orientation distribution function (ODF), representative of the orientations of grains in the polycrystal [18]. A scanning electron microscope (SEM), with an electron back

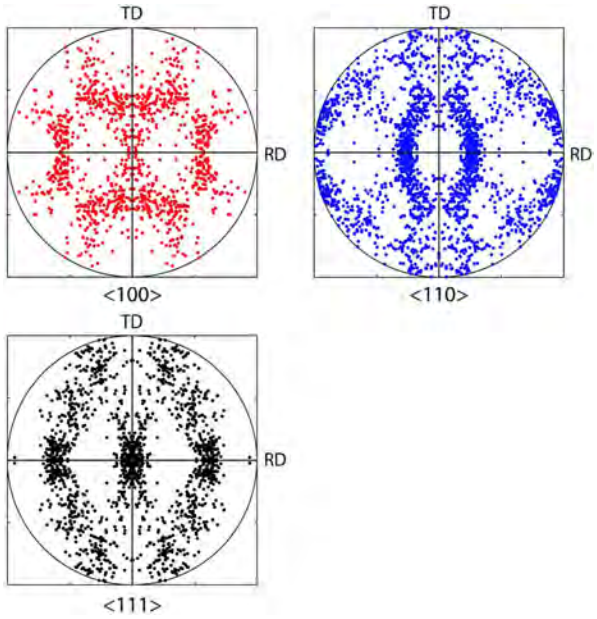

Fig. 5. $\langle 100\rangle$, $\langle 110\rangle$, and $\langle 111\rangle$ discrete pole figures for a nonoriented 3% silicon-iron steel.

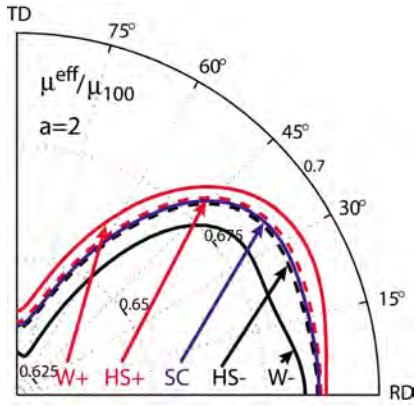

Fig. 6. Normalized magnetic permeability in the sheet plane: Wiener, Hashin & Shtrikman bounds and self-consistent estimate for an anisotropy ratio $a = 2$.

scatter diffraction (EBSD) measurement system, can provide a discrete orientation data file for the crystallographic texture of a given material. An example of pole figures, using 396 orientations, is shown for a nonoriented 3% silicon-iron steel in Fig. 5.

This discrete ODF can be used in (28) or (30) for the calculation of the effective permeability of anisotropic polycrystals. The corresponding results, according to several estimates, are shown in Figs. 6 and 7, respectively, for a single crystal anisotropy ratio $a = 2$ and $a = 5$. It must be noticed that the scales of polar Figs. 6 and 7 are not centered on the origin. This choice has been made in order to highlight the differences between the estimates.

It can be seen that the proposed approach allows the description of the macroscopic anisotropy of texturized polycrystals. As expected, for low anisotropy ratio a, corresponding to low

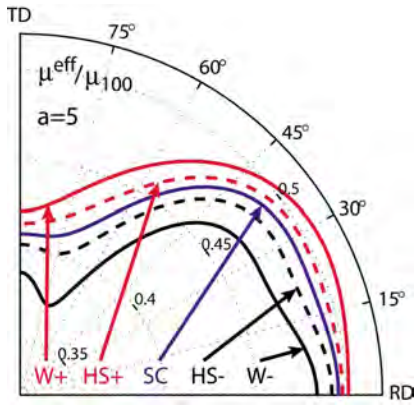

Fig. 7. Normalized magnetic permeability in the sheet plane: Wiener, Hashin & Shtrikman bounds and self-consistent estimate for an anisotropy ratio $a = 5$.

applied fields, the contrast between the several estimates is tiny. In Fig. 6, Hashin and Shtrikman bounds and self-consistent estimates are very close. But for higher anisotropy ratio, differences between the different approaches becomes significant. Moreover, the description of the macroscopic anisotropy is not strictly identical from one approach to another. Then, it becomes important to choose an appropriate homogenization model for the definition of the effective permeability.

VI. Discussion

The choice of the most appropriate model (namely the appropriate value of $\mu^{\mathbf{m}}$) for a given heterogeneous material is a key point, particularly for high anisotropy ratio of the single crystal.

Experimental results could help to evaluate the different possible choices. Unfortunately, the result is expected to be strongly dependent on the microstructure of the particular chosen material. Moreover, to our knowledge, no publication associates macroscopic polycrystalline permeability measurement to corresponding single crystals data. As an example, the experimental results from [19], for a material with a similar crystallographic texture of the one presented in Fig. 5, have been replotted[6] in Fig. 8, to highlight the anisotropic behavior.

For very low magnetic field, the relative anisotropy has a similar appearance in experiment and modeling. It corresponds to the linear behavior stage for the material. As soon as the magnetic field level reaches about 200 A/m, the nonlinear stage begins, and the hypotheses of the proposed model do not apply.

A second strategy to choose the value of $\mu^{\mathbf{m}}$ in the model would be to consider the particular microstructure of the modelled material. In the case of biphasic materials, if the microstructure is constituted of inclusions of phase 1 embedded in a continuous matrix of phase 2, the choice of the Hashin & Shtrikman bound with $\mu^{\mathbf{m}} = \mu_2$ is expected to give accurate results. In the case of polycrystals, the self-consistent scheme is known to be well suited to random grain microstructure. It is probably the method to recommend. Unfortunately, it is also the most complicated to implement since it is based on

[6]It must be noticed that the single crystal permeability has not been characterized, so that the measured permeability has been normalized to the value obtained in the rolling direction (RD).

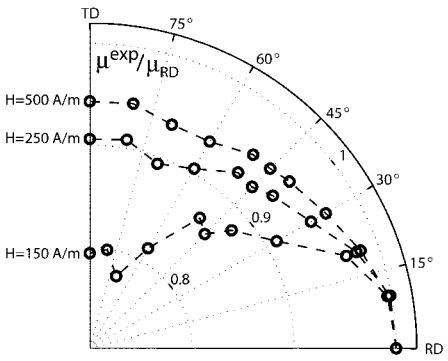

Fig. 8. Normalized magnetic permeability in the sheet plane: experimental results for a nonoriented 3% silicon-iron steel [19].

an iterative procedure. For simplicity reasons, the HS bounds can be preferred. If a rough estimate is sufficient, the formula given by (31) is particularly simple, but does not incorporate any anisotropy information.

VII. Conclusion

A model for the prediction of the effective magnetic permeability of heterogeneous linear materials has been presented. It is based on the solution of the basic inclusion problem. This approach enables to recover some classical estimates obtained under different assumptions for polyphasic materials. In the case of linear cubic polycrystals, the classical description of the permeability through a second order tensor has been shown to be inefficient. A formulation has been proposed to describe the local anisotropy of cubic single crystals. Combined with the grain orientations, this approach allows the prediction of the macroscopic anisotropy of polycrystals. Several estimates, classical in the case of biphasic materials, have been derived for polycrystals, and can lead to significantly different predictions for the macroscopic behavior.

However, the proposed approach is restricted to linear magnetic behavior. The case of nonlinear properties is much more complicated. Nevertheless, the resolution of nonlinear homogenization problems generally rely on the resolution of a linear comparison problem (see for example [20]). In that context, the knowledge of solutions for linear homogenization problems is essential.

References

[1] O. Wiener, "Die Theorie des Mischkörpers für das Feld des stationären Strömung. erste abhandlung die Mittelswertsätze für kraft, polarisation und energie," *Abh. Math. Phys. Kl. Konigl. Sach.*, vol. 32, pp. 509–604, 1912.

[2] Z. Hashin and S. Shtrikman, "A variational approach to the theory of the effective magnetic permeability of multiphase materials," *J. Appl. Phys.*, vol. 33, pp. 3125–3131, 1962.

[3] K. Lichtenecker, "Die dielektrizitats konstante naturlicher und kunstlicher mischkorper," *Physik. Z.*, vol. 27, pp. 115–158, 1926.

[4] J. C. M. Garnett, "Colours in metal glasses and in metallic films," *Phil. Trans. R. Soc.*, vol. 203, pp. 385–420, 1904.

[5] D. A. G. Bruggeman, "Berechnung verschiedener physikalischer konstanten von heterogenen substanzen," *Annalen der Physik*, vol. 5, pp. 636–664, 1935.

[6] R. Landauer, "The electrical resistance of binary metallic mixtures," *J. Appl. Phys.*, vol. 23, pp. 779–784, 1952.

[7] D. J. Bergman, "Exactly solvable microscopic geometries and rigorous bounds for the complex dielectric constant of a two-component composite material," *Phys. Rev. Lett.*, vol. 44, pp. 1285–1287, 1980.

[8] H. Waki, H. Igarashi, and T. Honma, "Estimation of effective permeability of magnetic composite materials," *IEEE Trans. Magn.*, vol. 41, no. 5, pp. 1520–1523, May 2005.

[9] D. Stroud, "Generalized effective-medium approach to the conductivity of an inhomogeneous material," *Phys. Rev. B*, vol. 12, pp. 3368–3373, 1975.

[10] M. Le Floc'h, J. L. Mattei, P. Laurent, O. Minot, and A. M. Konn, "A physical model for heterogeneous magnetic materials," *J. Magn. Magn. Mater.*, vol. 140–144, pp. 2191–2192, 1995.

[11] D. Bariou, P. Quéffélec, P. Gelin, and M. Le Floc'h, "Extension of the effective medium approximation for the determination of effective permeability tensor of unsaturated polycrystalline ferrites," *IEEE Trans. Magn.*, vol. 37, no. 6, pp. 3885–3891, Nov. 2001.

[12] P. Quéffélec, D. Bariou, and P. Gelin, "A predictive model for the permeability tensor of magnetized heterogeneous materials," *IEEE Trans. Magn.*, vol. 41, no. 1, pp. 17–23, Jan. 2001.

[13] J. A. Stratton, *Electromagnetic Theory*. New York: McGraw-Hill, 1941.

[14] K. Kärkkäinen, A. H. Sihvola, and K. Nikoskinen, "Effective permittivity of mixtures: Numerical validation by the FDTD method," *IEEE Trans. Geosci. Remote Sens.*, vol. 38, no. 3, pp. 1303–1308, May 2000.

[15] W. L. Webster, "Magnetostriction and change of resistance in single crystals of iron and nickel," *Proc. Phys. Soc.*, vol. 42, pp. 431–440, 1930.

[16] B. W. Wang, S. C. Busbridge, Y. X. Li, G. H. Wu, and A. R. Piercy, "Magnetostriction and magnetization process of $Tb_{0,27}Dy_{0,73}Fe_2$ single crystal," *J. Magn. Magn. Mater.*, vol. 218, pp. 198–202, 2000.

[17] R. M. Bozorth, *Ferromagnetism*. New York: Van Nostrand, 1951.

[18] H. J. Bunge, *Texture Analysis in Materials Science*. London, U.K.: Butterworth, 1982.

[19] O. Hubert, L. Daniel, and R. Billardon, "Experimental analysis of the magneto-elastic anisotropy of a non-oriented silicon iron alloy," *J. Magn. Magn. Mater.*, vol. 254–255, pp. 352–354, 2003.

[20] L. Daniel, O. Hubert, and B. Vieille, "Multiscale strategy for the determination of magneto-elastic behaviour: Discussion and application to Ni-Zn ferrites," *Int. J. Appl. Electromagn. Mech.*, 2007, to be published.

Manuscript received November 22, 2006; revised March 29, 2007. Corresponding author: L. Daniel (e-mail: laurent.daniel@lgep.supelec.fr).

Intraphase fluctuations in heterogeneous magnetic materials

Romain Corcolle,[a] Laurent Daniel, and Frédéric Bouillault
Laboratoire de Génie Electrique de Paris, CNRS UMR8507; SUPELEC; UPMC Univ Paris 06; Université de Paris-Sud; 11 rue Joliot-Curie, Plateau de Moulon, F-91192 Gif-sur-Yvette Cedex, France

(Received 12 January 2009; accepted 16 May 2009; published online 22 June 2009)

The main purpose of homogenization is the determination of the effective behavior (or macroscopic behavior) of heterogeneous materials. Mean fields per phase are generally used in homogenization and represent sufficient information in most cases. However, more information about the field distribution can be necessary, particularly in nonlinear cases. Then, intraphase fluctuations have to be determined. This paper presents a method, based on homogenization tools, for the determination of both estimates and bounds for the intraphase fluctuations. The presented applications deal with magnetic materials and the results obtained with homogenization are compared to those obtained using a finite element modeling. © *2009 American Institute of Physics*. [DOI: 10.1063/1.3152789]

I. INTRODUCTION

The determination of the effective properties of heterogeneous materials is a long-standing problem in physics. Unless the microstructure is fully described, the effective properties cannot be exactly determined. Analytical solutions exist for very simple microstructures. For more complex microstructures, finite element modeling is sometimes used to estimate the effective properties.

Homogenization is an alternative modeling approach that enables the determination of bounds or estimates on the effective properties from few pieces of information about the microstructure. Some optimal bounds for the effective properties have been derived.[1,2] Additional information on the effective property function have been studied by Bergman and Milton[3,4] to define more restrictive bounds. For example, from the knowledge of the effective properties for a given set of parameters, improved bounds have been derived by Milton and by Avellaneda.[4,5]

In the case of magnetic materials, homogenization enables the determination of the effective permeability $\tilde{\mu}$ (permeability of the equivalent homogeneous medium), linking the macroscopic magnetic field $\overline{\mathbf{H}}$ and the macroscopic magnetic induction $\overline{\mathbf{B}}$ in the real medium (RM) (see Fig. 1),

$$\overline{\mathbf{B}} = \langle \mathbf{B}(\mathbf{x}) \rangle = \langle \mu(\mathbf{x}) \cdot \mathbf{H}(\mathbf{x}) \rangle = \tilde{\mu} \cdot \langle \mathbf{H}(\mathbf{x}) \rangle = \tilde{\mu} \,.\, \overline{\mathbf{H}}, \qquad (1)$$

where $\mu(\mathbf{x})$ is the local permeability and $\mathbf{x}$ the spatial position. The operator $\langle \cdot \rangle$ represents an averaging operation over the whole volume of the RM [$\langle \mathbf{H}(\mathbf{x}) \rangle = 1/V \cdot \int_V \mathbf{H}(\mathbf{x}) \cdot dV$, with V the volume of the RM].

These techniques generally rely on a mean field approach. Indeed a first homogenization description of the local behavior can be obtained with the mean field per phase. In many cases, this piece of information can be sufficient. For example, in a magnetostriction problem, the local magnetic field has to be determined in order to define the local strain. If the constitutive law is linear (piezomagnetic behavior), the knowledge of the mean magnetic field is sufficient to determine the mean strain. But when the constitutive law is nonlinear, then the mean strain is not directly linked to the mean magnetic field through the constitutive law (see Fig. 2). This is the reason why the determination of intraphase fluctuations is necessary.

The study of the second order moments $\langle \mathbf{H}(\mathbf{x})^2 \rangle$ is a first approach for the description of field fluctuations. Although particularly important to study some nonlinear effects, these fluctuations have been less intensively studied. Axell[6] derived bounds for second order moments in two-phase materials for isotropic composites. Lipton[7] derived a lower bound for *n*th order moments. Cheng and Torquato[8] studied the field fluctuations in random composites through a finite element model. We propose in that paper a method to derive bounds and estimates for second order moments in the general case and in the particular case of isotropic composites.

In the first part, homogenization techniques are presented. The second part is dedicated to the use of homogenization tools to determine second order moments. The optimality of the derived bounds is discussed. In the last part, an application on biphasic composites is studied and the results obtained with the presented method are compared to the ones obtained from a finite element modeling. An example about the use of second order moments in a magnetostriction problem is finally presented.

II. HOMOGENIZATION

A. Theory

The distribution of the magnetic field in a heterogeneous material can be obtained by defining a localization operator $\mathbb{A}(\mathbf{x})$ linking the local magnetic field $\mathbf{H}(\mathbf{x})$ to the macroscopic one $\overline{\mathbf{H}}$,

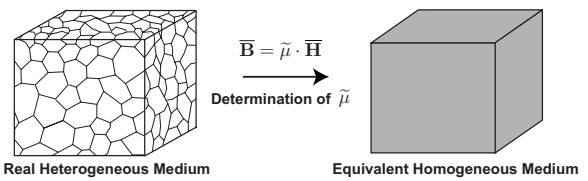

FIG. 1. Homogenization scheme.

[a]Electronic mail: romain.corcolle@lgep.supelec.fr.

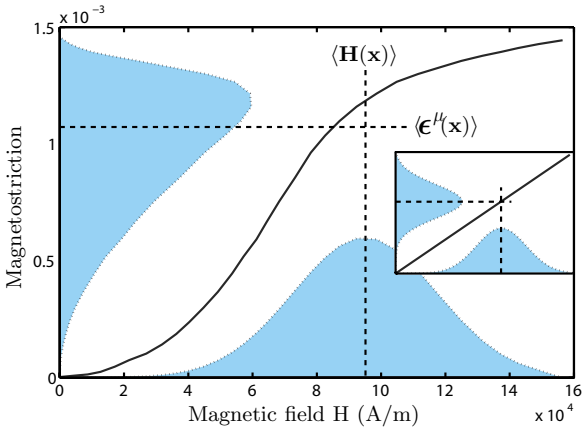

FIG. 2. (Color online) Field distributions and mean values. In the nonlinear case, the relationship between $\langle \boldsymbol{\epsilon}^{\mu}(\mathbf{x}) \rangle$ and $\langle \mathbf{H}(\mathbf{x}) \rangle$ is not directly given by the constitutive law.

$$\mathbf{H}(\mathbf{x}) = \mathbb{A}(\mathbf{x}) \cdot \overline{\mathbf{H}}. \tag{2}$$

This localization operator $\mathbb{A}(\mathbf{x})$ depends on the position $\mathbf{x}$, on the local permeability $\mu(\mathbf{x})$, and on the microstructure of the RM. Moreover, since $\langle \mathbf{H}(\mathbf{x}) \rangle = \overline{\mathbf{H}}$, it must verify Eq. (3) (with $\mathbb{I}$ the 3×3 identity tensor),

$$\langle \mathbb{A}(\mathbf{x}) \rangle = \mathbb{I}. \tag{3}$$

Then, combining Eqs. (1)–(3), the effective permeability $\tilde{\mu}$ can be written as

$$\tilde{\mu} = \langle \mu(\mathbf{x}) \cdot \mathbb{A}(\mathbf{x}) \rangle. \tag{4}$$

The homogenization approach classically relies on the determination of the mean local field per phase $\mathbf{H}_i$. This mean local field per phase $\mathbf{H}_i$ can also be linked to the macroscopic one $\overline{\mathbf{H}}$ [similarly to Eq. (2)],

$$\mathbf{H}_i = \langle \mathbf{H}(\mathbf{x}) \rangle_i = \langle \mathbb{A}(\mathbf{x}) \,.\, \overline{\mathbf{H}} \rangle_i = \langle \mathbb{A}(\mathbf{x}) \rangle_i \cdot \overline{\mathbf{H}} = \mathbb{A}_i \cdot \overline{\mathbf{H}}, \tag{5}$$

where $\langle \cdot \rangle_i$ represents an averaging operation over the only phase i and $\mathbb{A}_i$ the mean localization operator on phase i.

The effective permeability $\tilde{\mu}$ can be determined (for a n-phasic material),

$$\tilde{\mu} = \langle \mu(\mathbf{x}) \cdot \mathbb{A}(\mathbf{x}) \rangle = \sum_{i=1}^{n} f_i \cdot \mu_i \cdot \mathbb{A}_i \tag{6}$$

since $\mu(\mathbf{x})$ is constant per phase (considering linear behavior). f_i stands for the volumetric fraction of phase i.

In the particular case of a biphasic material, the localization tensors $\mathbb{A}_i$ can be conversely retrieved from the effective permeability $\tilde{\mu}$ [using Eqs. (3) and (6)],

$$\mathbb{A}_1 = \frac{1}{f_1}(\mu_1 - \mu_2)^{-1} \cdot (\tilde{\mu} - \mu_2),$$

$$\mathbb{A}_2 = \frac{1}{f_2}(\mu_2 - \mu_1)^{-1} \cdot (\tilde{\mu} - \mu_1). \tag{7}$$

Therefore, in the biphasic case, the mean field per phase can be estimated (or bounded) from the estimates (or bounds) on the effective permeability $\tilde{\mu}$. Many methods can be used to build these estimates (or bounds). We made the choice to use the homogenization techniques based on inclusion problems.

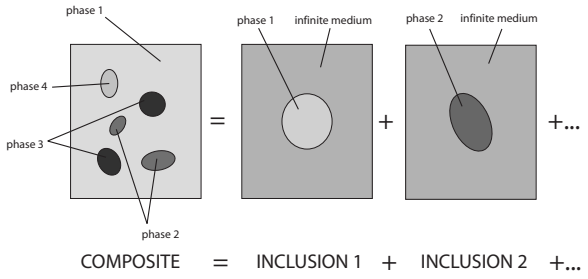

FIG. 3. Principle of homogenization based on inclusion problems.

B. Inclusion problems

Homogenization models based on inclusion problems rely on the hypothesis that the mean field in each phase i is similar to the corresponding field in a inclusion (with the same properties μ_i than in the RM) embedded in a infinite homogeneous medium with permeability μ_m.[9] Then, a n-phasic problem can be studied such as n uncorrelated inclusion problems (see Fig. 3).

The basic inclusion problem is defined by (i) an inclusion embedded in an infinite medium and (ii) an uniform magnetic field $\mathbf{H}^{\infty}$ applied at the infinity.

The inclusion shapes are linked to the distribution of the corresponding phases in the RM. For example, an isotropic distribution of one phase in the RM would be modeled by a spherical inclusion in the inclusion problem. It has to be noticed that, in the case of an ellipsoidal inclusion, the field in this inclusion is uniform and can be deduced analytically.[10]

For the sake of simplicity, we will focus on that paper on two dimensional (2D) composites with isotropic constituents (the permeability tensors can be reduced to scalars). In that case, the definition of the effective permeability $\tilde{\mu}$ is given by

$$\tilde{\mu} = \frac{\left\langle \dfrac{\mu_i}{\mu_i + \mu_m} \right\rangle}{\left\langle \dfrac{1}{\mu_i + \mu_m} \right\rangle}. \tag{8}$$

The choice of the infinite medium permeability μ_m is a degree of freedom in order to describe the microstructure. Some particular choices can lead to classical estimates in homogenization such as the Wiener (W) bounds, the Hashin and Shtrikman (HS) ones, or the self-consistent (SC) estimate.[9]

But homogenization techniques can also provide more information than estimates or bounds on the effective permeability $\tilde{\mu}$. Section III presents a method to determine second order moments of the magnetic field per phase.

III. SECOND ORDER MOMENTS

In a first part, the relation giving the second order moment of the magnetic field per phase $\langle \mathbf{H}(\mathbf{x})^2 \rangle_i$ is derived. In a

second part, some results are presented on particular microstructures for which analytical solutions are known. A method that enables to determine bounds on the derivative $\partial\tilde{\mu}/\partial\mu_i$, when bounds on the effective permeability $\tilde{\mu}$ are given, is then presented. The optimality of these bounds is discussed.

A. Theory

Homogenization can also be applied to energetic quantities.[4] Equation (9) is verified when uniform boundary conditions are applied (Tellegen's theorem),

$$\langle \mathbf{B}(\mathbf{x}) \cdot \mathbf{H}(\mathbf{x}) \rangle = \langle \mathbf{B}(\mathbf{x}) \rangle \cdot \langle \mathbf{H}(\mathbf{x}) \rangle = \overline{\mathbf{B}} \cdot \overline{\mathbf{H}}. \tag{9}$$

The first member is equal to

$$\langle \mathbf{B}(\mathbf{x}) \cdot \mathbf{H}(\mathbf{x}) \rangle = \frac{1}{V} \int_V \mu(\mathbf{x}) \cdot \mathbf{H}(\mathbf{x})^2 \cdot dV. \tag{10}$$

Since the permeability is constant per phase, this equation can be rewritten as

$$\langle \mathbf{B}(\mathbf{x}) \cdot \mathbf{H}(\mathbf{x}) \rangle = \sum_{i=1}^{n} f_i \cdot \mu_i \cdot \langle \mathbf{H}(\mathbf{x})^2 \rangle_i. \tag{11}$$

The last member in Eq. (9) can be rewritten with the introduction of the (isotropic) effective permeability $\tilde{\mu}$,

$$\overline{\mathbf{B}} \cdot \overline{\mathbf{H}} = (\tilde{\mu} \cdot \overline{\mathbf{H}}) \cdot \overline{\mathbf{H}} = \tilde{\mu} \cdot \overline{\mathbf{H}}^2. \tag{12}$$

Finally, Eq. (9) leads to

$$\tilde{\mu} \cdot \overline{\mathbf{H}}^2 = \sum_{i=1}^{n} f_i \cdot \mu_i \cdot \langle \mathbf{H}(\mathbf{x})^2 \rangle_i. \tag{13}$$

Considering that the effective applied magnetic field $\overline{\mathbf{H}}$ is a constant field, the last equation can be differentiated as

$$(\tilde{\mu} + \delta\tilde{\mu}) \cdot \overline{\mathbf{H}}^2 = \sum_{i=1}^{n} f_i \cdot (\mu_i + \delta\mu_i) \cdot \langle (\mathbf{H}(\mathbf{x}) + \delta\mathbf{H}(\mathbf{x}))^2 \rangle_i. \tag{14}$$

Moreover, the use of a variational principle indicates that the second term in the second member of the following equation is equal to zero:

$$\sum_{i=1}^{n} f_i \cdot \mu_i \cdot \langle (\mathbf{H}(\mathbf{x}) + \delta\mathbf{H}(\mathbf{x}))^2 \rangle_i = \sum_{i=1}^{n} f_i \cdot \mu_i \cdot \langle \mathbf{H}(\mathbf{x})^2 \rangle_i + 2\sum_{i=1}^{n} f_i \cdot \mu_i \cdot \langle \mathbf{H}(\mathbf{x}) \cdot \delta\mathbf{H}(\mathbf{x}) \rangle_i + \sum_{i=1}^{n} f_i \cdot \mu_i \cdot \langle \delta\mathbf{H}(\mathbf{x})^2 \rangle_i \tag{15}$$

since the magnetic field minimizes the energy for a given configuration (configuration made of permeabilities μ_i). Moreover, the last term in the second member can be neglected (second order term).

Using Eq. (14) with Eq. (15) gives

$$(\tilde{\mu} + \delta\tilde{\mu}) \cdot \overline{\mathbf{H}}^2 = \sum_{i=1}^{n} f_i \cdot \mu_i \cdot \langle \mathbf{H}(\mathbf{x})^2 \rangle_i + \sum_{i=1}^{n} f_i \cdot \delta\mu_i \cdot \langle (\mathbf{H}(\mathbf{x}) + \delta\mathbf{H}(\mathbf{x}))^2 \rangle_i. \tag{16}$$

The second term in the second member can be simplified keeping only the first order term and neglecting second and third order terms,

$$\sum_{i=1}^{n} f_i \cdot \delta\mu_i \cdot \langle (\mathbf{H}(\mathbf{x}) + \delta\mathbf{H}(\mathbf{x}))^2 \rangle_i \approx \sum_{i=1}^{n} f \cdot \delta\mu_i \cdot \langle \mathbf{H}(\mathbf{x})^2 \rangle_i. \tag{17}$$

Then, using Eq. (16) with Eqs. (11) and (17) gives the following relation:

$$\delta\tilde{\mu} \cdot \overline{\mathbf{H}}^2 = \sum_{i=1}^{n} f_i \cdot \delta\mu_i \cdot \langle \mathbf{H}(\mathbf{x})^2 \rangle_i, \tag{18}$$

which provides us the following equation to determine the second order moment of the magnetic field per phase:

$$\langle \mathbf{H}(\mathbf{x})^2 \rangle_i = \frac{1}{f_i} \frac{\partial\tilde{\mu}}{\partial\mu_i} \overline{\mathbf{H}}^2. \tag{19}$$

This relation was derived earlier by Bergman.[3]

B. Exact solutions

For some particular microstructures, analytical solutions for the field distribution exist, as well as for the effective permeability.

The most simple example is the study of laminated composites. The magnetic field $\mathbf{H}(\mathbf{x})$ is uniform per phase. The Wiener bounds are exact estimates for the effective permeability $\tilde{\mu}$. The first case is obtained when the laminate direction is parallel to the field, then the magnetic field is uniform in the whole composite ($\mathbf{H}(\mathbf{x}) = \overline{\mathbf{H}}$). The effective permeability is equal to

$$\tilde{\mu} = \sum_{i=1}^{n} f_i \cdot \mu_i. \tag{20}$$

Applying Eq. (19) leads to

$$\langle \mathbf{H}(\mathbf{x})^2 \rangle_i = \overline{\mathbf{H}}^2 = \langle \mathbf{H}(\mathbf{x}) \rangle_i^2, \tag{21}$$

which is consistent with the fact that the magnetic field is uniform in the composite.

The second case is obtained when the laminate direction is perpendicular to the magnetic field, the magnetic induction is uniform in the whole composite ($\mathbf{B}(\mathbf{x}) = \overline{\mathbf{B}}$). The effective permeability is given by

$$\frac{1}{\tilde{\mu}} = \sum_{i=1}^{n} \frac{f_i}{\mu_i}. \tag{22}$$

Applying Eq. (19) leads to

$$\langle \mathbf{B}(\mathbf{x})^2 \rangle_i = \overline{\mathbf{B}}^2 = \langle \mathbf{B}(\mathbf{x}) \rangle_i^2, \tag{23}$$

which is consistent again.

Another example of microstructure with analytical solution is the Hashin cylinders (or spheres) assemblage.[2,11] The

composite is made of composite cylinders consisting of an inner cylinder (phase 2, volumetric fraction f_2) embedded in a concentric outer cylinder (phase 1, volumetric fraction $f_1 = 1 - f_2$). The whole space is filled with such composite cylinders sized down to the infinitesimally small. In that case, the magnetic field in phase 2 is uniform. The effective permeability is exactly equal to 1 of the Hashin and Shtrikman bound,

$$\tilde{\mu} = \mu_1 \cdot \frac{(1-f_2)\mu_1 + (1+f_2)\mu_2}{(1+f_2)\mu_1 + (1-f_2)\mu_2}. \tag{24}$$

Applying Eq. (19) leads to

$$\langle \mathbf{H}(\mathbf{x})^2 \rangle_1 = \frac{(\mu_2+\mu_1)^2 + f_2(\mu_2-\mu_1)^2}{((1+f_2)\mu_1 + (1-f_2)\mu_2)^2} \cdot \overline{\mathbf{H}}^2,$$

$$\langle \mathbf{H}(\mathbf{x})^2 \rangle_2 = \frac{4\mu_1^2}{((1+f_2)\mu_1 + (1-f_2)\mu_2)^2} \cdot \overline{\mathbf{H}}^2 = \langle \mathbf{H}(\mathbf{x}) \rangle_2^2. \tag{25}$$

The same relations can be extracted from the analytical field distribution given in Ref. 11.

C. Bounds on $\partial\tilde{\mu}/\partial\mu_i$

In the general case, the microstructure of materials is not exactly described, so that exact effective permeability cannot be given. Estimates can be built but bounds on the effective permeability can be preferred. Nevertheless, bounds on the effective permeability $\tilde{\mu}$ do not provide any information about the derivative $\partial\tilde{\mu}/\partial\mu_i$. However, more refined bounds on $\tilde{\mu}$ can be obtained from an additional piece of information and will help us to bound the derivative $\partial\tilde{\mu}/\partial\mu_i$. This point is the object of this section.

Let us suppose that the effective permeability is known for a given configuration (obtained from experimentation, for example). Then, for the same fixed microstructure and changing the phase properties (permeabilities), the effective permeability may vary. From the information on the effective permeability for this particular configuration, more restrictive bounds on the effective permeability $\tilde{\mu}$ can be obtained for the same microstructure[4] (see Fig. 4).

For example, some bounds (Wiener ones, Hashin and Shtrikman ones, etc.) can be determined for a composite if the phase permeabilities are known as well as the volumetric fractions f_i (an additional assumption could be isotropy). But, from an additional information, more restrictive bounds derived from the previous bounds can be written as the ratio of two polynomials. The following example is derived from Wiener bounds with a known value of the function $\tilde{\mu}(\mu_1^*, \mu_2^*) = \tilde{\mu}^*$:

$$\tilde{\mu}_1(\mu_1,\mu_2) = \frac{a_0\mu_2^2 + a_1\mu_2\mu_1}{\mu_2 + b_1\mu_1},$$

$$\tilde{\mu}_2(\mu_1,\mu_2) = \frac{a_1'\mu_2\mu_1 + a_2'\mu_1^2}{\mu_2 + b_1'\mu_1}, \tag{26}$$

where the a_i and b_i coefficients depend on the previous bounds and on the additional information.[4] For example, in this particular case, the coefficients are determined so that the effective permeability verifies: $\tilde{\mu}(1,1) = 1$, $\partial\tilde{\mu}/\partial\mu_1|_{\mu_1=\mu_2=1} = f_1$, and $\tilde{\mu}(\mu_1^*, \mu_2^*) = \tilde{\mu}^*$.

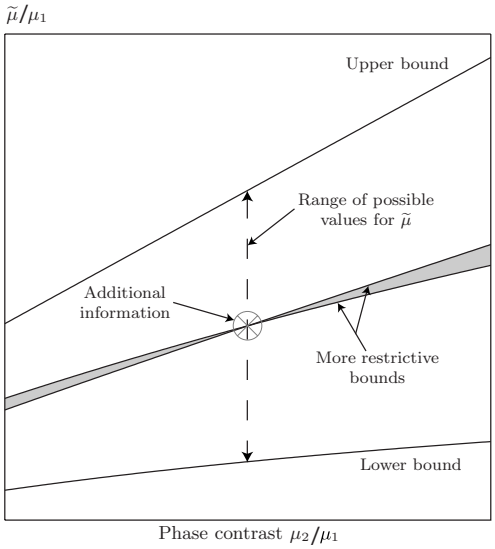

FIG. 4. More restrictive bounds from an additional information about $\tilde{\mu}$.

Until that point, more restrictive bounds have been obtained for the effective permeability $\tilde{\mu}$ but no information about the derivative $\partial\tilde{\mu}/\partial\mu_i$ is given. The noticeable point in Fig. 4 is that the new bounds (logically) cross. Then, the derivative $\partial\tilde{\mu}/\partial\mu_i$ is necessarily bounded by the derivatives of the new bounds at that point. In that way, when bounds are provided on the effective permeability, it is possible to determine some bounds on the derivative $\partial\tilde{\mu}/\partial\mu_i$ by scanning the full scale of possible values for $\tilde{\mu}$ and take these values for the additional information. Then, bounds for the derivative $\partial\tilde{\mu}/\partial\mu_i$ are obtained for each possible value of $\tilde{\mu}$. The optimality of such bounds will be discussed in the next paragraph.

D. Optimality

The optimality of the bounds on the derivative $\partial\tilde{\mu}/\partial\mu_i$ obtained from the proposed method is proven by the definition of a microstructure attaining these bounds. The bounds on the derivative $\partial\tilde{\mu}/\partial\mu_i$ obtained from the Wiener bounds on the effective permeability $\tilde{\mu}$ are attained for the confocal-ellipsoid assemblage defined in Ref. 7.

In the case of 2D isotropic composites, an additional property of the effective permeability can be used, known as the Keller's relation,[12]

$$\tilde{\mu}(\mu_1,\mu_2) \cdot \tilde{\mu}(\mu_2,\mu_1) = \mu_1 \cdot \mu_2. \tag{27}$$

Then, using this additional information for isotropic 2D composites, bounds on the derivative $\partial\tilde{\mu}/\partial\mu_i$ obtained from the Hashin and Shtrikman bounds on the effective permeability $\tilde{\mu}$ are attained for the composite consisting of densely packed, doubly coated circular cylinders defined in Ref. 13.

Unfortunately, for isotropic three dimensional (3D) composites, the Keller relation does not apply since some 3D

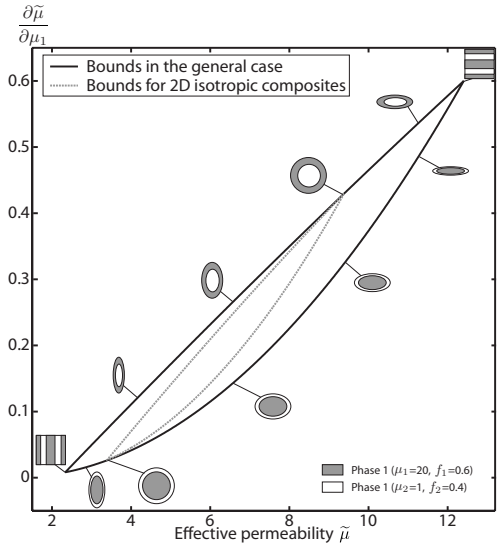

FIG. 5. Bounds on the derivative $\partial\tilde{\mu}/\partial\mu_1$ as a function of the effective permeability $\tilde{\mu}$ in the general case and in the case of 2D isotropic composites. The bounds are optimal since they are attained for some particular microstructures.

isotropic composites have been shown not to respect Keller's relation.[14] The relation becomes an inequality,

$$\tilde{\mu}(\mu_1,\mu_2)\cdot\tilde{\mu}(\mu_2,\mu_1)\geq\mu_1\cdot\mu_2. \tag{28}$$

Figures 5 and 6 present the derivative $\partial\tilde{\mu}/\partial\mu_i$ as the function of the effective permeability $\tilde{\mu}$. The phase properties are $\mu_1=20$, $\mu_2=1$, and $f_1=0.6$.

The corresponding microstructures attaining the bounds are also presented in the figures. These microstructures show a continuous way to transform, for a given composition, a "lower Wiener" microstructure into an "upper Wiener" one

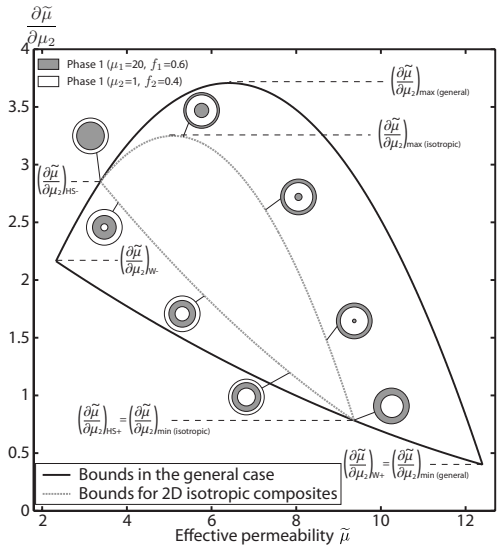

FIG. 6. Bounds on the derivative $\partial\tilde{\mu}/\partial\mu_2$ as a function of the effective permeability $\tilde{\mu}$ in the general case and in the case of 2D isotropic composites. The bounds are optimal since they are attained for particular microstructures.

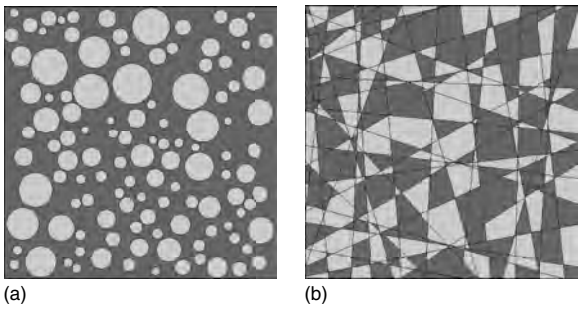

FIG. 7. Microstructures modeled with the finite element method.

passing through Hashin and Shtrikman microstructures, using confocal-ellipsoid assemblage (Fig. 5). Such a transformation can also be performed for isotropic composites using doubly coated circular cylinders (Fig. 6). These continuous transformations could also be applied, for a given effective permeability, with a variation of volumetric fraction f_1. A similar proposal, using an assemblage of two types of Hashin spheres, has been made by Gilormini[15] for the effective bulk modulus and conductivity of isotropic two-phase composite.

IV. RESULTS

In order to validate the presented method, results are compared to the ones obtained from a finite element modeling. The modeled materials are 2D biphasic magnetic materials with a phase contrast μ_2/μ_1 equal to 5. The finite element modeling models different types of microstructures (phase 1/phase 2): (i) type I: inclusions/matrix and matrix/inclusions [Fig. 7(a)]; (ii) type II: mosaic microstructure [Fig. 7(b)].

For these two types of microstructure, the finite element modeling has been realized for a large number of random microstructures (500 per volumetric fraction and per microstructure type, random position and radius for the disks in the first type, and random allocation of the phases in the second type).

A. Effective permeability

Figure 8 shows the results obtained from homogenization and finite element modeling about the effective permeability $\tilde{\mu}$ as a function of the volumetric fraction f_1 of phase 1.

Results for the mosaic microstructure are presented with error bars because the variability of the effective permeability $\tilde{\mu}$ is quite important. On the opposite, results for the matrix/inclusions (and inclusions/matrix) are presented with points representing the mean value of the different computations because the variability of the effective permeability $\tilde{\mu}$ is very low for this type of microstructure.

Classical estimates in homogenization are presented too. The Wiener bounds are obtained by choosing $\mu_m=0$ and $\mu_m\to\infty$ in the inclusion problems. The more restrictive HS bounds for isotropic composites are obtained by choosing $\mu_m=\mu_1$ and $\mu_m=\mu_2$ in the inclusion problems. The SC estimate can be a relevant estimate for microstructures where

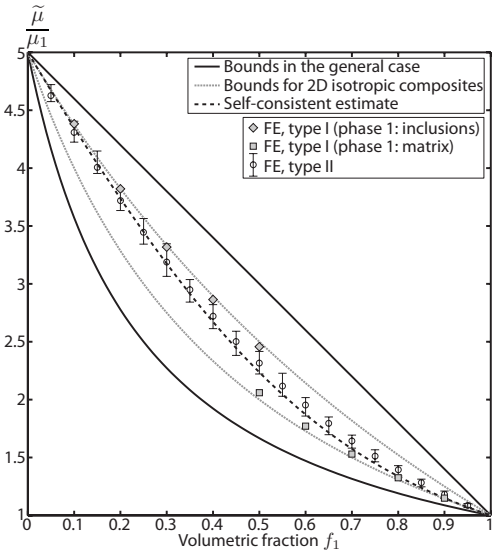

FIG. 8. Effective permeability $\tilde{\mu}$ as a function of the volumetric fraction of phase 1.

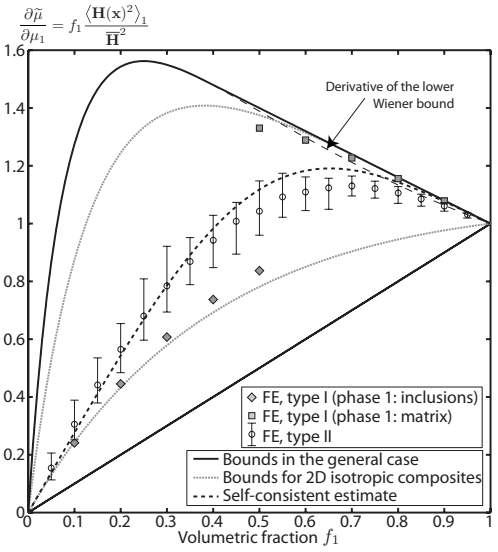

FIG. 9. Derivative of the effective permeability $\partial\tilde{\mu}/\partial\mu_1$ as a function of the volumetric fraction f_1 of phase 1, contrast $\mu_2/\mu_1=5$ (same legend for finite element results than Fig. 8).

none of the phase plays a particular role. They are obtained by choosing $\mu_m=\tilde{\mu}$ in the inclusion problems, leading to an iterative computation.

As expected, the finite element results are bounded by the Wiener bounds. Since the studied finite element microstructures can be considered isotropic, HS estimates should be bounds for the finite element results. A very few number of computations do not remain between these bounds, the isotropy of the corresponding microstructures may not be verified. In the following, the HS estimates will be considered as bounds. The first comment about Fig. 8 is that the effective permeability for the matrix/inclusions (and also inclusions/matrix) microstructures is quite close to the HS bounds. The HS bounds seem to be appropriate to give a quite accurate estimate for matrix/inclusion problems. The second comment is that the variability for the mosaic microstructure is quite high but the mean value for the effective permeability seems to be correctly estimated by the self-consistent estimate. This estimate seems well suited to this type of microstructure.

B. Derivatives of the effective permeability

Figure 9 shows the derivative of the effective permeability $\partial\tilde{\mu}/\partial\mu_1$ [determined in the finite element modeling by computing the value $f_1\langle\mathbf{H}(\mathbf{x})^2\rangle_1/\overline{\mathbf{H}}^2$ according to Eq. (19)] as a function of the volumetric fraction f_1 of phase 1 for a given phase contrast μ_2/μ_1 equal to 5. Figure 10 presents the same results for a contrast equal to 100. The homogenization results are given with two types of estimates: (i) estimates of $\partial\tilde{\mu}/\partial\mu_1$ obtained directly by deriving the estimates of $\tilde{\mu}$ (W and HS bounds, SC estimate), (ii) and bounds on $\partial\tilde{\mu}/\partial\mu_1$ obtained by scanning the range of possible values of $\tilde{\mu}$ (according to the bounds on the effective permeability $\tilde{\mu}$, see Fig. 8) and taking the minimum and maximum values of the derivative computed from Eq. (26) according to the method described in Sec. III C.

In one hand, these results illustrate that the derivatives of the previous effective permeability bounds cannot be considered as bounds on the derivative $\partial\tilde{\mu}/\partial\mu_1$. Some finite element results bypass these estimates (for example, some finite element results for the type I microstructures bypass the derivative $\partial\tilde{\mu}/\partial\mu_1$ of the W bound).

On the other hand, the finite element results for the type II microstructure seem to fit with the SC estimate (derivative of the SC estimate of $\tilde{\mu}$). For type I microstructures, the results are close to the bounds for isotropic composites for the contrast 5, whereas it is not really the case with the contrast 100 (at least, for the upper bound). This is due to the

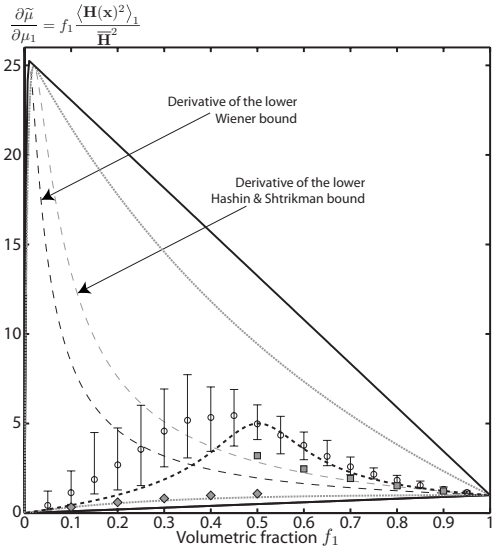

FIG. 10. Derivative of the effective permeability $\partial\tilde{\mu}/\partial\mu_1$ as a function of the volumetric fraction f_1 of phase 1, contrast $\mu_2/\mu_1=100$ (same legend than Fig. 9).

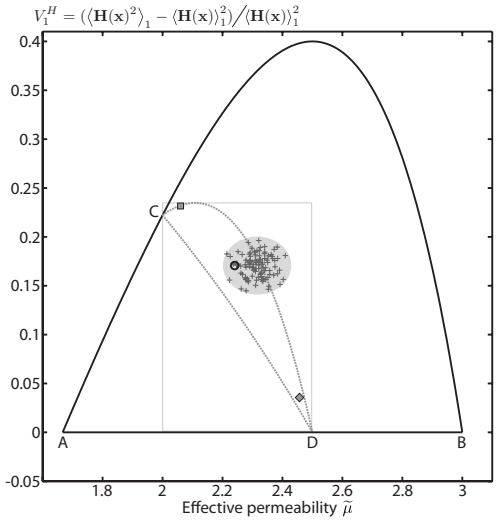

FIG. 11. Variance of the magnetic field $\mathbf{H}(\mathbf{x})$ in phase 1 as a function of the effective permeability $\tilde{\mu}$, contrast $\mu_2/\mu_1=5$ (see legend in Fig. 12).

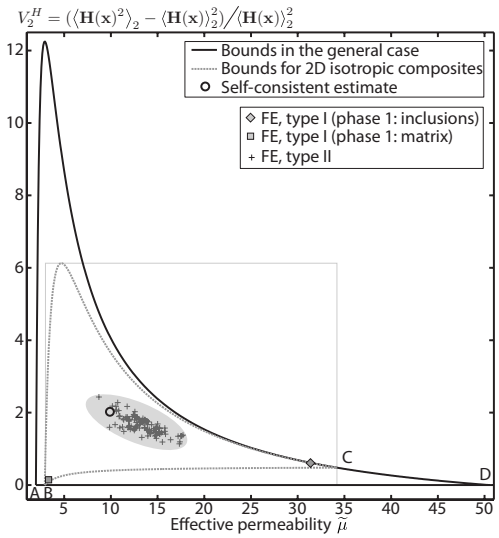

FIG. 12. Variance of the magnetic field $\mathbf{H}(\mathbf{x})$ in phase 2 as a function of the effective permeability $\tilde{\mu}$, contrast $\mu_2/\mu_1=100$.

fact that the maximum value for $\partial\tilde{\mu}/\partial\mu_1$ (depending on $\tilde{\mu}$) is quite high compared to its value when taking $\tilde{\mu}$ equal to the HS limit. This point appears clearly in Fig. 6.

It also appears in these figures, that in the case of a type I microstructure, the differentiation of HS estimate provides a satisfying approximation of the second order moment.

It must be noticed that the lower bounds for $\partial\tilde{\mu}/\partial\mu_1$ (both in the general case and isotropic composites) are exactly equal to the derivatives of the Wiener and Hashin and Shtrikman for $\tilde{\mu}$ (in that example with contrast μ_2/μ_1 higher than 1, it is equal to the derivatives of the upper bounds).

The bounds for the derivative $\partial\tilde{\mu}/\partial\mu_1$, for a given volumetric fraction f_1, are large due to the loss of the estimation of $\tilde{\mu}$.

C. Variance

It is convenient to present the evolution of the variance as a function of $\tilde{\mu}$. The variance of the magnetic field in phase i is defined as

$$V_i^H = \frac{\langle \mathbf{H}(\mathbf{x})^2 \rangle_i - \langle \mathbf{H}(\mathbf{x}) \rangle_i^2}{\langle \mathbf{H}(\mathbf{x}) \rangle_i^2}. \tag{29}$$

Figure 11 shows the variance of the magnetic field in phase 1 as a function of the effective permeability $\tilde{\mu}$ in the particular case of a volumetric fraction of phase 1 equal to $f_1=0.5$ and contrast $\mu_2/\mu_1=5$. Figure 12 is the variance of the magnetic field in phase 2 with contrast $\mu_2/\mu_1=100$ (volumetric fraction is still $f_1=0.5$). The end points A and B, respectively, correspond to the lower and upper Wiener bounds on the effective permeability, and the variance of the magnetic field (in both phases) is equal to zero in these cases. The end points C and D, respectively, correspond to the lower and upper HS bounds on the effective permeability; only one of the phases presents a zero variance for the magnetic field in these cases.

The value $\langle \mathbf{H}(\mathbf{x})^2 \rangle_i$ is computed from Eqs. (19) and (26) and the value $\langle \mathbf{H}(\mathbf{x}) \rangle_i^2$ is computed from Eq. (7).

These figures (particularly Fig. 12) show that taking minimum and maximum values for the derivative $\partial\tilde{\mu}/\partial\mu_i$ when scanning the range of possible values of $\tilde{\mu}$ is not judicious if the information about $\tilde{\mu}$ is known, since this information is lost. The corresponding bounds would be rectangles on these figures. It would be preferable to present bounds as a function of the volumetric fraction f and of the effective permeability $\tilde{\mu}$; but this kind of 3D curves cannot be presented easily.

The finite element results for type I microstructures show a low variability in variance and effective permeability. Moreover, the results are very close to the C and D end points, corresponding to HS estimates for the effective permeability and the use of the derivative $\partial\tilde{\mu}/\partial\mu_1$ of the HS bounds for the determination of the second order moment $\langle \mathbf{H}(\mathbf{x})^2 \rangle_1$. The SC estimate also seems to be a good estimate for type II microstructure.

D. Application

An example of application is presented in this paragraph. It deals with magnetostriction, including the nonlinear relationship between the magnetic field and the magnetostrictive strain. A classical model[16] gives the magnetostrictive strain $\boldsymbol{\epsilon}^{\mu}(\mathbf{x})$ as a function of the magnetic induction $\mathbf{B}(\mathbf{x})$,

$$\boldsymbol{\epsilon}^{\mu}(\mathbf{x}) = \alpha \cdot \begin{pmatrix} 1 & 0 & 0 \\ 0 & -1/2 & 0 \\ 0 & 0 & -1/2 \end{pmatrix} \cdot \mathbf{B}(\mathbf{x})^2 = \underline{\underline{\alpha}} \cdot \mathbf{B}(\mathbf{x})^2. \tag{30}$$

Let us study a composite made of two magnetostrictive phases. The two phases have different permeabilities μ_i and different magnetostriction coefficients α_i. Then, the macroscopic magnetostrictive strain $\overline{\boldsymbol{\epsilon}^{\mu}}$ can be deduced from the magnetic state in the composite (the composite is supposed to be elastically homogeneous),

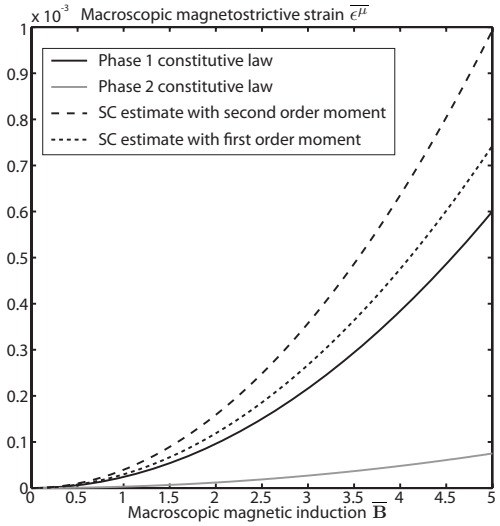

FIG. 13. Macroscopic magnetostrictive strain $\overline{\epsilon^\mu}$ as a function of the macroscopic magnetic induction $\overline{\mathbf{B}}$.

$$\overline{\epsilon^\mu} = \langle \epsilon^\mu(\mathbf{x}) \rangle = f_1 \cdot \alpha_1 \cdot \langle \mathbf{B}(\mathbf{x})^2 \rangle_1 + f_2 \cdot \alpha_2 \cdot \langle \mathbf{B}(\mathbf{x})^2 \rangle_2. \quad (31)$$

A classical approximation is the mean field approach, which assimilates the second order moments as the square of the first order moments $\langle \mathbf{H}(\mathbf{x})^2 \rangle_i \rightarrow \langle \mathbf{H}(\mathbf{x}) \rangle_i^2$, which is generally wrong (underestimation of the second order moment).

A better estimate can be obtained with the determination of second order moments. These second order moments can be computed from Eq. (19) and $\langle \mathbf{B}(\mathbf{x})^2 \rangle_i = \mu_i^2 \cdot \langle \mathbf{H}(\mathbf{x})^2 \rangle_i$.

Figure 13 presents the macroscopic magnetostrictive strain ϵ^μ as a function of the macroscopic magnetic induction $\overline{\mathbf{B}}$ for the two phases and an estimate for the composite. The phase properties are $\mu_1/\mu_2 = 15$, $\alpha_1 = 24 \times 10^{-4}$, $\alpha_2 = 3 \times 10^{-4}$, and $f_1 = 0.7$. We can see on this figure that approximating the second order moments as squares of first order moments underestimates the macroscopic strain for about 25% in this example. By the way, it is interesting to notice that the composite presents a higher magnetostriction than each of the two constituents (because of the concavity of the constitutive law [Eq. (30)].

V. CONCLUSION

Homogenization techniques can provide estimates or bounds for the effective behavior of composite materials with very low computational cost compared to the finite element method. In addition to mean field per phase, it can also provide estimates or bounds on the intraphase fluctuations. Such information can be decisive in the case of nonlinear behavior. In the example dealing with a magnetostriction model presented in this paper, the magnetostrictive strain can be about 25% underestimated when using only mean field approach, compared to the case introducing field fluctuations.

We presented in this paper a method to determine the intraphase fluctuations in heterogeneous materials using homogenization tools. The results have been compared to those obtained from a finite element modeling. It has been shown that the self-consistent estimate provides a satisfying approximation of both mean field and second order moment, for mosaic microstructure, where none of the phase plays a specific role. In the case of matrix/inclusion microstructure, the Hashin and Shtrikman estimate is well suited for both mean field and second order moment. If bounds rather than estimates are needed, we defined optimal bounds for the second order moments in the general case and more restrictive ones in the particular case of isotropic 2D composites.

[1] O. Wiener, Abhandlungen der Mathematisch-Physischen Klasse des Königlich Sächisischen Gesellschaft des Wissenschaften **32**, 509 (1912).
[2] Z. Hashin and S. Shtrikman, J. Appl. Phys. **33**, 3125 (1962).
[3] D. J. Bergman, Phys. Rep. **43**, 377 (1978).
[4] G. W. Milton, *The Theory of Composites* (Cambridge University Press, Cambridge, 2002).
[5] M. Avellaneda, A. V. Cherkaev, K. A. Lurie, and G. W. Milton, J. Appl. Phys. **63**, 4989 (1988).
[6] J. Axell, J. Appl. Phys. **72**, 1217 (1992).
[7] R. Lipton, J. Appl. Phys. **96**, 2821 (2004).
[8] H. Cheng and S. Torquato, Phys. Rev. B **56**, 8060 (1997).
[9] L. Daniel and R. Corcolle, IEEE Trans. Magn. **43**, 3153 (2007).
[10] A. H. Sihvola and I. V. Lindell, AEU, Int. J. Electron. Commun. **50**, 289 (1996).
[11] D. Cule and S. Torquato, Phys. Rev. B **58**, R11829 (1998).
[12] J. B. Keller, J. Math. Phys. **5**, 548 (1964).
[13] G. W. Milton, J. Appl. Phys. **52**, 5294 (1981).
[14] K. Schulgasser, J. Math. Phys. **17**, 378 (1976).
[15] P. Gilormini, C. R. Acad. Sci., Ser. IIb: Mec., Phys., Chim., Astron. **329**, 851 (2001).
[16] D. C. Jiles, *Introduction to Magnetism and Magnetic Materials* (Chapman and Hall, London, 1991).

Generic formalism for homogenization of coupled behavior: Application to magnetoelectroelastic behavior

Romain Corcolle,* Laurent Daniel,† and Frédéric Bouillault‡
Laboratoire de Génie Electrique de Paris, CNRS UMR8507; SUPELEC; UPMC Univ Paris 06; Univ Paris-Sud; 11 rue Joliot-Curie, Plateau de Moulon, F-91192 Gif-sur-Yvette Cedex, France
(Received 19 August 2008; published 30 December 2008)

Multiphysics couplings are at the origin of many applications. In order to design devices with optimal coupling effects, advanced modeling tools are necessary. In this paper a generic formalism for the homogenization of coupled magnetoelectrothermoelastic behavior is proposed. It is based on the decomposition in several contributions of the magnetic, electric, thermal, and mechanical fields. This decomposition makes it possible to use the classical homogenization tools developed in the framework of uncoupled behavior. The method is illustrated on the calculation of the effective properties of a magnetoelectric composite made of piezomagnetic and piezoelectric phases.

DOI: 10.1103/PhysRevB.78.214110 PACS number(s): 75.80.+q

I. INTRODUCTION

Coupled behavior is a long-standing domain of interest in physics. The possibility of applications such as sensors or actuators, relying on these multiphysics coupling effects have made these materials receive more and more attention in the past years. In order to design properly these different applications, advanced modeling tools are needed. Phenomenological macroscopic approaches can give a first description.[1] These approaches proved to be very efficient in the case of homogeneous materials. But a promising issue is the development of sensors and actuators made of composite materials. The properties of each constituent can then be combined to obtain optimal macroscopic properties. In those cases, all the more if the composition of the composite material has to be optimized, a phenomenological macroscopic approach is not suitable anymore. This is particularly true when the observed macroscopic coupling effect is not observed in any of the constituent of the composite (see the example of magnetoelectric composite in Sec. IV).

If the heterogeneity of the material is to be accounted for in the definition of the macroscopic constitutive law, a classical approach is the use of finite element modeling. This choice has been applied, for example, in the case of electrostrictive,[2] magnetostrictive,[3] or magnetoelectric[4,5] composites. Another convenient method is the use of homogenization techniques, leading to much lower computational times. Some authors applied these techniques in the case of electrostrictive,[6–8] magnetostrictive,[9,10] or magnetoelectric[11,12] behavior. These approaches are often based upon the adaptation to coupled phenomena of the classical homogenization tools designed in the framework of uncoupled behavior.

We show in this paper that an appropriate decomposition (Fig. 1) of the state variables of a coupled problem allows us to keep unchanged the classical-uncoupled-homogenization rules. The constitutive laws used in the problem are then very close to the classical-uncoupled ones, and the relative contribution of the coupled phenomena to the macroscopic response can be clearly identified.

In Sec. II, the constitutive laws are written, using the proposed decomposition of the state variables. In Sec. III, we develop in that framework the localization-homogenization rules, unchanged compared to the classical-uncoupled ones. In Sec. IV, an application of the proposed homogenization model is done on a piezomagnetic and piezoelectric composite. That composite exhibits a macroscopic magnetoelectric effect, whereas none of the phases exhibit such an effect. This behavior is shown to be well captured by the model and compared to another heterogeneous models.

II. CONSTITUTIVE LAWS

Coupled effects are often observed in the macroscopic behavior of materials. These effects are the manifestation of the interaction between mechanics, magnetism, electricity, thermics, etc. For example, the piezomagnetic behavior is observed when the apparent permeability of a material depends on the level of stress or when the strain depends on the level of the magnetic induction. The constitutive law of the material links the applied loading to the response of the material. The loading can be a mechanical strain, a magnetic,

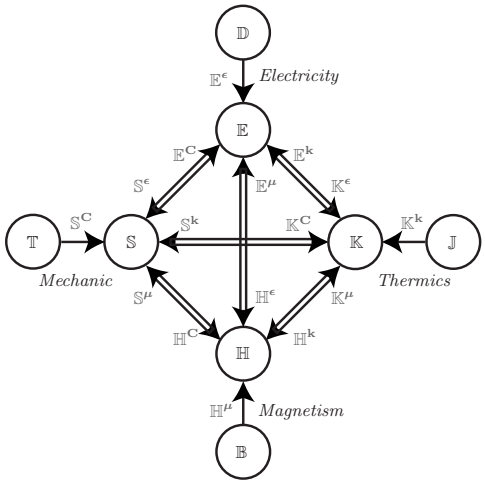

FIG. 1. Coupling effects decomposition.

electric or thermal field, or any combination of them. The response is then a stress, a magnetic, electric or thermal induction, or any combination of them. The constitutive laws are usually written separately for each uncoupled behavior. It is convenient to write a global constitutive law, intrinsically including the coupling effects. It is the objective of this section. We first summarize the classical expression for uncoupled behavior. We then define the general constitutive law from these expressions.

A. Uncoupled constitutive laws

1. Mechanics

For uncoupled-mechanical behavior, the dual state variables are the strain tensor $\mathbb{S}$ (linked to the displacement field $\mathbf{u}$, $\mathbb{S}=1/2(\nabla\mathbf{u}+{}^t\nabla\mathbf{u})$, the operator ${}^t\mathbf{X}$ denoting a transposition operation over $\mathbf{X}$), and the stress tensor $\mathbb{T}$. In a purely elastic problem, the relationship between these tensors (Hooke's law) is written as

$$\mathbb{T}=\mathbf{C}\cdot\mathbb{S}, \tag{1}$$

where $\mathbb{S}$ and $\mathbb{T}$ are second-order tensors (3×3) and $\mathbf{C}$ is the fourth-order stiffness tensor $(3\times3\times3\times3)$. The modified Voigt notation (Voigt-Mandel notation) can be used, thanks to the symmetries exhibited by these tensors (see Appendix A). Then, $\mathbb{S}$ and $\mathbb{T}$ are represented by (6×1) vectors and $\mathbf{C}$ is represented by a (6×6) matrix.

2. Magnetism

For uncoupled-magnetic behavior, the dual state variables are the magnetic field $\mathbb{H}$ (linked to the magnetic potential ϕ in absence of currents, $\mathbb{H}=-\nabla\phi$) and the magnetic induction $\mathbb{B}$. In a purely magnetic problem, the relationship between these fields is written as

$$\mathbb{B}=\boldsymbol{\mu}\cdot\mathbb{H}, \tag{2}$$

where $\mathbb{H}$ and $\mathbb{B}$ are vectors (3×1) and $\boldsymbol{\mu}$ is the second-order permeability tensor (3×3).

3. Electricity

For uncoupled-electric behavior, the dual state variables are the electric field $\mathbb{E}$ (linked to the electric potential φ, $\mathbb{E}=-\nabla\varphi$) and the electric induction $\mathbb{D}$. In a purely electric problem, the relationship between these fields is written as

$$\mathbb{D}=\boldsymbol{\epsilon}\cdot\mathbb{E}, \tag{3}$$

where $\mathbb{E}$ and $\mathbb{D}$ are vectors (3×1) and $\boldsymbol{\epsilon}$ is the second-order permittivity tensor (3×3).

4. Thermics

For uncoupled-thermal behavior, the dual state variables are the thermal field $\mathbb{K}$ (linked to the temperature θ, $\mathbb{K}=-\nabla\theta$) and the thermal induction $\mathbb{J}$. In a purely thermal problem, the relationship between these fields (Fourier's law) is written as

$$\mathbb{J}=\mathbf{k}\cdot\mathbb{K}, \tag{4}$$

where $\mathbb{K}$ and $\mathbb{J}$ are vectors (3×1) and $\mathbf{k}$ is the second-order thermal-conductivity tensor (3×3).

5. Global constitutive law

For a material with no coupling effects, the global constitutive law is just the superposition of the previous laws,

$$\begin{pmatrix}\mathbb{T}\\ \mathbb{B}\\ \mathbb{D}\\ \mathbb{J}\end{pmatrix}=\begin{pmatrix}\mathbf{C}&\mathbf{0}&\mathbf{0}&\mathbf{0}\\ \mathbf{0}&\boldsymbol{\mu}&\mathbf{0}&\mathbf{0}\\ \mathbf{0}&\mathbf{0}&\boldsymbol{\epsilon}&\mathbf{0}\\ \mathbf{0}&\mathbf{0}&\mathbf{0}&\mathbf{k}\end{pmatrix}\cdot\begin{pmatrix}\mathbb{S}\\ \mathbb{H}\\ \mathbb{E}\\ \mathbb{K}\end{pmatrix}. \tag{5}$$

The response vector ${}^t(\mathbb{T}\ \mathbb{B}\ \mathbb{D}\ \mathbb{J})$ is constituted of fields with null divergence $[\nabla\cdot\mathbb{T}=\mathbf{0}$ (in the absence of volumic forces), $\nabla\cdot\mathbb{B}=0$, $\nabla\cdot\mathbb{D}=0$ (in the absence of electric charges), and $\nabla\cdot\mathbb{J}=0$ (in the absence of own heating sources)]. On the other hand, the loading vector ${}^t(\mathbb{S}\ \mathbb{H}\ \mathbb{E}\ \mathbb{K})$ is constituted of fields that each derives from a potential.

B. Coupled constitutive laws

1. Global constitutive law

For a material exhibiting coupling phenomena, the global constitutive law includes coupling parameters $\boldsymbol{\alpha}$,

$$\begin{pmatrix}\mathbb{T}\\ \mathbb{B}\\ \mathbb{D}\\ \mathbb{J}\end{pmatrix}=\begin{pmatrix}\mathbf{C}&\boldsymbol{\alpha}^{\mathbf{C}\mu}&\boldsymbol{\alpha}^{\mathbf{C}\epsilon}&\boldsymbol{\alpha}^{\mathbf{C}k}\\ \boldsymbol{\alpha}^{\mu\mathbf{C}}&\boldsymbol{\mu}&\boldsymbol{\alpha}^{\mu\epsilon}&\boldsymbol{\alpha}^{\mu k}\\ \boldsymbol{\alpha}^{\epsilon\mathbf{C}}&\boldsymbol{\alpha}^{\epsilon\mu}&\boldsymbol{\epsilon}&\boldsymbol{\alpha}^{\epsilon k}\\ \boldsymbol{\alpha}^{k\mathbf{C}}&\boldsymbol{\alpha}^{k\mu}&\boldsymbol{\alpha}^{k\epsilon}&\mathbf{k}\end{pmatrix}\cdot\begin{pmatrix}\mathbb{S}\\ \mathbb{H}\\ \mathbb{E}\\ \mathbb{K}\end{pmatrix}. \tag{6}$$

This generic form for the constitutive laws is compact, but it is not well suited to the use of classical homogenization tools. Indeed homogenization models generally provide some so-called localization operators (for example, based on Eshelby inclusion problem in mechanics) linking the local fields to the macroscopic loading. But these localization operators usually apply to uncoupled behavior. In the case of coupling effects, some authors proposed to define some new coupled Eshelby tensors accounting for magnetoelectromechanical coupling.[13] This tensor depends on the nature of the coupling and on the distribution of the phases, meaning that it has to be computed for every studied configuration. We propose to keep using the well-known classical homogenization models: the adaptation to coupled behavior relying on an appropriate decomposition of the fields. This method is inspired from the usual strain decomposition in mechanics.[14,15]

2. Mechanics

In the case of coupled behavior, we divide the strain into several contributions. For a magnetoelectrothermomechanical coupling, the total strain tensor $\mathbb{S}$ can be decomposed in the following way:

$$\mathbb{S}=\mathbb{S}^{\mathbf{C}}+\mathbb{S}^{\boldsymbol{\mu}}+\mathbb{S}^{\boldsymbol{\epsilon}}+\mathbb{S}^{\mathbf{k}}, \tag{7}$$

where $\mathbb{S}^{\mathbf{C}}$, $\mathbb{S}^{\boldsymbol{\mu}}$, $\mathbb{S}^{\boldsymbol{\epsilon}}$, and $\mathbb{S}^{\mathbf{k}}$ represent, respectively, the purely mechanical, the magnetic, the electric, and the thermal strain tensors. The purely mechanical strain tensor $\mathbb{S}^{\mathbf{C}}$ is linked to the stress tensor $\mathbb{T}$ by the usual Hooke's law (in the case of elasticity),

$$\mathbb{T} = \mathbf{C} \cdot \mathbb{S}^{\mathbf{C}}. \tag{8}$$

The stiffness tensor $\mathbf{C}$ (in the case of a homogeneous material) is the same that the one introduced in Eq. (6). The definition of the stiffness tensor is given by Eq. (8) and $\mathbb{T} \neq \mathbf{C} \cdot \mathbb{S}$ in the general case.

The magnetic strain tensor $\mathbb{S}^{\boldsymbol{\mu}}$ (magnetostriction) is linked to the magnetic state, the electric strain tensor $\mathbb{S}^{\boldsymbol{\epsilon}}$ (electrostriction) to the electric state, and the thermal strain tensor $\mathbb{S}^{\mathbf{k}}$ (thermal dilatation) to the thermal state. Moreover Eq. (8) can be rewritten as

$$\mathbb{T} = \mathbf{C} \cdot (\mathbb{S} - \mathbb{S}^{\boldsymbol{\mu}} - \mathbb{S}^{\boldsymbol{\epsilon}} - \mathbb{S}^{\mathbf{k}}). \tag{9}$$

From Eqs. (6) and (9), the different contributions to the strain can be defined as

$$\begin{aligned} -\mathbf{C} \cdot \mathbb{S}^{\boldsymbol{\mu}} &= \boldsymbol{\alpha}^{\mathbf{C}\boldsymbol{\mu}} \cdot \mathbb{H}, \\ -\mathbf{C} \cdot \mathbb{S}^{\boldsymbol{\epsilon}} &= \boldsymbol{\alpha}^{\mathbf{C}\boldsymbol{\epsilon}} \cdot \mathbb{E}, \\ -\mathbf{C} \cdot \mathbb{S}^{\mathbf{k}} &= \boldsymbol{\alpha}^{\mathbf{C}\mathbf{k}} \cdot \mathbb{K}. \end{aligned} \tag{10}$$

3. Magnetism

In the case of coupled behavior, we divide the magnetic field into several contributions. For an electrothermomechanomagnetic coupling, the total magnetic field $\mathbb{H}$ can be decomposed in the following way:

$$\mathbb{H} = \mathbb{H}^{\mathbf{C}} + \mathbb{H}^{\boldsymbol{\mu}} + \mathbb{H}^{\boldsymbol{\epsilon}} + \mathbb{H}^{\mathbf{k}}, \tag{11}$$

where $\mathbb{H}^{\mathbf{C}}$, $\mathbb{H}^{\boldsymbol{\mu}}$, $\mathbb{H}^{\boldsymbol{\epsilon}}$, and $\mathbb{H}^{\mathbf{k}}$ represent, respectively, the mechanical, the purely, the electric, and the thermal magnetic fields. The purely magnetic field $\mathbb{H}^{\boldsymbol{\mu}}$ is linked to the magnetic induction $\mathbb{B}$ by the-uncoupled-magnetic constitutive law,

$$\mathbb{B} = \boldsymbol{\mu} \cdot \mathbb{H}^{\boldsymbol{\mu}}. \tag{12}$$

The definition of the magnetic permeability is given by Eq. (12) and $\mathbb{B} \neq \boldsymbol{\mu} \cdot \mathbb{H}$ in the general case.

The mechanical magnetic field $\mathbb{H}^{\mathbf{C}}$ is linked to the mechanical state, the electric magnetic field $\mathbb{H}^{\boldsymbol{\epsilon}}$ to the electric state, and the thermal magnetic field $\mathbb{H}^{\mathbf{k}}$ to the thermal state. Moreover Eq. (12) can be rewritten as

$$\mathbb{B} = \boldsymbol{\mu} \cdot (\mathbb{H} - \mathbb{H}^{\mathbf{C}} - \mathbb{H}^{\boldsymbol{\epsilon}} - \mathbb{H}^{\mathbf{k}}). \tag{13}$$

The different contributions to the magnetic field can be defined as

$$\begin{aligned} -\boldsymbol{\mu} \cdot \mathbb{H}^{\mathbf{C}} &= \boldsymbol{\alpha}^{\boldsymbol{\mu}\mathbf{C}} \cdot \mathbb{S}, \\ -\boldsymbol{\mu} \cdot \mathbb{H}^{\boldsymbol{\epsilon}} &= \boldsymbol{\alpha}^{\boldsymbol{\mu}\boldsymbol{\epsilon}} \cdot \mathbb{E}, \\ -\boldsymbol{\mu} \cdot \mathbb{H}^{\mathbf{k}} &= \boldsymbol{\alpha}^{\boldsymbol{\mu}\mathbf{k}} \cdot \mathbb{K}. \end{aligned} \tag{14}$$

4. Electricity

In the case of coupled behavior, we divide the electric field into several contributions. For a thermomechanomagnetoelectric coupling, the total electric field $\mathbb{E}$ can be decomposed in the following way:

$$\mathbb{E} = \mathbb{E}^{\mathbf{C}} + \mathbb{E}^{\boldsymbol{\mu}} + \mathbb{E}^{\boldsymbol{\epsilon}} + \mathbb{E}^{\mathbf{k}}, \tag{15}$$

where $\mathbb{E}^{\mathbf{C}}$, $\mathbb{E}^{\boldsymbol{\mu}}$, $\mathbb{E}^{\boldsymbol{\epsilon}}$, and $\mathbb{E}^{\mathbf{k}}$ represent, respectively, the mechanical, the magnetic, the purely, and the thermal electric fields. The purely electric field $\mathbb{E}^{\boldsymbol{\epsilon}}$ is linked to the electric induction $\mathbb{D}$ by the-uncoupled-electric constitutive law,

$$\mathbb{D} = \boldsymbol{\epsilon} \cdot \mathbb{E}^{\boldsymbol{\epsilon}}, \tag{16}$$

The definition of the electric permittivity is given by Eq. (16) and $\mathbb{D} \neq \boldsymbol{\epsilon} \cdot \mathbb{E}$ in the general case.

The mechanical electric field $\mathbb{E}^{\mathbf{C}}$ is linked to the mechanical state, the magnetic electric field $\mathbb{E}^{\boldsymbol{\mu}}$ to the magnetic state, and the thermal electric field $\mathbb{E}^{\mathbf{k}}$ to the thermal state. Moreover Eq. (16) can be rewritten as

$$\mathbb{D} = \boldsymbol{\epsilon} \cdot (\mathbb{E} - \mathbb{E}^{\mathbf{C}} - \mathbb{E}^{\boldsymbol{\mu}} - \mathbb{E}^{\mathbf{k}}). \tag{17}$$

The different contributions to the electric field can be defined as

$$\begin{aligned} -\boldsymbol{\epsilon} \cdot \mathbb{E}^{\mathbf{C}} &= \boldsymbol{\alpha}^{\boldsymbol{\epsilon}\mathbf{C}} \cdot \mathbb{S}, \\ -\boldsymbol{\epsilon} \cdot \mathbb{E}^{\boldsymbol{\mu}} &= \boldsymbol{\alpha}^{\boldsymbol{\epsilon}\boldsymbol{\mu}} \cdot \mathbb{H}, \\ -\boldsymbol{\epsilon} \cdot \mathbb{E}^{\mathbf{k}} &= \boldsymbol{\alpha}^{\boldsymbol{\epsilon}\mathbf{k}} \cdot \mathbb{K}. \end{aligned} \tag{18}$$

5. Thermics

In the case of coupled behavior, we divide the thermal field into several contributions. For a mechanomagnetoelectrothermal coupling, the total thermal field $\mathbb{K}$ can be decomposed in the following way:

$$\mathbb{K} = \mathbb{K}^{\mathbf{C}} + \mathbb{K}^{\boldsymbol{\mu}} + \mathbb{K}^{\boldsymbol{\epsilon}} + \mathbb{K}^{\mathbf{k}}, \tag{19}$$

where $\mathbb{K}^{\mathbf{C}}$, $\mathbb{K}^{\boldsymbol{\mu}}$, $\mathbb{K}^{\boldsymbol{\epsilon}}$, and $\mathbb{K}^{\mathbf{k}}$ represent, respectively, the mechanical, the magnetic, the electric, and the purely thermal fields. The purely thermal field $\mathbb{K}^{\mathbf{k}}$ is linked to the electric induction $\mathbb{J}$ by the Fourier's law,

$$\mathbb{J} = \mathbf{k} \cdot \mathbb{K}^{\mathbf{k}}. \tag{20}$$

The definition of the thermal conductivity is given by Eq. (20) and $\mathbb{J} \neq \mathbf{k} \cdot \mathbb{K}$ in the general case.

The mechanical thermal field $\mathbb{K}^{\mathbf{C}}$ is linked to the mechanical state, the magnetic thermal field $\mathbb{K}^{\boldsymbol{\mu}}$ to the magnetic state, and the electric thermal field $\mathbb{K}^{\boldsymbol{\epsilon}}$ to the electric state. Moreover Eq. (20) can be rewritten as

$$\mathbb{J} = \mathbf{k} \cdot (\mathbb{K} - \mathbb{K}^{\mathbf{C}} - \mathbb{K}^{\boldsymbol{\mu}} - \mathbb{K}^{\boldsymbol{\epsilon}}). \tag{21}$$

The different contributions to the thermal field can be defined as

$$\begin{aligned} -\mathbf{k} \cdot \mathbb{K}^{\mathbf{C}} &= \boldsymbol{\alpha}^{\mathbf{k}\mathbf{C}} \cdot \mathbb{S}, \\ -\mathbf{k} \cdot \mathbb{K}^{\boldsymbol{\mu}} &= \boldsymbol{\alpha}^{\mathbf{k}\boldsymbol{\mu}} \cdot \mathbb{H}, \\ -\mathbf{k} \cdot \mathbb{K}^{\boldsymbol{\epsilon}} &= \boldsymbol{\alpha}^{\mathbf{k}\boldsymbol{\epsilon}} \cdot \mathbb{E}. \end{aligned} \tag{22}$$

6. Summary

The following scheme shows the coupling effects and the different contributions to the loading fields in the general

case of magnetoelectrothermomechanical behavior. The global constitutive law can be rewritten as follows:

$$\begin{pmatrix} \mathbb{T} \\ \mathbb{B} \\ \mathbb{D} \\ \mathbb{J} \end{pmatrix} = \begin{pmatrix} \mathbf{C} & \mathbf{0} & \mathbf{0} & \mathbf{0} \\ \mathbf{0} & \boldsymbol{\mu} & \mathbf{0} & \mathbf{0} \\ \mathbf{0} & \mathbf{0} & \boldsymbol{\epsilon} & \mathbf{0} \\ \mathbf{0} & \mathbf{0} & \mathbf{0} & \mathbf{k} \end{pmatrix} \cdot \begin{pmatrix} \mathbb{S}^{\mathbf{C}} \\ \mathbb{H}^{\boldsymbol{\mu}} \\ \mathbb{E}^{\boldsymbol{\epsilon}} \\ \mathbb{K}^{\mathbf{k}} \end{pmatrix}. \tag{23}$$

This presentation must be completed by the coupling relations given by Eqs. (10), (14), (18), and (22). The basic decomposition given by Eqs. (7), (11), (15), and (19) is also needed. The number of relations appears to be higher than in the classical formalism, but each of them is much simpler.

C. Example of piezoelectricity

Piezoelectric materials exhibit a coupling between mechanics and electricity. The constitutive law is written in Eq. (24), according to the proposed formalism. This relation corresponds to Eq. (6) where the magnetoelastic, thermoelastic, thermomagnetic, thermoelectric, and magnetoelectric couplings have been canceled,

$$\begin{pmatrix} \mathbb{T} \\ \mathbb{B} \\ \mathbb{D} \\ \mathbb{J} \end{pmatrix} = \begin{pmatrix} \mathbf{C} & \mathbf{0} & \boldsymbol{\alpha}^{\mathbf{C}\boldsymbol{\epsilon}} & \mathbf{0} \\ \mathbf{0} & \boldsymbol{\mu} & \mathbf{0} & \mathbf{0} \\ \boldsymbol{\alpha}^{\boldsymbol{\epsilon}\mathbf{C}} & \mathbf{0} & \boldsymbol{\epsilon} & \mathbf{0} \\ \mathbf{0} & \mathbf{0} & \mathbf{0} & \mathbf{k} \end{pmatrix} \cdot \begin{pmatrix} \mathbb{S} \\ \mathbb{H} \\ \mathbb{E} \\ \mathbb{K} \end{pmatrix}. \tag{24}$$

It is interesting to compare this constitutive law to the classical piezoelectric relations given by Eqs. (25)–(28).

$$T_{ij} = c^E_{ijkl} S_{kl} - e_{kij} E_k,$$

$$D_i = e_{ikl} S_{kl} + \epsilon^S_{ik} E_k, \tag{25}$$

$$S_{ij} = s^E_{ijkl} T_{kl} + d_{kij} E_k,$$

$$D_i = d_{ikl} T_{kl} + \epsilon^T_{ik} E_k, \tag{26}$$

$$S_{ij} = s^D_{ijkl} T_{kl} + g_{kij} D_k,$$

$$E_i = -g_{ikl} T_{kl} + \beta^T_{ik} D_k, \tag{27}$$

$$T_{ij} = c^D_{ijkl} S_{kl} - h_{kij} D_k,$$

$$E_i = -h_{ikl} S_{kl} + \beta^S_{ik} D_k. \tag{28}$$

Each of these four systems is equivalent and can be identified to Eq. (24). Considering Eq. (25), we obtain that $\mathbf{c}^E$ is the elastic stiffness tensor $\mathbf{C}$, $\boldsymbol{\epsilon}^S$ is the permittivity tensor $\boldsymbol{\epsilon}$, and $\mathbf{e}$ is equal to $\boldsymbol{\alpha}^{\boldsymbol{\epsilon}\mathbf{C}}$. It leads also to the additional relation that under such hypotheses, $\boldsymbol{\alpha}^{\mathbf{C}\boldsymbol{\epsilon}} = -{}^t\boldsymbol{\alpha}^{\boldsymbol{\epsilon}\mathbf{C}}$. This relation is carried out from thermodynamics, dealing with reversible (linear) behavior. Equation (6) embraces a more general case and does not *a priori* present this kind of symmetry (or antisymmetry). It can also be noticed that an antisymmetric matrix can be changed into a symmetric one by choosing the sign of the state variables [for example, choosing $-\mathbb{S}$ instead of $\mathbb{S}$ in Eq. (25)]. Considering Eqs. (26)–(28), we obtain the following additional relations:

$$\mathbf{s}^E = \mathbf{C}^{-1},$$

$$\boldsymbol{\epsilon}^T = \boldsymbol{\epsilon} + \mathbf{C}^{-1} \cdot {}^t\boldsymbol{\alpha}^{\boldsymbol{\epsilon}\mathbf{C}} \cdot \boldsymbol{\alpha}^{\boldsymbol{\epsilon}\mathbf{C}},$$

$$\mathbf{d} = \boldsymbol{\alpha}^{\boldsymbol{\epsilon}\mathbf{C}} \cdot \mathbf{C}^{-1},$$

$$\mathbf{s}^D = (\mathbf{C} + {}^t\boldsymbol{\alpha}^{\boldsymbol{\epsilon}\mathbf{C}} \cdot \boldsymbol{\epsilon}^{-1} \cdot \boldsymbol{\alpha}^{\boldsymbol{\epsilon}\mathbf{C}})^{-1},$$

$$\boldsymbol{\beta}^T = (\boldsymbol{\epsilon} + \mathbf{C}^{-1} \cdot {}^t\boldsymbol{\alpha}^{\boldsymbol{\epsilon}\mathbf{C}} \cdot \boldsymbol{\alpha}^{\boldsymbol{\epsilon}\mathbf{C}})^{-1},$$

$$\mathbf{g} = \boldsymbol{\epsilon}^{-1} \cdot \boldsymbol{\alpha}^{\boldsymbol{\epsilon}\mathbf{C}} \cdot (\mathbf{C} + {}^t\boldsymbol{\alpha}^{\boldsymbol{\epsilon}\mathbf{C}} \cdot \boldsymbol{\epsilon}^{-1} \cdot \boldsymbol{\alpha}^{\boldsymbol{\epsilon}\mathbf{C}})^{-1},$$

$$\mathbf{c}^D = \mathbf{C} + {}^t\boldsymbol{\alpha}^{\boldsymbol{\epsilon}\mathbf{C}} \cdot \boldsymbol{\epsilon}^{-1} \cdot \boldsymbol{\alpha}^{\boldsymbol{\epsilon}\mathbf{C}},$$

$$\boldsymbol{\beta}^S = \boldsymbol{\epsilon}^{-1},$$

$$\mathbf{h} = \boldsymbol{\epsilon}^{-1} \cdot \boldsymbol{\alpha}^{\boldsymbol{\epsilon}\mathbf{C}}. \tag{29}$$

It can be noticed that the semantic ambiguousness risen on the definition of the material parameters in the classical formalism does not appear in the proposed formalism. For example, the elastic stiffness tensor definition is unique (link between stress $\mathbb{T}$ and purely elastic strain $\mathbb{S}^{\mathbf{C}}$), and there is no need to distinguish a stiffness tensor measured at a constant electric induction $\mathbf{c}^D$ and at a constant electric field $\mathbf{c}^E$. Moreover, these parameters become complicated to define when nonlinearity is encountered (e.g., the so-called ΔE effect in magnetoelasticity).

Using the proposed field decomposition for $\mathbb{S}$ and $\mathbb{E}$, we get

$$\mathbb{S} = \mathbb{S}^{\mathbf{C}} + \mathbb{S}^{\boldsymbol{\epsilon}},$$

$$\mathbb{E} = \mathbb{E}^{\boldsymbol{\epsilon}} + \mathbb{E}^{\mathbf{C}}. \tag{30}$$

The constitutive law can be rewritten as

$$\begin{pmatrix} \mathbb{T} \\ \mathbb{D} \end{pmatrix} = \begin{pmatrix} \mathbf{C} & \mathbf{0} \\ \mathbf{0} & \boldsymbol{\epsilon} \end{pmatrix} \cdot \begin{pmatrix} \mathbb{S}^{\mathbf{C}} \\ \mathbb{E}^{\boldsymbol{\epsilon}} \end{pmatrix} \tag{31}$$

with additional coupling relations,

$$-\mathbf{C} \cdot \mathbb{S}^{\boldsymbol{\epsilon}} = -{}^t\mathbf{e} \cdot \mathbb{E},$$

$$-\boldsymbol{\epsilon} \cdot \mathbb{E}^{\mathbf{C}} = \mathbf{e} \cdot \mathbb{S}. \tag{32}$$

These three latter equations are equivalent to any of the set of Eqs. (26)–(28). The proposed formalism is thus equivalent to the classical one in the case of the coupled behavior of homogeneous materials. But this formalism is very helpful to define the effective coupled behavior of heterogeneous materials. This point is the object of Sec. III.

III. HOMOGENIZATION

We now consider a heterogeneous material constituted of n phases. The constitutive law for each phase i is

$$\begin{pmatrix} \mathbb{T}_i \\ \mathbb{B}_i \\ \mathbb{D}_i \\ \mathbb{J}_i \end{pmatrix} = \begin{pmatrix} \mathbf{C}_i & \boldsymbol{\alpha}_i^{\mathbf{C}\boldsymbol{\mu}} & \boldsymbol{\alpha}_i^{\mathbf{C}\boldsymbol{\epsilon}} & \boldsymbol{\alpha}_i^{\mathbf{C}\mathbf{k}} \\ \boldsymbol{\alpha}_i^{\boldsymbol{\mu}\mathbf{C}} & \boldsymbol{\mu}_i & \boldsymbol{\alpha}_i^{\boldsymbol{\mu}\boldsymbol{\epsilon}} & \boldsymbol{\alpha}_i^{\boldsymbol{\mu}\mathbf{k}} \\ \boldsymbol{\alpha}_i^{\boldsymbol{\epsilon}\mathbf{C}} & \boldsymbol{\alpha}_i^{\boldsymbol{\epsilon}\boldsymbol{\mu}} & \boldsymbol{\epsilon}_i & \boldsymbol{\alpha}_i^{\boldsymbol{\epsilon}\mathbf{k}} \\ \boldsymbol{\alpha}_i^{\mathbf{k}\mathbf{C}} & \boldsymbol{\alpha}_i^{\mathbf{k}\boldsymbol{\mu}} & \boldsymbol{\alpha}_i^{\mathbf{k}\boldsymbol{\epsilon}} & \mathbf{k}_i \end{pmatrix} \cdot \begin{pmatrix} \mathbb{S}_i \\ \mathbb{H}_i \\ \mathbb{E}_i \\ \mathbb{K}_i \end{pmatrix}. \quad (33)$$

The objective is to deduce the constitutive law of the equivalent homogeneous medium (EHM). This EHM exhibits, for a given loading, the same macroscopic response than the real heterogeneous medium (RHM). The effective constitutive law is written in the form as

$$\begin{pmatrix} \overline{\mathbb{T}} \\ \overline{\mathbb{B}} \\ \overline{\mathbb{D}} \\ \overline{\mathbb{J}} \end{pmatrix} = \begin{pmatrix} \tilde{\mathbf{C}} & \tilde{\boldsymbol{\alpha}}^{\mathbf{C}\boldsymbol{\mu}} & \tilde{\boldsymbol{\alpha}}^{\mathbf{C}\boldsymbol{\epsilon}} & \tilde{\boldsymbol{\alpha}}^{\mathbf{C}\mathbf{k}} \\ \tilde{\boldsymbol{\alpha}}^{\boldsymbol{\mu}\mathbf{C}} & \tilde{\boldsymbol{\mu}} & \tilde{\boldsymbol{\alpha}}^{\boldsymbol{\mu}\boldsymbol{\epsilon}} & \tilde{\boldsymbol{\alpha}}^{\boldsymbol{\mu}\mathbf{k}} \\ \tilde{\boldsymbol{\alpha}}^{\boldsymbol{\epsilon}\mathbf{C}} & \tilde{\boldsymbol{\alpha}}^{\boldsymbol{\epsilon}\boldsymbol{\mu}} & \tilde{\boldsymbol{\epsilon}} & \tilde{\boldsymbol{\alpha}}^{\boldsymbol{\epsilon}\mathbf{k}} \\ \tilde{\boldsymbol{\alpha}}^{\mathbf{k}\mathbf{C}} & \tilde{\boldsymbol{\alpha}}^{\mathbf{k}\boldsymbol{\mu}} & \tilde{\boldsymbol{\alpha}}^{\mathbf{k}\boldsymbol{\epsilon}} & \tilde{\mathbf{k}} \end{pmatrix} \cdot \begin{pmatrix} \overline{\mathbb{S}} \\ \overline{\mathbb{H}} \\ \overline{\mathbb{E}} \\ \overline{\mathbb{K}} \end{pmatrix}, \quad (34)$$

where the macroscopic loadings and responses are defined by Eq. (35),

$$\overline{\mathbb{T}} = \langle \mathbb{T}_i \rangle, \quad \overline{\mathbb{S}} = \langle \mathbb{S}_i \rangle,$$

$$\overline{\mathbb{B}} = \langle \mathbb{B}_i \rangle, \quad \overline{\mathbb{H}} = \langle \mathbb{H}_i \rangle,$$

$$\overline{\mathbb{D}} = \langle \mathbb{D}_i \rangle, \quad \overline{\mathbb{E}} = \langle \mathbb{E}_i \rangle,$$

$$\overline{\mathbb{J}} = \langle \mathbb{J}_i \rangle, \quad \overline{\mathbb{K}} = \langle \mathbb{K}_i \rangle. \quad (35)$$

The operator $\langle \cdot \rangle$ denotes an averaging operation over the volume.

Homogenization tools have been mainly developed in the framework of uncoupled behavior. We present hereafter the homogenization model based on inclusion problems that will be used in the following.

A. Inclusion-based model (uncoupled)

For a *n*-phasic material with uncoupled behavior, the constitutive law for each phase *i* is

$$\begin{pmatrix} \mathbb{T}_i \\ \mathbb{B}_i \\ \mathbb{D}_i \\ \mathbb{J}_i \end{pmatrix} = \begin{pmatrix} \mathbf{C}_i & \mathbf{0} & \mathbf{0} & \mathbf{0} \\ \mathbf{0} & \boldsymbol{\mu}_i & \mathbf{0} & \mathbf{0} \\ \mathbf{0} & \mathbf{0} & \boldsymbol{\epsilon}_i & \mathbf{0} \\ \mathbf{0} & \mathbf{0} & \mathbf{0} & \mathbf{k}_i \end{pmatrix} \cdot \begin{pmatrix} \mathbb{S}_i \\ \mathbb{H}_i \\ \mathbb{E}_i \\ \mathbb{K}_i \end{pmatrix}. \quad (36)$$

The effective constitutive law is

$$\begin{pmatrix} \overline{\mathbb{T}} \\ \overline{\mathbb{B}} \\ \overline{\mathbb{D}} \\ \overline{\mathbb{J}} \end{pmatrix} = \begin{pmatrix} \overline{\mathbf{C}} & \mathbf{0} & \mathbf{0} & \mathbf{0} \\ \mathbf{0} & \overline{\boldsymbol{\mu}} & \mathbf{0} & \mathbf{0} \\ \mathbf{0} & \mathbf{0} & \overline{\boldsymbol{\epsilon}} & \mathbf{0} \\ \mathbf{0} & \mathbf{0} & \mathbf{0} & \overline{\mathbf{k}} \end{pmatrix} \cdot \begin{pmatrix} \overline{\mathbb{S}} \\ \overline{\mathbb{H}} \\ \overline{\mathbb{E}} \\ \overline{\mathbb{K}} \end{pmatrix}. \quad (37)$$

The effective properties are the effective elastic stiffness tensor $\overline{\mathbf{C}}$ in the purely elastic homogenization problem, the effective magnetic permeability tensor $\overline{\boldsymbol{\mu}}$ in the purely magnetic homogenization problem, the effective electric permittivity tensor $\overline{\boldsymbol{\epsilon}}$ in the purely electric homogenization problem, and the effective thermal-conductivity tensor $\overline{\mathbf{k}}$ in the purely thermal homogenization problem. These effective properties are deduced through a classical homogenization process.[16,17] This process relies on the definition of localization operators, defining the local fields in phase *i* from the knowledge of the macroscopic loading. Two types of localization operators are used. The localization tensors **A** [Eq. (38)] link the local fields deriving from potentials to the corresponding macroscopic fields, whereas the concentration tensors **B** [Eq. (39)] link the local fields with a null divergence to the corresponding macroscopic fields,

$$\mathbb{S}_i = \mathbf{A}_i^{\mathbf{C}} \cdot \overline{\mathbb{S}},$$

$$\mathbb{H}_i = \mathbf{A}_i^{\boldsymbol{\mu}} \cdot \overline{\mathbb{H}},$$

$$\mathbb{E}_i = \mathbf{A}_i^{\boldsymbol{\epsilon}} \cdot \overline{\mathbb{E}},$$

$$\mathbb{K}_i = \mathbf{A}_i^{\mathbf{k}} \cdot \overline{\mathbb{K}}, \quad (38)$$

$$\mathbb{T}_i = \mathbf{B}_i^{\mathbf{C}} \cdot \overline{\mathbb{T}},$$

$$\mathbb{B}_i = \mathbf{B}_i^{\boldsymbol{\mu}} \cdot \overline{\mathbb{B}},$$

$$\mathbb{D}_i = \mathbf{B}_i^{\boldsymbol{\epsilon}} \cdot \overline{\mathbb{D}},$$

$$\mathbb{J}_i = \mathbf{B}_i^{\mathbf{k}} \cdot \overline{\mathbb{J}}. \quad (39)$$

Moreover, these localization operators verify $\langle \mathbf{A}_i \rangle = \langle \mathbf{B}_i \rangle = \mathbf{I}$ (with **I** as the identity tensor (6×6) in mechanics or (3×3) in magnetism, electricity, or thermics). From these localization tensors, the effective properties can be deduced,

$$\overline{\mathbf{C}} = \langle \mathbf{C}_i \cdot \mathbf{A}_i^{\mathbf{C}} \rangle = \langle \mathbf{C}_i^{-1} \cdot \mathbf{B}_i^{\mathbf{C}} \rangle^{-1},$$

$$\overline{\boldsymbol{\mu}} = \langle \boldsymbol{\mu}_i \cdot \mathbf{A}_i^{\boldsymbol{\mu}} \rangle = \langle \boldsymbol{\mu}_i^{-1} \cdot \mathbf{B}_i^{\boldsymbol{\mu}} \rangle^{-1},$$

$$\overline{\boldsymbol{\epsilon}} = \langle \boldsymbol{\epsilon}_i \cdot \mathbf{A}_i^{\boldsymbol{\epsilon}} \rangle = \langle \boldsymbol{\epsilon}_i^{-1} \cdot \mathbf{B}_i^{\boldsymbol{\epsilon}} \rangle^{-1},$$

$$\overline{\mathbf{k}} = \langle \mathbf{k}_i \cdot \mathbf{A}_i^{\mathbf{k}} \rangle = \langle \mathbf{k}_i^{-1} \cdot \mathbf{B}_i^{\mathbf{k}} \rangle^{-1}. \quad (40)$$

In order to build these localization operators, a homogenization model based on inclusion problems is used (see Appendix B). This method divides the problem of a *n*-phasic material into *n*-independent basic inclusion problems (Fig. 2). Indeed the mean response of the phase *i* is supposed to be the same as the response of an inclusion of phase *i* embedded in an infinite-loaded medium.

The problem of the inclusion of phase *i* gives the localization operators $\mathbf{A}_i$ and $\mathbf{B}_i$ for phase *i*. The choice of the infinite medium properties ($\mathbf{C}_\infty$, $\boldsymbol{\mu}_\infty$, $\boldsymbol{\epsilon}_\infty$, and $\mathbf{k}_\infty$) gives a degree of freedom in order to account for the influence of the microstructure of the RHM. Some particular choices enable us to retrieve some classical homogenization estimates or bounds[18] (Wiener or Voigt & Reuss, Hashin & Shtrikman, Mori-Tanaka, self-consistent estimate, etc.).

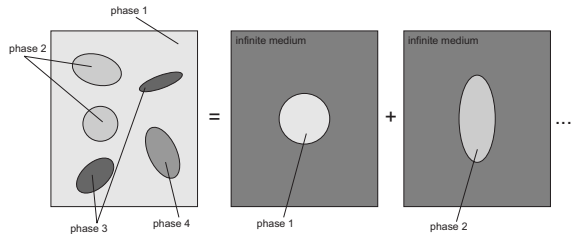

FIG. 2. Homogenization based on inclusion problems.

B. Coupled problems

If the behavior is coupled, such an approach is not directly tractable. Indeed the classical localization operators do not link the total macroscopic loading to the total local response. One method[13] is to redefine the localization operators in the case of coupling effects. Our proposal is to keep the usual localization operators but combined to the use of the decomposition of the loadings presented in Sec. II B. It can be noticed that the same kind of decomposition used in Eqs. (7), (11), (15), and (19) can be used with the macroscopic fields. Moreover, a constitutive law similar to the local one [Eq. (23)] can be written macroscopically as

$$\begin{pmatrix} \overline{\mathbb{T}} \\ \overline{\mathbb{B}} \\ \overline{\mathbb{D}} \\ \overline{\mathbb{J}} \end{pmatrix} = \begin{pmatrix} \overline{\mathbf{C}} & \mathbf{0} & \mathbf{0} & \mathbf{0} \\ \mathbf{0} & \overline{\boldsymbol{\mu}} & \mathbf{0} & \mathbf{0} \\ \mathbf{0} & \mathbf{0} & \overline{\boldsymbol{\epsilon}} & \mathbf{0} \\ \mathbf{0} & \mathbf{0} & \mathbf{0} & \overline{\mathbf{k}} \end{pmatrix} \cdot \begin{pmatrix} \overline{\mathbb{S}}^{\mathbf{C}} \\ \overline{\mathbb{H}}^{\boldsymbol{\mu}} \\ \overline{\mathbb{E}}^{\boldsymbol{\epsilon}} \\ \overline{\mathbb{K}}^{\mathbf{k}} \end{pmatrix}, \tag{41}$$

where the effective properties are the ones deduced in the-uncoupled problems [Eq. (40)].

But because of the coupling effects leading to local incompatibilities, one must pay attention to the fact that these decomposed macroscopic fields are not directly the mean values of the decomposed local fields [see Eqs. (42)–(45)]. Even if the total fields still respect $\overline{\mathbb{S}}=\langle \mathbb{S}_i \rangle$, $\overline{\mathbb{H}}=\langle \mathbb{H}_i \rangle$, $\overline{\mathbb{E}}=\langle \mathbb{E}_i \rangle$, and $\overline{\mathbb{K}}=\langle \mathbb{K}_i \rangle$, such a relationship does not apply to the decomposed fields. However, the macroscopic decomposed fields can be deduced from the local ones, using a modified averaging operation. This averaging operation introduces the-uncoupled-concentration tensors **B** (see proof in Appendix D),

$$\begin{aligned}
&\overline{\mathbb{S}} = \overline{\mathbb{S}}^{\mathbf{C}} + \overline{\mathbb{S}}^{\boldsymbol{\mu}} + \overline{\mathbb{S}}^{\boldsymbol{\epsilon}} + \overline{\mathbb{S}}^{\mathbf{k}}, \\
&\overline{\mathbb{S}}^{\mathbf{C}} = \overline{\mathbf{C}}^{-1} \cdot \overline{\mathbb{T}} \neq \langle \mathbb{S}_i^{\mathbf{C}} \rangle, \\
&\overline{\mathbb{S}}^{\boldsymbol{\mu}} = \langle {}^t\mathbf{B}_i^{\mathbf{C}} \cdot \mathbb{S}_i^{\boldsymbol{\mu}} \rangle \neq \langle \mathbb{S}_i^{\boldsymbol{\mu}} \rangle, \\
&\overline{\mathbb{S}}^{\boldsymbol{\epsilon}} = \langle {}^t\mathbf{B}_i^{\mathbf{C}} \cdot \mathbb{S}_i^{\boldsymbol{\epsilon}} \rangle \neq \langle \mathbb{S}_i^{\boldsymbol{\epsilon}} \rangle, \\
&\overline{\mathbb{S}}^{\mathbf{k}} = \langle {}^t\mathbf{B}_i^{\mathbf{C}} \cdot \mathbb{S}_i^{\mathbf{k}} \rangle \neq \langle \mathbb{S}_i^{\mathbf{k}} \rangle,
\end{aligned} \tag{42}$$

$$\begin{aligned}
&\overline{\mathbb{H}} = \overline{\mathbb{H}}^{\mathbf{C}} + \overline{\mathbb{H}}^{\boldsymbol{\mu}} + \overline{\mathbb{H}}^{\boldsymbol{\epsilon}} + \overline{\mathbb{H}}^{\mathbf{k}}, \\
&\overline{\mathbb{H}}^{\mathbf{C}} = \langle {}^t\mathbf{B}_i^{\boldsymbol{\mu}} \cdot \mathbb{H}_i^{\mathbf{C}} \rangle \neq \langle \mathbb{H}_i^{\mathbf{C}} \rangle, \\
&\overline{\mathbb{H}}^{\boldsymbol{\mu}} = \overline{\boldsymbol{\mu}}^{-1} \cdot \overline{\mathbb{B}} \neq \langle \mathbb{H}_i^{\boldsymbol{\mu}} \rangle, \\
&\overline{\mathbb{H}}^{\boldsymbol{\epsilon}} = \langle {}^t\mathbf{B}_i^{\boldsymbol{\mu}} \cdot \mathbb{H}_i^{\boldsymbol{\epsilon}} \rangle \neq \langle \mathbb{H}_i^{\boldsymbol{\epsilon}} \rangle, \\
&\overline{\mathbb{H}}^{\mathbf{k}} = \langle {}^t\mathbf{B}_i^{\boldsymbol{\mu}} \cdot \mathbb{H}_i^{\mathbf{k}} \rangle \neq \langle \mathbb{H}_i^{\mathbf{k}} \rangle,
\end{aligned} \tag{43}$$

$$\begin{aligned}
&\overline{\mathbb{E}} = \overline{\mathbb{E}}^{\mathbf{C}} + \overline{\mathbb{E}}^{\boldsymbol{\mu}} + \overline{\mathbb{E}}^{\boldsymbol{\epsilon}} + \overline{\mathbb{E}}^{\mathbf{k}}, \\
&\overline{\mathbb{E}}^{\mathbf{C}} = \langle {}^t\mathbf{B}_i^{\boldsymbol{\epsilon}} \cdot \mathbb{E}_i^{\mathbf{C}} \rangle \neq \langle \mathbb{E}_i^{\mathbf{C}} \rangle, \\
&\overline{\mathbb{E}}^{\boldsymbol{\mu}} = \langle {}^t\mathbf{B}_i^{\boldsymbol{\epsilon}} \cdot \mathbb{E}_i^{\boldsymbol{\mu}} \rangle \neq \langle \mathbb{E}_i^{\boldsymbol{\mu}} \rangle, \\
&\overline{\mathbb{E}}^{\boldsymbol{\epsilon}} = \overline{\boldsymbol{\epsilon}}^{-1} \cdot \overline{\mathbb{D}} \neq \langle \mathbb{E}_i^{\boldsymbol{\epsilon}} \rangle, \\
&\overline{\mathbb{E}}^{\mathbf{k}} = \langle {}^t\mathbf{B}_i^{\boldsymbol{\epsilon}} \cdot \mathbb{E}_i^{\mathbf{k}} \rangle \neq \langle \mathbb{E}_i^{\mathbf{k}} \rangle,
\end{aligned} \tag{44}$$

$$\begin{aligned}
&\overline{\mathbb{K}} = \overline{\mathbb{K}}^{\mathbf{C}} + \overline{\mathbb{K}}^{\boldsymbol{\mu}} + \overline{\mathbb{K}}^{\boldsymbol{\epsilon}} + \overline{\mathbb{K}}^{\mathbf{k}}, \\
&\overline{\mathbb{K}}^{\mathbf{C}} = \langle {}^t\mathbf{B}_i^{\mathbf{k}} \cdot \mathbb{K}_i^{\mathbf{C}} \rangle \neq \langle \mathbb{K}_i^{\mathbf{C}} \rangle, \\
&\overline{\mathbb{K}}^{\boldsymbol{\mu}} = \langle {}^t\mathbf{B}_i^{\mathbf{k}} \cdot \mathbb{K}_i^{\boldsymbol{\mu}} \rangle \neq \langle \mathbb{K}_i^{\boldsymbol{\mu}} \rangle, \\
&\overline{\mathbb{K}}^{\boldsymbol{\epsilon}} = \langle {}^t\mathbf{B}_i^{\mathbf{k}} \cdot \mathbb{K}_i^{\boldsymbol{\epsilon}} \rangle \neq \langle \mathbb{K}_i^{\boldsymbol{\epsilon}} \rangle, \\
&\overline{\mathbb{K}}^{\mathbf{k}} = \overline{\mathbf{k}}^{-1} \cdot \overline{\mathbb{J}} \neq \langle \mathbb{K}_i^{\mathbf{k}} \rangle.
\end{aligned} \tag{45}$$

The localization rules are similar to those defined by Hill[14] in mechanics (the tensors **A** and **B** are derived from this relation in the-uncoupled case),

$$\begin{aligned}
&\mathbf{N}_i^{\mathbf{C}} \cdot \mathbf{C}_\infty^{-1} \cdot (\overline{\mathbb{T}} - \mathbb{T}_i) = (\mathbf{N}_i^{\mathbf{C}} - \mathbf{I}) \cdot (\overline{\mathbb{S}} - \mathbb{S}_i), \\
&\mathbf{N}_i^{\boldsymbol{\mu}} \cdot \boldsymbol{\mu}_\infty^{-1} \cdot (\overline{\mathbb{B}} - \mathbb{B}_i) = (\mathbf{N}_i^{\boldsymbol{\mu}} - \mathbf{I}) \cdot (\overline{\mathbb{H}} - \mathbb{H}_i), \\
&\mathbf{N}_i^{\boldsymbol{\epsilon}} \cdot \boldsymbol{\epsilon}_\infty^{-1} \cdot (\overline{\mathbb{D}} - \mathbb{D}_i) = (\mathbf{N}_i^{\boldsymbol{\epsilon}} - \mathbf{I}) \cdot (\overline{\mathbb{E}} - \mathbb{E}_i), \\
&\mathbf{N}_i^{\mathbf{k}} \cdot \mathbf{k}_\infty^{-1} \cdot (\overline{\mathbb{J}} - \mathbb{J}_i) = (\mathbf{N}_i^{\mathbf{k}} - \mathbf{I}) \cdot (\overline{\mathbb{K}} - \mathbb{K}_i),
\end{aligned} \tag{46}$$

where $\mathbf{C}_\infty$, $\boldsymbol{\mu}_\infty$, $\boldsymbol{\epsilon}_\infty$, and $\mathbf{k}_\infty$ are the properties of the infinite medium in the inclusion problem and $\mathbf{N}_i^{\mathbf{C}}$, $\mathbf{N}_i^{\boldsymbol{\mu}}$, $\mathbf{N}_i^{\boldsymbol{\epsilon}}$, and $\mathbf{N}_i^{\mathbf{k}}$ are the corresponding depolarizing (or Eshelby) tensors (see Appendixes B and C). Adding the local coupling relations given by Eqs. (10), (14), (18), and (22) for each phase *i*, we obtain a system that can be solved in order to deduce the effective properties [Eq. (34)]. One should pay attention to the fact that the effective stiffness, permeability, permittivity, and thermal-conductivity tensors have different expressions than the ones defined in the-uncoupled problem [Eq. (37)]: for example, $\tilde{\boldsymbol{\mu}}$ links $\overline{\mathbb{B}}$ to $\overline{\mathbb{H}}$ when all the other total effective loadings are equal to zero. This permeability is not equal to $\overline{\boldsymbol{\mu}}$ obtained when the coupled effects are locally canceled because of local incompatibilities due to the coupled behavior.

TABLE I. Material properties (Ref. 4).

		$BaTiO_3$	$CoFe_2O_4$
$\mathbf{C}_{11}$	(GPa)	166	286
$\mathbf{C}_{12}$		77	173
$\mathbf{C}_{13}$		78	170.5
$\mathbf{C}_{33}$		162	26.95
$\mathbf{C}_{44}/2$		43	45.3
$\boldsymbol{\mu}_{11}$	$(10^{-6}\ \mathrm{N\,s^2/C^2})$	5	−590
$\boldsymbol{\mu}_{33}$		10	157
$\boldsymbol{\epsilon}_{11}$	$(10^{-10}\ \mathrm{C^2/N\,m^2})$	112	0.8
$\boldsymbol{\epsilon}_{33}$		126	0.93
$\mathbf{e}_{31}$	$(\mathrm{C/m^2})$	−4.4	0
$\mathbf{e}_{33}$		18.6	0
$\mathbf{e}_{15}/\sqrt{2}$		11.6	0
$\mathbf{q}_{31}$	(N/A m)	0	580.3
$\mathbf{q}_{33}$		0	699.7
$\mathbf{q}_{15}/\sqrt{2}$		0	550

The general resolution scheme in the case of a fully coupled *n*-phasic material is detailed in Appendix E. A particular case of biphasic composite (for which localization rules can significantly be simplified) is given hereafter as an illustration.

IV. APPLICATION TO MAGNETOELECTRIC COMPOSITES

The method is applied to a magnetoelectric composite made of piezomagnetic and piezoelectric materials. Composites made of magnetostrictive and electrostrictive phases exhibit a magnetoelectric effect. This effect is extrinsic since the coupling between electricity and magnetism appears through mechanics. Results in the literature show that the extrinsic magnetoelectric effect is larger in such composites than the intrinsic one[19,20] observed in some homogeneous materials. We will use the configuration and material properties (see Table I) proposed by Li and Dunn,[12] who proposed a homogenization model for those materials, and also taken by Lee *et al.*[4] who compared these results to the corresponding finite element computations.

In the following, subscript *m* stands for the piezomagnetic phase and subscript *e* for the piezoelectric phase. The local constitutive laws are

$$\begin{pmatrix} \mathbb{T}_m \\ \mathbb{B}_m \\ \mathbb{D}_m \end{pmatrix} = \begin{pmatrix} \mathbf{C}_m & -{}^t\mathbf{q}_m & \mathbf{0} \\ \mathbf{q}_m & \boldsymbol{\mu}_m & \mathbf{0} \\ \mathbf{0} & \mathbf{0} & \boldsymbol{\epsilon}_m \end{pmatrix} \cdot \begin{pmatrix} \mathbb{S}_m \\ \mathbb{H}_m \\ \mathbb{E}_m \end{pmatrix} \tag{47}$$

for the piezomagnetic material [$\mathbf{q}_m$ is the piezomagnetic matrix (3×6)] and

$$\begin{pmatrix} \mathbb{T}_e \\ \mathbb{B}_e \\ \mathbb{D}_e \end{pmatrix} = \begin{pmatrix} \mathbf{C}_e & \mathbf{0} & -{}^t\mathbf{e}_e \\ \mathbf{0} & \boldsymbol{\mu}_e & \mathbf{0} \\ \mathbf{e}_e & \mathbf{0} & \boldsymbol{\epsilon}_e \end{pmatrix} \cdot \begin{pmatrix} \mathbb{S}_e \\ \mathbb{H}_e \\ \mathbb{E}_e \end{pmatrix} \tag{48}$$

for the piezoelectric material [$\mathbf{e}_e$ is the piezoelectric matrix (3×6)].

We apply the field decomposition,

$$\begin{aligned} \mathbb{S}_m &= \mathbb{S}_m^{\mathbf{C}} + \mathbb{S}_m^{\boldsymbol{\mu}}, \\ \mathbb{H}_m &= \mathbb{H}_m^{\boldsymbol{\mu}} + \mathbb{H}_m^{\mathbf{C}}, \\ \mathbb{E}_m &= \mathbb{E}_m^{\boldsymbol{\epsilon}}, \\ \mathbb{S}_e &= \mathbb{S}_e^{\mathbf{C}} + \mathbb{S}_e^{\boldsymbol{\epsilon}}, \\ \mathbb{H}_e &= \mathbb{H}_e^{\boldsymbol{\mu}}, \\ \mathbb{E}_e &= \mathbb{E}_e^{\boldsymbol{\epsilon}} + \mathbb{E}_e^{\mathbf{C}}. \end{aligned} \tag{49, 50}$$

Then the homogenization equations can be written.

A. Equations

The mechanical system is

$$\begin{aligned} \overline{\mathbb{S}} &= \langle \mathbb{S}_i \rangle = f \cdot \mathbb{S}_e + (1-f) \cdot \mathbb{S}_m = f \cdot (\mathbb{S}_e^{\mathbf{C}} + \mathbb{S}_e^{\boldsymbol{\epsilon}}) + (1-f) \cdot (\mathbb{S}_m^{\mathbf{C}} + \mathbb{S}_m^{\boldsymbol{\mu}}), \\ \overline{\mathbb{S}} &= \overline{\mathbb{S}}^{\mathbf{C}} + \overline{\mathbb{S}}^{\boldsymbol{\epsilon}} + \overline{\mathbb{S}}^{\boldsymbol{\mu}} = \overline{\mathbf{C}}^{-1} \cdot \overline{\mathbb{T}} + \langle {}^t\mathbf{B}_i^{\mathbf{C}} \cdot \mathbb{S}_i^{\boldsymbol{\epsilon}} \rangle + \langle {}^t\mathbf{B}_i^{\mathbf{C}} \cdot \mathbb{S}_i^{\boldsymbol{\mu}} \rangle \\ &= \overline{\mathbf{C}}^{-1} \cdot \overline{\mathbb{T}} + f \cdot {}^t\mathbf{B}_e^{\mathbf{C}} \cdot \mathbb{S}_e^{\boldsymbol{\epsilon}} + (1-f) \cdot {}^t\mathbf{B}_m^{\mathbf{C}} \cdot \mathbb{S}_m^{\boldsymbol{\mu}}, \\ \overline{\mathbb{T}} &= \langle \mathbb{T}_i \rangle = \langle \mathbf{C}_i \cdot \mathbb{S}_i^{\mathbf{C}} \rangle \\ &= f \cdot \mathbf{C}_e \cdot \mathbb{S}_e^{\mathbf{C}} + (1-f) \cdot \mathbf{C}_m \cdot \mathbb{S}_m^{\mathbf{C}}, \end{aligned} \tag{51}$$

with f the volumetric fraction of the piezoelectric phase. Similarly, the magnetic system can be written as

$$\begin{aligned} \overline{\mathbb{H}} &= \langle \mathbb{H}_i \rangle = f \cdot \mathbb{H}_e + (1-f) \cdot \mathbb{H}_m = f \cdot \mathbb{H}_e^{\boldsymbol{\mu}} + (1-f) \cdot (\mathbb{H}_m^{\boldsymbol{\mu}} + \mathbb{H}_m^{\mathbf{C}}), \\ \overline{\mathbb{H}} &= \overline{\mathbb{H}}^{\boldsymbol{\mu}} + \overline{\mathbb{H}}^{\mathbf{C}} = \overline{\boldsymbol{\mu}}^{-1} \cdot \overline{\mathbb{B}} + \langle {}^t\mathbf{B}_i^{\boldsymbol{\mu}} \cdot \mathbb{H}_i^{\mathbf{C}} \rangle \\ &= \overline{\boldsymbol{\mu}}^{-1} \cdot \overline{\mathbb{B}} + (1-f) \cdot {}^t\mathbf{B}_m^{\boldsymbol{\mu}} \cdot \mathbb{H}_m^{\mathbf{C}}, \\ \overline{\mathbb{B}} &= \langle \mathbb{B}_i \rangle = \langle \boldsymbol{\mu}_i \cdot \mathbb{H}_i^{\boldsymbol{\mu}} \rangle = f \cdot \boldsymbol{\mu}_e \cdot \mathbb{H}_e^{\boldsymbol{\mu}} = (1-f) \cdot \boldsymbol{\mu}_m \cdot \mathbb{H}_m^{\boldsymbol{\mu}}. \end{aligned} \tag{52}$$

Finally, the electric system can be written as

$$\begin{aligned} \overline{\mathbb{E}} &= \langle \mathbb{E}_i \rangle = f \cdot \mathbb{E}_e + (1-f) \cdot \mathbb{E}_m = f \cdot (\mathbb{E}_e^{\boldsymbol{\epsilon}} + \mathbb{E}_e^{\mathbf{C}}) + (1-f) \cdot \mathbb{E}_m^{\boldsymbol{\epsilon}}, \\ \overline{\mathbb{E}} &= \overline{\mathbb{E}}^{\boldsymbol{\epsilon}} + \overline{\mathbb{E}}^{\mathbf{C}} = \overline{\boldsymbol{\epsilon}}^{-1} \cdot \overline{\mathbb{D}} + \langle {}^t\mathbf{B}_i^{\boldsymbol{\epsilon}} \cdot \mathbb{E}_i^{\mathbf{C}} \rangle = \overline{\boldsymbol{\epsilon}}^{-1} \cdot \overline{\mathbb{D}} + f \cdot {}^t\mathbf{B}_i^{\boldsymbol{\epsilon}} \cdot \mathbb{E}_e^{\mathbf{C}}, \\ \overline{\mathbb{D}} &= \langle \mathbb{D}_i \rangle = \langle \boldsymbol{\epsilon}_i \cdot \mathbb{E}_i^{\boldsymbol{\epsilon}} \rangle = f \cdot \boldsymbol{\epsilon}_e \cdot \mathbb{E}_e^{\boldsymbol{\epsilon}} + (1-f) \cdot \boldsymbol{\epsilon}_m \cdot \mathbb{E}_m^{\boldsymbol{\epsilon}}. \end{aligned} \tag{53}$$

Moreover, The coupling relations are given by Eqs. (54) and (55), respectively, for the piezomagnetic and piezoelectric phases,

$$\begin{aligned} -\mathbf{C}_m \cdot \mathbb{S}_m^{\boldsymbol{\mu}} &= -{}^t\mathbf{q}_m \cdot \mathbb{H}_m = -{}^t\mathbf{q}_m \cdot (\mathbb{H}_m^{\boldsymbol{\mu}} + \mathbb{H}_m^{\mathbf{C}}), \\ -\boldsymbol{\mu}_m \cdot \mathbb{H}_m^{\mathbf{C}} &= \mathbf{q}_m \cdot \mathbb{S}_m = \mathbf{q}_m \cdot (\mathbb{S}_m^{\mathbf{C}} + \mathbb{S}_m^{\boldsymbol{\mu}}), \end{aligned} \tag{54}$$

$$\begin{aligned} -\mathbf{C}_e \cdot \mathbb{S}_e^{\boldsymbol{\epsilon}} &= -{}^t\mathbf{e}_e \cdot \mathbb{E}_e = -{}^t\mathbf{e}_e \cdot (\mathbb{E}_e^{\boldsymbol{\epsilon}} + \mathbb{E}_e^{\mathbf{C}}), \\ -\boldsymbol{\epsilon}_e \cdot \mathbb{E}_e^{\mathbf{C}} &= \mathbf{e}_e \cdot \mathbb{S}_e = \mathbf{e}_e \cdot (\mathbb{S}_e^{\mathbf{C}} + \mathbb{S}_e^{\boldsymbol{\epsilon}}). \end{aligned} \tag{55}$$

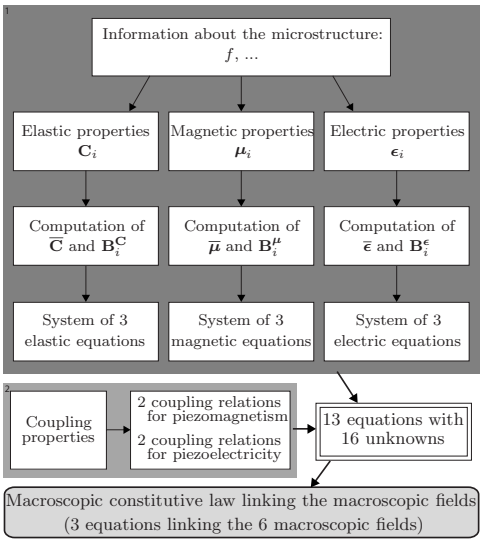

FIG. 3. Modeling scheme.

B. Modeling scheme

The system is constituted of 16 unknowns: (i) the macroscopic loading $\overline{\mathbb{S}}$, $\overline{\mathbb{H}}$, and $\overline{\mathbb{E}}$; (ii) the macroscopic response $\overline{\mathbb{T}}$, $\overline{\mathbb{B}}$, and $\overline{\mathbb{D}}$; (iii) the local decomposed strains $\mathbb{S}_e^{\mathbf{C}}$, $\mathbb{S}_m^{\mathbf{C}}$, $\mathbb{S}_e^{\boldsymbol{\epsilon}}$, and $\mathbb{S}_m^{\boldsymbol{\mu}}$; (iv) the local decomposed magnetic fields $\mathbb{H}_e^{\boldsymbol{\mu}}$, $\mathbb{H}_m^{\boldsymbol{\mu}}$, and $\mathbb{H}_m^{\mathbf{C}}$; (v) and the local decomposed electric fields $\mathbb{E}_e^{\boldsymbol{\epsilon}}$, $\mathbb{E}_m^{\boldsymbol{\epsilon}}$, and $\mathbb{E}_e^{\mathbf{C}}$.

These 16 unknowns are linked through 13 equations (three from mechanics [Eq. (51)], three from magnetism [Eq. (52)], three from electricity [Eq. (53)], two from piezomagnetism [Eq. (54)], and two from piezoelectricity [Eq. (55)]).

The effective properties of the composite can be deduced eliminating the local fields. Then the system reduces to three equations with six unknowns (the macroscopic fields) (Fig. 3). For a given applied loading (three parameters), the macroscopic response is given by the constitutive law [Eq. (56)]. If needed, the local fields and corresponding decomposition can also be calculated,

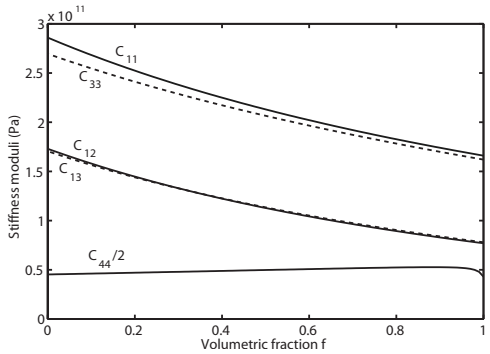

FIG. 4. Effective stiffness moduli depending on the volumetric fraction f of the piezoelectric phase.

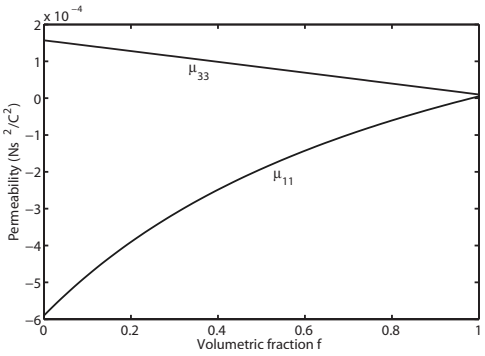

FIG. 5. Effective permeability depending on the volumetric fraction f of the piezoelectric phase.

$$\begin{pmatrix} \overline{\mathbb{T}} \\ \overline{\mathbb{B}} \\ \overline{\mathbb{D}} \end{pmatrix} = \begin{pmatrix} \tilde{\mathbf{C}} & -{}^t\tilde{\mathbf{q}} & -{}^t\tilde{\mathbf{e}} \\ \tilde{\mathbf{q}} & \tilde{\boldsymbol{\mu}} & {}^t\tilde{\boldsymbol{\alpha}} \\ \tilde{\mathbf{e}} & \tilde{\boldsymbol{\alpha}} & \tilde{\boldsymbol{\epsilon}} \end{pmatrix} \cdot \begin{pmatrix} \overline{\mathbb{S}} \\ \overline{\mathbb{H}} \\ \overline{\mathbb{E}} \end{pmatrix}. \tag{56}$$

C. Results

The modeled composite is a piezomagnetic matrix ($CoFe_2O_4$) reinforced with cylindrical piezoelectric fibers ($BaTiO_3$). For such a matrix and fibers microstructure, an appropriate choice for the infinite medium properties in the homogenization scheme is the properties of the matrix. This choice will correspond to a Mori-Tanaka-type estimate.[17] Some complementary elements to calculate the localization tensors in the case of infinite cylindrical inclusions are given in Appendix C. The volumetric fraction of the piezoelectric phase is f. The effective properties [Eq. (56)] obtained with the proposed homogenization model are shown in the following figures (Fig. 4–9).

These modeling results are the same than the ones obtained by Li and Dunn.[12] Their model is based upon a modified localization tensor for coupled properties. These results are also in good agreement with the ones obtained by Lee *et al.*[4] with a finite element modeling.

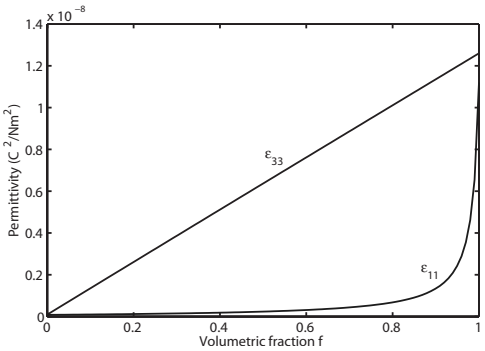

FIG. 6. Effective permittivity depending on the volumetric fraction f of the piezoelectric phase.

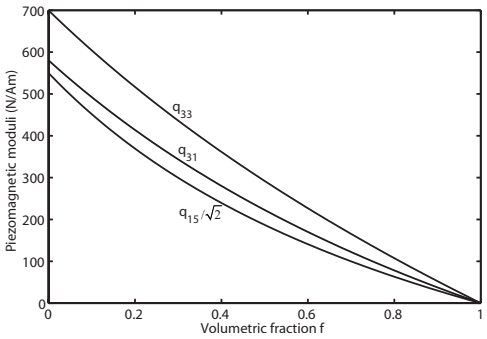

FIG. 7. Effective piezomagnetic moduli depending on the volumetric fraction f of the piezoelectric phase.

It is very noticeable that the effective properties of the composite made of piezomagnetic and piezoelectric materials exhibit a magnetoelectric effect, whereas none of the phases exhibit such an effect locally. This magnetoelectric effect in composites is typically a microstructure effect. In that sense it is particularly suited to validate homogenization tools.

V. CONCLUSION

We proposed a generic formalism for the homogenization of coupled behavior. It is based on the decomposition of the state variables into several contributions representing the coupling effects. That way, the classical rules of homogenization for uncoupled behavior can be maintained. They have to be completed by some additional coupling rules. This approach gives identical macroscopic results in the case of magnetoelectroelastic behavior with some previous results taken in the literature. The advantages of the proposed method are numerous: it applies to any kind of coupling among magnetoelectrothermoelastic couplings; it applies to any composite material, whatever the number of phases, and even for polycrystals (each phase being associated to a particular crystallographic direction); different types of microstructure are accounted for, through the choice of the properties of the infinite medium in the inclusion problem; it allows us to define the values of the local and macroscopic

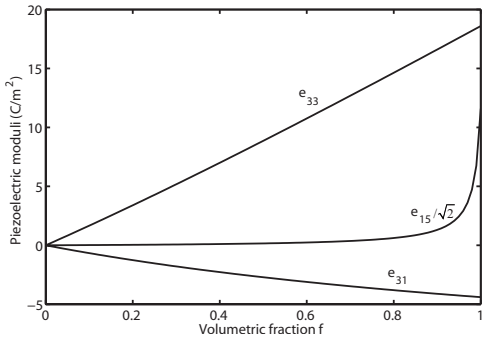

FIG. 8. Effective piezoelectric moduli depending on the volumetric fraction f of the piezoelectric phase.

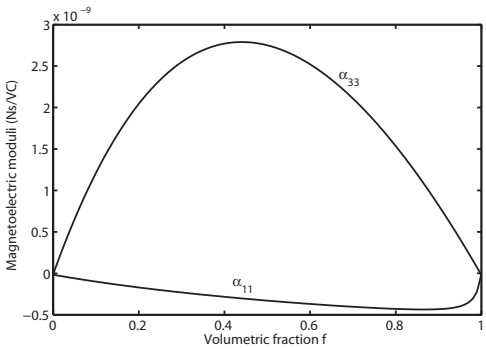

FIG. 9. Effective magnetoelectric moduli depending on the volumetric fraction f of the piezoelectric phase.

contributions of each coupling effect on the overall response of the material; and it does not introduce any ambiguousness concerning the properties linking the dual state variables (elastic stiffness, magnetic permeability, and electric permittivity and thermal-conductivity tensors) that are defined in a unique way.

The proposed approach considers linear behavior. Many smart materials exhibit nonlinear behavior; but in many cases, the linearization of the behavior around the operating point gives satisfying approximation. In the case when this nonlinearity cannot be neglected, for example, for devices used in a wide range of loadings, an extension of this method has to be achieved. This point is currently a work in progress. To conclude, we can emphasize the fact that the proposed decomposition for the state variables (already used in mechanics when dealing with thermal strain or plasticity) can be used in other context than homogenization and could give interesting results in other modeling techniques such as finite element methods.

APPENDIX A: MODIFIED VOIGT NOTATION

When second-, third-, and fourth-order tensors exhibit some symmetries, the modified Voigt notation (also named Voigt-Mandel notation) can be used in order to manipulate only matrices. For a second-order tensor $\mathbb{X}$ with symmetries so that $X_{ij}=X_{ji}$, the modified Voigt notation gives the following representation (6×1):

$$\mathbb{X}=\begin{pmatrix} X_{11} & X_{12} & X_{13} \\ X_{21} & X_{22} & X_{23} \\ X_{31} & X_{32} & X_{33} \end{pmatrix} \rightarrow \begin{pmatrix} X_{11} \\ X_{22} \\ X_{33} \\ \sqrt{2}X_{23} \\ \sqrt{2}X_{31} \\ \sqrt{2}X_{12} \end{pmatrix}. \tag{A1}$$

Similarly, a fourth-order tensor $\mathbf{F}$ exhibiting the following symmetries: $F_{ijkl}=F_{jikl}=F_{ijlk}=F_{jilk}$ can be written using modified Voigt notation. The (6×6) representation is given by Eq. (A2)

$$\mathbf{F} = (F_{ijkl}) \rightarrow \begin{pmatrix} F_{1111} & F_{1122} & F_{1133} & \sqrt{2}F_{1123} & \sqrt{2}F_{1131} & \sqrt{2}F_{1112} \\ F_{2211} & F_{2222} & F_{2233} & \sqrt{2}F_{2223} & \sqrt{2}F_{2231} & \sqrt{2}F_{2212} \\ F_{3311} & F_{3322} & F_{3333} & \sqrt{2}F_{3323} & \sqrt{2}F_{3331} & \sqrt{2}F_{3312} \\ \sqrt{2}F_{2311} & \sqrt{2}F_{2322} & \sqrt{2}F_{2333} & 2F_{2323} & 2F_{2331} & 2F_{2312} \\ \sqrt{2}F_{3111} & \sqrt{2}F_{3122} & \sqrt{2}F_{3133} & 2F_{3123} & 2F_{3131} & 2F_{3112} \\ \sqrt{2}F_{1211} & \sqrt{2}F_{1222} & \sqrt{2}F_{1233} & 2F_{1223} & 2F_{1231} & 2F_{1212} \end{pmatrix}. \quad \text{(A2)}$$

For a third-order tensor $\mathbf{d}$ exhibiting symmetries $d_{ijk}=d_{ikj}$, the (3×6) representation is used [Eq. (A3)],

$$\mathbf{d} = (d_{ijk}) \rightarrow \begin{pmatrix} d_{111} & d_{122} & d_{133} & \sqrt{2}d_{123} & \sqrt{2}d_{131} & \sqrt{2}d_{112} \\ d_{211} & d_{222} & d_{233} & \sqrt{2}d_{223} & \sqrt{2}d_{231} & \sqrt{2}d_{212} \\ d_{311} & d_{322} & d_{333} & \sqrt{2}d_{323} & \sqrt{2}d_{331} & \sqrt{2}d_{312} \end{pmatrix}. \quad \text{(A3)}$$

APPENDIX B: DEFINITION OF LOCALIZATION TENSORS

The basic-uncoupled-inclusion problem consists of an inclusion i embedded in an infinite medium ∞ with a uniform applied loading at the infinity. When the shape of the inclusion is ellipsoidal, then the field in the inclusion is uniform.[16] In a mechanical problem, noting $\mathbf{C}_i$ the stiffness tensor of the inclusion, $\mathbf{C}_\infty$ the stiffness tensor of the infinite medium, and $\mathbb{S}_\infty$ the uniform applied loading at the infinity, the (uniform) strain in the inclusion is given by

$$\mathbb{S}_i = [\mathbf{I} + \mathbf{N}_i^{\mathbf{C}} \cdot \mathbf{C}_\infty^{-1} \cdot (\mathbf{C}_i - \mathbf{C}_\infty)]^{-1} \cdot \mathbb{S}_\infty, \quad \text{(B1)}$$

where $\mathbf{N}_i^{\mathbf{C}}$ is the Eshelby tensor (6×6) depending on the shape of the inclusion and on the properties of the infinite medium (details to calculate the Eshelby tensor can be found in Mura's[21] monograph).

Homogenization techniques based on inclusion problems divide the n-phasic problem into n uncorrelated basic inclusion problems. The uniform applied loading at the infinity $\mathbb{S}_\infty$ in the basic inclusion problem is not directly the macroscopic loading[18] $\overline{\mathbb{S}}$. Indeed, the local strains must verify $\langle \mathbb{S}_i \rangle = \overline{\mathbb{S}}$. Then, the-uncoupled-mechanical localization tensor $\mathbf{A}_i^{\mathbf{C}}$ ($\mathbb{S}_i = \mathbf{A}_i^{\mathbf{C}} \cdot \overline{\mathbb{S}}$) can be deduced as

$$\mathbf{A}_i^{\mathbf{C}} = [\mathbf{I} + \mathbf{N}_i^{\mathbf{C}} \cdot \mathbf{C}_\infty^{-1} \cdot (\mathbf{C}_i - \mathbf{C}_\infty)]^{-1} \cdot \langle [\mathbf{I} + \mathbf{N}_i^{\mathbf{C}} \cdot \mathbf{C}_\infty^{-1} \cdot (\mathbf{C}_i - \mathbf{C}_\infty)]^{-1} \rangle^{-1}. \quad \text{(B2)}$$

The same way, the-uncoupled-magnetic localization tensor $\mathbf{A}_i^{\boldsymbol{\mu}}$ ($\mathbb{H}_i = \mathbf{A}_i^{\boldsymbol{\mu}} \cdot \overline{\mathbb{H}}$) can be obtained as

$$\mathbf{A}_i^{\boldsymbol{\mu}} = [\mathbf{I} + \mathbf{N}_i^{\boldsymbol{\mu}} \cdot \boldsymbol{\mu}_\infty^{-1} \cdot (\boldsymbol{\mu}_i - \boldsymbol{\mu}_\infty)]^{-1} \cdot \langle [\mathbf{I} + \mathbf{N}_i^{\boldsymbol{\mu}} \cdot \boldsymbol{\mu}_\infty^{-1} \cdot (\boldsymbol{\mu}_i - \boldsymbol{\mu}_\infty)]^{-1} \rangle^{-1}, \quad \text{(B3)}$$

where $\mathbf{N}_i^{\boldsymbol{\mu}}$ is the demagnetizing tensor (3×3) (equivalent to the Eshelby tensor in mechanics).

Similarly, the-uncoupled-electric localization tensor $\mathbf{A}_i^{\boldsymbol{\epsilon}}$ ($\mathbb{E}_i = \mathbf{A}_i^{\boldsymbol{\epsilon}} \cdot \overline{\mathbb{E}}$) can be obtained as

$$\mathbf{A}_i^{\boldsymbol{\epsilon}} = [\mathbf{I} + \mathbf{N}_i^{\boldsymbol{\epsilon}} \cdot \boldsymbol{\epsilon}_\infty^{-1} \cdot (\boldsymbol{\epsilon}_i - \boldsymbol{\epsilon}_\infty)]^{-1} \cdot \langle [\mathbf{I} + \mathbf{N}_i^{\boldsymbol{\epsilon}} \cdot \boldsymbol{\epsilon}_\infty^{-1} \cdot (\boldsymbol{\epsilon}_i - \boldsymbol{\epsilon}_\infty)]^{-1} \rangle^{-1} \quad \text{(B4)}$$

with $\mathbf{N}_i^{\boldsymbol{\epsilon}}$ the depolarizing tensor in the electric problem. The-uncoupled-thermal localization tensor $\mathbf{A}_i^{\mathbf{k}}$ ($\mathbb{K}_i = \mathbf{A}_i^{\mathbf{k}} \cdot \overline{\mathbb{K}}$) can be obtained as

$$\mathbf{A}_i^{\mathbf{k}} = [\mathbf{I} + \mathbf{N}_i^{\mathbf{k}} \cdot \mathbf{k}_\infty^{-1} \cdot (\mathbf{k}_i - \mathbf{k}_\infty)]^{-1} \cdot \langle [\mathbf{I} + \mathbf{N}_i^{\mathbf{k}} \cdot \mathbf{k}_\infty^{-1} \cdot (\mathbf{k}_i - \mathbf{k}_\infty)]^{-1} \rangle^{-1} \quad \text{(B5)}$$

with $\mathbf{N}_i^{\mathbf{k}}$ the depolarizing tensor as the thermal problem.

The choice of the infinite medium properties gives a degree of freedom for the construction of several homogenization models. This choice is directly connected to the type of microstructure of the real heterogeneous material. When the microstructure consists of inclusions embedded in a homogeneous matrix, then an appropriate choice for the infinite medium properties is the matrix properties (corresponding to the Mori-Tanaka estimate in mechanics).

APPENDIX C: ESHELBY AND DEPOLARIZING TENSORS IN THE CYLINDRICAL CASE

For an infinite cylindrical inclusion i (embedded in an infinite medium ∞ with transversely isotropic stiffness tensor $\mathbf{C}_\infty$), the Eshelby tensor $\mathbf{N}_i^{\mathbf{C}}$ is given by (cylinder along the axis 3)

$$\mathbf{N}_{i11}^{\mathbf{C}} = \mathbf{N}_{i22}^{\mathbf{C}} = \frac{5\mathbf{C}_{\infty 11} + \mathbf{C}_{\infty 12}}{8\mathbf{C}_{\infty 11}},$$

$$\mathbf{N}_{i12}^{\mathbf{C}} = \mathbf{N}_{i21}^{\mathbf{C}} = \frac{-\mathbf{C}_{\infty 11} + 3\mathbf{C}_{\infty 12}}{8\mathbf{C}_{\infty 11}},$$

$$\mathbf{N}_{i13}^{\mathbf{C}} = \mathbf{N}_{i23}^{\mathbf{C}} = \frac{\mathbf{C}_{\infty 13}}{2\mathbf{C}_{\infty 11}},$$

$$\mathbf{N}_{i44}^{\mathbf{C}} = \mathbf{N}_{i55}^{\mathbf{C}} = \frac{1}{2},$$

$$\mathbf{N}_{i66}^{\mathbf{C}} = \frac{3\mathbf{C}_{\infty 11} - \mathbf{C}_{\infty 12}}{4\mathbf{C}_{\infty 11}}. \quad \text{(C1)}$$

All others terms are null.

In the case of diagonal permeability, permittivity, or thermal-conductivity tensors, the depolarizing tensors only

depend on the shape of the inclusion. For a cylindrical inclusion (along axis 3),

$$\mathbf{N}_i^{\boldsymbol{\mu}} = \mathbf{N}_i^{\boldsymbol{\epsilon}} = \mathbf{N}_i^{\mathbf{k}} = \begin{pmatrix} 1/2 & 0 & 0 \\ 0 & 1/2 & 0 \\ 0 & 0 & 0 \end{pmatrix}. \quad \text{(C2)}$$

APPENDIX D: DECOMPOSITION OF THE MACROSCOPIC FIELDS

The following proof is given in mechanics[22] but it can be generalized to magnetism, electricity, and thermics:

$$\langle {}^t\mathbf{B}_i^{\mathbf{C}} \cdot \mathbb{S}_i \rangle = \langle {}^t\mathbf{B}_i^{\mathbf{C}} \cdot \mathbb{S}_i^{\mathbf{C}} \rangle + \langle {}^t\mathbf{B}_i^{\mathbf{C}} \cdot (\mathbb{S}_i^{\boldsymbol{\mu}} + \mathbb{S}_i^{\boldsymbol{\epsilon}} + \mathbb{S}_i^{\mathbf{k}}) \rangle. \quad \text{(D1)}$$

Using Eq. (8) leads to

$$\langle {}^t\mathbf{B}_i^{\mathbf{C}} \cdot \mathbb{S}_i^{\mathbf{C}} \rangle = \langle {}^t\mathbf{B}_i^{\mathbf{C}} \cdot \mathbf{C}_i^{-1} \cdot \mathbb{T}_i \rangle, \quad \text{(D2)}$$

which is equal to

$$\langle {}^t\mathbf{B}_i^{\mathbf{C}} \cdot \mathbb{S}_i^{\mathbf{C}} \rangle = {}^t\langle \mathbb{T}_i \cdot \mathbf{C}_i^{-1} \cdot \mathbf{B}_i^{\mathbf{C}} \rangle \quad \text{(D3)}$$

because $\mathbb{T}_i$ and $\mathbf{C}_i$ are symmetric tensors.

Moreover, the Hill theorem[22] enables us to write

$$\langle \mathbb{T}_i \cdot \mathbf{C}_i^{-1} \cdot \mathbf{B}_i^{\mathbf{C}} \rangle = \langle \mathbb{T}_i \rangle \cdot \langle \mathbf{C}_i^{-1} \cdot \mathbf{B}_i^{\mathbf{C}} \rangle = \overline{\mathbb{T}} \cdot \overline{\mathbf{C}}^{-1} \quad \text{(D4)}$$

with $\overline{\mathbf{C}}$ as the effective stiffness tensor introduced in the purely mechanical problem [Eq. (40)]. Then coming back to Eq. (D3), we obtain

$$\langle {}^t\mathbf{B}_i^{\mathbf{C}} \cdot \mathbb{S}_i^{\mathbf{C}} \rangle = {}^t(\overline{\mathbb{T}} \cdot \overline{\mathbf{C}}^{-1}) = \overline{\mathbf{C}}^{-1} \cdot \overline{\mathbb{T}} \quad \text{(D5)}$$

because $\overline{\mathbb{T}}$ and $\overline{\mathbf{C}}$ are symmetric tensors. Additionnaly, $\overline{\mathbf{C}}^{-1} \cdot \overline{\mathbb{T}}$ is equal to $\overline{\mathbb{S}}^{\mathbf{C}}$ according to Eq. (41). We can conclude that $\langle {}^t\mathbf{B}_i^{\mathbf{C}} \cdot \mathbb{S}_i^{\mathbf{C}} \rangle = \overline{\mathbb{S}}^{\mathbf{C}}$.

Moreover, the first equation also verifies

$$\langle {}^t\mathbf{B}_i^{\mathbf{C}} \cdot \mathbb{S}_i \rangle = \langle {}^t\mathbf{B}_i^{\mathbf{C}} \rangle \cdot \langle \mathbb{S}_i \rangle = \overline{\mathbb{S}} \quad \text{(D6)}$$

because of the Hill theorem. Finally, the following equalities are obtained:

$$\overline{\mathbb{S}} = \overline{\mathbb{S}}^{\mathbf{C}} + \overline{\mathbb{S}}^{\boldsymbol{\mu}} + \overline{\mathbb{S}}^{\boldsymbol{\epsilon}} + \overline{\mathbb{S}}^{\mathbf{k}},$$

$$\overline{\mathbb{S}}^{\mathbf{C}} = \langle {}^t\mathbf{B}_i^{\mathbf{C}} \cdot \mathbb{S}_i^{\mathbf{C}} \rangle = \overline{\mathbf{C}}^{-1} \cdot \overline{\mathbb{T}} \neq \langle \mathbb{S}_i^{\mathbf{C}} \rangle,$$

$$\overline{\mathbb{S}}^{\boldsymbol{\mu}} = \langle {}^t\mathbf{B}_i^{\mathbf{C}} \cdot \mathbb{S}_i^{\boldsymbol{\mu}} \rangle \neq \langle \mathbb{S}_i^{\boldsymbol{\mu}} \rangle,$$

$$\overline{\mathbb{S}}^{\boldsymbol{\epsilon}} = \langle {}^t\mathbf{B}_i^{\mathbf{C}} \cdot \mathbb{S}_i^{\boldsymbol{\epsilon}} \rangle \neq \langle \mathbb{S}_i^{\boldsymbol{\epsilon}} \rangle,$$

$$\overline{\mathbb{S}}^{\mathbf{k}} = \langle {}^t\mathbf{B}_i^{\mathbf{C}} \cdot \mathbb{S}_i^{\mathbf{k}} \rangle \neq \langle \mathbb{S}_i^{\mathbf{k}} \rangle. \quad \text{(D7)}$$

APPENDIX E: GENERAL RESOLUTION SCHEME

We define hereafter the system of equations to be solved in the general case of a fully coupled n-phasic composite.[23] The set of unknowns consists of eight macroscopic (total) fields,

$$\overline{\mathbb{T}}, \quad \overline{\mathbb{B}}, \quad \overline{\mathbb{D}}, \quad \overline{\mathbb{J}},$$

$$\overline{\mathbb{S}}, \quad \overline{\mathbb{H}}, \quad \overline{\mathbb{E}}, \quad \overline{\mathbb{K}},$$

$8n$ local (total) fields,

$$\mathbb{T}_i, \quad \mathbb{B}_i, \quad \mathbb{D}_i, \quad \mathbb{J}_i,$$

$$\mathbb{S}_i, \quad \mathbb{H}_i, \quad \mathbb{E}_i, \quad \mathbb{K}_i,$$

$16n$ local decomposed fields,

$$\mathbb{S}_i^{\mathbf{C}}, \quad \mathbb{H}_i^{\mathbf{C}}, \quad \mathbb{E}_i^{\mathbf{C}}, \quad \mathbb{K}_i^{\mathbf{C}},$$

$$\mathbb{S}_i^{\boldsymbol{\mu}}, \quad \mathbb{H}_i^{\boldsymbol{\mu}}, \quad \mathbb{E}_i^{\boldsymbol{\mu}}, \quad \mathbb{K}_i^{\boldsymbol{\mu}},$$

$$\mathbb{S}_i^{\boldsymbol{\epsilon}}, \quad \mathbb{H}_i^{\boldsymbol{\epsilon}}, \quad \mathbb{E}_i^{\boldsymbol{\epsilon}}, \quad \mathbb{K}_i^{\boldsymbol{\epsilon}},$$

$$\mathbb{S}_i^{\mathbf{k}}, \quad \mathbb{H}_i^{\mathbf{k}}, \quad \mathbb{E}_i^{\mathbf{k}}, \quad \mathbb{K}_i^{\mathbf{k}}.$$

The system of equations is given by (i) macroscopic applied loadings: four equations involving the macroscopic (total) fields, (ii) macroscopic decomposition of the fields: 4 equations [obtained from Eqs. (42)–(45)],

$$\overline{\mathbb{S}} = \overline{\mathbf{C}}^{-1} \cdot \overline{\mathbb{T}} + \langle {}^t\mathbf{B}_i^{\mathbf{C}} \cdot \mathbb{S}_i^{\boldsymbol{\mu}} \rangle + \langle {}^t\mathbf{B}_i^{\mathbf{C}} \cdot \mathbb{S}_i^{\boldsymbol{\epsilon}} \rangle + \langle {}^t\mathbf{B}_i^{\mathbf{C}} \cdot \mathbb{S}_i^{\mathbf{k}} \rangle,$$

$$\overline{\mathbb{H}} = \langle {}^t\mathbf{B}_i^{\boldsymbol{\mu}} \cdot \mathbb{H}_i^{\mathbf{C}} \rangle + \overline{\boldsymbol{\mu}}^{-1} \overline{\mathbb{B}} + \langle {}^t\mathbf{B}_i^{\boldsymbol{\mu}} \cdot \mathbb{H}_i^{\boldsymbol{\epsilon}} \rangle + \langle {}^t\mathbf{B}_i^{\boldsymbol{\mu}} \cdot \mathbb{H}_i^{\mathbf{k}} \rangle,$$

$$\overline{\mathbb{E}} = \langle {}^t\mathbf{B}_i^{\boldsymbol{\epsilon}} \cdot \mathbb{E}_i^{\mathbf{C}} \rangle + \langle {}^t\mathbf{B}_i^{\boldsymbol{\epsilon}} \cdot \mathbb{E}_i^{\boldsymbol{\mu}} \rangle + \overline{\boldsymbol{\epsilon}}^{-1} \overline{\mathbb{D}} + \langle {}^t\mathbf{B}_i^{\boldsymbol{\epsilon}} \cdot \mathbb{E}_i^{\mathbf{k}} \rangle,$$

$$\overline{\mathbb{K}} = \langle {}^t\mathbf{B}_i^{\mathbf{k}} \cdot \mathbb{K}_i^{\mathbf{C}} \rangle + \langle {}^t\mathbf{B}_i^{\mathbf{k}} \cdot \mathbb{K}_i^{\boldsymbol{\mu}} \rangle + \langle {}^t\mathbf{B}_i^{\mathbf{k}} \cdot \mathbb{K}_i^{\boldsymbol{\epsilon}} \rangle + \overline{\mathbf{k}}^{-1} \overline{\mathbb{J}}, \quad \text{(E1)}$$

(iii) local decomposition of the fields: $4n$ equations [Eqs. (7), (11), (15), and (19)], uncoupled local constitutive laws: $4n$ equations [Eqs. (8), (12), (16), and (20)], (iv) local coupling relations: $12n$ equations [Eqs. (10), (14), (18), and (22)], (v) localization relations: $4n$ equations [Eq. (46)]. We then obtain a linear system of $24n+8$ equations with $24n+8$ unknowns. The 16 macroscopic decomposed fields can be obtained *a posteriori* from Eqs. (42)–(45).

*romain.corcolle@supelec.fr
†laurent.daniel@supelec.fr
‡frederic.bouillault@supelec.fr

[1] IEEE Trans. Ultrason. Ferroelectr. Freq. Control **43** (5), 717 (1996).
[2] R. L. Goldberg, M. J. Jurgens, D. M. Mills, C. S. Henriquez, D. Vaughan, and S. W. Smith, IEEE Trans. Ultrason. Ferroelectr. Freq. Control **44**, 1204 (1997).
[3] M. Besbes, Z. Ren, and A. Razek, IEEE Trans. Magn. **32**, 1058 (1996).

[4] J. Lee, J. G. Boyd IV, and D. C. Lagoudas, Int. J. Eng. Sci. **43**, 790 (2005).
[5] N. Galopin, X. Mininger, F. Bouillault, and L. Daniel, IEEE Trans. Magn. **44**, 834 (2008).
[6] J. E. Huber, N. A. Fleck, C. M. Landis, and R. M. McMeeking, J. Mech. Phys. Solids **47**, 1663 (1999).
[7] C.-W. Nan and G. J. Weng, Phys. Rev. B **61**, 258 (2000).
[8] A. Haug, J. E. Huber, P. R. Onck, and E. Van der Giessen, J. Mech. Phys. Solids **55**, 648 (2007).
[9] C.-W. Nan and G. J. Weng, Phys. Rev. B **60**, 6723 (1999).
[10] R. Corcolle, L. Daniel, and F. Bouillault, IEEE Trans. Magn. **44**, 17 (2008).
[11] C.-W. Nan, Phys. Rev. B **50**, 6082 (1994).
[12] J. Y. Li and M. L. Dunn, Mech. Mater. **31**, 149 (1999).
[13] J. H. Huang, Y.-H. Chiu, and H.-K. Liu, J. Appl. Phys. **83**, 5364 (1998).
[14] R. Hill, J. Mech. Phys. Solids **13**, 89 (1965).
[15] J. W. Hutchinson, Proc. R. Soc. London, Ser. A **319**, 247 (1970).
[16] G. W. Milton, *The Theory of Composites* (Cambridge University Press, New York, 2001).
[17] M. Bornert, T. Bretheau, and P. Gilormini, *Homogenization in Mechanics of Materials* (Iste, London, 2008).
[18] L. Daniel and R. Corcolle, IEEE Trans. Magn. **43**, 3153 (2007).
[19] M. Avellaneda and G. Harshe, J. Intell. Mater. Syst. Struct. **5**, 501 (1994).
[20] C.-W. Nan, M. Li, X. Feng, and S. Yu, Appl. Phys. Lett. **78**, 2527 (2001).
[21] T. Mura, *Micromechanics of defects in solids* (Martinus Nijhoff, Boston, 1982).
[22] D. François, A. Pineau, and A. Zaoui, *Mechanical Behavior of Materials: Elasticity and Plasticity* (Kluwer, Norwell, 1998).
[23] The corresponding MATLAB routines can be obtained on request.

2.1.2 Modélisation par éléments finis *

Mon arrivée au LGEP, au sein d'une équipe investie de longue date dans le développement d'outils de simulation numérique pour l'électromagnétisme, m'a également conduit à m'impliquer dans des travaux de modélisation par éléments finis. En effet, si les méthodes numériques pour l'électromagnétisme ont beaucoup évolué ces dernières dizaines d'années, les lois de comportement qui alimentent ces outils de modélisation restent encore assez souvent relativement rudimentaire. En particulier, la prise en compte de la forte non-linéarité des comportements magnétique et magnétostrictif reste un sujet d'étude stimulant.

Nous nous sommes particulièrement intéressés au cas des matériaux magnéto-électriques composites [35]. Ces matériaux composites sont constitués d'une phase piézoélectrique et d'une phase magnétostrictive (voir les exemples de la figure 2.2). Une phase supplémentaire est parfois ajoutée en vue d'optimiser les propriétés mécaniques de l'ensemble. Ces matériaux composites sont le siège d'un effet de couplage magnéto-électrique, lié à des effets d'incompatibilité élastique. On peut décrire qualitativement l'effet magnéto-électrique direct de la manière suivante : plongé dans un champ magnétique, le matériau magnétostrictif se déforme. Il transmet cette déformation à la phase piézoélectrique, qui se polarise. Ce principe permet notamment la fabrication de capteurs de champ de grande sensibilité [36]. L'effet inverse peut également être utilisé pour piloter la perméabilité de la phase magnétostrictive en appliquant un champ électrique à la phase piézoélectrique. Ce principe permet notamment la fabrication d'inductances variables [37].

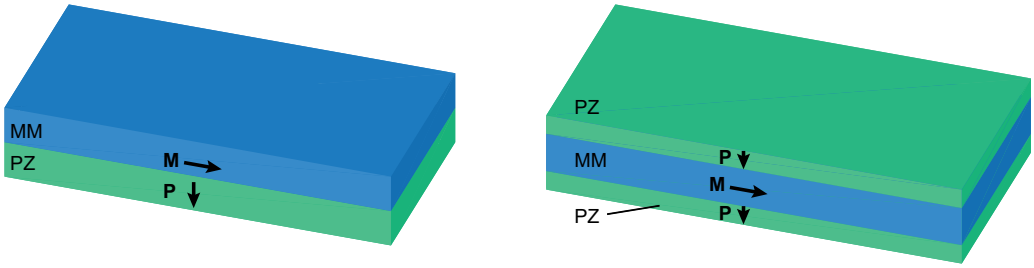

FIGURE 2.2 – Deux configurations classiques, bilame et multicouche, de matériaux magnéto-électriques composites (PZ : phase piézoélectrique, MM : phase magnétostrictive).

Nous avons tout d'abord cherché à proposer une modélisation de ces dispositifs composites magnéto-électriques en régime statique. Ces résultats sont présentés dans la publication [38] jointe ci-après. Ils ont notamment permis la comparaison, dans des configurations simples correspondant à la figure 2.2 des résultats numériques et de résultats analytiques. Dans un deuxième temps nous nous sommes intéressés au comportement des capteurs magnéto-électriques en régime harmonique. En effet, ces capteurs de champ magnétique sont en général soumis à un champ alternatif de faible amplitude superposé au champ statique à mesurer. Lorsque la fréquence de ce champ alternatif est placée à la fréquence de résonance mécanique du capteur, on observe une nette augmentation du coefficient de conversion magnéto-électrique (défini comme le rapport de la tension mesurée aux bornes de la phase piézoélectrique avec le champ magnétique mesuré). Nous avons proposé une méthode de modélisation pour ce type de sollicitation et montré que l'augmentation du coefficient magnéto-électrique à la résonance est directement lié à la non-linéarité des comportements magnétique et magnétostrictif. Ces résultats sont présentés dans la publication [39] ci-après.

Publications jointes

[RI.13,38] : N. Galopin, X. Mininger, F. Bouillault, L. Daniel, "Finite element modelling of magneto-electric sensors", *IEEE Transactions on Magnetics*, **44(6)** :834-837, 2008.

[RI.28,39] : T.T. Nguyen, F. Bouillault, L. Daniel, X. Mininger, "Finite element modeling of magnetic field sensors based on nonlinear magnetoelectric effect", *Journal of Applied Physics*, **109(8)** :084904, 2011.

∗. Les travaux présentés dans ce chapitre ont pour l'essentiel été menés dans le cadre des thèses de Nicolas Galopin [33] et Thu Trang Nguyen [34].

Finite Element Modeling of Magnetoelectric Sensors

Nicolas Galopin, Xavier Mininger, Frédéric Bouillault, and Laurent Daniel

Laboratoire de Génie Électrique de Paris, CNRS UMR 8507; SUPELEC; Univ Paris-Sud; UPMC Univ Paris 06; Plateau de Moulon, 91192 Gif-sur-Yvette Cedex, France

The magnetoelectric effect, stemming from piezoelectric and magnetostrictive materials composite, is studied. A model based on the association of magnetoelastic and piezo-electric constitutive laws is presented. This model is implemented in a finite element formulation and a comparison with analytical solutions for piezoelectric/magnetostrictive composite is realized. A magnetoelectric displacement sensor is finally studied.

***Index Terms*—Finite element formulation, magnetoelectric sensors, magnetostriction, piezoelectric.**

I. Introduction

SMART materials such as magnetostrictive (MM) and piezoelectric (PM) materials are usually used in a wide range of electromechanical systems. The strong coupling between electromagnetic and mechanical properties in this type of materials enables to control electric or magnetic (respectively mechanical) behavior by mechanical (respectively electric or magnetic) quantities. These materials are commonly employed separately but they can also be used together in a composite design. The presence of a magnetic field within a MM generates a magnetostriction strain, that transmitted to a PM, is associated to an electric polarization. Conversely, an electric field in a PM can create a modification of magnetization in a MM. This effect is called "magnetoelectric" effect.

Analytical studies of this effect, considering small variations of the fields, with MM/PM laminate composites as well as conception of such structures have been proposed [1][2]. The design of a novel generation of smart systems using this effect needs models describing accurately their behavior associated to robust modeling tools for solving coupled problems, in order to optimize efficiently such structures.

A magnetoelastic model built from a thermodynamical approach is presented. It is based on nonlinear constitutive laws which present the mutual interaction between magnetic and elastic properties. Piezoelectric constitutive laws, in the linear assumptions, are detailed. From the minimization of functional energy, finite element formulation of the magnetoelastic and electroelastic problems are established. Specific considerations allow to establish finite element formulation of magnetoelectric problem. Validation of the formulation is realized with comparison of analytical solutions of two MM/PM composite structures. Finally, study of a magnetoelectric displacement sensor is achieved.

II. Magnetoelectric Modeling

The behavior of active materials, when losses are neglected, is given by the knowledge of the dependence of the electric flux density d and the stress tensor σ on the electric field e and the strain tensor s for PM, and of the magnetic field h and the stress σ on the magnetic flux density b and the strain s for MM

$$\sigma(e,s) \qquad d(e,s) \tag{1}$$

$$\sigma(b,s) \qquad h(b,s). \tag{2}$$

The definition of expressions (1) and (2) requires the use of piezoelectric coefficients α [3] as well as piezomagnetic coefficients γ [4]

$$\alpha_{ikl} = \frac{\partial d_i}{\partial s_{kl}} = -\frac{\partial \sigma_{kl}}{\partial e_i} \tag{3}$$

$$\gamma_{ikl} = \frac{\partial h_i}{\partial s_{kl}} = \frac{\partial \sigma_{kl}}{\partial b_i}. \tag{4}$$

A. Electroelastic Behavior

PM are usually used around a polarization point. In this case, all the material parameters are constant and the behavior is taken linear. A simple integration of the piezoelectric coefficients (3) gives the following expression [3] of the electroelastic behavior:

$$\begin{aligned} \sigma_{ij}(e,s) &= C^e_{ijkl}\, s_{kl} - \alpha^t_{kij}\, e_k \\ d_i(e,s) &= \alpha_{ikl}\, s_{kl} + \varepsilon^s_{ij}\, e_j \end{aligned} \tag{5}$$

where C^e and ε^s are respectively the stiffness tensor at constant electric field and the electrical permittivity at constant strain. In linear piezoelectricity, the equations of linear elasticity are coupled to the charge equation of electrostatics by the mean of the piezoelectric coefficients.

B. Magnetoelastic Behavior

The magnetostrictive behavior is highly non linear, and this non linearity has to be considered in the magnetoelastic constitutive laws. The mechanical behavior law is written in the framework of linear elasticity, using the decomposition of total strain into elastic strain s^e and magnetostriction strain s^μ, $s_{kl} = s^e_{kl} + s^\mu_{kl}$ [5]. Besides, magnetostriction strain induced by a magnetic field is assumed to depend only on the magnetic flux density. With these assumptions Hooke's law is expressed as follows:

$$\sigma_{ij}(b,s) = C_{ijkl}(s_{kl} - s^\mu_{kl}(b)) \tag{6}$$

with s_{kl} the total strain tensor and C_{ijkl} the usual stiffness tensor defined, in the case of isotropic material, by

$$C_{ijkl} = \frac{E^*}{1+\nu^*}\left(\frac{\nu^*}{1-2\nu^*}\delta_{kl}\delta_{ij} + \frac{1}{2}(\delta_{ik}\delta_{jl}+\delta_{il}\delta_{jk})\right) \tag{7}$$

Digital Object Identifier 10.1109/TMAG.2008.915781

Color versions of one or more of the figures in this paper are available online at http://ieeexplore.ieee.org.

where E^*, ν^* and δ are respectively Young's modulus, Poisson's ratio and the Kronecker's symbol.

From the definition of the piezomagnetic coefficients (4), integration of both terms between s^μ and s enables to express the magnetic behavior law $h(b,s)$. This law can be written by introducing a coercive magnetic field h^c which describes the effect of an applied stress

$$\begin{aligned} h_i(b,s) &= h_i^0(b,s^\mu) - C_{klnp}\frac{\partial s_{np}^\mu(b)}{\partial b_i}(s_{kl} - s_{kl}^\mu) \\ &= h_i^0(b,s^\mu) - h_i^c(b,s) \end{aligned} \tag{8}$$

$h_i^c(b,s)$ is the magnetic field induced along i axis by stress at given magnetic flux density and $h_i^0(b,s^\mu)$ is the magnetic field at free stress depending only on magnetic flux density.

C. Magnetostriction Strain Model

The magnetostriction strain tensor $(s_{//}^\mu, s_{\perp_1}^\mu, s_{\perp_2}^\mu)$ is expressed in the reference frame of the magnetic induction. The component $s_{//}^\mu$ can be approximated as a polynomial function versus the magnetic flux density [6]. Besides, assuming magnetostriction phenomena isochore and isotropic, the magnetostriction strain tensor can be expressed in the reference frame of the magnetic induction $(b_{//}, b_{\perp_1}, b_{\perp_2})$:

$$s_{//}^\mu = \sum_{n=0}^{N} \beta_n b^{2(n+1)} \quad s_{\perp_1}^\mu(b) = s_{\perp_2}^\mu(b) = -\frac{s_{//}^\mu}{2}. \tag{9}$$

To take into account the magnetic flux density distribution, the magnetostriction strain tensor in the material frame is given by the following indicial form:

$$s_{kl}^\mu(b) = \frac{1}{2}\sum_{n=0}^{N} \beta_n\, b^{2n}(3b_k b_l - \delta_{kl} b^2). \tag{10}$$

From the expression of the magnetostriction strain tensor, the coercive magnetic field (8) can be expressed as the product of an 'equivalent' reluctivity tensor with the magnetic flux density

$$h_i^c(b,s) = \nu_{ij}^c(b,s) b_j. \tag{11}$$

Due to the applied stress, the 'equivalent' reluctivity tensor is anisotropic. Its expression can be found in [6]. A reasonable first approximation for the magnetostriction strain tensor can be obtained by neglecting the terms up to $N = 1$.

III. Finite Element Formulation

A. Magnetoelastic Problem

In the static case, the finite element formulation integrating the magnetostrictive phenomena can be established from a minimization of the functional energy E in terms of b and s:

$$E(b,s) = W(b,s) - T \tag{12}$$

where $W(b,s)$ and T are respectively the magnetoelastic energy and the work of magnetic and mechanical sources, defined by

$$W(b,s) = \int_{\Omega_T}\left(\int_0^b h^0(b',s^\mu)db' + \int_{s^\mu}^{s}\sigma(b,s')ds'\right)d\Omega_T \tag{13}$$

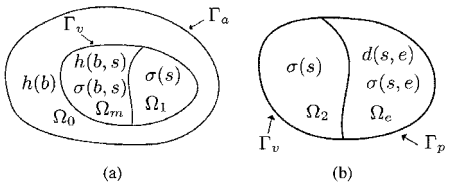

Fig. 1. The studied domains.

$$\begin{aligned} T = &\int_{\Omega_T} a\cdot j\, d\Omega + \int_{\Gamma_h} a\cdot(h\times n)\, d\Gamma_h \\ &+ \int_{\Omega_M} u\cdot f^\Omega\, d\Omega + \int_{\Gamma_\sigma} u\cdot(\sigma\cdot n)\, d\Gamma_\sigma \end{aligned} \tag{14}$$

with a the magnetic vector potential, u the vector displacement, j the current density, f^Ω the volume force density and n the normal vector. Boundary conditions associated to the magnetomechanical problem are of two types

$$\begin{aligned} h\times n = 0 \quad &\text{on} \quad \Gamma_h \qquad \sigma\cdot n = f^\Gamma \ \text{on} \quad \Gamma_\sigma \\ b\cdot n = 0 \quad &\text{on} \quad \Gamma_b \qquad u = 0 \quad \text{on} \quad \Gamma_u \end{aligned}$$

where $\Gamma_a = \Gamma_h \cup \Gamma_b$ and $\Gamma_v = \Gamma_\sigma \cup \Gamma_u$ are the boundaries of the study domains defined by $\Omega_T = \Omega_M \cup \Omega_0$ and $\Omega_M = \Omega_m \cup \Omega_1$ [Fig. 1(a)]. f^Γ is associated to surface force densities.

Application of variational principles, gives the following magnetic and mechanical formulation associated to arbitrary variations δ_a and δ_u:

$$\begin{aligned} &\int_{\Omega_T} \nabla\times\delta_a[\nu]\nabla\times a\, d\Omega_T + \int_{\Gamma_h}\delta_a\cdot(h\times n)d\Gamma_h \\ &\quad = \int_{\Omega_m} \nabla\times\delta_a\cdot h^c(b,s)\, d\Omega_T + \int_{\Omega_T}\delta_a\cdot j\, d\Omega_T \end{aligned} \tag{15}$$

$$\begin{aligned} &\int_{\Omega_1} s(\delta_u)[C]s\, d\Omega + \partial_u\left(\frac{1}{2}\int_{\Omega_T}\left(\int_0^b h^0(b',s^\mu)db'\right)d\Omega_T\right) \\ &\quad = \int_{\Omega_m} s(\delta_u)[C]s^\mu d\Omega + \int_{\Omega_m}\delta_u\cdot f^\Omega\, d\Omega + \int_{\Gamma_\sigma}\delta_u\cdot f^\Gamma d\Gamma_\sigma. \end{aligned} \tag{16}$$

The magnetic vector potential is discretized using edge and nodal elements, respectively in 3D and 2D cases, while the displacement vector is discretized with nodal elements. From this discretization, the algebraic equation system is defined by

$$\begin{aligned} [M](a) &= (J) + (J^c(b,s)) \\ [K](u) &= (F^\sigma) + (F^{mf}(b)) + (F^\mu(b)). \end{aligned} \tag{17}$$

The right-hand side of each equation (17) can be interpreted as a coercive current density J^C representing the effect of an applied stress and the 'equivalent' nodal magnetostriction forces F^μ resulting from an applied magnetic field. F^{mf} are the nodal magnetic forces determined by the local derivative of magnetic energy [7]. The obtained algebraic system is nonlinear. It can be solved by an iterative procedure based on fixed point algorithm, where the nonlinearity due to magnetic properties and magnetostriction effects is placed at the right-hand side of each equation. In this case, the magnetic $[M]$ and mechanical $[K]$ rigidity matrices are calculated only at the first iteration.

B. Electroelastic Problem

Electromechanical problem in the static condition can be defined, in a similar way, by minimization of a functional energy. This one, integrating piezoelectric phenomena, leads to solve the following equality of the electrical and mechanical problems associated to the variations $\delta\varphi$ and δu [8] [see (18) and (19)]

$$\int_{\Omega_e} \nabla\delta\varphi\,[\alpha]\,s\,d\Omega_p - \int_{\Omega_e} \nabla\delta\varphi\,[\varepsilon]\,\nabla\varphi\,d\Omega_p = \int_{\Gamma_d} \delta\varphi\,(d\cdot n)\,d\Gamma_p \tag{18}$$

$$\int_{\Omega_2} s(\delta u)\,[C]\,s\,d\Omega_p + \int_{\Omega_e} s(\delta u)\,[\alpha]^t\,\nabla\varphi\,d\Omega_p - \int_{\Omega_p} \cdot\delta u\cdot f^{\Omega}\,d\Omega_p - \int_{\Gamma_\sigma} \delta u\cdot f^{\Gamma}\,d\Gamma_\sigma = 0. \tag{19}$$

Boundary conditions relative to the electroelastic problem, where $\Omega_p = \Omega_e \cup \Omega_2$ and $\Gamma_p = \Gamma_d \cup \Gamma_e$ [Fig. 1(b)], are defined by

$$e\times n = 0 \quad \text{on} \quad \Gamma_e \qquad d\cdot n = 0 \ \text{ on } \ \Gamma_d$$
$$\sigma\cdot n = f^{\Gamma} \ \text{ on } \ \Gamma_\sigma \qquad u = 0 \ \text{ on } \ \Gamma_u.$$

After discretisation with nodal elements, the algebraic equation system relative to the electroelastic problem is

$$\begin{bmatrix} [K_{uu}] & [K_{u\phi}] \\ -[K_{u\phi}]^t & [K_{\phi\phi}] \end{bmatrix} \begin{pmatrix} u \\ \phi \end{pmatrix} = \begin{pmatrix} F \\ Q \end{pmatrix} \tag{20}$$

with ϕ the electric potential and Q the vector of the nodal electric charges. F can be taken equal to the external forces F^{σ}. For piezoelectric material the electrostatic forces, due to the form effect, can be neglected.

C. Magnetoelectric Problem

The sensor configuration of the piezoelectric materials is a particular case. In this situation, the total electrical charge Q can be considered equal to zero. The second equation of (20) is simplified and it is possible to write

$$(\phi) = [K_{\phi\phi}]^{-1}[K_{u\phi}]^t(u) \tag{21}$$
$$[K] = [K_{uu}] + [K_{u\phi}][K_{\phi\phi}]^{-1}[K_{u\phi}]^t. \tag{22}$$

Equation (22) gives, for the piezoelectric material, the effect of an equivalent piezoelectric stiffness induced by electric potentials on the sensor electrodes. It allows to consider the influence of the inverse piezoelectric effect in the global structure rigidity matrix during the mechanical resolution of a magnetomechanical problem. The rigidity matrix associated to piezoelectric material has to be modified considering (22) in the mechanical equation of the magnetomechanical problem (17). Consequently, magnetoelectromechanical problems are coupled into a single magnetomechanical code. Electrostatic potential is obtained after convergence of the magnetomechanical problem by use of (21).

IV. Model Validation

In order to validate the formulation, let us first consider two composite structures. The first one is a MM/PM bilayer [Fig. 2(a)], respectively of FeCo and PZT materials, while the second is a multilayer with one MM and two PM with the same materials [Fig. 2(b)].

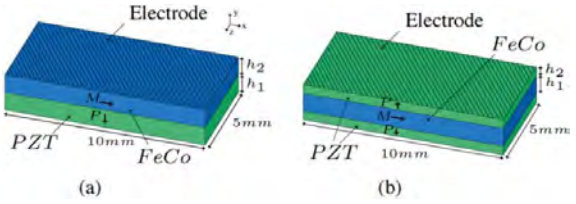

Fig. 2. Two configurations of MM/PM composite.

A. Analytical Solution

To obtain an analytical solution, some considerations are required. First, one dimension (along x axis) is significantly longer than the others, second, *Kirchhoff* assumption is used. Moreover, the volume of PM and MM are assumed identical (see Fig. 2). This gives the following composite strain expression versus y distance:

$$s(y) = s_0 - \frac{y}{r} \tag{23}$$

where s_0 is the mid plane strain and r the composite curvature. From the mechanical balance equations, forces and moments, equations closing PM strain to MM strain relative to the multilayer (24) and the bilayer (25) are defined by

$$\frac{s^{pzt}}{s^{\mu}} = \frac{E_1}{E_1 + E_2} \tag{24}$$
$$\frac{s^{pzt}}{s^{\mu}} = \frac{E_1(E_1 + E_2)}{E_1^2 + E_2^2 + 14E_1E_2} \tag{25}$$

where E_1 and E_2 are respectively the Young's modulus of the PM and MM. From the knowledge of strains, electric potential is deduced. To obtain these results, the inverse piezoelectric effect is neglected.

B. Comparison of Analytical and Numerical Solutions

PM and MM are made respectively of EB10 ceramic and FeCo ferromagnetic material. It appears that the electric potential (Fig. 3) is higher for the multilayer than for the bilayer, considering the same quantities of piezoelectric material in the two structures. Besides, it can be shown that the ratio between electric potential of the bilayer (V_b) and the multilayer (V_t), for the analytical and numerical solutions, are respectively of $V_b/V_t = 0.295$ and $V_b/V_t = 0.3$. Analytical and numerical solutions are in good agreement.

V. Magnetoelectric Displacements Sensor

Taking the MM/MP multilayer as a basis, design of novel smart material structures is possible. One of these, which will be taken as an example, is a magnetoelectric displacements sensor [9], intended to detect the displacement of ferromagnetic objects. This sensor is constituted of a laminate composite associated to two iron yokes and a permanent magnet (Fig. 4). The laminate composite is a MM plate bonded with two PM plates. Magnetic orientation and electric polarization are orthogonal, as indicated in Fig. 4. Both sides of the composite are stuck (not

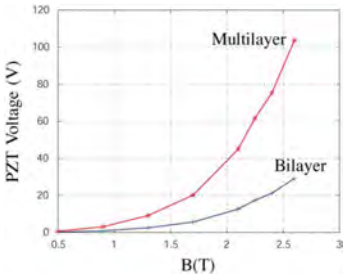

Fig. 3. Electric potential versus magnetic flux density.

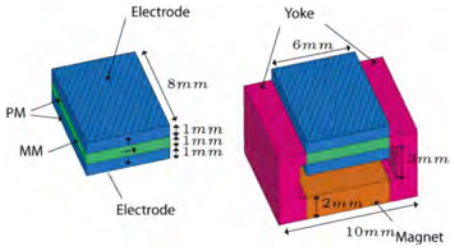

Fig. 4. Magnetoelectric displacements sensors.

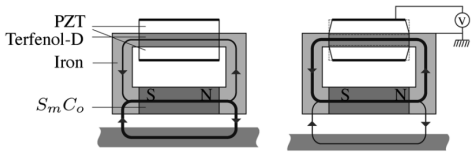

Fig. 5. Magnetic flux distribution (left) and its change with ferromagnetic plate displacement (right).

bonded) to the iron yokes with magnetic forces via flux path. In this structure, small part of the magnetic flux is derived between the mobile ferromagnetic plate and the MM (Terfenol-D). Thereafter, small variations of the air gap change the magnetic flux inside the MM, which is associated to magnetostriction strain variation. This strain is then responsible for an electric field. Thus, the magnetoelectric device converts the displacement into a voltage on the electrodes (Fig. 5). The multilayer composite has advantage to reduce bending deformation due to magnetostriction.

We intend to study the sensitivity of the sensor linked to the air gap variations. For that, in a first time MM is considered at free stress. Due to the magnetic flux distribution, electric potential are not equal into the two PM [Fig. 6(a)]. A small bending effect is present. In comparison with the experimental results, sensitivity of the lower PM is in good adequacy [Fig. 6(b)]. Differences are observed for the small air gaps. If the Terfenol-D is pre-stressed, magnetostriction strain developed is more important [6]. If we consider that, with an external set, the Terfenol-D layer of the sensor can be pre-stressed, it results in an increase of the electric potential [Fig. 6(a)] and a higher sensitivity of the sensor [Fig. 6(b)].

This analysis allows a good description of the operating mode of the sensor, and the developed model can be useful for design and optimization of new structures.

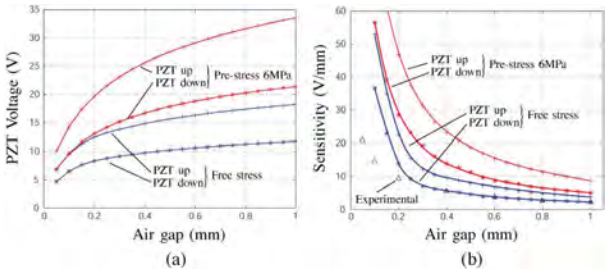

Fig. 6. Response of the magnetoelectric displacements sensor.

VI. Conclusion

A finite element model has been developed in order to study the magnetoelectric effect, stemming from magnetostrictive and piezoelectric materials composite. Standard piezoelectric behavior laws are considered, while the coupling of magnetic and elastic properties is ensured by nonlinear constitutive laws. Specific considerations allow a coupling between the magnetoelastic and the electroelastic problems, such that only the resolution of a magnetoelastic problem is necessary. To validate the approach, a comparison between analytical and numerical solutions of multilayers is globally satisfactory. Finally this model is successfully used to analyze a new device of magnetoelectric displacement sensor, based on the variations of the electric potential due to air gap changes. Some discrepancies are observed with experimental results. They may be due to the imperfect definition of mechanical boundary conditions. The properties of the permanent magnet may also not be identical to the experimental device and the influence of the PM sticking with the MM has not been taken into account.

References

[1] S. Dong, J. F. Li, and D. Viehland, "Longitudinal and transversal magnetoelectric voltage coefficients of magnetostrictive/piezoelectric laminate composite: Theory," *IEEE Trans. Ultrason., Ferroelect., Freq. Contr.*, vol. 50, no. 10, pp. 1253–1261, Oct. 2003.

[2] S. Dong, J. F. Li, and D. Viehland, "Longitudinal and transversal magnetoelectric voltage coefficients of magnetostrictive/piezoelectric laminate composite: Experiments," *IEEE Trans. Ultrason., Ferroelect., Freq. Contr.*, vol. 51, no. 7, pp. 793–798, 2004.

[3] IEEE Standard on Piezoelectricity 1988, ANSI/IEEE Std. 176-1987.

[4] M. Besbes, Z. Ren, and A. Razek, "A generalized finite element model of magnetostriction phenomenas," *IEEE Trans. Magn.*, vol. 37, no. 5, pp. 3324–3328, 2001.

[5] L. Hirsinger and R. Billardon, "Magneto-elastic finite element analysis including magnetic forces and magnetostriction effects," *IEEE Trans. Magn.*, vol. 31, no. 3, pp. 1877–1880, May 1995.

[6] K. Azoum, M. Besbes, F. Bouillault, and T. Ueno, "Modeling of magnetostrictive phenomena. application in magnetic force control," *Eur. Phys. J. Appl. Phys.*, vol. 36, no. 1, pp. 43–47, Oct. 2006.

[7] Z. Ren and A. Razek, "Local force computation in deformable bodies using edge elements," *IEEE Trans. Magn.*, vol. 28, no. 2, pp. 1212–1215, 1992.

[8] H. F. Tiersten, "Hamilton's principle for linear piezoelectric media," *IEEE Proc. Lett.*, vol. 55, no. 8, pp. 1523–1524, Aug. 1967.

[9] T. Ueno and T. Higuchi, "Magnetic sensor for high temperature using a laminate composite of magnetostrictive material and piezoelectric material," *SPIE Smart. Str. Mat.*, vol. 5761, pp. 156–163, May 2005.

Manuscript received June 24, 2007; revised October 24, 2007. Corresponding author: N. Galopin (e-mail: nicolas.galopin@lgep.supelec.fr).

JOURNAL OF APPLIED PHYSICS **109**, 084904 (2011)

Finite element modeling of magnetic field sensors based on nonlinear magnetoelectric effect

Thu Trang Nguyen,[a] Frédéric Bouillault, Laurent Daniel, and Xavier Mininger
Laboratoire de Génie Electrique de Paris, CNRS UMR8507; SUPELEC; UPMC; University Paris-Sud, 11 Rue Joliot-Curie, Plateau de Moulon, 91192 Gif-sur-Yvette Cedex, France

(Received 2 August 2010; accepted 7 January 2011; published online 21 April 2011)

Magnetoelectric effect in composite materials results from the combination of piezoelectric and magnetostrictive effects. This paper focuses on the development of a harmonic finite element formulation for such coupled problems, taking into account the nonlinearity of magnetostrictive behavior. An application to a magnetic sensor operating under dynamic excitation is presented in order to illustrate the formulation. The enhancement of the magnetoelectric coefficient when a low amplitude harmonic field is superimposed to the static field to be measured is shown to be related to the nonlinearity of magnetic and magnetostrictive behavior. © *2011 American Institute of Physics*. [doi:10.1063/1.3553855]

I. INTRODUCTION

Magnetoelectricity consists in the coupling between magnetic and electric fields even under static conditions.[1] The magnetoelectric (ME) effect can be either intrinsic, in single phase materials, or extrinsic, in composite materials. Up to now, the highest magnetoelectric coefficients have been observed for extrinsic ME effect. We consider here only the extrinsic effect resulting from the combination of magnetostrictive and piezoelectric effects. In composite materials, this ME effect can be written in a simple way either in the form of Eqs. (1) and (2):[2]

$$\mathrm{ME}_1 = \frac{\text{electrical}}{\text{mechanical}} \cdot \frac{\text{mechanical}}{\text{magnetic}}, \tag{1}$$

$$\mathrm{ME}_2 = \frac{\text{magnetic}}{\text{mechanical}} \cdot \frac{\text{mechanical}}{\text{electrical}}. \tag{2}$$

Recently, research activities on ME composite materials have increased rapidly,[1,3] but numerical approaches are still limited due to the lack of a complete theoretical formulation. A unified formulation is required to deal with nonlinearity and frequency dependence of the ME effect. Up to now, several numerical models have been developed: The frequency effect is integrated in the linear model of Liu *et al.*,[4] but only from the mechanical point of view, and the model of Galopin *et al.*[5] takes into account the nonlinear behavior of the magnetostrictive phase, but only under quasistatic loadings. Recently, a nonlinear dynamic scalar formulation has been proposed.[6]

The objective of this paper is to build a numerical vector model based on the finite element method, accounting for nonlinearities of both magnetostrictive and magnetic behavior. Magnetostriction is described as a quadratic function of magnetization. Constitutive laws coupling mechanical/electric/magnetic effects are first detailed, and then introduced into a finite element formulation. An application to the modeling of a ME sensor under different configurations is finally proposed. For such an application, it has been observed that the sensor sensitivity is enhanced when a harmonic field at the resonance frequency is superimposed to the static field to be measured.[7,8] The work reported in this paper proves that this enhanced sensitivity is directly related to the nonlinearity of magnetic and magnetostrictive behavior.

II. EQUILIBRIUM EQUATIONS

The variables used in the model are the stress tensor **T,** the strain tensor **S,** the displacement **u,** the volumic force **f,** the mass density ρ_m, the electric field **E,** the electric flux density **D,** the electrical voltage V, the charge density ρ, the electric conductivity σ, the magnetic field **H,** the magnetic induction **B,** the magnetic vector potential **a,** and the current density **J.** For a vector **X,** we note x_i the components of **X.**

A. Mechanical equilibrium

The mechanical equilibrium is given by

$$\operatorname{div}\mathbf{T} + \mathbf{f} = \rho_m \frac{\partial^2 \mathbf{u}}{\partial t^2}. \tag{3}$$

Noting $\mathbf{S}^e$ the elastic strain, we consider a 2D problem with plane stress conditions ($t_{31} = t_{32} = t_{33} = 0$) leading to the following relations:

$$\begin{aligned} s^e_{31} &= s^e_{32} = 0 \\ s^e_{33} &= \frac{\lambda^*}{2\mu^* + \lambda^*}\left(s^e_{11} + s^e_{22}\right). \end{aligned} \tag{4}$$

As s^e_{33} can be calculated afterwards, we only have to consider the mechanical strains in the working plane. In the finite element form, the mechanical variable chosen is then the displacement **u** in the working plane:

$$\mathbf{S} = \frac{1}{2}\left(\mathbf{grad}\,\mathbf{u} + \mathbf{grad}^{\mathrm{t}}\,\mathbf{u}\right) = D\mathbf{u}. \tag{5}$$

[a]Author to whom correspondence should be addressed. Electronic mail: thutrang.nguyen@supelec.fr.

B. Electromagnetic equilibrium

The electromagnetic equations are given by the standard magnetodynamic Maxwell's equations (neglecting the displacement currents):

$$\mathbf{curl}(\mathbf{H}) = \mathbf{J}, \tag{6}$$

$$\mathrm{div}\,\mathbf{D} = \rho, \tag{7}$$

$$\mathrm{div}\,\mathbf{B} = 0. \tag{8}$$

Moreover, at the frequencies and geometry considered in this paper (see Sec. V), eddy currents can be neglected because the skin depth calculated from analytical equation is much higher than the usual depth of magnetostrictive layers.[6] From Eq. (8), magnetic induction **B** can be written as: $\mathbf{B} = \mathbf{curl}(\mathbf{a})$, where **a** is the magnetic vector potential.

We consider a 2D problem with the following assumptions: Neither magnetic induction **B**, nor electric field **E**, are considered in the direction perpendicular to the working plane (z direction). Moreover, **B** and **E** are assumed to be invariant with z. These assumptions lead to the following simplifications.

(i) The magnetic vector potential is along the z direction and independent of z ($a_1 = a_2 = 0$).
(ii) The electric field in the working plane $E_{//}$ can be written: $\mathbf{E}_{//} = \mathbf{grad}\,V(x,y)$.

The electric voltage V and the magnetic vector potential along the z direction a_3 are chosen as the electromagnetic variables in the finite element formulation.

III. FINITE ELEMENT FORMULATION

Finite element method (FEM) is one of the most widespread tools used to solve the partial differential equations such as the given equilibrium equations (3), (6), and (7). The FEM is usually associated with the variational methods or residual methods. The variational method for such a coupled problem has been presented by Galopin *et al.*[5] by minimizing the energy function. The residual methods directly solve the equilibrium equations. It is an advantage compared to the variational methods, especially under harmonic loadings when the energy functions are not easy to determine. In this paper, a particular residual method—the Galerkin method—is chosen to establish the 2D finite element formulation. This formulation is well suited to our electro-magneto-elastic coupled problem. The constitutive law in the coupled problem can be written in the generic matrix form of the following equation [the caret denotes the use of Voigt notation (see Appendix A)]:

$$\begin{pmatrix} \hat{\mathbf{T}} \\ \mathbf{D} \\ \mathbf{H} \end{pmatrix} = \begin{bmatrix} \hat{\mathbb{c}} & -\hat{\mathbb{e}}^{\mathrm{t}} & -\hat{\mathbb{q}}^{\mathrm{t}} \\ \hat{\mathbb{e}} & \mathbb{\varepsilon} & \mathbb{\alpha}^{\mathrm{t}} \\ -\hat{\mathbb{q}} & \mathbb{\alpha} & \mathbb{\nu} \end{bmatrix} \begin{pmatrix} \hat{\mathbf{S}} \\ \mathbf{E} \\ \mathbf{B} \end{pmatrix}. \tag{9}$$

In the case of piezoelectric material, the constitutive law is expressed by

$$\begin{pmatrix} \hat{\mathbf{T}} \\ \mathbf{D} \\ \mathbf{H} \end{pmatrix} = \begin{bmatrix} \hat{\mathbb{c}} & -\hat{\mathbb{e}}^{\mathrm{t}} & \mathbb{0} \\ \hat{\mathbb{e}} & \mathbb{\varepsilon} & \mathbb{0} \\ \mathbb{0} & \mathbb{0} & \mathbb{\nu} \end{bmatrix} \begin{pmatrix} \hat{\mathbf{S}} \\ \mathbf{E} \\ \mathbf{B} \end{pmatrix}. \tag{10}$$

In the case of magnetostrictive material, the constitutive law is expressed by:

$$\begin{pmatrix} \hat{\mathbf{T}} \\ \mathbf{D} \\ \mathbf{H} \end{pmatrix} = \begin{bmatrix} \hat{\mathbb{c}} & \mathbb{0} & -\hat{\mathbb{q}}^{\mathrm{t}} \\ \mathbb{0} & \mathbb{\varepsilon} & \mathbb{0} \\ -\hat{\mathbb{q}} & \mathbb{0} & \mathbb{\nu} \end{bmatrix} \begin{pmatrix} \hat{\mathbf{S}} \\ \mathbf{E} \\ \mathbf{B} \end{pmatrix}. \tag{11}$$

The coefficients $\mathbb{e}$ and $\mathbb{q}$ are, respectively, the piezoelectric and magnetostrictive coefficients.

A. Mechanical formulation

The mechanical formulation is established by taking into account the mechanical equilibrium (3) and the constitutive law deduced from Eq. (9):

$$\mathbf{T} = \mathbb{c} : \mathbf{S} - \mathbb{e}^{\mathrm{t}}.\mathbf{E} - \mathbb{q}^{\mathrm{t}}.\mathbf{B}.$$

Noting Ω the study domain, Γ_s its boundaries, the weak formulation of the mechanical equilibrium equation is

$$\int_{\Omega} \mathbf{w}.\left(\mathrm{div}\mathbf{T} + \mathbf{f} - \rho_m \frac{\partial^2 \mathbf{u}}{\partial t^2}\right) d\Omega = 0, \tag{12}$$

where **w** is a vectorial test function. Integrating by parts, Eq. (12) leads to

$$\int_{\Omega} \left(D\mathbf{w} : \mathbf{T} - \mathbf{w}.\mathbf{f} + \rho_m \mathbf{w}.\frac{\partial^2 \mathbf{u}}{\partial t^2}\right) d\Omega = \oint_{\Gamma_s} \mathbf{T}.\mathbf{n}.\mathbf{w}\, d\Gamma \tag{13}$$

with **n** the normal vector to the boundary Γ_s. The term on the right-hand side of Eq. (13) is related to the boundary conditions. There are two types of boundary conditions we need to contend with.

(1) Dirichlet boundary condition: The values of **u** are known on a part of the boundary Γ_s
(2) Neumann condition: $\mathbf{T}.\mathbf{n} = 0$, the right-hand side of Eq. (13) is zero.

Replacing $\mathbf{S} = D\mathbf{u}$, $\mathbf{E} = \mathbf{grad}\,V$ and $\mathbf{B} = \mathbf{curl}(\mathbf{a})$, Eq. (13) can be written as

$$\begin{aligned} &\int_{\Omega} D\mathbf{w} : \mathbb{c} : D\mathbf{u}\, d\Omega - \int_{\omega} D\mathbf{w} : \mathbb{e}^{t}.\mathbf{grad}\, V\, d\Omega \\ &- \int_{\Omega} D\mathbf{w} : \mathbb{q}^{t}.\mathbf{curl}(\mathbf{a}) d\Omega + \int_{\Omega} \rho_m \mathbf{w} \frac{\partial^2 \mathbf{u}}{\partial t^2} d\Omega \\ &= \int_{\Omega} \mathbf{w}.\mathbf{f}\, d\Omega + \oint_{\Gamma_s} \mathbf{T}.\mathbf{n}.\mathbf{w}\, d\Gamma. \end{aligned} \tag{14}$$

In our mechanical problem no body force is considered ($\mathbf{f} = \mathbf{0}$). The magnetic vector potential **a** is along z direction, therefore: $\mathbf{curl}(\mathbf{a}) = \mathrm{r}^{*}\mathbf{grad}\, a_3$ with

$$\mathrm{r}^{*} = \begin{bmatrix} 0 & 1 \\ -1 & 0 \end{bmatrix}.$$

In the finite element formulation, the displacement **u,** the electric potential V, and the vector potential a_3 over an element are related to the corresponding node values $\{\mathbf{u}\}$, $\{V\}$, and $\{a_3\}$ using the shape functions $[\mathbf{w}]$, $[N_v]$, and $[N_a]$:

$$\begin{aligned} \mathbf{u} &= [\mathbf{w}]\{\mathbf{u}\} \\ V &= [N_V]\{V\} \\ a_3 &= [N_a]\{a_3\}. \end{aligned} \tag{15}$$

Therefore, the strain **S,** the electrical field **E**, and the magnetic induction **B** are associated to the nodal displacements and potentials by the derivatives $[G_u]$, $[G_v]$, and $[G_a]$ of the shape functions:

$$\begin{aligned} \hat{\mathbf{S}} &= D[\mathbf{w}]\{\mathbf{u}\} = [G_u]\{\mathbf{u}\} \\ \mathbf{E} &= \mathbf{grad}[N_V]\{V\} = [G_V]\{V\} \\ \mathbf{B} &= \mathrm{r}^*\mathbf{grad}[N_a]\{a_3\} = [\mathrm{r}^*][G_a]\{a_3\}. \end{aligned} \tag{16}$$

After discretization, Eq. (14) can be written in the matrix form:

$$\left([\mathbb{K}_{uu}] - \omega^2[\mathbb{M}]\right)\{\mathbf{u}\} + \left[\mathbb{K}_{up}\right]\{V\} + [\mathbb{K}_{ua}]\{a_3\} = [\mathbf{0}] \tag{17}$$

with

$$\begin{aligned} [\mathbb{K}_{uu}] &= \sum_e \int_{\Omega^e} [G_u]^t[\hat{\mathbb{c}}][G_u]d\Omega \\ [\mathbb{M}] &= \sum_e \int_{\Omega^e} \rho_m[\mathbf{w}]^t[\mathbf{w}]d\Omega \\ \left[\mathbb{K}_{up}\right] &= -\sum_e \int_{\Omega^e} [G_u]^t[\hat{\mathbb{e}}^t][G_V]d\Omega \\ [\mathbb{K}_{ua}] &= -\sum_e \int_{\Omega^e} [G_u]^t[\hat{\mathbb{q}}^t][\mathrm{r}^*][G_a]d\Omega \end{aligned} \tag{18}$$

where Ω^e is the partial domain associated to the mesh element e. Equation (17) can be complemented with a damping term $j\omega\alpha[\mathbb{K}_{uu}]\{\mathbf{u}\}$ with α the damping coefficient. Noting $\left[\mathbb{K}^*_{uu}\right] = [\mathbb{K}_{uu}] + j\omega\alpha[\mathbb{K}_{uu}] - \omega^2[\mathbb{M}]$ gives:

$$\left[\mathbb{K}^*_{uu}\right]\{\mathbf{u}\} + \left[\mathbb{K}_{up}\right]\{V\} + [\mathbb{K}_{ua}]\{a_3\} = [\mathbf{0}] \tag{19}$$

B. Electromagnetic formulation

In a similar way, equations div $\mathbf{D} = \rho$ and $\mathbf{curl}(\mathbf{H}) = \mathbf{J}$ gives the following expressions:

$$\begin{aligned} \left[\mathbb{K}_{up}\right]^t\{\mathbf{u}\} + \left[\mathbb{K}_{pp}\right]\{V\} &= [Q] + [Q_n] \\ [\mathbb{K}_{ua}]^t\{\mathbf{u}\} + [\mathbb{K}_{aa}]\{a_3\} &= [I] + [I_n] \end{aligned} \tag{20}$$

with

$$\begin{aligned} \left[\mathbb{K}_{pp}\right] &= \sum_e \int_{\Omega^e} [G_V]^t[\mathbb{\varepsilon}][G_V]d\Omega \\ [Q] &= \sum_e \int_{\Omega^e} \rho[N_V]^t d\Omega \\ [Q_n] &= \sum_e \oint_{\Gamma_s} D_n[N_V]^t d\Gamma \\ [\mathbb{K}_{aa}] &= \sum_e \int_{\Omega^e} [G_a]^t[\mathrm{r}^*]^t[\tilde{\mathrm{v}}][\mathrm{r}^*][G_a]d\Omega \\ [I] &= \sum_e \int_{\Omega^e} j_3[N_V]^t d\Omega \\ [I_n] &= \sum_e \oint_{\Gamma_s} H_t[N_V]^t d\Gamma \end{aligned} \tag{21}$$

where $\tilde{\mathrm{v}}$ is the equivalent reluctivity tensor accounting for the magnetoelastic coupling (see Sec. IV B 2), D_n is the component of **D** normal to Γ_s, j_3 is the electric current along the z direction, and H_t is the component of **H** tangent to Γ_s. In the case of the sensor studied in the following we will consider no electric charges ($\rho = 0$) and no current density (so that $j_3 = 0$). We finally obtain the following system:

$$\begin{bmatrix} \mathbb{K}^*_{uu} & \mathbb{K}_{up} & \mathbb{K}_{ua} \\ \mathbb{K}_{pu} & \mathbb{K}_{pp} & \mathbb{0} \\ \mathbb{K}_{au} & \mathbb{0} & \mathbb{K}_{aa} \end{bmatrix} \begin{Bmatrix} \mathbf{u} \\ V \\ a_3 \end{Bmatrix} = \begin{bmatrix} \mathbf{0} \\ \mathbf{0} \\ I_n \end{bmatrix}, \tag{22}$$

where $\mathbb{K}_{pu} = \mathbb{K}^{\mathrm{t}}_{up}$ describes the electro-mechanical coupling, $\mathbb{K}_{au} = \mathbb{K}^{\mathrm{t}}_{ua}$ describes the magnetomechanical coupling. Linear system (22) is solved using Gauss algorithm.

IV. CONSTITUTIVE LAWS

ME composite materials often consist in an assembly of piezoelectric (pz) and magnetostrictive (ms) materials. The electroelastic behavior is assumed to be linear. The magnetostrictive behavior is nonlinear.

A. Electroelastic behavior

Considering that the piezoelectric material is prepolarized, the constitutive law is assumed to be linear around the polarization point:

$$\begin{pmatrix} \tilde{\mathbf{T}} \\ \tilde{\mathbf{D}} \end{pmatrix} = \begin{bmatrix} \tilde{\mathbb{c}} & -\tilde{\mathbb{e}}^t \\ \tilde{\mathbb{e}} & \tilde{\mathbb{\varepsilon}} \end{bmatrix}_{pz} \begin{pmatrix} \tilde{\mathbf{S}} \\ \tilde{\mathbf{E}} \end{pmatrix}. \tag{23}$$

$\tilde{X}(\tilde{a}, \tilde{b})$—applied to a mechanical, electric or magnetic field—denotes the small variation of X around a polarization point $X_0(a_0, b_0)$:

$$\tilde{X} = \frac{\partial X}{\partial a}(a_0, b_0)\tilde{a} + \frac{\partial X}{\partial b}(a_0, b_0)\tilde{b}, \quad X = X_0 + \tilde{X}. \tag{24}$$

B. Magnetostrictive behavior

1. General form

The magnetostrictive material is not prepolarized, therefore its constitutive law is strongly nonlinear and has then to be investigated. The total strain **S** is divided[9] into the elastic strain $\mathbf{S}^e$ and the magnetostriction strain $\mathbf{S}^\mu$, $\mathbf{S} = \mathbf{S}^e + \mathbf{S}^\mu$. According to Hooke's law, the total stress is expressed by

$$t_{ij} = C^{ms}_{ijkl}\left(s_{kl} - s^\mu_{kl}\right) = C^{ms}_{ijkl}s_{kl} - t^\mu_{ij}, \tag{25}$$

where C^{ms}_{ijkl} is the usual stiffness tensor of the magnetostrictive material under static loading.

In the case of an isotropic material, Eq. (25) can be written using Lamé coefficients μ^* and λ^*:

$$t_{ij} = 2\mu^*\left(s_{ij} - s^\mu_{ij}\right) + \delta_{ij}\lambda^*\left(s_{kk} - s^\mu_{kk}\right), \tag{26}$$

where δ_{ij} is the Kronecker symbol ($\delta_{ij} = 1$ if $i = j$ and $\delta_{ij} = 0$ if $i \neq j$).

The magnetostriction phenomenon is assumed to be isochoric[10] (meaning $s^{\mu}_{kk}=0$) and isotropic. Magnetostriction strain is also assumed to be a parabolic function of the magnetization. Modifying the model of Galopin *et al.*,[5] who considered the magnetostriction strain **S** as a parabolic function of the magnetic induction **B,** and assuming that **B** and **M** are collinear, the magnetostriction strain can be expressed by

$$s^{\mu}_{ij}=\frac{\beta}{2\mu_0^2}\left(3b_ib_j-\delta_{ij}b_kb_k\right)\frac{\mathbf{m}^2}{\mathbf{b}^2}, \tag{27}$$

where $\mathbf{m}^2=m_im_i$, $\mathbf{b}^2=b_ib_i$, and β is deduced from experimental results.[11]

Using the thermodynamical approach of Besbes *et al.*[12] (writing $\partial t_{kl}/\partial b_i=\partial h_i/\partial s_{kl}$) with respect to the independent variables **S** and **B,** the magnetic field can be expressed as

$$h_i=\nu_{ij}b_j-\frac{\partial t^{\mu}_{kl}}{\partial b_i}\left(s_{kl}-s^{\mu}_{kl}\right), \tag{28}$$

where ν_{ij} is the reluctivity tensor of the magnetostrictive material.

2. Linearized form

In order to describe the constitutive law at a polarization point of the magnetostrictive material, the differentials of Eqs. (25) and (28) are calculated, leading, respectively, to Eqs. (29) and (30):

$$\tilde{t}_{ij}=C^{ms}_{ijkl}\tilde{s}_{kl}-\frac{\partial t^{\mu}_{ij}}{\partial b_k}\tilde{b}_k, \tag{29}$$

$$\tilde{h}_i=-\frac{\partial t^{\mu}_{kl}}{\partial b_i}\tilde{s}_{kl}+\left[\frac{\partial \nu_{ik}b_k}{\partial b_j}-\frac{\partial^2 t^{\mu}_{kl}}{\partial b_i\partial b_j}\left(s_{kl}-s^{\mu}_{kl}\right)+\frac{\partial t^{\mu}_{kl}}{\partial b_i}\frac{\partial s^{\mu}_{kl}}{\partial b_j}\right]\tilde{b}_j. \tag{30}$$

Equation (30) introduces the terms to be calculated: $\partial t^{\mu}_{kl}/\partial b_i$ and $\partial \nu_{ik}b_k/\partial b_j$ correspond respectively to the coupling matrix $\mathbb{q}$ and the equivalent reluctivity $\tilde{\nu}_{ij}$. Two additional terms $\left(\partial^2 t^{\mu}_{kl}/\partial b_i\partial b_j\right)\left(s_{kl}-s^{\mu}_{kl}\right)$ and $\left(\partial t^{\mu}_{kl}/\partial b_i\right)\left(\partial s^{\mu}_{kl}/\partial b_j\right)$ also need to be estimated.

(1) As $s^{\mu}_{kk}=0$ (isochoric magnetostriction), the coupling matrix $\partial t^{\mu}_{kl}/\partial b_i$ can be calculated as follows in the case of isotropic elasticity:

$$\frac{\partial t^{\mu}_{kl}}{\partial b_i}=2\mu^*\frac{\partial s^{\mu}_{kl}}{\partial b_i}. \tag{31}$$

Using Eq. (27) we obtain

$$\frac{\partial t^{\mu}_{kl}}{\partial b_i}=\frac{\mu^*\beta}{\mu_0^2}\left[\frac{\partial\left(3b_kb_l-\delta_{kl}b_jb_j\right)}{\partial b_i}\frac{\mathbf{m}^2}{\mathbf{b}^2}+\left(3b_kb_l-\delta_{kl}b_jb_j\right)\frac{\partial\left(\mathbf{m}^2/\mathbf{b}^2\right)}{\partial\mathbf{b}}\frac{\partial\mathbf{b}}{\partial b_i}\right] \tag{32}$$

with

$$\frac{\partial\mathbf{b}}{\partial b_i}=\frac{b_i}{\mathbf{b}}$$

and

$$\frac{\partial\left(3b_kb_l-\delta_{kl}b_jb_j\right)}{\partial b_i}=\begin{cases}4b_i & \text{if } k=l=i\\ -2b_i & \text{if } k=l\neq i\\ 3b_l & \text{if } k=i\neq l\\ 3b_k & \text{if } l=i\neq k\\ 0 & \text{else}\end{cases}.$$

(2) The nonlinear relationship between **M** and **H** is written using a Langevin-type equation:[13]

$$M=M_s\left[\operatorname{cotanh}(A_sHM_s)-\frac{1}{A_sHM_s}\right], \tag{33}$$

with M_s the saturation magnetization, the constant A_s can be defined as $A_s=3\mu_0\chi_0/M_s^2$ with χ_0 the initial susceptibility of the anhysteretic magnetization curve.[14] Replacing in Eq. (33) and using $B=\mu_0(H+M)$, it comes:

$$B=\mu_0\left[H+M_s\left(\frac{1}{\tanh(3\mu_0\chi_0H/M_s)}-\frac{M_s}{3\mu_0\chi_0H}\right)\right]. \tag{34}$$

(3) The first term of the equivalent reluctivity $\tilde{\nu}_{ij}$ can be expressed as follows:

$$\frac{\partial\nu_{ik}b_k}{\partial b_j}=\nu_{ij}+\frac{\partial\nu_{ii}}{\partial\mathbf{b}}\frac{b_ib_j}{\mathbf{b}}. \tag{35}$$

Unlike the initial reluctivity that is diagonal ($\nu_{ij}\neq 0$ only if $i=j$), this expression introduces extra diagonal terms, which may not be negligible.

(4) Additional terms $\left(\partial^2 t^{\mu}_{kl}/\partial b_i\partial b_j\right)\left(s_{kl}-s^{\mu}_{kl}\right)$ and $\left(\partial t^{\mu}_{kl}/\partial b_i\right)\left(\partial s^{\mu}_{kl}/\partial b_j\right)$ have to be estimated: Knowing $\left[\partial^2\left(3b_kb_l-\delta_{kl}b_pb_p\right)/\partial b_i\partial b_j\right]\left(s_{kl}-s^{\mu}_{kl}\right)=4\left(3s_{ij}-\delta_{ij}s_{kk}\right)$, the term $\left(\partial^2 t^{\mu}_{kl}/\partial b_i\partial b_j\right)\left(s_{kl}-s^{\mu}_{kl}\right)$ is calculated from the derivation of Eq. (32). In the case of no applied strain, $s_{kl}-s^{\mu}_{kl}=0$, therefore the term $\left(\partial^2 t^{\mu}_{kl}/\partial b_i\partial b_j\right)\left(s_{kl}-s^{\mu}_{kl}\right)$ vanishes. In a similar way, the term $\left(\partial t^{\mu}_{kl}/\partial b_i\right)\left(\partial s^{\mu}_{kl}/\partial b_j\right)$ can be calculated using Eq. (36):

$$\frac{\partial\left(3b_kb_l-\delta_{kl}b_pb_p\right)}{\partial b_i}\frac{\partial\left(3b_kb_l-\delta_{kl}b_pb_p\right)}{\partial b_j}=\begin{cases}6\left(b_i^2+3\mathbf{b}^2\right) & \text{if } i=j\\ 6b_ib_j & \text{if } i\neq j\end{cases}. \tag{36}$$

In the case of no applied magnetic field, $s^{\mu}_{kl}=0$, therefore $\left(\partial t^{\mu}_{kl}/\partial b_i\right)\left(\partial s^{\mu}_{kl}/\partial b_j\right)$ is reduced to zero. Introducing the effective reluctivity

$$\tilde{\nu}_{ij}=\left[\frac{\partial\nu_{ik}b_k}{\partial b_j}-\frac{\partial^2 t^{\mu}_{kl}}{\partial b_i\partial b_j}\left(s_{kl}-s^{\mu}_{kl}\right)+\frac{\partial t^{\mu}_{kl}}{\partial b_i}\frac{\partial s^{\mu}_{kl}}{\partial b_j}\right], \tag{37}$$

the constitutive law of magnetostrictive material can be expressed by the following system:

$$\begin{pmatrix}\tilde{\mathbf{T}}\\ \tilde{\mathbf{H}}\end{pmatrix}=\begin{bmatrix}\tilde{\mathbb{c}} & -\tilde{\mathbb{q}}^t\\ -\tilde{\mathbb{q}} & \tilde{\mathbb{v}}\end{bmatrix}\begin{pmatrix}\tilde{\mathbf{S}}\\ \tilde{\mathbf{B}}\end{pmatrix}. \tag{38}$$

The final local constitutive law of the system combined from Eqs. (38) and (23) is given by

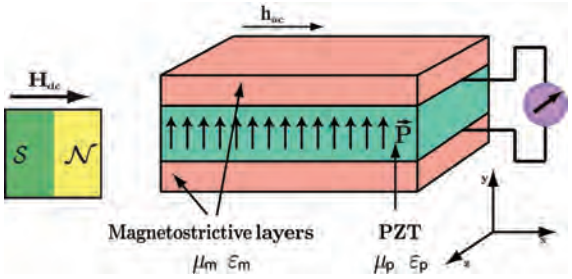

FIG. 1. (Color online) Magnetic sensor configuration.

$$\begin{pmatrix} \tilde{\mathbf{T}} \\ \tilde{\mathbf{D}} \\ \tilde{\mathbf{H}} \end{pmatrix} = \begin{bmatrix} \tilde{\mathbb{c}} & \tilde{\mathbb{e}}^t & -\tilde{\mathbb{q}}^t \\ -\tilde{\mathbb{e}} & \tilde{\mathbb{\varepsilon}} & \mathbb{0} \\ -\tilde{\mathbb{q}} & \mathbb{0} & \tilde{\mathbb{v}} \end{bmatrix} \begin{pmatrix} \tilde{\mathbf{S}} \\ \tilde{\mathbf{E}} \\ \tilde{\mathbf{B}} \end{pmatrix} \tag{39}$$

with $\tilde{\mathbb{e}} = \mathbb{0}$ for the magnetostrictive material and $\tilde{\mathbb{q}} = \mathbb{0}$ for the piezoelectric material.

V. APPLICATION—MAGNETIC SENSOR

A. Sensor configuration

The model has been applied to a magnetic sensor proposed by Huong Giang and Duc.[15] In order to estimate the performance of such a sensor, we focus on the numerical modeling of the corresponding sandwiched structure presented in Fig. 1. The material parameters correspond to those of Terfenol-D (Appendix B) bonded with PZT (Appendix C). A schematic view of the sensor in 2D configuration is presented in Fig. 2.

The sensor is a trilayer consisting in a piezoelectric layer between two magnetostrictive layers. In order to enhance the sensitivity of the sensor for the measurement of a static magnetic field $\mathbf{H}_{dc}$, a low harmonic magnetic field $\mathbf{h}_{ac}$ is usually superimposed using a coil surrounding the trilayer and excited at mechanical resonance frequency of the sensor ($\|\mathbf{h}_{ac}\| << \|\mathbf{H}_{dc}\|$). Therefore a harmonic electric voltage is obtained between the electrodes of the piezoelectric layer.

B. Modeling procedure

The numerical implementation of this magnetic sensor consists in two sequential finite element problems. The first is

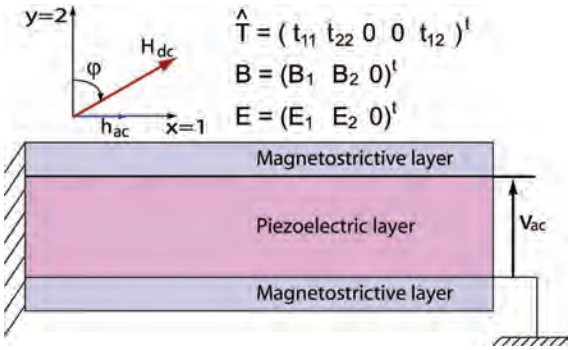

FIG. 2. (Color online) Magnetic sensor configuration.

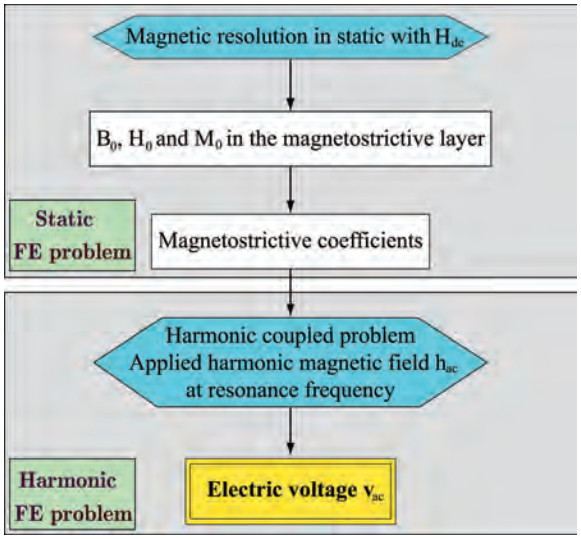

FIG. 3. (Color online) Modeling procedure.

a static problem allowing the calculation of the coefficients to establish the constitutive law of the magnetostrictive phase. The corresponding loading condition is no applied stress but initial magnetic induction due to the presence of the static magnetic field $\mathbf{H}_{dc}$. After obtaining all parameters of the magnetostrictive material under this specific loading, the second finite element problem is to solve the electric voltage under applied harmonic magnetic field at resonance frequency. The numerical procedure is detailed in Fig. 3.

C. Static FE problem

The magnetostrictive coefficients q_{ij} depend on the applied static magnetic field $\mathbf{H}_{dc}$. We first investigate with the proposed 2D model the value of these coefficients. Figures 4 and 5, respectively, plot the value of q_{11} and q_{21} as a function of the magnetic induction in the magnetostrictive layer. q_{11} (resp. q_{21}) links the component 11 (resp. 22) of the stress to the component 1 of the magnetic induction.

In the case of the sensor studied in this paper the magnetic induction in the sensor is redirected inside the magnetostrictive phase, whatever the orientation of the magnetic field outside the sensor. The induction is then mainly along direction 1 (in-plane). As shown in Figs. 4 and 5, the values of q_{11} and q_{21} are almost insensitive to the out-of-plane component when it is very low. Thus, the determination of the in-plane component of the induction will be sufficient to define the magnetostrictive parameters with good accuracy. Moreover, it can be shown that the in-plane component of the induction in the magnetostrictive layer is proportional to $\mathbf{H}_{eff} = \mathbf{H}_{dc} \sin\varphi$, where φ is defined on Fig. 6.

D. Harmonic FE problem

As the magnetostrictive material has a low conductivity, eddy currents have negligible effect at the resonance frequency,[6] therefore the resonance frequency is the same as the mechanical resonance frequency: 73 kHz for the first

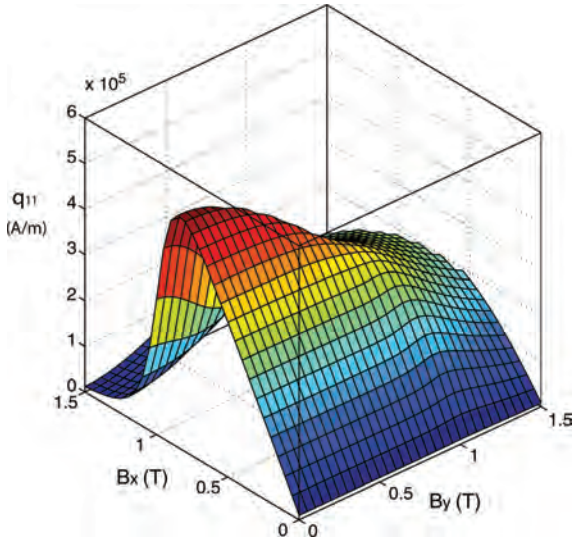

FIG. 4. (Color online) Magnetostrictive coefficient q_{11} as a function of the magnetic induction in the material.

longitudinal mode. The magnetostrictive parameter obtained with the static FE problem are implemented to solve the harmonic FE problem.

Figure 7 presents the electric voltage between the electrodes of the piezoelectric layer as a function of the applied in-plane static magnetic field. The electric voltage increases linearly in a first time and then decreases and approaches 0.

The numerical results have a shape very similar to the experimental results obtained by Huong Giang and Duc.[15] This shape is highly correlated to the coefficient q_{11}. Indeed considering the sensor configuration, the harmonic magnetic field $\mathbf{h}_{ac}$ in the magnetostrictive layer is only in the in-plane direction. In these conditions only the coefficients q_{11} and q_{21} play a role in the sensor response. The coefficient q_{21} links the in-plane component of the magnetic field to the strain along the direction normal to the layers. As the mechanical boundaries are free on the upper and lower borders of the sensor in the considered configuration, this strain along direction 2 will not be transmitted to the piezoelectric layer. Thus, for this particular sensor configuration and boundary conditions, the obtained electric voltage is mainly related to the coefficient q_{11}.

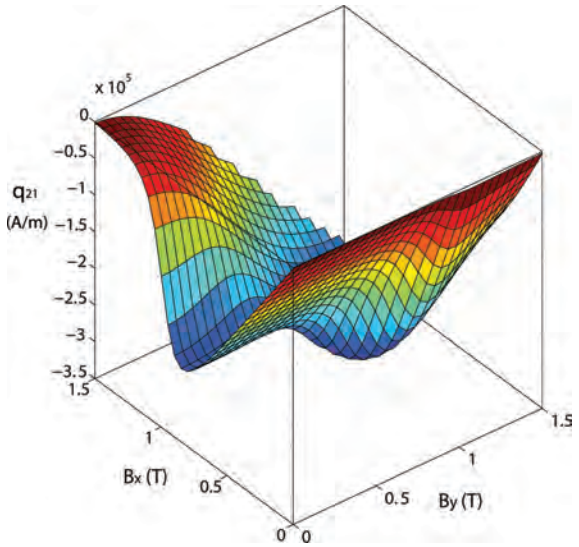

FIG. 5. (Color online) Magnetostrictive coefficient q_{21} as a function of the magnetic induction in the material.

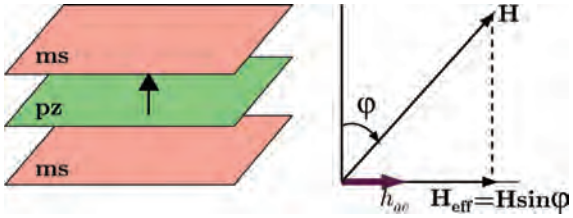

FIG. 6. (Color online) Rotation of the static field.

Moreover the obtained ME coefficients are much higher than those obtained in the static case. The static coefficients can be retrieved by moving the frequency of $\mathbf{H}_{dc}$ far from the resonance frequency. This enhancement of ME coefficients[7] by adding a small magnetic field oscillating at resonance frequency $\mathbf{h}_{ac}$ is due to the nonlinearity of magnetic and magnetostrictive behavior. Indeed if this behavior was linear, a superimposition principle would apply, and only the electric response corresponding to the alternative component of the magnetic field would be amplified by the resonant effect. The response corresponding to the static magnetic field would only be amplified in an amount corresponding to the static magnetoelectric coefficient. As the behavior is nonlinear, the static and resonant effects are coupled, and the magnetoelectric effect corresponding to the static field is enhanced through the resonance of the device.

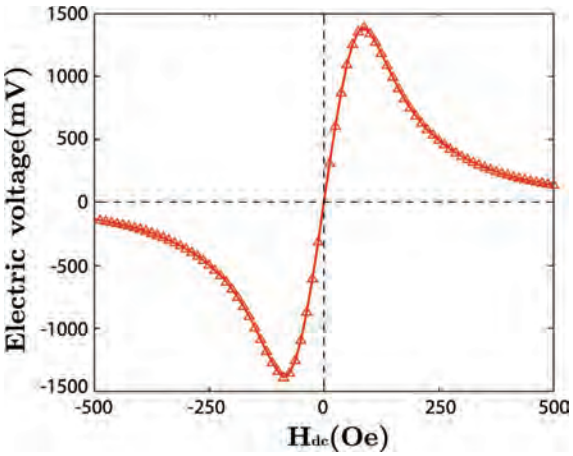

FIG. 7. (Color online) Electric voltage vs magnetic field applied in the in-plane direction.

E. Rotation of magnetic static field

The magnetic sensors can be used not only to measure the amplitude of static magnetic field but also its orientation. We consider the static magnetic field $\mathbf{H}_{dc}$ turning around the harmonic magnetic field $\mathbf{h}_{ac}$, which is along the polarization's direction of the magnetostrictive layers. φ is the angle between $\mathbf{H}_{dc}$ and the polarization's direction of the piezoelectric layer presented in Fig. 6. The rotation of $\mathbf{H}_{dc}$ can be simulated by orthogonal projections of $\mathbf{H}_{dc}$ onto x and y and writing the corresponding Neumann boundary conditions. Figure 8 (left hand side) shows the electric voltage as a function of the rotation angle. On the right-hand side, this voltage has been plotted as a function of the effective in-plane component $H_{dc} \sin \varphi$ of the applied magnetic field.

Again, there is a very satisfactory qualitative agreement with the experimental results of Huong Giang and Duc.[15] A quantitative comparison process should be undertaken, but the properties of the constituents have to be identified precisely. This is a work in progress. The right-hand side plots indicate that as far as the material remains in the linear stage of the magnetic behavior, the magnetoelectric response is proportional to $\sin \varphi$. The magnetic saturation modifies this dependence to the orientation of the applied magnetic field. The right-hand side plots indicate that the magnetoelectric response of the sensor when plotted as a function of $H_{dc} \sin \varphi$ is the same than the uniaxial characterization of Fig. 7. This result is consistent with the observation mentioned in the static analysis (Sec. V C) that—for this sensor configuration—the magnetic induction in the magnetostrictive layer is mainly directed in the in-plane direction and itself proportional to $H_{dc} \sin \varphi$. For this sensor configuration, a unique characterization with a static magnetic field in the in-plane direction is enough to define

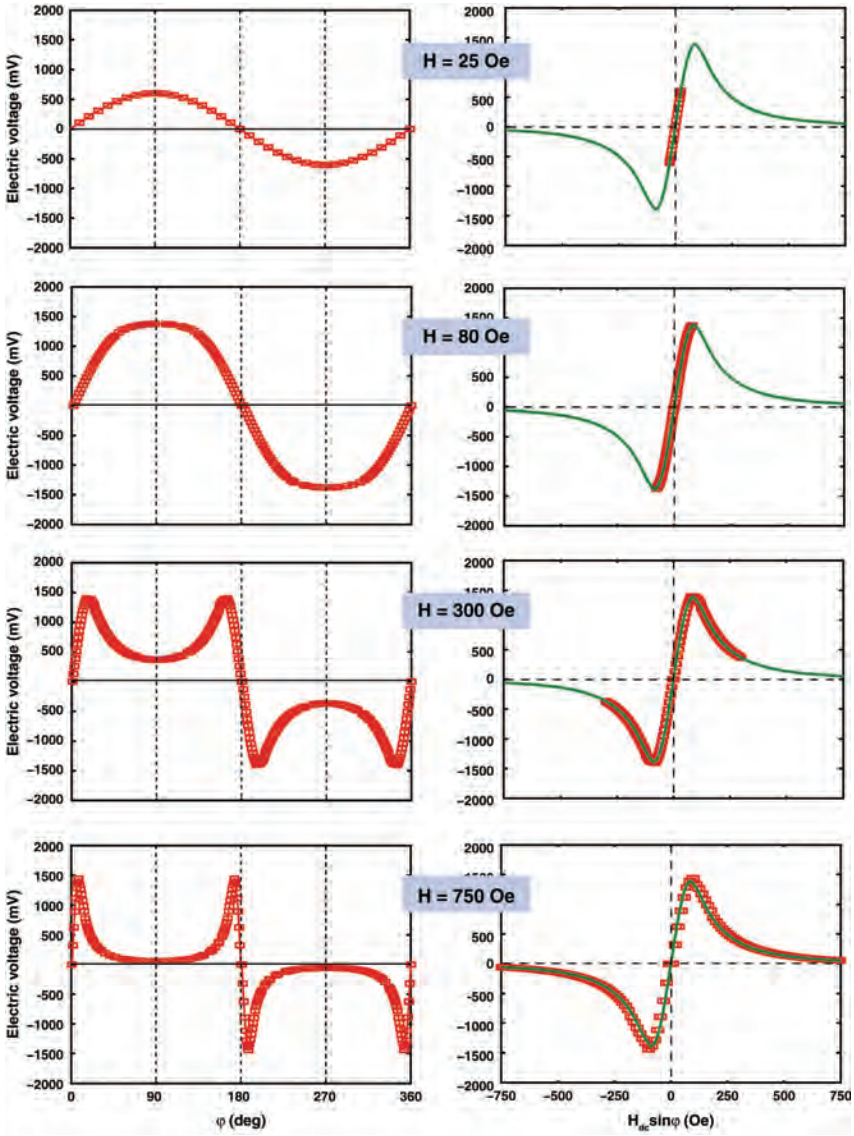

FIG. 8. (Color online) Electrical response of the ME sensor for different static magnetic-field values as a function of the rotation angle φ (left) and of the effective in-plane magnetic-field component $\mathbf{H}_{eff} = \mathbf{H}_{dc} \sin \varphi$ (right). The straight lines reproduce the result of Fig. 7 ($\varphi = 90°$).

the response for a static magnetic field in any direction. This sensor cannot be used to measure the orientation and the intensity of the magnetic field in a single measurement. A 2D magnetic sensor could be built using two multilayer devices (or performing two measurements in different directions). It could also be interesting to change the mechanical boundary conditions of the sensor in order to let the coefficient q_{21} play a role in the overall response of the sensor. The choice of another type of microstructure (for instance, matrix/inclusions instead of multilayers) could also be studied. The proposed modeling approach provides a tool to explore such an optimization of 2D magnetic sensors based on magnetoelectric effect.

VI. CONCLUSION

In this paper, we propose a 2D finite element model to investigate the magnetoelectric effect under harmonic loadings for high sensitivity magnetic field sensors. In such piezoelectric/magnetostrictive composites, the piezoelectric material is prepolarized. The corresponding constitutive law is thus defined as linear. The magnetostrictive material is not prepolarized, and a nonlinear constitutive law has to be used. An appropriate linearization procedure depending on the polarization point of the magnetostrictive material is presented. The model has been applied to a typical configuration of magnetic sensor, with very satisfying qualitative results, whatever the relative orientation between the sensor and the applied magnetic field. This approach gives a deepened insight on the magnetoelectric sensor working principle. The enhancement of the magnetoelectric coefficient when a low amplitude harmonic field is superimposed to the static field to be measured is shown to be related to the nonlinearity of magnetic and magnetostrictive behavior. The proposed modeling provides a tool to explore the possibility to build magnetic sensors with optimal configurations—topology, boundary conditions—for high sensitivity 2D or 3D measurements. An experimental validation in order to perform quantitative comparison is a work in progress. The development of a 3D model is the further step of this study.

APPENDIX A: VOIGT NOTATION

Voigt notation takes advantage of the symmetry properties of a tensor to reduce its order. The stress tensor $\hat{\mathbf{T}}$, the strain tensor $\hat{\mathbf{S}}$ and the stiffness tensor $\hat{\mathbb{c}}$ are presented as follows:

$$\hat{\mathbf{T}}=(t_{11} \quad t_{22} \quad 0 \quad 0 \quad 0 \quad t_{12})^{t},$$

$$\hat{\mathbf{S}} = (s_{11} \quad s_{22} \quad s_{33} \quad 2s_{23} \quad 2s_{31} \quad 2s_{12})^{t},$$

$$\hat{\mathbb{c}} = \begin{pmatrix} c_{1111} & c_{1122} & c_{1133} & c_{1123} & c_{1131} & c_{1112} \\ c_{2211} & c_{2222} & c_{2233} & c_{2223} & c_{2231} & c_{2212} \\ c_{3311} & c_{3322} & c_{3333} & c_{3323} & c_{3331} & c_{3312} \\ c_{2311} & c_{2322} & c_{3333} & c_{2323} & c_{2331} & c_{2312} \\ c_{3111} & c_{3122} & c_{3133} & c_{3123} & c_{3131} & c_{3112} \\ c_{1211} & c_{1222} & c_{1233} & c_{1223} & c_{1231} & c_{1212} \end{pmatrix}.$$

APPENDIX B: PROPERTIES OF MAGNETOSTRICTIVE MATERIAL

(1) Stiffness tensor:

$$\begin{bmatrix} 1.24 & 0.61 & 0.61 & 0 & 0 & 0 \\ 0.61 & 1.42 & 0.61 & 0 & 0 & 0 \\ 0.61 & 0.61 & 1.42 & 0 & 0 & 0 \\ 0 & 0 & 0 & 0.54 & 0 & 0 \\ 0 & 0 & 0 & 0 & 0.54 & 0 \\ 0 & 0 & 0 & 0 & 0 & 0.63 \end{bmatrix} \times 10^{10}\text{Pa};$$

(2) magnetic properties: $\mu_0 M_s = 1T$, $\chi_0 = 99$;
(3) magnetostrictive parameter: $\beta = 25 \times 10^{-6}$;
(4) density[4]: 9200 kg/m^3.

APPENDIX C: PROPERTIES OF PIEZOELECTRIC MATERIAL

(i) Stiffness tensor:

$$\begin{bmatrix} 3.19 & 1.43 & 1.43 & 0 & 0 & 0 \\ 1.43 & 3.19 & 1.43 & 0 & 0 & 0 \\ 1.43 & 1.43 & 2.67 & 0 & 0 & 0 \\ 0 & 0 & 0 & 0.68 & 0 & 0 \\ 0 & 0 & 0 & 0 & 0.58 & 0 \\ 0 & 0 & 0 & 0 & 0 & 0.58 \end{bmatrix} \times 10^{10}\text{Pa};$$

(ii) Dielectric permittivity[4]:

$$\begin{bmatrix} 15.92 & 0 & 0 \\ 0 & 15.92 & 0 \\ 0 & 0 & 15.92 \end{bmatrix} \times 10^{-9}\text{A(s/V m)};$$

(iii) Piezoelectric matrix[4]:

$$\begin{bmatrix} 0 & -5.9 & 0 \\ 0 & -5.9 & 0 \\ 0 & 15.2 & 0 \\ 0 & 0 & 10.5 \\ 0 & 0 & 0 \\ 10.5 & 0 & 0 \end{bmatrix} \times \text{N/(V m)};$$

(iv) Density[4]: 7700 kg/m^3.

[1]C. W. Nan, M. I. Bichurin, S. Dong, D. Viehland, and G. Srinivasan, J. Appl. Phys. **103**, 031101 (2008).
[2]C. W. Nan, Phys. Rev. B **50**, 6082 (1994).
[3]M. Fiebig, J. Phys. D **38**, 123 (2005).
[4]Y. X. Liu, J. G. Wan, J. M. Liu, and C. W. Nan, J. Appl. Phys. **94**, 5111 (2003).
[5]N. Galopin, X. Mininger, F. Bouillault, and L. Daniel, IEEE Trans. Magn. **44**, 834 (2008).
[6]T. T. Nguyen, X. Mininger, F. Bouillault, and L. Daniel, IEEE Trans. Magn. (in press).
[7]M. I. Bichurin, D. A. Filippov, V. M. Petrov, V. M. Laletsin, N. Paddubnaya, and G. Srinivasan, Phys. Rev. B **68**, 132408 (2003).
[8]R. Grössinger, G. V. Duong, and R. Sato-Turtelli, J. Magn. Magn. Mater. **320**, 1972 (2008).
[9]L. Hirsinger and R. Billardon, IEEE Trans. Magn. **31**, 1877 (1995).
[10]E. du Trémolet de Lacheisserie, *Magnetostriction: Theory and Application of Magnetoelasticity* (CRC Press, Boca Raton, FL, 1993).
[11]K. Azoum, M. Besbes, F. Bouillault, and T. Ueno, Eur. Phys. J. Appl. Phys. **36**, 43 (2006).
[12]M. Besbes, Z. Ren, and A. Razek, IEEE Trans. Magn. **37**, 3324 (2001).
[13]R. M. Bozorth, *Ferromagnetism* (Van Nostrand, Princeton, NJ, 1951).
[14]L. Daniel, O. Hubert, N. Buiron, and R. Billardon, J. Mech. Phys. Solids **56**, 1018 (2008).
[15]D. T. Huong Giang, and N. H. Duc, Sensors Actuators A. **149**, 229 (2009).

2.2 Relations de comportement : cas du couplage magnéto-mécanique

L'application des règles de changement d'échelle présentées au chapitre précédent pour déterminer la réponse macroscopique d'un matériau hétérogène nécessite la connaissance de la loi de comportement locale. La réponse d'un matériau à une sollicitation résulte souvent de mécanismes physiques complexes. Dans le but de mettre en place des outils de modélisation prédictifs, il peut être utile de s'appuyer sur la description de ces mécanismes physiques pour déduire la relation de comportement macroscopique. Je me suis plus particulièrement intéressé dans mes travaux de recherche au comportement magnéto-élastique. Les phénomènes de couplage magnéto-élastique présentent deux manifestations principales. La première est l'effet des contraintes sur le comportement magnétique. La seconde est la déformation de magnétostriction, qui est la déformation spontanée induite dans les matériaux ferromagnétiques par la présence d'un champ magnétique. Ces manifestations macroscopiques trouvent leur explication à une échelle bien plus fine. En effet, la microstructure des matériaux magnétiques se divise en domaines magnétiques. Chacun de ces domaines magnétiques présente une aimantation uniforme, de norme M_S, orientée dans une direction particulière. La configuration en domaines magnétiques est liée aux propriétés du matériaux, en particulier à son anisotropie initiale, et aux sollicitations extérieures. Afin de décrire le comportement magnéto-élastique, différentes stratégies sont envisageables.

Les approches phénoménologiques macroscopiques sont les plus répandues. Elles consistent à identifier des relations entre réponse macroscopique et sollicitation à partir de résultats d'essais. Dans cette catégorie les modèles de type "Jiles-Atherton" et de type "Preisach" sont certainement les plus populaires. Les premiers décrivent le cycle d'hystérésis à l'aide d'une fonction différentielle macroscopique [40], et les seconds s'appuient sur une distribution d'opérateurs élémentaires, les hystérons, pour décrire ces mêmes cycles [41,42]. Initialement destinés au comportement magnétique découplé, ils ont été étendus au cas de sollicitations magnéto-mécaniques ([43–45] et [46–49]). D'autres approches macroscopiques ont également été proposées [50–53]. L'un des défauts majeurs de ces modèles, outre la nécessité d'identifier leurs paramètres sur des essais macroscopiques, est qu'ils limitent en général la contrainte à une grandeur scalaire, restreignant ainsi le domaine d'application aux sollicitations de compression ou traction simple. Cette restriction est souvent un handicap quand on s'intéresse aux dispositifs réels, soumis à des sollicitations complexes.

A une échelle bien différente, les approches micromagnétiques offrent un éclairage précis sur la formation et l'évolution des microstructures en domaines magnétiques [54]. Ces approches sont basées sur la résolution de l'équation de Landau-Lifshitz-Gilbert souvent combinée avec la méthode des différences finies ou des éléments finis [55]. Elles permettent la prise en compte des phénomènes de couplage magnéto-élastique par l'introduction de l'énergie élastique dans la définition de l'énergie libre du système [56–58]. Malgré la précision des prédictions obtenues concernant les microstructures en domaines magnétiques, l'usage de ces méthodes reste limité par le temps de calcul nécessaire si l'on souhaite caractériser le comportement de volumes élémentaires représentatifs.

Une troisième voie consiste à recourir aux approches micro-mécaniques pour déduire le comportement macroscopique des matériaux à partir d'une description locale des mécanismes physiques. Cette description locale, nécessairement simplifiée, pourra s'appuyer sur des résultats obtenus par des méthodes plus fondamentales, telles que les approches micromagnétiques. Ce type de modélisation micro-macro a été appliqué avec succès pour décrire la plasticité des polycristaux [59, 60], le comportement des alliages à mémoire de forme [61, 62] ou encore le comportement ferroélectrique [63, 64]. Pour ce qui concerne le comportement magnéto-élastique, des modèles micro-macro ont également été proposés [65–69]. Ces modèles se focalisent en général sur le comportement magnétique, et négligent souvent les hétérogénéités mécaniques des matériaux. Ainsi, par exemple, les effets de texture cristallographique ne sont pas pris en compte. A la suite des travaux entamés au LMT-Cachan [70], j'ai participé au développement d'approches micro-macro pour les phénomènes de couplage magnéto-élastique.

2.2.1 Une proposition de modèle multi-échelle *

La modélisation des phénomènes de couplage magnéto-élastique dans le cas des polycristaux fait classiquement apparaître trois échelles de description possible (figure 2.3) : l'échelle du Volume Elémentaire Représentatif (VER) à laquelle on souhaite obtenir la relation de comportement macroscopique, l'échelle du grain ou du monocristal, qui est celle de l'hétérogénéité mécanique, et l'échelle du domaine magnétique qui est l'échelle de l'hétérogénéité magnétique. On aurait pu ajouter de part et d'autre l'échelle de la structure étudiée, pour laquelle on écrira les équations d'équilibre, souvent dans une version discrétisée et l'échelle de l'atome ou du groupement d'atome à laquelle peuvent être décrits les mécanismes fondamentaux du comportement. On supposera en général, même si c'est parfois discutable, que ces différentes échelles sont bien distinctes.

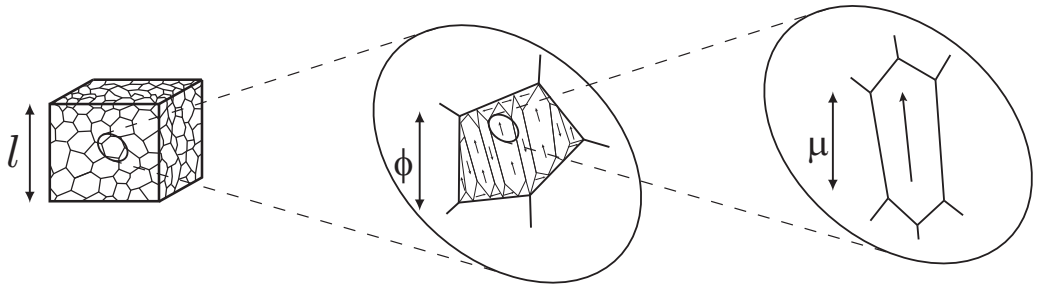

FIGURE 2.3 – Trois échelles de description des matériaux magnétiques ($l << \phi << \mu$).

A l'échelle du domaine magnétique, on considère une aimantation $\vec{M}_\alpha$ et une déformation de magnétostriction $\boldsymbol{\varepsilon}^\mu_\alpha$ uniformes (équations (2.9) et (2.10)) définies par la direction de l'aimantation $\vec{m}_\alpha$ et les paramètres matériaux M_S (aimantation à saturation) et λ_{100}, λ_{111} (coefficients de magnétostriction), dans le cas d'un matériau à symétrie cubique.

$$\vec{M}_\alpha = M_S\,\vec{m}_\alpha = M_S\ {}^T[\gamma_1\ \gamma_2\ \gamma_3] \tag{2.9}$$

$$\boldsymbol{\varepsilon}^\mu_\alpha = \frac{3}{2}\begin{pmatrix} \lambda_{100}(\gamma_1^2-\frac{1}{3}) & \lambda_{111}\gamma_1\gamma_2 & \lambda_{111}\gamma_1\gamma_3 \\ \lambda_{111}\gamma_1\gamma_2 & \lambda_{100}(\gamma_2^2-\frac{1}{3}) & \lambda_{111}\gamma_2\gamma_3 \\ \lambda_{111}\gamma_1\gamma_3 & \lambda_{111}\gamma_2\gamma_3 & \lambda_{100}(\gamma_3^2-\frac{1}{3}) \end{pmatrix} \tag{2.10}$$

L'énergie potentielle W_α d'un domaine magnétique peut s'écrire comme la somme de trois contributions majeures (équation (2.11)). L'énergie d'anisotropie W^{an}_α (équation (2.12)) tend à aligner l'aimantation suivant des directions particulières, dites directions de facile aimantation, liées à la cristallographie dans le cas de l'anisotropie magnétoscristalline (K_1 et K_2 sont les constantes d'anisotropie magnétocristalline). L'énergie magnétostatique (équation (2.13)) tend à aligner l'aimantation suivant le champ magnétique $\vec{H}_\alpha$ (μ_0 est la perméabilité du vide). Le troisième terme est l'énergie élastique W^σ_α qui permet d'introduire des effets magnéto-élastiques en raison des incompatibilités élastiques associées à la déformation de magnétostriction. Sous l'hypothèse de déformation uniforme dans un monocristal, l'énergie élastique peut se mettre sous la forme de l'équation (2.14) où $\boldsymbol{\sigma}_i$ est la contrainte moyenne dans le monocristal considéré. L'aimantation étant supposée uniforme dans un domaine, l'énergie d'échange n'est pas prise en compte dans cette formulation.

$$W_\alpha = W^{an}_\alpha + W^{mag}_\alpha + W^\sigma_\alpha \tag{2.11}$$

$$W^{an}_\alpha = K_1(\gamma_1^2\gamma_2^2+\gamma_2^2\gamma_3^2+\gamma_3^2\gamma_1^2) + K_2(\gamma_1^2\gamma_2^2\gamma_3^2) \tag{2.12}$$

$$W^{mag}_\alpha = -\mu_0\,\vec{H}_\alpha.\vec{M}_\alpha \tag{2.13}$$

$$W^\sigma_\alpha = -\boldsymbol{\sigma}_i : \boldsymbol{\varepsilon}^\mu_\alpha \tag{2.14}$$

∗. Les travaux présentés dans ce chapitre ont été menés à la suite des travaux entamés il y a une vingtaine d'années au LMT-Cachan autour de René Billardon. J'ai pu m'associer à ces travaux au cours de ma thèse de doctorat et les poursuivre ensuite au LGEP, le plus souvent en collaboration avec le LMT-Cachan, et plus particulièrement Olivier Hubert. Ils se poursuivent actuellement dans le cadre de la thèse de Karl-Joseph Rizzo [71].

A partir de cette écriture, on peut introduire deux types de variables internes qui vont permettre de décrire le comportement magnéto-élastique. L'orientation $\vec{m}_\alpha$ de l'aimantation dans un domaine, initialement alignée avec une direction facile, peut être obtenue par minimisation de l'énergie W_α. La proportion f_α de ce type de domaines dans le monocristal peut être introduite à l'aide d'une fonction de type Boltzmann [70, 72] (équation 2.15). Cette équation fait intervenir un paramètre A_s dont on peut démontrer qu'il est directement relié à la pente à l'origine χ^0 de la courbe anhystérétique macroscopique du matériau (équation 2.16).

$$f_\alpha = \frac{\exp\left(-A_s.W_\alpha\right)}{\sum_\alpha \exp\left(-A_s.W_\alpha\right)} \tag{2.15}$$

$$A_s = \frac{3\,\chi^0}{\mu_0\, M_S^2} \tag{2.16}$$

Une fois connues les fractions volumiques des domaines magnétiques, le calcul de la réponse macroscopique (étape d'homogénéisation) se fait par des opérations de moyenne adaptées aux microstructures envisagées. En raison du caractère hétérogène des matériaux considérés, la détermination des champs locaux $\vec{H}_\alpha$ et $\boldsymbol{\sigma}_i$ (étape de localisation) doit également tenir compte de la microstructure des matériaux. Les opérations de localisation et d'homogénéisation sont menées en suivant les règles de changement d'échelle présentées préalablement dans la section 2.1.

La présentation détaillée du modèle multi-échelle brièvement ébauché dans ce paragraphe est proposée dans la référence [73] jointe ci-après. Ce modèle permet d'envisager des sollicitations magnéto-mécaniques multiaxiales, sans hypothèses particulières sur l'orientation relative du champ magnétique et de la contrainte. Son originalité réside notamment dans sa capacité à intégrer les effets de texture cristallographique sur le comportement macroscopique. Cette version initiale du modèle a par la suite été modifiée de manière à éviter l'étape de minimisation de l'énergie potentielle qui était relativement coûteuse en temps de calcul. Cette version modifiée, détaillée dans la référence [74] jointe ci-après, est basée sur les mêmes principes. Cependant, alors qu'on se limitait auparavant à un nombre restreint de familles de domaines orientés suivant les directions de facile aimantation, elle s'appuie sur le pavage d'une sphère unité pour discrétiser les directions de l'espace, et envisage toutes ces directions comme possibles supports de l'aimantation locale.

Ces travaux sur le comportement anhystérétique des matériaux magnétiques amènent naturellement à s'interroger sur l'intégration des mécanismes de dissipation dans la modélisation. En effet, l'hystérésis magnétique contribue significativement aux pertes dans les machines électriques. Il a fait l'objet de nombreux travaux de recherche [75]. Au moment où l'on cherche à faire fonctionner les machines électriques en environnement sévère, les effets magnéto-mécaniques pourraient participer de manière significative aux pertes globales. Dans l'objectif d'intégrer ces effets de dissipation dans le modèle multi-échelle , un projet de recherche (MAEL, MAgneto-ELastic behaviour characterisation and multiscale modelling, http ://www.lgep.supelec.fr/mael) regroupant quatre laboratoires (LGEP, LMT, LPCES, LPMTM) investis dans les domaines de l'électromagnétisme, de la mécanique, de la science des matériaux et de la métallurgie est en cours. Du point de vue de la modélisation du comportement magnéto-élastique, le programme propose de revenir à la caractérisation de monocristaux qui a permis d'établir les modèles anhystérétiques, mais en s'intéressant cette fois aux effets de dissipation. L'objectif est de mettre en place des modèles monocristallins pour l'hystérésis magnéto-mécanique, et de s'appuyer ensuite sur les règles de changement d'échelle déjà établies pour obtenir des modèles polycristallins. L'ambition est de permettre la définition de microstructures optimales pour le comportement magnéto-mécanique, à la fois du point de vue de la perméabilité magnétique et des pertes par hystérésis. L'état d'avancement du projet ne permet pas encore à ce jour de proposer un modèle de comportement magnéto-mécanique hystérétique satisfaisant, même si une première tentative, basée sur l'utilisation d'un modèle de Jiles-Atherton a été proposée [76].

Publications jointes

[RI.14, 73] : L. Daniel, O. Hubert, N. Buiron, R. Billardon, "Reversible magneto-elastic behavior : a multiscale approach", *Journal of the Mechanics and Physics of Solids*, **56(3)** :1018-1042, 2008.

[RI.15, 74] : L. Daniel, N. Galopin, "A constitutive law for magnetostrictive materials and its application to Terfenol-D single and polycrystals", *The European Physical Journal - Applied Physics*, **42(2)** :153-159, 2008.

Available online at www.sciencedirect.com
ScienceDirect
Journal of the Mechanics and Physics of Solids 56 (2008) 1018–1042
JOURNAL OF THE MECHANICS AND PHYSICS OF SOLIDS
www.elsevier.com/locate/jmps

Reversible magneto-elastic behavior: A multiscale approach

Laurent Daniel[a,*], Olivier Hubert[b], Nicolas Buiron[c], René Billardon[b]

[a]LGEP - CNRS (UMR 8507), Supélec, Univ Paris-Sud, UPMC-Paris6 Plateau du Moulon, 91192 Gif sur Yvette Cedex, France
[b]LMT-Cachan, ENS Cachan, CNRS (UMR 8535), UPMC-Paris6 61 avenue du Président Wilson, 94235 CACHAN Cedex, France
[c]Laboratoire Roberval, Université de Technologie de Compiègne BP 20529, 60205 COMPIEGNE Cedex, France

Received 5 February 2007; received in revised form 7 June 2007; accepted 11 June 2007

Abstract

Magnetic and mechanical behaviors are strongly coupled. But few models are able to describe magneto-mechanical coupling effects. We propose a multiscale approach for the modeling of the reversible magneto-elastic behavior of ferromagnetic materials. This approach stands between macroscopic phenomenological modeling and micromagnetic simulations. We detail first the definition of the magneto-elastic behavior of a single crystal, deduced from energetic considerations made at the scale of magnetic domains and hypotheses concerning the domains microstructure. This model is then applied to the description of the behavior of polycrystalline media, through a multiscale approach. The heterogeneity of stress and magnetic field is taken into account through a self-consistent localization–homogenization scheme, including crystallographic texture data. Results are discussed and compared to experimental data from the literature.

Keywords: Magneto-elastic couplings; Magnetostriction; Multiscale modeling; Single crystal; Polycrystal

1. Introduction

Ferro- and ferrimagnetic materials are used to produce and to transform energy or build actuators. The search for higher performance and lighter electrotechnical devices leads to a deeper need of predictive dimensioning tools, concerning optimization of materials, structures and forming processes. Consequently, advanced models are needed to describe the magnetic behavior. Especially, the accuracy of modeling has to be improved to account for coupled magneto-mechanical phenomena. This coupling is characterized by the influence of stress state on the magnetic susceptibility and by the magnetostriction[1] (i.e. the spontaneous deformation due to magnetization, Joule, 1847; Bozorth, 1951; Du Trémolet de Lacheisserie, 1993). These phenomena are linked to the existence of a magnetic domains microstructure (Hubert and Schäfer, 1998). Each magnetic domain is associated to a given saturation magnetization and magnetostriction strain. Macroscopic magnetization process and magnetostriction are explained by a variation in volume of domains

*Corresponding author. Tel.: +33 1 69 85 16 39; fax: +33 1 69 41 83 18.
E-mail address: laurent.daniel@lgep.supelec.fr (L. Daniel).

[1]The form effect will not be addressed in that paper. This elastic deformation—superimposed to the magnetostriction strain—results from the existence of magnetic forces, and is linked to boundary conditions and to the geometry of the considered specimen. Thus, it cannot be introduced into a magneto-elastic constitutive law.

0022-5096/$ - see front matter © 2007 Elsevier Ltd. All rights reserved.
doi:10.1016/j.jmps.2007.06.003

submitted to a magnetic field or stress. A concomitant magnetization process consists in a rotation of magnetization direction of the magnetic domains. A stress modifies the energetic equilibrium of domains structure as well, bringing a change of their volume, and as a consequence a change of susceptibility. At the macroscopic scale, the magnetostriction partly explains the noise emitted by electrical devices, and particularly transformers. The effect of stress on the magnetic behavior is responsible for the decrease of rates in electrical devices submitted to stress. The magnetic behavior cannot, therefore, be accurately determined unless the mechanical fields are taken into account. The difficulty of such a determination is increased by the multiaxiality of magnetic and mechanical loadings.

Up to now, two main approaches have been proposed to describe such coupling effects. On the one hand, several phenomenological macroscopic models (introducing the stress as a parameter in classical macroscopic models) have been proposed, extended from the Jiles–Atherton model (see for instance Sablik and Jiles, 1993), from the Preisach model (for instance Appino et al., 1999 or Bernard and Ossart, 2004) or based on thermodynamic arguments (for instance Hirsinger et al., 2000 or Azoum et al., 2004). The applicability of such approaches is often limited to a short range of loadings, to isotropic materials, and the multiaxiality of stress state is rarely accounted for. Moreover, these approaches do not allow the investigation of materials properties optimization, since the effect of a change in composition or crystallographic texture cannot be predicted. On the other hand, micromagnetic simulations allow the simulation of complex domain structures (DeSimone et al., 2000). They are based on the minimization of the potential energy of the single crystal modeled by a set of interacting magnetic moments, each of them representing a set of atoms. The number of degrees of freedom and interactions is growing very quickly with the number of magnetic moments, so that these simulations are always made for small size systems. Several authors have developed some magneto-elastic simulations that take into account uniaxial or cubic crystalline symmetries (for example He, 1999; DeSimone and James, 2002). This kind of strategy usually concerns 2D patterns and often leads to prohibitive calculation times, still not reasonable today concerning polycrystalline media.

Micro–macro approaches have been successfully developed in many fields of physics during the past years to deduce the overall behavior of heterogeneous materials from the behavior of their constituents. Concerning non-linear behaviors, these approaches have been developed first in the framework of polycrystals plasticity (Hill, 1965; Berveiller and Zaoui, 1978). Applications to coupled phenomena have been proposed for shape memory or ferroelectric polycrystals (see for instance Patoor et al., 2006; Lagoudas et al., 2006; Huber et al., 1999; Haug et al., 2007). But few models have been addressed in the framework of magneto-elasticity. The development of such approaches relies on two key points. The first one is the definition of transition scale rules, depending on the microstructure of the studied material, and allowing to estimate the fluctuation of the local fields for a given macroscopic loading. The second one is an appropriate description of the behavior of the constituents.

Our proposition is to use simplifying hypotheses allowing a fast estimation for the magneto-elastic behavior. Several scales can be chosen to define this behavior, leading to a multiscale calculation strategy, remaining in the framework of continuum mechanics. The first scale for which homogeneous magnetic and mechanical state can be considered is the magnetic domains scale. The next scale is the grain scale for which the elastic properties are homogeneous. We then define the polycrystalline representative volume element (RVE) scale. The studied zone is then large enough to consider that the RVE behavior defines the average material behavior and/or properties. It is not possible to define precisely this scale as its dimensions depend on the studied material and/or on the studied properties.

The polycrystal is seen as a single crystals aggregate, with respect to a given orientation distribution function (ODF), representative of the polycrystal texture. The proposed modeling considers homogeneous magnetic field and strain state within the single crystal. These hypotheses are maintained in each grain of a polycrystal. The fluctuations of magnetic field and stress within the polycrystal is not neglected since they significantly affect the predicted value for the magnetostriction strain. The self-consistent approach (Bruggeman, 1935; Hill, 1965), known to be suitable to polycrystals behavior (Bornert et al., 2007), will be used. Hypotheses of homogeneity of stress and magnetic field will be nevertheless used in order to obtain faster results in the framework of simplified approaches.

Hysteretic phenomena are not considered in this first approach. The proposed modeling is only relevant for reversible magneto-elastic behavior, associated to anhysteretic magnetic field strengthening. Assumptions hereafter have been developed for ferro- or ferrimagnetic materials with a cubic crystallographic symmetry.

The paper is divided into three parts. The first one presents the single crystal constitutive law. The second part is dedicated to the definition of polycrystalline media behavior, with the definition of scale transition rules. In the last part, modeling results are compared to experimental data.

2. Single crystals

2.1. Energetic equilibrium

At the scale of a group of atoms, the magnetic equilibrium state is the result of the competition between several energetic terms. The potential energy of a group of atoms can be written (Hubert and Schäfer, 1998)

$$W = W_{\mathrm{ex}} + W_{\mathrm{an}} + W_{\mathrm{mag}} + W_{\sigma}, \tag{1}$$

where W_{ex} denotes the exchange energy; W_{an} denotes the magneto-crystalline energy; W_{mag} denotes the magneto-static energy; W_{σ} denotes the elastic energy.

2.1.1. Exchange energy

The exchange energy is related to the ferromagnetic coupling effect between neighboring atoms, tending to uniformize the magnetization in a volume element. It can be written

$$W_{\mathrm{ex}} = A(\mathrm{grad}\,\vec{\gamma})^2, \tag{2}$$

A is the exchange constant of the material, and $\vec{\gamma}$ denotes the magnetization direction

$$\vec{M} = M_{\mathrm{s}}\vec{\gamma} \tag{3}$$

M_{s} is the magnetization saturation value of the material.

Exchange energy is minimum when the spatial variations of the magnetization direction are minimum.

2.1.2. Magneto-crystalline energy

The magneto-crystalline energy tends to force the magnetization to be aligned along particular directions, called easy axes. These directions are mostly connected to crystallographic structure. In the case of cubic crystallographic symmetry, the magneto-crystalline energy can be written

$$W_{\mathrm{an}} = K_0 + K_1(\gamma_1^2\gamma_2^2 + \gamma_2^2\gamma_3^2 + \gamma_3^2\gamma_1^2) + K_2(\gamma_1^2\gamma_2^2\gamma_3^2) \tag{4}$$

$[\gamma_1, \gamma_2, \gamma_3]$ are the direction cosines of $\vec{\gamma}$. K_0 is an arbitrary constant, K_1 and K_2 denote the magneto-crystalline anisotropy constants of the material. Magneto-crystalline energy is minimum when $\vec{\gamma}$ is an easy axis.

2.1.3. Magneto-static energy

The magneto-static energy can be written

$$W_{\mathrm{mag}} = -\mu_0\vec{H}.\vec{M}, \tag{5}$$

$\vec{H}$ and $\vec{M}$ are, respectively, the local magnetic field and magnetization. This term tends to align the magnetization with the magnetic field. It is minimum when $\vec{H} = \|\vec{H}\|\vec{\gamma}$.

2.1.4. Elastic energy

In the case of a linear elastic behavior, Hooke's law defines a proportional relation between elastic strain ($\boldsymbol{\varepsilon}_{\mathrm{e}}$) and stress ($\boldsymbol{\sigma}$). The elastic energy is then defined as

$$W_{\sigma} = \tfrac{1}{2}\boldsymbol{\varepsilon}_{\mathrm{e}} : \mathbb{C}^I : \boldsymbol{\varepsilon}_{\mathrm{e}} = \tfrac{1}{2}\boldsymbol{\sigma} : \mathbb{C}^{-1} : \boldsymbol{\sigma} \tag{6}$$

$\mathbb{C}^I$ is the material stiffness tensor, uniform within a single crystal.

In magnetic materials, the magnetostriction strain[2] $\boldsymbol{\varepsilon}_\mu$ is a source of incompatibility, involved in the definition of $\boldsymbol{\sigma}$ and thus in the definition of W_σ.

In the case of cubic crystallographic symmetry, the magnetostriction strain $\boldsymbol{\varepsilon}_\mu$ can be described with three parameters. Assuming that this strain is isochore (Du Trémolet de Lacheisserie, 1993), the number of parameters is reduced to two. In the crystallographic frame (CF), the magnetostriction strain tensor can be written

$$\boldsymbol{\varepsilon}_\mu = \frac{3}{2}\begin{pmatrix} \lambda_{100}(\gamma_1^2-\frac{1}{3}) & \lambda_{111}\gamma_1\gamma_2 & \lambda_{111}\gamma_1\gamma_3 \\ \lambda_{111}\gamma_1\gamma_2 & \lambda_{100}(\gamma_2^2-\frac{1}{3}) & \lambda_{111}\gamma_2\gamma_3 \\ \lambda_{111}\gamma_1\gamma_3 & \lambda_{111}\gamma_2\gamma_3 & \lambda_{100}(\gamma_3^2-\frac{1}{3}) \end{pmatrix}_{\mathrm{CF}} \tag{7}$$

where λ_{100} and λ_{111} denote the magnetostrictive constants. λ_{100} (resp. λ_{111}) is the magnetostriction strain along the direction $\langle 1\,0\,0\rangle$ (resp. $\langle 1\,1\,1\rangle$) of a single crystal when it is magnetized at saturation along this direction.

2.2. Definition of the magneto-elastic behavior

If we consider a volume element V, the total potential energy becomes

$$W = \frac{1}{V}\int_V (W_{\mathrm{ex}} + W_{\mathrm{an}} + W_{\mathrm{mag}} + W_\sigma)\,\mathrm{d}V. \tag{8}$$

The resolution of a problem of magneto-elasticity involves the minimization of this potential energy for the volume element. This point is the base of the so-called micro-magnetic approaches. The macroscopic quantities ($\boldsymbol{\Sigma}$, $\boldsymbol{E}$, $\vec{M}^{\mathbf{m}}$, $\vec{H}_{\mathbf{ext}}$) are defined by an averaging operation of the local quantities ($\boldsymbol{\sigma}$, $\boldsymbol{\varepsilon}$, $\vec{M}$, $\vec{H}$) over the volume. Such an approach, involving a large number of degrees of freedom, appears to be difficult to implement, particularly if the heterogeneity scale is much smaller than the volume of interest.

In the present case, the volume of interest is the single crystal. If a single crystal is seen as a domains aggregate, the potential energy of a single crystal can be defined as the sum of its domains potential energies and of a wall energy, related to the transition zone between magnetic domains

$$W^{\mathbf{sc}} = \frac{1}{V}\left(\int_{V_{\mathrm{d}}} W^\alpha\,\mathrm{d}V + \int_{V_{\mathrm{w}}} W^{\mathrm{w}}\,\mathrm{d}V\right) \tag{9}$$

V_{d} being the domains volume and V_{w} the magnetic walls volume ($V_{\mathrm{d}} + V_{\mathrm{w}} = V$). However, the definition of W^{w}, of the wall volume V_{w}, and of the boundary between domains and walls are quite difficult. Actually, the formulation (9), although seducing, is practically very difficult to use, unless one gets back to a micromagnetic formulation.

We propose a model that uses the uniformity of magnetization and stress in magnetic domains and neglects the fast variations of exchange and magneto-crystalline energies in the domain walls, joining on that point the "no-exchange" formulation (James and Kinderlehrer, 1990; DeSimone, 1993). This model is simple enough to be implemented in a polycrystalline modeling.

2.3. Energetic equilibrium of a magnetic domain α and related hypotheses

In a magnetic domain α, with magnetization direction $\vec{\gamma}^\alpha = [\gamma_1, \gamma_2, \gamma_3]$, spatial variations of magnetization are inexistent, the exchange energy is consequently zero.

The magnetization being uniform in a domain, the magneto-crystalline energy is also uniform, and the integration over the volume becomes easy. Eq. (4) remains unchanged

$$W_{\mathrm{an}}^\alpha = K_0 + K_1(\gamma_1^2\gamma_2^2 + \gamma_2^2\gamma_3^2 + \gamma_3^2\gamma_1^2) + K_2(\gamma_1^2\gamma_2^2\gamma_3^2). \tag{10}$$

[2] ε_μ denotes the free magnetostriction strain, meaning the magnetostriction strain that would appear if the material was able to deform without any incompatibility.

The magnetic field being supposed uniform in a domain, the magneto-static energy is uniform too, and can be written

$$W^{\alpha}_{\mathrm{mag}} = -\mu_0 \vec{M}^{\alpha}.\vec{H}^{\alpha}, \tag{11}$$

$\vec{H}^{\alpha}$ is the magnetic field at the domain scale. $\vec{M}^{\alpha}$ is the magnetization in the domain, defined by Eq. (12)

$$\vec{M}^{\alpha} = M_{\mathrm{s}}\vec{\gamma}^{\alpha}. \tag{12}$$

A first simplification is related to the definition of the local magnetic field $\vec{H}$. The magneto-static energy is defined assuming that $\vec{H}$ is uniform within a single crystal (or grain) and noted $\vec{H}^{\mathbf{I}}$ ($\vec{H}^{\alpha} = \vec{H}^{\mathbf{I}}$).

A domain is supposed to be a substructure of a zone for which elastic properties are uniform. Magnetostriction strain is also uniform in the domain. We assume that the stress is uniform in a magnetic domain. The elastic energy can then be written

$$W^{\alpha}_{\sigma} = \tfrac{1}{2}\boldsymbol{\sigma}^{\alpha} : \mathbb{C}^{I^{-1}} : \boldsymbol{\sigma}^{\alpha}. \tag{13}$$

A second assumption is related to the expression of the elastic energy. We choose an uniform strain hypothesis within a single crystal, so that the elastic energy expression is simplified (see Appendix A), and can be written

$$W^{\alpha}_{\sigma} = W^{\mathrm{o}}_{\sigma} - \boldsymbol{\sigma}^{I} : \boldsymbol{\varepsilon}^{\alpha}_{\mu}, \tag{14}$$

$\boldsymbol{\sigma}^{I}$ being the mean stress within the single crystal (i.e. the applied stress at the grain scale) and W^{o}_{σ} a constant over the single crystal. The expression obtained by neglecting the constant term is usually called the magneto-elastic energy (Bozorth, 1951; Hubert and Schäfer, 1998)

$$W^{\alpha}_{\sigma\mu} = -\boldsymbol{\sigma}^{I} : \boldsymbol{\varepsilon}^{\alpha}_{\mu}. \tag{15}$$

The potential energy of each domain is then written, except for a constant

$$W^{\alpha} = -\mu_0 \vec{M}^{\alpha}.\vec{H}^{\mathbf{I}} - \boldsymbol{\sigma}^{I} : \boldsymbol{\varepsilon}^{\alpha}_{\mu} + K_1(\gamma_1^2\gamma_2^2 + \gamma_2^2\gamma_3^2 + \gamma_3^2\gamma_1^2) + K_2(\gamma_1^2\gamma_2^2\gamma_3^2). \tag{16}$$

2.4. A semi-phenomenological modeling for single crystals

2.4.1. State variables

We consider a single crystal. We define domain families (α), each of them being associated to a particular—initial—easy axis ($\vec{\gamma}^{\alpha}_0$).

The chosen state variables are defined for each family and can be divided into two sets:

- The orientation of the magnetization in each domain family, defined by two usual spherical angles θ^{α} and δ^{α}.
- The volumetric fraction f^{α} of the α domain family in the single crystal.

2.4.2. State variables calculation

Magnetic field and stress tensor being known, the variables θ^{α} and δ^{α} are calculated by minimization of the domain potential energy W^{α}

$$W^{\alpha}(\theta^{\alpha}, \delta^{\alpha}) = \min(W^{\alpha}). \tag{17}$$

Variables f^{α} cannot be estimated by such a minimization because of the mean magnetic field approach. f^{α} is then obtained using a Boltzmann function,[3] proposed by Buiron et al. (1999) following Chikazumi (1997)

$$f^{\alpha} = \frac{\exp(-A_{\mathrm{s}}.W^{\alpha})}{\sum_{\alpha}\exp(-A_{\mathrm{s}}.W^{\alpha})}, \tag{18}$$

[3]Statistical approach for the determination of a specific state depending on its energy compared to the energy of the other states.

A_s is a parameter that introduces the "inertial" effects ignored by the modeling.[4] Its value can be analytically calculated (see paragraph 2.4.4 and Appendix B). f^α satisfies

$$\sum_\alpha f^\alpha = 1. \tag{19}$$

2.4.3. Single crystal behavior

The mean magnetization over the single crystal is defined by

$$\vec{M}^{\mathbf{I}} = \langle \vec{M}^\alpha \rangle = \sum_\alpha f^\alpha \vec{M}^\alpha. \tag{20}$$

Assuming homogeneous elastic properties for the single crystal, the magnetostriction strain can be defined the same way

$$\boldsymbol{\varepsilon}^I_\mu = \langle \boldsymbol{\varepsilon}^\alpha_\mu \rangle = \sum_\alpha f^\alpha \boldsymbol{\varepsilon}^\alpha_\mu. \tag{21}$$

2.4.4. Identification of A_s parameter

If the magnetization rotation mechanism is ignored, a simplified modeling can be derived (see Appendix B). This modeling, applicable only for low applied magnetic fields allows to link the parameter A_s to the initial slope of the anhysteretic magnetization curve χ^0. We find

$$A_s = \frac{3\chi^0}{\mu_0 M_s^2}. \tag{22}$$

This parameter is found to be independent of the magnetic field direction. Under this assumption, the only adjustable parameter of the modeling is directly obtained from a single anhysteretic magnetization curve (without mechanical loading).

3. Polycrystals

Let us consider a RVE of a polycrystalline material. Grains orientation in the polycrystal is given[5] and the whole properties of the single crystal are known. Depending on these properties and on some hypotheses concerning the microstructure, we want to link the macroscopic response (mean magnetization $\vec{M}^{\mathbf{m}}$ and macroscopic strain $\boldsymbol{E}$) of this RVE to the macroscopic loading (the applied magnetic field $\vec{H}_{\mathbf{ext}}$ and macroscopic stress $\boldsymbol{\Sigma}$). The determination of this constitutive law is based on a localization-homogenization strategy. The generic principle of such a multiscale approach is illustrated on Fig. 1.

3.1. Localization scheme

3.1.1. Definition of the local stress

The aim of this step is to derive the local stress $\boldsymbol{\sigma}^I$ from the external loading, postulating a particular form for the function g in relation (23)

$$\boldsymbol{\sigma}^I = g(\boldsymbol{\Sigma}, \vec{H}_{\mathbf{ext}}). \tag{23}$$

The function g is deduced from a self-consistent approach. Each grain is considered as an inclusion in the homogeneous medium equivalent to the polycrystal, so that the problem can be linked to the solution of the Eshelby inclusion problem (Eshelby, 1957).

The magnetostriction strain $\boldsymbol{\varepsilon}^I_\mu$ is considered as a free strain. The Eshelby tensor $\mathbb{S}^E$ is calculated[6] following Mura (1982). $\mathbb{S}^E$ links the free strain ($\boldsymbol{\varepsilon}^I_\mu$) in a region (the inclusion) of the infinite media to the total strain $\boldsymbol{\varepsilon}^I$ in

[4] Such as the magnetic walls effect, the effect of the non-uniformity of the exchange energy, of the magnetic field or of the stress tensor in the single crystal.

[5] It can be either simulated or measured thanks to X-rays diffraction or electron back scattering diffraction (EBSD) measurements.

[6] For the applications considered in this paper inclusions are taken spherical, assuming an isotropic distribution of the grains.

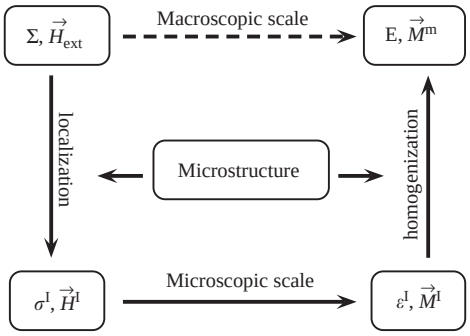

Fig. 1. Multiscale approach—principle.

this region

$$\boldsymbol{\varepsilon}^I = \mathbb{S}^{\mathrm{E}} : \boldsymbol{\varepsilon}_\mu^I. \tag{24}$$

Hill's formula (Hill, 1965) is applied, giving the local stress $\boldsymbol{\sigma}^I$ (at the single crystal scale) as a function of the applied stress $\boldsymbol{\Sigma}$ (at the VER scale), the total strain $\boldsymbol{E}$ and the grain total strain $\boldsymbol{\varepsilon}^I$

$$\boldsymbol{\sigma}^I = \boldsymbol{\Sigma} + \mathbb{C}^* : (\boldsymbol{E} - \boldsymbol{\varepsilon}^I). \tag{25}$$

$\mathbb{C}^*$ is the so-called Hill's constraint tensor, defined according to the Eshelby solution for the inclusion problem

$$\mathbb{C}^* = \mathbb{C} : (\mathbb{S}^{\mathrm{E}^{-1}} - \mathbb{I}), \tag{26}$$

$\mathbb{C}$ is the polycrystal stiffness tensor, and $\mathbb{I}$ the fourth order identity tensor.

Strains are then separated into elastic and magnetostrictive parts:

$$\begin{cases} \boldsymbol{E} = \boldsymbol{E}_{\mathrm{e}} + \boldsymbol{E}_\mu = \mathbb{C}^{-1} : \boldsymbol{\Sigma} + \boldsymbol{E}_\mu, \\ \boldsymbol{\varepsilon}^I = \boldsymbol{\varepsilon}_{\mathrm{e}}^I + \boldsymbol{\varepsilon}_\mu^I = \mathbb{C}^{I^{-1}} : \boldsymbol{\sigma}^I + \boldsymbol{\varepsilon}_\mu^I \end{cases} \tag{27}$$

leading to the relation

$$\boldsymbol{\sigma}^I = \mathbb{B}^I : \boldsymbol{\Sigma} + \mathbb{L}_{\mathrm{inc}}^* : (\boldsymbol{E}_\mu - \boldsymbol{\varepsilon}_\mu^I). \tag{28}$$

The local stress is written as the sum of two terms:

- The first term depends on the macroscopic stress tensor $\boldsymbol{\Sigma}$ and on the stress concentration law. $\mathbb{B}^I$ is the stress concentration tensor in the purely elastic problem. It can be written

$$\mathbb{B}^I = \mathbb{C}^I : \mathbb{A}^I : \mathbb{C}^{-1} \quad \text{with } \mathbb{A}^I = (\mathbb{C}^I + \mathbb{C}^*)^{-1} : (\mathbb{C} + \mathbb{C}^*). \tag{29}$$

- The second term is linked to the elastic incompatibilities due to the existence of the free strain $\boldsymbol{\varepsilon}_\mu^I$ in the grain, and to the stiffness of the surrounding medium. $\boldsymbol{E}_\mu$ is the macroscopic magnetostriction strain. $\mathbb{L}_{\mathrm{inc}}^*$ is defined by

$$\mathbb{L}_{\mathrm{inc}}^* = \mathbb{C}^I : (\mathbb{C}^I + \mathbb{C}^*)^{-1} : \mathbb{C}^*. \tag{30}$$

The proposed expression for this incompatibility stress supposes that the overall behavior remains in the elastic domain.[7] Otherwise relaxation terms would have to be accounted for.[8]

A third term $\boldsymbol{\sigma}_{\mathbf{res}}^I$ can be added in order to account for residual stresses associated to other incompatibility phenomena. These incompatibilities can be linked to plasticity, thermal or transformation strain. Eq. (28)

[7]This condition is verified for most of ferro and ferrimagnetic materials, for which magnetostriction magnitude is about 10^{-6}–10^{-4}, and maximum elastic strain magnitude is about 10^{-3}–10^{-2}.

[8]The approach would then join plasticity or phase transformation micro–macro modeling.

becomes

$$\boldsymbol{\sigma}^I = \mathbb{B}^I : \boldsymbol{\Sigma} + \mathbb{L}^*_{\text{inc}} : (\boldsymbol{E}_\mu - \boldsymbol{\varepsilon}^I_\mu) + \boldsymbol{\sigma}^I_{\mathbf{res}} \tag{31}$$

with

$$\frac{1}{V}\int_{\mathbf{VER}} \boldsymbol{\sigma}^I_{\mathbf{res}}\, \mathrm{d}V = \langle \boldsymbol{\sigma}^I_{\mathbf{res}} \rangle = \boldsymbol{O}. \tag{32}$$

It must be noticed that relation (28) (or (31)) is implicit, since $\boldsymbol{\varepsilon}^I_\mu$ and $\boldsymbol{E}_\mu$ are functions of $\boldsymbol{\sigma}^I$ and $\boldsymbol{\Sigma}$.

3.1.2. Definition of the local magnetic field

The aim of this step is to derive the local magnetic field $\vec{H}^{\mathbf{I}}$ from the external loading, postulating a given form for the function h in relation (33)

$$\vec{H}^{\mathbf{I}} = h(\boldsymbol{\Sigma}, \vec{H}_{\mathbf{ext}}). \tag{33}$$

This equation is usually written (in electrotechnical engineering) in the form of relation (34)

$$\vec{H}^{\mathbf{I}} = \vec{H}_{\mathbf{ext}} + \vec{H}^{\mathbf{I}}_{\mathrm{d}}, \tag{34}$$

where the local perturbation of the macroscopic magnetic field is taken into account through the demagnetizing field $\vec{H}^{\mathbf{I}}_{\mathrm{d}}$. As we must verify

$$\frac{1}{V}\int_{\mathbf{VER}} \vec{H}^{\mathbf{I}}\, \mathrm{d}V = \langle \vec{H}^{\mathbf{I}} \rangle = \vec{H}_{\mathbf{ext}}, \tag{35}$$

we have

$$\frac{1}{V}\int_{\mathbf{VER}} \vec{H}^{\mathbf{I}}_{\mathrm{d}}\, \mathrm{d}V = \langle \vec{H}^{\mathbf{I}}_{\mathrm{d}} \rangle = \vec{0}. \tag{36}$$

Assuming that the mean values for the magnetization and the magnetic fields are sufficient to define the magnetic state of a grain, the demagnetizing field is written

$$\vec{H}^{\mathbf{I}}_{\mathrm{d}} = \boldsymbol{K}_{\mathrm{d}}(\vec{M}^{\mathbf{m}} - \vec{M}^{\mathbf{I}}) \tag{37}$$

with $\vec{M}^{\mathbf{m}}$ the mean magnetization in the material, $\vec{M}^{\mathbf{I}}$ the mean magnetization for the considered grain and $\boldsymbol{K}_{\mathrm{d}}$ a second order operator.

In the case of stress independent linear isotropic magnetic behavior, and spherical inclusions, the tensor $\boldsymbol{K}_{\mathrm{d}}$ can be replaced by a scalar value N_{c} (see Appendix C).

$$N_{\mathrm{c}} = \frac{1}{3 + 2\chi^{\mathbf{m}}}, \quad \chi^{\mathbf{m}} \text{ is the equivalent media susceptibility.} \tag{38}$$

Herein, as a first approximation, we choose to extend this relation to anisotropic non-linear magnetic behavior. We use a variable value of N_{c} computed from the value of $\chi^{\mathbf{m}}$ recalculated at each step of the iterative scheme (secant definition)

$$\chi^{\mathbf{m}} = \frac{\|\vec{M}^{\mathbf{m}}\|}{\|\vec{H}_{\mathbf{ext}}\|}. \tag{39}$$

The localization law[9] (Eq. (34)) is then written

$$\vec{H}^{\mathbf{I}} = \vec{H}_{\mathbf{ext}} + \frac{1}{3 + 2\chi^{\mathbf{m}}}(\vec{M}^{\mathbf{m}} - \vec{M}^{\mathbf{I}}). \tag{40}$$

[9]The adopted modeling is similar to the secant approach used in the framework of micro–macro modeling of plasticity, and exhibits the same limitations, particularly for high levels of non-linearity (Gilormini, 1995).

3.2. Local behavior

Local behavior is defined according to Section 2. The local loading—applied to a grain—being known, the local behavior law can be applied, and the grain response (magnetization and strain) deduced.

3.3. Homogenization

The last step in the micro–macro modeling is the homogenization step to go back to the macro-scale. We define:

$$\begin{cases} \vec{M}^{\mathbf{m}} = \dfrac{1}{V}\displaystyle\int_{\mathbf{VER}} \vec{M}\,\mathrm{d}V = \langle \vec{M}^{\mathbf{I}} \rangle, \\ \boldsymbol{E} = \dfrac{1}{V}\displaystyle\int_{\mathbf{VER}} \boldsymbol{\varepsilon}\,\mathrm{d}V = \langle \boldsymbol{\varepsilon}^{I} \rangle. \end{cases} \tag{41}$$

As the scheme is self-consistent, an iterative procedure has to be built up. The calculation is then done until convergence.

The resolution of a complete coupled magneto-elastic problem requires a numerical implementation of the modeling, including discrete ODF data. An example is given on Section 4.2 in the case of isotropic polycrystalline iron. Nevertheless, analytical solutions can be found in the case of isotropic polycrystals, using similar ideas. The particular case of magnetic saturation, leading to an usual thermo-elastic problem, is treated in Appendix D.

4. Modeling results

4.1. Single crystals

We compare in this section the results of modeling to the experimental data obtained by Webster (1925a,b) for pure iron single crystals.

Low fields measurements give the necessary data to identify the parameter A_s. The initial susceptibility of the single crystal is approximatively estimated thanks to the $\langle 1\,0\,0 \rangle$ magnetization curve

$$\chi^0_{\mathbf{exp}} \backsimeq 2000 \quad \text{leading to } A_s = 1.6 \times 10^{-3}\,\mathrm{m^3\,J^{-1}}. \tag{42}$$

This result is obviously approximative since it is based only on the behavior along the $\langle 1\,0\,0 \rangle$ axis. Experimental data indicate that the initial susceptibility in other directions is a little lower, in disaccordance with our initial hypotheses. The material constants used are defined in Table 1.

Fig. 2(a) (resp. 2(b)) shows the magnetization (resp. the magnetostriction strain) measured in the direction parallel to the magnetic field, when magnetic field is applied along a $\langle 1\,0\,0 \rangle$, $\langle 1\,1\,0 \rangle$ or $\langle 1\,1\,1 \rangle$ axis of the single crystal. We observe a very good agreement between numerical and experimental results, both for magnetic and magnetostrictive behaviors. Strong non-linearity and anisotropy are well reproduced.

4.2. Polycrystals

In the case of polycrystals, the choice of a discrete modeling seems quite natural as the texture data (ODF) are often available under the form of discrete data.

Table 1
Pure iron single crystal characteristics—bibliographic data

Constant	Value	Reference
M_s	$1.71 \times 10^6\,\mathrm{A/m}$	Bozorth (1951), Cullity (1972), Jiles (1991)
$(K_1; K_2)$	$(42.7; 15)\,\mathrm{kJ/m^3}$	Bozorth (1951)
$(\lambda_{100}; \lambda_{111})$	$(21; -21)10^{-6}$	Cullity (1972), Jiles (1991)
(C_{11}, C_{12}, C_{44})	(238;142;232) GPa	McClintock and Argon (1966)

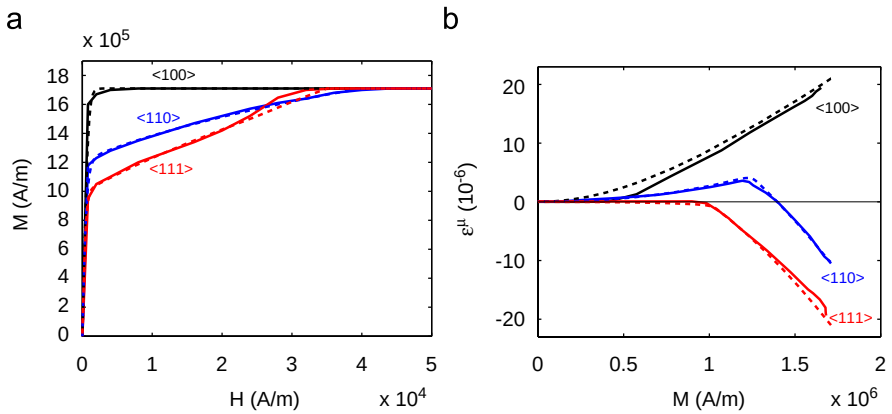

Fig. 2. Pure iron single crystal behaviour. Experimental data (Webster, 1925a,b) (line) and numerical results (dashed line): (a) magnetization curve; (b) magnetostrictive curve.

Modeling results are illustrated in the case of isotropic pure iron polycrystal. The material parameters used are listed in Table 1. They are relative to the single crystal, except A_s. The experimental results of Kuruzar and Cullity (1971) allow to define the parameter A_s in the case of iron: $A_s = 2 \times 10^{-3}\,\mathrm{m^3\,J^{-1}}$.

The first possible way to describe the crystallographic orientation distribution function is to choose of a random orientation for each grain. This choice leads to a great uncertainty on the results obtained for the magnetostriction strain as it is illustrated in Fig. 3.[10]

For a number of 100 orientations, the obtained value of the saturation magnetostriction strain lies in a wide band—150% around the theoretical value. This dispersion (defined with a six standard deviation width) is very slowly decreasing when increasing the number of orientations. A 1000 orientations distribution function does not allow to define the magnetostriction in a band thinner than 50% around the theoretical value. The mean value over the 200 random distribution functions leads approximatively to the correct value for the saturation strain, whatever the—reasonable—number of orientations chosen. A solution to get precise results would be to define a great number of random distribution functions, and to define the mean value for the obtained results. This solution appears to be expensive in terms of computation time.

Another choice, already used by Buiron (2000), is to build a regular zoning in the space of possible orientations. Each crystal is defined by three Euler angles (φ_1, ψ, φ_2) following Bunge notation. Each angle takes values regularly distributed in their variation domain, following Table 2.

The number of values taken in each space domain gives the precision of the texture isotropy. Limitation is still linked to the number of orientations which has to be low in order to get reasonable computation times. One possible ODF is made of 546 different orientations. The corresponding poles figures are given in Fig. 4.

This regular distribution exhibits a weak but obvious isotropic transverse symmetry. As shown in Fig. 3, the Reuss magnetostriction saturation strain is a good indicator of anisotropy for a given texture. It has been calculated for the 546 orientations texture, considering a great number (2000) of random directions of the magnetic field. The obtained mean value is -4.18×10^{-6}, which is very near from the theoretical value (-4.20×10^{-6}). Standard deviation reaches $S = 6.8 \times 10^{-8}$, so that the dispersion reported in Fig. 3 is associated to an error bar of ± 0.05. This dispersion corresponds to a number of random orientations more than 5000. As a conclusion, the constructed data file leads to quasi-isotropic behavior and will be kept to describe isotropic materials.

The multiscale approach presented in Section 3 has been applied using this "isotropic" texture data, and the iron single crystal characteristics (Table 1).

[10]The sensibility of the results to the texture data is highly dependent on the contrast between the constants λ_{100} and λ_{111}.

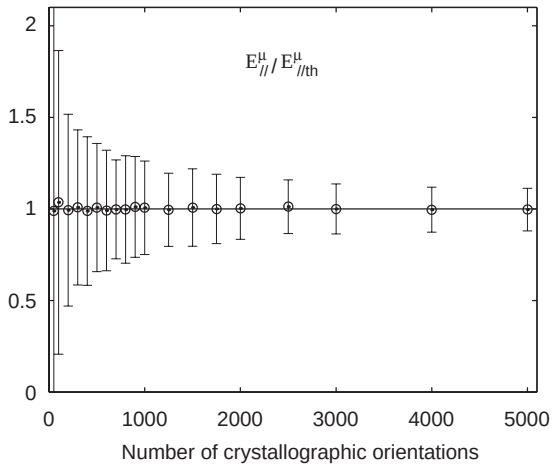

Fig. 3. Dispersion obtained—for 200 random orientation distribution functions—on the Reuss estimate value for the saturation magnetostriction strain, depending on the number of orientations considered for this distribution function.

Table 2
Values chosen for the Euler angle for the "isotropic" texture

Variable	Domain	Number of values
φ_1	$[0, 2\pi]$	13
$\cos\psi$	$[0, 1]$	7
φ_2	$[0, 2\pi]$	6

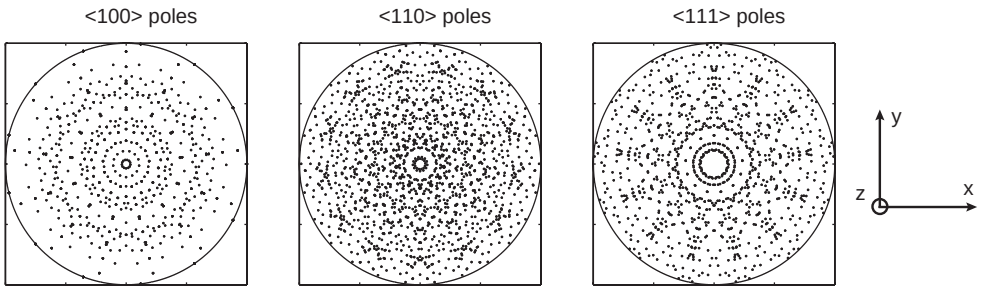

Fig. 4. Pole figures for the "isotropic" polycrystal obtained by regular zoning of the crystallographic orientations space (stereographic projection).

4.2.1. Elastic behavior

Self-consistent and Voigt estimates for the shear modulus associated to this (discrete) virtual material have been calculated:

$$\mu^{\mathbf{eff}\,\mathbf{SC}} \simeq 82.1\,\mathrm{GPa} \quad \text{and} \quad \mu^{\mathbf{eff}\,\mathbf{V}} \simeq 88.8\,\mathrm{GPa}. \tag{43}$$

The calculation of the corresponding theoretical values is presented in Appendix D. If no more significant figure is needed, the results given by the discrete approach are exactly the same than the analytical ones (Table D.1). From that observation, we can conclude that the 546 orientations distribution allows an accurate description of the elastic behavior of an isotropic polycrystal.

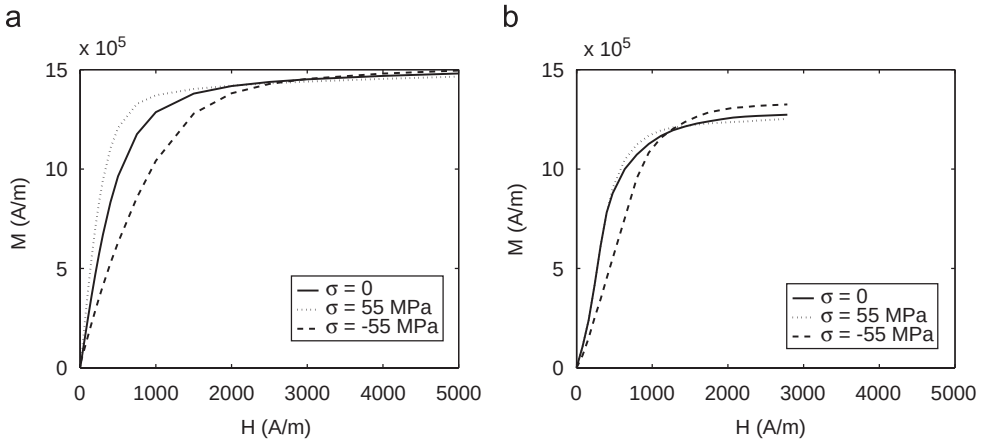

Fig. 5. Effect of uniaxial stress on the magnetization curve: (a) numerical results; (b) experimental results (Kuruzar and Cullity, 1971).

4.2.2. Saturation magnetostriction strain

The saturation magnetostriction strain is obtained using a very high applied magnetic field along the $\vec{z}$ axis.[11] Self-consistent and Reuss estimates have been calculated

$$\boldsymbol{E}^{\|546}_{\mu_{\mathbf{SC}}} = -8.95 \times 10^{-6} \quad \text{and} \quad \boldsymbol{E}^{\|546}_{\mu_{\mathbf{R}}} = -4.41 \times 10^{-6}. \tag{44}$$

These results are close to the analytical ones presented in Table D.2, but the agreement is less accurate than for elastic properties: magnetostrictive properties of polycrystals are much more texture dependent than elastic properties.

4.2.3. Magnetic behavior

The multiscale modeling allows to predict both the magnetic and magnetostrictive behaviors of the material for different values of the external field and stress. In this case, no analytical solution are available, since linear behavior and field homogeneity assumptions cannot be made anymore. Results obtained for the anhysteretic magnetization curves are shown in Fig. 5(a) for several levels of uniaxial applied stress. Fig. 5(b) shows corresponding experimental results obtained by Kuruzar and Cullity (1971) for pure polycrystalline iron (see also Cullity, 1972).

Comparison between experimental and numerical results shows that the multiscale model seems to describe correctly the effect of an applied stress. For low levels of magnetic field, a tensile stress increases the magnetic susceptibility whereas a compression decreases it, in a stronger way. This effect is inversed for higher levels of the applied magnetic field (Villari reversal), and the modeling reproduces it. The crossover between the magnetization curves for different stress levels is usually explained by an inversion of the evolution of the magnetostriction strain, introducing a change in the sense of variation for the magneto-elastic energy. This point is directly related to the magnetization rotation mechanism.

Nevertheless, the modeling tends to overestimate the magnetic behavior, and the crossover point between the different magnetization curves is obtained for higher magnetic field levels. However, the quantitative comparison is hazardous, since the results of Kuruzar and Cullity (1971) are first magnetization curves (meaning hysteretic measurements). Moreover the material used by Kuruzar and Cullity (1971) is supposed to be isotropic, but the grain orientation distribution is actually unknown.

4.2.4. Magnetostrictive behavior

Experimental observations (Fig. 6(b)) show that the magnetostriction strain first increases with the applied field and then decreases until a saturation point is reached. The effect of the magnetic field on the strain is

[11] $\vec{z}$ is the direction normal to the plane of poles figures.

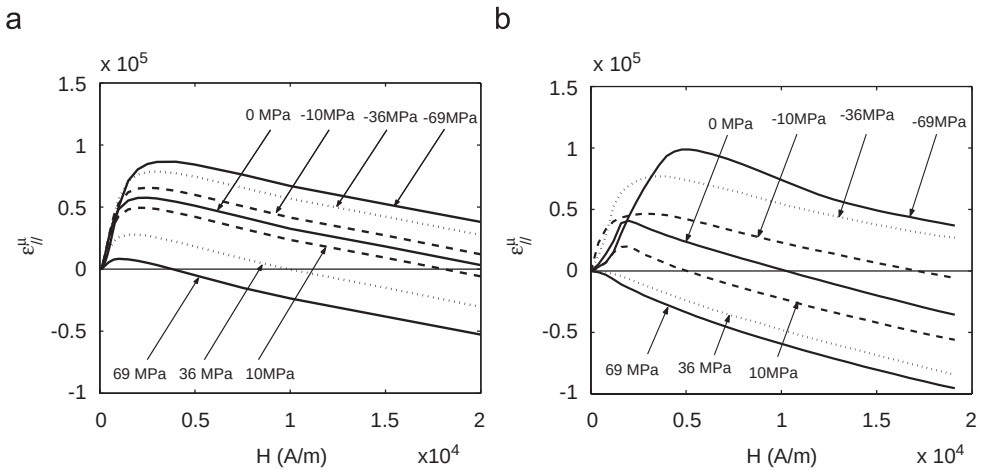

Fig. 6. Effect of uniaxial stress on the magnetostriction curve: (a) numerical results; (b) experimental results (Kuruzar and Cullity, 1971).

correctly reproduced by the modeling[12] (Fig. 6(a)), qualitatively concerning the general level, and quantitatively concerning the slopes of the curves. The effect of uniaxial stress on the strain level is correctly reproduced, even if the observed amplitude for the strain variations is higher than the predicted one.

5. Conclusion

In this paper, a model for the reversible magneto-mechanical behavior of magnetic materials, accounting for 3D magnetization and multiaxial stress state has been presented.

The multiscale model can be described as a simplified micro-magnetic model. Several scales are chosen to define the magneto-elastic behavior, leading to a multiscale calculation strategy. The first scale is the magnetic domains scale, at which the magnetization can be considered as homogeneous. The next scale is the single crystal scale where elastic properties are homogeneous. The last scale is the RVE scale, which is large enough to define the average material behavior and properties. Calculation of whole magneto-elastic behavior requires the use of a single crystal modeling.

Potential energy is written at domain scale considering three energetic terms: magnetostatic energy, magnetocrystalline energy and elastic energy. The internal variables are volumetric fraction and magnetization orientation of each magnetic domain family: it means 18 internal variables for crystals with $\langle 1\,0\,0\rangle$ easy directions and 24 for crystal with $\langle 1\,1\,1\rangle$ easy directions. Each internal variable is calculated thanks to a two steps procedure: energetic minimization for orientations calculation and explicit Boltzmann formulation for the calculation of volumetric fractions. Single crystal magnetization and magnetostriction are calculated thanks to averaging operations over the domains.

Specific localization and homogenization procedures from RVE to grain scale are nevertheless required for local magnetic and mechanical fields calculation. Secant approach is used for magnetic behavior, which is strongly non-linear; elastic behavior remains linear and convergence is easily reached.

The multiscale model is able to predict: (1) magnetic behavior; (2) elastic behavior; (3) influence of multiaxial stress state on magnetization; (4) magnetostrictive behavior; (5) influence of multiaxial stress state on the magnetostrictive behavior; isotropic material as well as strongly textured material (Hubert et al., 2003) can be considered. Comparisons to experimental data obtained from iron-silicon sheets (Daniel et al., 2003), or isotropic ferrimagnetic NiZn ferrite (Vieille et al., 2004; Daniel et al., 2007) are conclusive.

The main shortcomings of the model are first that magnetic and mechanical fields are considered homogeneous within a single crystal; second that domain walls are not taken into account (domain walls lead

[12]For which the reference strain is put to zero at zero magnetic field, whatever the stress level. It is imposed by the presentation of the experimental data.

to an increase of energy due to exchange energy contribution). A third important limitation is that the domain configuration is only seen through volumetric fractions, which is insufficient when considering the importance of the domains distribution on the local demagnetizing fields. Finally, surface effect has to be considered when the grain size is comparable to the thickness of material (Hubert et al., 2003; Daniel et al., 2004).

Future developments will consist in introducing residual stresses effects such as plasticity or thermal stresses, and dynamic and dissipative phenomena.

Appendix A

A.1. Definition of the elastic energy

The elastic energy for a domain is written

$$W_\sigma = \tfrac{1}{2}\boldsymbol{\varepsilon}_e^\alpha : \mathbb{C}^I : \boldsymbol{\varepsilon}_e^\alpha = \tfrac{1}{2}\boldsymbol{\sigma}^\alpha : \mathbb{C}^{I^{-1}} : \boldsymbol{\sigma}^\alpha. \tag{A.1}$$

Several cases can be considered:

- If the stress is supposed uniform over the grain, $\boldsymbol{\sigma}^\alpha = \boldsymbol{\sigma}^I$, and then

$$W_\sigma^\alpha = \tfrac{1}{2}\boldsymbol{\sigma}^I : \mathbb{C}^{I^{-1}} : \boldsymbol{\sigma}^I. \tag{A.2}$$

  This term is uniform over a single crystal, no magneto-elastic interaction appears.
- If the strain is supposed uniform over the grain, $\boldsymbol{\varepsilon}^\alpha = \boldsymbol{\varepsilon}^I$, and then

$$\begin{aligned} W_\sigma^\alpha &= \tfrac{1}{2}\boldsymbol{\varepsilon}_e^\alpha : \mathbb{C}^I : \boldsymbol{\varepsilon}_e^\alpha \\ &= \tfrac{1}{2}(\boldsymbol{\varepsilon}^\alpha - \boldsymbol{\varepsilon}_\mu^\alpha) : \mathbb{C}^I : (\boldsymbol{\varepsilon}^\alpha - \boldsymbol{\varepsilon}_\mu^\alpha) \\ &= \tfrac{1}{2}\boldsymbol{\varepsilon}^\alpha : \mathbb{C}^I : \boldsymbol{\varepsilon}^\alpha + \tfrac{1}{2}\boldsymbol{\varepsilon}_\mu^\alpha : \mathbb{C}^I : \boldsymbol{\varepsilon}_\mu^\alpha - \boldsymbol{\varepsilon}_\mu^\alpha : \mathbb{C}^I : \boldsymbol{\varepsilon}^\alpha \\ &= \tfrac{1}{2}\boldsymbol{\varepsilon}^I : \mathbb{C}^I : \boldsymbol{\varepsilon}^I + \tfrac{1}{2}\boldsymbol{\varepsilon}_\mu^\alpha : \mathbb{C}^I : \boldsymbol{\varepsilon}_\mu^\alpha - \boldsymbol{\varepsilon}_\mu^\alpha : \mathbb{C}^I : (\boldsymbol{\varepsilon}_\mu^I + \boldsymbol{\varepsilon}_e^I) \\ &= \tfrac{1}{2}\boldsymbol{\varepsilon}^I : \mathbb{C}^I : \boldsymbol{\varepsilon}^I + \tfrac{1}{2}\boldsymbol{\varepsilon}_\mu^\alpha : \mathbb{C}^I : \boldsymbol{\varepsilon}_\mu^\alpha - \boldsymbol{\varepsilon}_\mu^\alpha : \mathbb{C}^I : \boldsymbol{\varepsilon}_\mu^I - \boldsymbol{\sigma}^I : \boldsymbol{\varepsilon}_\mu^\alpha. \end{aligned} \tag{A.3}$$

  A magneto-elastic interaction appears. If we neglect the second order terms (considering that $\mathbb{C}^I : \boldsymbol{\varepsilon}_\mu^\alpha$ and $\mathbb{C}^I : \boldsymbol{\varepsilon}_\mu^I$ are much smaller than $\boldsymbol{\sigma}^I$), we get the usual magneto-elastic interaction term (Hubert and Schäfer, 1998)

$$W_\sigma^\alpha = W_\sigma^o - \boldsymbol{\sigma}^I : \boldsymbol{\varepsilon}_\mu^\alpha, \tag{A.4}$$

  W_σ^o being a constant over the grain, whatever the magnetization state

$$W_\sigma^o = \tfrac{1}{2}\boldsymbol{\varepsilon}^I : \mathbb{C}^I : \boldsymbol{\varepsilon}^I. \tag{A.5}$$

- Hill's approach can also be used (Hill, 1965) to treat an intermediate situation. Hill's formula is applied, giving the local stress $\boldsymbol{\sigma}^\alpha$ as a function of the applied stress $\boldsymbol{\sigma}^I$ (at the single crystal scale), the single crystal total strain $\boldsymbol{\varepsilon}^I$ and the domain total strain $\boldsymbol{\varepsilon}^\alpha$

$$\boldsymbol{\sigma}^\alpha = \boldsymbol{\sigma}^I + \mathbb{C}^* : (\boldsymbol{\varepsilon}^I - \boldsymbol{\varepsilon}^\alpha). \tag{A.6}$$

  $\mathbb{C}^*$ is the so-called Hill's constraint tensor, defined after the Eshelby solution for the inclusion problem (Eshelby, 1957)

$$\mathbb{C}^* = \mathbb{C}^I : (\mathbb{S}^{E^{-1}} - \mathbb{I}). \tag{A.7}$$

  $\mathbb{S}^E$ is the so-called Eshelby tensor, and $\mathbb{I}$ the fourth order identity tensor. The strain is then separated into elastic and magnetostrictive parts

$$\begin{cases} \boldsymbol{\varepsilon}^I = \boldsymbol{\varepsilon}_e^I + \boldsymbol{\varepsilon}_\mu^I = \mathbb{C}^{I^{-1}} : \boldsymbol{\sigma}^I + \boldsymbol{\varepsilon}_\mu^I, \\ \boldsymbol{\varepsilon}^\alpha = \boldsymbol{\varepsilon}_e^\alpha + \boldsymbol{\varepsilon}_\mu^\alpha = \mathbb{C}^{I^{-1}} : \boldsymbol{\sigma}^\alpha + \boldsymbol{\varepsilon}_\mu^\alpha \end{cases} \tag{A.8}$$

leading to the relation

$$\boldsymbol{\sigma}^{\alpha} = \boldsymbol{\sigma}^{I} + \mathbb{C}^{I} : (\mathbb{I} - \mathbb{S}^{\mathrm{E}}) : (\boldsymbol{\varepsilon}_{\mu}^{I} - \boldsymbol{\varepsilon}_{\mu}^{\alpha}). \tag{A.9}$$

The elastic energy can now be written

$$\begin{aligned} W_{\sigma}^{\alpha} &= \tfrac{1}{2}\boldsymbol{\sigma}^{\alpha} : \mathbb{C}^{I^{-1}} : \boldsymbol{\sigma}^{\alpha} \\ &= \tfrac{1}{2}\boldsymbol{\sigma}^{I} : \mathbb{C}^{I^{-1}} : \boldsymbol{\sigma}^{I} + \tfrac{1}{2}(\boldsymbol{\varepsilon}_{\mu}^{I} - \boldsymbol{\varepsilon}_{\mu}^{\alpha}) : \mathbb{C}^{I} : (\mathbb{I} - \mathbb{S}^{\mathrm{E}}) : (\boldsymbol{\varepsilon}_{\mu}^{I} - \boldsymbol{\varepsilon}_{\mu}^{\alpha}) + \boldsymbol{\sigma}^{I} : (\mathbb{I} - \mathbb{S}^{\mathrm{E}}) : (\boldsymbol{\varepsilon}_{\mu}^{I} - \boldsymbol{\varepsilon}_{\mu}^{\alpha}) \\ &= W_{\sigma}^{\mathrm{o}} - \boldsymbol{\sigma}^{I} : (\mathbb{I} - \mathbb{S}^{\mathrm{E}}) : \boldsymbol{\varepsilon}_{\mu}^{\alpha} + \tfrac{1}{2}\boldsymbol{\varepsilon}_{\mu}^{\alpha} : \mathbb{C}^{I} : (\mathbb{I} - \mathbb{S}^{\mathrm{E}}) : \boldsymbol{\varepsilon}_{\mu}^{\alpha} - \boldsymbol{\varepsilon}_{\mu}^{I} : \mathbb{C}^{I} : (\mathbb{I} - \mathbb{S}^{\mathrm{E}}) : \boldsymbol{\varepsilon}_{\mu}^{\alpha}. \end{aligned} \tag{A.10}$$

If $\mathbb{S}^{\mathrm{E}}$ is supposed constant, W_{σ}^{o} is a constant over the grain, whatever the magnetization state

$$W_{\sigma}^{\mathrm{o}} = \tfrac{1}{2}\boldsymbol{\sigma}^{I} : \mathbb{C}^{I^{-1}} : \boldsymbol{\sigma}^{I} + \tfrac{1}{2}\boldsymbol{\varepsilon}_{\mu}^{I} : \mathbb{C}^{I} : (\mathbb{I} - \mathbb{S}^{\mathrm{E}}) : \boldsymbol{\varepsilon}_{\mu}^{I} + \boldsymbol{\sigma}^{I} : (\mathbb{I} - \mathbb{S}^{\mathrm{E}}) : \boldsymbol{\varepsilon}_{\mu}^{I}. \tag{A.11}$$

Only the non-uniform part of W_{σ}^{α} plays a role in the energetic equilibrium. The latter assumptions leads to intermediate estimates, but is associated to more complicated calculations (to get the Eshelby tensor).

Appendix B. A simplified approach for the identification of A_{s} parameter

B.1. Single crystal

B.1.1. A simplified approach

When the description of the magnetic behavior is restricted to low fields and stress states, the rotation mechanism is usually neglected. A way to define the validity range of such an hypothesis is to consider the so-called "anisotropy" field (Chikazumi, 1997). The anisotropy magnetic and stress fields are defined by Eq. (B.1)

$$H_K = \frac{K_1}{\mu_0 M_{\mathrm{s}}} \quad \text{and} \quad \sigma_K = \frac{K_1}{\lambda_S}. \tag{B.1}$$

The rotation mechanism can be neglected until magnetic field or stress levels stand far from the anisotropy fields.[13]

Under these conditions, the potential energy of a domain can be written

$$W^{\alpha} = -\mu_0 \vec{M}^{\alpha}.\vec{H}^{\mathbf{I}}. \tag{B.2}$$

The volumetric fraction of each domain family is still defined by Eq. (18). We note, for further simplifications

$$\begin{cases} \vec{M}^{\alpha} = M_{\mathrm{s}}\vec{\gamma}^{\alpha}, \\ H = \|\vec{H}^{\mathbf{I}}\|, \\ S = \sum\limits_{\alpha} \exp(-A_{\mathrm{s}}.W^{\alpha}), \\ K = A_{\mathrm{s}}\mu_0 H M_{\mathrm{s}}. \end{cases} \tag{B.3}$$

In the crystallographic frame, using spherical coordinates for the magnetic field ($\vec{H}^{\mathbf{I}} = H[\sin\varphi\cos\theta, \sin\varphi\sin\theta, \cos\varphi]$), the potential energy of the domain families can be explicitly written, and S is deduced:

$$S = 2(\cosh(K\sin\varphi\cos\theta) + \cosh(K\sin\varphi\sin\theta) + \cosh(K\cos\varphi)). \tag{B.4}$$

The single crystal magnetization is given by

$$\vec{M}^{\mathbf{I}} = \frac{2M_{\mathrm{s}}}{S} \begin{vmatrix} \sinh(K\sin\varphi\cos\theta), \\ \sinh(K\sin\varphi\sin\theta), \\ \sinh(K\cos\varphi). \end{vmatrix} \tag{B.5}$$

[13] H_K (resp. σ_K) corresponds to a situation when the magnetic energy (resp. the elastic energy) totally compensate the magneto-crystalline energy. In the case of iron $H_K \simeq 20\,\mathrm{kA/m}$ and $\sigma_K \simeq 2\,\mathrm{GPa}$. In the case of nickel $H_K \simeq 5.5\,\mathrm{kA/m}$ and $\sigma_K \simeq 73\,\mathrm{MPa}$.

The single crystal magnetostriction can also be written

$$\varepsilon_{\mu}^{I}=\frac{\lambda_{100}}{S}\begin{pmatrix} 2\cosh(K\sin\varphi\cos\theta) & 0 & 0 \\ -(\cosh(K\sin\varphi\sin\theta)+\cosh(K\cos\varphi)) & & \\ 0 & 2\cosh(K\sin\varphi\sin\theta) & 0 \\ & -(\cosh(K\sin\varphi\cos\theta)+\cosh(K\cos\varphi)) & \\ 0 & 0 & 2\cosh(K\cos\varphi) \\ & & -(\cosh(K\sin\varphi\cos\theta)+\cosh(K\sin\varphi\sin\theta)) \end{pmatrix}. \tag{B.6}$$

These relations can be considered as a simplified modeling for the magnetization and magnetostriction of a single crystal as a function of the applied magnetic field. This modeling is anisotropic, as coordinates θ and φ are involved. Its validity area is however very tiny as it does not account for rotation mechanisms nor effect of an applied stress.

Experimental data obtained by Webster (1925a) for pure iron are reported in Fig. B.1 and compared to modeling results. Since the modeling does not account for the out of easy directions rotation mechanism, the simplified model will not be able to predict a saturation state if the applied field is oriented along a $\langle 1\,1\,0\rangle$ or $\langle 1\,1\,1\rangle$ direction, or more generally in a direction that is not an easy magnetization direction.

B.1.2. Initial susceptibility definition

The assumptions made in the previous paragraph do not allow to use this modeling for high magnetic fields. But interesting informations can be obtained in the vicinity of a null applied field. We can observe the evolution of the magnetization in the vicinity of zero by calculating its derivative with H. After calculation, we obtain

$$\left.\frac{\partial\vec{M}^{\mathbf{1}}}{\partial H}\right|_{H=0}=\frac{\mu_0 A_s M_s^2}{3}\frac{\vec{H}}{H}. \tag{B.7}$$

Near the origin, the magnetization rises and keeps its direction parallel to the applied magnetic field. The material initial susceptibility, defined as the slope at the origin of the magnetization curve, can thus be written

$$\chi^0=\tfrac{1}{3}A_s\mu_0 M_s^2. \tag{B.8}$$

The constant A_s can therefore be identified using a single magnetization curve of the crystal

$$A_s=\frac{3\chi^0}{\mu_0 M_s^2}. \tag{B.9}$$

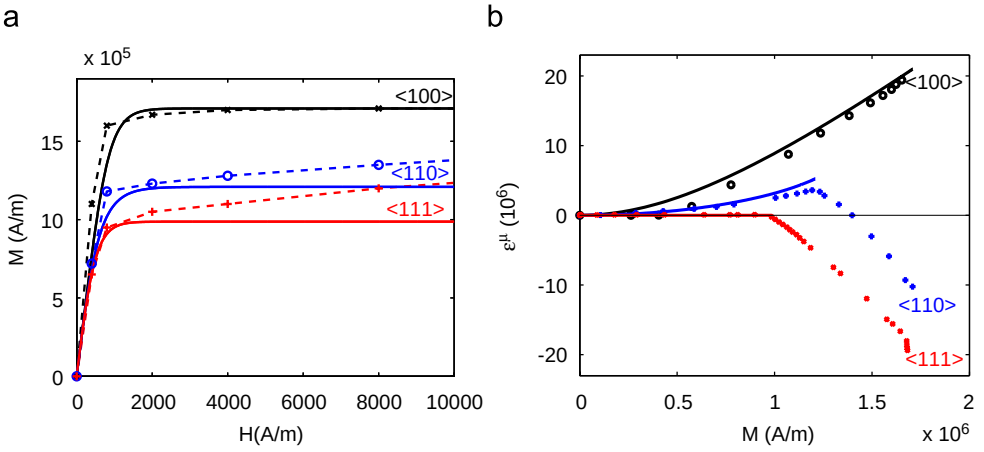

Fig. B.1. Simplified modeling for the iron single crystal behavior: experimental data (Webser, 1925a,b) (lines) and numerical results (dots): (a) magnetization; (b) magnetostriction.

The proposed simplified modeling is isotropic near the origin, as the predicted initial susceptibility is the same for every direction of the single crystal, and the predicted magnetization is parallel to the applied magnetic field. The anisotropic character of the behavior only appears for higher magnetic fields.

B.2. Polycrystals

B.2.1. A simplified approach

Let us consider an—ideal—unstressed bulk isotropic ferromagnetic material. The polycrystal microstructure is seen as an assembly of magnetic domains. By opposition to the single crystal, all the possible orientations in space are considered equiprobable, and the domains are randomly distributed. The macroscopic behavior is then isotropic.

We will estimate the polycrystal behavior by considering that a polycrystal is a single crystal for which all space directions are easy magnetization directions. For each domain α, we can write

$$\vec{M}^{\alpha} = M_s \vec{\gamma}^{\alpha}. \tag{B.10}$$

The macroscopic magnetization is written

$$\vec{M} = \frac{1}{V}\int_V \vec{M}^{\alpha}\,\mathrm{d}V = M_s \int_{\alpha} f^{\alpha}\vec{\gamma}^{\alpha}\,\mathrm{d}\alpha. \tag{B.11}$$

Using the same notations and simplifications than in Section B.1, we define

$$f^{\alpha} = \frac{1}{S}\exp(K\cos\varphi) \tag{B.12}$$

with

$$S = \int_{\alpha} \exp(-A_s W^{\alpha})\,\mathrm{d}\alpha = \int_{\alpha} \exp(A_s \mu_0 M_s \vec{\gamma}^{\alpha}.\vec{H})\,\mathrm{d}\alpha. \tag{B.13}$$

If the magnetic field is aligned with the $\vec{z}$ direction ($\vec{H} = H[0,0,1]$), we get

$$S = \frac{4\pi\sinh K}{K} \tag{B.14}$$

so that

$$\vec{M} = M_s \frac{K\cosh(K) - \sinh(K)}{K\sinh(K)}\vec{z}. \tag{B.15}$$

B.2.2. Initial susceptibility definition

This macroscopic modeling does not take into account the magnetization rotation mechanism, and thus, its validity domain is limited to the low applied fields area. Furthermore, only unstressed material has been considered. An interesting quantity to be studied is the initial susceptibility χ^0

$$\chi^0 = \left.\frac{\partial M_z}{\partial H}\right|_{H=0}. \tag{B.16}$$

We get

$$\frac{\partial M_z}{\partial H} = A_s \mu_0 M_s^2 \frac{\sinh^2(K) - K^2}{K^2\sinh^2(K)} \tag{B.17}$$

leading to, for $K = 0$

$$\chi^0 = \tfrac{1}{3} A_s \mu_0 M_s^2. \tag{B.18}$$

We obtain for a polycrystal, the same definition for χ^0 as in the case of a single crystal. This point results from the fact that, in the simplified approach, the polycrystal is seen as a single crystal with an infinity of easy magnetization directions (all directions of space being easy magnetization directions). A way to identify the value for A_s is to get the initial slope of the macroscopic anhysteretic magnetization curve, and to deduce the

value of A_s from it

$$A_s = \frac{3\chi^0}{\mu_0 M_s^2}. \tag{B.19}$$

B.3. Simplified modeling for the anhysteretic magnetostriction curve

As for the magnetization curve, it is possible to define a simplified modeling for the magnetostriction curve. This approach neglects the magnetization rotation phenomenon, so that the extreme value for magnetostriction is identical to its saturation value.

The definition of the volumetric fractions given by Eq. (B.12) is still correct. The single crystal magnetostriction strain can be written, considering that the stress is uniformly zero within the material:

$$\boldsymbol{E}_\mu = \int_\alpha f^\alpha \boldsymbol{\varepsilon}_\mu^{\alpha\prime}\, \mathrm{d}\alpha. \tag{B.20}$$

The definition of $\boldsymbol{\varepsilon}_\mu^{\alpha\prime}$ has to be specified. This definition is different from the usual definition of the magnetostriction strain in a domain (given in Eq. (D.9)) in order to account for the fact that crystallographic data has been totally neglected in this simplified modeling. $\boldsymbol{\varepsilon}_\mu^{\alpha\prime}$ must satisfy the two following properties:

- When the applied field is zero, the macroscopic magnetostriction strain is zero.
- When saturation is reached, $\boldsymbol{E}_\mu$ reaches a maximum value $\mathbf{E}_{\mu_{\mathbf{max}}}$ (that can be taken from Appendix D).

Considering the saturation state, for which the volumetric fraction of a domain—the one whose magnetization is parallel to the applied field—becomes 1, and the others become zero, we get

$$\boldsymbol{\varepsilon}_\mu^{\alpha\prime} = \mathbf{E}_{\mu_{\mathbf{max}}}. \tag{B.21}$$

As it is shown in Appendix D, this value can be written

$$\boldsymbol{\varepsilon}_\mu^{\alpha\prime} = \frac{2}{5}\lambda_{100} k^{\mathbf{a}} \begin{pmatrix} 1 & 0 & 0 \\ 0 & -\frac{1}{2} & 0 \\ 0 & 0 & -\frac{1}{2} \end{pmatrix}. \tag{B.22}$$

This strain tensor, initially written in the macroscopic frame, becomes the strain tensor of each domain family, in their own local frame.

The magnetostriction strain component $\mathbf{E}_{\mu_{zz}}$, parallel to the magnetic field can then be written

$$\mathbf{E}_{\mu_{zz}} = \int_\alpha f^\alpha ({}^t\vec{z}\,\boldsymbol{\varepsilon}_\mu^{\alpha\prime}\vec{z})\, \mathrm{d}\alpha. \tag{B.23}$$

Using the definition of f^α and $\boldsymbol{\varepsilon}_\mu^{\alpha\prime}$, we get

$$\mathbf{E}_{\mu_{zz}} = \int_0^{2\pi}\int_0^{\pi} \frac{2\lambda_{100} k^{\mathbf{a}}}{5S} \exp(K\cos\varphi)\left(1 - \frac{3}{2}\sin^2\varphi\right)\sin\varphi\, \mathrm{d}\varphi\, \mathrm{d}\theta \tag{B.24}$$

leading to, after calculation

$$\mathbf{E}_{\mu_{zz}} = \frac{2}{5}\lambda_{100} k^{\mathbf{a}}\left[1 - \frac{3\cosh(K)}{K\sinh(K)} + \frac{3}{K^2}\right]. \tag{B.25}$$

As shown in Appendix D, several estimates can be chosen to calculate the value of $k^{\mathbf{a}}$. For instance, the self-consistent estimate can be used. In the case of iron

$$\tfrac{2}{5}\lambda_{100} k^{\mathbf{a}} = 6.13 \times 10^{-6}. \tag{B.26}$$

Appendix C. Determination of the magnetic field localization operator

Relations (37) and (38) defining the localization law for the magnetic field are derived from the solution of a magnetostatic problem for an inclusion.

We consider a spherical isotropic magnetic region embedded in an infinite isotropic magnetic medium (Fig. C.1). This medium is submitted to an uniform (at the boundary) magnetic field $\vec{H}^{\infty} = H^{\infty}\vec{x}$.

The behavior law for the spherical region (of radius R) is written

$$\vec{M}^{\mathbf{I}} = \chi^{I}\vec{H}^{\mathbf{I}}. \tag{C.1}$$

The behavior law for the infinite medium is written

$$\vec{M}^{\mathrm{o}} = \chi^{\mathrm{o}}\vec{H}^{\mathrm{o}}. \tag{C.2}$$

Without any current density, the Maxwell equations can be written

$$\begin{cases} \operatorname{div}\vec{B} = 0, & \text{where } \vec{B} \text{ denotes the magnetic induction,} \\ \vec{\operatorname{rot}}\,\vec{H} = \vec{0}, & \text{where } \vec{H} \text{ denotes the magnetic field.} \end{cases} \tag{C.3}$$

Under these conditions, the magnetic field can be derived from a scalar potential:

$$\vec{H} = -\vec{\operatorname{grad}}\,\varphi. \tag{C.4}$$

Applying the isotropic behavior law ($\vec{B} = \mu\vec{H}$) leads to the Poisson equation for the potential:

$$\Delta\varphi = 0. \tag{C.5}$$

The solutions for the potential φ can be written

$$\begin{cases} \varphi^{\mathrm{I}} = -H^{\mathrm{I}}\, r\cos\theta, & \text{inside the sphere,} \\ \varphi^{\mathrm{o}} = -H^{\infty} r\left(1 - \dfrac{k}{r^3}\right)\cos\theta, & \text{outside the sphere,} \end{cases} \tag{C.6}$$

H^{∞} being the value for the magnetic field very far from the inclusion. The magnetic field can then be written, following Eq. (C.4):

- Inside the sphere:

$$\vec{H}^{\mathbf{I}} = H^{\mathrm{I}}\vec{x}. \tag{C.7}$$

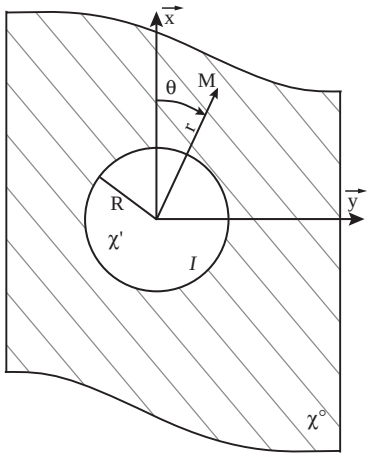

Fig. C.1. Schematic representation of the inclusion problem.

- Outside the sphere:

$$\vec{H}^{\mathrm{o}} = H^{\infty}\left[\left(1+\frac{k}{r^3}(3\cos^2\theta-1)\right)\vec{x}+\frac{3k}{r^3}\cos\theta\sin\theta\,\vec{y}\right]. \tag{C.8}$$

The boundary conditions at the interface of the inclusion give ($\vec{n}$ is the unit vector normal to the sphere surface):

(a) For $\theta=\pi/2$ and $r=R$:

$$[\vec{H}]\wedge\vec{n}=0 \;\Rightarrow\; H^{\mathrm{I}} = H^{\infty}\left(1-\frac{k}{R^3}\right), \tag{C.9}$$

where the symbol $[\vec{H}]$ denotes the jump of $\vec{H}$ through the surface ($[\vec{H}]=\vec{H}^{\mathrm{ext}}-\vec{H}^{\mathrm{int}}$).

From Eq. (C.9) we can deduce

$$k=\left(1-\frac{H^{\mathrm{I}}}{H^{\infty}}\right)R^3. \tag{C.10}$$

(b) For $\theta=0$ and $r=R$

$$\begin{aligned}[\vec{B}].\vec{n}=[\vec{H}+\vec{M}].\vec{x}=0 \;&\Rightarrow\; M^{\mathrm{I}}+H^{\mathrm{I}}=M^{\mathrm{o}}(0,R)+H^{\mathrm{o}}(0,R)\\ &\Rightarrow\; M^{\mathrm{I}}+H^{\mathrm{I}}=(\chi^{\mathrm{o}}+1)H^{\infty}\left(1+\frac{2k}{R^3}\right).\end{aligned} \tag{C.11}$$

Replacing the value of k in Eq. (C.11) leads to

$$M^{\mathrm{I}}+H^{\mathrm{I}}=(\chi^{\mathrm{o}}+1)H^{\infty}\left(3-\frac{2H^{\mathrm{I}}}{H^{\infty}}\right) \tag{C.12}$$

that can also be written:

$$M^{\mathrm{I}}+3H^{\mathrm{I}}+2\chi^{\mathrm{o}}H^{\mathrm{I}}=2\chi^{\mathrm{o}}H^{\infty}+M^{\infty}+3H^{\infty} \tag{C.13}$$

finally leading to the expression

$$H^{\mathrm{I}}-H^{\infty}=\frac{1}{3+2\chi^{\mathrm{o}}}(M^{\infty}-M^{\mathrm{I}}). \tag{C.14}$$

As both magnetization and magnetic fields appearing in Eq. (C.14) are parallel to the direction $\vec{x}$, this relation can be written in a vectorial way

$$\vec{H}^{\mathbf{I}}-\vec{H}^{\infty}=\frac{1}{3+2\chi^{\mathrm{o}}}(\vec{M}^{\infty}-\vec{M}^{\mathbf{I}}). \tag{C.15}$$

This relation justifies the choice made for relation (37), and the particular value of N_{c} in Eq. (38).

Appendix D. Magnetic saturation for isotropic polycrystal

The case of infinite isotropic polycrystal is interesting because it allows to obtain analytical results to the homogenization problem when magnetic saturation is reached. Such a configuration can help to define the parameters sensibility of the model.

The considered material is an isotropic polycrystal. Each grain exhibits a cubic crystalline symmetry. All crystallographic orientations are equiprobable, randomly distributed in the material, and the grains are equiaxial, so that the macroscopic behavior is isotropic.

D.1. Elastic behavior

The determination of the effective stiffness tensor of an isotropic polycrystal is a classical problem (see for example Bornert et al., 2007) rapidly summarized hereafter. Isotropic stiffness tensor is defined by two

constants: the shear modulus μ and the compressibility modulus k are often chosen. The stiffness tensor is then written

$$\mathbb{C} = 2\mu\mathbb{K} + 3k\mathbb{J}. \tag{D.1}$$

The stiffness tensor of a cubic single crystal is written using three constants

$$\mathbb{C}^I = 2\mu_a^I\mathbb{K}^a + 2\mu_b^I\mathbb{K}^b + 3k^I\mathbb{J}. \tag{D.2}$$

The base tensors are defined as

$$\begin{aligned} &J_{ijkl} = \frac{1}{3}\delta_{ij}\delta_{kl}, \quad P_{ijkl} = \delta_{ij}\delta_{kl}\delta_{ik}, \\ &\mathbb{K}^a = \mathbb{P} - \mathbb{J}, \quad \mathbb{K}^b = \mathbb{I} - \mathbb{P}, \\ &\mathbb{K} = \mathbb{K}^a + \mathbb{K}^b = \mathbb{I} - \mathbb{J}. \end{aligned} \tag{D.3}$$

Several hypotheses can be made to determinate the polycrystal effective elastic properties.

Voigt and Reuss hypotheses (respectively, uniform strain and uniform stress within the material) leads to

$$\begin{cases} \mu^{\mathbf{V}} = \dfrac{2\mu_a^I + 3\mu_b^I}{5}, \\ \mu^{\mathbf{R}} = \dfrac{5\mu_a^I\mu_b^I}{3\mu_a^I + 2\mu_b^I}. \end{cases} \tag{D.4}$$

We can also calculate the Hashin and Shtrikman bounds

$$\begin{cases} \mu^{\mathbf{HS}+} = \dfrac{\mu_b^I(3k^I(16\mu_a^I + 9\mu_b^I) + 4\mu_b^I(19\mu_a^I + 6\mu_b^I))}{\mu_b^I(57k^I + 64\mu_b^I) + 18\mu_a^I(k^I + 2\mu_b^I)}, \\ \mu^{\mathbf{HS}-} = \dfrac{\mu_a^I(3k^I(6\mu_a^I + 19\mu_b^I) + 4\mu_a^I(4\mu_a^I + 21\mu_b^I))}{\mu_a^I(63k^I + 76\mu_a^I) + 12\mu_b^I(k^I + 2\mu_a^I)}. \end{cases} \tag{D.5}$$

The self-consistent estimates can also be obtained, verifying the following third-order polynomial equation:

$$8\mu^{\mathbf{SC}^3} + (9k^I + 4\mu_a^I)\mu^{\mathbf{SC}^2} - (12\mu_a^I\mu_b^I + 3k^I\mu_b^I)\mu^{\mathbf{SC}} - 6k^I\mu_a^I\mu_b^I = 0. \tag{D.6}$$

In the case of iron

$$\mu_a^I = 48\,\mathrm{GPa}, \quad \mu_b^I = 116\,\mathrm{GPa}, \quad \text{and} \quad k^I = 174\,\mathrm{GPa} \tag{D.7}$$

leading to the results presented in Table D.1.

All these estimates leads to the same compressibility modulus for the polycrystal

$$k^{\mathbf{V}} = k^{\mathbf{R}} = k^{\mathbf{HS}+} = k^{\mathbf{HS}-} = k^{\mathbf{SC}} = k^I. \tag{D.8}$$

Fig. D.1 shows the sensibility of the result to the single crystal anisotropy.

As expected, the more anisotropic the single crystal is, the more different the estimate becomes. They are of course equal when the single crystal is isotropic. In the case of iron, all these estimates are still quite similar.

D.2. Saturation magnetostriction strain

The magnetic saturation state enables to calculate an analytical form for the macroscopic strain. The material being magnetized at saturation, the magnetization in the material is uniformly aligned along the external field direction, and its norm is M_s. Under these conditions the magnetostriction strain in each grain is

Table D.1
Several estimates for the shear modulus of an isotropic iron polycrystal

	Reuss	HS−	Self-consistent	HS+	Voigt
$\mu^{\mathbf{eff}}$	74.0 GPa	80.4 GPa	82.1 GPa	83.1 GPa	88.8 GPa

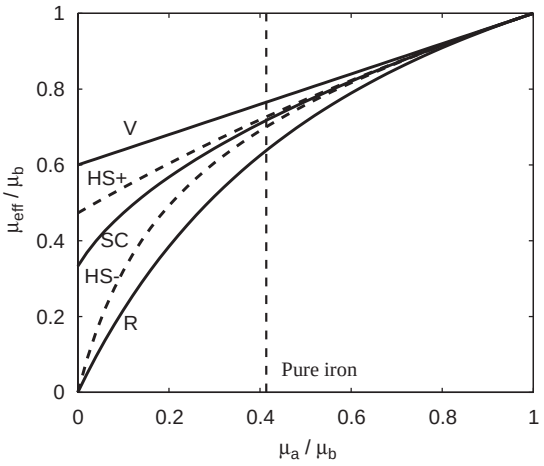

Fig. D.1. Several estimates for the shear modulus of an isotropic polycrystal depending on the single crystal anisotropy—Voigt (V), Reuss (R), Hashin and Shtrikman (HS+ and HS−) and self-consistent (SC) estimates.

uniform and is written, in the crystallographic frame

$$\boldsymbol{\varepsilon}_{\mu}^{I} = \frac{3}{2}\begin{pmatrix} \lambda_{100}(\gamma_1^2 - \frac{1}{3}) & \lambda_{111}\gamma_1\gamma_2 & \lambda_{111}\gamma_1\gamma_3 \\ \lambda_{111}\gamma_1\gamma_2 & \lambda_{100}(\gamma_2^2 - \frac{1}{3}) & \lambda_{111}\gamma_2\gamma_3 \\ \lambda_{111}\gamma_1\gamma_3 & \lambda_{111}\gamma_2\gamma_3 & \lambda_{100}(\gamma_3^2 - \frac{1}{3}) \end{pmatrix}_{\mathrm{CF}}. \tag{D.9}$$

From a macroscopic point of view, the magnetostriction strain can be obtained by the resolution of a thermo-elasticity problem

$$\boldsymbol{E}_{\mu_{\mathbf{sat}}} = \langle {}^{t}\mathbb{B}^{I} : \boldsymbol{\varepsilon}_{\mu}^{I} \rangle, \tag{D.10}$$

$\mathbb{B}^I$ is the stress concentration tensor and $\langle\cdot\rangle$ denotes the averaging operation over the volume.

The magnetostriction strain being isochore (Du Trémolet de Lacheisserie, 1993), and the macroscopic behavior being isotropic, the magnetostriction strain tensor is written

$$\boldsymbol{E}_{\mu} = \boldsymbol{E}_{\mu}^{\parallel}\begin{pmatrix} 1 & 0 & 0 \\ 0 & -\frac{1}{2} & 0 \\ 0 & 0 & -\frac{1}{2} \end{pmatrix}, \quad \boldsymbol{E}_{\mu}^{\parallel} \text{ being a function of the magnetic field.} \tag{D.11}$$

The analytical calculation of $\boldsymbol{E}_{\mu_{\mathbf{sat}}}$ finally leads to the following form for $\boldsymbol{E}_{\mu_{\mathbf{sat}}}^{\parallel}$ (the component of $\boldsymbol{E}_{\mu_{\mathbf{sat}}}$ parallel to the applied magnetic field):

$$\boldsymbol{E}_{\mu_{\mathbf{sat}}}^{\parallel} = \tfrac{2}{5}\lambda_{100}k^{\mathbf{a}} + \tfrac{3}{5}\lambda_{111}k^{\mathbf{b}}. \tag{D.12}$$

As for the shear modulus, different estimates can be obtained, leading to different values for $k^{\mathbf{a}}$ and $k^{\mathbf{b}}$.

Table D.2
Several estimates for the saturation magnetostriction strain of an isotropic iron polycrystal

	Reuss	HS−	Self-consistent	HS+	Voigt
$\boldsymbol{E}^{\parallel \mathbf{sat}}_{\mu_{\mathbf{sat}}}$	-4.20×10^{-6}	-7.90×10^{-6}	-8.75×10^{-6}	-9.25×10^{-6}	-11.9×10^{-6}

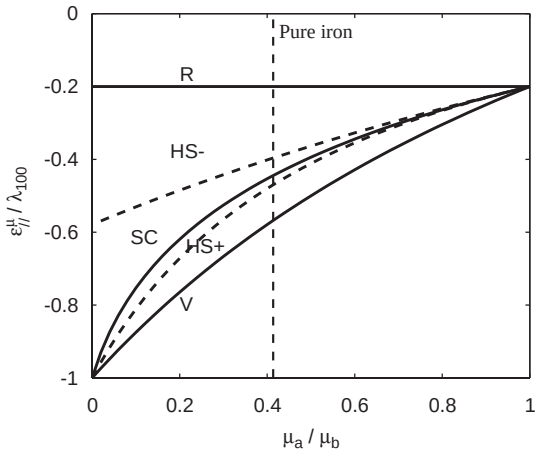

Fig. D.2. Several estimates for the saturation magnetostriction strain depending on the single crystal elastic anisotropy—Voigt (V), Reuss (R), Hashin and Shtrikman (HS+ and HS−) and self-consistent (SC) estimates.

The Voigt and Reuss hypotheses leads to

$$\boldsymbol{E}^{\parallel \mathbf{V}}_{\mu_{\mathbf{sat}}} = \frac{2\mu_a^I\lambda_{100} + 3\mu_b^I\lambda_{111}}{2\mu_a^I + 3\mu_b^I} \quad \text{and} \quad \boldsymbol{E}^{\parallel \mathbf{R}}_{\mu_{\mathbf{sat}}} = \frac{2\lambda_{100} + 3\lambda_{111}}{5}. \tag{D.13}$$

Hashin and Shtrikman and self-consistent estimates can also be obtained (leading to more complicated expressions for $k^{\mathbf{a}}$ and $k^{\mathbf{b}}$).

In the case of iron, we have

$$\lambda_{100} = 21\times10^{-6} \quad \text{and} \quad \lambda_{111} = -21\times10^{-6}. \tag{D.14}$$

The corresponding estimates for the saturation magnetostriction strain are given in Table D.2.

Fig. D.2 shows the sensibility of this result to the single crystal elastic anisotropy.

As expected, all these estimates give the same result when the single crystal is isotropic.

Fig. D.3 shows the saturation magnetostriction strain depending on the magnetostrictive anisotropy of the single crystal. When the single crystal is isotropic, all these estimates are equal. But they rapidly become different when the anisotropy increases. For specific cases, different estimates can lead to different signs for the strain. A situation of elastic isotropy or magnetostrictive anisotropy lead to great simplifications, and give identical estimates whatever the chosen hypotheses (lower and upper bounds are equal). The divergence of these estimates appear as a result of the combination of both elastic and magnetostrictive anisotropy.

D.3. Maximum magnetostriction strain

Maximum magnetostriction strain is obtained, for a material with high level of magnetocrystalline anisotropy, when the wall displacements are stabilized and the magnetization rotation mechanism not started (we suppose here $\lambda_{100} > \lambda_{111}$). Assuming that these two mechanisms are successive (and not simultaneous as they are actually), the maximal magnetostriction strain is obtained by prohibiting in the modeling of the

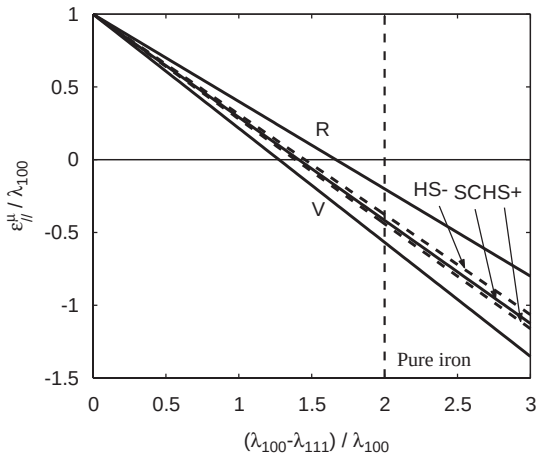

Fig. D.3. Several estimates for the saturation magnetostriction strain depending on the single crystal magnetostrictive anisotropy—Voigt (V), Reuss (R), Hashin and Shtrikman (HS+ and HS−) and self-consistent (SC) estimates.

Table D.3
Several estimates for the maximum magnetostriction strain of an isotropic iron polycrystal

	Reuss	HS−	Self-consistent	HS+	Voigt
$\boldsymbol{E}^{\parallel}_{\mu\mathbf{max}}$	8.40×10^{-6}	6.55×10^{-6}	6.13×10^{-6}	5.87×10^{-6}	4.54×10^{-6}

rotation mechanism, i.e. by giving arbitrary high values for the anisotropy constants. For the calculation of analytical values presented in the previous section, it is equivalent to use $\lambda_{111} = 0$ in Eq. (D.12).

Assuming that the relations obtained in the case of magnetic saturation are still valid (even if the magnetization is no more uniform within the material), we obtain several estimates for the maximum magnetostriction strain

$$\boldsymbol{E}_{\mu\mathbf{max}} = \frac{2}{5}\lambda_{100} k^{\mathbf{a}} \begin{pmatrix} 1 & 0 & 0 \\ 0 & -\frac{1}{2} & 0 \\ 0 & 0 & -\frac{1}{2} \end{pmatrix}. \tag{D.15}$$

Results are listed in Table D.3.

References

Appino, C., Durin, G., Basso, V., Beatrice, C., Pasquale, M., Bertotti, G., 1999. Effect of stress anisotropy on hysteresis and Barkhausen noise in amorphous materials. J. Appl. Phys. 85 (8), 4412–4414.

Azoum, K., Besbes, M., Bouillault, F., 2004. Three dimensional finite element model of magnetostriction phenomena using coupled constitutive laws. Int. J. Appl. Electromagn. Mech. 19, 367–371.

Bernard, Y., Ossart, F., 2004. Comparison between two models of magnetic hysteresis accounting for stress. Int. J. Appl. Electromagn. Mech. 19, 551–556.

Berveiller, M., Zaoui, A., 1978. An extension of the self-consistent scheme to plastically-flowing polycrystals. J. Mech. Phys. Solids 26 (5–6), 325–344.

Bornert, M., Bretheau, T., Gilormini, P., 2007. Homogenization in Mechanics of Material. Iste Publishing Company.

Bozorth, R.M., 1951. Ferromagnetism. Van Nostrand, Princeton, NJ.

Bruggeman, D.A.G., 1935. Berechnung verschiedener physikalischer konstanten von heterogenen substanzen. Annalen der Physik 5 (24), 636–664.

Buiron, N., 2000. Modélisation multi-échelle du comportement magnéto-mécanique couplé des matériaux ferromagnétiques doux. PhD Thesis, Ecole Normale Supérieure de Cachan, France.
Buiron, N., Hirsinger, L., Billardon, R., 1999. A multiscale model for magneto-elastic couplings. J. Phys. IV 9, 139–141.
Chikazumi, S., 1997. Physics of Ferromagnetism, second ed. Clarendon Press, Oxford.
Cullity, B.D., 1972. Introduction to Magnetic Materials. Addison-Wesley Publishing Company, London.
Daniel, L., Hubert, O., Ossart, F., Billardon, R., 2003. Experimental analysis and multiscale modelling of the anisotropic mechanical and magnetostrictive behaviours of electrical steels. J. Phys. IV 105, 247–253.
Daniel, L., Hubert, O., Billardon, R., 2004. Multiscale modelling of the magnetostrictive behaviour of electrical steels—demagnetising surface effect and texture gradient. Int. J. Appl. Electromagn. Mech. 19, 293–297.
Daniel, L., Hubert, O., Vieille, B., 2007. Multiscale strategy for the determination of magneto-elastic behaviour: discussion and application to Ni–Zn ferrites. Int. J. Appl. Electromagn. Mech. 25, 31–36.
DeSimone, A., 1993. Energy minimizers for large ferromagnetic bodies. Arch. Ration. Mech. Anal. 125, 99–143.
DeSimone, A., James, R.D., 2002. A constrained theory of magnetoelasticity. J. Mech. Phys. Solids 50, 283–320.
DeSimone, A., Kohn, R.V., Müller, S., Otto, F., 2000. Magnetic microstructures—a paradigm of multiscale problems. In: Ball, J.M., Hunt, J.C.R. (Eds.), ICIAM 99. Oxford University Press, Oxford, pp. 175–190.
Du Trémolet de Lacheisserie, E., 1993. Magnetostriction—Theory and Applications of Magnetoelasticity. CRC Press, Boca Raton.
Eshelby, J.D., 1957. The determination of the elastic field of an ellipsoidal inclusion, and related problems. Proc. R. Soc. London A 421, 376.
Gilormini, P., 1995. Insuffisance de l'extension classique du modèle autocohérent au comportement non linéaire. C. R. Acad. Sci. Paris, Série IIb 320, 115–122.
Haug, A., Huber, J.E., Onck, P.R., Van der Giessen, E., 2007. Multi-grain analysis versus self-consistent estimates of ferroelectric polycrystals. J. Mech. Phys. Solids 55 (3), 648–665.
He, S., 1999. Modélisation et simulation numérique de matériaux magnétostrictifs. PhD Thesis, Université Pierre et Marie Curie, France.
Hill, R., 1965. Continuum micro-mechanics of elastoplastic polycrystals. J. Mech. Phys. Solids 13, 89–101.
Hirsinger, L., Barbier, G., Gourdin, C., Billardon, R., 2000. Application of the internal variable formalism to the modelling of magneto-elasticity. In: Yang, J.S., Maugin, G.A. (Eds.), Mechanics of Electromagnetic Materials and Structures. IOS Press, pp. 54–67.
Huber, J.E., Fleck, N.A., Landis, C.M., McMeeking, R.M., 1999. A constitutive model for ferroelectric polycrystals. J. Mech. Phys. Solids 47 (8), 1663–1697.
Hubert, A., Schäfer, R., 1998. Magnetic Domains. Springer, Berlin.
Hubert, O., Daniel, L., Billardon, R., 2003. Multiscale modelling and demagnetising surface effect: application to the prediction of magnetostriction of Grain Oriented silicon irons. In: Proceedings of the 16th Soft Magnetic Materials Conference.
James, R., Kinderlehrer, D., 1990. Frustration in ferromagnetic materials. Cont. Mech. Therm. 2, 215–239.
Jiles, D.C., 1991. Introduction to Magnetism and Magnetic Materials. Chapman & Hall, London.
Joule, J.P., 1847. On the effects of magnetism upon the dimensions of iron and steel bars. Philos. Mag. Sér. 3 30 (199), 76–87.
Kuruzar, M.E., Cullity, B.D., 1971. The magnetostriction of iron under tensile and compressive tests. Int. J. Magn. 1, 323–325.
Lagoudas, D.C., Entchev, P.B., Popov, P., Patoor, E., Brinson, L.C., Gao, X., 2006. Shape memory alloys, part II: modeling of polycrystals. Mech. Mater. 38 (5–6), 430–462.
McClintock, F.A., Argon, A.S., 1966. Mechanical Behavior of Materials. Addison-Wesley, New York.
Mura, T., 1982. Micromechanics of Defects in Solids. Martinus Nijhoff Publishers, Dordrecht, MA.
Patoor, E., Lagoudas, D.C., Entchev, P.B., Brinson, L.C., Gao, X., 2006. Shape memory alloys, part I: general properties and modeling of single crystals. Mech. Mater. 38 (5–6), 391–429.
Sablik, M.J., Jiles, D.C., 1993. Coupled magnetoelastic theory of magnetic and magnetostrictive hysteresis. IEEE Trans. Magn. 29 (3), 2113–2123.
Vieille, B., Buiron, N., Pellegrini, Y.P., Billardon, R., 2004. Modelling of the magnetoelastic behaviour of a polycrystalline ferrimagnetic material. J. Phys. IV 115, 129.
Webster, W.L., 1925a. The magnetic properties of iron crystals. Proc. R. Soc. London 107A, 496–509.
Webster, W.L., 1925b. Magnetostriction in iron crystals. Proc. R. Soc. London 109A, 570–584.

Eur. Phys. J. Appl. Phys. **42**, 153–159 (2008)
DOI: 10.1051/epjap:2008031

THE EUROPEAN PHYSICAL JOURNAL APPLIED PHYSICS

A constitutive law for magnetostrictive materials and its application to Terfenol-D single and polycrystals

L. Daniel[a] and N. Galopin

Laboratoire de Génie Électrique de Paris, CNRS UMR 8507; SUPELEC; Univ. Paris-Sud; UPMC Univ. Paris 06; 11 rue Joliot-Curie, Plateau de Moulon, 91192 Gif-sur-Yvette Cedex, France

Received: 9 August 2007 / Received in final form 12 October 2007/ Accepted: 18 January 2008
Published online: 28 March 2008 –

Abstract. This paper addresses a multiscale strategy for the prediction of anhysteretic magneto-elastic behavior and its application to the definition of a magneto-elastic constitutive law for Terfenol-D. The multiscale modeling is based on an energetic procedure at the single crystal scale. Localization and homogenization procedures are then applied to deduce the constitutive law of polycrystalline media from the behavior of the corresponding single crystal. The method is applied first to define the magneto-elastic behavior of single crystals, and the application to polycrystalline samples is then considered. Modeling results are compared to experimental data.

PACS. 75.80.+q Magnetomechanical and magnetoelectric effects, magnetostriction – 46.25.Hf Thermoelasticity and electromagnetic elasticity (electroelasticity, magnetoelasticity)

1 Introduction

Magnetostriction is the spontaneous strain that occurs when a magnetic material is subjected to a magnetic field. In the case of rare-earth alloys such as Terfenol-D ($Tb_{0.27}Dy_{0.73}Fe_2$), this strain is far larger (about 10^{-3}) than for most materials, and finds applications in transducer and actuator design [1]. However, the magnetostrictive behavior of Terfenol-D is very sensitive to the application of stress. The prediction of the magneto-elastic behavior of Terfenol-D, including this sensitivity to stress, can lead to optimum design for giant magnetostrictive transducers and actuators. A multiscale strategy for the description of magneto-elastic couplings phenomena has been recently proposed [2,3]. In this approach, a time consuming minimization is necessary to define the single crystal behavior. This minimization procedure can be avoided thanks to the discretization of the single crystal problem. After the presentation of this approach, it is applied to the case of Terfenol-D, firstly by considering single crystals and then polycrystalline media. It must be noticed that the proposed modeling is restricted to reversible (anhysteretic) magneto-elastic behavior.

[a] e-mail: laurent.daniel@lgep.supelec.fr

2 Multi-scale modeling principle

Three distinct scales can be considered in the study of magneto-elastic behavior[1] (Fig. 1):

- the magnetic domains scale (μ);
- the single crystal (or grain) scale (ϕ),;
- the Representative Volume Element (RVE) scale (ℓ).

The modeling principle is based on the description, for each of these scales, of the mechanisms responsible for magneto-elastic couplings.

2.1 Magnetic domain scale

In a magnetic domain, magnetization $\boldsymbol{M}_\alpha$ and magnetostriction $\boldsymbol{\varepsilon}^\mu_\alpha$ are supposed uniform:

$$\boldsymbol{M}_\alpha = M_S\, \boldsymbol{m}_\alpha = M_S\, {}^T[\gamma_1\ \gamma_2\ \gamma_3] \tag{1}$$

$$\boldsymbol{\varepsilon}^\mu_\alpha = \frac{3}{2}\begin{pmatrix} \lambda_{100}(\gamma_1^2-\frac{1}{3}) & \lambda_{111}\gamma_1\gamma_2 & \lambda_{111}\gamma_1\gamma_3 \\ \lambda_{111}\gamma_1\gamma_2 & \lambda_{100}(\gamma_2^2-\frac{1}{3}) & \lambda_{111}\gamma_2\gamma_3 \\ \lambda_{111}\gamma_1\gamma_3 & \lambda_{111}\gamma_2\gamma_3 & \lambda_{100}(\gamma_3^2-\frac{1}{3}) \end{pmatrix}. \tag{2}$$

[1] In most of practical cases, the separation of scales is verified. A notable exception is the grain oriented iron-silicon steels for which magnetic domain size can be of the order of the grain size.

Article published by EDP Sciences

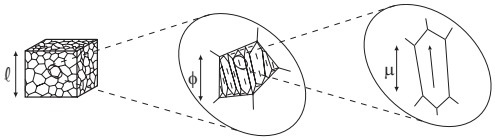

Fig. 1. Scales (polycrystal-grain-domain) for the modeling of magneto-elastic behavior – $\ell \gg \phi \gg \mu$.

Equation (2) is the classical expression for the magnetostriction strain tensor in the case of cubic crystalline symmetry (see for instance [4]). $\boldsymbol{m}_\alpha$ is the direction of the magnetization (unit vector) and $(\gamma_1\ \gamma_2\ \gamma_3)$ its direction cosines, M_S is the saturation magnetization of the material, λ_{100} and λ_{111} its magnetostrictive constants.

The potential energy of a domain is supposed to be the sum of three contributions:

$$W_\alpha = W_\alpha^{mag} + W_\alpha^{an} + W_\alpha^{\sigma}. \tag{3}$$

The expression of these energetic contributions can be written as follows [5]:

– W_α^{mag} is the magneto-static energy, tending to align the magnetization $\boldsymbol{M}_\alpha$ along the magnetic field $\boldsymbol{H}_\alpha$:

$$W_\alpha^{mag} = -\mu_0\, \boldsymbol{H}_\alpha \boldsymbol{M}_\alpha. \tag{4}$$

– W_α^{an} is the magneto-crystalline anisotropy energy tending to prevent the rotation of the magnetization out of the easy axes. This energetic term describes the existence of easy magnetization directions, and thus the existence of domains microstructure:

$$W_\alpha^{an} = K_1(\gamma_1^2\gamma_2^2 + \gamma_2^2\gamma_3^2 + \gamma_3^2\gamma_1^2) + K_2(\gamma_1^2\gamma_2^2\gamma_3^2) \tag{5}$$

K_1 and K_2 denote the anisotropy constants.

– W_α^{σ} is the elastic energy:

$$W_\alpha^{\sigma} = \frac{1}{2}\boldsymbol{\sigma}_\alpha : \boldsymbol{\varepsilon}_\alpha^e \tag{6}$$

$\boldsymbol{\sigma}_\alpha$ and $\boldsymbol{\varepsilon}_\alpha^e$ are respectively the stress and the elastic strain[2] tensors in the domain, linked by the single crystal stiffness tensor $\mathbb{C}_i$ in the usual Hooke law:

$$\boldsymbol{\sigma}_\alpha = \mathbb{C}_i : \boldsymbol{\varepsilon}_\alpha^e. \tag{7}$$

If the magneto-mechanical loading is known, namely the magnetic field $\boldsymbol{H}_\alpha$ and the stress $\boldsymbol{\sigma}_\alpha$, the knowledge of $\boldsymbol{m}_\alpha$ is required to define the magnetization $\boldsymbol{M}_\alpha$ and the magnetostriction strain $\boldsymbol{\varepsilon}_\alpha^\mu$ in the considered magnetic domain.

2.2 Single crystal scale

A single crystal (or grain) is defined as a zone where elastic properties are uniform (stiffness tensor $\mathbb{C}_i$). From the magnetic point of view, the crystal is divided into domain families, each corresponding to a particular direction of the magnetization. For any possible magnetization direction $\boldsymbol{m}_\alpha$, the lower the potential energy W_α, the higher the existence probability. The existence probability f_α of a magnetization direction $\boldsymbol{m}_\alpha$ in a single crystal is defined thanks to a Boltzmann explicit relation [2,6] given by equation (8)

$$f_\alpha = \frac{\exp(-A_s.W_\alpha)}{\displaystyle\int_\alpha \exp(-A_s.W_\alpha)} \tag{8}$$

A_s is an additional modeling parameter. It has been shown [3] to be proportional to the initial slope of the anhysteretic magnetic curve when no stress is applied. The identification of A_s can be made using one magnetic curve. All the other parameters are classical physical constants of the material, identified with independent experimentations.

Once the existence probability for each direction $\boldsymbol{m}_\alpha$ is known, magnetization $\boldsymbol{M}_i$ and magnetostriction $\boldsymbol{\varepsilon}_i^\mu$ in the single crystal are obtained thanks to an averaging operation over all possible directions:

$$\boldsymbol{M}_i = \langle \boldsymbol{M}_\alpha \rangle = \int_\alpha f_\alpha\, \boldsymbol{M}_\alpha \tag{9}$$

$$\boldsymbol{\varepsilon}_i^\mu = \langle \boldsymbol{\varepsilon}_\alpha^\mu \rangle = \int_\alpha f_\alpha\, \boldsymbol{\varepsilon}_\alpha^\mu. \tag{10}$$

From a practical point of view, this integral is evaluated numerically after discretization of the directions $\boldsymbol{m}_\alpha$ in space. The possible directions for $\boldsymbol{m}_\alpha$ are described through the mesh of a unit radius sphere S (N unit vectors $\boldsymbol{x}_n$ with components x_{ni}, $i = 1, 2, 3$). We used a 10242 point mesh. The — approximative — isotropy of the mesh is verified to avoid mesh anisotropy effects in the proposed modeling. For that purpose, the values given in Table 1 are compared to their theoretical value.

The size of the mesh is chosen to ensure a sufficiently small difference between discrete and numerical values. Using such a mesh, equations (8), (9) and (10) can be discretized, and the — time consuming — minimization of the potential energy (proposed in [2,3] in order to determine the direction of magnetization in the magnetic domains) is not required. Indeed the directions corresponding to high (resp. low) energy levels will be associated to low (resp. high) existence probability in equation (8).

2.3 Representative volume element scale

The Representative Volume Element (RVE), or macroscopic scale, is the scale at which the constitutive law is written, and at which the applied solicitations (magnetic field and stress) are known. It is a zone large enough so that its magneto-elastic behavior is representative for the whole material behavior. Since the material is heterogeneous, localization-homogenization rules, depending on

[2] The relationship between the elastic strain and the magnetostriction strain is not trivial, and can be estimated using appropriate localization-homogenization procedures [3].

Table 1. Verification of the mesh isotropy – $N = 10242$, $i = 1, 2, 3$, $j = 1, 2, 3$.

Discrete integral Di	Reference integral Ri	$\lvert Ri - Di\rvert$
$\frac{1}{N}\sum_{n=1}^{N} x_{ni}$	$\frac{1}{4\pi}\iint_S \gamma_i dS$	$<10^{-16}$
$\frac{1}{N}\sum_{n=1}^{N} x_{ni}^2$	$\frac{1}{4\pi}\iint_S \gamma_i^2 dS$	$<10^{-8}$
$\frac{1}{N}\sum_{n=1}^{N} x_{ni}x_{nj},\ i \neq j$	$\frac{1}{4\pi}\iint_S \gamma_i\gamma_j dS,\ i \neq j$	$< 10^{-9}$
$\frac{1}{N}\sum_{n=1}^{N} x_{ni}^3$	$\frac{1}{4\pi}\iint_S \gamma_i^3 dS$	$<2 \times 10^{-16}$
$\frac{1}{N}\sum_{n=1}^{N} x_{n1}x_{n2}x_{n3}$	$\frac{1}{4\pi}\iint_S \gamma_1\gamma_2\gamma_3 dS$	$< 10^{-17}$
$\frac{1}{N}\sum_{n=1}^{N} x_{ni}^4$	$\frac{1}{4\pi}\iint_S \gamma_i^4 dS$	$<2 \times 10^{-8}$
$\frac{1}{N}\sum_{n=1}^{N} x_{ni}^2x_{nj}^2,\ i \neq j$	$\frac{1}{4\pi}\iint_S \gamma_i^2\gamma_j^2 dS,\ i \neq j$	$<2 \times 10^{-8}$
$\frac{1}{N}\sum_{n=1}^{N} x_{ni}^6$	$\frac{1}{4\pi}\iint_S \gamma_i^6 dS$	$<2 \times 10^{-4}$
$\frac{1}{N}\sum_{n=1}^{N} x_{n1}^2x_{n2}^2x_{n3}^2$	$\frac{1}{4\pi}\iint_S \gamma_1^2\gamma_2^2\gamma_3^2 dS$	$<10^{-4}$

the microstructure, are necessary to deduce the local loadings from the macroscopic ones. In the proposed modeling, a self-consistent scheme is used [3].

The local magnetic field $\boldsymbol{H}_i$ is deduced from the macroscopic magnetic field $\boldsymbol{H}_m$ according to equation (11) deduced from the resolution of an inclusion problem[3].

$$\boldsymbol{H}_i = \frac{3 + 3\chi_m}{3 + \chi_i + 2\chi_m}\boldsymbol{H}_m \tag{11}$$

χ_m and χ_i are respectively the magnetic susceptibility of the polycrystal and of the single crystal. Since the magnetic behavior is usually non-linear, a secant definition is used:

$$\chi_m = \frac{||\boldsymbol{M}_m||}{||\boldsymbol{H}_m||} \qquad \chi_i = \frac{||\boldsymbol{M}_i||}{||\boldsymbol{H}_i||}. \tag{12}$$

The local stress tensor $\boldsymbol{\sigma}_i$ is deduced from the macroscopic stress tensor $\boldsymbol{\sigma}_m$ according to equation (13).

$$\boldsymbol{\sigma}_i = \mathbb{B} : \boldsymbol{\sigma}_m. \tag{13}$$

The fourth order tensor $\mathbb{B}$ is the so-called stress concentration tensor. In the self-consistent case, the tensor $\mathbb{B}$ can be calculated according to equation (14).

$$\mathbb{B} = \mathbb{C}_i : (\mathbb{C}_i + \mathbb{C}^*)^{-1} : (\mathbb{C}_m + \mathbb{C}^*) : {\mathbb{C}_m}^{-1} \tag{14}$$

[3] Inclusion based models rely on the hypothesis that mean fields in each phase i are similar to corresponding fields of an inclusion of phase i embedded in an infinite homogeneous medium with magnetic property χ_m [7]. In the self-consistent case, χ_m is the magnetic susceptibility of the polycrystal.

$\mathbb{C}_m$ is the stiffness tensor of the polycrystal and $\mathbb{C}^*$ is the Hill constraint tensor deduced from the resolution of the Eshelby's inclusion problem (see for example [8]). Once the local loading is known, the local modeling can be applied. The macroscopic response (macroscopic magnetization $\boldsymbol{M}_m$ and macroscopic magnetostriction strain $\boldsymbol{\varepsilon}_m^\mu$) is then deduced thanks to a classical homogenization step, according to equations (15) and (16).

$$\boldsymbol{M}_m = \langle \boldsymbol{M}_i \rangle \tag{15}$$

$$\boldsymbol{\varepsilon}_m^\mu = \langle {}^t\mathbb{B} : \boldsymbol{\varepsilon}_i^\mu \rangle. \tag{16}$$

Since the single crystal is usually anisotropic, the knowledge of the crystallographic texture of the polycrystal is required. The crystallographic texture can be described through an Orientation Distribution Function (ODF), representative of the orientations of grains in the polycrystal [9]. A Scanning Electron Microscope (SEM), with an Electron Back Scatter Diffraction (EBSD) measurement system, can provide a discrete Orientation Data File for the crystallographic texture of a given material.

2.4 Summary of the multiscale scheme

The principle of the multiscale modeling is summarized on Figure 2. Entry data are material parameters for the single crystal (elastic, magnetic and magnetostrictive constants), texture data and A_s parameter for the polycrystal, and the macroscopic magneto-mechanical loading. Since the localization procedure requires an estimation of macroscopic magnetization and strain, an initial solution is also needed. This initial solution can be arbitrarily chosen, but the closest to the solution, the faster the convergence of the calculation. The hypotheses of uniform magnetic field and stress within the polycrystal can be used for the definition of that initial solution. The classical multiscale scheme is then performed until convergence, including the localization step, the local constitutive law application and the homogenization step.

3 Application to Terfenol-D single crystals

The multiscale modeling is applied first to Terfenol-D single crystals for which experimental results can be found in the literature. The material properties of the Terfenol-D single crystal have also been collected in the literature. They are summarized in Table 2. Both magnetic and magnetostrictive properties have been investigated. The value of the parameter A_s has been taken to 2×10^{-3} m^3/J.

3.1 Magnetic behavior

In order to exhibit the anisotropy of the magnetic behavior, the M-H curves have been plotted for a magnetic field applied in three directions of the single crystal, namely

Table 2. Terfenol-D properties: Saturation magnetization, anisotropy, magnetostrictive and elastic constants.

Constant	M_S	(K_1, K_2)	$(\lambda_{100}, \lambda_{111})$	(C_{11}, C_{12}, C_{44})
Value	8 10^5 A/m	$(-0.8, -1.8)$ 10^5 J/m^3	(9, 164) 10^{-5}	(141, 65, 49) GPa
Reference	[10]	[1]	[11]	[12]

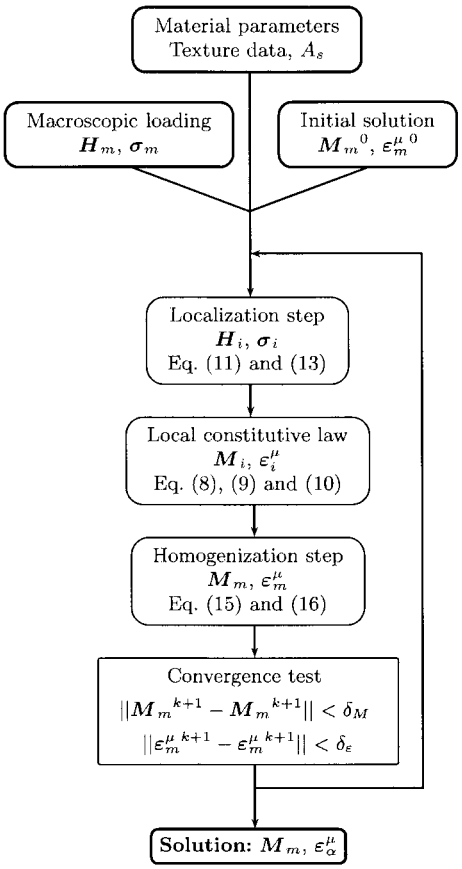

Fig. 2. Multiscale scheme: principle.

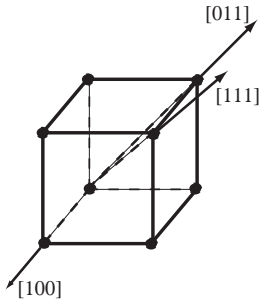

Fig. 3. Crystallographic frame in the cubic symmetry.

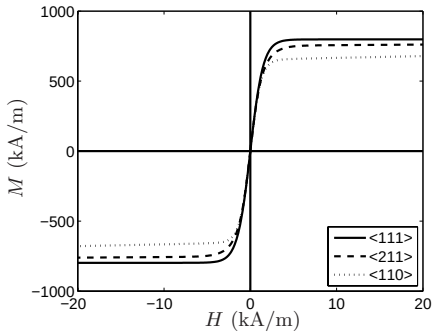

Fig. 4. Predicted anhysteretic magnetic behavior in different crystallographic directions for Terfenol-D single crystal in the stress-free case.

$\langle 111 \rangle$, $\langle 211 \rangle$ and $\langle 110 \rangle$ direction. These directions are defined with respect to the crystallographic frame (Fig. 3).

The modeling results are plotted in Figure 4.

The relative anisotropy of the single crystal is in good agreement with the results reported by Wang et al. [13]. The best magnetization directions are the $\langle 111 \rangle$ directions. However, the magnetic field levels do not correspond to those obtained experimentally. The value of the magnetic field H is defined in the simulation as the mean value of the magnetic field over the material. Concerning the experimental results, this value is difficult to define precisely and is often calculated from the value of the current intensity in the windings used to create the magnetic field. Such a calculation usually neglects the strong macroscopic demagnetizing field effects involved in such experimental apparatus. This point could explain the discrepancies between the magnetic field levels in experimental and numerical results. Unfortunately, data concerning the evaluation of the magnetic field are usually not given in the corresponding experimental papers.

3.2 Magnetostrictive behavior

The magnetostrictive behavior has also been evaluated. The magnetostriction curves have been plotted for a magnetic field applied in different directions of the single crystal. The results are plotted in Figure 5.

Here again, the predicted relative anisotropy is in good agreement with the results reported in [13], but the magnetic field axes do still not correspond, probably due to demagnetizing field effects.

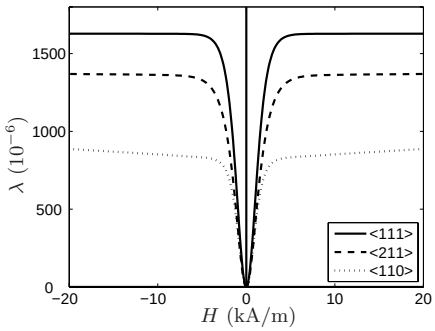

Fig. 5. Predicted anhysteretic magnetostrictive behavior in different crystallographic directions for Terfenol-D single crystal in the stress-free case.

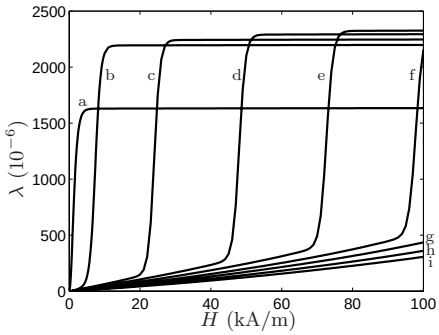

Fig. 6. Predicted anhysteretic magnetostrictive behavior of Terfenol-D single crystal: effect of a compression stress along a ⟨111⟩ direction (a:0, b:2, c:7, d:14, e:21, f:28, g:34, h:41, i:48 MPa).

3.3 Magnetostriction under stress

The magnetostriction strain is known to be dependent on stress. The ε^{μ}-H curves have been plotted for different levels of compressive stress. Both stress and magnetic field are applied along a ⟨111⟩ direction. The results are plotted in Figure 6.

Two tendencies are observed. For low magnetic field levels, the application of a stress tends to decrease the magnetostriction amplitude. On the other hand, the saturation magnetostriction strain is increasing with the applied stress. This latter effect is sensitive for low applied stress but saturates for higher levels. As a consequence, the magnetostriction curves are crossing each others. Such an effect has been observed experimentally by Clark et al. [14]. Unfortunately, a quantitative comparison is not possible because of the unknown definition of the magnetic field in the experimental data. Moreover, a small disorientation angle of the magnetic field (or stress) from the ⟨111⟩ direction can significantly modify the results, both experimental and numerical.

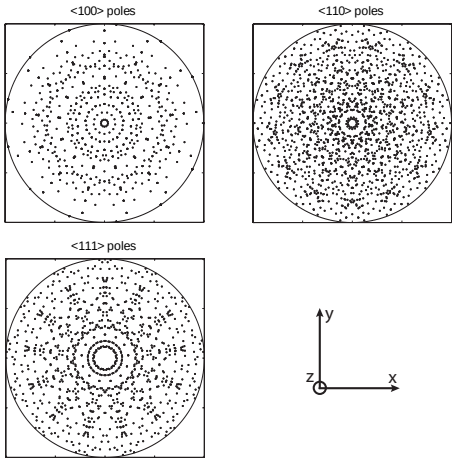

Fig. 7. Pole figures for an isotropic polycrystal obtained by regular zoning of the crystallographic orientations space (stereographic projection).

However, the single crystal modeling has been shown to capture the main magneto-elastic properties, at least qualitatively. We can apply the proposed constitutive law to a polycrystalline specimen.

4 Application to polycrystalline Terfenol-D

In most applications, Terfenol-D is used in its polycrystalline form. A polycrystal can be seen as a crystallite aggregate. The only additional data needed for the modeling are the crystallites orientation. These orientations are given by an Orientation Distribution Function. This ODF can be represented in stereographic projection on a pole figure (see for instance [9]). In the case of an isotropic polycrystalline Terfenol-D sample, the crystallites orientation is random. The crystallographic texture represented by the discrete pole figure of Figure 7 can be used to describe such an isotropic behavior [3].

The results obtained for the magnetostriction strain as a function of the magnetic field for several levels of stress are presented in Figure 8.

The same kind of effect than for the single crystal is observed: for a given level of magnetic field, the application of a compressive stress tends first to increase the magnetostriction strain and then to decrease it. It is consistent with the existence of an optimal pre-load stress for magnetostrictive actuators. The qualitative evolution of the magnetostriction with respect to stress is in agreement with experimental results previously reported in the literature [1,15] or by giant magnetostrictive material manufacturers [16]. Since a quantitative comparison is difficult unless the precise experimental conditions are known, particularly for the magnetic field level definition, a specific experimental setup has been developed [17]. Anhysteretic measurements have been performed on a 10 mm diameter Terfenol-D rod. The sample is placed in

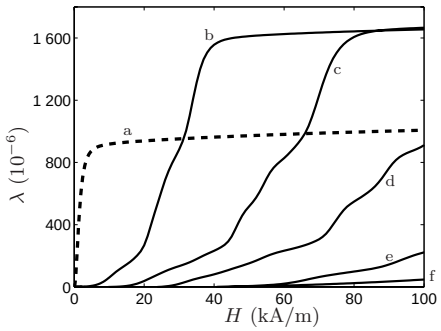

Fig. 8. Predicted anhysteretic magnetostrictive behavior of Terfenol-D polycrystal: effect of a compression stress along the magnetization direction (a:0, b:10, c:20, d:30, e:50, f:80 MPa).

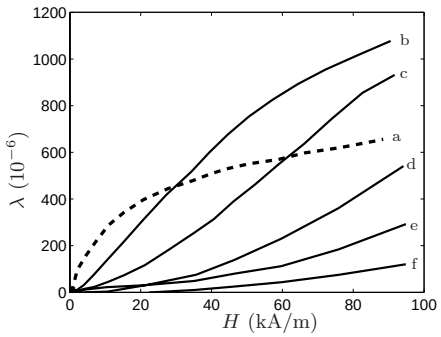

Fig. 9. Experimental anhysteretic magnetostrictive behavior of Terfenol-D polycrystal: effect of a compression stress along the magnetisation direction (a:0, b:10, c:20, d:30, e:50, f:80 MPa).

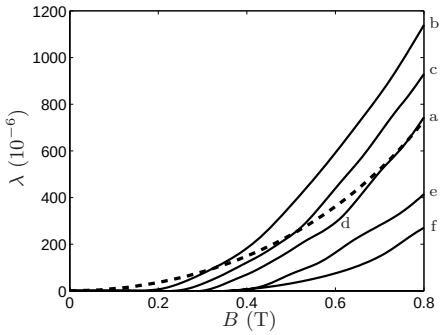

Fig. 10. Predicted anhysteretic magnetostrictive behavior of Terfenol-D polycrystal: effect of a compression stress along the magnetization direction (a:0, b:10, c:20, d:30, e:50, f:80 MPa).

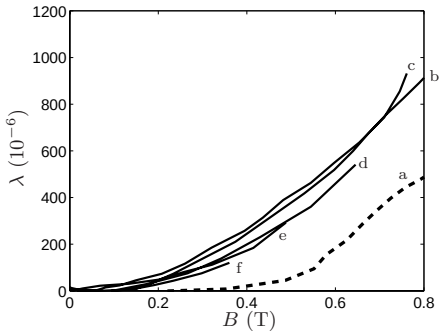

Fig. 11. Experimental anhysteretic magnetostrictive behavior of Terfenol-D polycrystal: effect of a compression stress along the magnetization direction (a:0, b:10, c:20, d:30, e:50, f:80 MPa).

a tension-compression test machine equipped with a magnetic solicitation apparatus. Stress and strain are respectively measured thanks to a standard load cell and strain gages. The applied magnetic field is measured thanks to Hall effect sensors, and the magnetic induction B in the sample is obtained through the integration of the induced voltage on a B-coil surrounding the specimen. The results are presented in Figure 9.

Except for the maximum strain level that is over-estimated by the model, the agreement is satisfying. Indeed, it must be recalled that the proposed multiscale approach does not use the modeled curves for any adjustment operation. The material parameters are taken from the literature (see Tab. 2).

The magnetostriction strain is often written as a function of the magnetic induction $\boldsymbol{B}$. The corresponding curves are plotted in Figure 10, assuming that the material is isotropic, so that the magnetic induction $\boldsymbol{B}$, the magnetic field $\boldsymbol{H}$ and the magnetisation $\boldsymbol{M}$ are parallel (and then $B = \mu_0(H + M)$).

The corresponding experimental data is plotted in Figure 11.

Both modeling and experimental results show that the magnetostriction strain first increase for low applied stress and then decrease. But this decrease is very significant according to the model whereas experiments shows that the compressive stress, after a minimal pre-load, has no strong influence on the $B(H)$ curve. This is in accordance with an usual hypothesis for macroscopic magnetostriction strain modeling of Terfenol-D (see for instance [18]) assuming that the $\lambda(B)$ curve is not stress-dependent. However, it seems to be very particular to Terfenol-D, for which the effect of stress on magnetostriction saturates very early, and should not be taken as a general property.

5 Conclusion

A multiscale approach for magnetostrictive behavior modeling has been presented. It is based on a statistical energetic description of the domain microstructure evolution. This approach has been applied to Terfenol-D single crystals and polycrystals. It has been shown to capture the

main features of this material's behavior. One of the objective of such an approach would be to replace experiments for the identification of macroscopic models used in numerical simulation for the design of electromagnetic devices. However this approach is limited to anhysteretic behavior. The extension to hysteretic behavior is necessary and supposes to modify the formulation in an incremental way. It can be done by using the variation of the existence probability of a given magnetization direction δf_α instead of f_α in the model. The definition of δf_α is given by differentiation of equation (8):

$$\delta f_\alpha = \frac{e^{-A_s.W_\alpha} - \int_\alpha e^{-A_s.W_\alpha}}{\int_\alpha e^{-A_s.W_\alpha}} A_s\, f_\alpha\, \delta W_\alpha. \qquad (17)$$

This extension is presently a work in progress and will lead to a full magneto-elastic modeling including hysteresis.

References

1. G. Engdahl, *Handbook of Giant Magnetostrictive Materials* (Academic Press, 2000)
2. N. Buiron, L. Hirsinger, R. Billardon, J. Phys. IV France **9**, 187 (1999)
3. L. Daniel, N. Buiron, O. Hubert, R. Billardon, J. Mech. Phys. Solids, in press, available on-line: doi:10.1016/j.jmps.2007.06.003
4. E. du Trémolet de Lacheisseirie, *Magnetostriction — Theory and applications of magnetoelasticity* (CRC Press, 1993)
5. A. Hubert, R. Schäfer, *Magnetic domains* (Springer, 1998)
6. S. Chikazumi, *Physics of Ferromagnetism*, 2nd edn. (Clarendon Press, 1997)
7. L. Daniel, R. Corcolle, IEEE Trans. Magn. **43**, 3153 (2007)
8. M. Bornert, T. Bretheau, P. Gilormini, *Homogenization in Mechanics of Materials* (ISTE Publishing Company, 2007)
9. H.J. Bunge, *Texture Analysis in Materials Science* (Butterworths, 1982)
10. L. Sandlund, M. Fahlander, T. Cedell, A.E. Clark, J.B. Restorff, M. Wun-Fogle, *Proc. 4th Conf. New Actuators* (Bremen, Germany, 1994), pp. 210–213
11. D.C. Jiles, *Introduction to Magnetism and Magnetic Materials* (Chapman & Hall, 1991)
12. A.E. Clark, in *Ferromagnetic Materials*, edited by E.P. Wohlfarth (North-Holland Publishing Company, 1980)
13. B.W. Wang, S.C. Busbridge, Y.X. Li, G.H. Wu, A.R. Piercy, J. Magn. Magn. Mater. **218**, 198 (2000)
14. A.E. Clark, H.T. Savage, M.L. Spano, IEEE Trans. Magn. **20**, 1443 (1984)
15. M. Wun-Fogle, J.B. Restorff, K. Leung, J.R. Cullen, A.E. Clark, IEEE Trans. Magn. **35**, 3817 (1999)
16. Etrema - Terfenol-D Data Sheet. http://etrema-usa.com/documents/Terfenol.pdf
17. N. Galopin, L. Daniel, F. Bouillault, M. Besbes, Przegląd Elektrotechnic. **6**, 44 (2007)
18. K. Azoum, M. Besbes, F. Bouillault, T. Ueno, Eur. Phys. J. Appl. Phys. **36**, 43 (2006)

2.2.2 Caractérisation expérimentale *

Afin d'aider à la construction, à l'identification et la validation des approches proposées, mes travaux de modélisation ont toujours été accompagnés de travaux de caractérisation. En ce qui concerne le comportement magnéto-élastique, les mesures consistent en l'acquisition de la déformation et de l'induction magnétique (ou de l'aimantation) sur des échantillons soumis simultanément à une contrainte et un champ magnétique. L'une des principales difficultés de ce type de mesure, outre parfois la faible amplitude des signaux à mesurer, réside dans la difficulté à maîtriser simultanément la stabilité des conditions aux limites magnétiques et mécaniques. Dans le cadre de mes travaux menés au LMT-Cachan, j'ai participé au développement d'un banc de caractérisation magnéto-élastique dédié aux tôles magnétiques soumises à des sollicitations de traction (figure 2.4(a)). Ces travaux ont notamment fourni des résultats originaux sur la mise en évidence de l'anisotropie magnéto-élastique des tôles de fer-silicium pour machines tournantes, pourtant réputées isotropes (pour le comportement découplé). Ces travaux sont présentés dans la référence [78] jointe ci-après. Plus récemment, dans le cadre du projet MAEL, ce banc de mesure a permis la caractérisation du comportement magnéto-élastique sous contrainte de traction de monocristaux de fer-silicium [79]. A mon arrivée au LGEP, j'ai piloté, dans le cadre de la thèse de Nicolas Galopin [33], la mise en place d'un banc de caractérisation magnéto-élastique orienté vers la caractérisation de matériaux magnétostrictifs soumis à des sollicitations de compression (figure 2.4(b)). Ces travaux sont présentés dans la référence [80] jointe ci-après. Ce banc de mesure a notamment permis d'établir les mesures de déformations de magnétostriction du Terfenol-D utilisées dans la référence [74] déjà mentionnée dans la section 2.2.1.

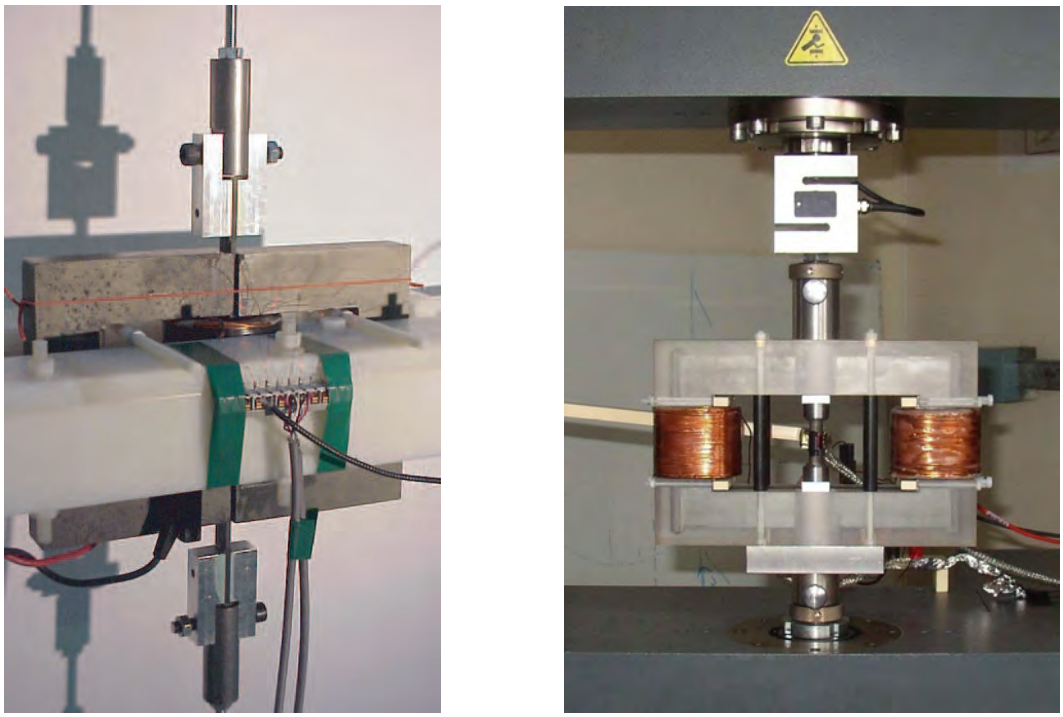

(a) Banc LMT-Cachan (b) Banc LGEP

FIGURE 2.4 – Bancs de caractérisation expérimentale du comportement magnéto-élastique

La demande de résultats expérimentaux pour la caractérisation du comportement magnéto-mécanique est assez forte. En particulier la prise de conscience de la multiaxialité des contraintes, et de son importance dans la définition du comportement macroscopique est finalement relativement récente. Il est en général exigé que les propositions de modèles multiaxiaux soient validées sur la base de mesures sous sollicitations complexes. Dans ce domaine, le LMT-Cachan s'est fortement investi dans le développement d'un banc de caractérisation magnéto-élastique sous sollicitations biaxiales [81, 82]. Si mon affectation au LGEP ne me permet pas de participer activement à ces essais, qui exigent un très fort investissement en temps, je participe à leur interprétation et à leur utilisation, notamment dans le cadre de la thèse de Mahmoud Rekik, démarrée en 2010 en co-tutelle

∗. Plusieurs doctorants ont contribué aux résultats présentés dans ce chapitre, notamment Nicolas Galopin [33] et Karl-Joseph Rizzo [71]. Pour l'avenir, Mahmoud Rekik se lance également dans un travail expérimental ambitieux [77].

entre le LMT-Cachan et le LGEP [77]. Ces essais multiaxiaux ont également permis la validation de modèles de contraintes équivalentes pour le comportement magnéto-élastique présentées dans la partie suivante.

Publications jointes

[RI.1, 78] : O. Hubert, L. Daniel, R. Billardon, "Experimental analysis of the magnetoelastic anisotropy of a non-oriented silicon iron alloy". *Journal of Magnetism and Magnetic Materials*, **254-255C** :352-354, 2003.

[RI.9,80] N. Galopin, L. Daniel, F. Bouillault et M. Besbes, "Numerical analysis for the design of a magneto-elastic characterization device", *Prezgląd Elektrotechniczny*, **83(6)** :44-47, 2007.

[RI.24,79] : K.J. Rizzo, O. Hubert, L. Daniel, "Magnetic and magnetostrictive behavior of iron-silicon single crystals under uniaxial stress", *IEEE Transactions on Magnetics*, **46(2)** :270-273, 2010.

ELSEVIER

Journal of Magnetism and Magnetic Materials 254–255 (2003) 352–354

Journal of magnetism and magnetic materials

www.elsevier.com/locate/jmmm

Experimental analysis of the magnetoelastic anisotropy of a non-oriented silicon iron alloy

O. Hubert*, L. Daniel, R. Billardon

LMT, ENS-Cachan/CNRS/University Paris 6, 61, Avenue du Président Wilson, 94235 Cachan Cedex, France

Abstract

This paper deals with experimental measurements of the mechanical, magnetic and magnetostrictive behaviours of a non-oriented 3%SiFe alloy. The results show that the low crystallographic texture of the material brings important anisotropic effects and that the coupled magnetomechanical properties are much more sensitive than uncoupled ones.

Keywords: Silicon steels; Magnetic measurements; Magnetostriction; Magnetoelastic anisotropy

1. Introduction

Non-oriented (NO) silicon iron laminations are widely used in the electric construction for their isotropic magnetic behaviour in the sheet plane. Anisotropy nevertheless exists and could explain an important part of noise linked to the magnetostriction in the electromagnetic devices, like for grain-oriented materials [1]. An experimental analysis of the influence of the texture for an NO material on the magnetic, mechanical and coupled properties is proposed.

2. Experimental procedure and results

A commercial 0.5 mm thick Fe–3%Si NO alloy has been employed, indicating no morphologic texture of the grains. Electron back-scattered diffraction measurements (EBSD) show that the forming process brought about a $\{1\,1\,1\}\langle 1\,1\,\bar{2}\rangle$ type crystallographic texture (Fig. 1). Samples for all experiments consist of 250 mm long and 12.5 mm wide bands. They were cut by electroerosion machining in the lamination each 10° from the rolling direction (RD). Standard tensile tests have been carried out to measure the Young's modulus and Poisson's ratio thanks to usual strain gauges. Magnetic measurements were implemented using a non-standard experimental frame [2]. The magnetisation characteristics have been investigated under quasistatic excitation conditions (0.1 Hz), and a special procedure allowed to build the anhysteretic curve ($M_{an}(H_{an})$) [2]. The magnetostriction characteristics have been measured simultaneously. The samples have been instrumented with longitudinal and transverse constantan strain gauges (low magnetoresistive sensitivity [3], gauge factor $K = 2.07 \pm 0.5\%$). Different configurations of measurements have been tested: quarter or half bridge systems (using a free gauge put on the other side of the sample and submitted to the same level of magnetic field), with temperature compensation. They give rise to similar results. The highest problem is the non-negligible level of the electromagnetic noise compared to the very low level of e.m.f. signal in the bridge. An efficient low pass filtering is consequently necessary (LP frequency less than 10 Hz) that implies the excitation system to work at very low frequency to avoid any distortion ($f = 0.1$ Hz). The measurement of the anhysteretic magnetostriction is another efficient solution, even if the duration of measurement is much longer.

Fig. 2a shows the main measured magnetic characteristics of the material (first magnetisation, anhysteretic and hysteretic curves) for a 70° oriented sample in sheet plane. Fig. 2b allows to compare the anhysteretic curves for all directions. A strong anisotropic magnetic

*Corresponding author. Tel.: +33-1-4740-2224; fax: +33-1-4740-2240.

E-mail address: hubert@lmt.ens-cachan.fr (O. Hubert).

0304-8853/03/$ - see front matter
PII: S0304-8853(02)00850-8

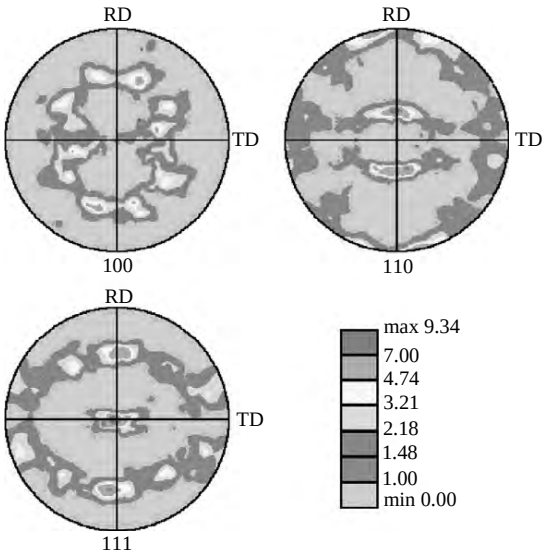

Fig. 1. Poles figure of a NO 3%SiFe alloy (EBSD method).

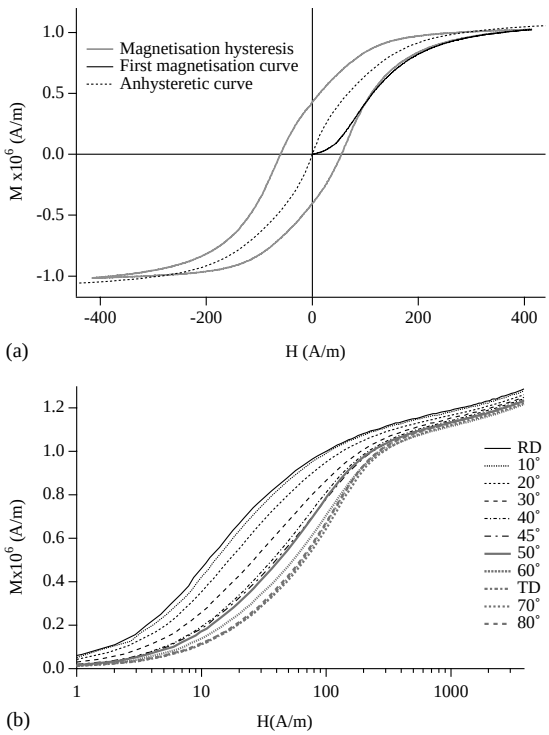

Fig. 2. (a) First magnetisation, hysteresis and anhysteretic curve for a 70° specimen; (b) anhysteretic curve $M_{anh}(H_{anh})$ of the material in the sheet plane.

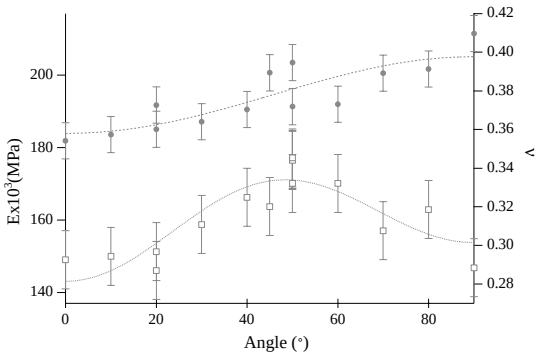

Fig. 3. Young's modulus and Poisson's ratio of the material in the sheet plane.

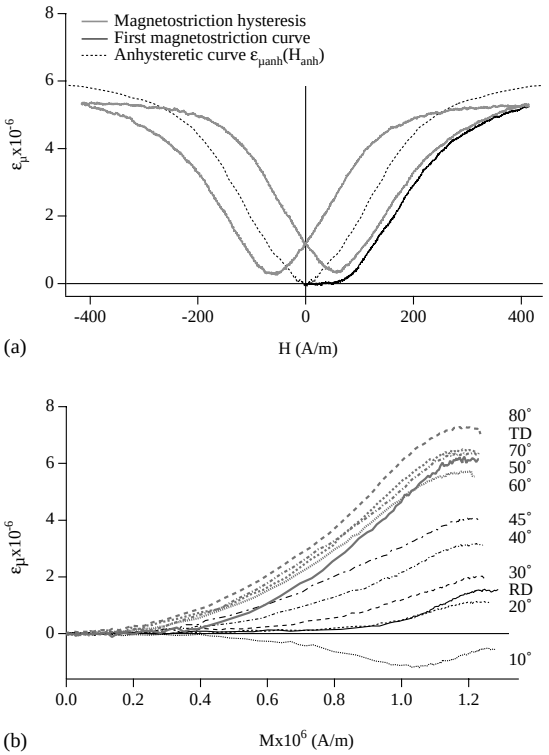

Fig. 4. (a) First longitudinal magnetostriction, hysteresis and anhysteretic magnetostriction curve for a 70° specimen; (b) longitudinal anhysteretic magnetostriction curve $\varepsilon_{\mu anh}$ (M_{anh}) in the sheet plane.

behaviour is clearly shown especially for low magnetic field strengths ($H < 200$ A/m): the magnetic permeability is decreasing between the rolling (RD) and transverse (TD) directions. At higher levels the differences are not exceeding 15%. The same variations are roughly obtained for the other uncoupled magnetic character-

istics. Young's modulus and Poisson's ratio evolution in the sheet plane are shown in Fig. 3. The highest stiffness is for TD and it roughly decreases monotonously to RD, highlighting a similar level of anisotropy than for uncoupled magnetic characteristics. Poisson's ratio is very sensitive to the crystallographic texture considering the non-monotonous variations and amplitudes between RD and TD.

Fig. 4a shows the main measured magnetostriction characteristics of the material (first magnetostriction, anhysteretic and hysteretic curves) for the previous 70° oriented sample. Longitudinal anhysteretic magnetostriction evolution in the sheet plane is drawn as a function of the magnetisation level in Fig. 4b. Only the relative variations have to be taken into account because the elastic deformations ($\approx 1 \times 10^{-6}$) due to the magnetic forces [4] have not been removed. The amplitude of variations of $\varepsilon_{\mu an}(M_{an})$ reaches a maximum of about 8×10^{-6} ($H < 4000$ A/m). The anisotropy of the magnetostrictive behaviour in the sheet plane is much stronger than for uncoupled behaviours. The observed anisotropy and variations for the transverse magnetostriction are of same order than the longitudinal one (Fig. 5a).

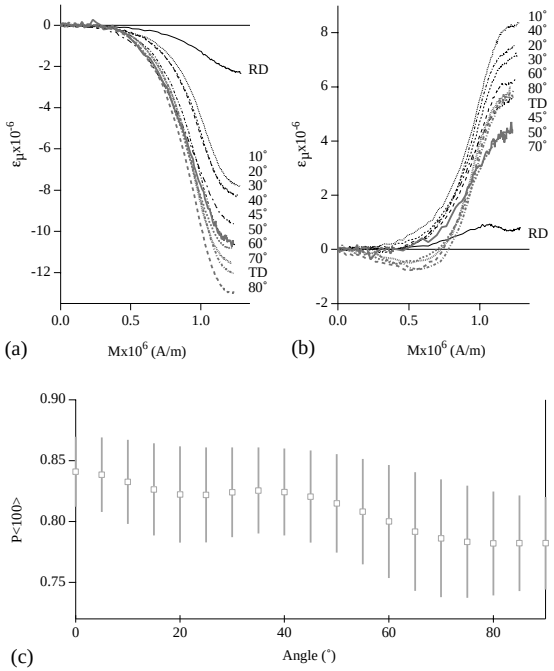

Fig. 5. (a) Transverse anhysteretic magnetostriction curve $\varepsilon_{\mu anh}$ (M_{anh}) in the sheet plane; (b) calculated anhysteretic magnetostriction through the thickness; (c) ⟨1 0 0⟩ direction projection in the sheet plane.

3. Discussion and conclusion

The magnetostriction through the thickness has been calculated (Fig. 5b) using the hypothesis that magnetostriction is an isochore deformation for this material [2]. This strain is highly non-monotonous facing to either the magnetisation orientation, or the magnetisation level. The associated high frequency deformation harmonics could be an important source of noise in a rotating field machine. Let us finally consider the observed various anisotropies facing the crystallographic texture. A simple treatment of the previous orientation data file is proposed: a triplet of Euler's angles $\{\phi_1, \theta, \phi_2\}$ corresponds to six ⟨1 0 0⟩ orientations. The closest ⟨1 0 0⟩ direction is projected along each orientation of the previous measurements between RD and TD (Fig. 5c). A good agreement appears between the variations of uncoupled properties and this projection: the ⟨1 0 0⟩ direction is first an easy magnetic direction and second a "soft" mechanical direction [5]. The tendency for magnetostriction is correct considering that the motion of 180° magnetic walls at low field occurs easily for ⟨1 0 0⟩ oriented crystals without magnetostriction [5]. The higher density of ⟨1 0 0⟩ directions corresponds to the lower magnetostriction amplitude. Anisotropy is just highly amplified.

References

[1] B. Weiser, H. Pfützner, IEEE Trans. Magn. 36 (2000) 3759.
[2] C. Gourdin, Ph.D., University Paris, Vol. 6, 1998.
[3] B. Hoekstra, E.M. Gyorgy, G. Zydzik, P.J. Flanders, Rev. Sci. Instrum. 48 (1977) 1253.
[4] R. Billardon, L. Hirsinger, J. Magn. Magn. Mater. 140–144 (1995) 2199.
[5] R.M. Bozorth, Ferromagnetism, Van Norstand, New York, 1951.

Nicolas GALOPIN, Laurent DANIEL, Frédéric BOUILLAULT, Mondher BESBES

Laboratoire de Génie Electrique de Paris,

Numerical analysis for the design of a magneto-elastic characterisation device

Abstract. *A specific experimental platform, dedicated to magneto-mechanical behaviour measurement, is presented. The specifications of the characterisation system are listed and the technical choices made described. Numerical aspects concerning the conception stage, in order to match the specifications, are highlighted.*

Abstract. *Opisano specjalny system do badania właściwości magnetomechanicznych. Przedstawiono specyfikację systemu oraz jego techniczne możliwości. Szczególny nacisk położono na numeryczne aspekty systemu. (**Numeryczna analiza urządzenia do badań właściwości magnetoelastycznych**).*

Keywords: magnetoelastic phenomena, measuring device.
Słowa kluczowe: zjawiska magnetoelastyczne, urządzenie pomiarowe.

1. Introduction[1]

Magnetic and mechanical behaviours of ferromagnetic materials are strongly coupled. This coupling has two main manifestations. On one hand, magnetic properties are modified by the application of a stress, and, on the other hand, the application of a magnetic field creates a deformation. This deformation is the sum of an elastic strain called "form-effect" (associated to magnetic forces created in the material) and of the magnetostriction strain (spontaneous deformation of magnetised bodies [1]). The high amplitude of magnetostriction in some materials, such as Giant Magnetostrictive Materials (GMM), allows the development of innovating sensors and actuators based on magneto-elastic properties [2, 3]. The optimal design of such smart materials based devices supposes the use of appropriate constitutive laws for the magneto-elastic behaviour. The definition of these constitutive laws requires magneto-elastic properties measurements, associated to the development of dedicated experimental setups.

After a presentation of the specifications related to the design of a characterisation device, a specific device, matching these specifications, is described. Numerical results, leading to the proposed solution are detailed. Finally, the first experimental results obtained on a Terfenol-D specimen are shown.

2. Specifications for a magneto-elastic measurements setup

The objective of the magneto-elastic characterisation setup is the measurement of magnetisation and strain in a ferromagnetic specimen submitted simultaneously to magnetic field and stress. The sollicitations considered in that study are uniaxial, but the response measurement should be multiaxial. The range of materials to be tested is large, from Terfenol-D, a giant magnetostrictive material for actuator applications, to iron-cobalt alloys for high speed rotating machines. The specimens should be mainly rod shaped polycrystalline materials, but ferromagnetic sheets or bulk single crystals could also be studied. Two main requirements for the device design have been expressed.

First, the experimental setup should ensure the homogeneity of the magneto-elastic sollicitations (namely the magnetic field and the stress) and response (namely the magnetic induction and the strain) in the specimen measurement area. This measurement area is defined as a 15mm long zone in the center of the specimen. The criterions used for the homogeneity of sollicitations (magnetic field H and stress σ) are defined by equation (1).

$$C_H = \left(H_{max} - H_{min}\right) / H_{max} < 5\% \qquad C_\sigma = \left(\sigma_{max} - \sigma_{min}\right) / \sigma_{max} < 5\% \tag{1}$$

H_{max} and H_{min} are the maximum and minimum value of the longitudinal component of the magnetic field H. σ_{max} and σ_{min} are the maximum and minimum value of the longitudinal component of the stress σ.

Moreover, the form-effect [4,5] should be controlled. This effect appears in all magneto-elastic measurements: the measured strain ε^m is the combination of the magnetostriction strain ε^μ, the elastic strain ε^e due to the applied stress and the elastic strain ε^{fe} due to the magnetic forces associated to magnetisation variations (the so-called form effect). Thus, the correct deduction of the magnetostriction strain from the strain measurement requires the control of the two latter terms of equation (2).

$$\varepsilon^m = \varepsilon^\mu + \varepsilon^e + \varepsilon^{fe} \tag{2}$$

3. Characterisation device description

The characterisation setup is divided into two parts, a mechanical tensile test machine (ZWICK/ROELL Z030) for the application of the stress, and a magnetic circuit for the application of the magnetic field. The mechanical loading apparatus can produce active efforts until 30 kN, controlled thanks to a servo-control. The electromagnetic device (figure 1(a)) is constituted of two U-shaped ferrite yokes, ensuring the closure of the magnetic flux density. The magnetic setup (figure 1(b)) is placed and kept in position on the testing machine thanks to an amagnetic fixation set. Associated to a power amplifier, four primary coils (one wounded around each yoke - 600 turns each - and two around the specimen - 265 turns each) produce the magnetic field. Two magnetic columns connect the specimen to the loading apparatus and close the magnetic circuit. Four small airgaps are present in the magnetic circuit, between the columns and the yokes, but can be controlled thanks to the fixation set.

This experimental setup is equipped with measurement devices for loadings control and responses acquisition (figure 2). The applied stress σ is measured thanks to a standard load cell, and the magnetic field H in the measurement area thanks to Hall effect sensors. The magnetic induction B in the sample is obtained through the integration of the induced voltage of a B-coil surrounding the specimen. The strain ε^m is given by strain gages, both in the directions parallel and perpendicular to the specimen long axis. The centralisation of measurements and loading

[1] This paper is an extended version of the previous paper presented in Przeglad Elektrotechniczny No. 4 (2007), 101-102

control is ensured under Labview environment thanks to a computer equipped with a Data Acquisition System.

a)

b)

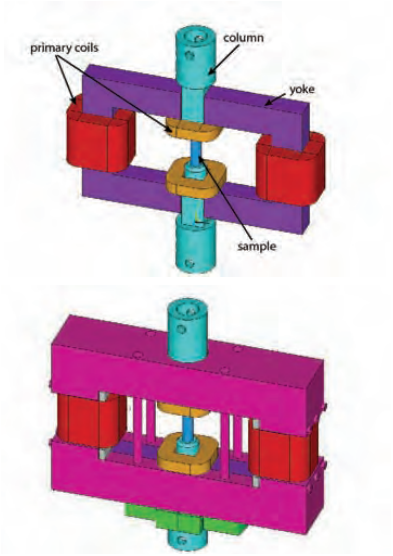

Fig. 1. Magneto-mechanical characterisation device: a) magnetic circuit, b) magnetic circuit with its fixation set

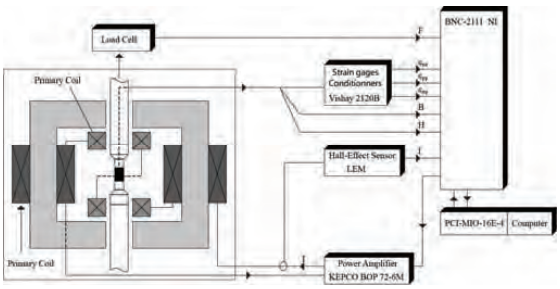

Fig. 2. Measurement setup synoptic

4. Numerical analysis

The numerical analysis was done with ANSYS finite element software. The properties of the materials have to be specified. The set up design step has focused on two materials for the specimens: an iron-cobalt alloy from IMPHY society and a Terfenol-D ceramic from ETREMA company. The iron-cobalt alloy (AFK-502: $Fe_{49}Co_{49}V_2$) has been characterised using another magneto-mechanical test bench [6]. The corresponding - non linear - results have been used for the magnetic behaviour of this material. The Terfenol-D properties have been defined after Etrema products information [7]. A pre-design step has been made in order to choose the specimen section (about 100 mm^2), the section for the ferrite yokes (20 × 27mm^2) and for the columns (15 mm diameter mini), preventing from the saturation of the magnetic circuit. The magnetic properties of the yokes and the columns are taken linear (the non-saturation of the magnetic circuit - except in the specimen - is controlled at each calculation step). Table 1 gives the magnetic properties taken for the magnetic analysis as well as the elastic properties for the mechanical calculation[2]. The materials have been assumed isotropic.

Table 1. Magnetic and mechanical properties

	B_{sat} (T)	μ_r	E (GPa)	ν
Terfenol-D	1	4	100	0.3
Fe-Co	2.2	n.l.	210	0.29
XC-48	1.6	1500	220	0,29
Ferrite	0.5	3500	-	-

Once the device is meshed (one eighth of the geometry for symmetry reasons), and the materials properties known, the sollicitations heterogeneity in the measurement area can be evaluated. Since dimensional uncertainties are not taken into account, the calculated heterogeneity will be related to the specimen length L_{spec}, to the friction coefficient f between the specimen and the column for the mechanical behaviour, and to the gaps width e for the magnetic behaviour. The finite element calculation also permits the determination of magnetic forces (see section 4.1). Figure 3 shows an example of magnetic results in the case of a Terfenol-D specimen, highlighting the leak of magnetic induction out of the specimen.

a) b)

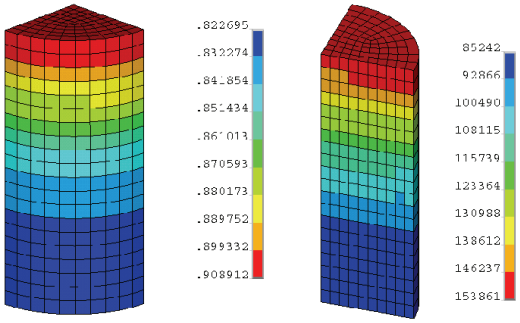

Fig.3. Numerical results in the case of a Terfenol-D sample for $I = 5A$: a) Magnetic induction (T), b) Magnetic field (A/m)

4.1 Magnetic forces calculation

The measured strain is the sum of three contributions (see equation (2)). The magnetostriction strain is obtained after a correction of the total - measured - strain. The elastic strain associated to the macroscopic applied stress is simply deduced from the Hooke law. The part due to magnetic forces (form effect) has to be estimated. The distributions of magnetic field H and magnetic induction B create a distribution of magnetic forces concentrated on the specimen faces. The surfacic forces density can be obtained integrating the Maxwell tensor [8,9]. The pressure p on the specimen surfaces is then defined by equation (3).

$$p = \frac{1}{2}\left[\left(\frac{1}{\mu_0} - \frac{1}{\mu_1}\right)b_n^2 - (\mu_0 - \mu_1)h_t^2\right] \tag{3}$$

b_n and h_t are respectively the component normal and tangent to the free surfaces of the specimen for respectively the magnetic induction and the magnetic field, μ_0 and μ_1 are the magnetic permeability of vacuum and of the specimen.

[2] B_{sat} is the maximum magnetic induction, μ_r is the relative magnetic permeability, E is the Young modulus and ν the Poisson ratio.

4.2 Influence of airgap width

As expected, the airgaps width e, for a given intensity in the windings, affects the level of the magnetic field in the measurement area (figure 4(a)). But as illustrated on figure 4(b) in the case of a Terfenol-D sample, the homogeneity of the magnetic field is not sensitive to the airgap width, whatever the specimen length. The -very low - effect of e on the level of magnetic forces is illustrated on figure 6.

a)

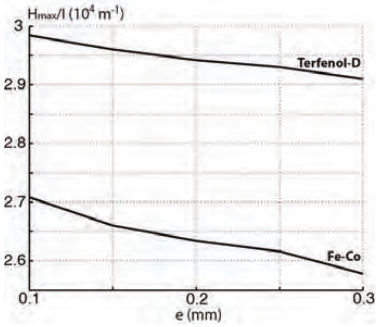

b)

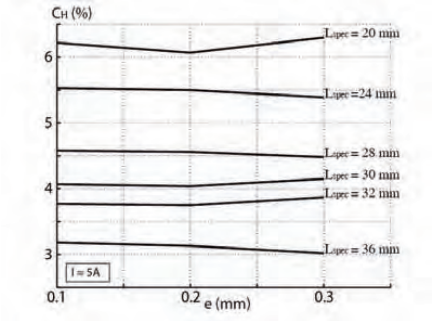

Fig. 4. Effect of the airgap width e on the level and on the heterogeneity of the magnetic field in the measurement area ($I = 5A$): a) magnetic field level, b) magnetic field homogeneity

4.3 Influence of friction coefficient between columns and specimen

The influence of the friction coefficient f between the columns and the specimen has also been studied. It appears that the value of f, taken from 0 to 0.3, has nearly no incidence on the stress homogeneity. Nonhomogeneity of stress could arise from setup dissymmetry - such as excentration of loading columns - but these effects have not been considered in that paper. They can be controlled using two strain gages sticked on the opposite sides of the specimen.

4.4 Influence of specimen length

The effect of the length of the specimen has also been investigated. As illustrated on figure 5(a), in the case of a section of 100 mm^2, the homogeneity of the magnetic field (as defined by equation (1)) cannot be guaranteed if the length of the specimen is too small. The case of Terfenol-D is more critical than the case of AFK-502. The stress homogeneity criterion is always respected for specimen longer than 20 mm (figure 5(b)).

The effect of the specimen length on the magnetic forces has also been evaluated (figure 6). The level of the pressure appears to be so weak that the form effect can be neglected in that configuration.

a)

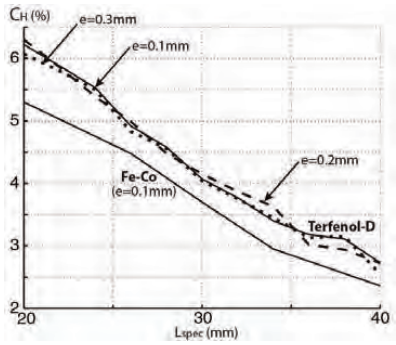

b)

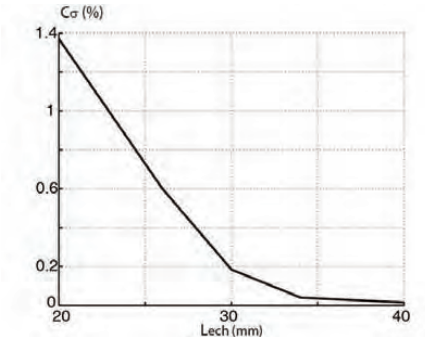

Fig. 5. Effect of the specimen length L_{spec} on the homogeneity criterions in the measurement area: a) magnetic field homogeneity, b) stress homogeneity (Terfenol-D)

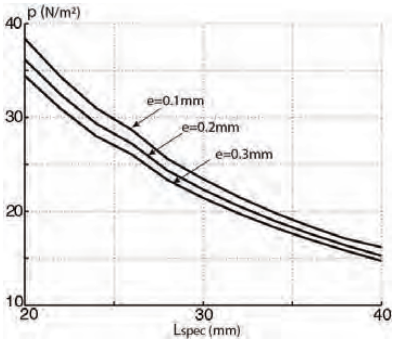

Fig. 6. Mean magnetic induced pressure on the lateral sides of the specimen (Terfenol-D)

Finally, a 30 mm length for the specimen ensures the homogeneity of the magnetic field and of the stress in the measurement area (as defined in section 2) for both Terfenol-D and iron-cobalt alloy specimens.

5 Conclusion

The first experimental results obtained on a Terfenol-D rod show the importance of a direct measurement of the applied magnetic field. Figure 7 highlights the fact that this magnetic field cannot be simply deduced from the knowledge of the current in the primary coils. Two different and nearly linear stages appear on that curve. During the first stage, for low magnetic field, most of the ampere-turns are concentrated in the airgaps. For higher magnetic fields, the magnetic induction in the specimen is getting non-linear and gets close to the saturation. Ampere-turns consumed in the specimen area are getting higher, changing the slope of the $H(I)$ curve.

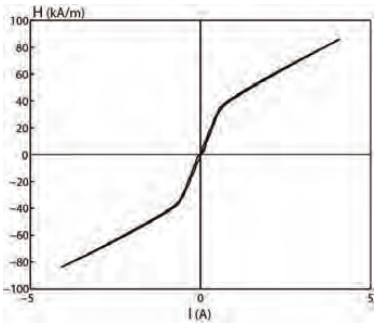

Fig. 7. Current-magnetic field relationship in the case of a Terfenol-D sample

a)

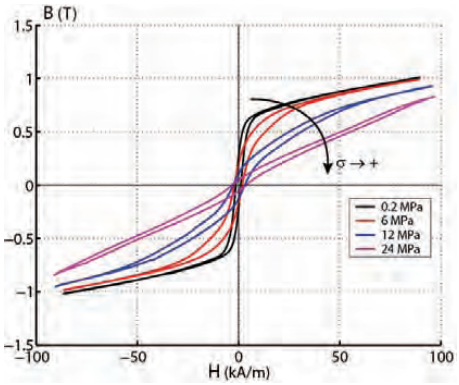

b)

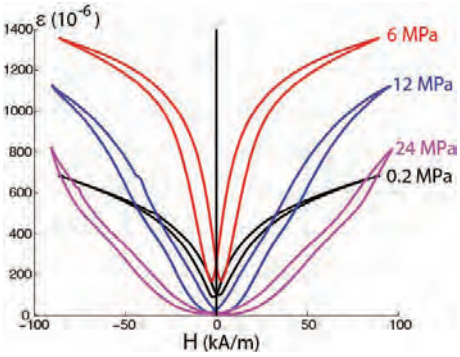

Fig. 8. Magneto-elastic characterisation of a Terfenol-D rod specimen for various uniaxial applied stress: a) Magnetic behaviour $B(H)$, b) Magnetostrictive behaviour $\varepsilon^{u}(H)$.

As an illustration, the first magneto-mechanical results for a Terfenol-D specimen are plotted on figure 5. The classical strong and non-linear effect of stress on the magnetisation and on the magnetostriction strain is recovered. The non-monotonous effect of an uniaxial stress on the magnetostriction is also highlighted: a low applied stress tends to increase the magnetostriction magnitude while a higher applied stress finally decreases it.

In that paper, a specific test bench dedicated to magneto-elastic characterisation has been presented. The numerical analysis step for the design of the magnetic circuit has been discussed. It was shown that the homogeneity of the magnetic field in the measurement area of the sample can be ensured by an appropriate choice of the length of the specimens. In the chosen configuration, the homogeneity of stress in the measurement area is attained and the effect of magnetic forces is weak. This numerical analysis design step has significantly reduced the time necessary to obtain an operational measurement setup system. This magneto-mechanical benchmark will be used for the development, identification and validation of magneto-mechanical behaviour models.

REFERENCES

[1] E. du Trémolet de Lacheisserie, *Magnetostriction, Theory and applications of magnetoelasticity*, CRC Press, 1993.
[2] G. Engdahl, *Handbook of Giant Magnetostrictive Materials*, Academic Press, 2000.
[3] M. Pasquale, *Sensors and Actuators A: Physical*, **106**, pp.142-148, 2003.
[4] R. Billardon and L. Hirsinger, *J. Magn. Magn. Mater.*, **140-144**(3), pp.2199-2200, 1995.
[5] A.C. Eringen and G.A. Maugin, *Electrodynamics of Continua*, Springer, New York, 1990.
[6] O. Hubert et al., *Przeglad Elektrotechniczny*, **81**(5), pp.19-23, 2005.
[7] http://www.etrema-usa.com/documents/Terfenol.pdf
[8] E. Durand, *Magnétostatique*, Masson, Paris, 1968.
[9] J.R. Melcher, *Continuum electromechanics*, MIT Press, 1981.

Authors:
N. Galopin, L. Daniel, F. Bouillault and M. Besbes; Laboratoire de Génie Electrique de Paris; 11 rue Joliot-Curie 91192 Gif-sur-Yvette Cedex, France, nicolas.galopin@lgep.supelec.fr

Magnetic and Magnetostrictive Behavior of Iron-Silicon Single Crystals Under Uniaxial Stress

Karl-Joseph Rizzo[1,2], Olivier Hubert[1], and Laurent Daniel[2]

[1]LMT-Cachan ENS-Cachan/CNRS/UPMC/UniverSud Paris, Cachan cedex F-94235, France
[2]LGEP Supelec/CNRS/Univ Paris-Sud/UPMC, Gif-sur-Yvette Cedex F-91192, France

This paper presents the full characterization of the reversible magneto-mechanical behavior of iron-silicon single crystals. Magnetostriction and magnetization measurements under tensile mechanical loading have been performed on specimen collected along the $\langle 100\rangle$, $\langle 110\rangle$ and $\langle 111\rangle$ crystallographic axes. A theoretical interpretation of the results is attempted.

***Index Terms*—Magnetoelasticity, silicon steel.**

I. Introduction

THE search for weight optimization of electromechanical systems leads to build more compact and high speed systems. These systems generate high levels of multiaxial mechanical stress, that strongly change the magnetic behavior of materials. In order to reach optimal design for electromagnetic devices, this magneto-mechanical coupling effect need to be introduced in advanced modeling tools. Macroscopic phenomenological approach (see for instance [1]) does not provide a sufficient description of such complex phenomena. An alternative way is the requirement of multiscale approaches introducing the coupling effect at the single crystal scale [2], and considering the effect of stress on the magnetic domains distribution. The full characterization of the magneto-mechanical behavior of single crystals is the first step necessary for the development of such a multiscale approach. We present in this paper the measurements of reversible magnetic and magnetostrictive behavior of an iron-silicon steel (3%Si-Fe) single crystal cut along the $\langle 100\rangle$, $\langle 110\rangle$ and $\langle 111\rangle$ crystallographic axes. Samples are submitted to both a magnetic excitation and a mechanical tensile loading. In a second part, these results are discussed from a theoretical point of view.

II. Magneto-Mechanical Characterization

An industrial grain-oriented silicon steel (3%Si-Fe GO, 0.3 mm thick) has been used for the experiments. This material exhibits a very large grain size (around 40 mm) and a strong crystallographic GOSS texture (rolling direction (RD)//[001], transverse direction (TD)//$[\bar{1}10]$) [3]. 200 mm long and 12.5 mm wide bands have been cut in sheet at 0°, 90° and 54.7° from RD, ideally corresponding to the crystallographic axes $\langle 100\rangle$, $\langle 110\rangle$ and $\langle 111\rangle$. The cutting area has been selected so that a large grain stands in the middle of the sample (see Fig. 1). The strips are equipped with heads in order to apply a pure mechanical tensile loading using weights. The selected grain is equipped with a pick-up coil for magnetic induction measurement. Strain gages are stuck on both sides of the sample in order to measure the magnetostriction along sample length and width. A specific procedure allows the measurement of the anhysteretic behavior of the material [4].

Fig. 1. Specimen, view of grain, coil and strain gage.

The anhysteretic magnetization and magnetostriction measurements in stress free conditions are presented in Fig. 2. The results obtained under tensile stress are presented in Fig. 3 for the three directions 0°, 90° and 54.7°. We note $\Delta\lambda_{//}$ the deformation measured along the sample length and $\Delta\lambda_{\perp}$ the deformation measured along the sample width.

III. Results Interpretation

The interpretation of these measurements is based on a schematic representation of the domain configuration and its evolution under external magneto-mechanical loading (Fig. 4). This schematic interpretation has already been presented in stress free configurations [3] (Fig. 4(b)–(i)) and is extended here to the case where a tensile stress is applied in free magnetic field configurations (Fig. 4(b')–(i')).

We focus on the relationship between the change of the magnetic domain structure and the measured magnetostriction. A domain α is an area inside the single crystal with uniform magnetization $\vec{M}_\alpha$ and uniform magnetostriction strain ε_μ^α given by (1) and (2)

$$\vec{M}_\alpha = M_S\vec{\gamma}_\alpha = M_S{}^t[\gamma_1\ \gamma_2\ \gamma_3] \tag{1}$$

$$\varepsilon_\mu^\alpha = \frac{3}{2}\begin{pmatrix} \lambda_{100}\left(\gamma_1^2-\frac{1}{3}\right) & \lambda_{111}\gamma_1\gamma_2 & \lambda_{111}\gamma_1\gamma_3 \\ \lambda_{111}\gamma_1\gamma_2 & \lambda_{100}\left(\gamma_2^2-\frac{1}{3}\right) & \lambda_{111}\gamma_2\gamma_3 \\ \lambda_{111}\gamma_1\gamma_3 & \lambda_{111}\gamma_2\gamma_3 & \lambda_{100}\left(\gamma_3^2-1\frac{1}{3}\right) \end{pmatrix}_{\mathrm{CF}}. \tag{2}$$

M_S is the saturation magnetization of the material, $\vec{\gamma}_\alpha$ the direction of the magnetization in the domain α, with direction cosines γ_1, γ_2, and γ_3 in the crystallographic frame CF. λ_{100} and λ_{111} are the magnetostriction constants of the material. In the case of 3%Si-Fe, these constants are $\lambda_{100} = 23 \times 10^{-6}$ and $\lambda_{111} = -4.5 \times 10^{-6}$. The initial distribution of magnetic domains is strongly dependent on the magnetocrystalline energy

Manuscript received June 20, 2009; revised August 30, 2009; accepted September 02, 2009. Current version published January 20, 2010. Corresponding author: O. Hubert (e-mail: hubert@lmt.ens-cachan.fr).

Color versions of one or more of the figures in this paper are available online at http://ieeexplore.ieee.org.

Digital Object Identifier 10.1109/TMAG.2009.2032146

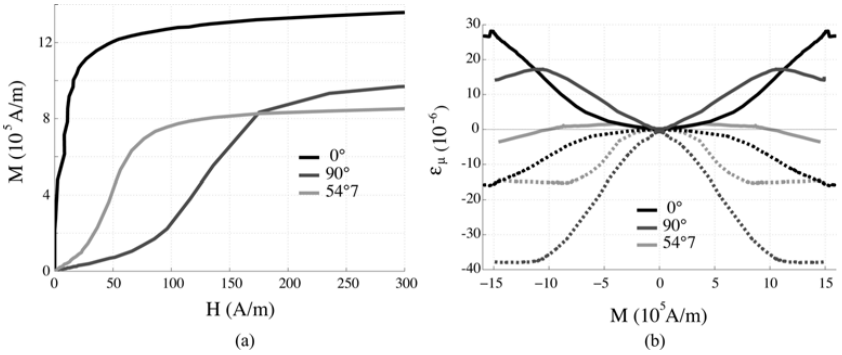

Fig. 2. Anhysteretic behavior for sample directions 0°, 90° and 54.7°—(b) full lines: $\Delta\lambda_{//}$; dashed lines: $\Delta\lambda_{\perp}$. (a) Magnetization, (b) Magnetostriction strain.

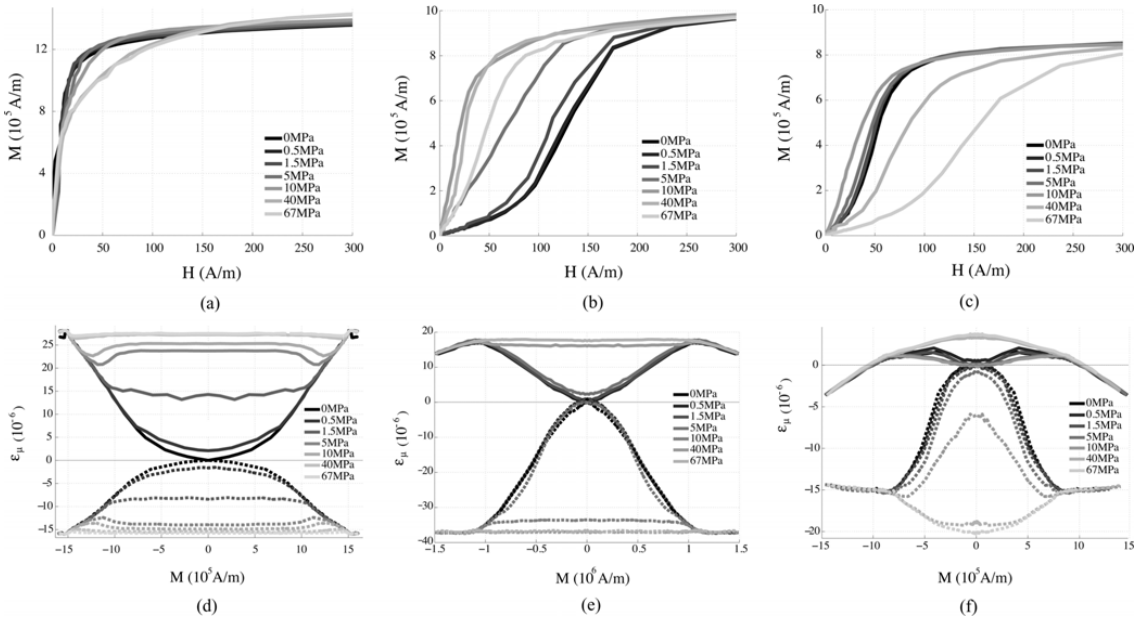

Fig. 3. Tensile stress influence on the anhysteretic behavior for sample directions 0°, 90°, and 54.7°—(d)-(e)-(f) full lines: $\Delta\lambda_{//}$; dashed lines: $\Delta\lambda_{\perp}$. (a) 0° Magnetization, (b) 90° Magnetization, (c) 54.7° Magnetization, (d) 0° Magnetostriction strain, (e) 90° Magnetostriction strain, (f) 54.7° Magnetostriction strain.

W_K^{α}, given by (3) in the case of a cubic crystal. K_1 and K_2 are the anisotropy constants of the material, respectively 35 kJ/m^3 and almost zero in the case of 3%Si-Fe

$$W_K^{\alpha} = K_1\left(\gamma_1^2\gamma_2^2 + \gamma_2^2\gamma_3^2 + \gamma_3^2\gamma_1^2\right) + K_2\left(\gamma_1^2\gamma_2^2\gamma_3^2\right). \quad (3)$$

This energetic term explains why the ideal single crystal can be divided into six domain families with magnetization respectively aligned along the six $\langle 100\rangle$ directions. But the presence of free surfaces on the sheet unbalances the ideal configuration [3] and leads to a two-domain structure along the rolling direction, schematically presented in Fig. 4(a). Starting from this initial GOSS distribution, we can write the associated magnetostriction tensor (without any loading) of the single crystal in the crystallographic frame:

$$\boldsymbol{\varepsilon}^{\mu}_{\text{ini}} = \begin{pmatrix} -\frac{1}{2}\lambda_{100} & 0 & 0 \\ 0 & -\frac{1}{2}\lambda_{100} & 0 \\ 0 & 0 & \lambda_{100} \end{pmatrix}_{\text{CF}}. \quad (4)$$

If a magnetic or mechanical loading is applied, this magnetostriction tensor is changed in $\boldsymbol{\varepsilon}^{\mu}_{\text{new}}$. The correspondence with experimental measurements is so that $\Delta\lambda_{//} = {}^t\vec{n}\cdot(\boldsymbol{\varepsilon}^{\mu}_{\text{new}} - \boldsymbol{\varepsilon}^{\mu}_{\text{ini}})\cdot\vec{n}$ and $\Delta\lambda_{\perp} = {}^t\vec{t}\cdot(\boldsymbol{\varepsilon}^{\mu}_{\text{new}} - \boldsymbol{\varepsilon}^{\mu}_{\text{ini}})\cdot\vec{t}$ where $\vec{n}$ and $\vec{t}$ denote the directions along sample length and width, respectively (see Fig. 4).

A. Magnetic Field Influence

The influence of the magnetic field $\vec{H}$ on the magnetic microstructure is driven by the Zeeman energy:

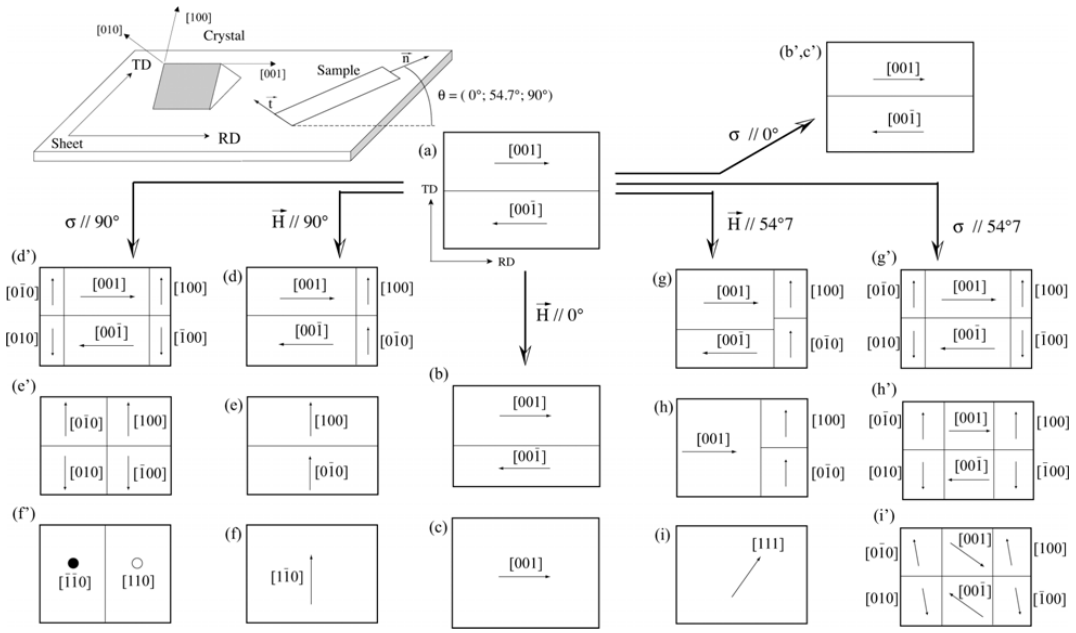

Fig. 4. Schematic representation of magnetic domain structure under magneto-mechanical loadings along three selected directions of the sheet plane (RD $=$ $0^\circ \approx [001]$, TD $= 90^\circ \approx [1\bar{1}0]$, $54.7^\circ \approx [1\bar{1}1]$).

$$W_H^\alpha = -\mu_0 \vec{H} \cdot \vec{M}_\alpha. \tag{5}$$

The application of a magnetic field will increase the size of domains with magnetization oriented nearby the direction of the field and favor the rotation of magnetization towards this orientation.

1) $\vec{H}//0^\circ$: domain wall motion 4(b) until magnetic saturation 4(c). Since the magnetostriction is not sensitive to the sign of the magnetization but only to its direction, this loading should not modify the magnetostriction so that $\Delta\lambda_{//} = \Delta\lambda_\perp = 0$. Our measurement (Fig. 3(d)) is not consistent with this scenario and rather looks like the behavior of a classical single crystal [3]. The possible explanations are the proximity of a grain boundary and/or influence of residual stresses, leading to closure domains and lancets with magnetization oriented orthogonally to the sample length in the area of the strain gage.

2) $\vec{H}//90^\circ$: nucleation of domains in two easy magnetization directions close to the magnetic field direction 4(d); then disappearance of the initial domains 4(e); finally rotation of the two remaining domains towards the magnetic field direction 4(f). At intermediate configuration 4(e), magnetostriction tensor is given by (6), we then have: $\Delta\lambda_{//} = (3)/(4)\lambda_{100} \approx 17\times10^{-6}$ and $\Delta\lambda_\perp = -(3)/(2)\lambda_{100} \approx -34 \times 10^{-6}$. Experimental results are in good agreement with this scenario. The small difference can be explained by a nonideal initial configuration, for instance due to a weak crystal disorientation. At saturation 4(f), magnetostriction tensor is given by (7): we obtain $\Delta\lambda_{//} = (3)/(4)\lambda_{100}+(3)/(4)\lambda_{111} \approx 14\times10^{-6}$; theoretical value along width is unchanged: $\Delta\lambda_\perp = -(3)/(2)\lambda_{100} \approx -34 \times 10^{-6}$. This is consistent with the fact that we observe on Fig. 3(e) a small variation for the magnetostriction along sample length at high magnetic fields whereas the magnetostriction along sample width remains constant

$$\varepsilon_{4e}^\mu = \begin{pmatrix} \frac{1}{4}\lambda_{100} & 0 & 0 \\ 0 & \frac{1}{4}\lambda_{100} & 0 \\ 0 & 0 & -\frac{1}{2}\lambda_{100} \end{pmatrix}_{\mathrm{CF}} \tag{6}$$

$$\varepsilon_{4f}^\mu = \begin{pmatrix} \frac{1}{4}\lambda_{100} & -\frac{3}{4}\lambda_{111} & 0 \\ -\frac{3}{4}\lambda_{111} & \frac{1}{4}\lambda_{100} & 0 \\ 0 & 0 & -\frac{1}{2}\lambda_{100} \end{pmatrix}_{\mathrm{CF}}. \tag{7}$$

3) $\vec{H}//54.7^\circ$: nucleation of domains in two easy magnetization directions close to the magnetic field direction 4(g); then coexistence of the three most favorably oriented domains 4(h); final rotation of magnetization towards the magnetic field direction at high fields 4(i). At intermediate configuration 4(h), magnetostriction tensor is given by (8): we have: $\Delta\lambda_{//} = 0$ and $\Delta\lambda_\perp = -(1)/(2)\lambda_{100} \approx -11 \times 10^{-6}$. At saturation 4(i), magnetostriction tensor is given by (9). Then $\Delta\lambda_{//} = \lambda_{111} \approx -4.5 \times 10^{-6}$ and $\Delta\lambda_\perp = -(1)/(2)\lambda_{100} - (1)/(3)\lambda_{111} \approx -10 \times 10^{-6}$. This scenario is in good agreement with the measurements of Fig. 3(f)

$$\varepsilon_{4h}^\mu \approx \varepsilon_{4e}^\mu \tag{8}$$

$$\varepsilon_{4i}^\mu = \begin{pmatrix} 0 & -\frac{\lambda_{111}}{2} & \frac{\lambda_{111}}{2} \\ -\frac{\lambda_{111}}{2} & 0 & -\frac{\lambda_{111}}{2} \\ \frac{\lambda_{111}}{2} & -\frac{\lambda_{111}}{2} & 0 \end{pmatrix}_{\mathrm{CF}}. \tag{9}$$

B. Tensile Stress Influence

The influence of the stress $\boldsymbol{\sigma}$ on the magnetic microstructure is driven by the magneto-elastic energy:

$$W_\sigma^\alpha = -\boldsymbol{\sigma} : \boldsymbol{\varepsilon}_\mu^\alpha. \tag{10}$$

In the case of 3%Si-Fe GO, the application of a tensile stress will increase the size of domains with magnetization oriented nearby the direction of the applied stress and can induce magnetization rotation. These two mechanisms are sequenced (volume variation at low stress, rotation at high stress) which allows a two-step analysis. The wall motion mechanism under stress is not sensitive to the sign of the magnetization but only to its direction. The mechanism of magnetization rotation under stress is much more difficult to handle than rotation under the action of a magnetic field. Let us consider a two-dimensional case and a domain initially oriented along [001] (corresponding to the case of GO sheet), and a stress σ applied along direction $\vec{n}$. The angle between $\vec{n}$ and [001] is noted ϕ_c and the angle between the magnetization and its initial position [001] is noted ϕ_1. The angle ϕ_1 can be written [5] according to

$$\phi_1(\sigma) = \frac{\operatorname{atan}(\frac{3}{2}\lambda_{111}\sigma\sin(2\phi_c))}{2K_1 + 3\lambda_{100}\sigma\cos(2\phi_c)}. \tag{11}$$

In the case of 3%Si-Fe (high K_1, $\phi_c > 0$ and $\lambda_{111} < 0$), a tensile stress will deviate the magnetization from the loading direction. The effect of stress on the magnetic behavior can finally be deduced indirectly from the observation of the evolution with stress of the projection along the magnetic field direction of the magnetization of favorably oriented domains: the stronger the projection, the higher the susceptibility. Moreover, one can remark that the effect of stress on magnetostriction leads to an initial deformation associated to the so-called ΔE effect [6].

1) $\sigma//0°$: the stress has no effect, structure is unchanged 4(b')–(c') so that $\Delta\lambda_{//} = \Delta\lambda_\perp = 0$. The magnetic behavior is expected to be unchanged. The experimental results [Fig. 3(d)] are not in agreement with this scenario for the same reasons detailed in Section III-A1. The application of a small tensile stress seems to realign the structure into a GOSS configuration. After the preload, we obtain $\Delta\lambda_{//} = \Delta\lambda_\perp = 0$ as expected. The decrease of susceptibility for stress level beyond 40 MPa is on the other hand the signature of a disorientation of the grain compared to the ideal orientation.

2) $\sigma//90°$: nucleation of orthogonal domains 4(d'); then disappearance of the initial domains 4(e'); finally rotation of magnetization away from the stress direction 4(f'). For the intermediate situation 4(e'), the magnetostriction tensor is identical to the one given by (6). It means that it is possible to mechanically saturate the magnetostriction strain to the value $\Delta\lambda_{//} = (3)/(4)\lambda_{100} \approx 17 \times 10^{-6}$ and $\Delta\lambda_\perp = -(3)/(2)\lambda_{100} \approx -34\times10^{-6}$. The magnetic saturation leads to the same configuration than without mechanical loading $\Delta\lambda_{//} = ((3)/(4)\lambda_{100} + (3)/(4)\lambda_{111}) \approx 14 \times 10^{-6}$. The magnetostriction along the sample width is unchanged compared to intermediate configuration 4(e'). The experimental measurements (Fig. 3(e)) confirm that it is possible to mechanically saturate magnetostriction in the absence of magnetic field. The magnetization rotation under stress is limited by free surface effect. This latter process should decrease the material susceptibility. Thus, we expect the magnetic susceptibility to increase with stress until the rotation process appears and then to decrease. This schematic view is in good agreement with the results of Fig. 3(b).

3) $\sigma//54.7°$: nucleation of orthogonal domains 4(g'); then the structure tends towards a six-domain structure similar to a single crystal structure 4(h'); finally rotation of the magnetization away from the stress direction 4(i'). For the intermediate situation 4(h'), the magnetostriction tensor is probably similar to the one obtained under a magnetic field ((8)). Consequently a magnetic loading will only introduce 180° wall motion, without deformation: the longitudinal measurement will remain zero and will undergo a rotation identical to the one observed without stress. The stress will induce an initial deformation along the sample width $\Delta\lambda_\perp = -(1)/(2)\lambda_{100} \approx -11 \times 10^{-6}$, corresponding to a mechanical saturation (no effect of field level except for the rotation). The rotation at high stress is more favorable for this orientation than for the 90° direction. It is difficult to express analytically the intermediate configuration. We expect saturation values identical to those obtained with no applied stress. Concerning the magnetic behavior, we expect a susceptibility increasing with stress until rotation occurs, and then a decrease, stronger than in the case of a loading along the 90° direction. The experimental measurements [Fig. 3(c)] are in good agreement with this scenario, and reveals that rotation occurs as soon as a 10 MPa stress is reached.

IV. Conclusion

In this paper, measurements of magnetization and magnetostriction strain of iron-silicon single crystals submitted to tensile stress have been presented. Results are roughly in accordance with theoretical interpretations based on domains structure evolution. The discrepancies observed denote the crucial role of the initial domains configuration and the extreme sensitivity of results to experimental procedure.

References

[1] M. J. Sablik and D. C. Jiles, *IEEE Trans. Magn.*, vol. 29, no. 3, p. 2113, May 1993.
[2] L. Daniel, O. Hubert, N. Buiron, and R. Billardon, *J. Mech. Phys. Solids*, vol. 56, p. 1018, 2008.
[3] O. Hubert and L. Daniel, *J. Magn. Magn. Mater.*, vol. 320, p. 1412, 2008.
[4] O. Hubert, L. Daniel, and R. Billardon, *J. Magn. Magn. Mater.*, vol. 254–255, p. 352, 2003.
[5] S. Lazreg and O. Hubert, in *Proc. Colloque national MECAMAT*, Aussois, 2009.
[6] L. Daniel and O. Hubert, *EPJ Appl. Phys.*, vol. 45, p. 31101, 2009.

2.3 Les approches multi-échelles au service des modèles macroscopiques

On est parfois tenté d'opposer les approches macroscopiques et les approches multi-échelles. Les premières ont l'avantage du pragmatisme, mais sont limitées par leur faible prédictivité, en raison de la nécessité d'identifier leurs paramètres sur des essais macroscopiques. On reproche souvent aux secondes leur difficulté de mise en œuvre. Pourtant, loin d'être incompatibles, ces approches peuvent au contraire s'avérer très complémentaires.

Les approches micro-macro, reposant sur une description des mécanismes physiques à une échelle supposée pertinente, constituent des outils prédictifs du comportement. Leur domaine de validité concerne un type de comportement, quel que soit le matériau considéré, pourvu que les caractéristiques physiques du matériau soient accesibles par ailleurs. Le domaine de validité des approches macroscopiques concerne en revanche à la fois un type de comportement et un matériau particulier. Les outils de modélisation multi-échelle peuvent ainsi être utilisés de manière efficace comme des "machines d'essais numériques" permettant l'identification des paramètres matériau des modèles macroscopiques. Cela peut permettre de faire l'économie d'essais d'identification parfois coûteux. Cela permet également de tester des gammes de sollicitations beaucoup plus larges, pour lesquelles les outils expérimentaux ne sont parfois pas disponibles. Cela permet surtout de tester l'effet de modification de composition ou de microstructure sur un matériau, sans procéder à l'élaboration de différentes nuances. Le passage à l'élaboration proprement dite peut être limité aux nuances prometteuses.

Dans certaines situations, les approches multi-échelles peuvent aussi constituer un investissement permettant la construction de modèles macroscopiques performants. Ces modèles macroscopiques ne sont pas des outils multi-échelles mais leur construction s'appuie sur un raisonnement micro-macro. Dans les parties qui suivent, une telle démarche a été appliquée pour la mise en place d'un modèle macroscopique pour l'effet ΔE dans les matériaux magnétiques, pour l'implantation de lois de comportement magnéto-mécanique dans des outils de calcul de structures, et pour la définition de contraintes équivalentes pour le comportement magnéto-mécanique. A chaque fois, les modèles présentés n'auraient pas pu être obtenus sans recourir à un raisonnement micro-macro, même si ce raisonnement peut finalement être mis de côté lors de l'utilisation de ces modèles.

2.3.1 Modélisation de l'effet ΔE

Le module d'Young est le rapport entre la contrainte σ et la déformation élastique ε^e (mesurée dans la direction parallèle à la contrainte appliquée) dans le cas d'un essai de traction ou de compression uniaxiale (équation 2.17).

$$E = \frac{\sigma}{\varepsilon^e} \tag{2.17}$$

Lorsqu'on pratique un essai de traction ou de compression sur un matériau magnétique aimanté à saturation, on obtient le comportement élastique linéaire usuel, où le module d'Young E est la pente de la courbe contrainte-déformation. Si le matériau est préalablement désaimanté, une non-linéarité apparaît dans les premiers stades de la courbe de traction (voir figure 2.5(a)). Cette non-linéarité, plus ou moins détectable en fonction des matériaux et de la précision des instruments de mesure, est appelée effet ΔE [83]. Elle est souvent interprétée comme une dépendance du module d'Young au niveau d'aimantation : le module d'Young d'un matériau désaimanté apparaît plus faible (dans les premiers stades de déformation) que celui d'un matériau aimanté à saturation. Cependant, l'effet ΔE peut aussi s'expliquer par la sensibilité de la déformation de magnétostriction à l'application d'une contrainte. En effet, lors d'un essai de traction, la déformation de magnétostriction, dont l'évolution en fonction de la contrainte est non-linéaire, se superpose à la déformation élastique ($\varepsilon = \varepsilon^\mu + \varepsilon^e$). Le module d'Young apparent E^a calculé d'après l'équation (2.18) semble alors dépendre du niveau d'aimantation, mais également du niveau de contrainte.

$$E^a = \frac{\sigma}{\varepsilon^\mu + \varepsilon^e} \tag{2.18}$$

Dans le cas d'un matériau aimanté à saturation, la microstructure en domaines magnétiques a atteint un stade de saturation, et la déformation de magnétostriction ne peut plus évoluer. Le module d'Young apparent à saturation E^a_{sat} est alors défini par l'équation (2.19), identique à l'équation (2.17).

$$E^a_{\text{sat}} = \frac{\sigma}{\varepsilon^e} = E \tag{2.19}$$

Dans une configuration magnétique donnée, l'effet ΔE peut être défini quantitativement comme une fonction de la contrainte appliquée σ par l'équation (2.20).

$$\frac{\Delta E}{E} = \frac{E - E^a(\sigma)}{E^a(\sigma)} = \frac{\varepsilon^\mu(\sigma)}{\varepsilon^e(\sigma)} \tag{2.20}$$

La valeur E du module d'Young peut-être identifiée sans ambiguïté à partir d'un essai de traction standard, quel que soit l'état magnétique de l'échantillon, en prenant la pente de la courbe contrainte-déformation dans la zone où elle est linéaire.

$$E = \frac{d\sigma}{d\varepsilon} \tag{2.21}$$

Un modèle prédictif pour l'effet ΔE est alors un modèle décrivant l'effet de la contrainte sur la déformation de magnétostriction. En s'appuyant sur le modèle multi-échelle présenté en partie 2.2.1, nous avons proposé un modèle analytique pour l'effet ΔE dans les monocristaux cubiques. Ce modèle a été étendu au cas des matériaux polycristallins. Il conduit à une définition explicite de la déformation de magnétostriction sous contraintes en l'absence de champ magnétique appliqué [84]. Dans le cas d'un essai de traction d'amplitude σ, la déformation de magnétostriction dans la direction de traction est donnée par l'équation (2.22).

$$\varepsilon^\mu(\sigma) = \frac{\pi\, \lambda_{\text{m}}\, I_1}{S}\ \exp\left(\frac{1}{2} A_s \lambda_{\text{m}} \sigma\right) \tag{2.22}$$

λ_{m} est, pour le polycristal, la déformation maximale que l'on peut obtenir sous chargement mécanique. A_s est un paramètre du modèle multi-échelle défini précédemment par l'équation (2.16). I_1 et S sont deux intégrales définies par les équations (2.23) et (2.24).

$$I_1 = \int_0^\pi (3\ \cos^2\varphi - 1)\ \exp\left(\frac{3}{2} A_s \lambda_{\text{m}} \sigma \cos^2\varphi\right)\ \sin\varphi\, d\varphi \tag{2.23}$$

$$S = 2\pi\ \mathrm{e}^{\left(-\frac{1}{2} A_s \lambda_{\text{m}} \sigma\right)} \int_0^\pi \exp\left(\frac{3}{2} A_s \lambda_{\text{m}} \sigma \cos^2\varphi\right)\ \sin\varphi\, d\varphi \tag{2.24}$$

La construction de ce modèle est détaillée dans la référence [84] jointe ci-après. Cette description est accompagnée d'une proposition de protocole expérimental pour la caractérisation de l'effet ΔE. L'ensemble de la

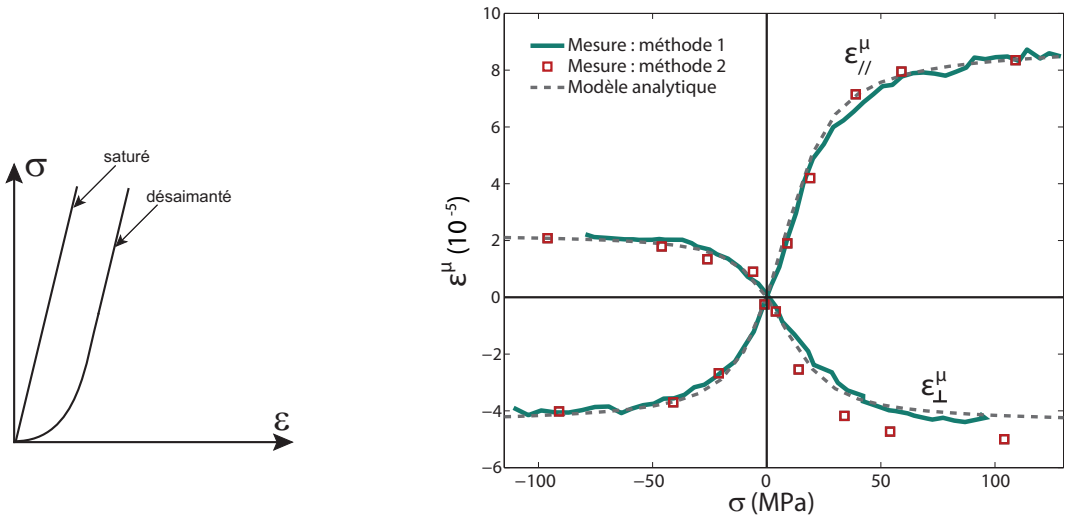

(a) Principe (b) 49%Co-49%Fe-2%V

FIGURE 2.5 – Effet ΔE : (a) Principe (b) Modélisation et résultats expérimentaux pour un alliage 49%Co-49%Fe-2%V (déformation de magnétostriction dans les directions longitudinale et transverse en fonction de la contrainte appliquée).

démarche a été appliqué avec succès dans des configurations uniaxiales pour différents matériaux. Une illustration est proposée sur la figure 2.5(b) pour un alliage fer-cobalt [85].

Ce modèle macroscopique semi-analytique, qui s'appuie initialement sur la modélisation multi-échelle, fournit un outil simple et direct pour décrire l'effet des contraintes sur la déformation de magnétostriction. Dans le domaine du Génie Electrique, il pourrait être utilisé pour compléter les modèles magnéto-élastiques macroscopiques disponibles qui négligent souvent l'effet de la contrainte sur la déformation de magnétostriction.

Publication jointe

[RI.21, 84] : L. Daniel, O. Hubert, "An analytical model for the ΔE effect in magnetic materials", *The European Physical Journal - Applied Physics*, **45** :31101 (11p), 2009.

Eur. Phys. J. Appl. Phys. **45**, 31101 (2009)
DOI: 10.1051/epjap/2009012

THE EUROPEAN PHYSICAL JOURNAL APPLIED PHYSICS

An analytical model for the ΔE effect in magnetic materials

L. Daniel[1,a] and O. Hubert[2]

[1] LGEP, CNRS-UMR 8507, Supélec, Univ. Paris-Sud, UPMC Paris 6, Plateau de Moulon, 11 rue Joliot-Curie, 91192 Gif-sur-Yvette Cedex, France
[2] LMT-Cachan – ENS Cachan, CNRS-UMR 8535, UPMC Paris 6, 61 avenue du Président Wilson, 94235 Cachan Cedex, France

Received: 23 November 2007 / Received in final form: 16 December 2008 / Accepted: 22 December 2008
Published online: 6 February 2009 –

Abstract. The ΔE effect is often presented as the dependency of the Young's modulus of a material on its state of magnetization. Nevertheless, the elastic properties of a magnetic material do not depend on the magnetization state. Actually, the sensitivity of the magnetostriction strain to the application of a stress explains the ΔE effect. According to this statement, a semi-analytical model for the ΔE effect is proposed, in which magnetization rotation is not considered. An experimental procedure to measure the ΔE effect in magnetic materials is then built-up. Experimental and modeling results are finally compared, with satisfying agreement.

PACS. 75.80.+q Magnetomechanical and magnetoelectric effects, magnetostriction – 46.25.Hf Thermoelasticity and electromagnetic elasticity

1 Introduction

The Young's modulus E of a material is the ratio between the stress σ and the elastic strain ε^{el} – measured in the direction parallel to the applied stress – in the case of a tension or compression test (Eq. (1))

$$E = \frac{\sigma}{\varepsilon^{el}}. \tag{1}$$

When a stress is applied to a magnetic material, stress-strain response appears to be non-linear (Fig. 1). This effect is called the ΔE effect [1,2]. It is often presented as a dependency of the Young's modulus E to the stress level. On the other hand, the ΔE effect depends on the state of magnetization of the material as illustrated in Figure 1: the Young's modulus of a demagnetized specimen appears to be lower than the Young's modulus of the same specimen magnetized at saturation. Thus, the ΔE effect could be seen as an apparent loss of linearity in the elastic behavior of demagnetized specimens. But it can also be interpreted as a consequence of the effect of stress on the magnetostriction strain (magnetostriction is the spontaneous deformation associated to magnetic domain structure evolution). The ΔE effect can consequently be dissociated from the elastic behavior.

Indeed, the application of stress modifies the magnetization state of magnetic materials and generates a magnetostriction strain. This magnetostriction strain ε^{μ} is superimposed to the elastic strain ε^{el}, so that the total measured strain ε is defined by equation (2), all the strains being measured in the direction parallel to the applied stress

$$\varepsilon = \varepsilon^{\mu} + \varepsilon^{el}. \tag{2}$$

The apparent Young's modulus E_a is defined by equation (3)

$$E_a = \frac{\sigma}{\varepsilon^{\mu} + \varepsilon^{el}}. \tag{3}$$

In the case of a saturated material, the magnetic domain structure has reached a saturated configuration and the magnetostriction strain cannot evolve anymore. The apparent Young's modulus E_a^s is then defined by equation (4), corresponding to the original definition of the

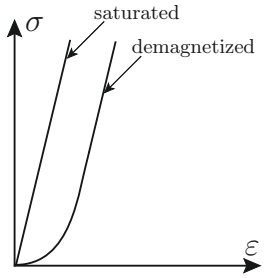

Fig. 1. Illustration of ΔE effect on a tensile stress-strain curve (ε is the total strain).

[a] e-mail: laurent.daniel@lgep.supelec.fr

Young's modulus given by equation (1)

$$E_a^s = \frac{\sigma}{\varepsilon^{el}} = E. \tag{4}$$

For a given initial magnetic configuration, the ΔE effect can be quantitatively defined as a function of the applied stress σ following equation (5):

$$\frac{\Delta E}{E} = \frac{E - E_a(\sigma)}{E_a(\sigma)} = \frac{\varepsilon^{\mu}(\sigma)}{\varepsilon^{el}(\sigma)}. \tag{5}$$

The value of the Young's modulus E can be easily identified thanks to an usual tensile test[1], for a stress level such that the stress-strain curve is linear. In the linearity area of the curve, we define:

$$E = \frac{d\sigma}{d\varepsilon}. \tag{6}$$

A predictive model for the ΔE effect should then rely on the description of the effect of stress on the magnetostriction strain. Very few models are available in the literature. Squire treated the case of amorphous ribbons [3], but did not address the case of crystalline materials. This latter point is the purpose of that paper. After a brief presentation of the energetic terms involved in the magnetic equilibrium of a ferro- or ferri-magnetic body volume element, a simplified approach for the ΔE effect in cubic single crystals is presented, in which magnetization rotation is not considered[2]. It is applied both for materials with positive and negative anisotropy constants. An extension to the behavior of polycrystals is then proposed and results are compared to original experimental ones.

2 Magneto-elastic equilibrium

The magneto-elastic equilibrium of a ferro- or ferrimagnetic body can be seen as the result of a competition between several energetic contributions [4].

- The exchange energy W^{ex} is related to the ferromagnetic coupling effect between neighboring atoms, tending to favor an uniform magnetization in a volume element.
- The magneto-crystalline energy W^K tends to align the magnetization along particular directions, called "easy axes". These easy magnetization directions are mostly connected to crystallographic structure. In the case of iron, whose crystallographic structure is body cubic centered, the anisotropy constant K_1 is positive and magnetization is aligned along $\langle 100 \rangle$ axes (six directions[3]). In the case of Nickel, whose crystallographic structure is face cubic centered, the easy axes are the eight $\langle 111 \rangle$ directions (Fig. 2).

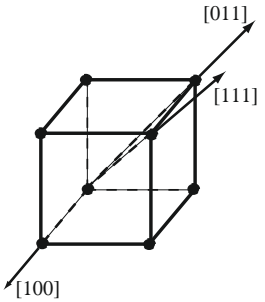

Fig. 2. Crystallographic directions in the cubic symmetry (Miller indices).

- The magneto-static energy W^{mag} tends to align the magnetization direction with the magnetic field direction, or, at least, to energetically favor domains for which the magnetization direction is close to the magnetic field direction.
- The elastic energy W^{el} introduces the magneto-elastic interactions in a ferromagnetic crystal. It is often called "magneto-elastic" energy.

The competition between these energetic contributions explains the existence of the typical magnetic domain microstructure of magnetic materials. Each magnetic domain is uniformly magnetized at saturation. For low magnetic field level, the magnetization of a magnetic domain is aligned along an easy axis.

The magnetization process is the result of two concomitant processes. On one hand, the magnetic walls, separating one domain from another, are moving, modifying the mean magnetization in the material. On the other hand, the magnetization direction can rotate out of its initial easy axis. This rotation mechanism is encountered when the energy given by the applied magnetic field is high enough to compensate the magneto-crystalline anisotropy energy. This situation is usually reached for medium to high magnetic fields. The application of a stress significantly modifies the magnetization of the material, through the contribution of the elastic energy.

Finally, the elastic energy strongly depends on the local magnetostriction strain, through the mechanical incompatibilities. This magneto-elastic coupling is at the origin of the ΔE effect.

3 A simplified approach for the ΔE effect in single crystals

We develop hereafter a simplified approach for the description of the ΔE effect in single crystals. This approach is inspired by a multiscale model for the prediction of magneto-elastic reversible behavior of ferromagnetic materials presented in [5]. The restriction to the case of no applied magnetic field allows an analytical derivation of the ΔE effect.

[1] Whatever the magnetic state of the specimen.

[2] Rotation is the mechanism considered in [3]. In that sense, our proposal is complementary to this previous one and will not apply to amorphous materials.

[3] The notation used for the crystallographic directions refers to the Miller indices.

The approach is limited to the case when no magnetic field is applied, so that the magneto-static energy does not appear in the definition of the magnetic equilibrium ($W^{mag} = 0$).

We suppose that no rotation mechanism occurs in the magnetic domains. The magneto-crystalline anisotropy energy is then uniform within a single crystal and does not participate to the evolution of the magnetostriction strain ($W^K = \text{const.}$). The magnetization in a domain is always aligned along an easy crystallographic direction.

We choose a simplified description of the single crystal microstructure. The crystal is seen as an aggregate of magnetic domains. Considering that only easy directions can be encountered for the magnetization in the domains, we divide the single crystal into domain families (num. α), each family being associated to the corresponding easy axis. In the case of $\langle 100\rangle$ easy axes, only six domain families are possible ($\alpha = \{1, \ldots, 6\}$), eight in the case of $\langle 111\rangle$ easy axes ($\alpha = \{1, \ldots, 8\}$).

The exchange energy W^{ex} is responsible for the local coupling between magnetic moments. It does not participate anymore in the energetic description of such an aggregate (wall energy is not considered, exchange energy is hidden in the concept of domain family).

In such conditions, the elastic energy will be the only energetic term explicitly considered in the description of the magnetic equilibrium of the single crystal, because this term is not identical from one domain family to another. The elastic energy W_α^{el} of a domain α can be written [5]:

$$W_\alpha^{el} = -\boldsymbol{\sigma}_c : \boldsymbol{\varepsilon}_\alpha^\mu \tag{7}$$

where $\boldsymbol{\sigma}_c$ is the mean stress – second order – tensor within the single crystal and $\boldsymbol{\varepsilon}_\alpha^\mu$ is the magnetostriction strain – second order – tensor in the domain family α. The latter, assumed to be homogeneous within a domain family, is written, in the crystallographic coordinate system of the cubic crystal (see for instance [6]):

$$\boldsymbol{\varepsilon}_\alpha^\mu = \frac{3}{2}\begin{pmatrix} \lambda_{100}(\gamma_1^2 - \frac{1}{3}) & \lambda_{111}\gamma_1\gamma_2 & \lambda_{111}\gamma_1\gamma_3 \\ \lambda_{111}\gamma_1\gamma_2 & \lambda_{100}(\gamma_2^2 - \frac{1}{3}) & \lambda_{111}\gamma_2\gamma_3 \\ \lambda_{111}\gamma_1\gamma_3 & \lambda_{111}\gamma_2\gamma_3 & \lambda_{100}(\gamma_3^2 - \frac{1}{3}) \end{pmatrix}. \tag{8}$$

(γ_1, γ_2, γ_3) are the direction cosines of magnetization in the domain family α, λ_{100} and λ_{111} are the magnetostrictive constants of the material. If we consider a multiaxial applied stress state $\boldsymbol{\sigma}_c$, written in the crystallographic coordinate system (Eq. (9)), the elastic energy (Eq. (7)) can be written in the form of equation (10).

$$\boldsymbol{\sigma}_c = \begin{pmatrix} \sigma_{11} & \sigma_{12} & \sigma_{13} \\ \sigma_{12} & \sigma_{22} & \sigma_{23} \\ \sigma_{13} & \sigma_{23} & \sigma_{33} \end{pmatrix} \tag{9}$$

$$\begin{aligned} W_\alpha^{el} = &-\tfrac{3}{2}\lambda_{100}\left[\sigma_{11}(\gamma_1^2 - \tfrac{1}{3}) + \sigma_{22}(\gamma_2^2 - \tfrac{1}{3}) + \sigma_{33}(\gamma_3^2 - \tfrac{1}{3})\right] \\ &-3\,\lambda_{111}\left(\sigma_{12}\,\gamma_1\,\gamma_2 + \sigma_{13}\,\gamma_1\,\gamma_3 + \sigma_{23}\,\gamma_2\,\gamma_3\right). \end{aligned} \tag{10}$$

It has to be emphasized that the condition on the magneto-crystalline energy ($W^K = \text{const.}$) supposes that no magnetization rotation occurs. In particular, it means that the level of stress is not high enough to generate magnetization rotation in the domains. This condition can be expressed as $|\boldsymbol{\sigma}_c : \boldsymbol{\varepsilon}_\alpha^\mu| \ll |K_1|$ in each domain.

The equilibrium configuration can be defined through the relative proportion of each domain family in the crystal. The volumetric fraction of a domain family is obtained using an explicit relation proposed by [7]:

$$f_\alpha = \frac{\exp(-A_s W_\alpha)}{\sum_\alpha \exp(-A_s W_\alpha)} = \frac{\exp(-A_s W_\alpha^{el})}{\sum_\alpha \exp(-A_s W_\alpha^{el})}. \tag{11}$$

A_s being a material parameter linked to the initial anhysteretic susceptibility χ_o and to the saturation magnetization M_s [5]:

$$A_s = \frac{3\chi_o}{\mu_o M_s^2}. \tag{12}$$

For further simplification, we introduce the quantity S:

$$S = \sum_\alpha \exp(-A_s W_\alpha^{el}). \tag{13}$$

An analytical model for the ΔE effect can then be derived from equation (11). Two cases are successively considered: material with $\langle 100\rangle$ easy magnetization axes (positive anisotropy constant) and material with $\langle 111\rangle$ easy magnetization axes (negative anisotropy constant).

3.1 Material with $\langle 100\rangle$ easy magnetization directions

3.1.1 Definition of variables

Six domain families have to be considered: they will be noted *abc*. The subscripts *abc* can take the value 100, $\overline{1}$00, 010, 0$\overline{1}$0, 001 and 00$\overline{1}$. The magnetization rotation mechanism being neglected, the magnetostriction strain tensor in each domain family is greatly simplified:

$$\boldsymbol{\varepsilon}_{abc}^\mu = \frac{1}{2}\lambda_{100}\begin{pmatrix} 3a^2 - 1 & 0 & 0 \\ 0 & 3b^2 - 1 & 0 \\ 0 & 0 & 3c^2 - 1 \end{pmatrix}. \tag{14}$$

The elastic energy for each domain family is then[4]:

$$W_{abc} = -\frac{1}{2}\lambda_{100}\big((3a^2-1)\sigma_{11} + (3b^2-1)\sigma_{22} + (3c^2-1)\sigma_{33}\big). \tag{15}$$

The quantity S is given by:

$$\begin{aligned} S = 2\Bigg[&\exp\left(A_s\lambda_{100}\left(\sigma_{11} - \frac{1}{2}\left(\sigma_{22} + \sigma_{33}\right)\right)\right) \\ &+\exp\left(A_s\lambda_{100}\left(\sigma_{22} - \frac{1}{2}\left(\sigma_{11} + \sigma_{33}\right)\right)\right) \\ &+\exp\left(A_s\lambda_{100}\left(\sigma_{33} - \frac{1}{2}\left(\sigma_{11} + \sigma_{22}\right)\right)\right)\Bigg]. \end{aligned} \tag{16}$$

[4] It can be noticed that the shear terms of the stress tensor, expressed in the crystal coordinate system, do not appear in the definition of the elastic energy.

We deduce the associated volumetric fractions for each domain family:

$$\begin{cases} f_{100} = f_{\overline{1}00} = \dfrac{1}{S}\exp\left(A_s\lambda_{100}\left(\sigma_{11} - \frac{1}{2}\left(\sigma_{22}+\sigma_{33}\right)\right)\right) \\ f_{010} = f_{0\overline{1}0} = \dfrac{1}{S}\exp\left(A_s\lambda_{100}\left(\sigma_{22} - \frac{1}{2}\left(\sigma_{11}+\sigma_{33}\right)\right)\right) \\ f_{001} = f_{00\overline{1}} = \dfrac{1}{S}\exp\left(A_s\lambda_{100}\left(\sigma_{33} - \frac{1}{2}\left(\sigma_{11}+\sigma_{22}\right)\right)\right). \end{cases} \tag{17}$$

We can verify that, in accordance with experimental observation, no magnetization is created in the single crystal by application of a stress:

$$\overrightarrow{M_{\mathbf{c}}} = \sum_{\alpha} f_\alpha \overrightarrow{M_\alpha} = M_s \begin{vmatrix} f_{100} - f_{\overline{1}00} \\ f_{010} - f_{0\overline{1}0} \\ f_{001} - f_{00\overline{1}} \end{vmatrix} = \overrightarrow{0}. \tag{18}$$

But a magnetostriction strain $\boldsymbol{\varepsilon}_c^\mu$ is created by application of a stress:

$$\boldsymbol{\varepsilon}_c^\mu = \sum_{\alpha} f_\alpha \, \boldsymbol{\varepsilon}_\alpha^\mu \neq 0\cdot \tag{19}$$

3.1.2 Uniaxial loadings

The case of a multiaxial applied stress can be first reduced to the simplified case of uniaxial loadings (tensile or compressive stress).

An uniaxial stress of amplitude σ along the [100] direction[5] leads to the strain ε_{100}^μ measured in the direction parallel to the applied stress[6]:

$$\varepsilon_{100}^\mu = \frac{\lambda_{100}\left[1 - \exp\left(-\frac{3}{2}A_s\lambda_{100}\,\sigma\right)\right]}{1 + 2\exp\left(-\frac{3}{2}A_s\lambda_{100}\,\sigma\right)}. \tag{20}$$

An uniaxial stress of amplitude σ along the [110] direction[7] leads to the strain ε_{110}^μ measured in the direction parallel to the applied stress:

$$\varepsilon_{110}^\mu = \frac{\lambda_{100}\left[1 - \exp\left(-\frac{3}{4}A_s\lambda_{100}\,\sigma\right)\right]}{2\left[2 + \exp\left(-\frac{3}{4}A_s\lambda_{100}\,\sigma\right)\right]}. \tag{21}$$

If an uniaxial stress of amplitude σ is applied along the [111] direction[8], we get:

$$f_{100} = f_{\overline{1}00} = f_{010} = f_{0\overline{1}0} = f_{001} = f_{00\overline{1}} = \frac{1}{6} \tag{22}$$

so that:

$$\boldsymbol{\varepsilon}_{111}^\mu = 0. \tag{23}$$

These results are plotted in Figure 3 in the case of iron for which $\lambda_{100} = 21 \times 10^{-6}$ [8]. The value for A_s is $5 \times 10^{-3}\,\mathrm{m^3\,J^{-1}}$.

[5] $\sigma_{ij} = 0$ except $\sigma_{11} = \sigma$.

[6] If ε_n^μ is the projection of the tensor $\boldsymbol{\varepsilon}^\mu$ in the direction $\boldsymbol{n}$, we have: $\varepsilon_n^\mu = {}^t\boldsymbol{n}\,\boldsymbol{\varepsilon}^\mu\,\boldsymbol{n}$.

[7] $\sigma_{ij} = 0$ except $\sigma_{11} = \sigma_{22} = \sigma_{12} = \frac{1}{2}\sigma$.

[8] $\sigma_{ij} = \frac{1}{3}\sigma$.

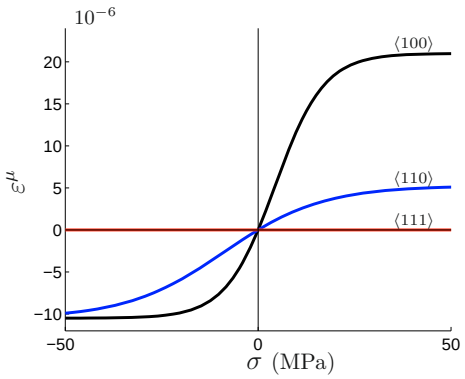

Fig. 3. (Color online) ΔE effect in the case of iron single crystal.

We can notice the dissymmetry between the tension and compression behaviors, visible for example in the values of the strain when – mechanical – saturation is reached:

$$\begin{cases} \lim_{(\sigma\to+\infty)} \varepsilon_{100}^\mu = \lambda_{100} \\ \lim_{(\sigma\to-\infty)} \varepsilon_{100}^\mu = -\dfrac{1}{2}\lambda_{100} \end{cases} \tag{24}$$

$$\begin{cases} \lim_{(\sigma\to+\infty)} \varepsilon_{110}^\mu = \dfrac{1}{4}\lambda_{100} \\ \lim_{(\sigma\to-\infty)} \varepsilon_{110}^\mu = -\dfrac{1}{2}\lambda_{100}. \end{cases} \tag{25}$$

3.1.3 Multiaxial loadings

More general and more complicated mechanical loadings can also be considered. We can study the particular cases of equi-bitension and hydrostatic pressure and compare them to uniaxial stress.

For example, under the hypotheses made, the magnetostriction strain in a ⟨100⟩ direction is defined, for any stress state, as:

$$\begin{aligned} \varepsilon_{100}^\mu &= \lambda_{100}\left(2f_{100} - f_{010} - f_{001}\right) \\ &= \frac{\lambda_{100}}{S}\left[2\exp\left(A_s\lambda_{100}\left(\sigma_{11} - \tfrac{1}{2}\left(\sigma_{22}+\sigma_{33}\right)\right)\right)\right. \\ &\qquad -\exp\left(A_s\lambda_{100}\left(\sigma_{22} - \tfrac{1}{2}\left(\sigma_{11}+\sigma_{33}\right)\right)\right) \\ &\qquad \left. -\exp\left(A_s\lambda_{100}\left(\sigma_{33} - \tfrac{1}{2}\left(\sigma_{11}+\sigma_{22}\right)\right)\right)\right]. \end{aligned} \tag{26}$$

The magnetostriction strain in a ⟨111⟩ direction is defined, for any stress state, as:

$$\varepsilon_{111}^\mu = 0. \tag{27}$$

Figure 4 shows the response of a single crystal under uniaxial[9], equibiaxial[10] and hydrostatic[11] loading along ⟨100⟩ directions.

We observe that a hydrostatic stress state has no effect on the magnetostriction strain.

[9] $\sigma_{ij} = 0$ except $\sigma_{11} = \sigma$.

[10] $\sigma_{ij} = 0$ except $\sigma_{11} = \sigma_{22} = \sigma$.

[11] $\sigma_{ij} = 0$ except $\sigma_{11} = \sigma_{22} = \sigma_{33} = \sigma$.

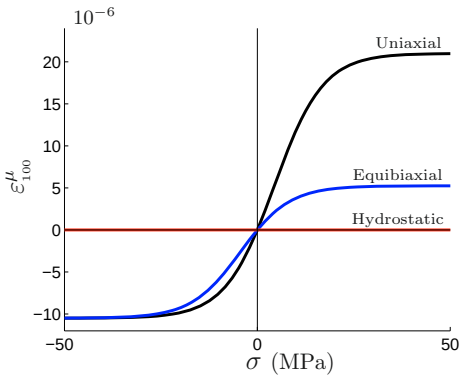

Fig. 4. (Color online) ΔE effect in the case of iron single crystal for a uniaxial, equibiaxial and hydrostatic loading along $\langle 100 \rangle$ directions.

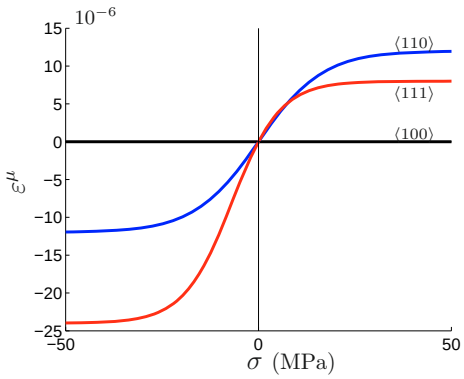

Fig. 5. (Color online) ΔE effect in the case of nickel single crystal.

3.2 Material with ⟨111⟩ easy magnetization directions

3.2.1 Definition of variables

In that case, eight domain families have to be considered: they will be noted *abc*. The subscripts *abc* take the values 111, $\overline{1}11$, $1\overline{1}1$, $11\overline{1}$, $\overline{1}\overline{1}1$, $\overline{1}1\overline{1}$, $1\overline{1}\overline{1}$ and $\overline{1}\overline{1}\overline{1}$. The magnetization rotation mechanism being neglected, the magnetostriction strain tensor in each domain family is also greatly simplified:

$$\boldsymbol{\varepsilon}^{\mu}_{abc} = \frac{1}{2}\lambda_{111}\begin{pmatrix} 0 & ab & ac \\ ab & 0 & bc \\ ac & bc & 0 \end{pmatrix}. \tag{28}$$

The elastic energy for each domain family is then[12]:

$$W_{abc} = -\lambda_{111}\,(ab\,\sigma_{12} + ac\,\sigma_{13} + bc\,\sigma_{23}). \tag{29}$$

The quantity S is given by:

$$\begin{aligned} S = 2\,[&\exp\left(A_s\lambda_{111}\left(\sigma_{12}+\sigma_{13}+\sigma_{23}\right)\right) \\ &+\exp\left(A_s\lambda_{111}\left(-\sigma_{12}-\sigma_{13}+\sigma_{23}\right)\right) \\ &+\exp\left(A_s\lambda_{111}\left(-\sigma_{12}+\sigma_{13}-\sigma_{23}\right)\right) \\ &+\exp\left(A_s\lambda_{111}\left(\sigma_{12}-\sigma_{13}-\sigma_{23}\right)\right)]\,. \end{aligned} \tag{30}$$

We deduce the associated volumetric fractions for each domain family:

$$\begin{cases} f_{111} = f_{\overline{1}\overline{1}\overline{1}} = \dfrac{1}{S}\exp\left(A_s\lambda_{111}\left(\sigma_{12}+\sigma_{13}+\sigma_{23}\right)\right) \\ f_{\overline{1}11} = f_{1\overline{1}\overline{1}} = \dfrac{1}{S}\exp\left(A_s\lambda_{111}\left(-\sigma_{12}-\sigma_{13}+\sigma_{23}\right)\right) \\ f_{1\overline{1}1} = f_{\overline{1}1\overline{1}} = \dfrac{1}{S}\exp\left(A_s\lambda_{111}\left(-\sigma_{12}+\sigma_{13}-\sigma_{23}\right)\right) \\ f_{11\overline{1}} = f_{\overline{1}\overline{1}1} = \dfrac{1}{S}\exp\left(A_s\lambda_{111}\left(\sigma_{12}-\sigma_{13}-\sigma_{23}\right)\right). \end{cases} \tag{31}$$

[12] It can be noticed that the diagonal terms of the stress tensor, expressed in the crystal coordinate system, do not appear in the definition of the elastic energy.

Here again, we verify that no magnetization can be created by application of a stress, but a magnetostriction strain $\boldsymbol{\varepsilon}^{\mu}_{c}$ appears:

$$\boldsymbol{\varepsilon}^{\mu}_{c} = \sum_{\alpha} f_{\alpha}\,\boldsymbol{\varepsilon}^{\mu}_{\alpha} \neq 0. \tag{32}$$

3.2.2 Uniaxial loadings

We study first the uniaxial case. An uniaxial stress of amplitude σ along the [111] direction leads to the strain ε^{μ}_{111} measured in the direction parallel to the applied stress:

$$\varepsilon^{\mu}_{111} = \frac{\lambda_{111}\,\left[1-\exp\left(-\frac{4}{3}A_s\lambda_{111}\,\sigma\right)\right]}{1+3\exp\left(-\frac{4}{3}A_s\lambda_{111}\,\sigma\right)}. \tag{33}$$

An uniaxial stress of amplitude σ along the [110] direction leads to the strain ε^{μ}_{110} measured in the direction parallel to the applied stress:

$$\varepsilon^{\mu}_{110} = \frac{1}{2}\lambda_{111}\tanh\left(\frac{1}{2}A_s\lambda_{111}\,\sigma\right). \tag{34}$$

If an uniaxial stress of amplitude σ is applied along the [100] direction, we get:

$$\begin{aligned} f_{111} &= f_{\overline{1}\overline{1}\overline{1}} = f_{\overline{1}11} = f_{1\overline{1}1} \\ &= f_{1\overline{1}\overline{1}} = f_{\overline{1}1\overline{1}} = f_{11\overline{1}} = f_{\overline{1}\overline{1}1} = \tfrac{1}{8} \end{aligned} \tag{35}$$

so that:

$$\boldsymbol{\varepsilon}^{\mu}_{100} = 0. \tag{36}$$

These results are reported in Figure 5 in the case of nickel for which $\lambda_{111} = -24\times10^{-6}$ [8]. The value for A_s is $5\times10^{-3}\,\mathrm{m^3\,J^{-1}}$ (the same than for the iron single crystal).

The dissymmetry between the tension and compression behaviors can also be noticed:

$$\begin{cases} \lim_{(\sigma\to+\infty)}\,\varepsilon^{\mu}_{111} = -\dfrac{1}{3}\lambda_{111} \\ \lim_{(\sigma\to-\infty)}\,\varepsilon^{\mu}_{111} = \lambda_{111} \end{cases} \tag{37}$$

$$\begin{cases} \lim_{(\sigma\to+\infty)} \varepsilon^{\mu}_{110} = -\dfrac{1}{2}\lambda_{111} \\ \lim_{(\sigma\to-\infty)} \varepsilon^{\mu}_{110} = \dfrac{1}{2}\lambda_{111}. \end{cases} \tag{38}$$

3.2.3 Multiaxial loadings

As previously said, the proposed modeling allows to consider more general and more complicated loadings.

The magnetostriction strain in a $\langle 100\rangle$ direction is defined, for any stress state, as:

$$\varepsilon^{\mu}_{100} = 0. \tag{39}$$

The magnetostriction strain in a $\langle 111\rangle$ direction is defined, for any stress state, as:

$$\begin{aligned} \varepsilon^{\mu}_{111} &= \frac{2}{3}\lambda_{111}\left(3f_{111} - f_{\overline{1}11} - f_{1\overline{1}1} - f_{11\overline{1}}\right) \\ &= \frac{2\lambda_{111}}{3S}\left[3\exp\left(A_s\lambda_{111}\left(\sigma_{12}+\sigma_{13}+\sigma_{23}\right)\right)\right. \\ &\quad -\exp\left(A_s\lambda_{111}\left(-\sigma_{12}-\sigma_{13}+\sigma_{23}\right)\right) \\ &\quad -\exp\left(A_s\lambda_{111}\left(-\sigma_{12}+\sigma_{13}-\sigma_{23}\right)\right) \\ &\quad \left.-\exp\left(A_s\lambda_{111}\left(\sigma_{12}-\sigma_{13}-\sigma_{23}\right)\right)\right]. \end{aligned} \tag{40}$$

We developed a fully analytical model of the effect of – uniaxial and multiaxial – stress on the magnetostriction strain of cubic single crystals. This modeling allows a description of the ΔE effect consistent with the independence of the elastic properties of materials on their magnetization. The same principles can be applied to the prediction of the behavior of polycrystals.

4 Extension to the behavior of polycrystals

The magnetostrictive behavior of a polycrystal is supposed, as a first approximation, to be isotropic. The contrast of behavior along different directions, exhibited for example in Figure 3 for the single crystal should not appear. The isotropic polycrystal can be seen as an aggregate of single crystals with random orientation. It can be defined as a single crystal for which all directions would be easy directions. In one domain of such a single crystal, the magnetostriction strain tensor can be written[13] (in the appropriate coordinate system):

$$\boldsymbol{\varepsilon}^{\mu}_{m} = \frac{1}{2}\lambda_{\mathrm{m}}\begin{pmatrix} 2 & 0 & 0 \\ 0 & -1 & 0 \\ 0 & 0 & -1 \end{pmatrix}, \tag{41}$$

λ_{m} denotes, for the polycrystal, the maximum magnetostriction strain that can be reached during a mechanical loading. The definition of its value requires a discussion.

[13] In accordance with the usual isochoric hypothesis for the magnetostriction strain [2].

4.1 Definition of λ_{m}

λ_{m} is the value of the maximum magnetostriction strain. This parameter can be identified from experimental measurements on unstrained specimen, but it can also be defined from the value of the single crystal magnetostriction coefficient λ_{100} or λ_{111}. It is shown in [5] that the maximum magnetostriction strain λ_{m} of a polycrystal, in the case when no magnetization rotation occurs can be written in the form:

$$\begin{aligned} \lambda_{\mathrm{m}} &= \tfrac{2}{5}\lambda_{100}k^{\mathbf{a}} \quad \text{for materials with} \\ &\qquad \langle 100\rangle \text{ easy directions,} \\ \lambda_{\mathrm{m}} &= \tfrac{3}{5}\lambda_{111}k^{\mathbf{b}} \quad \text{for materials with} \\ &\qquad \langle 111\rangle \text{ easy directions,} \end{aligned} \tag{42}$$

where $k^{\mathbf{a}}$ and $k^{\mathbf{b}}$ depend on the elastic properties of the single crystal and on the hypotheses chosen for the description of the material. For instance, if we choose uniform stress (Reuss) hypotheses, we have $k^{\mathbf{a}} = k^{\mathbf{b}} = 1$, and if we choose uniform strain (Voigt) hypotheses, we have $k^{\mathbf{a}} = 5\mu_a/(2\mu_a + 3\mu_b)$ and $k^{\mathbf{b}} = 5\mu_b/(2\mu_a + 3\mu_b)$, μ_a and μ_b being the cubic shear modulus of the single crystal. For the sake of simplicity, we will chose $k^{\mathbf{a}} = k^{\mathbf{b}} = 1$ in further numerical applications.

4.2 Multiaxial stress state

A general stress tensor is considered, with 6 independent components (see Eq. (9)). We choose to work in the principal coordinate system for the stress: in that particular framework, the stress tensor is diagonal and its components are called the principal stresses:

$$\boldsymbol{\sigma} = \begin{pmatrix} \sigma_{\mathrm{I}} & 0 & 0 \\ 0 & \sigma_{\mathrm{II}} & 0 \\ 0 & 0 & \sigma_{\mathrm{III}} \end{pmatrix}. \tag{43}$$

The definition of the magnetostriction strain of the polycrystal then follows the same strategy used for single crystals. Since a finite number of easy magnetization directions has been replaced by an infinite number, the symbol sum has to be replaced by an integral over the possible directions α.

The transformation matrix from the domain coordinate system to the principal coordinate system is noted $\boldsymbol{P}$ and defined by equation (44) where θ varies from 0 to 2π and φ from 0 to π

$$\boldsymbol{P} = \begin{pmatrix} \cos\theta\,\sin\varphi & \sin\theta & \cos\theta\cos\varphi \\ \sin\theta\,\sin\varphi & -\cos\theta & \sin\theta\sin\varphi \\ \cos\varphi & 0 & -\sin\varphi \end{pmatrix}. \tag{44}$$

The magnetostriction strain in a domain $\alpha(\theta,\,\varphi)$ can be expressed in the principal coordinate system according to equation (45)

$$\boldsymbol{\varepsilon}^{\mu}_{p} = {}^{t}\boldsymbol{P}\,\boldsymbol{\varepsilon}^{\mu}_{m}\,\boldsymbol{P}. \tag{45}$$

In such conditions:

$$\begin{cases} \varepsilon^{\mu}_{p11} = \dfrac{\lambda_{\mathrm{m}}}{2}\left(3\cos^2\theta\sin^2\varphi - 1\right) \\ \varepsilon^{\mu}_{p22} = \dfrac{\lambda_{\mathrm{m}}}{2}\left(3\sin^2\theta\sin^2\varphi - 1\right) \\ \varepsilon^{\mu}_{p33} = \dfrac{\lambda_{\mathrm{m}}}{2}\left(3\cos^2\varphi - 1\right) \\ \varepsilon^{\mu}_{p12} = \varepsilon^{\mu}_{21} = \dfrac{3\,\lambda_{\mathrm{m}}}{2}\ \cos\theta\ \sin\theta\sin^2\varphi \\ \varepsilon^{\mu}_{p13} = \varepsilon^{\mu}_{31} = \dfrac{3\,\lambda_{\mathrm{m}}}{2}\ \cos\theta\ \cos\varphi\ \sin\varphi \\ \varepsilon^{\mu}_{p23} = \varepsilon^{\mu}_{32} = \dfrac{3\,\lambda_{\mathrm{m}}}{2}\ \sin\theta\ \cos\varphi\ \sin\varphi. \end{cases} \tag{46}$$

The elastic energy in a domain α, defined by equation (47), can be developed according to equation (48).

$$W^{el}_{\alpha} = -\boldsymbol{\sigma} : \boldsymbol{\varepsilon}^{\mu}_{p} \tag{47}$$

$$\begin{aligned} W^{el}_{\alpha} = -\tfrac{1}{2}\lambda_{\mathrm{m}}\big[&\sigma_{\mathrm{I}}\left(3\cos^2\theta\sin^2\varphi - 1\right) \\ &+\sigma_{\mathrm{II}}\left(3\sin^2\theta\sin^2\varphi - 1\right) \\ &+\sigma_{\mathrm{III}}\left(3\cos^2\varphi - 1\right)\big]. \end{aligned} \tag{48}$$

Parameter S of equation (13) is now defined by equation (49)

$$S = \int_0^{2\pi}\!\!\int_0^{\pi} \exp\left(-A_s\, W^{el}_{\alpha}\right)\ \sin\varphi\, d\varphi\, d\theta. \tag{49}$$

The magnetostrictive response $\boldsymbol{E}^{\mu}$ of the polycrystal can be defined in a similar way to the one obtained in a direction $\langle 100\rangle$ of a single crystal with $\langle 100\rangle$ easy magnetization directions (since all directions are easy axes)

$$\boldsymbol{E}^{\mu} = \int_{\alpha} f_{\alpha}\, \boldsymbol{\varepsilon}^{\mu}_{p}\, d\alpha \tag{50}$$

with:

$$f_{\alpha} = \frac{1}{S}\exp\left(-A_s\, W^{el}_{\alpha}\right). \tag{51}$$

The magnetostriction strain tensor components, defined in the principal coordinate system, are then written:

$$E^{\mu}_{ij} = \frac{1}{S}\int_0^{2\pi}\!\!\int_0^{\pi} \varepsilon^{\mu}_{pij}\exp\left(-A_s\, W^{el}_{\alpha}\right)\ \sin\varphi\, d\varphi\, d\theta. \tag{52}$$

In accordance with experimental observation, the predicted magnetostriction strain is isochoric:

$$E^{\mu}_{11} + E^{\mu}_{22} + E^{\mu}_{33} = 0. \tag{53}$$

Moreover, we observe that the principal coordinate system for the magnetostriction strain tensor is the principal coordinate system for the stress tensor, so that:

$$\boldsymbol{E}^{\mu} = \begin{pmatrix} E^{\mu}_{11} & 0 & 0 \\ 0 & E^{\mu}_{22} & 0 \\ 0 & 0 & E^{\mu}_{33} \end{pmatrix} = \begin{pmatrix} E^{\mu}_{\mathrm{I}} & 0 & 0 \\ 0 & E^{\mu}_{\mathrm{II}} & 0 \\ 0 & 0 & E^{\mu}_{\mathrm{III}} \end{pmatrix}. \tag{54}$$

4.3 Uniaxial tension-compression

The case of uniaxial tension-compression[14] of amplitude σ brings significant simplifications. The elastic energy (Eq. (48)) reduces to:

$$W^{el}_{\alpha} = -\frac{1}{2}\lambda_{\mathrm{m}}\sigma\left(3\cos^2\varphi - 1\right). \tag{55}$$

Parameter S (Eq. (49)) is re-written:

$$S = 2\pi\ \mathrm{e}^{\left(-\frac{1}{2}A_s\lambda_{\mathrm{m}}\sigma\right)}\ \int_0^{\pi}\exp\left(\frac{3}{2}A_s\lambda_{\mathrm{m}}\sigma\cos^2\varphi\right)\ \sin\varphi\, d\varphi. \tag{56}$$

The magnetostriction strain in the direction parallel to the applied stress is then defined by equation (57)

$$E^{\mu}_{\mathrm{III}} = \frac{\pi\lambda_{\mathrm{m}}}{S}\exp\left(-\frac{1}{2}A_s\lambda_{\mathrm{m}}\sigma\right)\ I_1 \tag{57}$$

with:

$$I_1 = \int_0^{\pi}\left(3\cos^2\varphi - 1\right)\exp\left(\frac{3}{2}A_s\lambda_{\mathrm{m}}\sigma\cos^2\varphi\right)\ \sin\varphi\, d\varphi. \tag{58}$$

The calculation of the other terms of the tensor allows to verify the following expression for the magnetostriction strain tensor:

$$\boldsymbol{E}^{\mu} = \frac{\pi\,\lambda_{\mathrm{m}}\,I_1}{2\,S}\exp\left(\frac{1}{2}A_s\lambda_{\mathrm{m}}\sigma\right)\begin{pmatrix} -1 & 0 & 0 \\ 0 & -1 & 0 \\ 0 & 0 & 2 \end{pmatrix}. \tag{59}$$

5 Experimental characterization of ΔE effect

The measurement of ΔE effect usually consists in the evaluation of the stress-strain response of a demagnetized specimen (Fig. 1) thanks to a tensile-compressive machine. The ε^{μ} component of the total deformation is then extracted according to equation (2). This procedure is nevertheless very difficult to apply since amplitude of magnetostriction is most of the time much lower than the total deformation ε. Polycrystalline iron is a classical example: the amplitude of longitudinal magnetostriction is about 10^{-5}; considering a Young's modulus of about 200 GPa, a 2 MPa tensile stress produces the same elastic amplitude of deformation than magnetostriction. When stress overcomes 20 MPa, the deformation of magnetostriction only accounts for 10% of the total deformation. This way of measurement is consequently not accurate. Other methods can be used [9]. An alternative procedure, based on the hypothesis of magnetic saturation of the magnetostriction, is proposed in the next section.

5.1 Principle

The procedure is based on anhysteretic magnetostriction measurements under different levels of applied stress i.e.

[14] For example $\sigma_{\mathrm{I}} = \sigma_{\mathrm{II}} = 0$ and $\sigma_{\mathrm{III}} = \sigma$.

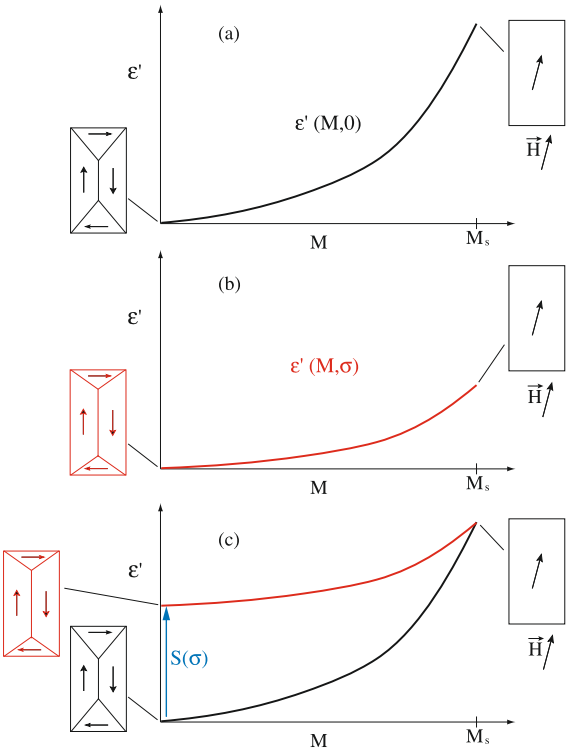

Fig. 6. (Color online) Schematic view of the measured deformation ε' and associated domain structure; (a) zero stress; (b) with σ applied stress; (c) shift of the σ applied stress curve to get the same saturation value.

$\varepsilon^{\mu}(M,\sigma)$ with σ constant. Accurate measurements require first to proceed to an efficient demagnetization under stress. This step leads to an initial deformation ε_i (Eq. (60)) that is practically not possible to measure.

$$\varepsilon_i(0,\sigma) = \varepsilon^{el}(\sigma) + \varepsilon^{\mu}(0,\sigma). \tag{60}$$

The deformation is then arbitrarily put to zero. Next step is to proceed to the anhysteretic magnetostriction measurement. Measurement is now corresponding to ε' given by equation (61):

$$\begin{aligned}\varepsilon'(M,\sigma) &= \varepsilon(M,\sigma) - \varepsilon_i(0,\sigma)\\ &= \varepsilon^{\mu}(M,\sigma) - \varepsilon^{\mu}(0,\sigma).\end{aligned} \tag{61}$$

The value of $\varepsilon'(M=0,\sigma)$ is artificially zero whatever the stress level. The extraction of magnetostriction behavior $\varepsilon^{\mu}(M,\sigma)$ requires consequently to evaluate $\varepsilon^{\mu}(0,\sigma)$.

Figure 6 gives a schematic view of $\varepsilon'(M,\sigma)$ for $\sigma = 0$ (a) and $\sigma \neq 0$ (b). A very simple 2D scheme of the domain configuration is associated. If we make the hypothesis that the magnetization reaches M_s at high magnetic field, the domain configurations and thus the values of magnetostriction are strictly identical whatever the stress level. The ultimate value $\varepsilon'(M_s,0) = \varepsilon^{\mu}(M_s,0)$ becomes a reference value that all the $\varepsilon'(M,\sigma)$ curves must reach. We finally proceed to a shift $S(\sigma)$ of the $\varepsilon'(M,\sigma)$ curves (Fig. 6c). $S(\sigma)$ is intrinsically corresponding to the magnetostriction at zero applied field i.e. $S(\sigma) = \varepsilon^{\mu}(0,\sigma)$, that is a direct observation of the ΔE effect. We note $S(\sigma) = \varepsilon^{\mu}(\sigma)$. Considering several stress levels σ, Figure 6c is consequently corresponding to the complete magnetostriction behavior $\varepsilon^{\mu}(M,\sigma)$[15].

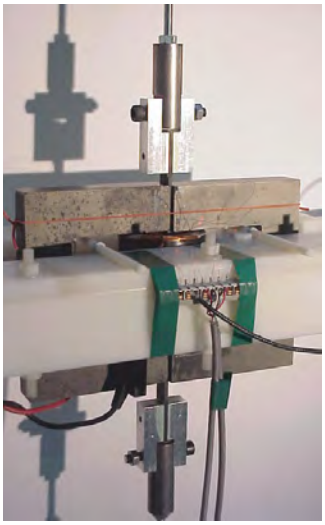

Fig. 7. (Color online) Apparatus for measurement of magnetostriction under applied stress – with articulated heads.

5.2 Experimental procedure

The benchmark for magneto-mechanical measurements is based on a non-standard experimental frame [10]. It is constituted of two face-to-face positioned ferrimagnetic U-yokes (Fig. 7). Samples are placed between the two yokes. Their shape and length depend on the nature of the investigated material. In order to measure magnetostriction, samples have been instrumented with longitudinal and transverse strain gages. A half Wheatstone bridge configuration with temperature compensation has been chosen for strain measurement (low-pass second order Butterworth filtering). A primary winding is placed on the specimen. B-coil and H-coil ensure the measurement of magnetic quantities.

We restrict the experiment to reversible behavior with usual methods (so-called anhysteretic measurement).

[15] It is not rigorously "pure" magnetostriction because the parasitic elastic deformation due to the magnetic forces still remains (i.e. form effect). This deformation is sometimes of same order of magnitude and has the same dynamic (frequency, even function) than magnetostriction. A second correction procedure should be applied especially with sheet specimen. But, because $\varepsilon^{\mu}(\sigma)$ is corresponding to a zero magnetization level, the correction is not necessary for this figure.

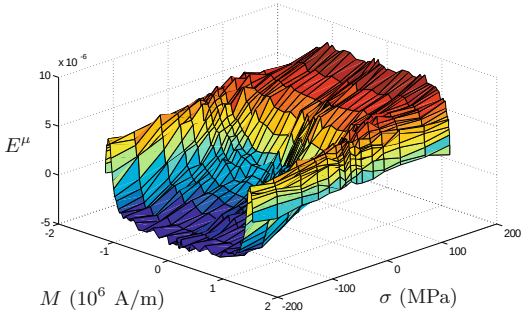

Fig. 8. (Color online) Influence of uniaxial stress on the anhysteretic longitudinal magnetostrictive behavior of pure iron [11].

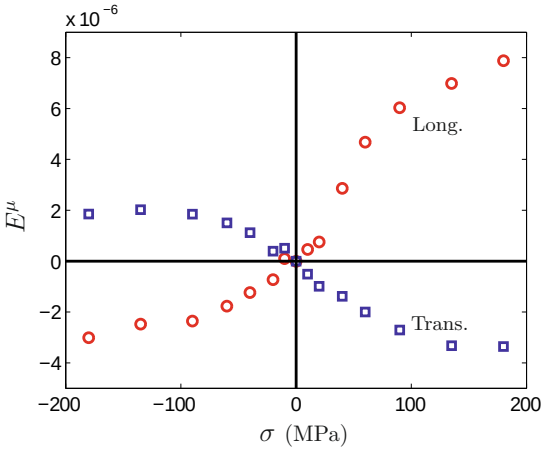

Fig. 9. (Color online) ΔE effect for pure iron – longitudinal and transverse behaviors.

The anhysteretic curves are measured point by point by applying a sinusoidal magnetic field of mean value H, and of exponentially decreasing amplitude.

Two solutions are possible to get uniaxial stress: the first solution is to suspend loads to the specimen, which is previously equipped with specific articulated heads (Fig. 7)[16]. This technique creates a pure uniaxial stress state and avoid vibrations, but compression is not possible; it is used for sheet format specimen (iron-silicon, iron-cobalt). The second solution is to use a hydraulic machine. This solution leads to noisy deformation measurements but enables compression. It is used for bulk materials (pure iron, Ni-Zn ferrite). The procedure detailed in Section 5.1 is finally applied.

Figure 8 gives an example of measurement carried out with the experimental set-up [11]. It shows the longitudinal magnetostrictive behavior of pure iron under tensile and compressive stress[17]. $\varepsilon^\mu(\sigma)$ is extracted from this measurement and plotted in Figure 9 for longitudinal and transverse directions.

Experimental results have been carried out with other materials: they are compared to the previsions of the model in the next section.

6 Comparison between experiments and modeling

The ΔE effect measurement has been performed on four different materials. Bulk specimens of pure iron and NiZn ferrite (composition $Ni_{0.48}Zn_{0.52}Fe_2O_4$), and sheet specimen of non-oriented 3%silicon-iron and 29%cobalt-iron alloys have been tested. The magnetostriction coefficients of the single crystals of these materials are reported in Table 1. The variables $k^{\mathbf{a}}$ and $k^{\mathbf{b}}$ (Eq. (42)) have been arbitrarily taken equal to 1, corresponding to uniform stress hypotheses. The data used for the modeling are given in Table 2.

Table 1. Magnetostriction constants of the materials used for experiments.

	λ_{100}	λ_{111}	K_1 (J m^{-3})	Ref.
Pure iron	21×10^{-6}	-21×10^{-6}	42 700	[6,8]
Ni-Zn ferrite	-26×10^{-6}	-5×10^{-6}	−1700	[12]
FeSi alloy	25×10^{-6}	-5×10^{-6}	38 000	[6,8]
FeCo alloy	100×10^{-6}	10×10^{-6}	35 000	[13]

Table 2. Modeling parameters.

	A_s (m^3/J)	λ_m
Pure iron	5×10^{-3}	8.4×10^{-6}
Ni-Zn ferrite	3×10^{-2}	-3.0×10^{-6}
FeSi alloy	3×10^{-2}	10×10^{-6}
FeCo alloy	5×10^{-3}	40×10^{-6}

6.1 Bulk specimens

The results for pure iron and Ni-Zn bulk specimens are respectively presented in Figures 10 and 11. Figure 10 exhibits a very good agreement between modeling and experimental results. Some significant discrepancies are observed for Ni-Zn ferrite. A higher value for λ_m would be necessary in the modeling to get a better agreement. Considering the elastic constants of the single crystal [12], another mechanical hypothesis than uniform stress state would not lead to a significant change of λ_m. The relatively low value of K_1 explains these discrepancies: indeed for such a low magnetocrystalline anisotropy, the hypothesis of no magnetization rotation under stress is not verified. The maximum value for the magnetostriction strain cannot be defined as simply as in equation (42). This results points out a limitation of the proposed approach. In such a case, where the behavior results from the combinaison

[16] The maximal load is about 50 kg leading to a maximal stress from 16 MPa to 100 MPa depending on the section of the specimen.

[17] The specimen is a 10 mm diameter plain cylinder of iron; form effect is negligible and so not withdrawn to the results.

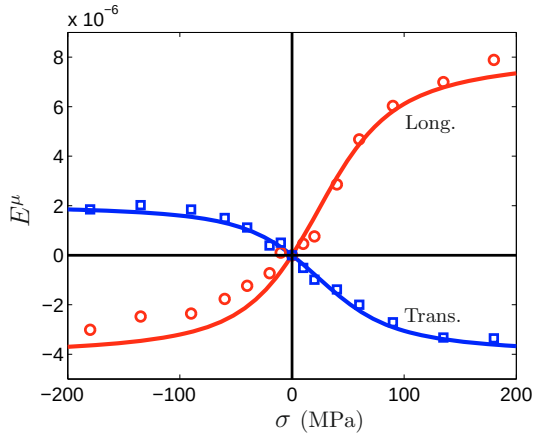

Fig. 10. (Color online) ΔE effect for pure iron: longitudinal and transverse magnetostriction strain as a function of the applied stress σ, modeling (line) and experimental results.

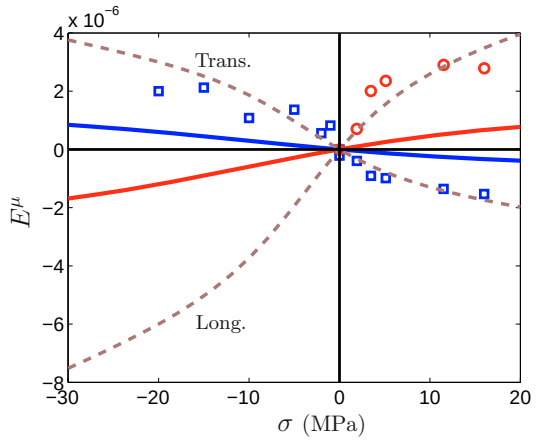

Fig. 11. (Color online) ΔE effect for Ni-Zn ferrite: longitudinal and transverse magnetostriction strain as a function of the applied stress σ, modeling (line) and experimental results. Dashed lines: results obtained with a full multiscale model [12].

of domain wall motion and magnetization rotation mechanisms, the full multiscale model [5] should be used. The corresponding results (presented in reference [12]) have been added in Figure 11.

6.2 Sheet specimens

The results for iron-silicon and iron-cobalt sheet specimens[18] are respectively presented in Figures 12 and 13.

The agreement between modeling (plain lines) and experimental (points) results is good considering the longitudinal direction, but the comparison is not satisfactory in the transverse direction. The explanation of these discrepancies may be found in the initial distribution of the magnetic domains in the material. Indeed the model is designed for bulk materials so that the initial distribution of the domains is assumed to be random into a uniform distribution (every domain directions have the same probability of existence). As a consequence, the behavior

[18] In both cases, the experimental data have been collected with a tensile stress applied in the direction TD perpendicular to the rolling direction of the sheet.

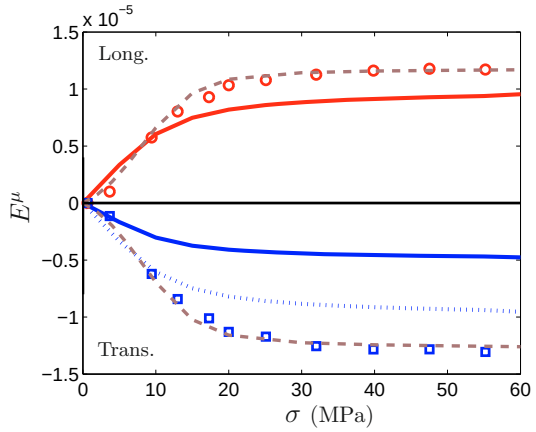

Fig. 12. (Color online) ΔE effect for an iron-silicon steel: longitudinal and transverse magnetostriction strain as a function of the applied stress σ, modeling (line) and experimental (points) results. Plain line for isotropic strain and dot line (transverse direction) for configuration energy effect. Dashed lines: results obtained with a full multiscale model with configuration energy effect [5,15,16].

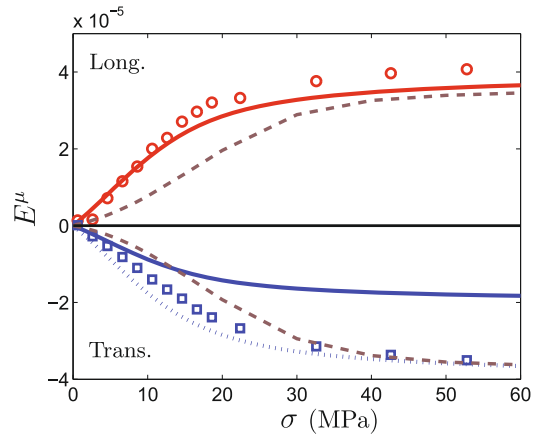

Fig. 13. (Color online) ΔE effect for an iron-cobalt alloy: longitudinal and transverse magnetostriction strain as a function of the applied stress σ, modeling (line) and experimental (points) results. Plain line for isotropic strain and dot line (transverse direction) for configuration energy effect. Dashed lines: results obtained with a full multiscale model with configuration energy effect [5,15,16].

is isotropic and the transverse magnetostriction is equivalent in any direction perpendicular to the longitudinal direction. Considering an isochoric strain, it comes:

$$E^{\mu}_{\text{Trans}} = -\frac{1}{2} E^{\mu}_{\text{Long}}. \tag{62}$$

This hypothesis obviously does not apply to sheet specimen. For such shapes, demagnetizing phenomena lead to a non-uniform distribution of domains [14,15]. This initial configuration is such that the domains with magnetization along the rolling direction of the sheet are in higher proportion than the others[19]. As a consequence, the behavior is anisotropic. The simplifying hypotheses used do not apply. However, the ΔE effect can be predicted using the full – numerical – multiscale model [5]. The initial configuration is taken into account in the model using configuration energy [15,16]. This procedure has been applied to iron-silicon and iron-cobalt alloys. Results are plotted in Figures 12 and 13 (dashed lines) showing a better agreement with experimental results.

It appears that the magnetostriction strain in the direction perpendicular to the sheet is close to zero (for these materials). The transverse magnetostriction strain satisfies the relation (63).

$$E^{\mu}_{\text{Trans}} = -E^{\mu}_{\text{Long}}. \tag{63}$$

Using this result as an hypothesis for the analytical model, the agreement between experimental and model data (dot line in Fig. 13 and 12) becomes better.

7 Conclusion

A model for the ΔE effect in magnetic materials has been proposed. This model is based on the description of the physical mechanisms responsible for magneto-elastic couplings at the single crystal scale. The proposed analytical approach does not include magnetization rotation as a source of magnetostriction strain. It is limited to material exhibiting high magneto-crystalline constants. A specific procedure for the experimental characterization of the ΔE effect has been proposed. Modeling and experimental results have been compared for bulk and sheet polycrystalline specimen. The results on Ni-Zn ferrite have allowed to illustrate the limitations and conditions of use of the model. In the case of sheet samples, an initial domain configuration has to be accounted for. This model provides a simple tool to describe the effect of stress on the magnetostriction strain. It could be used in electrical engineering to improve the macroscopic models for magneto-elastic coupling, that often neglect the effect of stress on magnetostriction.

[19] This change (compared to the uniform distribution) depends on the material composition, on the crystallographic texture, on the dimensions and on the forming process of the sheet.

References

1. B.D. Cullity, *Introduction to magnetic Materials* (Addison-Wesley Publishing Company, 1972)
2. E. du Trémolet de Lacheisserie, *Magnetostriction – Theory and applications of magnetoelasticity* (CRC Press, 1993)
3. P.T. Squire, J. Mag. Magn. Mat. **87**, 299 (1990)
4. A. Hubert, R. Schäfer, *Magnetic domains* (Springer, 1998)
5. L. Daniel, O. Hubert, N. Buiron, R. Billardon, J. Mech. Phys. Sol. **56**, 3, 1018 (2008)
6. R.M. Bozorth, *Ferromagnetism* (Van Nostrand, 1951)
7. N. Buiron, L. Hirsinger, R. Billardon, J. Phys. IV France **9**, 139 (1999)
8. D.C. Jiles, *Introduction to Magnetism and Magnetic Materials* (Chapman & Hall, 1991)
9. P.T. Squire, J. Mag. Magn. Mat. **160**, 11 (1996)
10. O. Hubert, L. Daniel, R. Billardon, J. Mag. Magn. Mat. **254–255**, 352 (2003)
11. L. Lollioz, S. Pattofatto, O. Hubert, J. Electr. Eng. **57**, 8, 15 (2006)
12. L. Daniel, O. Hubert, B. Vieille, Int. J. Appl. Electromagn. Mech. **25**, 31 (2007)
13. P. Brissonneau, *Magnétisme et matériaux magnétiques* (Hermès, 1997)
14. L. Daniel, O. Hubert, R. Billardon, Int. J. Appl. Electromagn. Mech. **19**, 293 (2004)
15. O. Hubert, L. Daniel, J. Mag. Magn. Mat. **320**, 7, 1412 (2008)
16. O. Hubert, L. Daniel, J. Mag. Magn. Mat. **304**, 489 (2006)

2.3.2 Introduction de l'approche multi-échelle dans les outils de calcul de structures

L'un des enjeux du développement de lois de comportement pour le comportement magnéto-mécanique est de permettre le développement de machines électriques fonctionnant en environnement sévère, en particulier du point de vue mécanique. Pour atteindre cet objectif, il est nécessaire d'intégrer les lois de comportement couplé dans les logiciels de dimensionnement des dispositifs électromagnétiques. Comme cela a déjà été dit, les méthodes macroscopiques présentent le défaut majeur d'être souvent limitées au cas de sollicitations mécaniques uniaxiales appliquées parallèlement au champ magnétique. Les outils multi-échelles développé dans le cadre de ces travaux s'appliquent dans des cas de chargement plus généraux, mais les temps de calcul qui leur sont associées ne permettent pas de les implanter élément par élément dans un calcul de structure.
La démarche proposée dans cette partie consiste à développer des modèles simplifiés. Ces modèles sont issus du modèle multi-échelle mais sont suffisamment compacts pour être compatibles avec les outils standards de calcul par éléménts finis. Nous nous sommes intéressés dans un premier temps à une approche 2D. On propose de considérer le matériau polycristallin comme un monocristal fictif. L'énergie de ce monocristal fictif (équation (2.25)) est écrite comme la somme d'une énergie de champ (équation (2.26)), d'une énergie élastique (équation (2.27)), et, si le matériau est macroscopiquement anisotrope, d'une énergie d'anisotropie associée à une direction particulière $\vec{\beta}$ (équation (2.28)).

$$W_\alpha = W_\alpha^{mag} + W_\alpha^{\sigma} + W_\alpha^{an} \tag{2.25}$$

$$W_\alpha^{mag} = -\mu_0 \vec{H}_\alpha . \vec{M}_\alpha \tag{2.26}$$

$$W_\alpha^{\sigma} = -\boldsymbol{\sigma}_i : \boldsymbol{\varepsilon}_\alpha^{\mu} \tag{2.27}$$

$$W_\alpha^{an} = K(\vec{\alpha}.\vec{\beta})^2 \tag{2.28}$$

La démarche est la même que dans le cas du modèle complet 3D, avec l'introduction des variables internes f_α identiques à celles définies par l'équation (2.15). Une différence notable est toutefois que dans le cas 2D, la constante A_s du modèle s'écrit :

$$A_s^{2D} = \frac{2\chi_0}{\mu_0 M_S^2} \tag{2.29}$$

Les paramètres "matériau" du monocristal fictif proposé peuvent être identifiés à partir du modèle multi-échelle complet. Le modèle monocristallin, compact, peut être implanté dans un code de calcul par éléments finis. Les résultats obtenus avec cette méthode ont été présentés dans la référence [86] jointe ci-après dans le cas d'une machine à réluctance variable tournant à haute vitesse. Les contraintes d'inertie sont alors relativement élevées (figure 2.6). L'effet sur la perméabilité du matériau est significative (figure 2.3.2), mais il est apparu que la valeur du couple de sortie était peu sensible à ces contraintes d'inertie. Ce résultat ne doit cependant pas être généralisé, car l'effet des contraintes sur les performances globales des machines électriques est fortement lié à l'architecture de la machine en question.

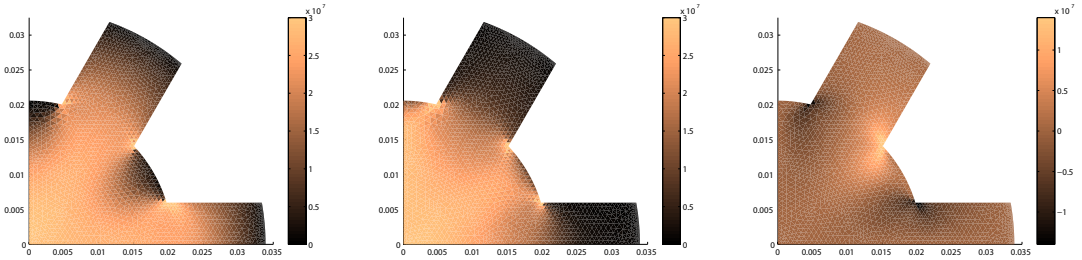

(a) σ_{rr} (b) $\sigma_{\theta\theta}$ (c) $\sigma_{r\theta}$

FIGURE 2.6 – Distribution des contraintes dans un rotor de machine tournante. Diamètre du rotor ϕ=34mm, vitesse de rotation N=30 000 tours/min.

L'outil de modélisation proposé permet de tester différentes architectures et différents dimensionnements, et autorise à terme l'intégration de critères magnéto-mécaniques dans la conception des dispositifs électromagnétiques. Enfin le passage à des calculs 3D permettra d'élargir la gamme de configurations accessibles à la

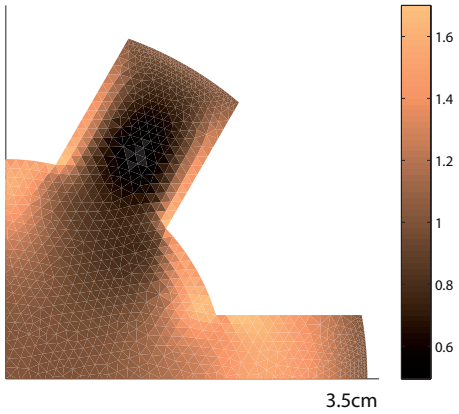

FIGURE 2.7 – Effet des contraintes d'inertie sur la perméabilité ($\mu/\mu(\sigma = 0)$).

modélisation. Ce passage ne pose pas de problème du point de vue de la loi de comportement (au contraire puisque le modèle simplifié est alors plus proche du modèle complet initial). Il faudra en revanche prévoir des durées plus longues pour les calculs de structure correspondants. Ces travaux font l'objet d'une collaboration mise en place avec une équipe de recherche au GRUCAD (Grupo de Concepção e Análise de Dispositivos Eletromagnéticos, Universidade Federal de Santa Catarina (UFSC), Florianopolis, Prof. Jhoe Batistela e Nelson Sadowski).

Publication jointe

[RI.30, 86] : L. Bernard, X. Mininger, L. Daniel, G. Krebs, F. Bouillault et M. Gabsi, "Effect of stress on switched reluctance motors : A magneto-elastic finite element approach based on multiscale constitutive laws", *IEEE Transactions on Magnetics*, 2011 (accepté).

Effect of Stress on Switched Reluctance Motors: A Magneto-Elastic Finite Element Approach Based on Multiscale Constitutive Laws

Laurent Bernard, Xavier Mininger, Laurent Daniel, Guillaume Krebs, Frédéric Bouillault and Mohamed Gabsi *

LGEP (CNRS(UMR 8507) ; SUPELEC ; Univ Paris-Sud ; UPMC Paris 6)
Plateau de Moulon, 11 rue Joliot-Curie ; F-91192 Gif sur Yvette Cedex ; France

* SATIE (ENS Cachan ; CNRS(UMR 8029) ; UniverSud)
61 avenue du Président Wilson ; F-94230 Cachan ; France

laurent.bernard@lgep.supelec.fr

***Abstract*—The design of electromagnetic devices submitted to high mechanical stress is a growing issue and requires consequently appropriate modeling tools. We propose in this paper to implement a multiscale model for magneto-elastic behavior into a finite element code. The 2D magneto-elastic constitutive law is derived from a multiscale model based on a local energetic approach. The method is applied to study the effect of stress on the magnetic behavior of a switched reluctance motor. This work provides a finite element tool for the modeling of the effect of multiaxial stress on electrotechnical devices.**

***Index Terms*—Magneto-elasticity, multiscale modeling, finite element method, effect of stress, electrical machines.**

I. Introduction

Magnetic materials in electrical machines or actuators are submitted to multiaxial mechanical loadings. These stress states can be inherited from forming and assembly processes (cutting, stacking, welding, ...) or appear in use (magnetic forces, inertial forces, ...). On the other hand, stress significantly modifies the magnetic and magnetostrictive behavior [1]. The increase of manufacturing constraints (for cost reduction) and operating constraints (for cost reduction or compacity purpose) emphasizes the need for appropriate coupled modeling tools in the design of electromagnetic systems. One possible choice is the introduction of coupled constitutive laws into finite element modeling. Unfortunately, most magneto-elastic models are restricted to uniaxial mechanical loadings (e.g. [2]–[5]). Some authors proposed to define a magneto-elastic equivalent stress, namely a (fictive) uniaxial stress that would change the magnetic behavior in a similar manner than the multiaxial one [6]–[10]. These approaches can be suited for certain particular multiaxial configuration of stress but did not succeed in giving a general description of the effect of stress on magneto-elastic behavior. Fully multiaxial magneto-elastic models, based on an energetic approach, have been proposed for single crystals [11] and for single and poly-crystalline media, including the effect of crystallographic texture [12]–[14]. The implementation of the latter models into a finite element simulation still leads to dissuasive computational times for engineering design applications. For an application of single crystals under uniaxial loadings, Graham *et al.* [15] proposed a finite element code using look-up text files containing scalar values of magnetostriction and magnetic field depending on stress and magnetic induction amplitudes (assuming the uniaxial stress to be parallel to the magnetic induction). They used the Armstrong model [16] to build these files. If a more general configuration is to be treated, such as a multiaxial stress combined to a magnetic field not aligned with a principal stress direction, the number of inputs for the precalculated data file is quickly increasing. We propose in this paper to define a simplified bi-dimensional version of the multiscale approach proposed in [14] and to implement it directly into a coupled magneto-mechanical numerical code. This approach provides an original finite element approach for the modeling of the effect of multiaxial stress on electrotechnical devices. It is applied to the calculation of the magnetic field in the rotor of a switched reluctance motor submitted to different sources of mechanical stress.

II. Local magneto-elastic constitutive law

The local magneto-elastic constitutive law is derived from the multiscale approach detailed in references [13] and [14]. This model is based on the description of the magnetic material as a set of magnetic domains with known magnetization (M_s) and random orientation. The local free energy of a magnetic domain is expressed as the sum of three contributions: the magneto-static, the magneto-crystalline anisotropy and the elastic energies. The magneto-elastic behavior is obtained by defining the volumetric fraction of a domain with a given magnetization through the use of a Boltzmann probability function. This model provides a multiaxial description of the magneto-elastic behavior and includes effects such as the dependence of magnetostriction strain on stress or crystallographic texture effects. However, due to computation time constraints, this approach cannot be easily implemented into motor design numerical tools. We propose to define a simplified version of the multiscale model (MSM) that allows to reduce by a factor greater than 1000 the computational burden due to the coupled constitutive law. The simplified model uses additional assumptions and gets close to Armstrong model [11].

The model is reduced to a 2-dimensional configuration. The material is assumed to be a collection of magnetic domains randomly oriented. The model defines the probability of existence of a domain oriented along a given direction $\vec{\alpha}$. The local potential energy W_α of the material is written using the same principle as the full MSM (Eq. (1)) [13]. It defines the magneto-static and elastic contributions (Eq. (2) and (3)). A macroscopic anisotropy can result from the

combination of crystalline anisotropy and crystallographic texture. This macroscopic anisotropy can be described through an anisotropy energy term (e.g. in Eq (4) for a uniaxial anisotropy along direction $\vec{\beta}$, K being a constant to be identified). If we assume macroscopic isotropy, this term vanishes.

$$W_\alpha = W_\alpha^{mag} + W_\alpha^{el} + W_\alpha^{an} \tag{1}$$

$$W_\alpha^{mag} = -\mu_0 \vec{H}.\vec{M}_\alpha \tag{2}$$

$$W_\alpha^{el} = -\boldsymbol{\sigma} : \boldsymbol{\varepsilon}_\alpha^\mu \tag{3}$$

$$W_\alpha^{an} = K(\vec{\alpha}.\vec{\beta})^2 \tag{4}$$

The following 2D definitions for the local magnetization $\vec{M}_\alpha$ and magnetostriction strain $\boldsymbol{\varepsilon}_\alpha^\mu$ are used:

$$\vec{M}_\alpha = M_s\,\vec{\alpha} = M_s \begin{bmatrix} \alpha_1 \\ \alpha_2 \end{bmatrix} \tag{5}$$

$$\boldsymbol{\varepsilon}_\alpha^\mu = \frac{3}{2}\begin{pmatrix} \lambda_{l_1}(\alpha_1^2 - \frac{1}{3}) & \lambda_t \alpha_1 \alpha_2 \\ \lambda_t \alpha_1 \alpha_2 & \lambda_{l_2}(\alpha_2^2 - \frac{1}{3}) \end{pmatrix} \tag{6}$$

μ_0 is the vacuum permeability. $\vec{H}$ and $\vec{M}_\alpha$ are the magnetic field and magnetization. $\boldsymbol{\sigma}$ and $\boldsymbol{\varepsilon}_\alpha^\mu$ are the stress and magnetostriction strain second order tensors. M_s is the saturation magnetization of the material, λ_{l_1}, λ_{l_2} and λ_t are magnetostriction constants. Assuming an isotropic behavior, we consider $\lambda_{l_1} = \lambda_{l_2} = \lambda_t = \lambda$.

The unknown of the problem is the local magnetization direction $\vec{\alpha}$. The probability f_α for the magnetization to be in the direction $\vec{\alpha}$ is calculated using a Boltzmann type relation:

$$f_\alpha = \frac{\exp(-A_s.W_\alpha)}{\int_\alpha \exp(-A_s.W_\alpha)} \tag{7}$$

A_s is a material parameter linked to the initial anhysteretic susceptibility χ_o [13]. Once the probability f_α is defined, the macroscopic magnetization $\vec{M}$ and magnetostriction $\boldsymbol{\varepsilon}^\mu$ are obtained thanks to an averaging operation over all possible directions:

$$\vec{M} = <\vec{M}_\alpha> = \int_\alpha f_\alpha\, \vec{M}_\alpha\, d\alpha \tag{8}$$

$$\boldsymbol{\varepsilon}^\mu = <\boldsymbol{\varepsilon}_\alpha^\mu> = \int_\alpha f_\alpha\, \boldsymbol{\varepsilon}_\alpha^\mu\, d\alpha \tag{9}$$

This integration step is performed numerically using a discretization of possible orientations $\vec{\alpha}$.

The material parameters for this simplified 2D modeling are M_s, λ, A_s in the case of macroscopic isotropy. The parameter K, the direction of anisotropy $\vec{\beta}$ and magnetostriction parameters are to be added for a material with a macroscopic uniaxial anisotropy. The identification of these material parameters can be made by using the full 3D MSM as a numerical testing machine in a few particular loading cases. These parameters can also be identified to fit experimental measurements. In the particular case of macroscopic isotropy, the parameter can be easily identified (see appendix): M_s is the saturation magnetization of the material, λ can be obtained from the macroscopic saturation magnetostriction strain λ_s of the material ($\lambda = 4\lambda_s/3$) and A_s can be deduced from the initial slope χ_0 of the anhysteretic magnetization curve under no applied stress ($A_s = 2\chi_0/(\mu_0\, M_s^2)$).

The description of the material as a collection of planar domains appears quite restrictive compared to the real 3D configuration, and we can expect the prediction of the behavior under multiaxial loadings to be less accurate than with the full 3D MSM. Moreover crystallographic texture effect cannot be addressed accurately with the simplified model: the description of macroscopic anisotropy can only be made through a macroscopic term. We can also notice that due to the 2D assumption, only external loadings consistent with the 2D symmetry of the problem can be handled.

The material parameters used for the application presented in this paper are given in Table I and have been identified from experimental measurements on an iron-cobalt alloy [10], [17].

Parameter	M_s	λ_s	A_s
Value	$1.8\ 10^6$	$50\ 10^{-6}$	$1.8\ 10^{-3}$
Unit	$A.m^{-1}$	-	$m^3.J^{-1}$

TABLE I
MATERIAL PARAMETERS USED IN THE CALCULATION

The evolution of the predicted susceptibility as a function of the applied stress has been plotted in Fig. 1 for different levels of magnetic field. The comparison to the experimental results excerpted from reference [10] is satisfying.

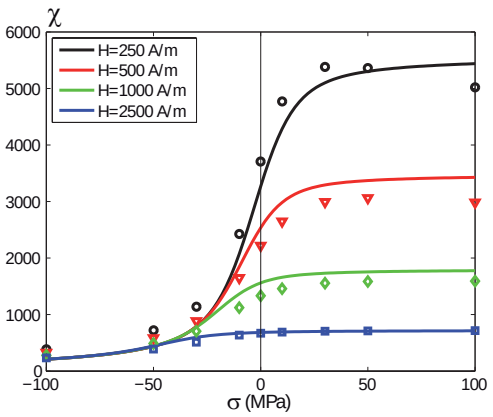

Fig. 1. Magnetic susceptibility under uniaxial mechanical stress: simplified 2D modeling (lines) and experimental results (dots) from [10]

The magnetostrictive behavior under uniaxial stress state has also been plotted in Fig. 2 and compared to the experimental results obtained on the same material [17]. The high sensitivity of the magnetostrictive behavior to the application of stress is well captured by the 2D model.

An example of the magnetic behavior under uniaxial stress state in the direction of the magnetic field, is given in Fig. 3,

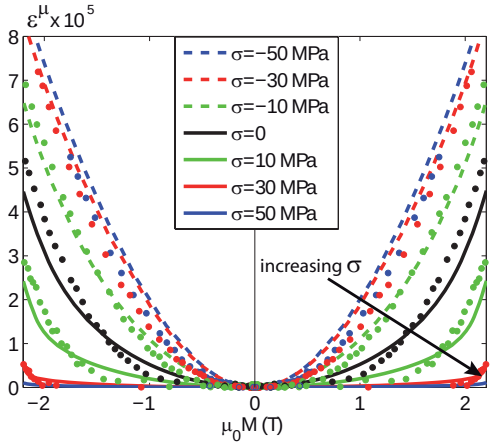

Fig. 2. Magnetostriction curve under uniaxial mechanical stress: simplified 2D modeling (lines) and experimental results (dots) from [17]

highlighting the strong effect of compressive stress on the magnetization curve.

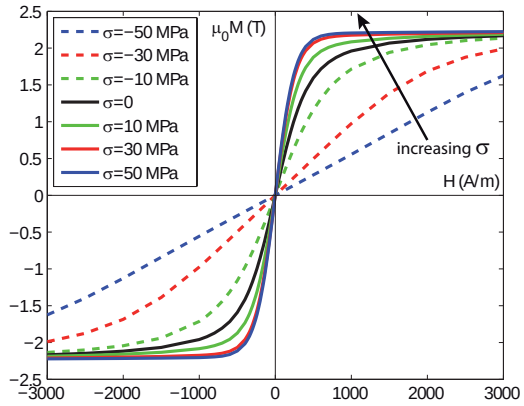

Fig. 3. Magnetization curve under uniaxial mechanical stress

The magneto-elastic behavior under multiaxial stress can also be defined. An illustration is given in Fig. 4 concerning the susceptibility of the material for an applied magnetic field of 250 A/m as a function of the applied bi-axial stress (σ_{11} and σ_{22} being the principal stresses with σ_{11} in the direction of the magnetic field). A compressive stress parallel to the magnetic field direction combined to a tensile stress perpendicular to the magnetic field direction results in a dramatic decrease of the material magnetic susceptibility. On the other hand a bitension mechanical loading hardly increases the susceptibility.

This simplification of the full MSM allows to define the magneto-elastic response of the material with very low computational cost. This constitutive law (illustrated in Fig. 5) is then implemented into a finite element formulation, and will be applied to each element of the mesh.

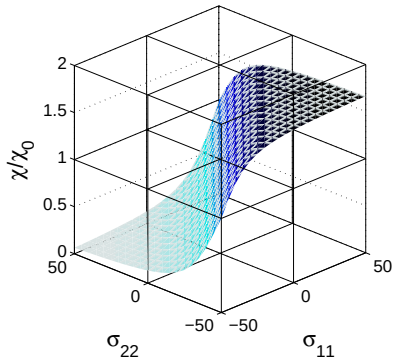

Fig. 4. Relative susceptibility in direction 1 as a function of the principal stresses σ_{11} and σ_{22} (H=250 A/m)

Fig. 5. Principle and parameters of the multiscale model (MSM)

III. Finite Element Formulation

The static finite element model (FE) is based on classical mechanical and magnetic formulations [18]. Hysteresis and eddy current effects are not taken into account. The mechanical problem with external forces f (see Section IV-A for more details on these forces):

$$div\,\boldsymbol{\sigma} = -f \tag{10}$$

is considered with the decomposition of the total strain $\boldsymbol{\varepsilon}$ into the elastic strain $\boldsymbol{\varepsilon}^e(\boldsymbol{\sigma})$ and the magnetostriction strain $\boldsymbol{\varepsilon}^\mu(\vec{H},\boldsymbol{\sigma})$:

$$\boldsymbol{\varepsilon} = \boldsymbol{\varepsilon}^e + \boldsymbol{\varepsilon}^\mu \tag{11}$$

and with the constitutive law:

$$\boldsymbol{\sigma} = [C]\boldsymbol{\varepsilon}^e \tag{12}$$

where $[C]$ the usual stiffness tensor[1]. The total strain $\boldsymbol{\varepsilon}$ corresponds to the symmetrical part of the displacement (U) gradient:

$$\boldsymbol{\varepsilon}_{ij} = \frac{1}{2}\left(\frac{\partial U_i}{\partial x_j} + \frac{\partial U_j}{\partial x_i}\right) \tag{13}$$

The resulting mechanical formulation contains an additional term $F^\mu(\vec{H},\boldsymbol{\sigma})$, corresponding to an equivalent force due to the magneto-elastic coupling. After discretization with nodal elements, this term is expressed with:

$$F^\mu(\vec{H},\boldsymbol{\sigma}) = \int_\Omega \nabla^s[C]\boldsymbol{\varepsilon}^\mu(\vec{H},\boldsymbol{\sigma})d\Omega \tag{14}$$

∇^s is the symmetrical gradient of the shape functions, Ω the study domain, and $\boldsymbol{\varepsilon}^\mu(\vec{H},\boldsymbol{\sigma})$ is the magnetostriction strain obtained from the multiscale model.

[1]Linear elasticity and small strains are assumed.

Similarly, the magnetic scalar potential Φ formulation contains an additional term equivalent to a magnetic charge. The current sources are accounted for by the use of a term $\vec{T_0}$ in the definition of the scalar potential [19]:

$$\vec{H} = -\overrightarrow{grad}\Phi + \vec{T_0} \tag{15}$$

The finite element formulation is expressed in terms of magnetic scalar potential and not with the magnetic vector potential so as to use directly the MSM model presented in Fig. 5. Indeed, the use of the vector potential would require an inversion of the magnetic part of the MSM model in order to get the convergence of the iterative process. The magnetic flux density $\vec{B}$ is defined from the magnetization $\vec{M}$:

$$\vec{B} = \mu_0(\vec{H} + \vec{M}) \tag{16}$$

Moreover, a modified fixed point (FP) iterative method is used to insure the convergence of the non-linear problem [20]. This method provides a slow but robust convergence. The method defines a fictive permeability μ_{FP}, the algorithm convergence depending on the choice of its value. It also introduces a fictive source term $\vec{M}_{FP}(\vec{H}, \boldsymbol{\sigma})$ such that:

$$\vec{B} = \mu_{FP}(\vec{H} + \vec{M}_{FP}) \tag{17}$$

Maxwell's flux conservation is written:

$$div(\mu_{FP}\overrightarrow{grad}\Phi) = div(\mu_{FP}(\vec{M}_{FP}(\vec{H}, \boldsymbol{\sigma}) + \vec{T_0})) \tag{18}$$

From Eq. (16) and (17), $\vec{M}_{FP}(\vec{H}, \boldsymbol{\sigma})$ is updated at each iteration using the magnetization obtained with the MSM. Thus, the coupling term in the magnetic formulation is finally:

$$Q^{\mu}(\vec{M}_{FP}) = \int_{\Omega} \mu_{FP} \nabla^m \vec{M}_{FP}(\vec{H}, \boldsymbol{\sigma}) d\Omega \tag{19}$$

with ∇^m the gradient of the shape functions. The coupled system is then defined by:

$$\begin{cases} [S](\Phi) = & (Q^{\mu}(M_{FP})) + (Q^0(T^0)) \\ [K](U) = & (F) + (F^{\mu}(\boldsymbol{\varepsilon}^{\mu})) \end{cases} \tag{20}$$

with S and K respectively the magnetic and mechanical stiffness matrices, U the displacement field and F the external forces. Finally, the resolution of the coupled non-linear system (20) is based on the algorithm presented in Fig. 6: values of magnetization and magnetostriction strain are updated using the MSM model at each step i for each element of the mesh, until the error criterion e falls below e_c. In this work a value of 1.10^{-4} has been used for e_c. For the calculations presented hereafter, the typical number of iterations to convergence is about 15, corresponding to a total computational time of a few minutes on a standard computer. The number of iterations is directly linked to the non-linearity of the problem. For low current sources, the material behavior is almost linear and the computation converges quickly. The computational cost is getting higher close to saturation.

$i \leftarrow 1$;
$e \leftarrow 1$; $\quad \Phi^0 \leftarrow 0$;
$e_c \leftarrow 1.10^{-4}$; $\quad U^0 \leftarrow 0$;
While $(e \geq e_c)$ **do**
  $[(M^i), (\boldsymbol{\varepsilon}^{\mu i})] = MSM(\vec{H}^{i-1}, \boldsymbol{\sigma}^{i-1})$;
  $M^i_{FP} = (\frac{\mu_0}{\mu_{FP}} - 1)H^{i-1} + \mu_0 M^i$;
  $[S^{FP}](\Phi^i) = (Q^{\mu}(M^i_{FP})) + Q^0(T^0)$;
  $[K](U^i) = (F) + (F^{\mu}(\boldsymbol{\varepsilon}^{\mu i}))$;
  $e = \frac{|U^i - U^{i-1}|}{|U^i|} + \frac{|\Phi^i - \Phi^{i-1}|}{|\Phi^i|}$;
  $i \leftarrow i + 1$;
done

Fig. 6. Modified fixed-point algorithm; i stands for the iteration number, MSM for the multiscale model.

IV. Application to the rotor of a switched reluctance motor

The modeling scheme has been applied to the calculation of the magnetic induction in the rotor of a high-speed switched reluctance motor (SRM). Indeed thanks to their passive rotor SRM are well-adapted for high speed applications, leading to high stress level in the rotating part. The considered configuration is given in Fig. 7. The radius of the rotor is $R = 34$ mm and the air gap is 0.4 mm. The electrical excitation is chosen considering the conjunction configuration in order to have an induction in the tooth corresponding to the beginning of the magnetic saturation (about 1.4 T for the considered material). In the following, when the conjunction configuration is considered, only one quarter of the machine is represented taking advantage of the symmetries.

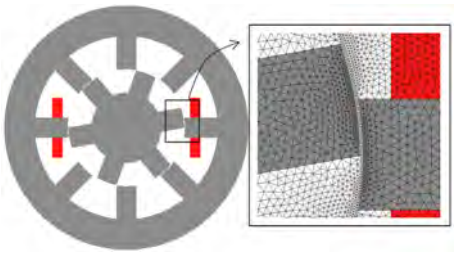

Fig. 7. Switched reluctance motor 2-D mesh

A. Mechanical loading

Several sources of external forces have been considered. A distinction has been made between initial forces (inherited from manufacturing process) and operating forces (appearing in use).

1) Operating forces: Three sources of operating stress have been identified.

Incompatibility stresses arise from the magnetostriction strain in the whole machine. An upper bound for the elastic energy corresponding to these incompatibility stresses is given by the knowledge of the magnetostriction strain. This upper bound would correspond to infinitely rigid boundary conditions[2]:

$$(\boldsymbol{\sigma} : \boldsymbol{\varepsilon}^e)^{incomp} \leq \max(\boldsymbol{\varepsilon}^\mu : C : \boldsymbol{\varepsilon}^\mu) \tag{21}$$

The calculated values of this energy correspond to stress levels lower than 7 MPa if considering tensile stress. This value, overestimating the real configuration, is very low compared to the level of the other operating stresses. This term will be neglected in the following.

Stresses induced by magnetic forces are then considered. A computation with no mechanical stress is done to get the magnetic state of the whole machine. Local forces are computed at each node of the mesh by derivation of the local magnetic co-energy [23]. These forces are mainly radial. The azimuthal component of these forces, that generates the torque, is small and its effect on the stress can be neglected. The radial component of the magnetic forces is taken as source term for an elastic computation on the rotor. It is found that all the components of the induced stress are lower than 2MPa. This source of operating stress will also be neglected in the following.

Inertial stresses are the third source of operating stress. The inertial stress has been calculated and discretized according to Eq. (22) and (23). A rotational speed N = 30 000 rpm ($\omega = 2\pi N/60$) has been chosen, which corresponds to a peripheral speed of 107 m/s. The density of the material is ρ = 7800 kg.m^{-3}. The inertial force density (22) leads to the expression of the external force F^ω.

$$f = \rho\omega^2 r \tag{22}$$

$$F^\omega = \int_\Omega v f d\Omega \tag{23}$$

where v is the test function for the mechanical displacement.

The resulting distribution of inertial stress in the rotor is given in Fig. 8, 9 and 10.

The stress state is mainly biaxial in the rotor, with very low shear stress, except in the lower corners of the rotor teeth. The amplitude of stress is significant (a few tens of MPa) but remains far from the yield stress of the material (about 300 MPa).

2) Initial forces: Residual stresses arise from the forming process of the machines. These residual stresses may be due to punching, cutting, stacking or welding processes [21], [22], [24], [25]. The estimation of these forces is very difficult since it is process dependent. However, these initial forces may significantly affect the magnetic behavior of materials. For the purpose of illustration we considered the stress resulting from the assembly process of the iron sheets. These stacking forces have been considered as a uniform compression along the z axis (orthogonal to the studied plane). This stress exists both in the stator and in the rotor and is assigned the value $\sigma_{zz} = -30$ MPa. For the practical calculation of the permeability, we consider a local coordinate system ($\vec{h}$,$\vec{z}$) where $\vec{h}$ is the direction of the magnetic field. The 2D constitutive law is applied in this plane, defining the permeability in direction $\vec{h}$. This calculation is valid only if the material is initially isotropic, otherwise a full 3D approach would be necessary.

[2]We then consider $\boldsymbol{\varepsilon}^e = -\boldsymbol{\varepsilon}^\mu$ so that the total strain is zero.

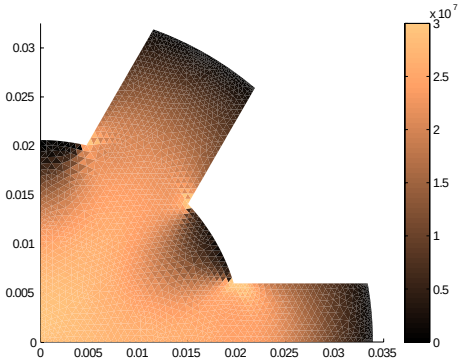

Fig. 8. Radial inertial stress σ_{rr} (Pa) in the rotor (N=30 000 rpm)

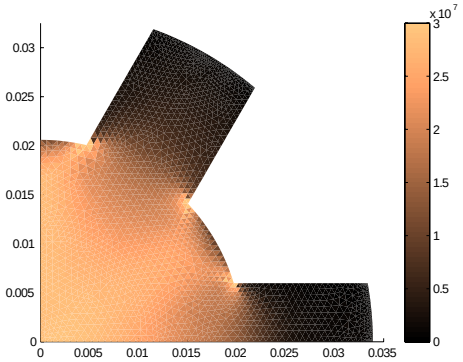

Fig. 9. Tangential inertial stress $\sigma_{\theta\theta}$ (Pa) in the rotor (N=30 000 rpm)

B. Effect of stress on the SRM behavior

In order to investigate the effect of stress on the behavior of the SRM, several calculations have been carried out. The first one is a magnetic calculation without any mechanical stress. It provides the reference magnetic state of the SRM based on the magnetization curve given in Fig. 3 for a stress $\sigma = 0$. A second calculation has been done using the MSM and considering only the inertial stress at $N = 30000$ rpm. A third calculation has been done considering only a uniform initial compressive stress in the direction normal to the sheet plane σ_{zz}=-30 MPa. These calculations have been carried out

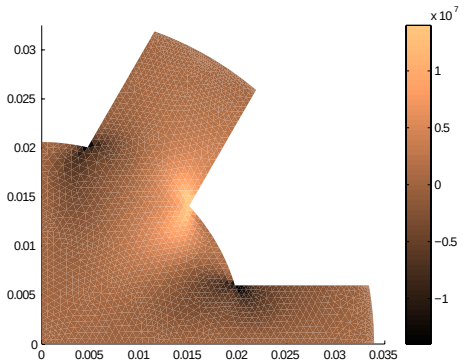

Fig. 10. Shear inertial stress $\sigma_{r\theta}$ (Pa) in the rotor (N=30 000 rpm)

in order to identify the most significant effects on the material permeability and on the machine torque. A full calculation with all sources of stress should be done if a design procedure is foreseen. Indeed no superimposition assumption can be made since the effect of stress on the magnetic behavior, as well as the magnetic behavior itself are strongly non-linear.

1) Material permeability: The effect of stress on the magnetic behavior can only be understood if the relative orientation between stress and magnetic field is known. Fig. 11, 12 and 13, plot the radial and tangential components of the magnetic field in the rotor for all the considered configurations. It can be seen that the magnetic field distribution is significantly modified by the stress. The level of magnetic field (a few hundreds A.m^{-1}) is relatively low and remains mostly below the saturation knee of the magnetization curves (Fig. 3).

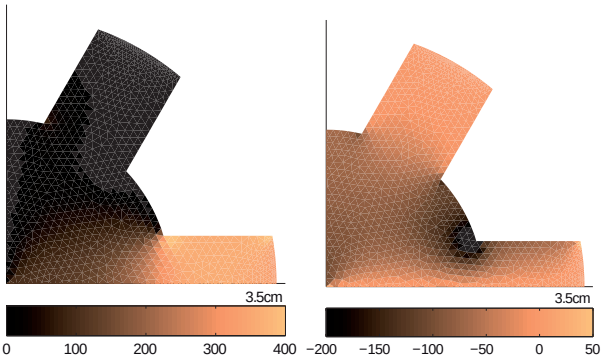

(a) Radial Magnetic field (b) Tangential Magnetic field

Fig. 11. Distribution of the magnetic field (A.m^{-1}) in the rotor - No applied stress

Fig. 14 plots the ratio between the predicted permeability $\mu_\sigma = \vec{B}.\vec{H}/\vec{H}^2$ considering the inertial stress and the reference permeability μ_{ref} (with no stress). The effect of stress is very significant, as can be expected from Fig. 4. The permeability is strongly increased, up to a factor 1.7, in areas in tension with a magnetic field parallel to the stress direction. It can be divided by a factor 2 in the areas of uniaxial tension

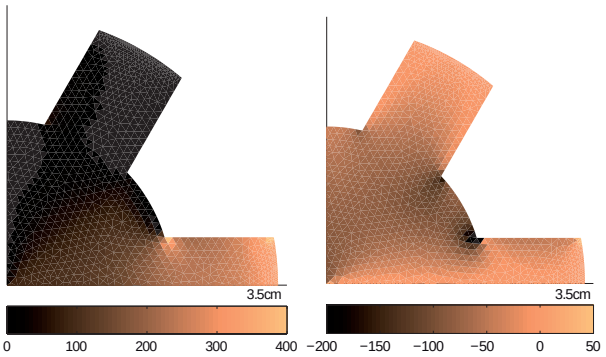

(a) Radial Magnetic field (b) Tangential Magnetic field

Fig. 12. Distribution of the magnetic field (A.m^{-1}) in the rotor - N = 30 000 rpm

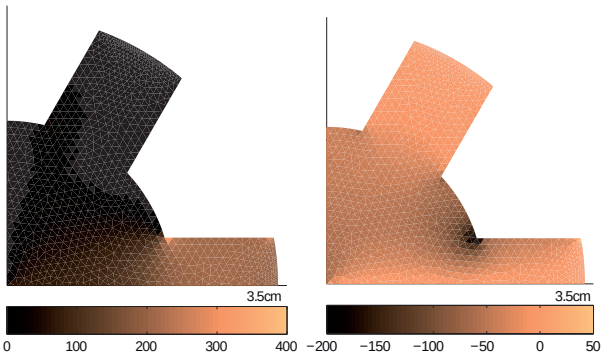

(a) Radial Magnetic field (b) Tangential Magnetic field

Fig. 13. Distribution of the magnetic field (A.m^{-1}) in the rotor - σ_{zz} = -30 MPa

in a direction perpendicular to the magnetic field.

The same analysis is then done for the effect of the initial stress on permeability. Fig. 15 plots the ratio between the predicted permeability $\mu_\sigma = \vec{B}.\vec{H}/\vec{H}^2$ for a uniform stress $\sigma_{zz} = -30$ MPa and the reference permeability on the rotor.

In this case, the compressive stress is normal to the magnetic field direction on the whole machine and consequently the magnetic permeability is increased up to a factor 1.8 on the rotor and the stator. The effect of stress on the permeability is non uniform owing to the non linearity of the magnetic behavior.

2) SRM torque calculation: A computation has been performed in order to evaluate the effect of stress on the SRM torque. A set of angular rotor positions between 0° (conjunction) and 30° is studied. The finite element mesh includes a circular line, in the air gap, with uniform nodes density that allows to generate the different configurations without remeshing. The magnetic excitation is maintained constant for all the rotor positions. The value of the torque T at each rotor position is computed from the flux of Maxwell's tensor

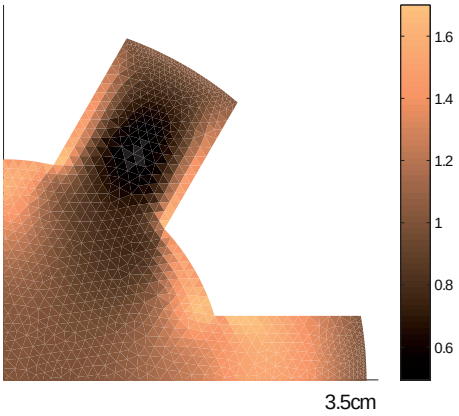

Fig. 14. Ratio μ_σ/μ_{ref} (inertial stress)

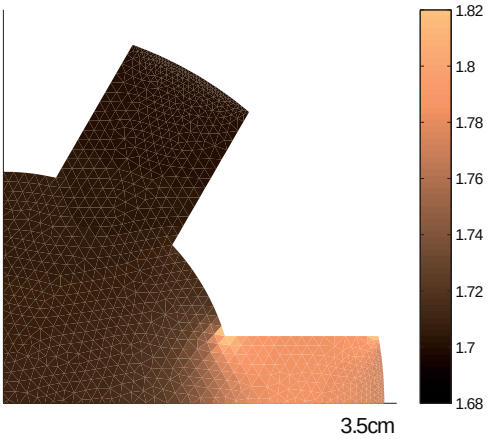

Fig. 15. Ratio μ_σ/μ_{ref} (initial stress $\sigma_{zz} = -30$ MPa)

through a circular surface γ in the air gap [23]:

$$T = r \oint_\gamma B_n.H_t d\gamma \tag{24}$$

where B_n and H_t are respectively the normal component of the magnetic flux density and the tangential component of the magnetic field and r the radius of γ. The relative change in the torque values under stress compared to the reference configuration is plotted in Fig. 16).

It is shown that the inertial stress has no significant influence and that the initial stress leads hardly to a 3% increase of the mean SRM torque (the mean torque values, between angular positions 2 and 20^o, are respectively 16.73, 16.80 and 17.16 N.m for the configuration with no stress, with inertial stress and with initial stress). Due to the high value of the permeability in the different cases, the torque is mainly related to the air-gap flux that is mainly controlled by the reluctivity of the air-gap. Thus, the great variation of the iron reluctivity due to the stress does not significantly influence the global reluctivity of the structure.

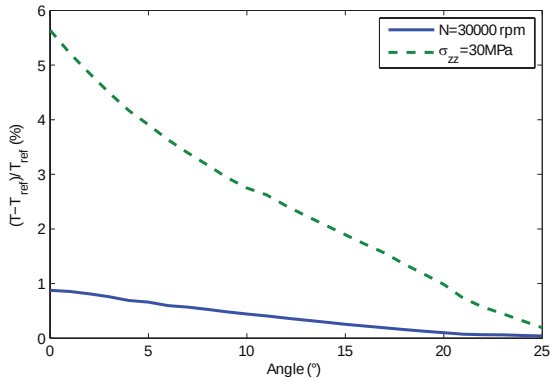

Fig. 16. Machine torque change (%) under stress

C. Discussion

Despite the significant effect on the permeability, the calculations show that the effect of stress on the SRM torque is very narrow. The inertial stress hardly modifies the machine torque. Calculation has also been carried out for a rotational speed of 60000 rpm with similar conclusions. Only the considered initial stress is shown to slightly modify the machine torque. A main difference between these two cases is that the initial stress modifies both the rotor and the stator permeability, affecting the whole magnetic circuit. It must be noticed that the obtained results strongly depend on the choice of motor architecture, material, and technological design - such as air gap width. Moreover the introduction of the hysteresis in the constitutive law of the magnetic material would certainly highlight a significant effect of stress on the overall losses of the machine. This dissipative calculation is a forthcoming challenge and will be the object of further publication.

V. Conclusion

In this paper, a 2-D magneto-elastic model for the behavior of magnetic materials has been proposed. It is based on a simplification of a full multiscale approach previously proposed. This simplified magneto-elastic model has been implemented into a finite element coupled magneto-mechanical formulation. Finally the proposed method for magneto-mechanical structural analysis has been applied to study a high rotation speed switched reluctance motor. Initial and operating forces have been considered for their effects on the machine behavior. The proposed model allows to understand how the relative configurations of stress and magnetic field modify the permeability. The considered stress and motor configuration have been shown to have slight influence on the SRM torque. The study of the effect of stress on the overall performance of electrical machine is still the object of on-going researches, notably concerning the modeling of hysteresis losses. In this context a structural analysis tool introducing the - multiaxial - magneto-elastic coupling into material constitutive laws constitutes a step towards a fully coupled design of electromagnetic devices.

APPENDIX: CONSTITUTIVE PARAMETER IDENTIFICATION FOR ISOTROPIC MATERIAL

In the case of isotropic materials, the constitutive parameters for the simplified 2D model reduce to M_s, λ and A_s.

1) M_s is the saturation magnetization of the material (this is also the case for anisotropic materials).

2) The determination of λ relies on the definition of the saturation magnetostriction strain λ_s as the difference between the strain at very high magnetic field and the strain at zero magnetic field under no applied stress:

$$\lambda_s = \varepsilon_l^{\mu}(H_{\text{sat}}, \mathbf{0}) - \varepsilon_l^{\mu}(\mathbf{0}, \mathbf{0}) \tag{25}$$

The saturation state is defined as a single domain configuration with magnetization parallel to the applied field. We then have:

$$\varepsilon_l^{\mu}(H_{\text{sat}}, \mathbf{0}) = \lambda \tag{26}$$

The demagnetized state is defined as a configuration for which each direction $\vec{\alpha}$ is equiprobable. The magnetostriction strain is then:

$$\varepsilon_l^{\mu}(\mathbf{0}, \mathbf{0}) = \frac{1}{2\pi}\int_0^{2\pi} \frac{3}{2}\lambda(\cos^2\alpha - \frac{1}{3})\, d\alpha = \frac{\lambda}{4} \tag{27}$$

We thus obtain:

$$\lambda = \frac{4}{3}\lambda_s \tag{28}$$

3) A_s can be deduced from the initial slope χ_0 of the anhysteretic magnetization curve under no applied stress following the idea presented in [13]. The principle is to write analytically the anhysteretic curve of the unstressed isotropic material. In this particular case, the potential energy of a domain reduces to:

$$W_\alpha = W_\alpha^{mag} = -\mu_0 \vec{H}.\vec{M}_\alpha = -\mu_0 H M_s \cos\alpha \tag{29}$$

The corresponding volumetric fraction is then:

$$f_\alpha = \frac{1}{S}\exp(A_s \mu_0 H M_s \cos\alpha) \tag{30}$$

with:

$$S = \int_0^{2\pi} \exp(A_s \mu_0 H M_s \cos\alpha)\ d\alpha \tag{31}$$

The macroscopic magnetization M of the material (parallel to the applied field) is then written:

$$\begin{aligned} M &= \int_0^{2\pi} f_\alpha M_s \cos\alpha\ d\alpha \\ &= \frac{M_s}{S}\int_0^{2\pi} \exp(A_s \mu_0 H M_s \cos\alpha)\ \cos\alpha\ d\alpha \end{aligned} \tag{32}$$

For very low applied magnetic field we can make use of the following approximation:

$$\exp(A_s \mu_0 H M_s \cos\alpha) \sim 1 + A_s \mu_0 H M_s \cos\alpha \tag{33}$$

We then obtain :

$$M \sim \frac{1}{2} A_s \mu_0 H M_s^2 \tag{34}$$

Defining the initial anhysteretic susceptibility χ_0 as the ratio between M and H for very low magnetic magnetic field, we obtain:

$$A_s = \frac{2\chi_0}{\mu_0 M_s^2} \tag{35}$$

The expression of A_s for the 2D model is very similar to the one obtained for the full 3D multiscale model: $A_s^{\text{3D}} = 3\chi_0/(\mu_0 M_s^2)$ [13].

The three parameters of the 2D constitutive law in the case of isotropic materials can then be very easily identified.

ACKNOWLEDGMENT

The authors acknowledge the ANR financial support under the grant MAEL BLAN08-2_367373.

REFERENCES

[1] R.M. Bozorth, *Ferromagnetism*, ed. D. Van Norstand Company, N.Y. 1951.
[2] M.J. Sablik and D.C. Jiles, "Coupled magnetoelastic theory of magnetic and magnetostrictive hysteresis" , *IEEE Trans. Magn.*, 29, pp. 2113, 1993.
[3] X.J. Zheng and X.E. Liu, "A nonlinear constitutive model for Terfenol-D rods", *J. Appl. Phys.*, 97, pp. 053901, 2005.
[4] O. Bottauscio, A. Lovisolo, P. E. Roccato, M. Zucca, C. Sasso and R. Bonin, "Modeling and Experimental Analysis of Magnetostrictive Devices: From the Material Characterization to Their Dynamic Behavior", *IEEE Trans. Magn.*, 44(11), pp. 3009-3012, 2008.
[5] D. Davino, A. Giustiniani and C. Visone, "A Magnetostrictive Model With Stress Dependence for Real-Time Applications", *IEEE Trans. Magn.*, 44(11), pp. 3193-3196, 2008.
[6] K. Kashiwaya, "Fundamentals of nondestructive measurement of biaxial stress in steel utilizing magnetoelastic effect under low magnetic field", *Jpn J. Appl. Phys.*, 30, pp. 2932, 1991.
[7] C.S. Schneider and J.M. Richardson, "Biaxial magnetoelasticity in steels", *J. Appl. Phys.*, 53, pp. 8136, 1982.
[8] M.J. Sablik, L. Riley, G. Burkhardt, H. Kwun, P. Cannel, K. Watts and R. Langman, "Micromagnetic model for biaxial stress effects on magnetic properties", *J. Appl. Phys.*, 75, pp. 5673, 1994.
[9] J.Pearson, P.T.Squire, M.G.Maylin, and J.G.Gore, "Biaxial stress effects on the magnetic properties of pure iron", *IEEE Trans. Magn.*, 38, pp. 3251, 2000.
[10] L. Daniel and O. Hubert, "Equivalent Stress Criteria for the Effect of Stress on Magnetic Behavior", *IEEE Trans. Magn.*, 46(8), pp. 3089, 2010.
[11] W.D. Armstrong, "A directional magnetization potential based model of magnetoelastic hysteresis", *J. Appl. Phys.*, 91, pp. 2202, 2002.
[12] N. Buiron, L. Hirsinger and R. Billardon, "A multiscale model for magneto-elastic couplings", *J. Phys. IV*, 9, pp. 187, 1999.
[13] L. Daniel, O. Hubert, N. Buiron and R. Billardon, "Reversible magneto-elastic behavior: a multiscale approach", *J. Mech. Phys. Solids*, 56, pp. 1018, 2008.
[14] L. Daniel and N. Galopin, "A constitutive law for magnetostrictive materials and its application to Terfenol-D single and polycrystals", *Eur. Phys. J. Appl. Phys.*, 42, pp. 153, 2008.
[15] F.C. Graham, C. Mudivarthi, S. Datta and A.B. Flatau, "Modeling of Galfenol transducer using the bidirectionally coupled magnetoelastic model", *Smart Mater. Struct.*, 18, pp. 104013, 2009.
[16] W.D. Armstrong, "Magnetization and magnetostriction processes in $\text{Tb}(0.27-0.30)\text{Dy}(0.73-0.70)\text{Fe}(1.9-2.0)$", *J. Appl. Phys.*, 81, pp.2321, 1997.
[17] O. Hubert and L. Daniel, "Measurement and analytical modeling of the ΔE effect in a bulk Iron-Cobalt alloy", *IEEE Trans. Magn.*, 46(2), pp. 401, 2010.
[18] M. Besbes, Z. Ren, and A. Razek,"A generalized finite element model of magnetostriction phenomena", *IEEE Trans. Magn.*, 37(5), pp. 3324-3328, 2001.
[19] A.G. Kladas, and J.A. Tegopoulos,"A new scalar potential formulation for 3-D magnetostatics necessitating no source field calculation", *IEEE Trans. Magn.*, 28(2), pp. 1103-1106, 1992.

[20] F. Ossart and V. Ionita, "Convergence de la méthode du point fixe modifiée pour le calcul de champ magnétique avec hystérésis", *Eur. Phys. J. Appl. Phys.*, 5, pp. 63-69, 1999.
[21] A. Schoppa, J. Schneider and C.D. Wuppermann, "Influence of the manufacturing process on the magnetic properties of non-oriented electrical steels", *J. Magn. Magn. Mater.*, 215-216, pp. 74-78, 2000.
[22] F. Ossart, E. Hug and O. Hubert, C. Buvat and R. Billardon, "Effect of Punching on Electrical Steels: Experimental and Numerical Coupled Analysis", *IEEE Trans. Magn.*, 36(5), pp. 3137-3140, 2000.
[23] J.L. Coulomb, "A methodology for the determination of global electromechanical quantities from a finite element analysis and its application to the evaluation of magnetic forces, torques and stiffness", *IEEE Trans. Magn.*, 19(6), pp. 2514-2519, 1983.
[24] A. Schoppa, J. Schneider, C.D. Wuppermann and T. Bakon, "Influence of welding and sticking of laminations on the magnetic properties of non-oriented electrical steels", *J. Magn. Magn. Mater.*, 254-255, pp. 367-369, 2003.
[25] E.G. Araujo, J. Schneider, K. Verbeken, G. Pasquarella and Y. Houbaert, "Dimensional Effects on Magnetic Properties of Fe-Si Steels Due to Laser and Mechanical Cutting", *IEEE Trans. Magn.*, 46(2), pp. 231-216, 2010.

2.3.3 Contrainte équivalente à un chargement multiaxial

On a vu qu'il est possible d'intégrer des relations de comportement magnéto-mécanique, éventuellement simplifiées, dans les codes de calcul de manière notamment à intégrer le caractère multiaxial des sollicitations en service. Cependant, les concepteurs sont parfois réticents à modifier en profondeur leurs outils de modélisation. Comme cela a déjà été mentionné en introduction de la partie 2.2, les outils de modélisation disponibles sont souvent limités au cas de sollicitations uniaxiales (contrainte uniaxiale dans la direction du champ magnétique). Cette configuration est évidemment extrêmement restrictive. Une solution alternative à une modification des outils de modélisation consiste à recourir à la notion de contrainte équivalente. Dans le cas du comportement magnéto-élastique, la contrainte équivalente pour un chargement multiaxial donné est la contrainte uniaxiale qui, appliquée parallèlement au champ magnétique, conduit au même effet sur le comportement magnéto-élastique que le chargement réel. Cette notion est forcément imparfaite, puisqu'il ne peut y avoir d'équivalence rigoureuse entre un état uniaxial et un état multiaxial, mais peut fournir dans certains cas une approximation acceptable. Différents auteurs ont proposé des contraintes équivalentes pour le comportement magnéto-élastique [87–89]. En s'appuyant sur une équivalence en énergie magnéto-élastique [90], nous avons proposé une contrainte équivalente sous la forme de l'équation (2.30).

$$\sigma_{\text{eq}} = \frac{3}{2}\, {}^t\boldsymbol{h}\, \boldsymbol{s}\, \boldsymbol{h} \tag{2.30}$$

$\boldsymbol{h}$ est le vecteur unitaire support du champ magnétique et $\boldsymbol{s}$ le déviateur des contraintes ($\boldsymbol{s}=\boldsymbol{\sigma} - \frac{1}{3}\text{tr}(\boldsymbol{\sigma})\boldsymbol{I}$). Les différentes contraintes équivalentes ont été comparées dans la référence [91] jointe ci-après. Plus récemment une nouvelle contrainte équivalente a été proposée, s'appuyant cette fois sur une équivalence en aimantation [92]. Cette dernière proposition peut être vue comme une généralisation de la contrainte équivalente donnée par l'équation (2.30). Elle offre une meilleure approximation du comportement magnéto-élastique sous sollicitations multiaxiales, mais son utilisation est rendue un peu plus complexe par le fait qu'elle fait intervenir des paramètres matériaux dans sa définition. Le détail de construction de cette contrainte est donné dans la publication [92] jointe ci-après.
Le principe d'utilisation d'une contrainte équivalente est très simple. Il faut disposer d'un outil de calcul de structure permettant de tenir compte de l'effet d'une contrainte uniaxiale dans la direction du champ magnétique, et connaître le comportement du matériau sous ce type de sollicitation. Ces courbes de comportement peuvent soit être identifiées expérimentalement, soit être issues d'un outil de prédiction du comportement, comme le modèle multi-échelle. Un calcul mécanique est nécessaire pour déterminer l'état de contraintes dans la structure, et un calcul magnétique doit être conduit pour connaître l'orientation du champ magnétique. La contrainte équivalent est ensuite calculée d'après l'équation (2.30). C'est cette contrainte qui est introduite dans la relation de comportement uniaxiale pour déterminer la perméabilité magnétique. Le calcul magnétique est ensuite relancé pour déterminer la distribution du champ magnétique. Si les distributions du champ magnétique et de la contrainte sont fortement dépendantes l'une de l'autre, un processus itératif doit être envisagé. L'utilisation de la contrainte équivalente a par exemple été mis en œuvre pour l'étude de faisabilité d'un système de défluxage basé sur l'utilisation de matériaux à magnétostriction géante sur une machine synchrone à aimants permanents [93].

Publications jointes

[RI.26, 91] : L. Daniel, O. Hubert, "Equivalent stress criteria for the effect of stress on magnetic behavior", *IEEE Transactions on Magnetics*, **46(8)** :3089-3092, 2010.

[RI.29, 92] : O. Hubert, L. Daniel, "Energetical and multiscale approaches for the definition of an equivalent stress for magneto-elastic couplings", *Journal of Magnetism and Magnetic Materials*, **323(13)** :1766-1781, 2011.

Equivalent Stress Criteria for the Effect of Stress on Magnetic Behavior

Laurent Daniel[1] and Olivier Hubert[2]

[1]Laboratoire de Génie Electrique de Paris (LGEP) CNRS (UMR 8507), Supelec-Univ Paris Sud-UPMC 11, Gif-sur-Yvette 91192, France

[2]LMT-Cachan ENS Cachan-CNRS (UMR8535)-UPMC-PRES UniverSud Paris 61, Cachan 94235, France

A main limitation of most models describing the effect of stress on the magnetic behavior is that they are restricted to uniaxial, tensile or compressive, stress. An idea to overcome this strong limitation is to define a fictive uniaxial stress, the equivalent stress that would affect the magnetic behavior in a similar manner than a multiaxial one. Several authors have tried to define such a criterion. We propose in this paper to compare several equivalent stress definitions, and to apply them in the case of uniaxial and biaxial mechanical loadings for which experimental results are available.

***Index Terms*—Effect of stress, equivalent stress, magneto-elasticity, multiaxiality.**

I. Introduction

In MOST practical electromagnetic applications, magnetic materials are submitted to multiaxial stress inherited from forming process or appearing in use. These stress states can change significantly the magnetic behavior of materials [1]. However, the few available models describing the effect of stress on the magnetic behavior are usually restricted to uniaxial (tensile or compressive) stress (see for instance [2]–[4]). A solution to introduce the multiaxiality of stress into modeling tools is the definition of an equivalent stress criterion. An equivalent stress for the magnetic behavior is a (fictive) uniaxial stress that would change the magnetic behavior in a similar manner than the multiaxial one[1] . This approach follows the classical equivalent stress definitions used in mechanics such as Von Mises or Tresca equivalent stresses for plasticity. Several equivalent stress for magneto-elasticity have been proposed in the past years [5]–[9]. We propose in this paper to compare these proposals. Experimental results carried out under biaxial mechanical loading will allow to validate these criteria.

II. Several Equivalent Stress Definitions

Several authors tried to define an equivalent stress for magneto-elastic behavior, usually thanks to energetic considerations and experimental observations of magnetic behavior of materials submitted to biaxial mechanical loadings.

Kashiwaya (K) [5] proposed the following definition for the equivalent stress $\sigma_{\rm eq}^{\rm K}$:

$$\sigma_{\rm eq}^{\rm K} = K(\sigma_1 - \sigma_{\max}) \tag{1}$$

with K a constant, σ_1 the eigenstress aligned with the magnetic field direction and $\sigma_{\max}$ the maximal value of the stress tensor eigenvalues. This equivalent stress is always negative or null. Iso-values are parallel lines in the (σ_1, σ_2) plane. If the magnetic field is applied along the direction of the maximum eigenstress, the equivalent stress is zero, so that a tensile stress or an equibiaxial tension or compression are supposed to have no effect on the magnetic behavior.

Schneider and Richardson (SR) [6] proposed the following definition for the equivalent stress $\sigma_{\rm eq}^{\rm SR}$:

$$\sigma_{\rm eq}^{\rm SR} = \sigma_1 - \sigma_2 \tag{2}$$

σ_1 and σ_2 are the eigenstresses in the sheet plane, the magnetic loading being aligned in the direction of σ_1. The main difference with K definition is that the area of the stress plane where $\sigma_1 > 0$ and $\sigma_2 < 0$ defines a positive equivalent stress. But an equibiaxial stress is still supposed to have no effect on the magnetic behavior.

Sablik and co-workers (S) [7] proposed the following definition for the equivalent stress $\sigma_{\rm eq}^{\rm S}$, based on previous magneto-mechanical measurements by Langman [10]:

$$\begin{cases} \sigma_{\rm eq}^{\rm S} = \frac{1}{3}(2\sigma_1 - \sigma_2) & \text{for } \sigma_1 < 0 \\ \sigma_{\rm eq}^{\rm S} = \frac{1}{3}(\sigma_1 - 2\sigma_2) & \text{for } \sigma_1 \geq 0 \end{cases} \tag{3}$$

σ_1 is still the stress aligned with the magnetic field. Equi-bitraction and equi-bicompression do not lead to the same result, that is a significant difference with K and SR approaches. But S model is discontinuous for $\sigma_1 = 0$.

Pearson and co-workers [8] also proposed an equivalent stress for a biaxial mechanical loading. In its simplest form this equivalent stress corresponds to SR proposal. The more refined form is a polynomial interpolation that reveals complicated to use because the parameter identification is sample dependent.

Daniel and Hubert (DH) [9] proposed the following definition $\sigma_{\rm eq}^{\rm DH}$, based on an equivalence in magneto-elastic energy:

$$\sigma_{\rm eq}^{\rm DH} = \frac{3}{2} t\vec{h}\boldsymbol{s}\vec{h} \tag{4}$$

$\vec{h}$ is the direction parallel to the applied magnetic field and $\boldsymbol{s}$ is the deviatoric part of the stress tensor $\boldsymbol{\sigma}(\boldsymbol{s} = \boldsymbol{\sigma} - 1/3\ \mathrm{tr}(\boldsymbol{\sigma})\boldsymbol{I})$. It can be noticed that the equivalent stress is zero when the stress is hydrostatic, meaning that a hydrostatic pressure has no effect on the magnetic behavior. A main advantage of this criterion is that it can be applied to a fully multiaxial mechanical loading, whereas the previous proposals only refer to biaxial stress state.

Manuscript received December 16, 2009; accepted February 21, 2010. Current version published July 21, 2010. Corresponding author: L. Daniel (e-mail: laurent.daniel@supelec.fr).

Color versions of one or more of the figures in this paper are available online at http://ieeexplore.ieee.org.

Digital Object Identifier 10.1109/TMAG.2010.2044561

[1]Meaning that an uniaxial stress with the amplitude defined by the equivalent stress criterion should lead to the same shift in magnetic susceptibility than the real multiaxial stress.

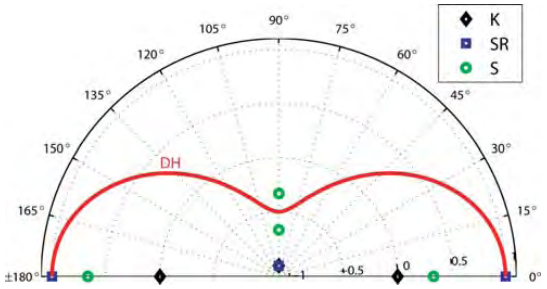

Fig. 1. Equivalent stress σ_{eq}/σ_o in the case of a uniaxial stress σ_o applied in a direction $\theta \in [0, \pi]$ with respect to the magnetic field (direction 0°).

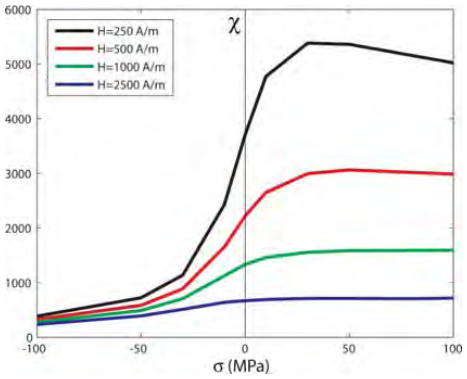

Fig. 2. Experimental secant susceptibility under mechanical loadings.

III. Application in the Case of Uniaxial Tension or Compression

As a first analysis, these equivalent stress criteria can be compared to each other in the case of a uniaxial mechanical loading (intensity σ_0). The result is presented in Fig. 1.

K criterion can only be applied if the maximum eigenstress is in the direction of the magnetic field. SR and S criteria can only be applied in the case when the direction of the magnetic field is a principal direction for the stress. DH criterion can be applied whatever the relative orientation between stress and magnetic field. In the uniaxial case, σ_{eq}^{DH} can be written:

$$\sigma_{eq}^{DH}(\theta) = \frac{3}{2}\sigma_o\left(\cos^2\theta - \frac{1}{3}\right). \quad (5)$$

It has to be noticed that in the case of an uniaxial stress applied in the direction of the magnetic field, K and S proposals differ from the applied stress. For SR and DH proposals, the equivalent stress reduces, as expected, to the applied stress. The discontinuity of S model for $\theta = \pi/2(\sigma_1 = 0)$ is also highlighted.

Some measurements of the susceptibility of an iron-cobalt under uniaxial stress loading have been carried out using a uniaxial magneto-mechanical set-up. The corresponding results are presented in Fig. 2 for several magnetic field levels. The susceptibility change is higher in compression $\sigma < 0$ than in tension $\sigma < 0$.

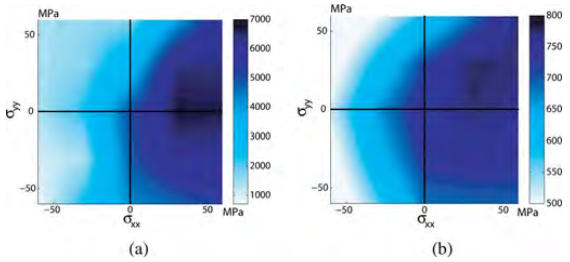

Fig. 3. Experimental secant susceptibility under mechanical loadings. (a) $H = 250$ A·m^{-1}, (b) $H = 2500$ A·m^{-1}.

IV. Application in the Case of Biaxial Mechanical Loadings

Experiments have been performed on iron-cobalt laminations (cross specimen) [11]. They consist in anhysteretic magnetic measurements carried out under biaxial mechanical stress in homogeneous magnetic and mechanical conditions, for stress levels varying from -60 MPa to $+60$ MPa. Magnetic field is applied along direction 1. The results are shown in Fig. 3.

Tension $(\sigma_1 > 0, \sigma_2 = 0)$ slightly increases the susceptibility, and compression $(\sigma_1 < 0, \sigma_2 = 0)$ strongly decreases it. An uniaxial stress in the direction orthogonal to the field $(\sigma_1 = 0, \sigma_2 \neq 0)$ deteriorates the magnetic behavior, with a stronger effect in tension. Equibiaxial stress $(\sigma_1 = \sigma_2)$, and shear stress $(\sigma_1 = -\sigma_2)$ strongly deteriorate the magnetic behavior when σ_1 is negative, and have a much lower effect when σ_1 is positive.

The expected susceptibility according to K, SR, S and DH criteria has been estimated (the experimental data for the susceptibility under uniaxial mechanical loading have been extracted from the measurements with $\sigma_2 = 0$) [2]. The experimental conditions correspond to biaxial stress (σ_1, σ_2) with the magnetic field applied along eigendirection 1 (DH equivalent stress is then defined by $\sigma_{eq} = \sigma_1 - (1/2)\sigma_2$). Fig. 4 shows a map of the relative error between predicted χ_p and measured χ_e susceptibilities $(e = 100 \times |\chi_p - \chi_e|/\chi_e)$ for a magnetic field of 250 A·m^{-1}.

For all criteria, the errors observed in equibicompression are very high. In the case of a stress $(\sigma_1, \sigma_2) = (-60\ \text{MPa}, -60\ \text{MPa})$ the error is up to 635% for K and SR, 371% for S and 238% for DH. All the proposed equivalent criteria fail in the prediction of the effect of a bicompressive stress. If the error values are truncated to 50% for reading convenience, Fig. 5 is obtained.

It appears that outside the bicompression area, DH criterion is closest to experimental results. Fig. 6 has been plotted for a magnetic field of 2500 A.m^{-1}. The same comments can be made. Errors are lower in that case. This decrease of the error is linked to the fact that for such a level of magnetic field, close to saturation, the effect of stress on the magnetic behavior is less sensitive (it can be observed from Figs. 2 and 3).

[2]Complementary measurements of Fig. 2 have been made mainly to ensure that the 1-D measurements with the cross specimen were consistent with a real 1-D configuration.

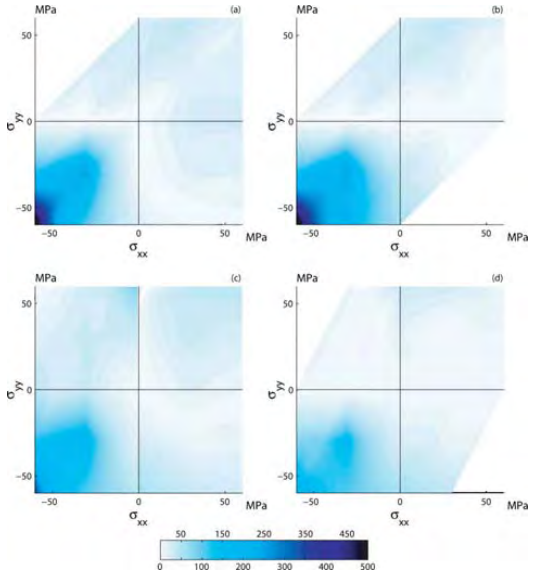

Fig. 4. Relative error (percent) for the predicted susceptibility ($H = 250$ A/m) according to several equivalent stress proposals. (a) K ($K = 1$), (b) SR, (c) S, (d) DH.

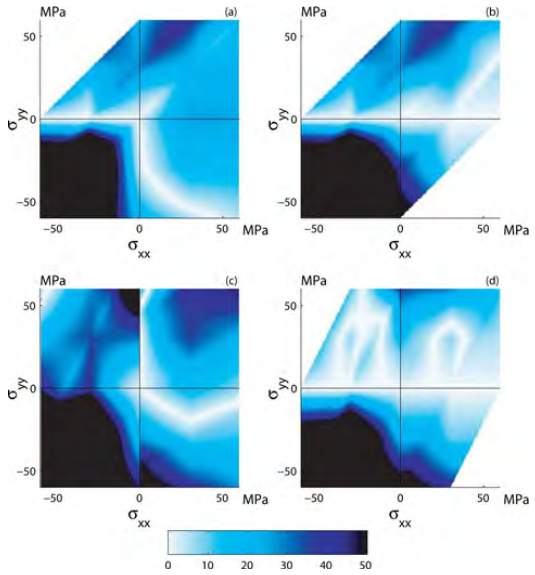

Fig. 5. Relative error (percent) for the predicted susceptibility ($H = 250$ A/m) according to several equivalent stress proposals. (a) K ($K = 1$), (b) SR, (c) S, (d) DH.

V. Guidelines for the Practical Implementation of an Equivalent Stress

The use of an equivalent stress criterion for magneto-elastic behavior is required when an electromagnetic device under significant mechanical loading is studied. As an example, we can consider the stress state inherited from a binding process. For the sake of simplicity, we will consider the very simple configu-

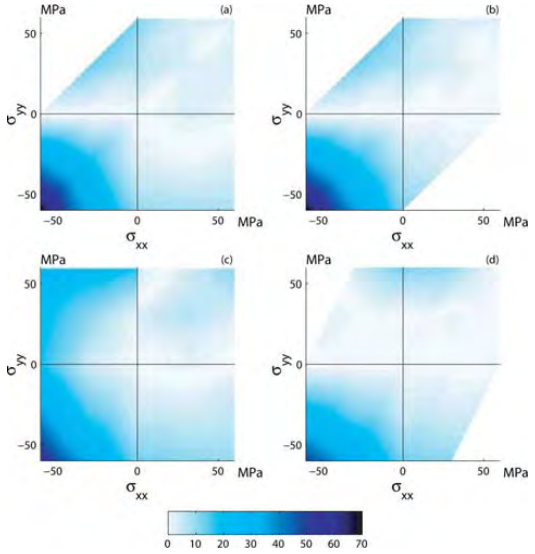

Fig. 6. Relative error (percent) for the predicted susceptibility ($H = 2500$ A/m) according to several equivalent stress proposals. (a) K ($K = 1$), (b) SR, (c) S, (d) DH.

ration of a rigid cylindrical yoke of internal diameter ϕ_0 binding a cylinder of external diameter $\phi_e = \phi_0 + 2\Delta$ and internal diameter ϕ_i. Under plain strain assumptions, the corresponding stress tensor in the cylinder as a function of the radius r is given in cylindrical coordinates by (6)

$$\boldsymbol{\sigma}(r) = \begin{pmatrix} \sigma_{rr} & 0 & 0 \\ 0 & \sigma_{\theta\theta} & 0 \\ 0 & 0 & \sigma_{zz} \end{pmatrix}_{r\theta z} \tag{6}$$

with

$$\begin{cases} \sigma_{rr} = -K\Delta\left(1 - \left(\dfrac{\phi_i}{2r}\right)^2\right), \\ \sigma_{\theta\theta} = -K\Delta\left(1 + \left(\dfrac{\phi_i}{2r}\right)^2\right), \\ \sigma_{zz} = -K\Delta\,\dfrac{\lambda}{\mu+\lambda}, \end{cases} \tag{7}$$

and

$$K = \frac{4\mu(\mu+\lambda)\phi_e}{\mu\phi_e^2 + (\mu+\lambda)\phi_i^2}. \tag{8}$$

λ and μ are the Lamé coefficients defining the elastic properties of the material (under isotropic assumption). Introducing the effect of such a triaxial stress state on the magnetic behavior would require to have an access to the characterization of the magnetic behavior under complex multiaxial mechanical loading. These experimental data are usually not available. The proposed alternative is to compute the equivalent uniaxial stress given by (4). From (6), and considering a magnetic field in the direction $\vec{h} = {}^t[h_r \;\; h_\theta \;\; h_z]$ we obtain:

$$\sigma_{\text{eq}}^{\text{DH}} = \frac{3}{2}\left(h_r^2\,\sigma_{rr} + h_\theta^2\,\sigma_{\theta\theta} + h_z^2\,\sigma_{zz}\right) - \frac{1}{2}\left(\sigma_{rr} + \sigma_{\theta\theta} + \sigma_{zz}\right). \tag{9}$$

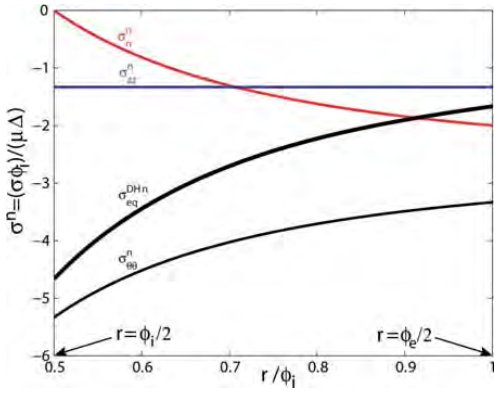

Fig. 7. Normalized values of $\sigma_{rr}, \sigma_{\theta\theta}, \sigma_{zz}$, and $\sigma_{\rm eq}^{\rm DH}$ for a simplified binding configuration with orthoradial magnetic field ($\phi_e/\phi_i = 2$ and $\nu = 0.25$).

It is then assumed that an uniaxial stress parallel to the local magnetic field, with amplitude $\sigma_{\rm eq}^{\rm DH}$, modifies the permeability as the real multiaxial stress. The only necessary data are the characterization of the magnetic behavior under uniaxial stress, that are rather classical measurements.

If we consider an even more simplified configuration where the field is orthoradial $\vec{h} = {}^t[0\ 1\ 0]$ (e.g., if a current along $\vec{z}$ is imposed in the central wire of diameter ϕ_i), the equivalent stress, applied in the orthoradial direction, reduces to (10)

$$\sigma_{\rm eq}^{\rm DH} = \sigma_{\theta\theta} - \frac{1}{2}(\sigma_{rr} + \sigma_{zz}) = -\frac{K\Delta}{2}\left(\frac{\mu}{\mu+\lambda} + 3\left(\frac{\phi_i}{2r}\right)^2\right). \quad (10)$$

This case is illustrated in Fig. 7, considering $\phi_e = 2\phi_i$ and a Poisson's ratio $\nu = 0.25$. It gives $\lambda = \mu$, $K = (8\mu)/(3\phi_i)$ and we obtain $\sigma_{\rm eq}^{\rm DH} = (-2\mu\Delta)/(3\phi_i)(1+6(\phi_i/2r)^2)$. It can be noticed that the equivalent stress is different from all the principal components of the stress tensor.

In the case of the structural analysis of a more complicated structure under more complicated loadings, the same scheme can be applied. The distribution of stress is first computed, so that the corresponding distribution of the equivalent stress can be calculated. The magnetic computation is then made using magnetization curves under uniaxial stress. The approach proposed in [12] can be used, the value for the uniaxial stress must just be replaced by the equivalent stress.

VI. Conclusion

Several equivalent stress criteria for the effect of multiaxial stress on the magnetic behavior have been compared. The main weakness of these models is their inability to describe the effect of a bicompression stress on the magnetic behavior. Only one equivalent stress (DH) can describe fully multiaxial stress state, without any hypothesis concerning the relative orientation of the magnetic field direction in the principal stress coordinate system. This latter proposal is also the closest to experimental results obtained in biaxial configurations. The guidelines for the use of such equivalent stress criteria have been given in the case of coupled magneto-mechanical structural analysis. These equivalent stress criteria are a strong approximation but they provide a significant—and easy to implement—improvement to the classical uniaxial approach of magneto-elastic couplings. If the corresponding predictions are not accurate enough—for example under bicompressive mechanical loadings—fully coupled multiaxial constitutive laws are required.

References

[1] R. M. Bozorth, *Ferromagnetism*. Walden, N.Y.: Van Norstand Distributors, 1951.

[2] M. J. Sablik and D. C. Jiles, "Coupled magnetoelastic theory of magnetic and magnetostrictive hysteresis," *IEEE Trans. Magn.*, vol. 29, no. 5, p. 2113, Sep. 1993.

[3] Y. Bernard and F. Ossart, "Comparison between two models of magnetic hysteresis accounting for stress," *Int. J, Appl. Electromagn. Mech.*, vol. 19, no. 1–4, pp. 551–556, 2004.

[4] O. Bottauscio, A. Lovisolo, P. E. Roccato, M. Zucca, C. Sasso, and R. Bonin, "Modeling and experimental analysis of magnetostrictive devices: From the material characterization to their dynamic behavior," *IEEE Trans. Magn.*, vol. 44, no. 11, pp. 3009–3012, Nov. 2008.

[5] K. Kashiwaya, "Fundamentals of nondestructive measurement of biaxial stress in steel utilizing magnetoelastic effect under low magnetic field," *Jpn. J. Appl. Phys.*, vol. 30, p. 2932, 1991.

[6] C. S. Schneider and J. M. Richardson, "Biaxial magnetoelasticity in steels," *J. Appl. Phys.*, vol. 53, p. 8136, 1982.

[7] M. J. Sablik, L. Riley, G. Burkhardt, H. Kwun, P. Cannel, K. Watts, and R. Langman, "Micromagnetic model for biaxial stress effects on magnetic properties," *J. Appl. Phys.*, vol. 75, p. 5673, 1994.

[8] J. Pearson, P. T. Squire, M. G. Maylin, and J. G. Gore, "Biaxial stress effects on the magnetic properties of pure iron," *IEEE Trans. Magn.*, vol. 38, no. 6, p. 3251, Nov. 2000.

[9] L. Daniel and O. Hubert, "An equivalent stress for the influence of multiaxial stress on the magnetic behavior," *J. Appl. Phys.*, vol. 105, p. 07A313, 2009.

[10] R. A. Langman, "Magnetic properties of mild steel under conditions of biaxial stress," *IEEE Trans. Magn.*, vol. 26, no. 4, p. 1243, Jul. 1990.

[11] O. Hubert, "Influence of biaxial stresses on the magnetic behaviour of an iron-cobalt sheet—Experiments and modelling," *Przedglad Elektrotecniczny*, vol. 83, p. 70, 2007.

[12] R. Billardon, L. Hirsinger, and F. Ossart, "Magneto-elastic coupled finite element analyses," *Revue européenne des éléments finis*, vol. 8, no. 5–6, p. 525, 1999.

Journal of Magnetism and Magnetic Materials 323 (2011) 1766–1781

Contents lists available at ScienceDirect

Journal of Magnetism and Magnetic Materials

journal homepage: www.elsevier.com/locate/jmmm

Energetical and multiscale approaches for the definition of an equivalent stress for magneto-elastic couplings

Olivier Hubert [a,*], Laurent Daniel [b]

[a] LMT-Cachan, ENS Cachan; CNRS; UPMC; PRES Universud Paris, 61, avenue du président Wilson, 94235 Cachan Cedex, France
[b] Laboratoire de Génie Electrique de Paris (LGEP), CNRS (UMR 8507); SUPELEC; Univ Paris-Sud; UPMC, Plateau du Moulon, 11 rue joliot-Curie, 91192 Gif sur Yvette Cedex, France

ARTICLE INFO

Article history:
Received 14 November 2010
Received in revised form
6 January 2011
Available online 4 February 2011

Keywords:
Equivalent stress
Magnetomechanical coupling
Magnetostriction

ABSTRACT

A main limitation of most models describing the effect of stress on the magnetic behavior is that they are restricted to uniaxial – tensile or compressive – stress. Nevertheless, stress is multiaxial in most of industrial applications. An idea to overcome the strong limitation of models is to define a fictive uniaxial stress, the equivalent stress, that would change the magnetic behavior in a similar manner than a multiaxial stress. A first definition of equivalent stress, called the deviatoric equivalent stress, is proposed. It is based on an equivalence in magneto-elastic energy. This formulation is first derived for isotropic materials under specific assumptions. An extension to orthotropic media under disoriented magneto-mechanical loading is made. A new equivalent stress expression, called generalized equivalent stress, is then proposed. It is based on an equivalence in magnetization. Inverse identification of equivalent stress is made possible thanks to a strong simplification of the description of the material seen as an assembly of elementary magnetic domains. It is shown that this second proposal is a generalization of the deviatoric expression. Equivalent stress proposals are compared to former proposals and validated using experimental results carried out on an iron–cobalt sheet submitted to biaxial mechanical loading. These results are compared to the predictions obtained thanks to the equivalent stress formulations. The generalized equivalent stress is shown to be a tool able to foresee the magnetic behavior of a large panel of materials submitted to multiaxial stress.

1. Introduction

In most practical electromagnetic applications, magnetic materials are submitted to multiaxial stress inherited from forming process or appearing in use. As an example, inertial stresses in high rotating speed systems for aeronautic equipments or new technologies of flywheel, stresses due to binding process (encapsulation) of electrical machines and actuators, residual stress associated to plastic straining (forming) or cutting process can be mentioned. Several examples that can be associated to some generic types of stress tensor are detailed in this paper. On the other hand, since the works of Mateucci [1] and Villari [2], mechanical stress is known to change significantly the magnetic behavior of materials (see for instance [3]) as well as their magnetostrictive behavior [4]. The design of electromagnetic systems consequently requires coupled and multiaxial models. However, the few available and practically implemented models describing the effect of stress on the magnetic behavior are restricted to uniaxial (tensile or compressive) stress. Jiles–Atherton type models [5–8] and Preisach type models [9–12] are the most popular but other approaches have also been proposed [13–15].

One way is to use energy-based models written at an appropriate scale. Indeed the development of fully multiaxial magneto-elastic models is a promising issue [16–22], but still leads to dissuasive computation times for engineering design applications. The second part of this paper briefly recalls such a multiscale magneto-elastic model for the prediction of the effect of multiaxial stress on magnetic and magnetostrictive behavior.

A second way is to implement multiaxial stress directly in a macroscopic model (see for instance [23]). Even sometimes effective, this solution is not fully satisfactory since the physics of coupling is not suitably described. Another approach combining uniaxial models and multiaxial stress is to define and calculate a "fictive" uniaxial stress, the equivalent stress that would change the magnetic behavior in a similar manner than the multiaxial one. The second step is to implement this scalar value into a uniaxial macroscopic magneto-mechanical model. Some authors proposed such an approach in the past years [24–27]. It is shown that in many cases these proposals are not fully satisfactory. Recently a definition of an equivalent stress based on an equivalence in magneto-elastic energy has been proposed [28,29]. Assuming that

* Corresponding author. Tel.: +33 1 47 40 22 24; fax: +33 1 47 40 22 40.
E-mail addresses: hubert@lmt.ens-cachan.fr (O. Hubert), laurent.daniel@supelec.fr (L. Daniel).

0304-8853/$ - see front matter © 2011 Elsevier B.V. All rights reserved.
doi:10.1016/j.jmmm.2011.01.041

the same magneto-elastic energy corresponds to the same magnetic behavior, the equivalent stress is defined as the uniaxial stress, applied along the magnetic field direction that leads to the same macroscopic magneto-elastic energy as the multiaxial one. This formulation is named as the deviatoric equivalent stress because it is expressed in terms of the deviatoric stress tensor. Its implementation is very simple; it is nevertheless involving some strong hypotheses on the behavior of the material and on the magneto-mechanical loading. Extension to orthotropic media and to a disoriented loading is proposed in this paper in order to solve some of the limitations of this approach. In the next section, a generalized equivalent stress is proposed, based on an equivalence in magnetization. Since magnetostatic and magnetoelastic terms cannot be easily dissociated in the expression of the free energy, the definition of the equivalent stress is made possible thanks to a strong simplification in the description of the material. Bulk magnetic material is seen as an assembly of elementary magnetic domains. The validation of these proposals requires to carry out magnetic measurements on materials submitted to multiaxial stress thanks to a multiaxial experimental set-up. The proposed validation is based on biaxial experiments.

Biaxial testing in mechanics is usually associated to traction–torsion, internal pressure, and/or traction–traction (along two orthogonal axes) experiments. Considering that sheet format is the most popular format for magnetic materials constitutive of electrical machines [3], only the latter experiment is suitable to study the magnetic behavior under biaxial mechanical conditions. Previous experiments from different authors are available in the literature (see for instance [24–26,30] and more recently [31–33]). But all of them present some mismatches especially concerning the homogeneity of the stress in the measurement area (e.g. Langman's eight points bending system [30]) or the inaccurate evaluation of magnetic quantities [33]. A previous paper detailed a new experimental procedure and corresponding results [34,35]. The procedure, partially recalled in this paper, allowed to evaluate the influence of a biaxial stress state on the magnetic behavior under adequate magnetic and mechanical conditions.

The new experimental results have been used in order to test the validity of previous and new formulations of equivalent stress. A short review of previous experimental results is finally made. These results are compared to predictions obtained thanks to the new formulation of equivalent stress. The generalized equivalent stress is shown to be a tool able to foresee the magnetic behavior of a large panel of materials submitted to multiaxial stress.

The paper is divided into five sections. In the first part, some typical multiaxial stress states that can be encountered in electromagnetic devices are presented. Magneto-elastic modeling approaches able to account for the effect of multiaxial stress on the magnetic behavior are presented in the second part. In the third and fourth parts, two distinct proposals for the definition of an equivalent stress for the magnetic behavior are proposed: the deviatoric and the generalized equivalent stresses. A validation of these approaches is finally proposed by comparison to biaxial magneto-mechanical measurements.

2. Multiaxial stress in magnetic materials and structures

Forces, torques, stresses acting on the material are associated to any operating electromagnetic system. Multiaxial stresses are generally created due to the nature of loading, to the complex geometry of devices or to the manufacturing process. Several examples of typical loadings and associated stress tensors are given in this section. Elastic mechanical behavior is assumed.

2.1. Multiaxial stress "in use": centrifugal forces and torque

The first example concerns the effect of centrifugal forces. Indeed modern technologies of electrical machines especially for aeronautical applications involve higher and higher rotating speed and torque. Centrifugal forces are also critical in new technologies of high speed flywheels (Fig. 1) [36].

Let us consider a ferromagnetic full cylinder (external diameter ϕ_e—Fig. 2) submitted to a constant angular speed $\vec{\omega} = \omega \cdot \vec{e}_z$. The volumetric forces are radial and related to the radius r by $\vec{f}_v = \rho r \omega^2 \cdot \vec{e}_r$ (ρ is the mass density of the considered material). The corresponding stress tensor $\boldsymbol{\sigma}_0$ is diagonal (1). The definition of each term depends on the assumption on the stress and strain tensors. Plane stress approximation or plane strain approximation leads to two classical results in continuum

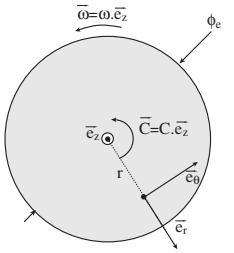

Fig. 2. Schematic view of a ferromagnetic full cylinder submitted to angular speed $\vec{\omega}$ and/or torque $\vec{C}$.

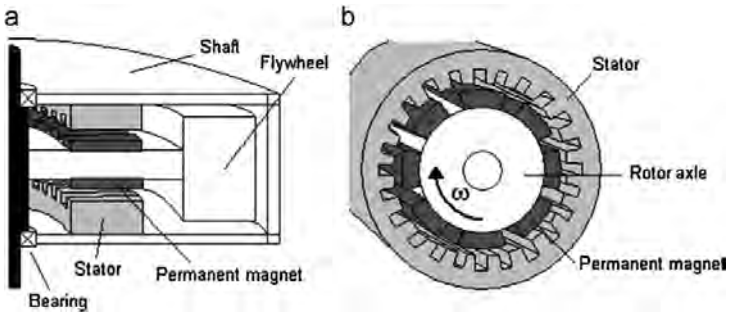

Fig. 1. Examples of flywheel systems: (a) axial-flux and, (b) radial-flux permanent magnet machines [36].

mechanics:

$$\boldsymbol{\sigma}_0 = \begin{pmatrix} \sigma_{rr} & 0 & 0 \\ 0 & \sigma_{\theta\theta} & 0 \\ 0 & 0 & \sigma_{zz} \end{pmatrix}_{(r,\theta,z)} \quad (1)$$

- In the case of plane stress conditions (free deformation through the thickness), the stress tensor is biaxial and its components are given by

$$\begin{cases} \sigma_{rr} = -K' \cdot (3-2\nu-4\nu^2)\left(r^2 - \left(\frac{\phi_e}{2}\right)^2\right) \\ \sigma_{\theta\theta} = -K' \cdot \left((1+2\nu-4\nu^2)r^2 - (3-2\nu-4\nu^2)\left(\frac{\phi_e}{2}\right)^2\right) \\ \sigma_{zz} = 0 \end{cases}$$

- In the case of plane strain conditions:

$$\begin{cases} \sigma_{rr} = -K' \cdot (3-2\nu)\left(r^2 - \left(\frac{\phi_e}{2}\right)^2\right) \\ \sigma_{\theta\theta} = -K' \cdot \left((1+2\nu)r^2 - (3-2\nu)\left(\frac{\phi_e}{2}\right)^2\right) \\ \sigma_{zz} = -2\nu K'\left(2r^2 - (3-2\nu)\left(\frac{\phi_e}{2}\right)^2\right) \end{cases}$$

with $K' = \rho\omega^2/(8(1-\nu))$, ν denoting Poisson's ratio of the material. The stress is multiaxial and increases with the square of the angular speed.

The second example deals with the stress associated to the torque acting on the rotor of the rotating machine. The torque occurs during a transient period of the system, when rotating speed is increasing or decreasing. Stress due to pure torque is usually added to the stress due to centrifugal forces.

Let us consider the previous ferromagnetic full cylinder (Fig. 2) submitted to a constant torque $\vec{C} = C \cdot \vec{e}_z$. The associated stress tensor $\boldsymbol{\sigma}_1$ is null except the shear term $\sigma_{\theta z}$:

$$\boldsymbol{\sigma}_1 = \begin{pmatrix} 0 & 0 & 0 \\ 0 & 0 & \sigma_{\theta z} \\ 0 & \sigma_{\theta z} & 0 \end{pmatrix}_{(r,\theta,z)} \quad (2)$$

with

$$\sigma_{\theta z} = \frac{8rC}{\pi\phi_e^2}$$

r denoting the radial position (Fig. 2). Such a shear stress is associated to a biaxial principal stress tensor, with opposite eigen stresses $\sigma^E = \pm\sigma_{\theta z}$.

2.2. Initial multiaxial stress due to forming process: binding and coiling processes

Multiaxial stress can occur during the forming process of the magnetic material, during the assembly of the electrical machine, or during the machining of a part of the machine (usually the magnetic sheets).

The binding process is usually employed to stack together the magnetic sheets of the stator of an electrical machine. It also ensures a protection of the magnetic circuit. This binding is usually realized on an axisymetric stator: the ring is heated to dilate and placed around the stator. The thermal contraction ensures the mechanical anchoring (see Fig. 3).

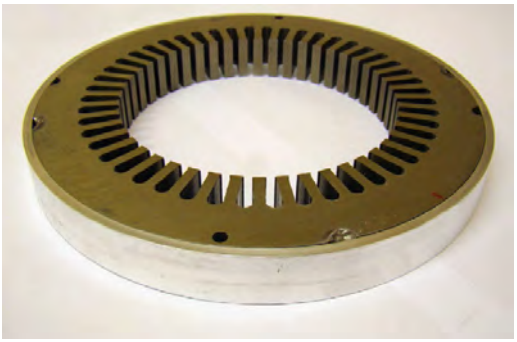

Fig. 3. Example of binding of a stator using an aluminum ring.

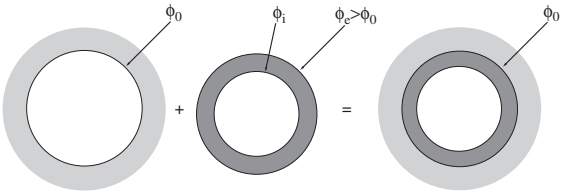

Fig. 4. Theoretical binding of a cylinder inside a rigid yoke.

The stress due to binding can be calculated under plane strain assumption, and using simplified geometric conditions. Let us consider a rigid cylindrical yoke of internal diameter ϕ_0, binding an iron cylinder of external diameter $\phi_e = \phi_0 + 2\delta$ and internal diameter ϕ_i (Fig. 4). Binding strength depends on these three geometric parameters and on material constants (the so-called Lamé coefficients μ and λ in the case of isotropic elasticity). After calculation we get the stress tensor $\boldsymbol{\sigma}_2$ as a function of the radius r (Eq. (3)). The stress state is triaxial, non-homogeneous and linearly depends on δ parameter:

$$\boldsymbol{\sigma}_2 = \begin{pmatrix} \sigma_{rr} & 0 & 0 \\ 0 & \sigma_{\theta\theta} & 0 \\ 0 & 0 & \sigma_{zz} \end{pmatrix}_{(r,\theta,z)} \quad (3)$$

with

$$\begin{cases} \sigma_{rr} = -K\delta\left(4 - \left(\frac{\phi_0}{r}\right)^2\right) \\ \sigma_{\theta\theta} = -K\delta\left(4 + \left(\frac{\phi_0}{r}\right)^2\right) \\ \sigma_{zz} = -K\delta\left(\frac{4\lambda}{\mu+2\lambda}\right) \end{cases}$$

and

$$K = \frac{\mu(\mu+2\lambda)\cdot\phi_e}{\mu(\phi_e^2+\phi_i^2)+2\lambda\phi_i^2}$$

Multiaxial stress can also appear in a magnetic material after plastic straining. Associated stresses are commonly called "internal stresses" if the scale of fluctuation of stress is lower than the grain size and "residual stresses" if the scale of fluctuation of stress is of the order of the specimen size. Effect of plasticity on magnetic materials can be interpreted as an effect of these internal or residual stresses [37,38]. Plastic strains occur for example at the cutting edge of sheets [39,40], or after bending during the forming process. We can consider the case of the

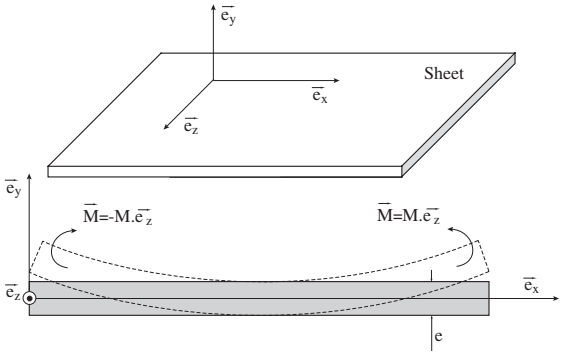

Fig. 5. Schematic view of a plane sheet submitted to a torque $\vec{M} = \pm M \cdot \vec{e}_z$.

Fig. 6. Residual curvature of an iron–cobalt sheet after severe coiling curvature denotes internal stresses.

coiling of a sheet around a cylinder: an irreversible deformation may occur if the diameter of the cylinder is too small. The mechanical state associated to the coiling is complex. A usual simplification plotted in Fig. 5 is to consider a pure bending of the sheet (thickness e and plane $(\vec{e}_z,\vec{e}_x)$) due to a torque $\vec{M} = \pm M \cdot \vec{e}_z$ associated to a dry friction condition on the lower surface (relative slip speed considered as zero). We can evaluate a stress tensor $\boldsymbol{\sigma}_3$ through the thickness of the sheet (depth y) as follows:

$$\boldsymbol{\sigma}_3 = \begin{pmatrix} K''(y)\cdot(2\mu+\lambda) & 0 & 0 \\ 0 & K''(y)\cdot\lambda & 0 \\ 0 & 0 & K''(y)\cdot\lambda \end{pmatrix}_{(x,y,z)} \quad (4)$$

with

$$K''(y) = \frac{M}{EI}\left(y+\frac{e}{2}\right)$$

E is the Young's modulus and I the moment of inertia of the section $(\vec{e}_y,\vec{e}_z)$ around $\vec{e}_z$ axis. When the yield stress is reached on the upper surface, stress tensor brings multiaxial plasticity, leading to residual stresses after unloading. Fig. 6 shows an iron–cobalt sheet deformed by bending after a coiling.

The previous simple examples show the need of magneto-elastic models considering multiaxial macroscopic stresses in order to predict their effects and optimize the design of electromagnetic devices. In industrial magnetic systems, the distribution of stress can be more complex and is often estimated using finite element techniques (see for instance [41,42]).

3. Multiaxial magneto-elastic models

The prediction of the influence of multiaxial stress on magnetic behavior supposes the introduction of the complete mechanical loading into a magnetoelastic modeling. As already mentioned, the few practically implemented models describing the effect of stress on magnetic behavior are restricted to uniaxial mechanical loadings (tension or compression) [5–15]. A first approach to build multiaxial magneto-elastic models consists in the definition of magneto-elastic constitutive laws including the multiaxiality of stress at the local scale. A multiscale model following this requirement is briefly presented in the first part. A second approach consists in the definition of a uniaxial equivalent stress, defined from the multiaxial loading and implemented into a uniaxial constitutive law. Such an approach is presented in the second part.

3.1. Multiaxial magneto-elastic constitutive laws: the multiscale model

At lower scales, micromagnetics offers a deep insight on the dynamics of magnetic structures—magnetic domains and domain walls. Micromagnetic approaches [43] are based on the local resolution of Landau–Lifshitz–Gilbert equation of motion often in combination with finite element methods [44]. In order to account for magneto-elastic coupling, the elastic energy can be introduced with respect to the balance equations and the boundary conditions [45–48]. This point remains a complex issue particularly in the context of multiaxial stress. Despite an accurate prediction of local magnetic microstructures, the small volumes considered and the high computation time associated to these calculations remain a significant drawback.

Following the early works of Néel [49], the development of multiscale magneto-elastic models is a promising issue [16–22]. These models are inspired from the equations of micromagnetics with the use of an energetic functional to be minimized but take benefit from the results of micromagnetic calculations in order to define simplifying assumptions. The computation times are then significantly improved. The multiaxiality of stress can usually be naturally accounted for in such approaches. Such a multiscale model is briefly presented hereafter. It is a three scale model – domain, grain and macroscopic scales – for the prediction of the reversible magneto-elastic behavior of heterogeneous materials [21,22].

A ferromagnetic medium can be seen as an aggregate of single crystals assembled following an orientation distribution function. Each single crystal can itself be seen as an aggregate of magnetic domains following another distribution function. The single crystal can be divided into domain families, each family α corresponding to a given orientation for the magnetization. The modeling scheme is based on the calculation of the volumetric fraction f_α of each domain family α. The volumetric fraction corresponding to the domain family α depends on the internal energy W_α classically defined (Eq. (5)) as the sum of the magneto-crystalline (Eq. (6)), Zeemann (Eq. (7)) and elastic (Eq. (8)) energies:

$$W_\alpha = W_\alpha^K + W_\alpha^H + W_\alpha^\sigma \quad (5)$$

$$W_\alpha^K = K_1(\gamma_1^2\gamma_2^2+\gamma_2^2\gamma_3^2+\gamma_3^2\gamma_1^2)+K_2(\gamma_1^2\gamma_2^2\gamma_3^2) \quad (6)$$

$$W_\alpha^H = -\mu_0\,\vec{H}_\alpha\cdot\vec{M}_\alpha \quad (7)$$

$$W_\alpha^\sigma = \tfrac{1}{2}\,\boldsymbol{\sigma}_\alpha : \mathbb{C}_\alpha^{-1} : \boldsymbol{\sigma}_\alpha \quad (8)$$

K_1 and K_2 are the magnetocrystalline constants, μ_0 denotes the vacuum permeability. $\vec{M}_\alpha = M_s\vec{\gamma}_\alpha = M_s\gamma_i.\vec{e}_i$ is the magnetization of the domain family α with M_s the saturation magnetization of the material and γ_i the direction cosines of the magnetization in the crystallographic coordinate system. $\vec{H}_\alpha$ and $\boldsymbol{\sigma}_\alpha$ denote the magnetic field and the stress tensor at domain scale. $\mathbb{C}_\alpha$ is the local stiffness tensor. If no specific information is known about magnetic domain topology, the assumption of a uniform magnetic field within a grain (single crystal) can be employed. The assumption of a uniform strain within a grain leads to further simplification of the elastic energy (Eq. (9)) introducing the magnetostriction strain tensor ε_α^μ in a domain (Eq. (10)), the

average stress tensor $\boldsymbol{\sigma}_g$ over the grain and a constant W_0^σ [21]. This latter constant, uniform over a grain does not participate in the energetic balance and is usually removed [4,51] leading to the classical expression for the so-called magneto-elastic energy (Eq. (11)):

$$W_\alpha^\sigma = -\boldsymbol{\sigma}_g : \varepsilon_\alpha^\mu + W_0^\sigma \tag{9}$$

$$\varepsilon_\alpha^\mu = \frac{3}{2}\begin{pmatrix} \lambda_{100}(\gamma_1^2-\frac{1}{3}) & \lambda_{111}\gamma_1\gamma_2 & \lambda_{111}\gamma_1\gamma_3 \\ \lambda_{111}\gamma_1\gamma_2 & \lambda_{100}(\gamma_2^2-\frac{1}{3}) & \lambda_{111}\gamma_2\gamma_3 \\ \lambda_{111}\gamma_1\gamma_3 & \lambda_{111}\gamma_2\gamma_3 & \lambda_{100}(\gamma_3^2-\frac{1}{3}) \end{pmatrix} \tag{10}$$

$$W_\alpha^\sigma = -\boldsymbol{\sigma}_g : \varepsilon_\alpha^\mu \tag{11}$$

λ_{100} and λ_{111} are the magnetostrictive coefficients of the single crystal. Following Chikazumi [51] and Buiron [18] the volumetric fraction f_α is calculated using a Boltzmann type function (Eq. (12)). The parameter S is defined by Eq. (13) and calculated using a spatial discretization of the possible directions for the magnetization [22]. The parameter A_s has been shown [21] to be proportional to the initial susceptibility χ_0 of the material (Eq. (14)):

$$f_\alpha = \frac{1}{S}\exp(-A_s \cdot W_\alpha) \tag{12}$$

$$S = \int_\alpha \exp(-A_s \cdot W_\alpha)\, d\alpha \approx \sum_\alpha \exp(-A_s \cdot W_\alpha) \tag{13}$$

$$A_s = \frac{3\chi_0}{\mu_0 M_s^2} \tag{14}$$

Magnetization $\vec{M}_g$ and magnetostriction ε_g^μ at the grain scale are finally defined as the average values of magnetization and magnetostriction over a grain (Eqs. (15) and (16)):

$$\vec{M}_g = \langle \vec{M}_\alpha \rangle = \int_\alpha f_\alpha \vec{M}_\alpha\, d\alpha \approx \sum_\alpha f_\alpha \vec{M}_\alpha \tag{15}$$

$$\varepsilon_g^\mu = \langle \varepsilon_\alpha^\mu \rangle = \int_\alpha f_\alpha \varepsilon_\alpha^\mu\, d\alpha \approx \sum_\alpha f_\alpha \varepsilon_\alpha^\mu \tag{16}$$

This calculation has to be made for each grain of a polycrystalline aggregate. The knowledge of magneto-elastic loading at the grain scale ($\vec{H}_g$,$\boldsymbol{\sigma}_g$) is required to process this calculation. This local loading can be obtained from the knowledge of the macroscopic loading and some assumptions on the microstructure using an appropriate micro–macro scheme. The model presented in [21,22] is based on a self-consistent scheme derived from Hill's formulation [53]. Once the response at the grain scale ($\vec{M}_g$,ε_g^μ) is calculated, the macroscopic response ($\vec{M}$,ε^μ) of the material is simply obtained from averaging operations (Eqs. (17) and (18)):

$$\vec{M} = \langle \vec{M}_g \rangle \tag{17}$$

$$\varepsilon^\mu = \langle \varepsilon_g^\mu \rangle \tag{18}$$

Such an approach is fully multiaxial since the macroscopic mechanical loading $\boldsymbol{\sigma}$ is multiaxial. However, the corresponding computation time can be dissuasive for engineering design applications, particularly if a structural analysis is foreseen. However, in the particular case of a macroscopically isotropic material a simplified procedure can be defined [21]. It consists first in neglecting the fluctuations of magnetic field and stress over the volume (uniform magnetic field and stress assumptions). The heterogeneity of the elastic properties is also neglected. The polycrystal is then seen as an aggregate of randomly distributed magnetic domains, each macroscopic direction being considered as a possible easy direction [54]. The definition of the magnetization (Eq. (19)) and magnetostriction strain (Eq. (20)) of the polycrystal then follows the procedure used for single crystals:

$$\vec{M} = \int_\alpha f_\alpha \vec{M}_\alpha\, d\alpha \tag{19}$$

$$\varepsilon^\mu = \int_\alpha f_\alpha \varepsilon_\alpha^\mu\, d\alpha \tag{20}$$

Such a simplified description can provide analytical results in certain particular configurations and will be helpful for the definition of the generalized equivalent stress.

3.2. Equivalent stress methods

Another way to account for the multiaxiality of stress in magneto-elastic modeling is to define an equivalent stress. An equivalent stress for magnetic behavior is a fictive uniaxial stress that would change the magnetic behavior in a similar manner than the real multiaxial one. This equivalent stress can be implemented into a macroscopic uniaxial magneto-mechanical model. This method has been followed by several authors in the past years [24–27]. These equivalent stresses have been compared recently [29], we only briefly recall their definition hereafter.

Schneider and Richardson [24] proposed an equivalent stress for biaxial loadings applied to sheet specimen (Eq. (21)). It introduces σ_1 and σ_2 the eigenvalues of the stress tensor in the sheet plane, the magnetic field being applied along direction 1. Equibiaxial tension or compression is supposed to have no effect on the magnetic behavior:

$$\sigma_{eq}^{\mathrm{SR}} = \sigma_1 - \sigma_2 \tag{21}$$

On the basis of experimental biaxial measurements, Kashiwaya [25] proposed a slightly different definition (Eq. (22)), σ_1 being the eigenstress parallel to the magnetic field and $\sigma_{\max}$ the maximum eigenvalue of the stress tensor. K is a constant that can be adjusted for a better fitting of experimental results. This equivalent stress is always negative. Tensile stress or equi-biaxial compression is supposed to have no effect on the magnetic behavior:

$$\sigma_{eq}^{\mathrm{K}} = K(\sigma_1 - \sigma_{\max}) \tag{22}$$

Based on biaxial measurement results [30], Sablik et al. [26] proposed another definition (Eq. (23)). σ_1 and σ_2 are still the eigenvalues of the stress tensor in the sheet plane, the magnetic field being applied along direction 1. It can be noticed that the definition is discontinuous for $\sigma_1 = 0$ and that in the case of a uniaxial loading the equivalent stress does not reduce to the applied stress:

$$\begin{cases} \sigma_{eq}^{\mathrm{S}} = \frac{1}{3}(2\sigma_1 - \sigma_2) & \text{if } \sigma_1 < 0 \\ \sigma_{eq}^{\mathrm{S}} = \frac{1}{3}(\sigma_1 - 2\sigma_2) & \text{if } \sigma_1 \geq 0 \end{cases} \tag{23}$$

Pearson et al. [27], under similar assumptions and using the notations of Schneider and Richardson's proposal, make use of a function $g(\boldsymbol{\sigma})$ (Eq. (24)). The equivalent stress is not explicitly defined but using $\sigma_{eq} = \sigma_1$ for a uniaxial loading, an explicit expression can be obtained. Although more accurate than the previous proposals, this definition does not address the case of a magnetic field not aligned along an eigendirection of the stress tensor. Moreover this criterion is highly material and specimen dependent, and complicated to implement due to the large number of parameters to identify:

$$g(\boldsymbol{\sigma}) = k\sqrt{\sigma_1^2 + \sigma_2^2} + \sum_{n=1}^{6} a_n (f\sigma_1 - \sigma_2)^n + b\sigma_1 \tag{24}$$

In the configuration corresponding to a biaxial stress with eigenvalues in directions 1 and 2, and a magnetic field applied

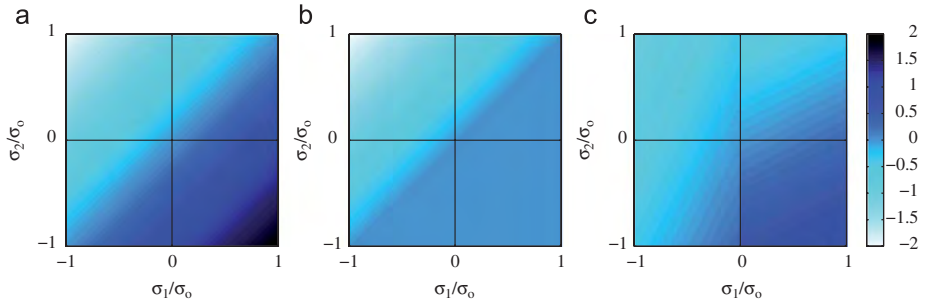

Fig. 7. Adimensional iso-values of several equivalent stress proposals (σ_{eq}/σ_0): (a) Schneider and Richardon [24]; (b) Kashiwaya [25] (with $K=1$); (c) Sablik et al. [26].

along direction 1, the different equivalent stress proposals have been compared in Fig. 7 (the adimensional ratio σ_{eq}/σ_0 is plotted as a function of σ_1/σ_0 and σ_2/σ_0. Pearson et al. proposal has not been reported due to the complexity of the parameter identification.

The former proposals for an equivalent stress exhibit strong limitations: the mechanical loading is restricted to biaxial stress, the magnetic field is necessarily applied along an eigendirection of the stress tensor and they are restricted to isotropic materials. The definition of a more general equivalent stress is requisite considering the much more complex range of combined magnetic and mechanical loadings that can be encountered in practical applications (see Section 1). The multiscale model in its continuous form gives directions of investigation. Homogeneous field and stress conditions over the grain are considered.

4. Equivalent stress definition from an equivalence in magneto-elastic energy

The following proposal of equivalent stress for isotropic materials based on an equivalence in magnetoelastic energy has been recently published [28].

Let us consider the definition of the magneto-elastic energy at the domain scale (Eq. (9)). An integration of the magneto-elastic energy over the volume leads to the macroscopic magneto-elastic energy so that

$$W^{\sigma} = -\int_{\alpha} f_{\alpha}\, \boldsymbol{\sigma}_g : \varepsilon^{\mu}_{\alpha}\, d\alpha \tag{25}$$

Since homogeneous stress condition ($\boldsymbol{\sigma}_g = \boldsymbol{\sigma}$) is assumed over the volume and using Eq. (20) we get

$$W^{\sigma} = -\int_{\alpha} f_{\alpha}\, \boldsymbol{\sigma} : \varepsilon^{\mu}_{\alpha}\, d\alpha = -\boldsymbol{\sigma} : \int_{\alpha} f_{\alpha}\, \varepsilon^{\mu}_{\alpha}\, d\alpha = -\boldsymbol{\sigma} : \varepsilon^{\mu} \tag{26}$$

$\boldsymbol{\sigma}$ is taken as multiaxial (six independent terms) in the orthonormal coordinate system ($\vec{e}_x$, $\vec{e}_y$, $\vec{e}_z$):

$$\boldsymbol{\sigma} = \begin{pmatrix} \sigma_{xx} & \sigma_{xy} & \sigma_{xz} \\ \sigma_{xy} & \sigma_{yy} & \sigma_{yz} \\ \sigma_{xz} & \sigma_{yz} & \sigma_{zz} \end{pmatrix} \tag{27}$$

Hypotheses must now be given on the macroscopic magnetostriction strain. The major hypothesis is to consider macroscopic magnetostriction as independent from stress, neglecting the so-called ΔE effect [54]. ε^{μ} is then only linked to the magnetic field strength and direction $\vec{H}$. Moreover magnetostriction is considered as isovolumetric (following a usual hypothesis for standard magnetic materials). Complementary hypotheses concern the symmetries of the material.

4.1. Isotropic material

In the case of an isotropic material, and considering a magnetic field applied along direction $\vec{e}_z$, ε^{μ} is given by

$$\varepsilon^{\mu} = \begin{pmatrix} -\frac{1}{2}\lambda(H) & 0 & 0 \\ 0 & -\frac{1}{2}\lambda(H) & 0 \\ 0 & 0 & \lambda(H) \end{pmatrix} \tag{28}$$

where $\lambda(H)$ is the deformation measured along the magnetic field direction. The magnetoelastic energy is given by

$$W^{\sigma} = \tfrac{1}{2}\sigma_{xx}\lambda(H) + \tfrac{1}{2}\sigma_{yy}\lambda(H) - \sigma_{zz}\lambda(H) = -\lambda(H)(\tfrac{3}{2}\sigma_{zz} - \tfrac{1}{2}(\sigma_{xx}+\sigma_{yy}+\sigma_{zz})) \tag{29}$$

In order to get a definition independent from the chosen coordinate system, the stress component in the direction of the magnetic field is written as $\sigma_{zz} = {}^t\vec{h}\boldsymbol{\sigma}\vec{h}$ where $\vec{h}$ denotes the direction of the applied field and ${}^t\vec{h}$ the transpose of $\vec{h}$. The frame associated to the magnetic field is $(\vec{h},\vec{t}_1,\vec{t}_2)$. We also recognize the trace of the stress tensor in Eq. (29): $\mathrm{tr}(\boldsymbol{\sigma}) = \sigma_{xx}+\sigma_{yy}+\sigma_{zz}$. The expression for the magnetoelastic energy is finally written, for any stress tensor $\boldsymbol{\sigma}$:

$$W^{\sigma} = -\lambda(H)(\tfrac{3}{2}{}^t\vec{h}\boldsymbol{\sigma}\vec{h} - \tfrac{1}{2}\,\mathrm{tr}(\boldsymbol{\sigma})) \tag{30}$$

Let now consider a uniaxial stress σ_u applied in the direction parallel to the magnetic field $\vec{h}$:

$$\boldsymbol{\sigma} = \begin{pmatrix} 0 & 0 & 0 \\ 0 & 0 & 0 \\ 0 & 0 & \sigma_u \end{pmatrix}_{(\vec{t}_1,\vec{t}_2,\vec{h})} \tag{31}$$

The corresponding magnetoelastic energy, according to Eq. (26) is simply

$$W^{\sigma}_u = -\lambda(H)\sigma_u \tag{32}$$

If we assume that the same magnetoelastic energy leads to the same magnetic behavior, the equivalent stress σ_{eq} is corresponding to the component σ_u once Eqs. (30) and (32) are considered equivalent. The following expression for the equivalent stress is finally obtained as

$$\sigma_{eq} = \sigma_u = \tfrac{3}{2}{}^t\vec{h}\boldsymbol{\sigma}\vec{h} - \tfrac{1}{2}\,\mathrm{tr}(\boldsymbol{\sigma}) = \tfrac{3}{2}{}^t\vec{h}\mathbf{s}\vec{h} \tag{33}$$

where $\mathbf{s}$ is the deviatoric part of the stress tensor $\boldsymbol{\sigma}$ ($\mathbf{s} = \boldsymbol{\sigma} - \frac{1}{3}\,\mathrm{tr}(\boldsymbol{\sigma})\mathbf{I}$, with $\mathbf{I}$ the identity second order tensor).

4.2. Orthotropic material

In the case of an orthotropic material, ε^{μ} has not a unique definition: it depends on the direction of the magnetic field with respect to the orthotropic frame. We consider first a magnetic field applied along a direction of orthotropy $\vec{e}_z$; ε^{μ} is diagonal in

the frame of orthotropy so that

$$\varepsilon^{\mu}=\begin{pmatrix}-\frac{(1+\beta)}{2}\lambda(H) & 0 & 0\\ 0 & -\frac{(1-\beta)}{2}\lambda(H) & 0\\ 0 & 0 & \lambda(H)\end{pmatrix}_{(\vec{e}_x,\vec{e}_y,\vec{e}_z)} \tag{34}$$

where coefficient β indicates a degree of orthotropy. Since orthotropy and magnetic field frame are coincident $((\vec{e}_x,\vec{e}_y,\vec{e}_z)=(\vec{t}_1,\vec{t}_2,\vec{h}))$, β can formally be defined as a ratio:

$$\beta=\frac{{}^t\vec{t}_2\varepsilon^{\mu}\vec{t}_2-{}^t\vec{t}_1\varepsilon^{\mu}\vec{t}_1}{{}^t\vec{t}_2\varepsilon^{\mu}\vec{t}_2+{}^t\vec{t}_1\varepsilon^{\mu}\vec{t}_1} \tag{35}$$

When $\beta=0$, the isotropic situation is recovered. $\beta=1$ condition is frequently encountered for sheet form specimens where the material exhibits a very low deformation through the thickness (non-oriented silicon–iron, iron–cobalt) due to a specific domain configuration [55]. Grain-oriented silicon–iron sheets exhibit on the other hand a value for β higher than 1 when the material is magnetized along the transversal direction for example [56]. The magnetoelastic energy is given by

$$W^{\sigma}=\frac{(1+\beta)}{2}\sigma_{xx}\lambda(H)+\frac{(1-\beta)}{2}\sigma_{yy}\lambda(H)-\sigma_{zz}\lambda(H) \tag{36}$$

Following the same mathematical developments than in the previous paragraph, we get a more complex definition of the equivalent stress:

$$\sigma_{eq}=\frac{3}{2}{}^t\vec{h}\mathbf{s}\vec{h}+\frac{\beta}{2}({}^t\vec{t}_2\mathbf{s}\vec{t}_2-{}^t\vec{t}_1\mathbf{s}\vec{t}_1) \tag{37}$$

This definition is limited to the cases where magnetic field is aligned with an orthotropic direction. This criterion is for example not applicable when the field is applied in a direction between the rolling or transverse direction for GO silicon steels. It is not applicable to the single crystalline situation when a direction other than $\langle 1\,0\,0\rangle$ or $\langle 1\,1\,0\rangle$ is considered.

We consider now that the magnetic field is not applied along a direction of orthotropy, ε^{μ} is nevertheless diagonal in its own eigenframe $(\vec{e}_I,\vec{e}_{II},\vec{e}_{III})$.[1] Eigenvalues are noted ε^{μ}_I, ε^{μ}_{II} and ε^{μ}_{III}, and verify $\varepsilon^{\mu}_I+\varepsilon^{\mu}_{II}+\varepsilon^{\mu}_{III}=0$. Parameters β_1 and β_2 are introduced so that $\varepsilon^{\mu}_I=\beta_1\lambda(H)$, $\varepsilon^{\mu}_{II}=\beta_2\lambda(H)$ and $\varepsilon^{\mu}_{III}=-(\beta_1+\beta_2)\lambda(H)$. The magnetostriction strain tensor is finally

$$\varepsilon^{\mu}=\begin{pmatrix}\beta_1\lambda(H) & 0 & 0\\ 0 & \beta_2\lambda(H) & 0\\ 0 & 0 & -(\beta_1+\beta_2)\lambda(H)\end{pmatrix}_{(\vec{e}_I,\vec{e}_{II},\vec{e}_{III})} \tag{38}$$

The magnetic field is not applied along $\vec{e}_I$, $\vec{e}_{II}$ or $\vec{e}_{III}$. It is written in the coordinate system using two spherical angles θ and ϕ:

$$\vec{h}=\begin{pmatrix}\cos\phi\,\sin\theta\\ \sin\phi\,\sin\theta\\ \cos\theta\end{pmatrix}_{(\vec{e}_I,\vec{e}_{II},\vec{e}_{III})} \tag{39}$$

Considering a stress tensor written in the eigenframe, the magnetoelastic energy is given by

$$W^{\sigma}=-\beta_1\sigma_{xx}\lambda(H)-\beta_2\sigma_{yy}\lambda(H)+(\beta_1+\beta_2)\sigma_{zz}\lambda(H) \tag{40}$$

The uniaxial stress σ_u considered for the expression of equivalent stress is applied along the magnetic field vector $\vec{h}$. The corresponding magnetoelastic energy is

$$W^{\sigma}_u=(-\beta_1\cos^2\phi\,\sin^2\theta-\beta_2\sin^2\phi\,\sin^2\theta+(\beta_1+\beta_2)\cos^2\theta)\sigma_u\lambda(H) \tag{41}$$

[1] The eigenframe is not rotating since magnetization rotation is not considered in the magnetization process. If magnetization rotation occurs, the frame is moving and a general formulation of equivalent stress is no more reachable.

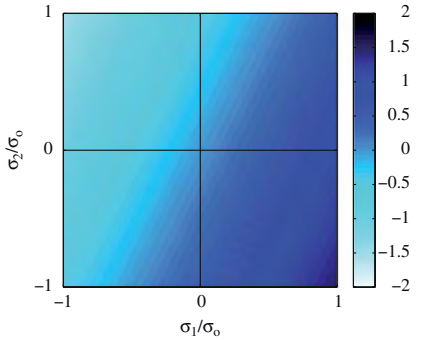

Fig. 8. Adimensional iso-values of deviatoric equivalent stress (σ_{eq}/σ_0).

A final form of equivalent stress is finally obtained, based on an equivalence in magneto-elastic energy and considering no magnetization rotation.

$$\sigma_{eq}=\frac{-\beta_1\sigma_{xx}-\beta_2\sigma_{yy}+(\beta_1+\beta_2)\sigma_{zz}}{-\beta_1\cos^2\phi\,\sin^2\theta-\beta_2\sin^2\phi\,\sin^2\theta+(\beta_1+\beta_2)\cos^2\theta} \tag{42}$$

The equivalent stress can be written as a function of the deviatoric stress tensor:

$$\sigma_{eq}=\frac{-\beta_1^t\vec{e}_I\,\mathbf{s}\,\vec{e}_I-\beta_2^t\vec{e}_{II}\,\mathbf{s}\,\vec{e}_{II}+(\beta_1+\beta_2)^t\vec{e}_{III}\,\mathbf{s}\,\vec{e}_{III}}{-\beta_1\cos^2\phi\,\sin^2\theta-\beta_2\sin^2\phi\,\sin^2\theta+(\beta_1+\beta_2)\cos^2\theta} \tag{43}$$

This final form is more general than the previous one. The major difficulty is to define the eigenframe of magnetostriction with respect to the directions of magnetic and mechanical loadings.

4.3. Discussion about the deviatoric equivalent stress—isotropic media

We are considering the simplest form of equivalent stress (Eq. (33)) defined by an equivalence in magneto-elastic energy for an isotropic material. The following properties can be highlighted:

- in the case of a uniaxial stress applied in the direction of the magnetic field, the equivalent stress is the applied stress;
- the definition can be applied to a fully multiaxial mechanical loading, not only biaxial;
- any orientation of the stress tensor with respect to the magnetic field can be considered;
- a hydrostatic pressure leads to an equivalent stress equal to zero, in agreement with the noneffect of hydrostatic pressure on magnetic behavior.

In the case of a biaxial mechanical loading (σ_1,σ_2), with $\vec{h}$ aligned with direction $\vec{e}_1$, the equivalent stress is given by

$$\sigma_{eq}=\sigma_1-\frac{\sigma_2}{2} \tag{44}$$

Results have been plotted in Fig. 8 (the adimensional ratio σ_{eq}/σ_0 is plotted as a function of σ_1/σ_0 and σ_2/σ_0). Comparison to experimental data will be presented in the final section.

5. Equivalent stress definition from an equivalence in magnetization

We look back to the original definition of the equivalent stress: it is the uniaxial stress that leads to a magnetic behavior corresponding to the magnetic behavior of the material submitted to the multiaxial stress. The magnetic field being imposed, the

magnetic response is the magnetization. The major difficulty is that magnetization depends on stress and magnetic field: effects cannot be easily separated. We propose here an approach using a surrogate multiscale model, only focused on the magneto-mechanical behavior of *one grain*, defined as an assembly of magnetic domains.

5.1. General formulation

Eq. (19) recalled here after (Eq. (45)) gives the definition of the macroscopic magnetization of the polycrystal using the surrogate multiscale model: isotropic material is seen as an assembly of magnetic domains equally distributed in the volume. The definition of the volumetric fraction follows the same approach (Eq. (46)):

$$\vec{M} = \int_\alpha f_\alpha \vec{M}_\alpha \, d\alpha \tag{45}$$

$$f_\alpha = \frac{\exp(-A_s \cdot W_\alpha)}{\int_\alpha \exp(-A_s \cdot W_\alpha)} \tag{46}$$

We suppose now that only the energetical terms associated to the loading have to be taken into account. This assumption means neglecting the role of magnetocrystalline anisotropy energy in the magnetization process. Moreover stress and magnetic field are supposed to be uniform within the material. We obtain the following definition of the volumetric fraction of a domain α:

$$f_\alpha = \frac{\exp(A_s\boldsymbol{\sigma} : \varepsilon_\alpha^\mu + A_s\mu_0\vec{H}\cdot\vec{M}_\alpha)}{\int_\alpha \exp(A_s\boldsymbol{\sigma} : \varepsilon_\alpha^\mu + A_s\mu_0\vec{H}\cdot\vec{M}_\alpha)} \tag{47}$$

Magnetization under multiaxial stress condition $\boldsymbol{\sigma}$ is given by

$$\vec{M} = \int_\alpha \frac{\exp(A_s\boldsymbol{\sigma} : \varepsilon_\alpha^\mu + A_s\mu_0\vec{H}\cdot\vec{M}_\alpha))}{\int_\alpha \exp(A_s\boldsymbol{\sigma} : \varepsilon_\alpha^\mu + A_s\mu_0\vec{H}\cdot\vec{M}_\alpha))\, d\alpha} \vec{M}^\alpha \, d\alpha \tag{48}$$

It has to be compared to the magnetization obtained under uniaxial stress condition $\boldsymbol{\sigma}_u$ applied in the direction of the magnetic field:

$$\vec{M}_u = \int_\alpha \frac{\exp(A_s\boldsymbol{\sigma}_u : \varepsilon_\alpha^\mu + A_s\mu_0\vec{H}\cdot\vec{M}_\alpha))}{\int_\alpha \exp(A_s\boldsymbol{\sigma}_u : \varepsilon_\alpha^\mu + A_s\mu_0\vec{H}\cdot\vec{M}_\alpha))\, d\alpha} \vec{M}^\alpha \, d\alpha \tag{49}$$

The uniaxial stress $\boldsymbol{\sigma}_u$ is finally corresponding to the equivalent stress $\boldsymbol{\sigma}_{eq}$ when $\vec{M} = \vec{M}_u$ so that σ_{eq} is a solution of the following equation:

$$\int_\alpha \frac{\exp(A_s\boldsymbol{\sigma}_{eq} : \varepsilon_\alpha^\mu + A_s\mu_0\vec{H}\cdot\vec{M}_\alpha))}{\int_\alpha \exp(A_s\boldsymbol{\sigma}_{eq} : \varepsilon_\alpha^\mu + A_s\mu_0\vec{H}\cdot\vec{M}_\alpha))d\alpha} \vec{M}^\alpha \, d\alpha = \int_\alpha \frac{\exp(A_s\boldsymbol{\sigma} : \varepsilon_\alpha^\mu + A_s\mu_0\vec{H}\cdot\vec{M}_\alpha))}{\int_\alpha \exp(A_s\boldsymbol{\sigma} : \varepsilon_\alpha^\mu + A_s\mu_0\vec{H}\cdot\vec{M}_\alpha))d\alpha} \vec{M}^\alpha \, d\alpha \tag{50}$$

with $\sigma_{eq} = {}^t\vec{h}\boldsymbol{\sigma}_{eq}\vec{h}$.

This equation is rather difficult to solve. Some previous works showed that an integration can be analytically done considering magnetic field or stress as zero [21,54]. A combination of the two loadings is necessary in the present case. A numerical resolution would be possible but our objective here is to propose an analytical expression for the equivalent stress. We then have to simplify Eq. (50) in order to identify σ_{eq}.

5.2. Multidomain model and application to the definition of the equivalent stress

The idea is to replace the volume integral by a discrete sum over a finite number of domains [57]. The domains must be equally distributed. The first admissible distribution is a cubic distribution (first terms of the spherical decomposition), where only six domain families are considered with magnetization along the six $\langle 1\,0\,0\rangle$ axes of an elementary cube (Fig. 9) in $(\vec{x},\vec{y},\vec{z})$ coordinate system. The coordinate system is supposed to be defined from the direction of the applied field so that: $(\vec{x},\vec{y},\vec{z}) = (\vec{h},\vec{t}_1,\vec{t}_2)$. This structure is simultaneously submitted to a magnetic field $\vec{H}$ (Eq. (51)) and to a multiaxial stress tensor $\boldsymbol{\sigma}$ (Eq. (52)):

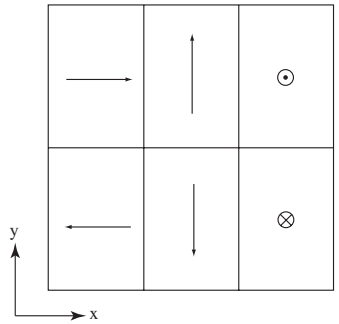

Fig. 9. Domain assembly representative for the material submitted to magnetic field and stress.

$$\vec{H} = H\vec{x} \tag{51}$$

$$\boldsymbol{\sigma} = \begin{pmatrix} \sigma_{xx} & \sigma_{xy} & \sigma_{xz} \\ \sigma_{xy} & \sigma_{yy} & \sigma_{yz} \\ \sigma_{xz} & \sigma_{yz} & \sigma_{zz} \end{pmatrix}_{xyz} \tag{52}$$

The definition of the magnetostriction strain tensor differs from the definition generally used for a domain because the average behavior has to be in accordance with the behavior of the isotropic material that this simple assembly of "domains" is supposed to model. Considering no rotation mechanism, the definition of the magnetostriction strain tensor in the domain frame (DF) is given by

$$\varepsilon'^\mu_\alpha = \begin{pmatrix} \lambda_m & 0 & 0 \\ 0 & -\frac{1}{2}\lambda_m & 0 \\ 0 & 0 & -\frac{1}{2}\lambda_m \end{pmatrix}_{DF} \tag{53}$$

λ_m is the maximum magnetostriction that can be reached by the isotropic material. This parameter can be identified from experimental measurements, but it can also be defined from the value of the single crystal magnetostriction coefficient λ_{100} or λ_{111}. In the previous work [54] it has been shown that the definition of λ_m depends on the material crystalline symmetry: $\lambda_m = 2/5\lambda_{100}\cdot k_a$ for positive magnetocrystalline constant materials (such as iron) and $\lambda_m = 3/5\lambda_{111}\cdot k_b$ for negative magnetocrystalline constant materials (such as nickel). k_a and k_b depend on the elastic properties of the single crystal [21] and on the hypotheses chosen for the description of the material. For instance, if we choose uniform stress (Reuss) hypotheses, we have $k_a = k_b = 1$, and if we choose uniform strain (Voigt) hypotheses, we have $k_a = 5\mu_a/(2\mu_a + 3\mu_b)$ and $k_b = 5\mu_b/(2\mu_a + 3\mu_b)$, μ_a and μ_b being the cubic shear moduli of the single crystal. For the sake of simplicity, we will choose $k_a = k_b = 1$, in further numerical applications.

The equivalent stress must now verify a discrete version of Eq. (50) so that

$$\sum_{\alpha=1\ldots6} \frac{\exp(A_s\boldsymbol{\sigma}_{eq} : \varepsilon'_\alpha\mu + A_s\mu_0\vec{H}\cdot\vec{M}_\alpha))}{\sum_{\alpha=1\ldots6}\exp(A_s\boldsymbol{\sigma}_{eq} : \varepsilon'_\alpha\mu + A_s\mu_0\vec{H}\cdot\vec{M}_\alpha))\vec{M}_\alpha} = \sum_{\alpha=1\ldots6} \frac{\exp(A_s\boldsymbol{\sigma} : \varepsilon'_\alpha\mu + A_s\mu_0\vec{H}\cdot\vec{M}_\alpha))}{\sum_{\alpha=1\ldots6}\exp(A_s\boldsymbol{\sigma} : \varepsilon'_\alpha\mu + A_s\mu_0\vec{H}\cdot\vec{M}_\alpha))\vec{M}_\alpha} \tag{54}$$

The potential energy of a domain family is now

$$W_\alpha = -\mu_0 \vec{H}\cdot\vec{M}_\alpha - \boldsymbol{\sigma} : \varepsilon'^{\mu}_{\alpha} \tag{55}$$

This energy term can be written for each of the six domain families submitted to the multiaxial stress:

$$W_1 = -\mu_0 H\cdot M_s - \sigma_{xx}\cdot\lambda_m + \sigma_{yy}\cdot\frac{\lambda_m}{2} + \sigma_{zz}\cdot\frac{\lambda_m}{2}$$

$$W_2 = \mu_0 H\cdot M_s - \sigma_{xx}\cdot\lambda_m + \sigma_{yy}\cdot\frac{\lambda_m}{2} + \sigma_{zz}\cdot\frac{\lambda_m}{2}$$

$$W_3 = W_4 = -\sigma_{yy}\cdot\lambda_m + (\sigma_{xx}+\sigma_{zz})\cdot\frac{\lambda_m}{2}$$

$$W_5 = W_6 = -\sigma_{zz}\cdot\lambda_m + (\sigma_{xx}+\sigma_{yy})\cdot\frac{\lambda_m}{2}$$

It can be noticed that the shear stresses σ_{xy}, σ_{xz} and σ_{yz} do not appear in the result. After calculation, the right hand term of Eq. (54) becomes

$$M_s\,\frac{\sinh(\mu_0 M_s A_s H)\,\exp\left(A_s\lambda_m\left(\sigma_{xx}-\frac{\sigma_{yy}}{2}-\frac{\sigma_{zz}}{2}\right)\right)}{\mathrm{A}+\mathrm{B}+\mathrm{C}}\,\vec{x} \tag{56}$$

with

$$\mathrm{A} = \cosh(\mu_0 M_s A_s H)\,\exp\left(A_s\lambda_m\left(\sigma_{xx}-\frac{\sigma_{yy}}{2}-\frac{\sigma_{zz}}{2}\right)\right)$$

$$\mathrm{B} = \exp\left(A_s\lambda_m\left(\sigma_{yy}-\frac{\sigma_{xx}}{2}-\frac{\sigma_{zz}}{2}\right)\right)$$

$$\mathrm{C} = \exp\left(A_s\lambda_m\left(\sigma_{zz}-\frac{\sigma_{xx}}{2}-\frac{\sigma_{yy}}{2}\right)\right)$$

Considering the equivalent uniaxial stress, the potential energy of a domain family is

$$W_\alpha = -\mu_0 \vec{H}\cdot\vec{M}_\alpha - \boldsymbol{\sigma}_{eq} : \varepsilon'^{\mu}_{\alpha} \tag{57}$$

We obtain the following energy terms for the six domain families:

$$W_1 = -\mu_0 H\cdot M_s - \sigma_{eq}\cdot\lambda_m$$

$$W_2 = \mu_0 H\cdot M_s - \sigma_{eq}\cdot\lambda_m$$

$$W_3 = W_4 = \sigma_{eq}\cdot\frac{\lambda_m}{2}$$

$$W_5 = W_6 = \sigma_{eq}\cdot\frac{\lambda_m}{2}$$

After calculation, the left hand term of Eq. (54) becomes

$$M_s\,\frac{\sinh(\mu_0 M_s A_s H)\,\exp(A_s\lambda_m\sigma_{eq})}{\cosh(\mu_0 M_s A_s H)\,\exp(A_s\lambda_m\sigma_{eq}) + 2\,\exp(-1/2A_s\lambda_m\sigma_{eq})}\vec{x} \tag{58}$$

Expressions (56) and (58) can be rewritten respectively in

$$M_s\frac{\sinh(\mu_0 M_s A_s H)}{\cosh(\mu_0 M_s A_s H) + \dfrac{\exp\left(A_s\lambda_m\left(\sigma_{yy}-\frac{\sigma_{xx}}{2}-\frac{\sigma_{zz}}{2}\right)\right)+\exp\left(A_s\lambda_m\left(\sigma_{zz}-\frac{\sigma_{xx}}{2}-\frac{\sigma_{yy}}{2}\right)\right)}{\exp\left(A_s\lambda_m\left(\sigma_{xx}-\frac{\sigma_{yy}}{2}-\frac{\sigma_{zz}}{2}\right)\right)}}\vec{x} \tag{59}$$

and

$$M_s\frac{\sinh(\mu_0 M_s A_s H)}{\cosh(\mu_0 M_s A_s H) + \dfrac{2\exp\left(-\frac{1}{2}A_s\lambda_m\sigma_u\right)}{\exp(A_s\lambda_m\sigma_u)}}\vec{x} \tag{60}$$

σ_{eq} being solution of Eq. (54), the equality of expressions (59) and (60) leads to

$$\exp\left(\frac{3}{2}A_s\lambda_m\sigma_{eq}\right) = \frac{2\exp\left(A_s\lambda_m\left(\sigma_{xx}-\frac{\sigma_{yy}}{2}-\frac{\sigma_{zz}}{2}\right)\right)}{\exp\left(A_s\lambda_m\left(\sigma_{yy}-\frac{\sigma_{xx}}{2}-\frac{\sigma_{zz}}{2}\right)\right)+\exp\left(A_s\lambda_m\left(\sigma_{zz}-\frac{\sigma_{xx}}{2}-\frac{\sigma_{yy}}{2}\right)\right)} \tag{61}$$

and finally after few calculations

$$\sigma_{eq} = \frac{2}{3A_s\lambda_m}\ln\left[\frac{2\exp\left(A_s\lambda_m\left(\sigma_{xx}-\frac{\sigma_{yy}}{2}-\frac{\sigma_{zz}}{2}\right)\right)}{\exp\left(A_s\lambda_m\left(\sigma_{yy}-\frac{\sigma_{xx}}{2}-\frac{\sigma_{zz}}{2}\right)\right)+\exp\left(A_s\lambda_m\left(\sigma_{zz}-\frac{\sigma_{xx}}{2}-\frac{\sigma_{yy}}{2}\right)\right)}\right] \tag{62}$$

This definition can be generalized to any frame $(\vec{h},\ \vec{t}_1,\ \vec{t}_2)$ associated to the magnetic field direction $\vec{h}$. We note k the product $A_s\lambda_m$ as a material dependent parameter:

$$\sigma_{eq} = {}^t\vec{h}\mathbf{s}\vec{h} - \frac{2}{3k}\ln\left[\frac{\exp\left(\frac{3k}{2}{}^t\vec{t}_1\mathbf{s}\vec{t}_1\right)+\exp\left(\frac{3k}{2}{}^t\vec{t}_2\mathbf{s}\vec{t}_2\right)}{2}\right] \tag{63}$$

Considering the definitions of A_s and λ_m, and using the hypothesis of uniform stress ($k_a = k_b = 1$) we get

$$k = \frac{6\chi_0\lambda_{100}}{5\mu_0 M_s^2} \tag{64}$$

for positive magnetocrystalline anisotropy materials and

$$k = \frac{9\chi_0\lambda_{111}}{5\mu_0 M_s^2} \tag{65}$$

for negative magnetocrystalline anisotropy materials. χ_0 denotes the initial anhysteretic susceptibility of the material, μ_0 the permeability of vacuum and M_s the saturation magnetization of the material. This definition of equivalent stress finally requires to know some relatively usual material parameters and *no supplementary adjusting parameter*. This new expression for the equivalent stress generalizes the deviatoric expression (Eq. (33)) and is applicable to cases of more intense loadings and/or highly magnetostrictive materials. The effect of stress on magnetostriction (ΔE effect) is taken into account. An extension to anisotropic materials is possible following the strategy developed in Section 3.2. This new expression will be referred to as the generalized equivalent stress in the following.

5.3. Discussion about the generalized equivalent stress

The properties that can be highlighted are very similar to the properties of the deviatoric equivalent stress:

- in the case of a uniaxial stress applied in the direction of the magnetic field, the equivalent stress is the applied stress;
- the definition can be applied to a fully multiaxial mechanical loading, not only biaxial;
- any orientation of the stress tensor with respect to the magnetic field can be considered;
- a hydrostatic pressure leads to an equivalent stress equal to zero, in agreement with the noneffect of hydrostatic pressure on magnetic behavior.

In the case of a biaxial mechanical loading with eigenstresses (σ_1,σ_2), the deviatoric tensor is

$$\mathbf{s} = \begin{pmatrix} \frac{2}{3}\sigma_1 - \frac{1}{3}\sigma_2 & 0 & 0 \\ 0 & \frac{2}{3}\sigma_2 - \frac{1}{3}\sigma_1 & 0 \\ 0 & 0 & -\frac{1}{3}(\sigma_1+\sigma_2) \end{pmatrix} \tag{66}$$

If $\vec{h}$ is aligned with direction $\vec{e}_1$ the equivalent stress is given by

$$\sigma_{eq} = \frac{2}{3}\sigma_1 - \frac{1}{3}\sigma_2 - \frac{2}{3k}\ln\left[\frac{\exp(k(\sigma_2-\frac{1}{2}\sigma_1))+\exp(k(-\frac{1}{2}\sigma_2-\frac{1}{2}\sigma_1))}{2}\right] \tag{67}$$

that can be simplified into

$$\sigma_{eq} = \sigma_1 - \frac{2}{3k}\ln\left[\frac{\exp\left(\frac{3k}{2}\sigma_2\right)+1}{2}\right] \tag{68}$$

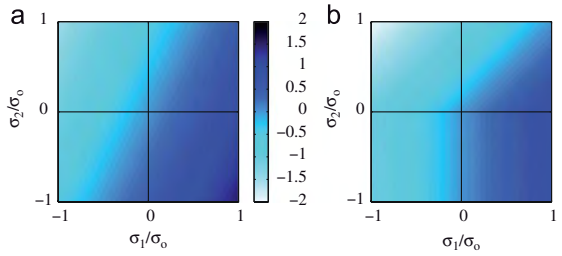

Fig. 10. Adimensional iso-values of generalised equivalent stress (σ_{eq}/σ_0)—for $k>0$ and (a) $|k\sigma_2| \ll 1$; (b) $|k\sigma_2| \gg 1$.

A direct plot of the generalized equivalent stress is not possible since parameter k is material dependent. We observe that the final expression is more or less complex depending on the stress value along $\vec{e}_2$ axis:

- for $\sigma_2 = 0$, $\sigma_{eq} = \sigma_1$;
- for $|k\sigma_2 \ll 1|$, a Taylor expansion of exponential and logarithm gives

$$\sigma_{eq} \sim \sigma_1 - \frac{2}{3k}\ln\left[\frac{\frac{3k}{2}\sigma_2+2}{2}\right] \sim \sigma_1 - \frac{2}{3k}\ln\left[\frac{3k}{4}\sigma_2+1\right] \sim \sigma_1 - \frac{1}{2}\sigma_2$$

  reducing to the deviatoric equivalent stress (no assumption is necessary concerning the stress level along $\vec{e}_1$ axis). This situation is illustrated in Fig. 10a (the adimensional ratio σ_{eq}/σ_0 is plotted as a function of σ_1/σ_0 and σ_2/σ_0). The deviatoric equivalent stress can be seen as a particular case of the generalized equivalent stress;
- for $k\sigma_2 \gg 1$, $\frac{1}{2}$ can be neglected compared to the exponential. We obtain the following estimation:

$$\sigma_{eq} \sim \sigma_1 - \frac{2}{3k}\ln\left[\frac{\exp\left(\frac{3k}{2}\sigma_2\right)}{2}\right] \sim \sigma_1 - \sigma_2 + \frac{2\ln 2}{3k}$$

  close to Schneider–Richardson proposal. This situation is illustrated in Fig. 10b for positive values of σ_2 (the adimensional ratio σ_{eq}/σ_0 is plotted as a function of σ_1/σ_0 and σ_2/σ_0. The Schneider–Richardson equivalent stress can be seen as a particular case of the generalized equivalent stress;
- for $k\sigma_2 \ll -1$, the exponential becomes negligible. We obtain the following estimation:

$$\sigma_{eq} \sim \sigma_1 - \frac{2}{3k}\ln\left(\frac{1}{2}\right) \sim \sigma_1 + \frac{2\ln 2}{3k}$$

  The criterion is now strongly associated to the value of σ_1. This situation is illustrated by vertical lines in Fig. 10b for negative values of σ_2 (the adimensional ratio σ_{eq}/σ_0 is plotted as a function of σ_1/σ_0 and σ_2/σ_0). This situation was not covered by any criterion of literature;
- intermediate values of $k\sigma_2$ will give a continuous criterion between the previous extremal solutions;
- a change of sign of k (*i.e.* change of sign of magnetostriction) will give a symmetric plot with respect to $\vec{e}_1$ axis.

A comparison to experimental data is presented in the next section.

6. Comparison experiments-modeling—magnetic behavior of Fe–Co thin sheet submitted to biaxial mechanical loading

The material used for experiments is a 49%Co–49%Fe–2%V alloy delivered in 0.5 mm thick sheets format (industrial denomination: AFK 502-R from Imphy Alloys). Cobalt-based alloys are usually known to exhibit a strong saturation magnetization ($M_s = 1.91 \times 10^6$ A/m), that promotes high torque/weight performances for aeronautic equipments. Experiments consist in anhysteretic magnetic measurements carried out under uniaxial and biaxial mechanical stress in homogeneous magnetic and mechanical conditions. A full description of the two set-ups used for measurements can be found in [54] for uniaxial set-up (Fig. 11a) and in [35] for biaxial set-up (Fig. 11b).

6.1. Magnetic and magnetostrictive measurements under uniaxial mechanical loading

The benchmark for magneto-mechanical measurements is detailed in [54]. Measurements carried out are anhysteretic (reversible) magnetic behavior $M(H)$, "parallel" (parallel to the magnetic field direction) and "perpendicular" (perpendicular to the magnetic field direction) magnetostrictive behavior (resp. $\varepsilon^{\mu}_{\parallel}$ and $\varepsilon^{\mu}_{\perp}$).[2] The applied stress is positive (tension). Fig. 12 shows the evolution of the magnetization curve with respect to the applied stress: we observe a clear increase in susceptibility with increasing stress. Corresponding magnetostrictive behavior has been plotted in Figs. 13a and b. The behavior seems roughly isotropic since perpendicular magnetostriction is negative and about half the amplitude of parallel magnetostriction. Influence of stress is also illustrated: tensile stress progressively saturates the magnetostriction.

Measurements have been carried out on a sample cut along the rolling direction. Measurements along the transverse direction (TD) give similar results. As expected from magnetostrictive measurements, the magneto-mechanical behavior can be considered as isotropic.

6.2. Magnetic measurements under biaxial mechanical loading

These experimental results have already been published in [35]. We recall the main results. Seventeen biaxial stress conditions (σ_1, σ_2) have been tested, for stress level varying from -60 to $+60$ MPa. The magnetic field is applied along direction 1. Mechanical loading can be divided into parallel uniaxial tests ($\sigma_1 \neq 0, \sigma_2 = 0$), orthogonal uniaxial tests ($\sigma_1 = 0, \sigma_2 \neq 0$), equibiaxial tests ($\sigma_1 = \sigma_2$), and shear tests ($\sigma_1 = -\sigma_2$) in order to map the stress plane.

Fig. 14 shows the evolution of the anhysteretic $M(H)$ curve for the parallel uniaxial situation ($\sigma_1 \neq 0, \sigma_2 = 0$). Results are in accordance with measurements carried out using uniaxial set-up: improvement of the magnetization behavior with positive stress. We observe a stronger opposite effect due to compression. Fig. 15 shows the evolution of the anhysteretic $M(H)$ curve for the orthogonal uniaxial situation ($\sigma_1 = 0, \sigma_2 \neq 0$). The effect of the stress level is strongly reduced compared to the previous situation. The sign of the stress is not a dominant parameter since magnetic susceptibility is deteriorated whatever the situation. The deterioration seems a little stronger with positive stress. The equibiaxial situation (Fig. 16) is characterized by a relative insensitivity to stress when the stress value is positive (equibitraction). The equibicompression on the contrary sharply deteriorates the magnetic behavior. The shear situation (Fig. 17) is the worst situation for the magnetic behavior except when σ_1 remains positive. The lowest susceptibility is reached with $\sigma_1 = -60$ MPa and $\sigma_2 = +60$ MPa.

[2] The readers will find in [54] all experimental details in order to carry out precise measurement of magnetostriction avoiding the difficulties due to the tensile loading.

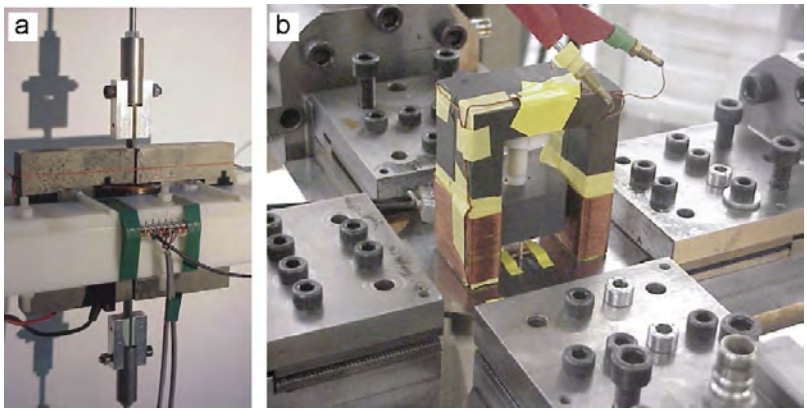

Fig. 11. (a) Benchmark for magnetic and magnetostrictive measurements under tensile stress; (b) general view of the experimental apparatus for magnetic measurement under biaxial stress loading.

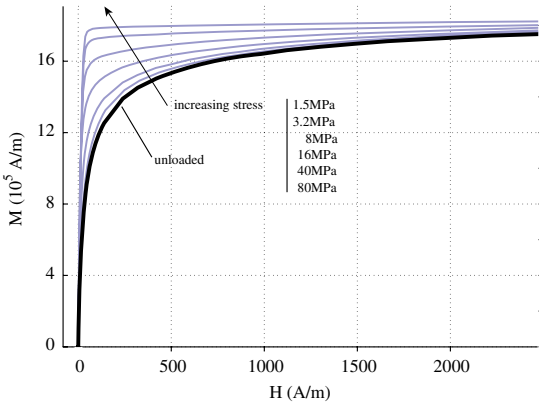

Fig. 12. Anhysteretic curve of Fe–Co submitted to uniaxial stress.

A dominant influence of stress level along the axis of magnetic measurement (σ_1) seems to be observed for equibiaxial ($\sigma_1=\sigma_2$) and shear ($\sigma_1=-\sigma_2$) conditions; it is especially sensitive when the stress along the orthogonal axis is negative. This analysis also applies for experiments carried out under uniaxial stress. We draw the evolution of the secant susceptibility $\chi=M/H$ in the stress plane in order to illustrate the main trends: $\chi(\sigma_1,\sigma_2)$. Fig. 18a and b plot χ for $H=250$ and 2500 A/m respectively. The level of magnetic field does not seem a determinant factor. The tension-compression asymmetry is easily perceptible on both graphs. The figures show that a bitraction hardly changes the susceptibility while a bicompression can divide it by two. A compression in a direction perpendicular to the magnetic field has a weak effect, while a tension notably decreases the susceptibility. The lowest values of χ are reached in the upper left side of the graph, corresponding to the shear situation with negative σ_1.

6.3. Equivalent stresses validation by comparison to biaxial experimental data

In this section, a validation of the several equivalent stress proposals is proposed. Kashiwaya (K), Schneider and Richardson (SR), Sablik et al. (S), deviatoric (d) and generalized (g) equivalent stress proposals have been detailed in sections 2.2, 3.1 and 4.2. The validation is based on a comparison to biaxial magneto-mechanical measurements. The loading configuration consists in a biaxial stress tensor $\boldsymbol{\sigma}$ superimposed to a magnetic field $\vec{H}$ aligned in the direction parallel to the first principal stress. This

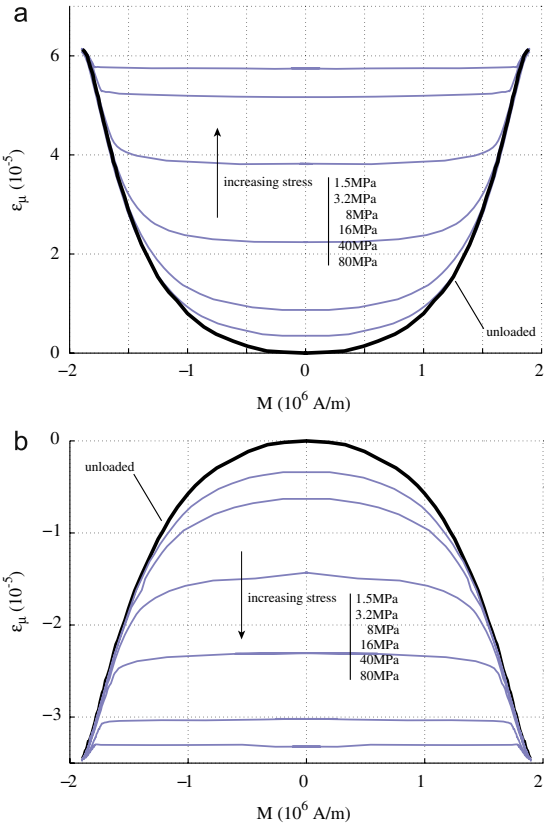

Fig. 13. Anhysteretic magnetostriction curves of Fe–Co submitted to uniaxial stress. (a) Parallel magnetostriction, (b) perpendicular magnetostriction.

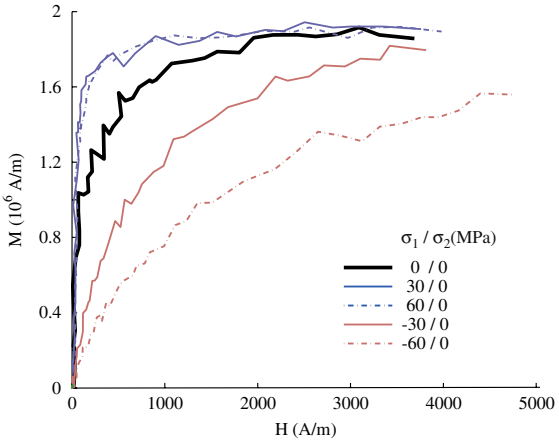

Fig. 14. Anhysteretic $M(H)$ behavior under uniaxial stress: $\vec{\sigma} \| \vec{H}$.

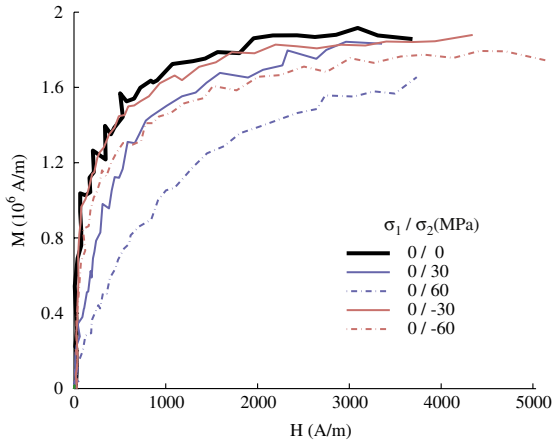

Fig. 15. Anhysteretic $M(H)$ behavior under uniaxial stress: $\vec{\sigma} \perp \vec{H}$.

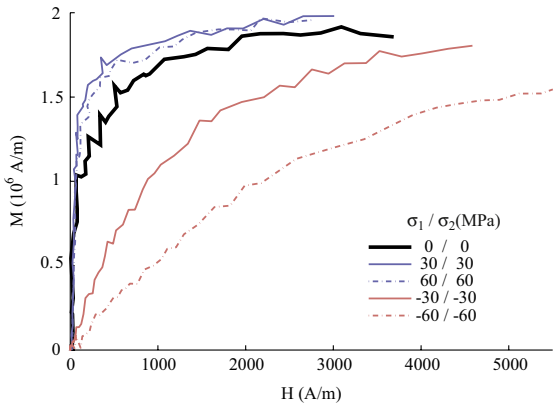

Fig. 16. Anhysteretic $M(H)$ behavior under equibiaxial stress: $\sigma_1 = \sigma_2$.

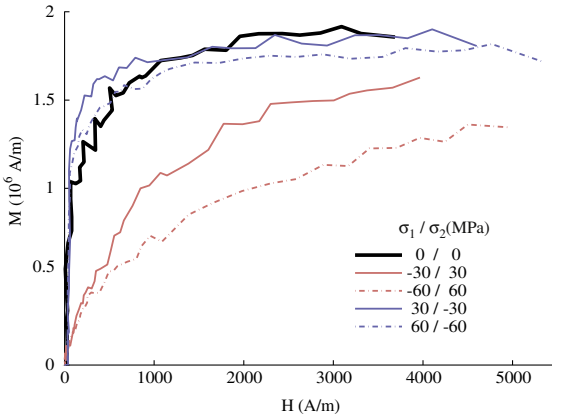

Fig. 17. Anhysteretic $M(H)$ behavior under shearing stress: $\sigma_1 = -\sigma_2$.

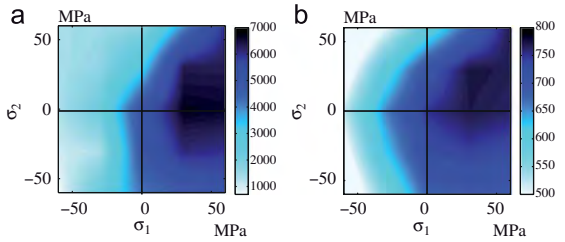

Fig. 18. Normalized susceptibility (experimental results) – H=250 A/m (a) H=2500 A/m (b) – $\vec{H} \| \vec{1}$.

configuration is given by

$$\boldsymbol{\sigma} = \begin{pmatrix} \sigma_1 & 0 \\ 0 & \sigma_2 \end{pmatrix} \text{and } \vec{H} = \begin{pmatrix} H \\ 0 \end{pmatrix} \tag{69}$$

The magnetic property of interest for this comparison is the magnetic susceptibility under stress. The validation process is based on four steps:

1. The magnetic susceptibility under uniaxial stress needs to be identified first. It has been collected from various sources (Sections 5.1 and 5.2, and Ref. [50]) for samples exhibiting the same composition. These different results are very consistent. They have been plotted in Figs. 19 and 20 respectively for an applied magnetic field of H=250 and 2500 A/m. It is reminded that the magnetic field H is applied in the direction parallel to the – uniaxial – applied stress σ. For modeling purpose, the evolution of the susceptibility as a function of stress has been interpolated, plotted as a full line in Figs. 19 and 20. The interpolation function $\chi = p(\sigma)$ will be used in the following steps.
2. The predicted susceptibility under biaxial stress is then calculated. For K, SR and S and deviatoric equivalent stresses, formulas (21)–(23) and (33) are applied directly. In the case of the generalized equivalent stress, some material parameters are necessary to apply Eq. (63). These material parameters can be identified from unloaded measurements of Figs. 12 and 13: $\lambda_m \approx 65 \times 10^{-6}$, $\chi_0 \approx 3000$ and $M_s = 1.91 \times 10^6$ A/m. Once each equivalent stress σ_{eq} is calculated for a given multiaxial stress $\boldsymbol{\sigma}$, the corresponding predicted susceptibility χ^p is calculated using the polynomial interpolation: $\chi^p = p(\sigma_{eq})$.

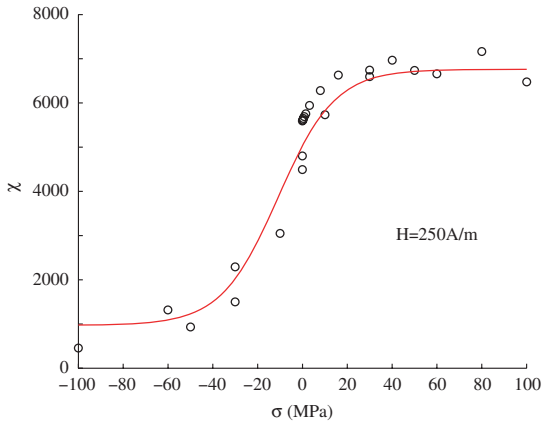

Fig. 19. Magnetic secant susceptibility of iron–cobalt as a function of uniaxial stress for $H=250$ A/m.

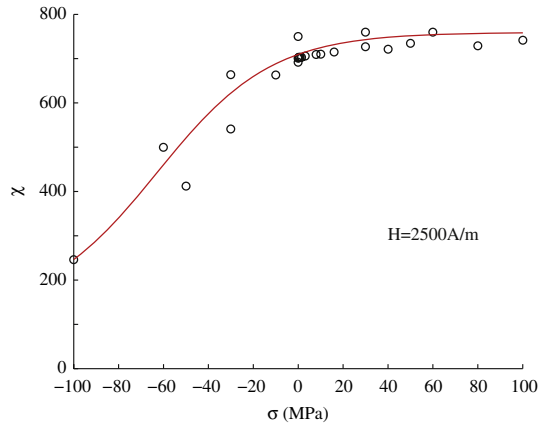

Fig. 20. Magnetic secant susceptibility of iron–cobalt as a function of uniaxial stress for $H=2500$ A/m.

3. Experimental results for the susceptibility χ^e under biaxial stress need to be collected. Such biaxial magneto-mechanical measurements have been detailed in Ref. [35] and recalled in Section 5.2. They are reported in Fig. 18, for $H=250$ and 2500 A/m.
4. The modeling results of step (2) are compared to independent experimental results of step (3) by the calculation of an error indicator. For each equivalent stress proposal the quantity e (Eq. (70)) is calculated. The lower this indicator, the more accurate the equivalent stress:

$$e = 100 \times \frac{|\chi_p - \chi_e|}{\chi_e} \tag{70}$$

Figs. 21 and 22 plot the error criterion e for K, SR, S, d and g equivalent stresses respectively for $H=250$ A/m and $H=2500$ A/m.

For all criteria except the generalized equivalent stress under high magnetic field, the errors observed are higher in equibicompression than for other loadings. In the case of a stress (σ_1, σ_2)=(−60 MPa, −60 MPa) and for a magnetic field $H=250$ A/m, the error is up to 635% for K and SR, 371% for S, 238% for d and 117% for g equivalent stress. For reading convenience the error values have been truncated at 100% to highlight the prediction out of the bicompression area. If the field is increased to $H=2500$ A/m, the error is up to 70% for K and SR, 57% for S, 50% for d and 44% for g equivalent stress. In that case, the generalized stress proposal exhibits higher error levels in the upper right part of the plot, in an area of strong shear stress. The error values have been truncated at 50% for reading convenience. Errors are lower in that latter case because the effect of stress on the magnetic behavior is less sensitive close to magnetic saturation (see for instance Fig. 12).

The deviatoric stress had already been shown to provide a significant improvement of the predicted susceptibility compared to K, SR and S proposals [29]. This result could be reinforced by taking into account the weak anisotropy of the material and choosing the orthotropic version of the deviatoric equivalent stress criterion. Compared to all previous proposals, adding a few material dependent parameters (λ_m, χ_0 and M_s) in the equivalent stress definition, the generalized equivalent stress is a significant improvement for the definition of the magnetic susceptibility under bicompression. These latter equivalent stress definitions make conceivable the use of equivalent stress models even in the case of bi-compressive mechanical loadings. Moreover it is to be recalled that the definition of deviatoric and generalized proposals are applicable for any multiaxial configuration—not only biaxial.

7. Conclusion

In this paper new proposals of equivalent stress for magneto-mechanical behavior have been presented. Equivalent stress is defined as the uniaxial mechanical loading, applied in the direction parallel to the applied magnetic field, that induces the same effect on the magnetic behavior than the corresponding multiaxial stress. The first proposal called "deviatoric equivalent stress" is defined thanks to an equivalence in magnetoelastic energy. The second proposal called "generalized equivalent stress" is defined thanks to an equivalence in magnetization for a given magnetic field. This proposal can be seen as a generalization of the deviatoric equivalent stress. Some stronger simplifications allow on the other hand to build the Schneider and Richardson criterion. The generalized equivalent stress has been constructed after simplification of a full 3D magneto-elastic multiscale model, neglecting the impact of magnetocrystalline energy and thanks to a cubic reconstruction of an idealized isotropic distribution of domains. It must be noticed that the deviatoric definition is easier to use; it may be preferred when $|k\sigma_2| \ll 1$ condition can be assumed (σ_2 is the eigenstress orthogonal to the magnetization direction).

Comparisons to experimental results carried out under biaxial loading show that the generalized equivalent stress gives more accurate predictions than the previous proposals. The criterion reflects the major influence of the stress level along the magnetization axis, especially when stress along the second axis is negative. The deviatoric and generalized equivalent stresses are not restricted to biaxial mechanical loadings and do not require any assumption on the magnetic field direction. The generalized form accounts for the magnetostrictive and magnetic constants of the material and thus reflects the different sensitivity of the magnetic behavior to a mechanical loading depending on the considered material.

This new definition can help to revisit and discuss some previous results of the literature. The results of Pearson et al. [27] and Maurel et al. [33] are accessible and can be re-interpreted. Pearson et al. obtained maps of the relative variation of the coercive field (%) in the biaxial stress plane for a pure iron. Fig. 23a shows the corresponding results. Maurel et al.

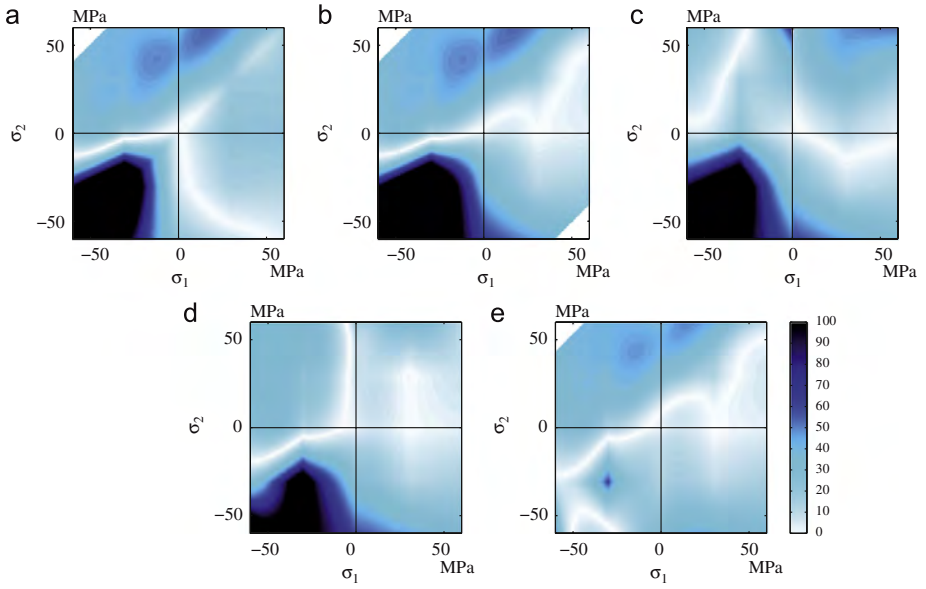

Fig. 21. Error (%) on the magnetic susceptibility estimates in the stress plane for $H=250$ A/m: (a) Kashiwaya (with $K=1$), (b) Schneider and Richardson, (c) Sablik et al., (d) deviatoric and (e) generalized ($k=1.277\times10^{-7}$ m^3 J^{-1}) equivalent stresses.

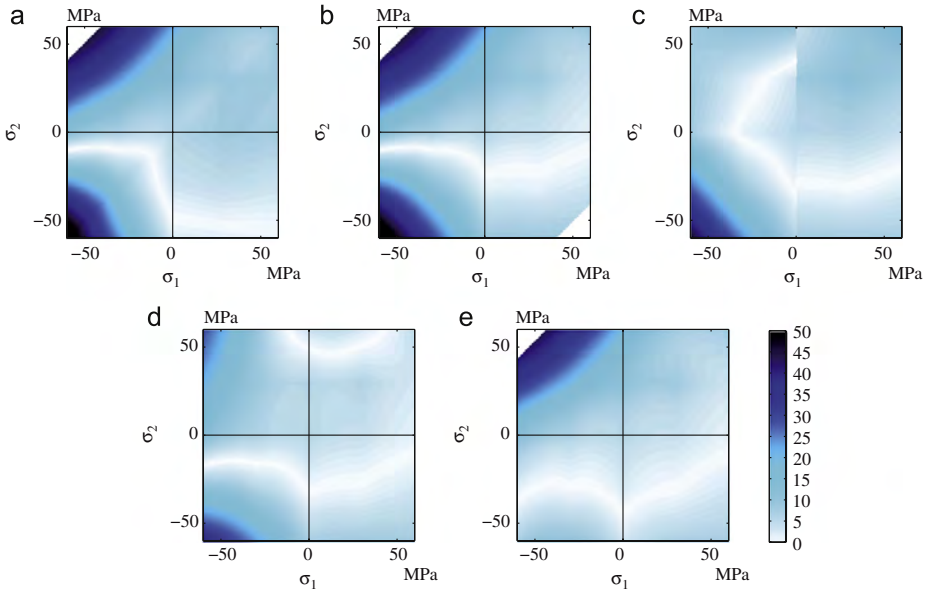

Fig. 22. Error (%) on the magnetic susceptibility estimates in the stress plane for $H=2500$ A/m: (a) Kashiwaya (with $K=1$), (b) Schneider and Richardson, (c) Sablik et al., (d) deviatoric and (e) generalized ($k=1.277\times10^{-7}$ m^3 J^{-1}) equivalent stresses.

plotted the evolution of a normalized initial permeability (ratio of initial permeability under stress with initial permeability of the unloaded material) in the biaxial stress plane for a 3%Si–Fe electrical steel. Fig. 23b shows the corresponding results. These results can be compared with the prediction of the generalized equivalent stress. Fig. 23c shows the equivalent stress associated to a parameter $k=1.96\times10^{-8}$ m^3 J^{-1} in adequation with the two materials investigated (arbitrary units have been chosen). The main difference with the experiments reported in this paper is the low magnitude of λ_m estimated to $\lambda_m=10\times10^{-6}$. The variations of the equivalent stress in the sheet plane seem to be in accordance with experimental results. This simulation confirms the ability of prediction of the new generalized equivalent stress.

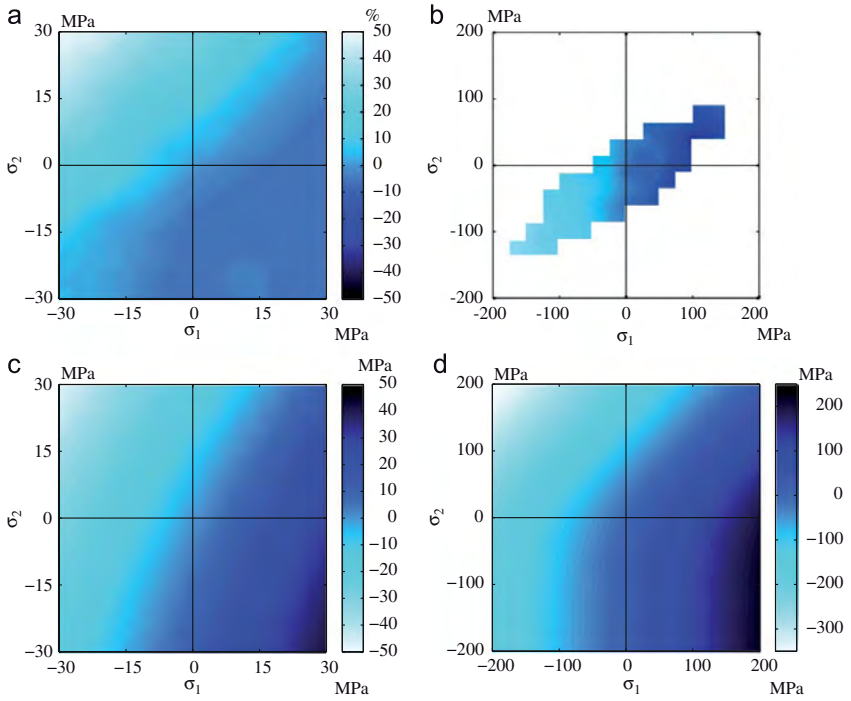

Fig. 23. Prediction of equivalent stress in the stress plane from generalized criterion, applied to iron-based alloys and comparison to previous experimental data – (a) Results from Pearson [27] – coercivity change as a function of biaxial stress. The color scale gives percentage of the stress-free coercivity; (b) results from Maurel [33] – initial normalized permeability – defined as the ratio between permeability under stress and stress-free permeability; (c) equivalent stress map – $k=1.96\times10^{-8}\ m^3\,J^{-1}$ for $\{\sigma_1,\sigma_2\}\in$ [-30 MPa,30 MPa] – comparison to results from Pearson; (d) equivalent stress map $-k=1.96\times10^{-8}\ m^3\,J^{-1}$ for $\{\sigma_1,\sigma_2\}\in$ [-200 MPa,200 MPa] – comparison to results from Maurel.

Complementary experiments are foreseen in order to validate or extend the equivalent stress proposals:

- experiments involving a magnetic field direction out of the mechanical eigenaxes;
- experiments involving measurement of the hysteresis losses and magnetostriction;

Acknowledgments

The authors wish to thank C. Doudard and V. Blanc for their contribution in experimental measurements. They wish to thank ArcelorMittal Stainless & Nickel Alloys for providing material and heat treatments after machining. This work was supported by French council for research (CNRS).

References

[1] C. Mateucci, Ann. Chim. Phys. 53 (1858) 358.
[2] E. Villari, Ann. Phys. Chem. 126 (1865) 87.
[3] R.M. Bozorth, in: D. Van (Ed.), Ferromagnetism, Norstand Company, NY, 1951.
[4] B.D. Cullity, Introduction to Magnetic Materials, Addison-Wesley, 1972.
[5] D.L. Atherton, D.C. Jiles, IEEE Trans. Magn. 19 (1983) 2021.
[6] D.C. Jiles, D.L. Atherton, J. Phys. D Appl. Phys. 17 (1984) 1265.
[7] M.J. Sablik, D.C. Jiles, IEEE Trans. Magn. 29 (1993) 2113.
[8] M. Zucca, P.E. Roccato, O. Bottauscio, C. Beatrice, IEEE Trans. Magn. 46 (2010) 183.
[9] A. Bergqvist, G. Engdahl, IEEE Trans. Magn. 27 (1991) 2623.
[10] A. Bergqvist, G. Engdahl, J. Appl. Phys. 72 (1994) 5496.
[11] D. Davino, A. Giustiniani, C. Visone, IEEE Trans. Magn. 44 (2008) 3193.
[12] O. Bottauscio, P.E. Roccato, M. Zucca, IEEE Trans. Magn. 46 (2010) 3022.
[13] C.P. Sasso, V. Basso, M. Lobue, G. Bertotti, J. Appl. Phys. 87 (2000) 4774.
[14] X.J. Zheng, X.E. Liu, J. Appl. Phys. 97 (2005) 053901.
[15] O. Perevertov, J. Phys. D Appl. Phys. 40 (2007) 949.
[16] H. Hauser, J. Appl. Phys. 75 (1994) 2584.
[17] W.D. Armstrong, J. Appl. Phys. 81 (1997) 2321.
[18] N. Buiron, L. Hirsinger, R. Billardon, J. Phys. IV 11 (1999) 187.
[19] W.D. Armstrong, J. Appl. Phys. 91 (2002) 2202.
[20] Y. Wan, D. Fang, K.C. Hwang, Int. J. Non-Linear Mech. 38 (2003) 1053.
[21] L. Daniel, O. Hubert, N. Buiron, R. Billardon, J. Mech. Phys. Solids 56 (2008) 1018.
[22] L. Daniel, N. Galopin, Eur. Phys. J. Appl. Phys. 42 (2008) 153–159.
[23] M.J. Sablik, B. Augustyniak, M. Chmielewski, J. Appl. Phys. 85 (1999) 4391.
[24] C.S. Schneider, J.M. Richardson, J. Appl. Phys. 53 (1982) 8136.
[25] K. Kashiwaya, Jpn. J. Appl. Phys. 30 (1991) 2932.
[26] M.J. Sablik, L.A. Riley, G.L. Burkhardt, H. Kwun, P.Y. Cannell, K.T. Watts, R.A. Langman, J. Appl. Phys. 75 (1994) 5673.
[27] J. Pearson, P.T. Squire, M.G. Maylin, J.G. Gore, IEEE Trans. Magn. 36 (2000) 3251.
[28] L. Daniel, O. Hubert, J. Appl. Phys. 105 (2009) 07A313.
[29] L. Daniel, O. Hubert, IEEE Trans. Magn. 46 (2010) 3089.
[30] R.A. Langman, IEEE Trans. Mag. 26 (1990) 1243.
[31] M.J. Sablik, M.Q. Smith, C.J. Waldhart, D.A. McKee, B. Augustyniak, J. Appl. Phys. 84 (1998) 6239.
[32] J. Pearson, P.T. Squire, M.G. Maylin, J.G. Gore, IEEE Trans. Magn. 36 (2000) 3599.
[33] V. Maurel, F. Ossart, Y. Marco, R. Billardon, J. Appl. Phys. 93 (2003) 7115.
[34] O. Hubert, M. Chaabane, J. Jumel, V. Maurel, F. Alves, A.D. Bensalah, M. Besbes, K. Azoum, L. Daniel, F. Bouillault, Przeglad Elektrotechniczny 81 (2005) 19.
[35] O. Hubert, Przeglad Elektrotechniczny 83 (2007) 70.
[36] B. Bolund, H. Bernhoff, M. Leijon, Renew. Sust. Energy Rev. 11 (2007) 235.
[37] O. Hubert, M. Clavel, I. Guillot, E. Hug, J. Phys. IV 9 (1999) 207.
[38] E. Hug, O. Hubert, J.J. Van Houtte, Mater. Sci. Eng. A 332 (2002) 193.
[39] O. Hubert, E. Hug, Mater. Sci. Technol. 11 (1995) 482.
[40] F. Ossart, E. Hug, O. Hubert, C. Buvat, R. Billardon, IEEE Trans. Magn. 36 (2000) 3137.
[41] A. Daikoku, M. Nakano, S. Yamaguchi, Y. Tani, Y. Toide, H. Arita, T. Yoshioka, C. Fujino, in: IEEE International Conference on Electric Machines and Drives, 2005, p. 366.

[42] L. Bernard, X. Mininger, L. Daniel, G. Krebs, F. Bouillault, M. Gabsi, Effect of stress on switched reluctance motors: a magneto-elastic finite element approach based on multiscale constitutive laws, IEEE Trans. Magn. submitted for publication.
[43] W.F. Brown, Micromagnetics, Wiley, New York, USA, 1963.
[44] J. Fidler, T. Schre, J. Phys. D 33 (2000) R135.
[45] S. He, Ph.D Thesis, University Paris, vol. 6, 1999.
[46] A. De Simone, R.D. James, J. Mech. Phys. Solids 50 (2002) 283.
[47] Y.C. Shu, M.P. Lin, K.C. Wu, Mech. Mater. 36 (2004) 975.
[48] C.M. Landis, J. Mech. Phys. Solids 56 (2008) 3059.
[49] L. Néel, J. Phys. Radiat. 5 (1944) 241.
[50] O. Hubert, R. Waberi, S. Lazerg, K. Huyn-Soo, R. Billardon, Measurement and two-scales modeling of the ΔE effect, in: 7th EUROMECH Solid Mechanics Conference, 2009.
[51] S. Chikazumi, Introduction to Ferromagnetic Materials, Addison-Wesley, 1997.
[53] R. Hill, J. Mech. Phys. Solids 13 (1965) 89.
[54] L. Daniel, O. Hubert, Eur. Phys. J. Appl. Phys. 45 (2009) 31101.
[55] O. Hubert, L. Daniel, R. Billardon, J. Magn. Magn. Mater. 254–255 (2003) 352.
[56] O. Hubert, L. Daniel, J. Magn. Magn. Mater. 320 (2008) 1412.
[57] S. Lazreg, O. Hubert, J. Appl. Phys. 109 (2011), doi:10.1063/1.3540416.

2.4 Conclusion

Mes travaux de recherche ont donc porté sur l'étude des phénomènes de couplage entre comportement mécanique et comportement électromagnétique. Ce travail s'est focalisé sur le développement d'outils de modélisation multi-échelle permettant de définir le comportement à l'échelle des mécanismes physiques. Des règles de changement d'échelle ont été définies pour permettre le passage de cette échelle locale à l'échelle macroscopique. Ce travail s'est accompagné de développements expérimentaux pour l'élaboration, l'identification et la validation des outils de modélisation proposés. Du point de vue des matériaux étudiés, cette démarche de modélisation micro-macro a été appliquée aux matériaux classiques pour machines tournantes [94, 95], pour transformateurs [96], à des ferrites Nickel-Zinc [97], à des matériaux à magnétostriction géante tel le Terfenol-D [74], à des composites magnétostrictifs [98] ou magnéto-électriques [32].

La mise à disposition de tels outils de modélisation permet d'envisager des démarches d'optimisation pour la définition de compositions ou de microstructures des matériaux sous sollicitations multiphysiques. C'est notamment l'objet du projet MAEL évoqué dans ce mémoire. Cette démarche de modélisation ouvre également la voie à une meilleure intégration des phénomènes de couplage électro-magnéto-mécanique dans les outils de conception de dispositifs électromagnétiques. Les modélisations micro-macro peuvent alors être utilisées soit comme "machine d'essais numériques" pour l'identification de modèles macroscopiques, soit comme point de départ à la définition de modèles simplifiés plus facilement implantables dans des codes de calcul numérique.

L'échelle locale retenue dans le cas des matériaux ferromagnétiques est celles des domaines magnétiques. On aurait choisi celle des domaines ferroélectriques dans le cas des matériaux ferroélectriques. On pourra arguer qu'il existe des échelles inférieures permettant d'expliquer plus fondamentalement ces comportements complexes, et que nous n'avons fait que descendre d'une échelle le niveau de description phénoménologique. Cette remarque est fondée. Mais il nous a semblé qu'un positionnement à l'échelle des domaines permet un bon compromis entre richesse du contenu physique et souplesse des moyens de calcul mis en œuvre. Ce choix d'échelle microscopique nous a permis de décrire de manière prédictive, et avec un niveau de précision relativement fin le comportement magnéto-mécanique des matériaux polycristallins.

Quand les phénomènes à modéliser sont un peu plus complexes, les modélisations multi-échelles se prêtent assez naturellement à l'incorporation d'ingrédients physiques supplémentaires. Ainsi, en introduisant dans le modèle multi-échelle un modèle local de plasticité cristalline, nous avons pu modéliser l'effet de la déformation plastique sur le comportement magnétique ou magnétostrictif des matériaux magnétiques [99, 100]. De même en introduisant un modèle local de magnéto-résistance anisotrope, il a été possible d'établir un modèle polycristallin pour l'effet AMR permettant notamment de prévoir l'effet de la texture cristallographique et de la contrainte sur les modifications de résistivité sous champ magnétique [101]. Ces deux dernières références sont jointes ci-après.

De manière plus générale, le parti pris des approches multi-échelles est un moyen de mettre en avant les mécanismes responsables des phénomènes couplés observés et ainsi de mieux en appréhender les causes et les effets. Du point de vue de l'élaboration des matériaux, ces méthodes ouvrent des perspectives pour l'optimisation des microstructures. Dans le domaine de la conception des dispositifs électromagnétiques, il est possible désormais de dépasser des procédures de dimensionnement séquencées (mécanique puis électomagnétique, etc) au profit d'une démarche réellement multiphysique. J'espère donc que ces travaux trouveront un écho notamment auprès de ces deux communautés.

Publications jointes

[RI.8,100] : O. Hubert, L. Daniel, "Effect of plastic straining on magnetostriction of ferromagnetic polycrystals - experiments and multiscale modelling", *Journal of Magnetism and Magnetic Materials*, **304(2)** :489-491, 2006.

[RI.31,101] : A. Bartók, L. Daniel, A. Razek, "Micro-macro modeling of stress-dependent anisotropic magnetoresistance", *Journal of Physics D : Applied Physics*, **44** :135001, 2011.

Available online at www.sciencedirect.com
SCIENCE DIRECT®
Journal of Magnetism and Magnetic Materials 304 (2006) e489–e491
www.elsevier.com/locate/jmmm

Effect of plastic straining on magnetostriction of ferromagnetic polycrystals—experiments and multiscale modeling

Olivier Hubert[a,*], Laurent Daniel[b]

[a]LMT-Cachan (ENS-Cachan - CNRS UMR 8535 - University Paris 6), 61 Avenue du Président Wilson, 94235 Cachan Cedex, France
[b]LGEP (SUPELEC - CNRS UMR 8507 - University Paris 6 and Paris 11), Plateau du Moulon, 11 rue Joliot-Curie 91192 Gif-sur-Yvette Cedex, France

Available online 15 March 2006

Abstract

The influence of plastic deformations on magnetostriction of NO–3% Si–Fe alloy is studied. Experimental measurements are presented. The magnetostriction is strongly anisotropic before deformation and plastic strain tends to homogenize this behavior. The modeling consists in the calculation of a specific residual stresses field and its introduction in the magnetic model. Experiments and modeling are in good agreement.

PACS: 72.80; 75.50; 81.70

Keywords: Magnetostriction; Plastic strains; Multiscale modeling

1. Introduction

The influence of plastic deformations on magnetic behavior has been studied intensively in past years [1]. It is characterized by a strong degradation of magnetic behavior especially for weak plastic strain levels [2] and associated to intergranular stresses [3]. A model was recently proposed to describe the influence of plastic strain on the magneto-mechanical behavior of ferromagnetic materials and experiments showed the ability of this model to predict the degradation of magnetization behavior [4]. On the other hand the magnetostriction measurement is often proposed as a suitable indicator of mechanical state [5], but few experimental results of the influence of plastic strain on magnetostriction are available since Cullity in 1972 [6]. The first objective of this paper is to carry out magnetostriction measurements of plastic strained samples. The second objective is to evaluate the ability of the model to predict these experimental results.

2. Experimental procedure

NO 3% silicon–iron (0.5 mm thick) laminations have been used. Mechanical and magnetic experiments have been performed on 250 mm length and 12.5 mm width specimens cut by electroerosion along the rolling and transverse directions (RD and TD). Uniaxial tensile tests have been carried out at room temperature and constant strain rate $\dot{\varepsilon} = 1 \times 10^{-4}\,\mathrm{s}^{-1}$. Strain measurement were performed by strain gauges. Five plastic strain levels have been reached. Anhysteretic measurements of magnetization and magnetostriction have been carried out for increasing plastic strain levels at unloaded state. Description of employed device and measurement procedures can be found in Ref. [7]. Magnetostriction has been measured along both longitudinal and transverse direction of tensile strained specimen. The so-called form effect has been numerically removed[1] [8].

3. Experimental results

Despite a very low plastic strain levels (Table 1), the plastic deformation is homogeneous over the specimens.

*Corresponding author. Tel.: +33 1 4740 2224; fax: +33 1 4740 2240.
E-mail address: hubert@lmt.ens-cachan.fr (O. Hubert).

[1]Measured deformation = magnetostriction + form effect.

0304-8853/$ - see front matter © 2006 Elsevier B.V. All rights reserved.
doi:10.1016/j.jmmm.2006.02.132

Table 1
Plastic strain levels ε_p per direction

ε_p - RD (%)	0.003	0.005	0.021	0.090	0.160
ε_p - TD (%)	0.002	0.004	0.017	0.075	0.145

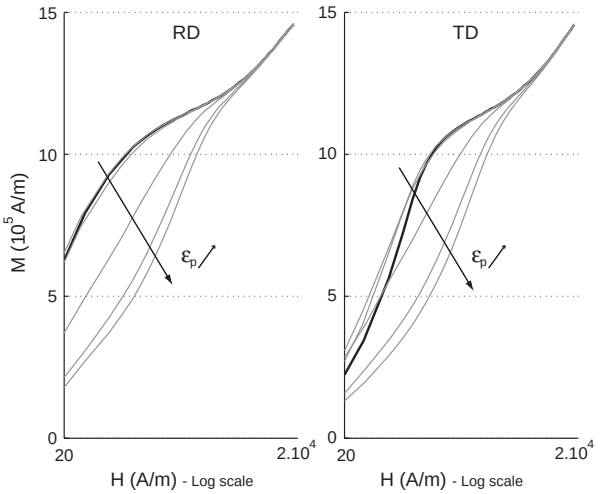

Fig. 1. Anhysteretic magnetic behavior.

Two first straining levels are below the macroscopic yield stress Σ_e: they are referred to as "microplasticity". Three higher levels correspond to usual plasticity. Fig. 1 shows the variations of magnetization behavior as function of strain level for RD and TD (thick lines: unstrained). The increasing strain levels roughly lead to a nonlinear degradation of the anhysteretic behavior as foreseen. This is especially sensitive for the weak and medium magnetic field strength, where maximal decreasing reaches 60%! We note that the two first plastic strain levels lead to a first weak improvement of the magnetization behavior especially along TD for $H < 100\,\mathrm{A/m}$. Fig. 2 shows the experimental results obtained for magnetostriction. Several points are remarkable: the initial behavior is strongly anisotropic (e.g. $\varepsilon_\mu^{\max}(\mathrm{RD}-\mathrm{long.}) = 3.5\times10^{-6}$ and $\varepsilon_\mu^{\max}(\mathrm{TD}-\mathrm{long.}) = 12\times10^{-6}$); at low levels, plastic straining has an opposite effect on RD and TD behaviors: magnetostriction amplitude increases for RD and decreases for TD. A global homogenization of the magnetostriction behavior occurs as major consequence; higher plastic strain level leads to progressively the same change for RD and TD. Amplitudes are increasing so that magnetostrictive behavior along TD before and after plastic straining is roughly equivalent (for investigated levels).

4. Micromechanical model of plasticity and multiscale modeling

The modeling procedure is divided in calculation of local stress field first, and multiscale (domain, grain, polycrystal) magnetic modeling, second. Magnetization and magnetostriction behaviors are finally calculated. Ref. [4] explains in detail how the local plastic straining is calculated using microplasticity tools. An orientation data file obtained by EBSD measurement and containing 396 orientations has been used. The multiscale magnetic modeling has been presented in detail elsewhere [9]. It is based on an energetic approach for the equilibrium state of a magnetic domain. Each grain is supposed be divided into domain families associated to "easy" directions. Localization procedures are first required in order to get the local loading at this scale. The volumetric fraction and magnetization of each family are evaluated thanks to a microscopic model. Averaging operations finally allow one to get the mean magnetization and magnetostriction strain across the grains and at macroscale. Fig. 3 plots the modelled magnetization behavior for RD and TD. Initial anisotropy

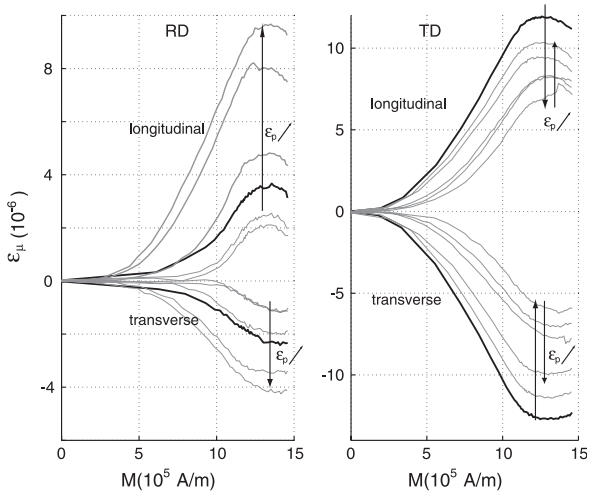

Fig. 2. Anhysteretic magnetostrictive behavior.

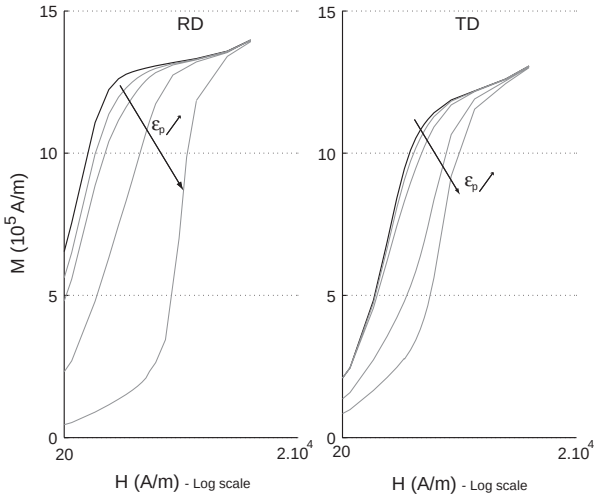

Fig. 3. Multiscale model: magnetization behavior.

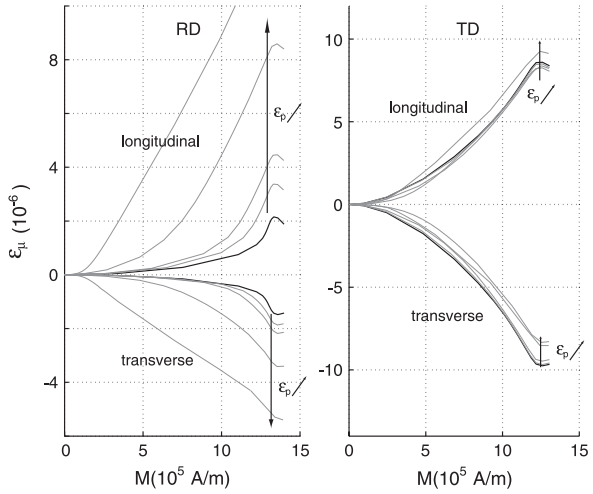

Fig. 4. Multiscale model: magnetostrictive behavior.

and drastic degradation due to plasticity are well described. The rate of degradation is nevertheless different from experiments at various strain levels. Fig. 4 plots the modeled longitudinal and transverse magnetostriction behavior for RD and TD. Initial anisotropy is well fitted even if amplitudes are lower. Influence of plastic straining is in good agreement with experimental results for RD. Initial and final TD behaviors are in accordance with experiments, but the decrease of amplitude at very low straining level is not modeled for TD.

5. Discussion and conclusion

Initial anisotropy was already discussed in a previous paper [7]. It is linked to low anisotropic crystallographic texture associated to initial configuration of domains mainly distributed along RD (same effect occurs for grain-oriented materials). This initial distribution is predicted by the model. The local stress tensor associated to the plastic strain completely destroys this weak configuration and two consequences are the degradation of magnetization behavior in the direction of the tensile test and the homogenization of magnetostriction. Finally higher plastic strain levels lead to an increase of amplitude of magnetostriction. This is in accordance with Cullity's and more recent Makar's observations [6,10], and associated with a major compressive effect along the straining direction.

References

[1] A. Seeger, et al., J. Appl. Phys. 35 (1964) 740.
[2] M.J. Sablik, J. Appl. Phys. 89 (2001) 5610.
[3] E. Hug, et al., Mater. Sci. Eng. A 332 (2002) 193.
[4] O. Hubert, et al., Int. J. Steel Res. 6 (2005) 400.
[5] T. Yamasaki, et al., NDT&E Int. 29 (5) (1996) 263.
[6] B.D. Cullity, Introduction to Magnetic Materials, Addison-Wesley, Reading, MA, 1972.
[7] O. Hubert, et al., J. Magn. Magn. Mater. 254–255C (2003) 352.
[8] L. Daniel, et al., J. Phys. IV 105 (2003) 247.
[9] L. Daniel, et al., Comput. Appl. Math. 23 (2–3) (2004) 285.
[10] J.M. Makar, et al., J. Magn. Magn. Mater. 222 (2000) 291.

IOP Publishing Journal of Physics D: Applied Physics
J. Phys. D: Appl. Phys. **44** (2011) 135001 (8pp) doi:10.1088/0022-3727/44/13/135001

Micro–macro modelling of stress-dependent anisotropic magnetoresistance

A Bartók, L Daniel and A Razek

Laboratoire de Génie Electrique de Paris (LGEP), CNRS (UMR 8507)-SUPELEC-UPMC Paris 6-Univ Paris-Sud 11, 11 rue Joliot-Curie, Plateau de Moulon, 91192 Gif-sur-Yvette, France

E-mail: andras.bartok@lgep.supelec.fr and laurent.daniel@u-psud.fr

Received 29 November 2010, in final form 30 January 2011
Published 16 March 2011
Online at stacks.iop.org/JPhysD/44/135001

Abstract
Anisotropic magnetoresistance (AMR) is the basic phenomenon of a spread class of sensors. AMR effect has a strong mechanical stress dependence. Micromagnetic simulations are often used for modelling the magnetoresistance of ferromagnetic materials, but these approaches do not allow us to investigate macroscopic effects (for example behaviour of a polycrystal under stress) due to the high number of interactions and degrees of freedom. On the other hand macroscopic phenomenological approaches fail in describing the main role of microstructure on the effective behaviour. In this work a micro–macro model is proposed to describe the effect of stress on the AMR in ferromagnetic polycrystals. Results are discussed and compared with experimental data from the literature.

(Some figures in this article are in colour only in the electronic version)

Introduction

The anisotropic magnetoresistance (AMR) effect in ferromagnetic materials (FM) was first discovered by William Thomson in 1857. Due to its high sensitivity and flexibility of design it is still used in a wide array of sensors for measurement of Earth's magnetic field (electronic compass) [1], for electrical current measuring (by measuring the magnetic field created around the conductor) [2], for traffic detection [3] and for linear position and angle sensing [4].

The electrical resistivity in FM depends on the angle between the direction of electrical current and orientation of the magnetization in the material. This anisotropic dependence lies in spin–orbit coupling. It is fundamentally related to the larger probability of s–d scattering for electrons travelling parallel to the magnetization [5]. As the magnetization rotates, the electron cloud about each nucleus deforms slightly and this deformation changes the amount of scattering undergone by the conduction electrons in their passage through the lattice [6]. Thus the AMR effect is strongly dependent on the local magnetization in the material. In that sense it has some similarities with the magnetostriction effect as discussed later in this paper. On the other hand, owing to the magnetic domain structure of FM, the distribution of magnetization within FM is very heterogeneous. This is the reason why numerical models for AMR effect are mostly based on micromagnetic calculations [7–9]. In these approaches the number of degrees of freedom and interactions are growing quickly with the number of magnetic moments, so that these simulations can only address small volumes corresponding to a limited number of domains. If the effect of the microstructure on the overall AMR properties is to be investigated—for example the effect of crystallographic texture in polycrystalline media—these methods are not relevant.

It is also known that the AMR effect has a strong mechanical stress dependence [10]. Indeed mechanical stress applied to a magnetic media changes the distribution of domain orientations. As a consequence it modifies the local resistivity, and thus the overall resistivity. This effect of stress on magnetoresistance is for instance used as the basis for a particular type of strain measurement gauges [11].

Some macroscopic phenomenological models for AMR effect have also been proposed [12–14] but they cannot account for microstructure or composition related effects. They have to be identified on macroscopic measurements and cannot be used as predictive tools for material design.

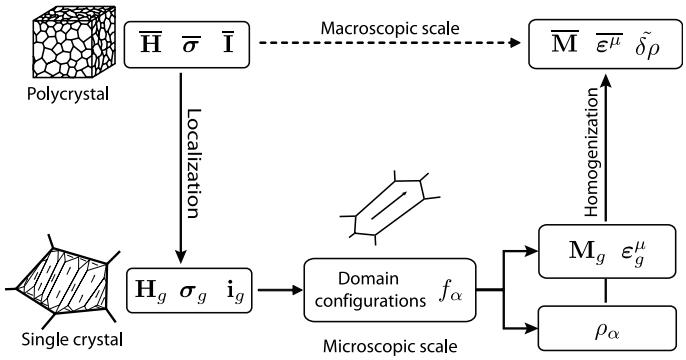

Figure 1. Modelling strategy.

An intermediate approach, standing between micro-magnetic and macroscopic modelling, would be useful in order to provide a design tool sensitive to complex microstructural effects, and notably accounting for the crystallographic texture. Indeed this microstructural parameter can be controlled and significantly modifies the overall AMR properties of FM. In this work a micro–macro model for stress-dependent AMR is proposed. This model is based on a magneto-elastic multiscale model allowing the definition of the local stress and magnetic field in heterogeneous materials from the knowledge of the macroscopic loading. A phenomenological law for AMR effect is then used at the local scale. A homogenization step is finally performed to define the macroscopic change in resistivity. This model can naturally account for the effect of stress on the overall AMR effect, and includes the influence of microstructural parameters such as the crystallographic texture.

The paper is divided into three parts. In the first part the micro–macro model is detailed. In the second part the approach is validated thanks to experimental measurements on iron, nickel and permalloy polycrystals taken from the literature. The approach is finally applied in the third part to the investigation of the effect of crystallographic texture on AMR.

1. Micro–macro modelling

AMR effect depends on the local magnetization orientation, itself depending on local magnetic field and stress (at the magnetic domain scale). Owing to the heterogeneity of materials, stress and magnetic field are not uniform within the material. Their local values have to be determined through an appropriate micro–macro scheme. Once these values for the local loading are known, the magnetic domain structure has to be determined, in order to define the local magnetization (at the domain scale). A model for the AMR effect can then be applied. The overall response of the material (polycrystalline scale) is then obtained through appropriate averaging operations. Thus, the model proposed in this paper is based on a three-scale description (polycrystal, single crystal, magnetic domain) and follows the scheme presented in figure 1.

The uppermost calculation scale in the model—called macroscopic scale—is the polycrystalline representative volume element (RVE) which is seen as an assembly of single crystals or grains (g) with respect to a given orientation function. The intermediate scale—called mesoscopic scale—is the single crystal or grain, that is seen as a collection of magnetic domains (α) with given magnetization orientation. The lowest scale—called microscopic scale—is the magnetic domain, that is an area with uniform magnetostriction strain[1] and magnetization.

The main steps of this model are divided as follows.

(i) The localization steps aims at defining the local loading (magnetic field $\boldsymbol{H}_\alpha$, stress $\boldsymbol{\sigma}_\alpha$ and current $\boldsymbol{i}_\alpha$) at the microscopic scale as a function of the macroscopic loading (magnetic field $\overline{\boldsymbol{H}}$, stress $\overline{\boldsymbol{\sigma}}$ and current $\overline{\boldsymbol{I}}$). The loading at the mesoscopic scale (magnetic field $\boldsymbol{H}_g$, stress $\boldsymbol{\sigma}_g$ and current $\boldsymbol{i}_g$) is calculated as an intermediate step. These localization steps highly depend on the microstructure of the material.

(ii) The microscopic magneto-elastic model allows us to define in a statistical way the domain configuration, introducing as an internal variable the volumetric fraction f_α of domains with orientation $\boldsymbol{\alpha}$ in a grain g. In each domain, depending on the considered orientation $\boldsymbol{\alpha}$, the magnetization $\boldsymbol{M}_\alpha$ and magnetostriction strain $\boldsymbol{\varepsilon}^\mu_\alpha$ are known.

(iii) The microscopic AMR model allows us to define the local resistivity (ρ_α) depending on the magnetization orientation $\boldsymbol{\alpha}$ in the considered domain.

(iv) The homogenization step allows us to retrieve the overall response of the material at the polycrystal scale (magnetization at the macroscopic scale $\overline{\boldsymbol{M}}$, macroscopic magnetostriction strain $\overline{\boldsymbol{\varepsilon}}^\mu$ and the variation of the macroscopic resistivity $\tilde{\delta\rho}$) depending on the local values of the response at the microscopic scale.

These steps are detailed hereafter. The magneto-elastic part of the model is based on a reversible magneto-elastic model previously published [15, 16].

[1] Magnetostriction strain is the spontaneous strain undertaken by magnetic materials.

Table 1. Physical constants used for the modelling.

Coefficient	M_S	K_1, K_2	λ_{100}, λ_{111}	A_s	C_{11}, C_{12}, C_{44}
Unit	$\mathrm{A\,m^{-1}}$	$\mathrm{kJ\,m^{-3}}$	—	$\mathrm{m^3\,J^{-1}}$	GPa
Iron [6, 10, 24]	1.71×10^6	42.7, 15	21, -21 ($\times 10^{-6}$)	0.0020	238, 142, 232
Nickel [10, 25]	4.91×10^5	-5.7, -2.3	-45.9, -24.3 ($\times 10^{-6}$)	0.016	250, 160, 118
$Fe_{11}Ni_{89}$ [10, 26]	7.50×10^5	-1, -2	-15, -10 ($\times 10^{-6}$)	0.032	243, 148, 122

1.1. Localization step

The simplest assumption to define the microscopic loading ($\boldsymbol{H}_\alpha$, $\boldsymbol{\sigma}_\alpha$, $\boldsymbol{i}_\alpha$) as a function of the macroscopic loading ($\overline{\boldsymbol{H}}$, $\overline{\boldsymbol{\sigma}}$, $\overline{\boldsymbol{I}}$) would be to consider uniform field hypotheses. Under such hypotheses the localization rules are very simple ($\boldsymbol{H}_\alpha = \overline{\boldsymbol{H}}$, $\boldsymbol{\sigma}_\alpha = \overline{\boldsymbol{\sigma}}$, $\boldsymbol{i}_\alpha = \overline{\boldsymbol{I}}$). However, due to the heterogeneity of the materials, these assumptions are often inappropriate.

1.1.1. Macro–meso scale transition. In a polycrystal the susceptibility from one grain to another can vary very significantly. For instance in pure iron the permeability of a grain can vary up to 70% at 400 A m^{-1} or 60% at 2000 A m^{-1} depending on its relative orientation with respect to the magnetic field [17]. This heterogeneity results in a significant heterogeneity of the magnetic field within the material. In the case of polycrystals, the self-consistent scheme is known to provide satisfying results. The macro–meso localization rule is written as follows [16]:

$$\boldsymbol{H}_g = \overline{\boldsymbol{H}} + \frac{1}{3 + 2\chi^m}(\overline{\boldsymbol{M}} - \boldsymbol{M}_g) \tag{1}$$

$\overline{\boldsymbol{M}}$ and $\boldsymbol{M}_g$ are the magnetization, respectively at the macroscopic and mesoscopic scales. In the case of self-consistent hypothesis χ^m is the overall magnetic susceptibility of the material.

The elastic response to a given mechanical loading also significantly differs from one grain to another in a polycrystal. As an example in the case of pure iron Young's modulus can vary up to 115% depending on the crystallographic orientation (see the elastic constants in table 1). The self-consistent localization scheme is known to provide satisfying estimates for polycrystalline media [18]. Under such hypotheses, the macro–meso localization rule can be written in the following form [16]:

$$\boldsymbol{\sigma}_g = \mathcal{B}_\sigma : \overline{\boldsymbol{\sigma}} + \mathcal{L}^{\mathrm{inc}} : (\overline{\varepsilon}^\mu - \varepsilon_g^\mu) \tag{2}$$

$\overline{\varepsilon}^\mu$ and ε_g^μ are the magnetostriction strain, respectively, at the macroscopic and mesoscopic scale. $\mathcal{B}_\sigma$ denotes the so-called concentration tensor and $\mathcal{L}^{\mathrm{inc}}$ is a tensor accounting for elastic incompatibilities due to magnetostriction. The way to calculate these fourth order tensor can be found in [18, 16] and is briefly recalled in the appendix.

In the case of the electrical resistivity, and as will be shown in the following, the heterogeneity is weak. Depending on the orientation of the single crystal, the electrical resistivity does not vary more than a few percent. This is why we applied uniform electric current conditions.

$$\boldsymbol{i}_g = \overline{\boldsymbol{I}}. \tag{3}$$

1.1.2. Meso–micro scale transition. In the case of the localization rules from the grain to the domain scale, an accurate definition of the microstructure, namely the magnetic domain structure, would be requisite[2]. This information is unknown. For the sake of simplicity we assumed uniform magnetic field, uniform strain and uniform current within the single crystal. However in the proposed microscopic magneto-elastic model, the mean values at the single crystal scale are often sufficient data.

1.2. Microscopic magneto-elastic model

The magneto-elastic model for the single crystal is derived from [15]. The single crystal is seen as an assembly of magnetic domains. The potential energy of a domain α is written:

$$W_\alpha = W_\alpha^K + W_\alpha^\sigma + W_\alpha^H \tag{4}$$

where W_α^K denotes the magnetocrystalline energy, W_α^σ denotes the elastic energy and W_α^H denotes the magneto-static energy.

In the case of cubic crystallographic structure the magnetocrystalline energy can be written

$$W_\alpha^K = K_1(\alpha_1^2\alpha_2^2 + \alpha_2^2\alpha_3^2 + \alpha_3^2\alpha_1^2) + K_2(\alpha_1^2\alpha_2^2\alpha_3^2) \tag{5}$$

where K_1 and K_2 denote the magnetocrystalline anisotropy constants of the cubic crystal and $\boldsymbol{\alpha} = {}^t[\alpha_1\alpha_2\alpha_3]$ the direction cosines of the magnetization ($\boldsymbol{M}_\alpha = M_s\,\boldsymbol{\alpha}$ with M_s the saturation magnetization of the material).

Under uniform strain hypotheses the elastic energy can be written [16]:

$$W_\alpha^\sigma = -\boldsymbol{\sigma}_g : \varepsilon_\alpha^\mu \tag{6}$$

In the case of cubic crystallographic symmetry, the magnetostriction strain tensor ε_α^μ can be written as

$$\varepsilon_\alpha^\mu = \frac{3}{2}\begin{pmatrix} \lambda_{100}\left(\alpha_1^2 - \frac{1}{3}\right) & \lambda_{111}\alpha_1\alpha_2 & \lambda_{111}\alpha_1\alpha_3 \\ \lambda_{111}\alpha_1\alpha_2 & \lambda_{100}\left(\alpha_2^2 - \frac{1}{3}\right) & \lambda_{111}\alpha_2\alpha_3 \\ \lambda_{111}\alpha_1\alpha_3 & \lambda_{111}\alpha_2\alpha_3 & \lambda_{100}\left(\alpha_3^2 - \frac{1}{3}\right) \end{pmatrix} \tag{7}$$

where λ_{100} and λ_{111} are the magnetostrictive constants of the single crystal.

The magneto-static energy of a domain is written as

$$W_\alpha^H = -\mu_0 \boldsymbol{M}_\alpha.\boldsymbol{H}_\alpha \tag{8}$$

where μ_0 is the vacuum permeability.

We then introduce the volumetric fractions f_α of domains with magnetization orientation $\boldsymbol{\alpha}$ [16, 19–21]. These internal

[2] Except for the electric current since the hypotheses of weak heterogeneity of the resistivity are still valid.

variables are obtained through the numerical integration of the following Boltzmann-type relation [15]:

$$f_\alpha = \frac{\exp(-A_s.W_\alpha)}{\int_\alpha \exp(-A_s.W_\alpha)\,\mathrm{d}\alpha} \tag{9}$$

where A_s is an adjustable parameter that can be deduced from low field measurement of the anhysteretic magnetization curve [16] ($A_s = 3\chi_0/\mu_0 M_s^2$ where χ_0 is the initial anhysteretic susceptibility of the material).

The magnetostriction strain and the magnetization over the single crystal are defined by an averaging operation over the single crystal (volume V_g):

$$\varepsilon_g^\mu = \langle \varepsilon^\mu \rangle_g = \frac{1}{V_g}\int_{V_g} \varepsilon^\mu \,\mathrm{d}V = \sum_\alpha f_\alpha\, \varepsilon_\alpha^\mu \tag{10}$$

$$M_g = \langle M \rangle_g = \frac{1}{V_g}\int_{V_g} M \,\mathrm{d}V = \sum_\alpha f_\alpha\, \vec{M}_\alpha. \tag{11}$$

If needed, the elastic strain ε_g^e in the single crystal can be easily calculated from Hooke's law (equation (12)) using the single crystal stiffness tensor $\mathcal{C}_g$. This elastic strain is superimposed to the magnetostriction strain to obtain the total strain of the single crystal ($\varepsilon = \varepsilon^e + \varepsilon^\mu$).

$$\varepsilon_g^e = \mathcal{C}_g^{-1} : \boldsymbol{\sigma}_g. \tag{12}$$

At this stage, the macroscopic magnetization and magnetostriction strain could also be calculated thanks to an averaging operation over the whole volume of the RVE.

1.3. Single-domain model of AMR

Let $\beta = {}^t[\beta_1\,\beta_2\,\beta_3]$ be the direction cosines determining the orientation of the current used for measuring the electrical resistance ($\boldsymbol{\alpha} = {}^t[\alpha_1\,\alpha_2\,\alpha_3]$ are still the direction cosines of the magnetization in the considered domain). The general expression for the magnetoresistance in any direction of a cubic crystal can be written in a series form of $\boldsymbol{\alpha}$ and β [13]. Döring used the following form [10] for cubic crystals with negative magnetocrystalline anisotropy constant[3] K_1 (such as nickel and $Fe_{11}Ni_{89}$ permalloy):

$$\begin{aligned}\rho_\alpha = \rho_0\big[1 &+ k_1\big(\alpha_1^2\beta_1^2 + \alpha_2^2\beta_2^2 + \alpha_3^2\beta_3^2 - \tfrac{1}{3}\big)\\ &+ 2k_2(\alpha_1\alpha_2\beta_1\beta_2 + \alpha_2\alpha_3\beta_2\beta_3 + \alpha_3\alpha_1\beta_3\beta_1) + k_3\big(s - \tfrac{1}{3}\big)\\ &+ k_4\big(\alpha_1^4\beta_1^2 + \alpha_2^4\beta_2^2 + \alpha_3^4\beta_3^2 + \tfrac{2s}{3} - \tfrac{1}{3}\big) + 2k_5(\alpha_1\alpha_2\beta_1\beta_2\alpha_3^2\\ &+ \alpha_2\alpha_3\beta_2\beta_3\alpha_1^2 + \alpha_3\alpha_1\beta_3\beta_1\alpha_2^2)\big]\end{aligned} \tag{13}$$

in which $s = \alpha_1^2\alpha_2^2 + \alpha_2^2\alpha_3^2 + \alpha_3^2\alpha_1^2$, ρ_0 is the resistivity in the demagnetized state and k_1,k_2,k_3,k_4,k_5 are material constants. For a crystal with positive magnetocrystalline anisotropy constant[4] K_1 (such as iron) the expression is the same except that the term $k_3/3$ is absent.

[3] In that case easy magnetization directions are ⟨1 1 1⟩ directions.
[4] In that case easy magnetization directions are ⟨1 0 0⟩ directions.

1.4. Effective properties

The macroscopic magnetization and strain are obtained through an averaging operation over the whole volume V of the RVE.

$$\overline{M} = \langle M \rangle_V = \langle M_g \rangle_V \tag{14}$$

$$\overline{\varepsilon} = \langle \varepsilon \rangle_V = \langle \varepsilon^e + \varepsilon^\mu \rangle_V = \langle \varepsilon_g \rangle_V. \tag{15}$$

If needed, the macroscopic magnetostriction strain can be obtained using the following relation [16]:

$$\overline{\varepsilon}^\mu = \langle {}^t\mathcal{B}_\sigma : \varepsilon^\mu \rangle_V = \langle {}^t\mathcal{B}_\sigma : \varepsilon_g^\mu \rangle_V \tag{16}$$

Since the local electric conductivity ς_α in a domain is known ($\varsigma_\alpha = 1/\rho_\alpha$), the effective macroscopic conductivity $\tilde{\varsigma}$ can be obtained through a self-consistent approach, applying the classical Bruggeman relation [17, 22, 23]. $\tilde{\varsigma}$ is solution of equation (17) that can be solved easily using a fixed point method.

$$\tilde{\varsigma} = \frac{\left\langle \dfrac{\varsigma_\alpha}{2\tilde{\varsigma} + \varsigma_\alpha} \right\rangle_V}{\left\langle \dfrac{1}{2\tilde{\varsigma} + \varsigma_\alpha} \right\rangle_V} \tag{17}$$

where the operation $\langle . \rangle_V$ is an averaging operation over the whole volume of the RVE. The effective resistivity $\tilde{\rho}$ is deduced from the effective conductivity ($\tilde{\rho} = 1/\tilde{\varsigma}$). In the following the variation of the macroscopic resistivity $\delta\tilde{\rho}$ (equation (18)) will be plotted. It can be noticed from equations (13) and (17) that $\delta\tilde{\rho}$ does not depend on the value of ρ_0.

$$\delta\tilde{\rho} = \frac{\tilde{\rho} - \rho_0}{\rho_0}. \tag{18}$$

2. Validation on isotropic polycrystals

The proposed micro–macro approach has been validated on isotropic iron, nickel and permalloy ($Fe_{11}Ni_{89}$) polycrystals.

2.1. Model parameters

The mechanical and magnetic characteristics of iron, nickel and a permalloy ($Fe_{11}Ni_{89}$) single crystal were used[5] for the calculations. At the single crystal scale, for the calculation of the volumetric fractions f_α, a 10242 orientation (α) data file was used [15]. The material constants are defined in tables 1 and 2. The distribution function for crystal orientation in the case of isotropic polycrystals has been obtained by a regular zoning of the crystallographic space [16]. The corresponding pole figures are given in figure 2.

2.2. Prediction of the AMR effect

The similarity in the phenomena of magnetostriction and magnetoresistance has been known for a long time. This similarity is linked to the strong dependence of both phenomena on the local magnetization state and thus on the magnetic domain configuration. Our model is based on a

[5] The accurate data of the constants of Döring expression of $Fe_{11}Ni_{89}$ were not found. The constants of the $Fe_{15}Ni_{85}$ permalloy were used instead.

Table 2. Constants of Döring expression.

Coefficient	k_1	k_2	k_3	k_4	k_5
Iron [10]	0.00153	0.00593	0.00194	0.00053	0.00269
Nickel [10]	0.0654	0.0266	−0.032	−0.054	0.020
$Fe_{15}Ni_{85}$ [27]	0.0518	0.0478	−0.0243	−0.0139	0.0259

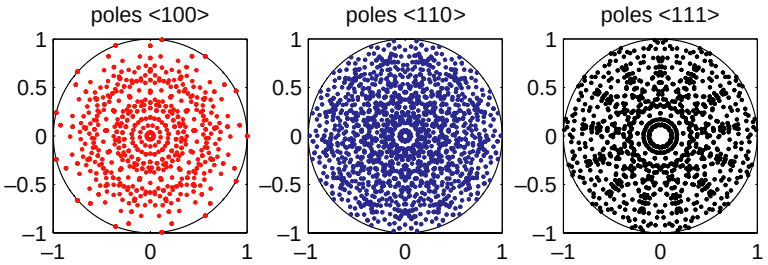

Figure 2. Pole figures for an isotropic polycrystal obtained from a regular zoning of the crystallographic space.

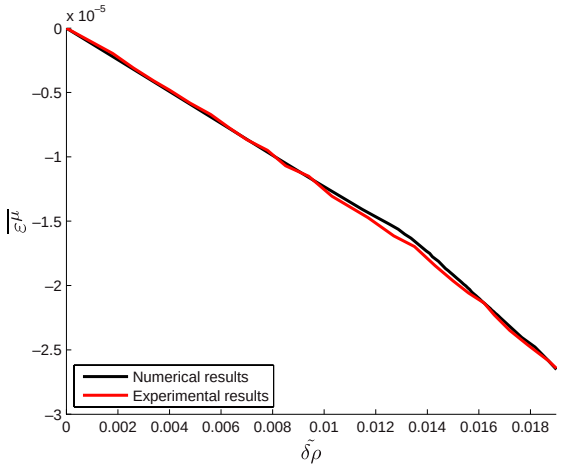

Figure 3. Magnetostriction strain of nickel polycrystal as a function of the change of resistivity (current and applied magnetic field are parallel)—experimental data [10] and obtained numerical results.

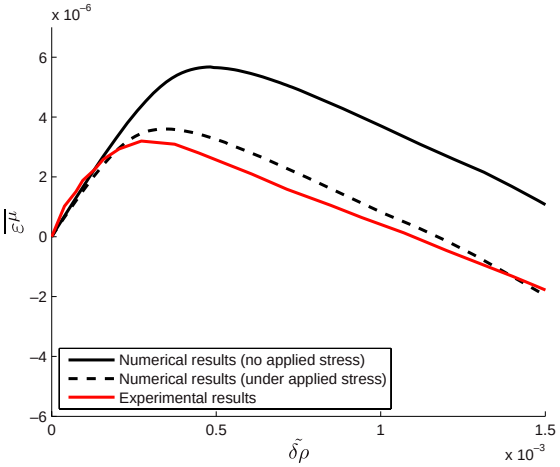

Figure 4. Magnetostriction strain of iron polycrystal as a function of the change of resistivity (current and applied magnetic field are parallel)—experimental data [10] and obtained numerical results (dashed line: under 25 MPa tension applied in the direction of magnetic field).

micro–macro approach of the magneto-elastic behaviour of the materials which can give the magnetostriction ($\lambda(H)$) and the magnetoresistance curves ($\delta\rho(H)$). From these results the relation between the change in resistivity and the magnetostriction strain can be easily obtained. It is illustrated in the case of isotropic nickel and pure iron polycrystals without external stress and compared with experimental data from the literature [10] in figures 3 and 4. These figures plot the effective magnetostriction strain as a function of the effective change in resistivity for parallel configuration (magnetic field and electrical current are parallel). Experimental observations show that magnetostriction strain first increases with magnetoresistance and then decreases in the case of iron, and magnetostriction decreases continuously in the case of nickel. The different behaviour of these materials results from the different sign in their material constants (magnetostriction and Döring expression). The experimental curve is accurately predicted by the model in the case of nickel. The experimental curve for iron is qualitatively predicted, but quantitatively overestimated. It is shown by the dot plot in figure 4 that a macroscopic tension of amplitude 25 MPa applied in the direction of the magnetic field provides a numerical result closer to the experimental observation. This point shows that a residual stress in the material could explain the discrepancies in the case of the iron specimen.

2.3. Prediction of the effect of stress on the AMR

In order to study the effect of an applied uniaxial stress on the magnetoresistance, modelling results were compared with experimental results [10] on a permalloy ($Fe_{11}Ni_{89}$) polycrystal. In this case the $\tilde{\delta\rho}(B)$ curves were calculated

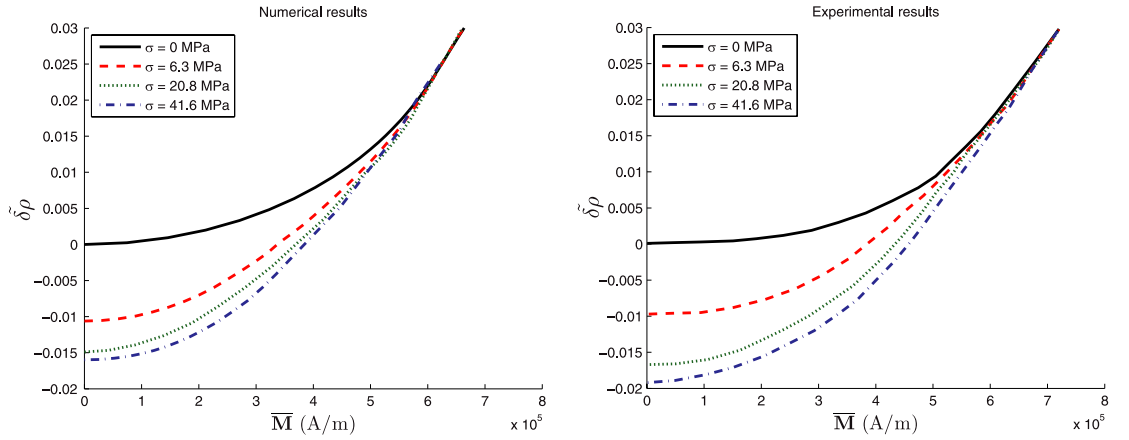

Figure 5. Change in resistivity (current and applied magnetic field are parallel) with change in magnetization of permalloy polycrystals ($Fe_{11}Ni_{89}$), effect of the level of applied uniaxial stress (compression)—obtained numerical results (left) and experimental data [10] (right).

from the combination of $B(H)$ and $\tilde{\delta\rho}(H)$ modelling results. This permalloy has negative magnetostriction so that the tension orients its domains perpendicularly to the direction of tension and this effect decreases the initial resistivity. The comparison between numerical and experimental results (figure 5) gives very satisfying results. It shows the nonlinear stress dependence as well. The stress decreases the initial resistivity and increases the slope of the curves which is important in the sensor application (higher sensibility in low field measurement). The model can predict the effect of a multiaxial stress as well but these results are not presented in this paper due to the lack of experimental results for validation.

3. Investigation of crystallographic texture effect

The magnetoresistance in a single crystal is strongly anisotropic. Figure 6 shows the change in resistivity in a pure iron single crystal as a function of the angle between its easy magnetization direction ⟨1 0 0⟩ and the applied magnetic field in the {0 1 1} crystallographic plane. The change in resistivity (under no applied stress) can vary up to several hundred percent depending on the orientation of the magnetic field with respect to the crystal orientation, both in parallel and perpendicular configurations. As a consequence, the AMR effect can be expected to be very sensitive to crystallographic texture.

In order to investigate this effect, the crystallographic texture of an Armco specimen (pure iron), known as isotropic, has been obtained from electron back-scattered diffraction (EBSD) measurement. The corresponding pole figures are given in figure 7. It shows a weak texture compared with the calculated isotropic crystal orientation distribution used previously and showed in figure 2.

The prediction of the AMR effect for pure iron using this latter crystallographic texture has been compared with the prediction using the isotropic orientation data file. Figure 8 shows the change in resistivity in the parallel current/applied magnetic field configuration as a function of current orientation in the polycrystal. In the case of Armco specimen two planes (XY and YZ) have been investigated.

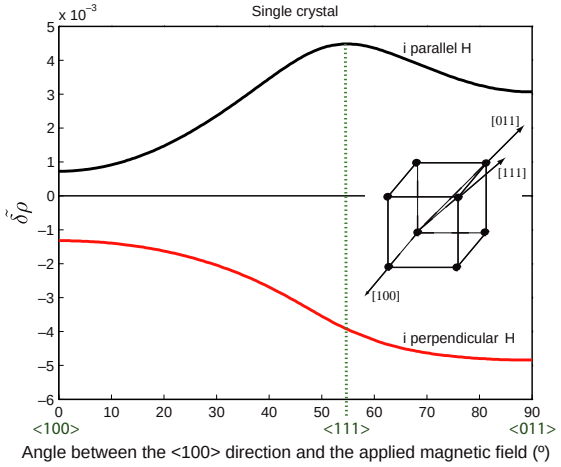

Figure 6. Change in resistivity as a function of the angle between the ⟨1 0 0⟩ direction and the applied magnetic field (10^5 A m^{-1}) in the {0 1 1} crystallographic plane—pure iron single crystal in parallel (parallel magnetic field and electrical current) and perpendicular (perpendicular magnetic field and electrical current) configurations.

It is shown that even for this very weakly textured material the magnetoresistance can vary up to 10% depending on the orientation of the solicitation (parallel configuration). The magnetoresistance is confirmed to be strongly dependent on crystallographic texture.

4. Conclusion

A micro–macro model for the effect of stress on the anisotropic magnetoresistance has been presented. It is based on a description of the magneto-mechanical coupling at several scales (domain, single crystal, polycrystal). The behaviour of iron, nickel and a permalloy ($Fe_{11}Ni_{89}$) polycrystal has been calculated. Numerical results have been compared with experimental results from the literature with very satisfying

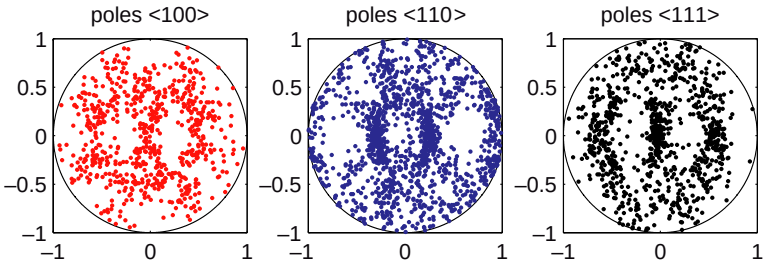

Figure 7. Pole figures of an Armco steel obtained from EBSD measurement.

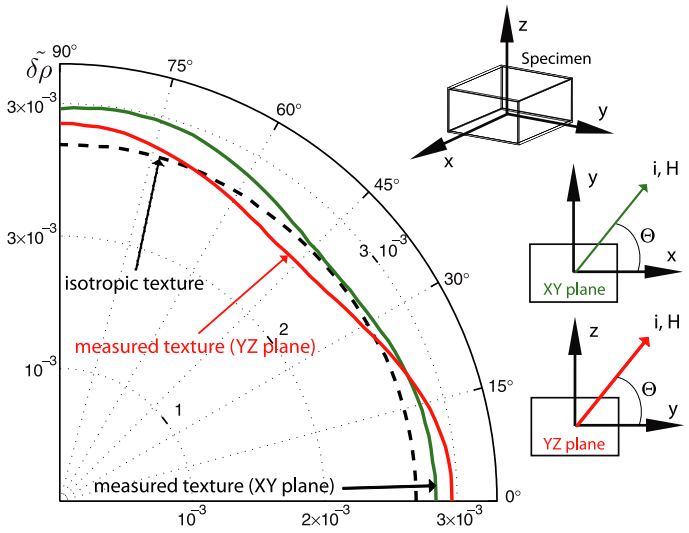

Figure 8. Change in resistivity (current and applied magnetic field are parallel) with change in the orientation of the applied magnetic field (10^5 A m^{-1}) for pure iron polycrystal using an isotropic texture (dotted line) and texture data from EBSD measurement in different planes (lines).

agreement. This model enables us to investigate the effect of crystallographic texture on AMR effect and it highlights the strong influence of crystallographic texture on it. It also enables us to investigate the effect of stress, and notably multiaxial stress on magnetoresistance. The development of micro–macro models accounting for microstructure and stress dependence of effective magnetoresistive properties should allow the design of high precision AMR devices.

Acknowledgments

The authors are greatly indebted to Dr Anne-Laure Helbert (ICMMO, Univ Paris-Sud) for the EBSD measurement of the Amrco steel.

Appendix. Calculation of mechanical localization operators

We briefly give hereafter the way to obtain the fourth order tensors $\mathcal{B}_\sigma$ and $\mathcal{L}^{\text{inc}}$ appearing in section 1.1. More detailed explanations can be found in [16, 18].

$\mathcal{B}_\sigma$ is defined by equation (19) that introduces the single crystal stiffness tensor $\mathcal{C}_g$, the polycrystal effective stiffness tensor $\tilde{\mathcal{C}}$ and the strain localization tensor $\mathcal{A}_\sigma$.

$$\mathcal{B}_\sigma = \mathcal{C}_g : \mathcal{A}_\sigma : \tilde{\mathcal{C}}^{-1}. \tag{19}$$

$\mathcal{A}_\sigma$ is defined by equation (21) where $\mathcal{C}^*$ is the so-called Hill constraint tensor [18] that can be obtained from the Eshelby tensor $\mathcal{S}^E$ according to equation (21), $\mathcal{I}$ being the fourth order identity tensor.

$$\mathcal{A}_\sigma = (\mathcal{C}_g + \mathcal{C}^*)^{-1} : (\tilde{\mathcal{C}} + \mathcal{C}^*) \tag{20}$$

$$\mathcal{C}^* = \tilde{\mathcal{C}} : (\mathcal{S}^{E^{-1}} - \mathcal{I}). \tag{21}$$

$\mathcal{L}^{\text{inc}}$ is defined by equation (22).

$$\mathcal{L}^{\text{inc}} = \mathcal{C}_g : (\mathcal{C}_g + \mathcal{C}^*)^{-1} : \mathcal{C}^*. \tag{22}$$

References

[1] Vcelak J, Ripka P, Kubik J, Platil A and Kaspar P 2005 AMR navigation systems and methods of their calibration *Sensors Actuators* A **123–124** 122

[2] Mlejnek P, Vopalensky M and Ripka P 2008 AMR current measurement device *Sensors Actuators* A **141** 649
[3] Application Note 2005 Vehicle detection and compass applications using AMR magnetic sensors *Technical Report* AN218, Honeywell SSEC, www.ssec.honeywell.com
[4] Adelerhof D J and Geven W 2000 New position detectors based on AMR sensors *Sensors Actuators* **85** 48
[5] Smit J 1951 Magnetoresistance of ferromagnetic metals and alloys at low temperatures *Physica* **17** 612
[6] Cullity B D 1972 *Introduction to Magnetic Materials* (London: Addison-Wesley)
[7] Adeyeyea A O and White R L 2004 Magnetoresistance behavior of single castellated $Ni_{80}Fe_{20}$ nanowires *J. Appl. Phys.* **95** 2025
[8] Hafner M *et al* 2009 Theory of anisotropic magnetoresistance in atomic-sized ferromagnetic metal contacts *Phys. Rev.* B **79** 140410(R)
[9] Serrano-Guisan S, Rott K, Reiss G and Schumacher H W 2008 Inductive and magneto-resistive measurements of gilbert damping in $Ni_{81}Fe_{19}$ thin films and microstructures *J. Phys. D: Appl. Phys.* **41** 164015
[10] Bozorth R M 1951 *Ferromagnetism* (Princeton, NJ: Van Nostrand)
[11] Sonehara M, Shinohara M, Sato T, Yamasawa T and Miura K 2010 Strain sensor using stress-magnetoresistance effect of NiFe/MnIr exchange-coupled magnetic film *J. Appl. Phys.* **107** 09E718
[12] Kwiatkowski W, Stabrowski M and Tumanski S 1983 Numerical analysis of the shape anisotropy and anisotropy dispersion in thin film permalloy magnetoresistors *IEEE Trans. Magn.* **MAG-19** 2502
[13] McGuire T R and Potter R I 1975 Anisotropic magnetoresistance in ferromagnetic 3d alloys *IEEE Trans. Magn.* **11** 1018
[14] Li J, Li S L, Wu Z W, Li S, Chu H F, Wang J, Zhang Y, Tian H Y and Zheng D N 2010 A phenomenological approach to the anisotropic magnetoresistance and planar hall effect in tetragonal $La_{2/3}Ca_{1/3}MnO_3$ thin films *J. Phys.: Condens. Matter* **22** 146006
[15] Daniel L and Galopin N 2008 A constitutive law for magnetostrictive materials and its application to Terfenol-d single and polycrystals *Eur. Phys. J. Appl. Phys.* **42** 153
[16] Daniel L, Hubert O, Buiron N and Billardon R 2008 Reversible magneto-elastic behavior: A multiscale approach *J. Mech. Phys. Solids* **56** 1018
[17] Daniel L and Corcolle R 2007 A note on the effective magnetic permeability of polycrystals *IEEE Trans. Magn.* **43** 3153
[18] Hill R 1965 Continuum micro-mechanics of elastoplastic polycrystals *J. Mech. Phys. Solids* **13** 213
[19] Néel L 1944 Les lois de l'aimantation et de la subdivision en domaines élémentaires d'un monocristal de fer *J. Phys. Radiat.* **5** 241
[20] Chikazumi S 1997 *Introduction to Ferromagnetic Materials* (Reading, MA: Addison-Wesley)
[21] Buiron N, Hirsinger L and Billardon R 1999 A multiscale model for magneto-elastic couplings *J. Phys. IV* **9** Pr9-187–Pr9–196
[22] Bruggeman D A G 1935 Berechnung verschiedener physikalischer konstanten von heterogenen substanzen *Annal. Phys. Lpz.* **416** 636
[23] Stroud D 1975 Generalized effective-medium approach to the conductivity of an inhomogeneous material *Phys. Rev.* B **12** 3368
[24] McClintock F A and Argon A S 1966 *Mechanical Behavior of Materials* (New York Addison-Wesley)
[25] Hausch G and Warlimont H 1973 Single crystalline elastic constants of ferromagnetic face centered cubic Fe-Ni invar alloys *Acta Metal.* **21** 401
[26] Kanrar A and Ghosh U S 1983 The variation of elastic constants of nickel-iron single crystal alloys from 78.76 to 300 K *J. Phys. Chem. Solids* **44** 457–62
[27] Berger L and Friedberg S A 1968 Magnetoresistance of a permalloy single crystal and effect of 3d orbital degeneracies *Phys. Rev.* **165** 670

Partie 3

Perspectives

Mes perspectives de recherche s'inscrivent dans la continuité des travaux réalisés sur l'étude et la modélisation des phénomènes de couplage multiphysique, abordés sous l'angle de la physique des matériaux hétérogènes. L'objectif est d'une part de permettre l'optimisation des microstructures (et donc des propriétés) des matériaux du Génie Electrique et de l'électronique, et d'autre part de fournir des modèles de comportement pertinents pour le calcul de structures (par exemple par éléments finis). Ces travaux orientés vers les outils de modélisation doivent continuer à s'appuyer sur une démarche expérimentale. La plate-forme de caractérisation du comportement des matériaux actifs développée ces dernières années au LGEP semble en mesure désormais d'atteindre son rythme de croisière, mais de nouveaux développements, ainsi que la mise en place de collaborations extérieures seront nécessaires. Les principales perspectives identifiées à ce jour sont présentées ci-dessous suivant quatre axes.

Dispositifs électrotechniques sous sollicitations extrêmes

La sévérité grandissante des cahiers des charges imposés aux dispositifs du Génie Electrique rend de plus en plus fréquentes les situations dans lesquelles les phénomènes de couplage multiphysique interviennent au premier plan.

Ainsi, la multiplication des systèmes embarqués dans le domaine des transports automobiles et aéronautiques rend indispensable une diminution drastique de la masse de ces systèmes. Ces nouvelles contraintes amènent à solliciter les dispositifs électromagnétiques dans des conditions de plus en plus sévères. Par exemple, dans le cas des machines tournantes, une des pistes pour améliorer la puissance massique consiste à augmenter les vitesses de rotation. Cette augmentation de vitesse a pour conséquence une augmentation de l'intensité des contraintes en service. Par ailleurs, dans l'objectif de proposer des propriétés optimales pour les matériaux magnétiques, les procédés de fabrication sont adaptés, d'autres sont mis au point. Ces procédés génèrent souvent des contraintes résiduelles qui influent sur les propriétés en service. Si on s'intéresse au cas des transformateurs électriques, ce sont plutôt les vibrations d'origine électromagnétique que l'on cherche à mieux maîtriser. Dans toutes ces situations, les phénomènes de couplage magnéto-mécanique apparaissent en première ligne et les approches multi-échelles développées dans le cadre de ces travaux sont des outils d'analyse intéressants. Ces problèmes, posés notamment par l'industrie automobile et aéronautique, sont autant de motivations pour poursuivre les recherches sur la modélisation micro-mécanique du comportement magnéto-élastique. La maturité des outils est même aujourd'hui suffisante pour fournir de premières réponses sur les aspects anhystérétiques. Une meilleure diffusion de ces méthodes auprès des fabricants de matériaux et des concepteurs de machines électriques est un effort indispensable à mener. Les choses évoluent cependant comme en témoigne par exemple le démarrage du projet 3MT (Matériaux Magnétiques pour Machines et Transformateurs) qui intégre les aspects magnéto-mécaniques pour le développement de nouveaux matériaux pour dispositifs électromagnétiques embarqués. Une première perspective de travail consiste donc à contribuer à faire vivre et à diffuser cette thématique de recherche et ces nouveaux outils pour la description du comportement magnéto-mécanique.

Un autre volet à aborder est celui des sollicitations thermiques. Les sollicitations en service subies par les dispositifs électromagnétiques couvrent en effet une gamme de température de plus en plus large, avec des fluctuations dont l'amplitude et la fréquence peuvent être relativement élevées. La prise en compte des sollicitations thermiques est importante à deux titres : d'une part les propriétés des matériaux dépendent de la température, et, d'autre part, les fluctuations de température peuvent donner naissance à des phénomènes de fatigue. Les outils de modélisation multi-échelle développés dans le cadre de mes travaux, s'ils ne permettent pas en l'état de traiter directement ces problèmes de fatigue, peuvent en revanche être utiles pour clarifier la nature et l'amplitude des sollicitations locales. En effet, la dépendance à la température des paramètres matériaux peut être introduite naturellement dans le modèle multi-échelle. Ce travail ne nécessite pas de développement majeur. Il requiert toutefois la connaissance de l'évolution en fonction de la température des grandeurs physiques telles que l'aimantation à saturation, les coefficients élastiques ou encore les coefficients de magnétostriction. Ces données ne sont pas faciles à recueillir, mais si elles sont connues, le modèle multi-échelle devrait permettre de prédire les effets de la température sur les propriétés macroscopiques des matériaux magnétiques. Le paramètre température pourra ainsi être intégré à terme dans la démarche d'optimisation des microstructures. Les effets de

la température - et des variations de température - sur les fluctutations du champ de contraintes dans le matériau pourront également être traités, ouvrant la voie à une modélisation plus fine des phénomènes de fatigue. Du point de vue expérimental, l'achat d'une enceinte thermique permettant le pilotage d'essais de caractérisation sous température contrôlée est à l'étude. Ce dispositif devra être facilement adaptable au dispositif de caractérisation magnéto-mécanique du LGEP. Cette acquisition permettrait une extension de la zone de validation du modèle multi-échelle. Les enceintes envisagées couvrent une gamme de température variant de -50^{o}C à 250^{o}C. Cette évolution de la plateforme de caractérisation nécessite toutefois un travail de fond, car la sensibilité des systèmes de mesures à ces variations de température doit être étudiée et prise en compte.

Comportement dynamique des matériaux et effets de dissipation

Les travaux de modélisation présentés dans ce mémoire ont pour l'essentiel été menés dans un cadre non-dissipatif et quasi-statique. Le caractère dynamique et la dissipation sont pourtant des aspects essentiels dans beaucoup d'applications électroniques et électrotechniques, et devront donc faire l'objet de travaux dédiés.

Concernant les effets de dissipation, des travaux de modélisation de l'hystérésis magnéto-mécanique ont déjà été entamés dans le cadre du projet MAEL et de la thèse de Karl-Joseph Rizzo [71] en co-encadrement avec le LMT-Cachan. La complexité mais aussi l'enjeu du problème sont tels qu'on peut penser que cette thématique sera poursuivie pendant encore plusieurs années. La piste suivie actuellement est d'implanter un modèle de dissipation à l'échelle locale dans le modèle multi-échelle. Le principal mécanisme de pertes par hystérésis est en effet lié à l'interaction entre les parois de domaines magnétiques et les défauts du matériau. Il paraît donc légitime de s'appuyer sur les variables internes du modèle multi-échelle pour décrire ce phénomène. On envisage par exemple d'introduire une relation entre un terme de dissipation et les variations des fractions volumiques des familles de domaines, ces variations étant bien représentatives du mouvement des parois. Ce type de démarche devrait permettre de décrire l'hystérésis statique des matériaux magnétiques sous sollicitations magnéto-mécaniques. L'enjeu est ici aussi de proposer des outils d'optimisation de microstructure pour le développement de nouveaux matériaux magnétiques, la grandeur à optimiser étant cette fois les pertes par hystérésis.

Les régimes de sollicitations dynamiques doivent également faire l'objet de développements significatifs. En effet, les sollicitations électromagnétiques en régime harmonique conduisent au développement de courants de Foucault dans les matériaux. Ces effets sont des effets macroscopiques, et l'échelle de description pertinente n'est vraisemblablement pas celle des domaines magnétiques mais plutôt celle de la structure. Cependant ces courants de Foucault sont dépendants des propriétés du matériau dans lequel ils se développent. Ces matériaux étant souvent hétérogènes, il est utile de disposer d'outils d'homogénéisation qui permettent de déterminer leurs propriétés effectives. Ces propriétés peuvent ensuite être introduites dans les codes de calcul de structures. Ce besoin se manifeste particulièrement dans le domaine de l'aéronautique où on cherche à remplacer certains boîtiers pour composants électroniques habituellement conçus en alliage d'aluminium par des boîtiers composites, plus légers. La fonction de blindage électromagnétique, qui était facilement réalisée par l'alliage d'aluminium, très bon conducteur, devient plus sensible dans le cas des matériaux composites. C'est pourquoi il est nécessaire de s'intéresser au comportement électromagnétique de matériaux composites sous sollicitations harmoniques. Les fréquences envisagées appartiennent à une gamme très large, puisqu'une tenue à la foudre (proche d'une sollicitation impulsionnelle) est même parfois envisagée. Le développement d'outils d'homogénéisation du comportement des matériaux composites pour application en compatibilité électromagnétique fait l'objet d'un projet de recherche, en partenariat avec la société SAGEM, qui s'inscrit dans un plus vaste programme de recherche portant sur les systèmes de régulation de moteurs pour l'aéronautique (SYRENA). La thèse de Valentin Préault [102] fait partie de ce programme.

Nous nous intéressons également, mais avec une approche différente, aux courants de Foucault dans les matériaux magnétiques polycristallins soumis à des sollicitations mécaniques. L'objectif est de tenir compte de l'état de contraintes (il s'agit souvent de contraintes résiduelles) dans les matériaux soumis à des procédures de Contrôle Non Destructif (CND) par courants de Foucault. En effet, l'état de contraintes modifie sensiblement la perméabilité magnétique et affecte ainsi directement le processus de CND lorsqu'il est conduit sur des matériaux magnétiques. Dans un premier temps, l'objectif consiste à prédire l'effet des contraintes sur les mesures d'impédances des dispositifs CND. Le développement d'une méthode de caractérisation expérimentale à l'aide des dispositifs de mesure disponibles au LGEP est prévue dans un avenir proche. Ce travail s'inscrit notamment dans les travaux de thèse d'András Bartók [103]. A terme ces travaux pourraient permettre de développer, par une méthode inverse, des dispositifs d'estimation des contraintes par mesures magnétiques.

L'introduction du caractère dynamique des sollicitations électromagnétiques est aussi nécessaire pour l'étude des capteurs magnéto-électriques présentés dans la partie 2.1.2. On a en effet vu que ces dispositifs fonctionnent de manière optimale lorsqu'un signal harmonique, à la fréquence de résonance du dispositif, est superposé au signal à mesurer. Si les outils de modélisation en 2D sont désormais disponibles grâce aux travaux de thèse de Thu Trang Nguyen [34], des outils 3D doivent encore être mis au point. Du point de vue des méthodes d'homogénéisation, les fortes non-linéarités du comportement, notamment pour la phase magnétique, sont encore insuffisament prises en compte dans les outils de modélisation multi-échelle. Recruté dernièrement au LGEP, Romain Corcolle a pour ambition de proposer des modèles d'homogénéisation pour les comportements couplés qui tiennent compte à la fois de ces non-linéarités et du caractère dynamique des sollicitations. J'espère avoir la chance de pouvoir l'assister dans ses travaux. Sur le plan expérimental, une collaboration est désormais mise en place avec le "Laboratory for Micro-Nano Technology" de l'Université Nationale du Vietnam. La mise en place de cette collaboration n'est pas seulement due à mon goût immodéré pour les voyages au Vietnam, mais surtout à la présence sur place d'une équipe renommée pour le développement de capteurs de champ magnétique basés sur l'utilisation de l'effet magnéto-électrique [36]. Un partenariat Hubert Curien (PHC Hoa Sen Lotus) pourrait fournir un cadre approprié à cette collaboration.

Echelles nanométriques

Les composites magnéto-électriques, on l'a vu, permettent la fabrication de capteurs de champ magnétique de forte sensibilité ou d'inductances variables. Ces matériaux ouvrent aussi des perspectives dans le domaine des micro voire nano-dispositifs. Une application particulièrement prometteuse concerne le stockage de données par mémoires magnétiques. Pour ce type de mémoires, l'écriture de données repose sur l'application d'un champ magnétique qui permet, dans une zone monodomaine, de faire basculer l'aimantation d'une position à la position opposée. L'encombrement, la masse des dispositifs nécessaires pour générer ce champ magnétique, et les dégagements de chaleur qui leur sont associés sont des facteurs limitants à une miniaturisation accrue. Les dispositifs magnéto-électriques permettent d'apporter une réponse à ce problème. On sait en effet que l'application d'une contrainte modifie l'équilibre magnétique dans un domaine magnétique. L'application d'une contrainte ne permet pas à elle seule de procéder à un retournement à 180^o de l'aimantation dans un domaine (et donc de procéder à l'écriture magnétique). En revanche, la contrainte peut significativement diminuer l'amplitude du champ magnétique nécessaire au retournement de l'aimantation, et ainsi diminuer la taille des dispositifs d'écriture magnétique. Pour procéder à l'application de la contrainte, les matériaux piézoélectriques sont de bons candidats. Ainsi, on réalise aujourd'hui des multi-couches ferromagnétiques/piézoélectriques très compacts. Les outils de modélisation développés pour les matériaux massifs peuvent être adaptés pour permettre l'étude de ces microsystèmes. Les dispositifs de stockage magnétique, constitués de cellules monodomaines dont l'aimantation bascule de manière approximativement uniforme, se prêtent bien à la mise en œuvre du modèle multi-échelle. On peut ainsi évaluer l'optimalité de différentes architectures pour ces dispositifs d'écriture magnétique assistée par la contrainte, et déterminer les états de contraintes les plus appropriés pour un retournement d'aimantation facilité. Jusqu'à présent les états de contraintes uniaxiaux ont été privilégiés dans les dispostifs expérimentaux, mais la modélisation pourrait permettre d'étudier la pertinence d'états de contraintes multiaxiaux. Des travaux exploratoires ont été menés dans le cadre d'une collaboration avec une équipe de l'Institut d'Electronique Fondamentale (IEF) à Orsay. Cette équipe dispose notamment des équipements pour l'élaboration et la caractérisation de ces dispositifs multicouches. Il manque encore à cette collaboration un cadre formel, mais de premiers résultats devraient être proposés dans un avenir proche.

Comportement ferroélectrique

J'ai consacré une grande part de ces dix dernières années de recherche à l'étude des phénomènes de couplage magnéto-mécanique. Même s'il reste encore beaucoup de pistes à explorer, ces travaux sont suffisamment avancés pour étendre l'étude à d'autres phénomènes de couplage multiphysique en adoptant le même parti pris de modélisation micro-macro. Comme cela a déjà été mentionné, l'étude de l'effet AMR dans les matériaux polycristallins est accessible grâce aux outils développés [101]. De même l'intégration des effets de la température dans les modélisations proposées sera un passage obligé pour mieux rendre compte des conditions de fonctionnement des dispositifs électromagnétiques. La poursuite de ces deux projets semble une perspective naturelle de ce travail.

Une autre perspective de recherche concerne la modélisation du comportement ferroélectrique. En effet, l'optimisation des microstructures et une meilleure maîtrise du comportement en environnement sévère sont aussi des enjeux de taille dans le domaine des matériaux ferroélectriques. C'est notamment le cas pour les applications capteurs ou actionneurs pour lesquelles les contraintes de dimensionnement sont souvent fortes. Depuis quelques années, de nouvelles contraintes environnementales visant à réduire l'utilisation du plomb poussent à une recherche accrue dans le domaine des matériaux ferroélectriques. Le plomb est en effet un élément de base des principaux matériaux ferroélectriques d'usage courant, comme le PZT. Le remplacement de ces matériaux par de nouveaux matériaux sans plomb nécessitera de l'ingéniosité dans la conception et l'élaboration pour obtenir des performances de bon niveau. Les travaux de modélisation développés ces dernières années peuvent contribuer aux recherches dans ce domaine. Le comportement ferroélectrique présente en effet de nombreux points communs avec le comportement ferromagnétique. En particulier, ces deux types de comportement s'articulent autour d'une microstructure en domaines, dont l'évolution en fonction des sollicitations extérieures permet de déduire les propriétés macroscopiques. Il est tentant de transposer les outils de modélisation développés dans le cadre de la magnéto-élasticité au cas des matériaux ferroélectriques. La transposition ne peut se faire de manière trop brutale cependant car les deux comportements présentent aussi des dissemblances. Par exemple, le mécanisme de rotation uniforme de l'aimantation dans les domaines magnétiques n'a pas son équivalent dans les domaines ferroélectriques. Inversement la dépendance de la polarisation locale au champ électrique appliqué (effet piézoélectrique) ne se retrouve pas dans le cas des matériaux ferromagnétiques. Dans le cas des matériaux ferroélectriques, l'utilisation de la diffraction des rayons X à haute énergie a récemment rendu possible le suivi de la microstructure en domaines dans des matériaux ferroélectriques sous sollicitations electro-mécaniques [104,105]. Il est notamment possible de détecter "en moyenne" la réorientation des domaines en cours de sollicitation. Ce type de méthode expérimentale pourrait donner accès aux fractions volumiques des différentes orientations de domaines ferroélectriques, et à leur évolution. Il s'agit d'une opportunité unique pour le développement et la validation de modèles micro-mécaniques. Les comparaisons peuvent en effet être ménées à partir de résultats expérimentaux à l'échelle de la microstructure, et plus seulement à l'échelle macroscopique. Je me suis rapproché de la "School of Materials" à l'Université de Manchester, pionnière dans ce domaine, pour monter un projet de recherche sur ce thème. L'exploitation des relevés de diffraction disponibles fournit déjà une base de données conséquente pour la validation locale des approches multi-échelles, et des essais complémentaires sont programmés. Il faut noter que ces relevés fournissent des informations en volume sur les microstructures en domaines, alors que les outils classiques d'investigation locale ne fournissent souvent qu'une information de surface - en général non représentative. La mise au point d'outils de modélisation micromécanique du comportement des matériaux ferroélectriques, en parallèle avec l'acquisition et l'analyse de résultats de diffraction en volume sur ces matériaux est donc une piste prometteuse pour mieux comprendre et quantifier les phénomènes de couplage multiphysique dont les mécanismes reposent sur une microstructure évolutive. Ces travaux devraient à terme pouvoir s'appliquer au cas des matériaux ferromagnétiques. On peut même rêver, à relativement courte échéance, à des expériences similaires de diffraction des rayons X sur les matériaux ferromagnétiques.

La fin de ce document est donc aussi le début d'une nouvelle aventure.

Bibliographie

[1] J.P.A. Bastos et N. Sadowski : *Electromagnetic Modeling by Finite Element Method*. Marcel Dekker, Electrical Engineering and Electronic Series, 2003.

[2] L. Hirsinger et R. Billardon : Magneto-elastic finite element analysis including magnetic forces and magnetostriction effects. *IEEE Transactions on Magnetics*, 31(3):1877–1880, 1995.

[3] M. Besbes, Z. Ren et A. Razek : Finite element analysis of magnetomechanical coupled phenomena in magnetostriction materials. *IEEE Transactions on Magnetics*, 32:1058–1061, 1996.

[4] M. Besbes, Z. Ren et A. Razek : A generalized finite element model of magnetostriction phenomena. *IEEE Transactions on Magnetics*, 37(5):3324–3328, 2001.

[5] O.A. Mohammed, T. Calvert et R. McConnell : Coupled magnetoelastic finite element formulation including anisotropic reluctivity tensor and magnetostriction effects for machinery applications. *IEEE Transactions on Magnetics*, 37(5):3388–3392, 2001.

[6] K. Azoum, M. Besbes, F. Bouillault et T. Ueno : Modeling of magnetostrictive phenomena. application in magnetic force control. *The European Physical Journal - Applied Physics*, 36:43–47, 2006.

[7] K. Fonteyn, A. Belahcen, R. Kouhia, P. Rasilo et A. Arkkio : Fem for directly coupled magneto-mechanical phenomena in electrical machines. *IEEE Transactions on Magnetics*, 46(8):2923–2926, 2010.

[8] R. Lerch : Simulation of piezoelectric devices by two- and threedimensional finite elements. *IEEE Trans. Ultrasonics Ferroelectr. Frequency Control*, 37:233–247, 1990.

[9] K.Y. Lam, X.Q. Peng, G.R. Liu et J.N. Reddy : A finite-element model for piezoelectric composite laminates. *Smart Materials and Structures*, 6:583–591, 1997.

[10] Y.H. Lim, V.V. Varadan et V.K. Varadan : Finite-element modeling of the transient response of mems sensors. *Smart Materials and Structures*, 6:53–61, 1997.

[11] A. Benjeddou : Advances in piezoelectric finite element modeling of adaptive structural elements : a survey. *Computer and Structures*, 76:347–363, 2000.

[12] D.H. Wu, W.T. Chien, C.J. Yang et Y.T. Yen : Coupled-field analysis of piezoelectric beam actuator using fem. *Sensors and Actuators A*, 118:171–176, 2005.

[13] M. Elhadrouz, T. Ben Zineb et E. Patoor : Finite element analysis of a multilayer piezoelectric actuator taking into account the ferroelectric and ferroelastic behaviors. *Int. J. Eng. Sci.*, 44:996–1006, 2006.

[14] Y.X. Liu, J.G. Wan, J.M. Liu et C.W. Nan : Numerical modeling of magnetoelectric effect in a composite structure. *Journal of Applied Physics*, 94(8):5111–5117, 2003.

[15] J. Lee, J.G. Boyd et D.C. Lagoudas : Effective properties of three-phase electro-magneto-elastic composites. *Int. J. Eng. Sci.*, 43(10):790–825, 2005.

[16] P. Suquet et H. Moulinec : A fast numerical method for computing the linear and nonlinear mechanical properties of composites. *Comptes Rendus des Séances de l'Académie des Sciences. Série II*, 318:1417–1423, 1994.

[17] R. Brenner : Numerical computation of the response of piezoelectric composites using fourier transform. *Physical Review B*, 79(18):184106, 2009.

[18] R. Brenner et J. Bravo-Castillero : Response of multiferroic composites inferred from a fast-fourier-transform based numerical scheme. *Smart Materials and Structures*, 19:115004, 2010.

[19] L. Daniel : *Modélisation multi-échelle du comportement magnéto-mécanique des matériaux ferromagnétiques texturés*. Thèse de doctorat, Ecole Normale Supérieure de Cachan, France, 2003.

[20] G.W. Milton : *The Theory of Composites*. Cambridge University Press, 2002.

[21] P. Wiener : *Abh. Math. Phys. Kl. Konigl. Sach.*, 32:509, 1912.

[22] Z. Hashin et S. Shtrikman : A variational approach to the theory of the effective magnetic permeability of multiphase materials. *Journal of Applied Physics*, 33(10):3125–3131, 1962.

[23] M. Bornert, T. Bretheau et P. Gilormini : *Homogénéisation en mécanique des matériaux. Tome 1 : Matériaux aléatoires élastiques et milieux périodiques.* Hermès Science, 2001.

[24] M. Bornert, T. Bretheau et P. Gilormini : *Homogénéisation en mécanique des matériaux. Tome 2 : Comportements non linéaires et problèmes ouverts.* Hermès Science, 2001.

[25] A.H. Sihvola : *Electromagnetic mixing formulas and applications.* Institution of Electrical Engineers, 1999.

[26] A.P. Vinogradov, L.V. Panina et A.K. Sarychev : Method for calculating the dielectric constant and magnetic permeability in percolating systems. *Sov. Phys. Dokl.*, 34(6):530–532, 1989.

[27] M. Le Floc'h, J.L. Mattei, P. Laurent, O. Minot et A.M. Konn : A physical model for heterogeneous magnetic materials. *Journal of Magnetism and Magnetic Materials*, 140-144:2191–2192, 1995.

[28] D. Bariou, P. Quéffélec, P. Gelin et M. Le Floc'h : Extension of the effective medium approximation for determination of the permeability tensor of unsaturated polycrystalline ferrites. *IEEE Transactions on Magnetics*, 37(6):3885–3891, 2001.

[29] R. Corcolle : *Détermination de lois de comportement couplé par des techniques d'homogénéisation : Application aux matériaux du Génie Electrique.* Thèse de doctorat, Université Paris-Sud, France, 2009.

[30] L. Daniel et R. Corcolle : A note on the effective magnetic permeability of polycrystals. *IEEE Transactions on Magnetics*, 43(7):3153–3158, 2007.

[31] R. Corcolle, L. Daniel et F. Bouillault : Intraphase fluctuations in heterogeneous magnetic materials. *Journal of Applied Physics*, 105(12):123913, 2009.

[32] R. Corcolle, L. Daniel et F. Bouillault : Generic formalism for homogenization of coupled behaviors : application to magnetoelectroelastic behavior. *Physical Review B*, 78(21):214110, 2008.

[33] N. Galopin : *Modélisation et caractérisation de matériaux actifs pour la conception de dispositifs magnéto-électriques.* Thèse de doctorat, Université Paris-Sud, France, 2007.

[34] T.T. Nguyen : *Modélisation de l'effet magnétoélectrique dans les matériaux composites.* Thèse de doctorat, Université Paris-Sud, France, à soutenir en 2011.

[35] C.W. Nan, M.I. Bichurin, S. Dong, D. Viehland et G. Srinivasan : Multiferroic magnetoelectric composites : Historical perspective, status, and future directions. *Journal of Applied Physics*, 103:031101, 2008.

[36] D.T. Huong Giang et N.H. Duc : Magnetoelectric sensor for microtesla magnetic-fields based on $(fe_{80}co_{20})_{78}si_{12}b_{10}$/pzt laminates. *Sensors and Actuators A*, 149:229–232, 2009.

[37] J. Lou, D. Reed, M. Liu et N.X. Sun : Electrostatically tunable magnetoelectric inductors with large inductance tunability. *Appl. Phys. Lett.*, 94:112508, 2009.

[38] N. Galopin, X. Mininger, F. Bouillault et L. Daniel : Finite element modelling of magneto-electric sensors. *IEEE Transactions on Magnetics*, 44(6):834–837, 2008.

[39] T.T. Nguyen, F. Bouillault, L. Daniel et X. Mininger : Finite element modeling of magnetic field sensors based on nonlinear magnetoelectric effect. *Journal of Applied Physics*, 109(8):084904, 2011.

[40] D.C. Jiles et D.L. Atherton : Theory of the magnetisation process in ferromagnets and its application to the magnetomechanical effect. *J. Phys. D : Appl. Phys.*, 17:1265–1281, 1984.

[41] F. Preisach : uber die magnetische nachwirkung,. *Z. Phys.*, 94:277, 1935.

[42] I.D. Mayergoyz : Mathematical models of hysteresis. *Physical Review Letters*, 56(15):1518, 1986.

[43] D.L. Atherton et D.C. Jiles : Effects of stress on the magnetization of steel. *IEEE Transactions on Magnetics*, 19:2021–2023, 1983.

[44] D.C. Jiles et D.L. Atherton : Theory of ferromagnetic hysteresis. *Journal of Applied Physics*, 55(6): 2115–2120, 1984.

[45] M.J. Sablik et D.C. Jiles : Coupled magnetoelastic theory of magnetic and magnetostrictive hysteresis. *IEEE Transactions on Magnetics*, 29(3):2113–2123, 1993.

[46] A. Bergqvist et G. Engdahl : A stress-dependent magnetic preisach hysteresis model. *IEEE Transactions on Magnetics*, 27(6):4796–4798, 1991.

[47] A. Bergqvist et G. Engdahl : A phenomenological magnetomechanical hysteresis model. *Journal of Applied Physics*, 75(10):5496–5498, 1994.

[48] D. Davino, A. Giustiniani et C. Visone : A magnetostrictive model with stress dependence for real-time applications. *IEEE Transactions on Magnetics*, 44(11):3193–3196, 2008.

[49] O. Bottauscio, P.E. Roccato et M. Zucca : Modeling the dynamic behavior of magnetostrictive actuators. *IEEE Transactions on Magnetics*, 46(8):3022–3028, 2010.

[50] F. Ossart, L. Hirsinger et R. Billardon : Computation of electromagnetic losses including stress dependence of magnetic hysteresis. *Journal of Magnetism and Magnetic Materials*, 196-197:924–926, 1999.

[51] C.P. Sasso, V. Basso, M. Lo Bue et G. Bertotti : Vector model for the study of hysteresis under stress. *Journal of Applied Physics*, 87(9):4774–4776, 2000.

[52] X.J. Zheng et X.E. Liu : A nonlinear constitutive model for terfenol-d rods. *Journal of Applied Physics*, 97:053901, 2005.

[53] O. Perevertov : Influence of the residual stress on the magnetization process in mild steel. *J. Phys. D : Appl. Phys.*, 40:949–954, 2007.

[54] W.F. Brown : *Micromagnetics*. Wiley, 1963.

[55] J. Fidler et T. Schrefl : Micromagnetic modelling - the current state of the art. *J. Phys. D : Appl. Phys.*, 33:R135–R156, 2000.

[56] A. DeSimone et R.D. James : A constrained theory of magnetoelasticity. *J. Mech. Phys. Solids*, 50:283–320, 2002.

[57] Y.C. Shu, M.P. Lin et K.C. Wu : Micromagnetic modeling of magnetostrictive materials under intrinsic stress. *Mechanics of Materials*, 36:975–997, 2004.

[58] C.M. Landis : A continuum thermodynamics formulation for micro-magnetomechanics with applications to ferromagnetic shape memory alloys. *J. Mech. Phys. Solids*, 56:3059–3076, 2008.

[59] R. Hill : Continuum micro-mechanics of elastoplastic polycrystals. *J. Mech. Phys. Solids*, 13:89–101, 1965.

[60] M. Berveiller et A. Zaoui : An extension of the self-consistent scheme to plastically-flowing polycrystals. *J. Mech. Phys. Solids*, 26:325–344, 1978.

[61] E. Patoor, D.C. Lagoudas, P.B. Entchev, L.C. Brinson et X. Gao : Shape memory alloys, part i : General properties and modeling of single crystals. *Mechanics of Materials*, 38:391–429, 2006.

[62] D.C. Lagoudas, P.B. Entchev, P. Popov, E. Patoor, L.C. Brinson et X. Gao : Shape memory alloys, part ii : Modeling of polycrystals. *Mechanics of Materials*, 38:430–462, 2006.

[63] J.E. Huber, N.A. Fleck, C.M. Landis et R.M. McMeeking : A constitutive model for ferroelectric polycrystals. *J. Mech. Phys. Solids*, 47:1663–1697, 1999.

[64] A. Haug, J.E. Huber, P.R. Onck et E. Van der Giessen : Multi-grain analysis versus self-consistent estimates of ferroelectric polycrystals. *J. Mech. Phys. Solids*, 55:648–665, 2007.

[65] H. Hauser : Energetic model of ferromagnetic hysteresis. *Journal of Applied Physics*, 75:2584–2596, 1994.

[66] W.D. Armstrong : Magnetization and magnetostriction processes in $tb_(0.27-0.30)dy_(0.73-0.70)fe_(1.9-2.0)$. *Journal of Applied Physics*, 81(5):2321–2326, 1997.

[67] W.D. Armstrong : A directional magnetization potential based model of magnetoelastic hysteresis. *Journal of Applied Physics*, 91(4):2202–2210, 2002.

[68] Y. Wan, D. Fang et K.C. Hwang : Non-linear constitutive relations for magnetostrictive materials. *International Journal of Non-linear Mechanics*, 38:1053–1065, 2003.

[69] A. van den Berg, L. Dupré, B. Van de Wiele et G. Crevecoeur : A mesoscopic hysteresis model based on the unconstrained minimization of the gibbs free energy. *IEEE Transactions on Magnetics*, 46(2):220–224, 2010.

[70] N. Buiron, L. Hirsinger et R. Billardon : A multiscale model for magneto-elastic couplings. *J. Phys. IV*, 9:139–141, 1999.

[71] K.J. Rizzo : *Modélisation multi-échelle du comportement magnéto-mécanique : prise en compte des phénomènes de dissipation*. Thèse de doctorat, Ecole Normale Supérieure de Cachan, France, à soutenir en 2011.

[72] S. Chikazumi : *Introduction to ferromagnetic materials*. Addison-Wesley, 1997.

[73] L. Daniel, O. Hubert, N. Buiron et R. Billardon : Reversible magneto-elastic behavior : a multiscale approach. *J. Mech. Phys. Solids*, 56(3):1018–1042, 2008.

[74] L. Daniel et N. Galopin : A constitutive law for magnetostrictive materials and its application to terfenol-d single and polycrystals. *The European Physical Journal - Applied Physics*, 42(2):153–159, 2008.

[75] G. Bertotti : *Hysteresis in Magnetism : For Physicists, Materials Scientists, and Engineers*. Academic Press, 1998.

[76] K.J. Rizzo, O. Hubert et L. Daniel : A multiscale model for piezomagnetic behavior. *European Journal of Electrical Engineering*, 12(4):525–540, 2009.

[77] M. Rekik : *Mesure et modélisation du comportement magnéto-mécanique dissipatif des matériaux ferromagnétiques à haute limite d'élasticité sous chargement multiaxial - Application aux machines électriques à grande vitesse*. Thèse de doctorat, Ecole Normale Supérieure de Cachan, France, à soutenir en 2013.

[78] O. Hubert, L. Daniel et R. Billardon : Experimental analysis of the magnetoelastic anisotropy of a non-oriented silicon iron alloy. *Journal of Magnetism and Magnetic Materials*, 254-255C:352–354, 2003.

[79] K.J. Rizzo, O. Hubert et L. Daniel : Magnetic and magnetostrictive behavior of iron-silicon single crystals under uniaxial stress. *IEEE Transactions on Magnetics*, 46(2):270–273, 2010.

[80] N. Galopin, L. Daniel, F. Bouillault et M. Besbes : Numerical analysis for the design of a magneto-elastic characterization device. *Prezgląd Elektrotechniczny*, 83(6):44–47, 2007.

[81] V. Maurel, F. Ossart, Y. Marco et R. Billardon : Setup to test biaxial stress effect on magneto-mechanic coupling. *Journal of Applied Physics*, 93(10):7115–7117, 2003.

[82] O. Hubert : Influence of biaxial stresses on the magnetic behaviour of an iron-cobalt sheet - experiments and modelling. *Prezgląd Elektrotechniczny*, 83(4):70–77, 2007.

[83] B.D. Cullity : *Introduction to magnetic Materials*. Addison-Wesley Publishing Company, London, 1972.

[84] L. Daniel et O. Hubert : An analytical model for the δe effect in magnetic materials. *The European Physical Journal - Applied Physics*, 45:31101, 2009.

[85] O. Hubert et L. Daniel : Measurement and analytical modeling of the δe effect in a bulk iron-cobalt alloy. *IEEE Transactions on Magnetics*, 46(2):401–404, 2010.

[86] L. Bernard, X. Mininger, L. Daniel, G. Krebs, F. Bouillault et M. Gabsi : Effect of stress on switched reluctance motors : A magneto-elastic finite element approach based on multiscale constitutive laws. *IEEE Transactions on Magnetics*, 2011 (accepté).

[87] C. Schneider et J. Richardson : Biaxial magnetoelasticity in steels. *Journal of Applied Physics*, 53:8136–8138, 1982.

[88] K. Kashiwaya : Fundamentals of nondestructive measurement of biaxial stress in steel utilizing magnetoelastic effect under low magnetic field. *Japanese Journal of Applied Physics*, 11A:2932–2942, 1991.

[89] M. Sablik, L. Riley, G. Burkhardt, H. Kwun, P. Cannell, K. Watts et R. Langman : Micromagnetic model for biaxial stress effects on magnetic properties. *Journal of Magnetism and Magnetic Materials*, 132, 1994.

[90] L. Daniel et O. Hubert : An equivalent stress for the influence of multiaxial stress on the magnetic behavior. *Journal of Applied Physics*, 105(7):07A313, 2009.

[91] L. Daniel et O. Hubert : Equivalent stress criteria for the effect of stress on magnetic behavior. *IEEE Transactions on Magnetics*, 46(8):3089–3092, 2010.

[92] O. Hubert et L. Daniel : Energetical and multiscale approaches for the definition of an equivalent stress for magneto-elastic couplings. *Journal of Magnetism and Magnetic Materials*, 323(13):1766–1781, 2011.

[93] G. Krebs et L. Daniel : A magneto-elastic proposal for field weakening in pmsm. *14th International IGTE Symposium on Numerical Field Calculation in Electrical Engineering (IGTE2010)*, Graz, Autriche, 2010.

[94] L. Daniel, O. Hubert, F. Ossart et R. Billardon : Experimental analysis and multiscale modelling of the anisotropic mechanical and magnetostrictive behaviours of electrical steels. *J. Phys. IV*, 105:247–253, 2003.

[95] L. Daniel, O. Hubert et R. Billardon : Magnetic behaviour of electrical steels : demagnetising surface effect and texture gradient. *International Journal of Applied Electromagnetics and Mechanics*, 1-4(19):293–297, 2004.

[96] O. Hubert et L. Daniel : Multiscale modeling of the magneto-mechanical behavior of grain oriented silicon steels. *Journal of Magnetism and Magnetic Materials*, 320(7):1412–1422, 2008.

[97] L. Daniel, O. Hubert et B. Vieille : Multiscale strategy for the determination of magneto-elastic behaviour : discussion and application to ni-zn ferrites. *International Journal of Applied Electromagnetics and Mechanics*, 25:31–36, 2007.

[98] R. Corcolle, L. Daniel et F. Bouillault : Optimal design of magnetostrictive composites : an analytical approach. *IEEE Transactions on Magnetics*, 44(1):17–23, 2008.

[99] O. Hubert, N. Jendly et L. Daniel : Modelling of the influence of micro-plasticity on the magnetic behaviour of ferromagnetic polycrystals through a multiscale approach. *Steel Research International*, 76(6):440–447, 2005.

[100] O. Hubert et L. Daniel : Effect of plastic straining on magnetostriction of ferromagnetic polycrystals - experiments and multiscale modelling. *Journal of Magnetism and Magnetic Materials*, 304(2):489–491, 2006.

[101] A. Bartók, L. Daniel et A. Razek : Micro-macro modeling of stress-dependent anisotropic magneto-resistance. *J. Phys. D : Appl. Phys.*, 44:135001, 2011.

[102] V. Préault : *Modélisation et caractérisation de matériaux composites pour boîtier d'équipement électronique.* Thèse de doctorat, Université Paris-Sud, France, à soutenir en 2013.

[103] A. Bartók : *Modélisation de dispositifs électromagnétiques sous sollicitations multiphysiques.* Thèse de doctorat, Université Paris-Sud, France, à soutenir en 2012.

[104] D.A. Hall, A. Steuwer, B. Cherdhirunkorn, T. Mori et P.J. Withers : A high energy synchrotron x-ray study of crystallographic texture and lattice strain in soft lead zirconate titanate ceramics. *Journal of Applied Physics*, 96:4245, 2004.

[105] D.A. Hall, J.D.S. Evans, E.C. Oliver, P.J. Withers et T. Mori : In-situ neutron diffraction study of the rhombohedral to orthorhombic phase transformation in lead zirconate titanate ceramics produced by uniaxial compression. *Philosophical Magazine Letters*, 87:41–52, 2007.

Nota : cette bibliographie ne reprend que les références d'articles mentionnés dans le texte d'introduction des publications. La bibliographie des publications qui constituent la partie 2 du document n'a pas été répétée ici.